

UNCLASSIFIED

AD NUMBER

**AD482069**

NEW LIMITATION CHANGE

TO

**Approved for public release, distribution  
unlimited**

FROM

**Distribution authorized to U.S. Gov't.  
agencies and their contractors;  
Administrative/Operational Use; 03 FEB  
1966. Other requests shall be referred to  
Commanding Officer, Army Engineer Research  
and Development Labs., Fort Belvoir, VA  
22060.**

AUTHORITY

**USAMRDC ltr, 20 Aug 1969**

THIS PAGE IS UNCLASSIFIED

AD482069

FINAL  
**ENGINEERING REPORT**

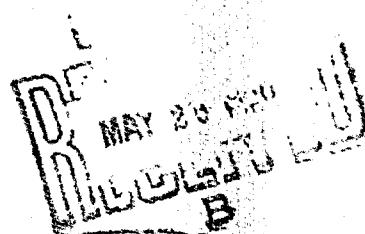
ACOUSTICAL CHARACTERISTICS OF THE  
AIRESEARCH MODEL GTP331-30 GAS TURBINE  
ENGINE AND DEVELOPMENT OF HIGH-TEMPERATURE  
VIBRATION-DAMPING COATINGS  
FOR NOISE CONTROL  
[U.S. ARMY CONTRACT DA-44-009-AMC-838(T)]

GT-7615-R, Rev. 1

February 3, 1966

Each transmittal of this document outside the agencies  
of the U. S. Government must have prior approval of  
Commanding Officer, Army Engineer Research & Development  
Labs, Fort Belvoir, Va. 22060

EA



AIRESEARCH MANUFACTURING COMPANY OF ARIZONA  
A DIVISION OF THE GARRETT CORPORATION  
PHOENIX, ARIZONA



Best Available Copy

**FINAL**  
**ENGINEERING REPORT**

ACOUSTICAL CHARACTERISTICS OF THE  
AIRESEARCH MODEL GTP331-30 GAS TURBINE ENGINE  
AND DEVELOPMENT OF HIGH-TEMPERATURE  
VIBRATION-DAMPING COATINGS  
FOR NOISE CONTROL  
[U.S. ARMY CONTRACT DA-44-009-AMC-838(T)]  
GT-7615-R, Rev. 1 February 3, 1966

Prepared by L. S. Wirt, R. W. Passage, D. Morro  
DGC, JLB

Initial Issue  
Approved by

J. W. McDonald

D. G. Furst  
D. G. Furst



AIRESEARCH MANUFACTURING COMPANY  
A DIVISION OF THE GARRETT CORPORATION

REPORT NO. GT-7615-R, Rev. 1

TOTAL PAGES 351

ATTACHMENTS: Appendices I, II, III, and IV

#### PREFACE

This study was authorized by the U.S. Army Engineer Development Laboratories, Fort Belvoir, Virginia; and was conducted under Contract DA-44-009-AMC-838(T), issued on November 6, 1964. The work reported herein was conducted during the period between the issuance of the contract and the date of this report, December 13, 1965. Those participating in the investigation were Messrs. L. S. Wirt, R. W. Passage, D. L. Morrow, R. L. Orr, J. C. Wahl, and J. E. McGlothin of AiResearch. A consultant, Professor B. J. Lazan, Head of the Aeronautics Department of the University of Minnesota, was retained to assist in a portion of this study. Frequent reference is made throughout this report to the work of others, which is documented in a bibliography in the Appendix Section.

Revision 1 was prepared to correct errors of omission and commission found after initial publication. As a large number of pages were affected, the entire document was reissued, rather than releasing only the revised pages. DGC 2-3-66



## TABLE OF CONTENTS

	<u>Page</u>
1.0 INTRODUCTION	1-1
2.0 SUMMARY	2-1
3.0 CONCLUSIONS AND RECOMMENDATIONS	3-1
3.1 Conclusions	3-1
3.1.1 Sound Survey	3-1
3.1.2 Damping Study	3-4
3.1.3 Micromechanisms and Models	3-4
3.2 Recommendations	3-5
3.2.1 Sound Survey	3-5
3.2.2 Damping Materials	3-5
3.2.3 Micromechanisms and Models	3-6
3.2.4 Improvements to the Model GTP331 Engine	3-7
4.0 BASE-LINE SOUND SURVEY OF THE MODEL GTP331 ENGINE	4-1
4.1 Background	4-1
4.1.1 Quantities Measured	4-1
4.1.2 Testing Performed	4-2
4.2 The Measuring Environments	4-3
4.3 Free-Field Turbine Exhaust Noise Test	4-4
4.3.1 Determination of Sound Power by the Free-Field Method	4-4
4.3.2 Axi-Symmetrical Noise Source Radiating in a Half Space	4-7
4.3.3 Non-Axi-Symmetrical Noise Source	4-8
4.3.4 Turbine Exhaust Noise Test	4-10
4.3.5 Interpretation of the Turbine Exhaust Acoustic Power Spectrum	4-15
4.4 Reverberant-Room Engine Noise Test	4-23
4.4.1 Determination of Sound Power	4-23
4.4.2 Reverberant-Room Measurements	4-24
4.4.3 Engine Noise Test	4-25
4.4.4 Oil-Cooler Fan Acoustic Power Level	4-28



TABLE OF CONTENTS (CONTD.)

	<u>Page</u>
4.4.5 Interpretation of the Acoustic Power Spectra of the Bare Engine	4-39
4.5 Frequency Analyses of the Engine Components	4-44
4.5.1 Component Summary	4-54
4.5.2 Frequency Analysis	4-56
5.0 SOUND AND VIBRATION DAMPING COATINGS	5-1
5.1 Groundwork	5-1
5.1.1 State of the Art Survey	5-1
5.1.2 Materials Selection	5-7
5.1.3 Tuning Fork Test	5-23
5.2 Test Apparatus	5-25
5.2.1 Introduction	5-25
5.2.2 Apparatus Design	5-25
5.2.3 Instrumentation	5-30
5.2.4 Calibration	5-41
5.3 Test Procedure	5-42
5.3.1 Operational Procedure	5-42
5.3.2 Base-Line Test	5-44
5.4 Data Analysis	5-54
5.4.1 Terminology	5-54
5.4.2 Objectives	5-56
5.4.3 Derivation of Data Programming Methods	5-57
5.4.4 Error Analysis	5-72
5.5 Test Results	5-77
5.5.1 Introduction	5-77
5.5.2 Observations	5-128
5.5.3 The Refined Data	5-132
5.6 Other Physical Properties	5-138
5.6.1 Base Material	5-138
5.6.2 Coatings	5-139
5.6.3 Fabrication Philosophy	5-149



TABLE OF CONTENTS (CONTD.)

	<u>Page</u>
5.7 Discussion	5-151
5.7.1 Temperature Band Width	5-151
5.7.2 Frequency Band Width	5-158
5.7.3 Applications	5-161
6.0 MICROMECHANISM AND MODELS	6-1
6.1 Introduction	6-1
6.2 Some Known Micromechanisms	6-3
6.2.1 Anelasticity	6-3
6.2.2 Viscoelasticity	6-4
6.2.3 Nonlinear Damping	6-5
6.3 Micromechanisms in the Specimens	6-6
6.3.1 Hastelloy X	6-6
6.3.2 Vitreous Enamels	6-6
6.3.3 Manganese Alloys	6-8
6.3.4 Aluminum Cermets	6-8
6.4 Micromechanism and Fatigue	6-9
6.5 Rheological Epicycles	6-17
6.5.1 Introduction	6-17
6.5.2 Ptolemaic Formulation	6-25
6.5.3 Synthesis of Hysteresis Loops by Means of a Computer	6-66
6.5.4 The Generalized Hysteresis Loop and Its Representation by Means of Power Series	6-86

Appendix I - Review of Polar Formulas

Appendix II - Vendor Information

Appendix III - The Elastic and Anelastic Properties of Refractory Material for High-Temperature Applications

Appendix IV - List of References



## LIST OF FIGURES

<u>Figure</u>	<u>Title</u>	<u>Page</u>
4-1	Microphone Locations Used for Free Field Measurements	4-9
4-2	Microphone Locations Used for Free Field Measurements	4-11
4-3	Straight Exhaust Duct	4-13
4-4	Right-Angle Exhaust Duct	4-13
4-5	Right-Angle Exhaust Duct Attached to Straight Exhaust Duct	4-14
4-6	Engine Completely Enclosed with Air Inlet Silencers	4-26
4-7	Bare Engine, Panels Removed from Enclosure	4-27
4-8	Turbine Plenum Section	4-29
4-9	Compressor Section	4-30
4-10	Accessory Section	4-31
5-1	Idealized Damping Relations and Values for Different Categories of Materials	5-12
5-2	Properties of Alclad Materials	5-14
5-3	Manganese Alloys (Cold Worked)	5-15
5-4	Decay Rate of Cantilever Beams	5-18
5-5	Properties of XAP Alloys	5-19
5-6	Vibration-Damping Test Apparatus	5-26
5-7	Vibration-Damping Test Instrumentation	5-27
5-8	Test Apparatus with Oven and Instrumentation	5-31
5-9	Test Apparatus and Modified Oven Opening	5-32
5-10	Schematic of Driver and Optical Pickup	5-33
5-11	Test Apparatus with Driver Coils	5-35
5-12	Schematic Diagram of Driver Circuit	5-35
5-13	Instrumentation Used With Vibration Damping Test	5-39
5-14	Flexure No. 14 Mn Cu Alloy Coating after Heat Treat	5-47



AIRESEARCH MANUFACTURING COMPANY OF ARIZONA  
A DIVISION OF THE GARRETT CORPORATION  
PHOENIX, ARIZONA

LIST OF FIGURES (CONTD.)

<u>Figure</u>	<u>Title</u>	<u>Page</u>
5-15	Flexure No. 14 Mn Cu Alloy after Heat Treat	5-48
5-16	Flexure No. 18 after Test No. 3, Mn Cu Alloy Coating	5-50
5-17	Flexure No. 18 after Test No. 3, Mn Cu Alloy Coating	5-51
5-18	Classification of Recommended Damping Units, Their Interrelations, and Their Relations to the Measured Quantities of Damping Testing Systems	5-55
5-19	Longitudinal Section of a Sheet-Metal Strip with Two Damping Layers	5-65
5-20	Hastelloy Alloy X - Union Carbide Corp.	5-71
5-21	Test Data From Mystik Tape No. 7402	5-92
5-22	Test Data From Type B <sub>b</sub> Vitreous Coating	5-93
5-23	Test Data From XAPOOL Alloy	5-94
5-24	Test Data From Mn Cu Alloy No. 780	5-95
5-25	Test Data From Bare Flexure	5-96
5-26 thru 5-43	Computer Analysis of Test Data	5-97 thru 5-114
5-44	Actual versus Theoretical Loss Modulus for Type C Vitreous Coating	5-153
5-45	Porcelain Enamels	5-156
5-46	Frequency Range Between Loss-Modulus Half Values for Type C Vitreous Coating	5-162
6-1	Typical Changes in Stress-Strain Hysteresis Loops Occurring With Type BC Specimen During Fatigue Tests at High Stress Amplitude, $\pm 2940$ psi	6-11
6-2	Electron Micrographs of Chemically Polished Specimens	6-12
6-3	Electron Micrograph from Surface Replica of Tapered Specimen at $\pm 2500$ psi Level, After 1000 Cycles	6-13



AIRESEARCH MANUFACTURING COMPANY OF ARIZONA  
A DIVISION OF THE GARRETT CORPORATION  
PHOENIX, ARIZONA

### LIST OF FIGURES (CONTD.)

<u>Figure</u>	<u>Title</u>	<u>Page</u>
6-4	Electron Micrograph From Surface Replica of Tapered Specimen at 2500 psi Level, After $10^4$ Cycles	6-14
6-5	Electron Micrograph From Surface Replica of Tapered Specimen at $\pm 2500$ psi Level, After $10^5$ Cycles	6-15
6-6	Shaft Motions	6-21
6-7	An Arbitrary Hysteresis Loop in a Complex Plane	6-28
6-8	The Zero Order Term Which Represents the Preload	6-33
6-9	The Components of $\bar{R}_n$ At $t=0$	6-33
6-10	The Components of $\bar{R}_n$ At $t=0$	6-35
6-11	Angular Relations of $\bar{R}_n$ And $\bar{R}_n$	6-38
6-12	Increment of Area Swept Out by the Vector $\bar{H}_n$	6-42
6-13	Relative Position of $E$ , $E^*$ , And $\bar{E}$ Vectors	6-46
6-14	Determination of Direction of $E$ And $\bar{E}$	6-48
6-15	A Circular Hysteresis Loop in The Real Stress-Strain Plane	6-49
6-16	A Elliptical Hysteresis Loop for Stress And Strain	6-52
6-17	Equivalent Circular Hysteresis Loops for the Elliptical Loop in Figure 6-16.	6-52
6-18	Effect of Phase Parameters, $\alpha_n$ and $\beta_n$	6-55
6-19	Construction of $\bar{R}_n$ and $\bar{R}_n$ From a Time Mark on the nth Ellipse	6-57
6-20	Coulomb Damping	6-59
6-21	First Component Ellipse for a Square Hysteresis Loop	6-63
6-22	The $n = 3$ Component of a Square Hysteresis Loop	6-64
6-23	The $n = 5$ Component of a Square Hysteresis Loop	6-64



LIST OF FIGURES (CONTD.)

<u>Figure</u>		<u>Page</u>
6-24	Successive Approximations of a Square Hysteresis Loop as n Increases from 1 to 7	6-65
6-25	Analog Computer	6-67
6-26	$\bar{R}_1$ Circle (upper) and $\bar{Y}_1$ Circle (lower)	6-68
6-27	Computer Mechanization For Simulation of $\bar{R} = A (\sin \omega t + j \cos \omega t)$	6-70
6-28	Computer Mechanization For Simulation of $\bar{Y} = B (\sin \omega t + j \cos \omega t)$	6-72
6-29	Combined $\bar{R}$ and $\bar{Y}$ Circles	6-73
6-30	Lower: The Third Harmonic $\bar{R}_3 + \bar{Y}_3$ , ( $R_3 = Y_3$ ) Upper: Effect of Adding the Third Harmonic to the Combined $\bar{R}$ and $\bar{Y}$ Circles	6-74
6-31	Computer Mechanization for Simulation of: $\bar{R} + \bar{Y}_3 = A_3 [\sin (3 \omega t + j \cos (3 \omega t = \alpha))]$	6-76
6-32	Summing Amplifiers	6-77
6-33	Effect of $\bar{R}_3 + \bar{Y}_3 = A_3 \sin (3 \omega t + 0)$	6-78
6-34	Effect of $\bar{R}_3 + \bar{Y}_3 = A_3 \sin (3 \omega t - 30^\circ)$	6-79
6-35	$\bar{R}_3 + \bar{Y}_3 = A_3 \sin (3 \omega t - 60^\circ)$	6-80
6-36	$\bar{R}_3 + \bar{Y}_3 = A_3 \sin (3 \omega t - 90^\circ)$	6-81
6-37	Normalization of The First Order Ellipse, Shown for Input $\epsilon = a \cos \theta$	6-88
6-38	Relation of Stress Input to Strain Input for a Viscoelastic Material	6-90
6-39	The Construction of $\bar{F}$ , $\bar{G}$ , and $\bar{H}$ - $\frac{\bar{F} - \bar{G}}{2}$ at $t = 0$	6-91
6-40	$\bar{F}$ , $\bar{G}$ , and $\bar{H}$ for the Case $\delta = 0$	6-96
6-41	$\bar{F}$ , $\bar{G}$ , and $\bar{H}$ for the Case $\delta = \frac{\pi}{2}$	9-98



AIRESEARCH MANUFACTURING COMPANY OF ARIZONA  
A DIVISION OF THE GARRETT CORPORATION  
PHOENIX, ARIZONA

LIST OF TABLES

<u>Table</u>	<u>Title</u>	<u>Page</u>
4-1	Turbine Exhaust Directivity Index (db) GTP331-30 With Straight Exhaust Duct	4-18
4-2	Turbine Exhaust Directivity Index (db) GTP331-30 With Right-Angle Exhaust Duct - No Load Condition	4-19, 20
4-3	Turbine Exhaust Directivity Index (db) GTP331-30 With Right-Angle Exhaust Duct - Full Load Condition	4-21, 22
5-1	Physical Properties of Alcoa's Sintered Aluminum Powder Alloys	5-141
5-2	Typical Mechanical Properties of Sintered Aluminum Power Extrusions at Progressively Elevated Temperatures	5-142
5-3	Nominal Chemical Composition of Manganese Alloys, Percent by Weight	5-143
5-4	Manganese Alloy Physical Properties	5-143
5-5	Typical Mechanical Properties Manganese Alloys At Room Temperature	5-144
5-6	Ceramic Coating Compositions	5-146
6-1	Values for $R_n$ , $\bar{R}_n$ , $\alpha_n$ , and $s_n$ versus n	6-62
6-2	Values for $\bar{R}_1$ and $\bar{R}_1$ versus $\delta'$	6-108



AIRESEARCH MANUFACTURING COMPANY OF ARIZONA  
A DIVISION OF THE GARRETT CORPORATION  
PHOENIX, ARIZONA

LIST OF GRAPHS

<u>Graph</u>	<u>Title</u>	<u>Page</u>
4-1	1/3 Octave Band Sound Power Level Spectrum GTP331-30 Exhaust Noise - No Load Condition	4-16
4-2	1/3 Octave Band Sound Power Level Spectrum GTP331-30 Exhaust Noise - Full Load Condition	4-17
4-3	1/3 Octave Band Sound Power Level Spectrum GTP331-30 - Turbine Plenum Radiated Noise No Load Condition-Exhaust Noise Excluded	4-32
4-4	1/3 Octave Band Sound Power Level Spectrum GTP331-30 - Turbine Plenum Radiated Noise - Full Load Condition - Exhaust Noise Excluded	4-33
4-5	1/3 Octave Band Sound Power Level Spectrum GTP331-30 Compressor Inlet Noise - No Load Condition - Exhaust Noise Excluded	4-34
4-6	1/3 Octave Band Sound Power Level Spectrum GTP331-30 Compressor Inlet Noise - Full Load Condition - Exhaust Noise Excluded	4-35
4-7	1/3 Octave Band Sound Power Level Spectrum GTP331-30 Accessory Case Noise - No Load Condition - Exhaust Noise Excluded	4-36
4-8	1/3 Octave Band Sound Power Level Spectrum GTP331-30 Accessory Case Noise - Full Load Condition - Exhaust Noise Excluded	4-37
4-9	1/3 Octave Band Sound Power Level Spectrum GTP331-30 Accessory Case Noise - No Load Condition	4-38
4-10	1/3 Octave Band Sound Power Level Spectrum GTP331-30 Oil Cooler Fan - Determined by Close-In Measurement	4-40
4-11	1/3 Octave Band Sound Power Level Spectrum GTP331-30 Bare Engine Noise - No Load Condition - Exhause Noise Excluded	4-42



AIRRESEARCH MANUFACTURING COMPANY OF ARIZONA  
A DIVISION OF THE GARRETT CORPORATION  
PHOENIX, ARIZONA

LIST OF GRAPHS (CONTD.)

<u>Graph</u>	<u>Title</u>	<u>Page</u>
4-12	1/3 Octave Band Sound Power Level Spectra GTP331-30 - Bare Engine Noise - Full Load Condition-Exhaust and Oil-Cooler Fan Noise Excluded	4-43
4-13	1/3 Octave Band Sound Power Level Spectrum of GTP331-30 Accessory Case with Oil Cooler Fan - No Load Condition	4-45
4-14	1/3 Octave Band Sound Power Level Spectrum of the Total Power Radiated from the Model GTP331-30	4-46
4-15	Turbine Section - No Load - Close-In Sound Measurement	4-47
4-16	Turbine Section - Full Load - Close-In Sound Measurement	4-48
4-17	Compressor Section - No Load - Close-In Sound Measurement	4-49
4-18	Compressor Section - Full Load - Close-In Sound Measurement	4-50
4-19	Accessory Section - No Load (without Oil- Cooler Fan) - Close-In Sound Measurement	4-51
4-20	Accessory Section - Full Load (without Oil- Cooler Fan) - Close-In Sound Measurement	4-52
4-21	Accessory Section - No Load (with Oil-Cooler Fan) - Reverberant Sound Measurement	4-53
5-1	Optical System Output vs. Strain Measurements	5-43
5-2	Flexure No. 8, Coating = Vitreous Type A	5-78
5-3	Flexure No. 10, Coating = Vitreous Type B	5-79
5-4	Flexure No. 11, Coating = Vitreous Type B <sub>b</sub>	5-80
5-5	Flexure No. 12, Coating = Vitreous Type C	5-81
5-6	Flexure No. 18, Coating Mn Cu Alloy No. 780	5-82



AIRESEARCH MANUFACTURING COMPANY OF ARIZONA  
A DIVISION OF THE GARRETT CORPORATION  
PHOENIX, ARIZONA

LIST OF GRAPHS (CONTD.)

<u>Graph</u>	<u>Title</u>	<u>Page</u>
5-7	Flexure No. 18, Coating = Mn Cu Alloy No. 780	5-83
5-8	Flexure No. 23, Coating = Mn Cu Alloy No. 772	5-84
5-9	Flexure No. 16, Coating = Mn Cu Alloy No. 720	5-85
5-10	Flexure No. 22, Coating = Al Alloy XAP001	5-86
5-11	Flexure No. 17, Coating = Al Alloy XAP003	5-87
5-12	Flexure No. 27, Coating = Sperex VHT Coating	5-88
5-13	Flexure No. 27, Coating = Mystik Tape No. 7402	5-89
5-14	Flexure No. 27, Coating = Mystik Tape No. 7402	5-90
5-15	Damping Efficiency, Geiger Test Method	5-115
5-16	Hastelloy X Bare Flexure	5-116
5-17	Flexure No. 8, Coating = Vitreous Type A	5-117
5-18	Flexure No. 10, Coating = Vitreous Type B	5-118
5-19	Flexure No. 11, Coating = Vitreous Type B <sub>b</sub>	5-119
5-20	Flexure No. 12, Coating = Vitreous Type C	5-120
5-21	Vitreous Type Coatings	5-121
5-22	Flexure No. 18, Coating = Mn Cu Alloy No. 780	5-122
5-23	Flexure No. 23, Coating = Mn Cu Alloy No. 772	5-123
5-24	Flexure No. 16, Coating = Mn Cu Alloy No. 720	5-124
5-25	Flexure No. 22, Coating = Al Alloy XAP001	5-125
5-26	Flexure No. 17, Coating = Al Alloy XAP003	5-126
5-27	Flexure No. 27, Coating = Mystik Tape No. 7402	5-127
5-28	Mn Cu Alloy Data Comparison from Various Observers	5-129



AIRESEARCH MANUFACTURING COMPANY OF ARIZONA  
A DIVISION OF THE GARRETT CORPORATION  
PHOENIX, ARIZONA

ACOUSTICAL CHARACTERISTICS OF THE  
AIRESEARCH MODEL GTP331-30 GAS TURBINE ENGINE  
AND DEVELOPMENT OF HIGH-TEMPERATURE  
VIBRATION-DAMPING COATINGS  
FOR NOISE CONTROL  
[U.S. ARMY CONTRACT DA-44-009-AMC-838(T)]

#### 1.0 INTRODUCTION

This is the final report on the investigation of means and techniques for attenuating the sound level of single-shaft gas turbine engines in the 30/500-hp engine size conducted under Contract DA-44-009-AMC-838(T).

The work done under the contract had the objective to determine new or improved approaches for attenuating noise, as an extension of basic work done under Contract DA-44-009-ENG-5183, as follows:

- (a) Acoustical testing of the Model GTP331-30 Engine.
- (b) Analytical study, test, and evaluation of sound and vibration damping materials.
- (c) Investigation of the other physical properties of those materials found to show promise in sound damping.
- (d) Presentation of recommendations for future follow-on work.



AIRESEARCH MANUFACTURING COMPANY OF ARIZONA  
A DIVISION OF THE BARRETT CORPORATION  
PHOENIX, ARIZONA

This report presents the results of the testing and studies conducted and makes recommendations for further investigations. The work reported herein is a continuation of studies for developing practical methods of attenuating the noise of a Model GTP331 Gas Turbine Engine within its envelope. This prior work utilized vibration damping useful only at low metal temperatures (up to 500°F). Thus, there was still a lack of suitable means for vibration-damping the high-temperature structure, particularly its sheet-metal parts. This study, then, is an attempt to extend the field of knowledge of vibration-damping coatings. Previous damping coatings investigated were effective only up to 500°F; for this study, the object was to find coatings effective up to 2000°F.



## 2.0 SUMMARY

Acoustical power level spectra and directivity indices in one-third octave bands were measured by the free-field method, with use of both a straight exhaust duct and a right-angle duct. One-third octave acoustic power level spectra were obtained for the cooling fan, accessory case, compressor inlet, and turbine plenum by use of the reverberant-room method. Source isolation was accomplished by means of a special compartmented enclosure having removable panels. The method appears satisfactory and convenient, and the data obtained will be useful to installation designers and for the design of attenuating devices. The noise patterns and trends are in general similar to those observed in related engine models.

Two strong pure-tone spikes, which are not acoustically desirable, were observed. One occurs at main rotor speed and is symptomatic of unbalance. The second occurs at 100 to 125 cps in the exhaust noise. Tape recordings of each noise source were subjected to narrow-band analyses and local peaks correlated with engine processes.

The materials study began with a survey of literature, vendors, and authorities in the field of vibration damping, and very little information relating specifically to high-temperature vibration-damping coatings was found. A consultant, Dr. B. J. Lazan, was retained to provide the conceptual design of a test apparatus. The consultant was also able to demonstrate data processing methods determining fundamental parameters of vibration damping. Eventually, three types of coatings were tested:

- (a) Vitreous enamels
- (b) High-manganese alloys
- (c) Aluminum-alumina cermets



AIRESEARCH MANUFACTURING COMPANY OF ARIZONA  
A DIVISION OF THE GARRETT CORPORATION  
PHOENIX, ARIZONA

All of the vitreous enamels, when applied in thin coatings, exhibited very good damping ability within their usable temperature range. The least efficient enamel had far more damping at high temperatures than the best low-temperature material at its optimum. This includes the enamels commonly used for corrosion resistance at elevated temperatures. Some of the high-manganese alloys and aluminum-alumina cermets produced a significant but lesser amount of damping. Test results with manganese copper alloys showed unexplained irregularities which need further investigation. It was recommended that further study of these alloys be started in the near future so as to make available a larger variety of damping materials.

It is not uncommon for research in one field to uncover useful information only obliquely related to the original objectives. Occasionally such discoveries overshadow the original objectives of the study. Any material or system when cyclically stressed generates a hysteresis loop. These loops are studied because they indicate the types of micromechanisms at work in the material.

In particular, the nonlinear hysteresis loops generated at high stress levels are studied in attempts to learn the micro-mechanisms of fatigue failure. The literature searched revealed that this study of fatigue is seriously hampered by the lack of adequate mathematical models for nonlinear hysteresis loops.

It was noticed that these nonlinear hysteresis loops resembled the Lissajous Figures encountered in shaft dynamics. Adequate mathematical models for the shaft motions have recently appeared. These were found to be formulatable in a way capable of describing any hysteresis loop.



AIRESEARCH MANUFACTURING COMPANY OF ARIZONA  
A DIVISION OF THE GARRETT CORPORATION  
PHOENIX, ARIZONA

It is possible that this mathematical model for the nonlinear hysteresis loop can contribute to the understanding of fatigue. Ironically the lack of knowledge of metal fatigue is the major incentive for the use of damping coatings.

It is therefore possible that this unforeseen discovery will become the most significant aspect of this study, in spite of the success in attaining the original objectives.

It was recommended that work continue in the study of noise generation and transmission in gas turbine engines, with the Model GTP331 used as a typical example. The need for such information becomes more urgent as gas turbines attain broader usage and operate more frequently in proximity to personnel.

Current technological advances indicate that gas turbines will be operating at temperatures greater than 2000°F, and a demand will exist for damping materials in the range from 2000°F to 4000°F. The results of this study indicated that useful damping might be attained up to 3500°F. Development with this goal in mind should commence as soon as possible.

A detailed design study and development program should now be undertaken to incorporate vitreous enamels as vibration-damping coatings in the Model GTP331-30 engine structure, and into gas turbines in other size ranges.

It was recommended that generalized hysteresis loops and their power series representation be subjected to further study to explore their mathematical properties and to seek correlation with physical measurements and dislocation theory.



AIRESEARCH MANUFACTURING COMPANY OF ARIZONA  
A DIVISION OF THE GARRETT CORPORATION  
PHOENIX, ARIZONA

### 3.0 CONCLUSIONS AND RECOMMENDATIONS

#### 3.1 Conclusions

##### 3.1.1 Sound Survey

The method of source separation by means of a compartmented enclosure provided satisfactory acoustic power level spectra for the individual sources considered. The limiting factor in the method is the degree to which vibration isolation between the engine and its enclosure, in particular the bulkheads, is attained. The primary difficulty occurs at low frequencies.

The cooling fan used on this unit has an acoustic power level spectrum which differs from that of older models, due to increased blade count. A dominant peak of 115 db occurs in the acoustic power level at the blade-passage fundamental (5,750 cps). This represents a significant improvement over older four-bladed fans. The higher blade passage frequency lends itself to attenuation by a more compact inlet-duct silencing device.

The remaining accessory-section noise, in general, lies well below the base engine noise spectrum, such that it would become significant only on an engine that has been thoroughly attenuated at all other noise sources, including the fan. No acoustical indications of accessory malfunction were found in the narrow-band analyses.



The compressor inlet acoustic power level spectrum is dominated by a blade-passage-fundamental pure tone of 137 db. A substantial spike also occurs at main rotor speed. This is believed to be due mainly to a single-lobed spinning mode associated with synchronous precession of the impellers.

The acoustic power level spectrum for the turbine plenum is of the usual form. At low frequencies, plenum noise levels are substantially below those of the compressor inlet. In the 2,000 to 8,000-cps band the plenum becomes more "transparent" and noise levels approach those of the compressor inlet. The acoustic spectrum is dominated by a peak of 122 db, corresponding to the combined frequencies of the first- and second-stage compressor wheel blade counts.

The exhaust acoustic power level spectrum differs according to whether a straight or right-angle duct is used. Both feature a dominant low-frequency peak centered in the 100-to 200-cps region. The middle- and high-frequency regions feature moderate acoustic power levels which are relatively flat. The turbine-blade-passage fundamental occurs in the ultrasonic frequency range. The right angle duct attenuates the higher frequencies by several db, apparently by reflective processes. Only at no load there are strong pure-tone spikes projecting from the low-frequency broad-band hump. These extend more than 10 db above the surrounding spectrum and are the dominant spikes. A peak value of 140 db is attained with the right-angle exhaust pipe. This type of spike has been occasionally encountered before, but is not regarded as a normal exhaust noise component.



All attenuation hardware developed under ERDL Contract DA-44-009-ENG-5183 and described in Ref. 1 (SD 5011 - Vol. 2) is directly applicable to the Model GTP331-30 engine. The attenuation attainable thereby is well represented by the best results shown in SD 5011. This can be said with confidence because of refinements that have occurred in the intervening period. These include the adoption of Scottfelt and the production and additional testing of Slitmetal.

Appreciable weight reductions result from the substitution of Scottfelt for Feltmetal in the treatment of compressor inlets. This will be offset in part by a slightly bulkier turbine-plenum jacket necessitated by the lack of symmetry of a single-combustor plenum. See References 38 and 39.

As judged from an acoustical standpoint, the engine appears "normal", producing noise patterns typical of gas turbines, with two exceptions.

- (a) The shaft-speed components appear high, which indicates that improved balance is at least acoustically desirable as a means of internal sound attenuation.
- (b) The presence of the pure-tone spikes in the low-frequency exhaust noise at some load conditions, although previously observed, is not considered "normal" and its magnitude makes it acoustically undesirable.



### 3.1.2 Damping Study

It is concluded that vitreous enamels may be regarded as viscoelastic damping materials of extraordinary efficiency at elevated temperatures. These are commercially available in a wide variety, some of which are already specialized for corrosion resistance and other properties rendering them usable in the environments prevailing inside gas turbines. The literature reveals the likelihood that similar properties exist to some extent in refractory ceramics, such that immediate extension of the scope of useful application of 3500°F by means of refractory coatings seems feasible.

The high-manganese alloys exhibit broad-band high-temperature damping of unknown origin. Their behavior is complex, and substantial additional work would be required to develop coatings of a predictable nature.

The aluminum-alumina cermets (XAP) exhibit broad-band damping of modest but useful proportions over the temperature range up to 1000°F. This material can be applied with ordinary metal-spray equipment. Oxidation resistance was good.

### 3.1.3 Micromechanisms and Models

Recent technical literature reveals a lack of suitable mathematical models for stress-strain-time relations for materials in their nonlinear range. This lack impedes fundamental research into the micromechanisms of damping and fatigue. The 2,000-year-old Epicycles of Ptolemy are capable of providing such a model. These can be reformulated as power series reminiscent of Laurent's series. It is concluded that the classic sinusoidal stress or sinusoidal



AIRESEARCH MANUFACTURING COMPANY OF ARIZONA  
A DIVISION OF THE GARRETT CORPORATION  
PHOENIX, ARIZONA

strain test procedures cannot define a nonlinear material, but fundamental parameters can be deduced if both tests are performed.

Useful information concerning energy relations and other properties of hysteresis loops can be graphically demonstrated by the epicyclic model. When formulated as a power series, the concept of a unique generalized hysteresis loop, as a representation for a material, evolves. It is concluded that this mathematical model may prove useful to facilitate fundamental material research leading, for example, to better damping materials.

### 3.2 Recommendations

#### 3.2.1 Sound Survey

The mechanisms by which the low-frequency hump in the exhaust noise spectra is generated need fundamental investigation. This includes both the broad hump and the pure-tone spikes which occasionally arise out of it. The broad hump is commonly called "combustion rumble", but recent developments have cast doubt on the appropriateness of this term and have provided new hypotheses as a guide to specific research. This research should be pursued, because all known silencing devices of reasonable proportions fail to attenuate the low-frequency hump.

#### 3.2.2 Damping Materials

To facilitate the more rapid application of vitreous enamels as high-temperature damping coatings, greater knowledge should be acquired of the effects of composition on the location and width of the damping peak. It is recommended that screening tests such as the Harrison test be carefully explored to provide simple test procedures to fill this need.



AIRESEARCH MANUFACTURING COMPANY OF ARIZONA  
A DIVISION OF THE GARRETT CORPORATION  
PHOENIX, ARIZONA

It is recommended that the manganese alloys be further examined in several areas. Study is required to understand and control the high-temperature damping found in these materials. Development is needed of suitable coating processes, either by improved metal-spray procedures or perhaps by hot dip or sintering procedures. Attempts to apply the known room-temperature damping to the fabrication of quieter gearing, bearings, and seals seem likely to be profitable.

The aluminum cermets show promise as convenient broad-band dampers either as a coating or as a structural material. Fundamental research to establish the micromechanisms of their damping is needed.

Experimental evaluation of the acoustical effects of vibration-damped turbines is recommended, but only if the testing is intensive enough to accomplish such a complete source separation that the results are not masked by interfering noise. Such a test would be quite elaborate in nature. Tests to reveal reduction of resonant stress in hot sheet-metal parts are recommended as both simple to execute and meaningful.

### 3.2.3 Micromechanisms and Models

It is strongly recommended that the possible usefulness of the concepts of epicycles, generalized hysteresis loops, and power series be explored to establish the full extent of their value as research tools. This investigation would of necessity be of a highly academic nature. It could best be conducted by a team effort. Pure mathematics, metallurgy, and solid-state physics should be represented on such a team. Since the concepts seem to apply in any field in which hysteresis loops appear, academic-level attempts to apply them to electrical, magnetic, mechanical, and acoustical problems seem in order.



AIRESEARCH MANUFACTURING COMPANY OF ARIZONA  
A DIVISION OF THE GARRETT CORPORATION  
PHOENIX, ARIZONA

### 3.2.4 Improvements to the Model GTP331-30 Engine

The ultimate desireability of maximum noise reduction for the Model GTP331-30 engine is recognized. The concepts developed herein and those accomplished under the previous contract, DA-44-009-ENG-5183, provide a means whereby a lessening in engine noise can be achieved. It is recommended that a development program be undertaken with the purpose of incorporating into an engine all of the known noise-reducing methods. This program would include three basic phases.

In the first phase, development tests would be conducted on materials found to dampen vibration, to evaluate their physical properties at simulated engine operating conditions. These tests would determine such characteristics as corrosion resistance, thermal shock, erosion resistance, and resistance to the effects of oxidation and sulfidation.

With the above knowledge, an engine design study phase would be initiated. Each engine section would be designed to incorporate the optimum materials and concepts regarding noise reduction and operating conditions. Weight, cost, and size studies would be made to insure the best overall configuration.

In the final phase, an engine would be fabricated and subjected to an acoustical survey. These results would be compared to the baseline sound survey and the magnitude of sound reduction noted.



## 4.0 BASE-LINE SOUND SURVEY OF THE MODEL GTP331 ENGINE

### 4.1 Background

A fundamental acoustical survey of a new gas turbine engine model has several useful functions. The data obtained can be invaluable to the designer of a system that includes the engine and can cast light on fundamental characteristics of the gas turbine, thus contributing to its improvement. Finally, acoustical data on the bare engine is essential for the optimum design of silencing components to be added to it.

#### 4.1.1 Quantities Measured

How useful acoustical data is depends mainly on the quantities chosen for measurement and the degree of care with which the various sources of noise are separated from each other. Acoustical data consisting of overall sound pressure observations is, in general, of little value since it provides no information as to how the sound is distributed, in frequency, and no clues as to its sources. Sound-pressure-level spectra at arbitrary observation points are slightly more useful, but their magnitude at any other points in space cannot be readily predicted, and information as to the sources of the noise remains lacking.

Acoustic-power-level spectrum is a much more fundamental quality. It is the actual power radiated as sound by a noise source, expressed as a function of frequency. The power could be expressed directly in watts, but a decibel scale is more commonly used. Since acoustic power is essentially independent of both environment and the location of measuring equipment, it is the fundamental acoustical quantity. In principle, if the acoustic power level spectrum



AIRESEARCH MANUFACTURING COMPANY OF ARIZONA  
A DIVISION OF THE GARRETT CORPORATION  
PHOENIX, ARIZONA

plus a related quantity, directivity index is known, then the sound pressure level can be computed at any point in space, in any environment--be it outdoors or in a room of any size, shape, or construction.

Source separation is equally vital. The spectrum of a compressor inlet is totally different from that of a turbine exhaust. A compressor inlet handles ambient air; the turbine exhaust duct handles products of combustion at perhaps 1200°F. Thus, data on the combined inlet and exhaust noise will be of little use in the optimum design of either an inlet or an exhaust silencer.

Other noise sources -body radiation, gear case, and cooling fan--contribute significantly to the total disturbance. Detailed knowledge of each is essential to their proper individual treatment. In summary, a good acoustical study accomplishes the measurement of acoustical-power-level spectra for each individual noise source present. Directivity information on the bare engine, although desirable, is not as important as acoustic power data. Normally, the engine will be either enclosed or acoustically jacketed. Its compressor inlet and exhaust will be ducted; the directivity characteristics of such ducts and silencers are more important than those of the bare engine.

#### 4.1.2 Testing Performed

The base-line survey of the AiResearch Model GTP331-30 Gas Turbine Engine was conducted in three phases. The first is the determination of the turbine exhaust acoustic power level by the free-field method. Two exhaust configurations were used--a standard laboratory straight extension and a right-angle duct. The second phase determined the acoustic power level of the engine less the



AIRESEARCH MANUFACTURING COMPANY OF ARIZONA  
A DIVISION OF THE GARRETT CORPORATION  
PHOENIX, ARIZONA

exhaust noise by the reverberant-field method. This phase also included a noise separation of the three engine sections--the turbine plenum, the compressor inlet, and the accessory case.

A third phase was added for the acoustic-power-level estimation of the oil-cooler fan noise. The method used consisted of close-in or direct near-field measurements and were only approximate. Additional close-in measurements of the separate engine sections were tape-recorded for a detailed frequency analysis and source-component identification.

#### 4.2 The Measuring Environments

A laboratory test cell, specially modified for acoustic testing, was used for all three phases of this survey. The cell served as a soundproof enclosure for the engine during the free-field measurements, and the bare interior wall surfaces made the building suitable for reverberation measurements conducted within the cell.

The cell is constructed of reinforced concrete having a high transmission loss factor. All openings in the cell were either sealed or acoustically treated, and special commercial sound-proof doors were used on the outside entrance into the cell. The engine intake air was admitted into the cell through special air silencers. The air was also humidified, due to the fact that air absorption of sound can become significant at low humidities, especially at the high frequencies.



AIRESEARCH MANUFACTURING COMPANY OF ARIZONA  
A DIVISION OF THE GARRETT CORPORATION  
PHOENIX, ARIZONA

Free-field measurement of the exhaust noise was made in the outside space adjacent to the cell-wall exhaust-duct opening. The reverberant-field and direct near field measurements were made within the cell. A special engine enclosure was used whereby the three main engine sections--the turbine plenum, the compressor inlet, and the accessory case--were acoustically separated by compartmentation of the enclosure. Thus, the noise radiated from an engine section could be emitted into the room by removing the three outer panels (the two sides and top) that enclosed the section. With all side and top panels removed, the total engine noise less the turbine exhaust could be measured.

#### 4.3 Free-Field Turbine Exhaust-Noise Test

##### 4.3.1 Determination of Sound Power by the Free-Field Method

The determination of the sound power radiated by a noise source in a free field above a reflecting plane is based on these premises:

1. The reverberant field is negligible at the positions of measurement.
2. The radiated sound power is obtained by a space integration of the sound intensity over an imaginary hemisphere centered on the source of noise.
3. The surface of the hemisphere is in the far field of the source.



AIRESEARCH MANUFACTURING COMPANY OF ARIZONA  
A DIVISION OF THE GARRETT CORPORATION  
PHOENIX, ARIZONA

The equations utilized to convert the free-field sound pressure measurements to total sound power are briefly outlined below.

For a free progressive wave the sound intensity ( $I$ ) at a point is proportional to the sound pressure squared.

$$I = \frac{P^2}{\rho_0 C} \quad \text{where, } P = \text{sound pressure} \quad (1)$$

$\rho_0 = \text{density of air}$

$C = \text{local velocity of sound in air}$

The acoustic power ( $W$ ) is defined as the integral sound intensity ( $I$ ) over a surface area ( $S$ ).

$$dW = \int I \, ds \quad (2)$$

This integral can be evaluated approximately by choosing an array of sound-measuring locations ( $L$ ) that divide the total surface into small areas ( $\Delta S$ ). Each sound measurement will be associated with a particular area ( $\Delta S_L$ ) and the calculated sound intensity ( $I_L$ ) will be representative of that area.

therefore,

$$\Delta W = I_L \Delta S_L = \frac{P_L^2}{\rho_0 C} \Delta S_L \quad (3)$$



AIRESEARCH MANUFACTURING COMPANY OF ARIZONA  
A DIVISION OF THE GARRETT CORPORATION  
PHOENIX, ARIZONA

The space sound pressure level (SPL) over the small area is defined by the equation:

$$SPL_L = 20 \log_{10} \frac{P_L}{P_{ref}} = 10 \log_{10} \frac{P_L^2}{P_{ref}^2} \quad (4)$$

or  $P_L^2 = P_{ref}^2 \text{ antilog}_{10} \left( \frac{SPL_L}{10} \right)$  (5)

Substituting into Equation (3):

$$\Delta W_L = \frac{\Delta S_L P_{ref}^2}{\rho_0 C} \text{ antilog}_{10} \left( \frac{SPL_L}{10} \right) \quad (6)$$

The sound power level (PWL) in decibels of the small area is defined by the equation:

$$\Delta PWL_L = 10 \log_{10} \frac{\Delta W_L}{W_{ref}} = 10 \log_{10} \Delta W_L + 130 \text{db} \quad (7)$$

where,  $W_{ref} = 10^{-13}$  watt

Or substituting from Equation (6):

$$\Delta PWL_L = 10 \log_{10} \left[ \frac{\Delta S_L P_{ref}^2}{\rho_0 C} \text{ antilog}_{10} \left( \frac{SPL_L}{10} \right) \right] + 130 \text{db} \quad (8)$$

And evaluating the constants:

$$\Delta PWL_L = \log_{10} [9.08 \times 10^{-14} \Delta S_L \text{ antilog}_{10} \left( \frac{SPL_L}{10} \right)] + 130 \text{db} \quad (9)$$

where:  $\Delta S_L$  = small area in sq ft.

$\rho_0 C$  = 41 gms per  $\text{cm}^2 \text{ sec.}$

$P_{ref}^2$  = 0.0002 dynes per  $\text{cm}^2$



AIRESEARCH MANUFACTURING COMPANY OF ARIZONA  
A DIVISION OF THE GARRETT CORPORATION  
PHOENIX, ARIZONA

The third-octave sound power in each frequency band is

$$PWL_{1/3} \text{ Oct.} = 10 \log^{10} \sum_L [9.08 \times 10^{-14} \Delta S_L \text{ antilog}_{10}$$

$$\left( \frac{SPL_{1/3} \text{ Oct.}}{10} \right) ] + 130 \text{ db} \quad (10)$$

The total sound power is:

$$PWL = 10 \log_{10} \sum_{1/3} \text{ Oct.} \sum_L [9.08 \times 10^{-14} \Delta S_L \text{ antilog}_{10}$$

$$\left( \frac{SPL_{1/3} \text{ Oct.}}{10} \right) ] + 130 \text{ db} \quad (11)$$

The number of measuring locations needed will depend on the accuracy required and the directivity of the noise source. Symmetry in the directivity pattern may be utilized to reduce the number of necessary positions.

Once the sound power level is determined as a function of frequency, the directivity index (DI) of a directional source can be evaluated. By definition the directivity index is:

$$DI_{f\theta} = SPL_{f\theta} - SPL_s \text{ db.} \quad (12)$$

The  $SPL_{f\theta}$  is the sound pressure for a given frequency band ( $f$ ) in the direction ( $\theta$ ) at a distance ( $r$ ) from the source.  $SPL_s$  is the sound pressure that would be produced at the same distance ( $r$ ) by a nondirectional source radiating the same power for the given frequency band.

#### 4.3.2 Axi-Symmetrical Noise Source Radiating in a Half Space

Gas turbine engine exhaust noise, when radiation from a symmetrical duct, is symmetrical about its gas-flow axis.



AIRESEARCH MANUFACTURING COMPANY OF ARIZONA  
A DIVISION OF THE GARRETT CORPORATION  
PHOENIX, ARIZONA

The exhaust-noise characteristic directivity pattern exhibits pronounced maxima, usually between 30 to 60 degrees from the flow axis, and minima on the axis of flow. With the exhaust-flow axis in the horizontal plane, parallel to the ground, the total acoustic energy to a first approximation is radiated in the half space containing the gas flow. As a result, sound measurements made on the surface of the half hemisphere would suffice for the sound-power level determination. From the symmetry of the exhaust noise one can assume that the sound pressure is nearly constant for all points on a segment of area. The segment area  $S$  is defined as the area on the surface of the half-hemisphere with radius  $r$  that is bounded by the arcs of two spherical circles corresponding to different constant values of the angle ( $\theta$ ) measured from the axis of symmetry (exhaust axis).

$$S = \pi r (\cos \theta_1 - \cos \theta_2)$$

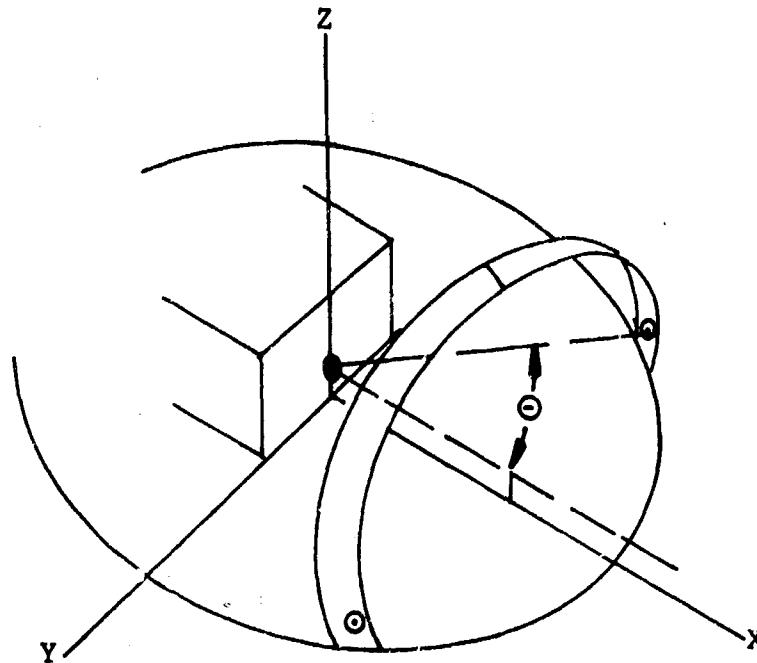
Figure 4-1 shows a typical area (spherical zone). Where a 180-degree ground arc is used, each segment of area (with the exception of the segment on the gas flow axis) is further divided by the XZ plane into two equal areas as shown in Figure 4-1. Also presented in the figure are the measuring locations on a 180-degree arc and the associated zone areas, which make up the 50-foot-radius half hemisphere used for the free-field test. The actual measuring positions are located approximately 5 feet above ground level on the horizontal arc.

#### 4.3.3 Non-Axi-Symmetrical Noise Source

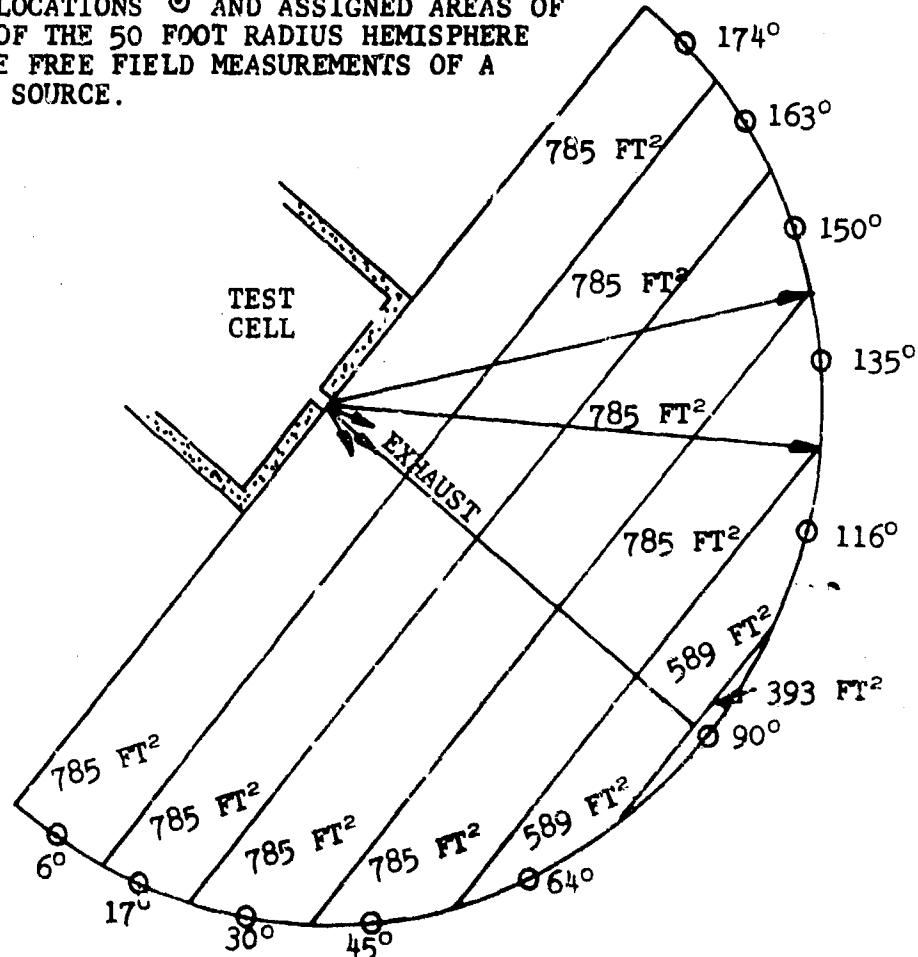
The previous discussion (section 4.3.2) has assumed a symmetrical noise source about the axis of the exhaust flow, and therefore the sound measurements on the ground arc were considered representative of an entire spherical zone (see Figure 4-1). Where the sound is nonsymmetrical, these spherical zones must be further divided. Ideally, this would be accomplished by rotating the



AIRESEARCH MANUFACTURING COMPANY / OF ARIZONA  
A DIVISION OF THE BARRETT CORPORATION  
PHOENIX, ARIZONA



MICROPHONE LOCATIONS  $\odot$  AND ASSIGNED AREAS OF HALF SPACE OF THE 50 FOOT RADIUS HEMISPHERE USED FOR THE FREE FIELD MEASUREMENTS OF A SYMMETRICAL SOURCE.



GT-7615-R  
Page 4-9

FIGURE 4-1



AIRESEARCH MANUFACTURING COMPANY OF ARIZONA  
A DIVISION OF THE GARRETT CORPORATION  
PHOENIX, ARIZONA

arc of measuring stations about the exhaust axis. Each measuring arc would sample a spherical triangle with apex on the exhaust axis and the area associated with each individual measuring point would be the overlap area between the spherical zone and the spherical triangle. Figure 4-2A shows a typical area.

Therefore the above method was modified to maintain the measuring stations on a ground arc and rotate the noise source instead. This practice accomplishes the same purpose but overcomes the difficulties of measuring stations that would be at considerable elevation above the ground. The right angle exhaust duct aft of its junction with the straight extension piece was rotated clockwise on its axis in 30-degree increments through 150 degrees.

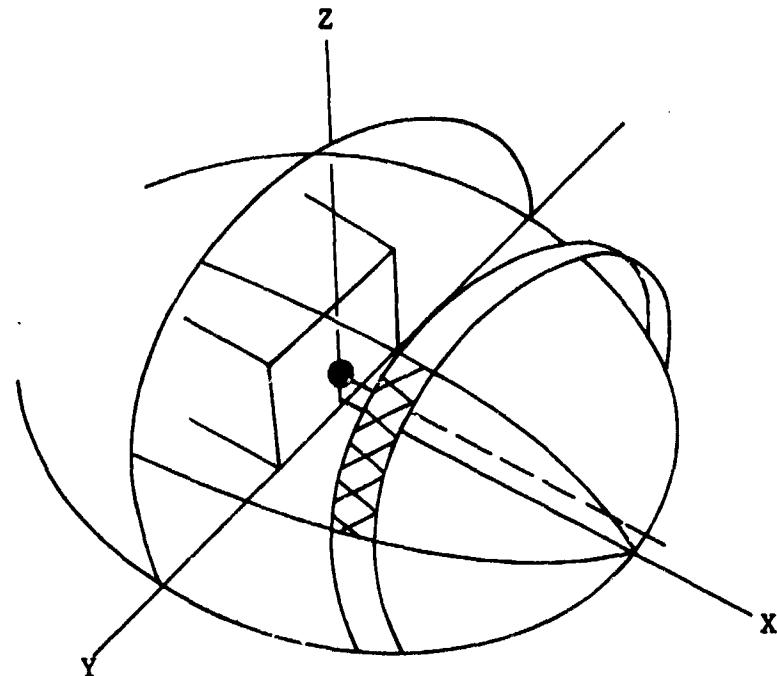
#### 4.3.4 Turbine Exhaust Noise Test

Two exhaust configurations were tested. The first was the straight exhaust extension shown in Figure 4-3. (as it protrudes through the cell wall). The extension was a 12-inch-diameter duct. The second configuration was the right-angle duct shown in Figure 4-4 viewed in the 90-degree position. The outlet end was approximately 26.5 inches by 5.4 inches. The right angle duct is attached to the straight exhaust extension as shown in Figure 4-5 viewed from the outlet end.

Because of the additional numerical complexities of the nonaxisymmetrical system, AiResearch has developed a digital computer program to convert the raw sound measurements into sound power levels and to calculate the directivity index.

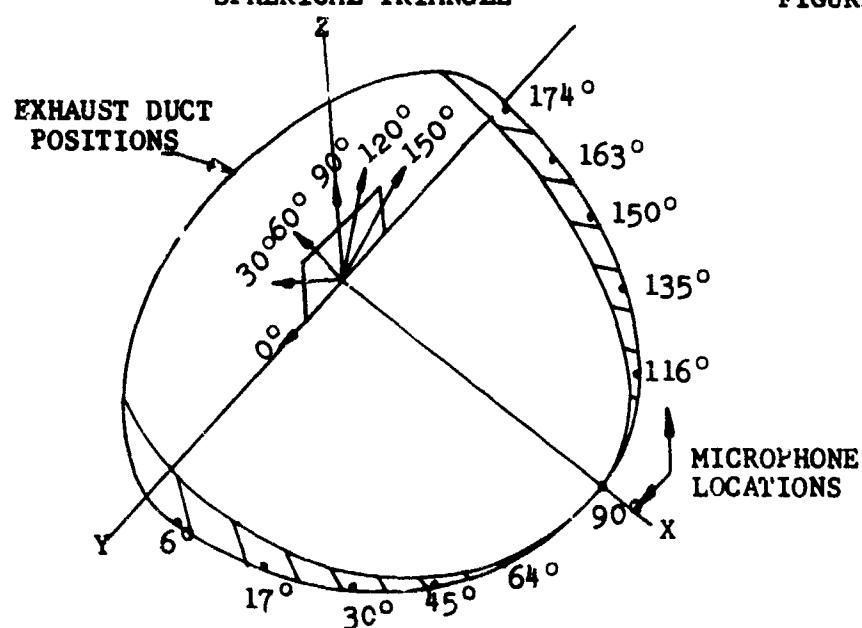


**AIRESEARCH MANUFACTURING COMPANY OF ARIZONA**  
A DIVISION OF THE GARRETT CORPORATION  
PHOENIX, ARIZONA

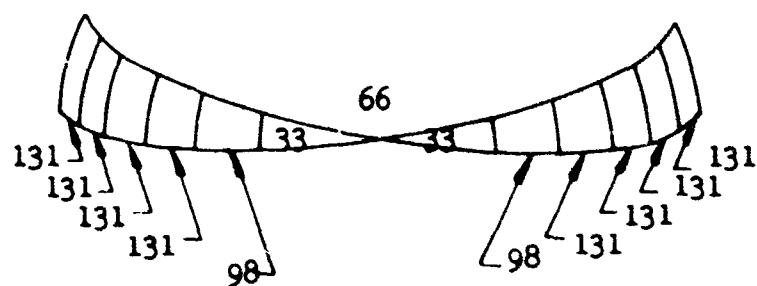


## OVERLAP AREA BETWEEN SPHERICAL ZONE AND SPHERICAL TRIANGLE

**FIGURE 4-2A**



**ASSIGNED AREAS IN SQUARE FEET  
FOR EACH MICROPHONE LOCATION  
AND EXHAUST DUCT POSITION**



GT-7615-R, Rev. 1 FIGURE 4-2B  
Page 4-11

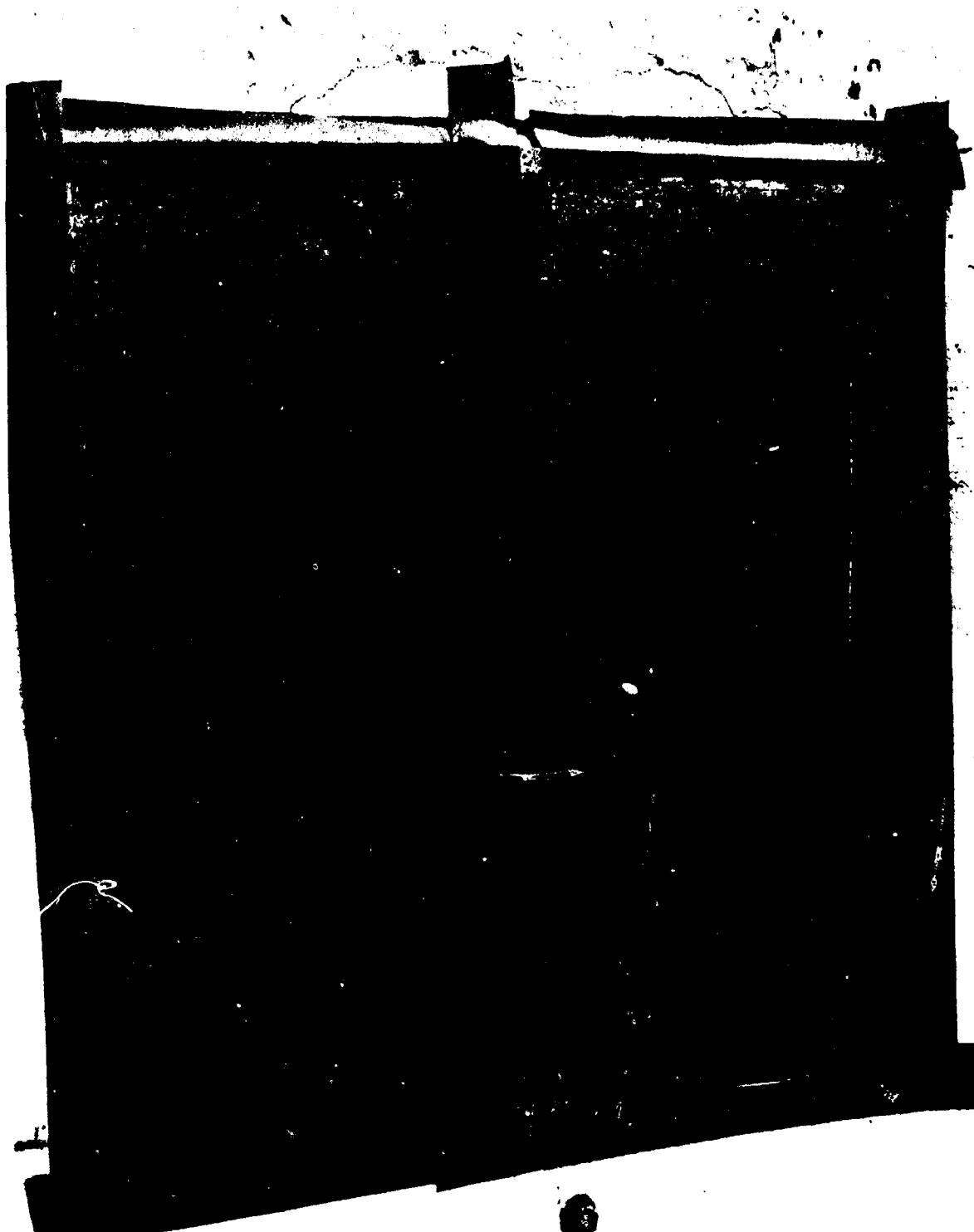


FIGURE 4-3

GT-7615-R  
Page 4-12

GT-331-30 EXHAUST NOISE TEST  
STRAIGHT EXHAUST DUCT

PHOTO NO. P-26172-5  
AERORESEARCH MANUFACTURING COMPANY



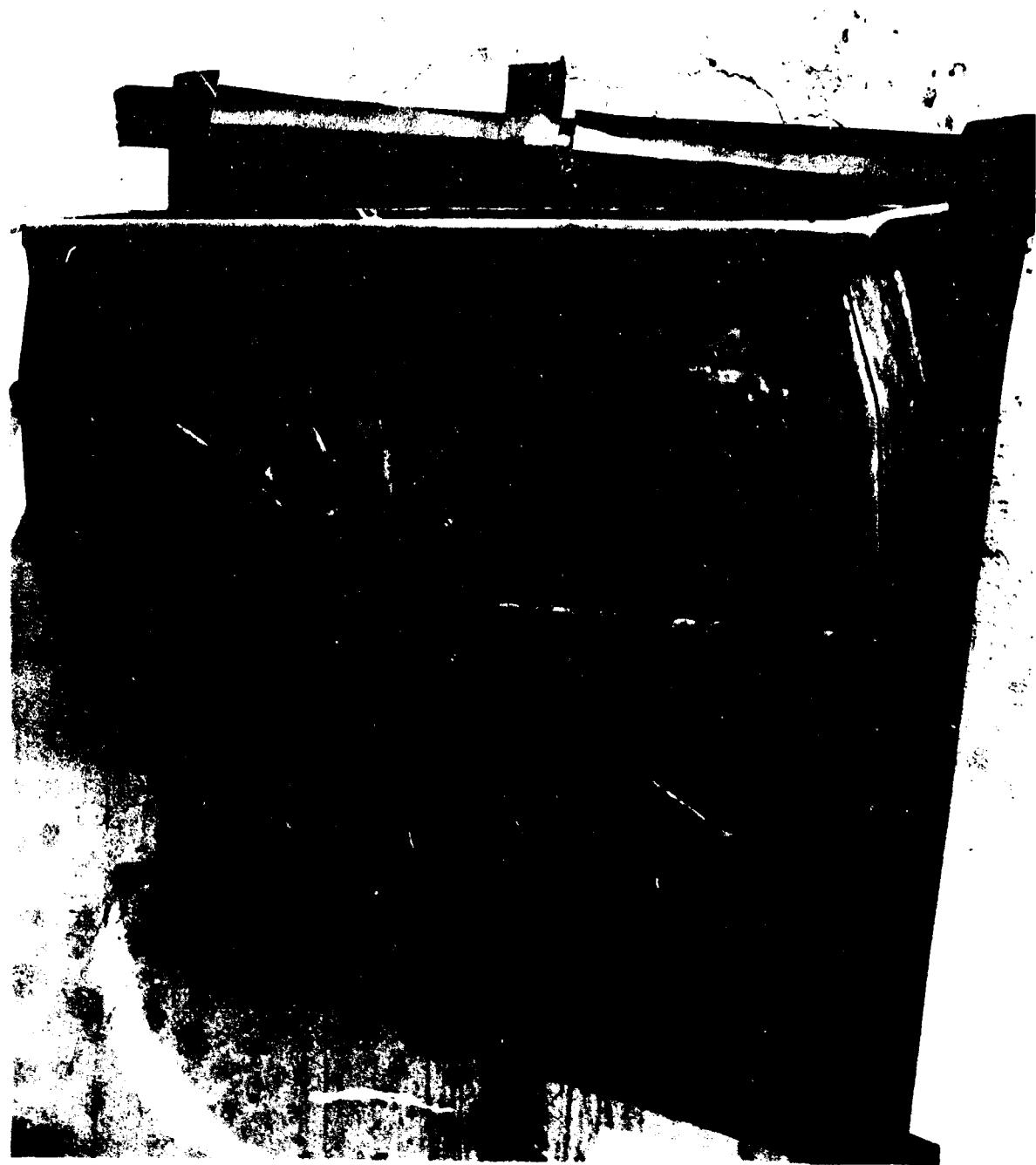


FIGURE 4-4

GT-7615-R  
Page 4-13

GTP331-30 EXHAUST NOISE TEST  
RIGHT ANGLE EXHAUST DUCT

PHOTO NO. P-26172-6  
AERESARCH MANUFACTURING COMPANY



FIGURE 4-5

GT-7615-R  
Page 4-14

GT-7615-R EXHAUST NOISE TEST  
RIGHT ANGLE DUCT ATTACHED  
TO STRAIGHT EXHAUST DUCT  
PHOTO NO. P-26172-7  
AERORESEARCH MANUFACTURING COMPANY



AIRESEARCH MANUFACTURING COMPANY OF ARIZONA  
A DIVISION OF THE BARRETT CORPORATION  
PHOENIX, ARIZONA

Graphs 4-1 and 4-2 present the sound power levels, in one-third octaves, of the turbine exhaust noise emitted from the straight exhaust extension and the right-angle duct, for the no-load and full-load operating conditions.

Tabulated in Tables 4-1 through 4-4 are the directivity indices of the exhaust noise for both exhaust configurations at the no-load and full-load conditions. The measuring locations are identified by the coordinate system used in Figures 4-1 and 4-2.

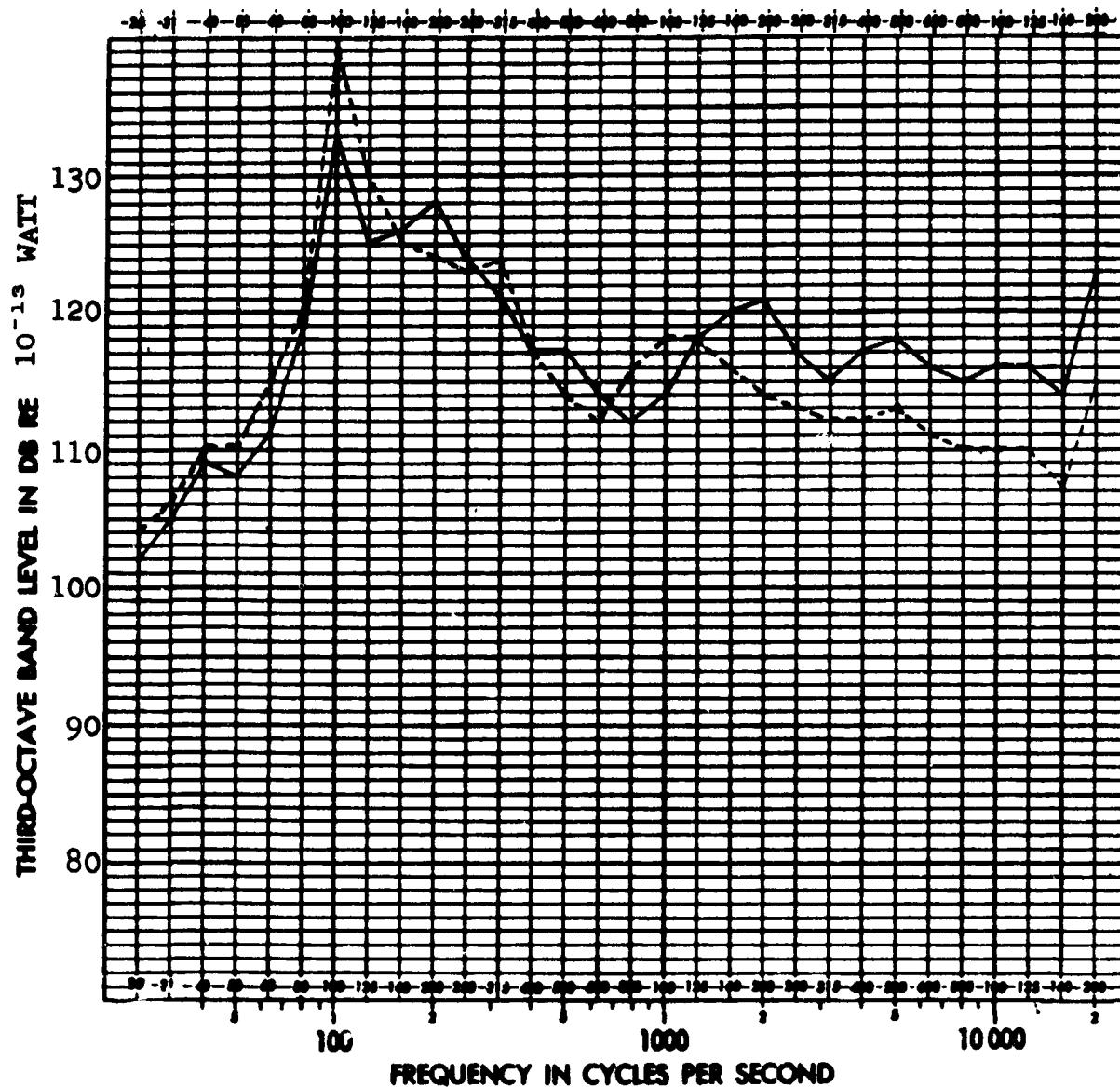
#### 4.3.5 Interpretation of the Turbine Exhaust Acoustic Power Spectrum

Presented in Graphs 4-1 and 4-2 are the acoustic power level spectra of the turbine exhaust noise emitted from the straight exhaust-duct extension and the right-angle exhaust duct. A broad-band low-frequency hump, which predominates the spectrum is observed for both duct configurations and load conditions. This hump is normally found with gas turbine engine exhaust noise and was assumed to be associated with the combustion process. Several hypotheses have been formulated to explain the hump. The first is the combustion process itself. A second is the acoustical network within the turbine having some form of band-pass character. A third is a combination of the combustion process and the acoustical network, whereby some type of feedback occurs between the two. These hypotheses have never been fully investigated.



AIRESEARCH MANUFACTURING COMPANY OF ARIZONA  
A DIVISION OF THE GARRETT CORPORATION  
PHOENIX, ARIZONA

Form No. PX1842

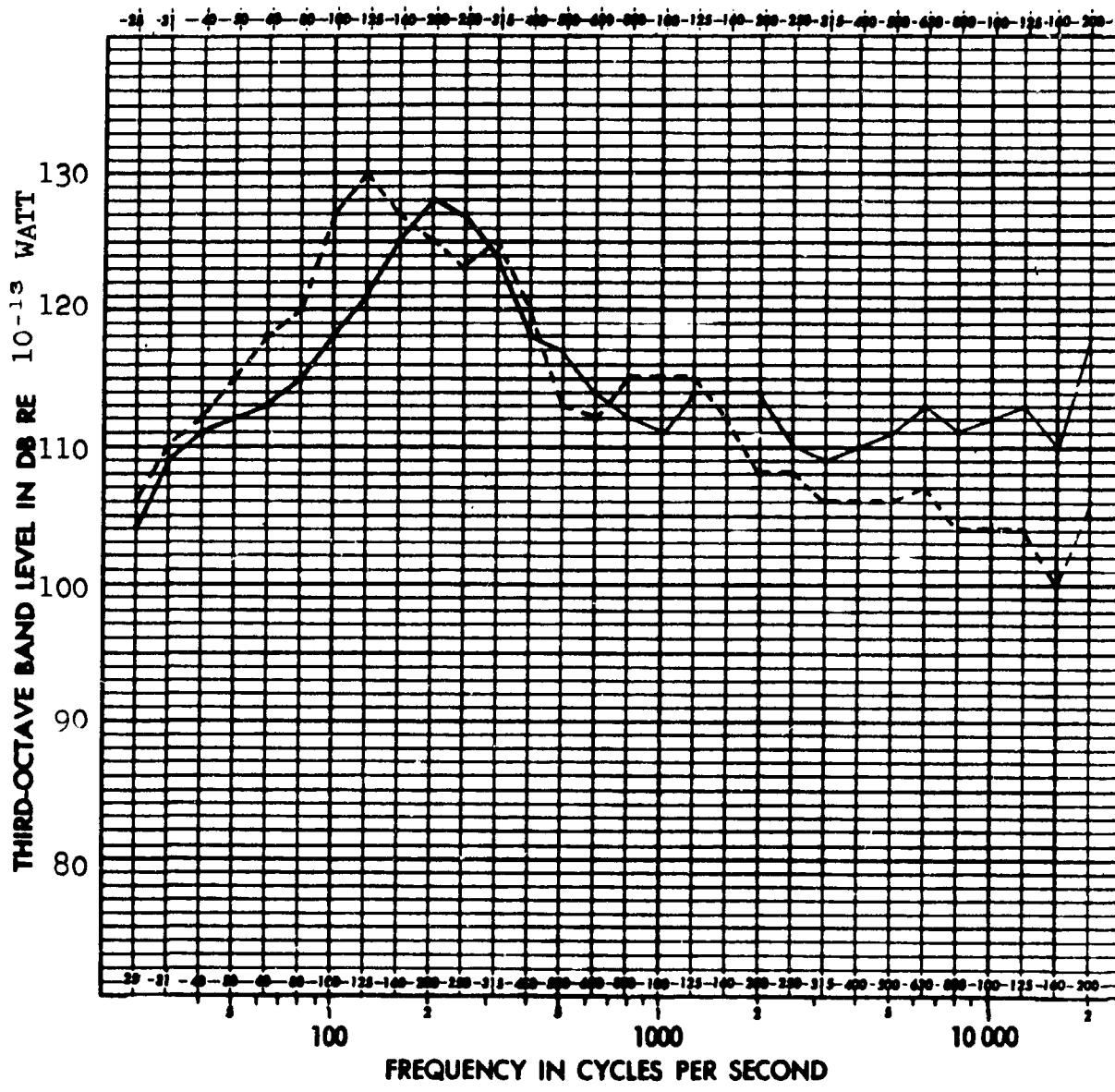


GRAPH 4-1      1/3 OCTAVE BAND SOUND POWER LEVEL SPECTRUM OF  
                  GTP331-30 EXHAUST NOISE  
                  NO LOAD CONDITION



AIRESEARCH MANUFACTURING COMPANY OF ARIZONA  
A DIVISION OF THE GARRETT CORPORATION  
PHOENIX, ARIZONA

Form No. PX1842





AIRESEARCH MANUFACTURING COMPANY OF ARIZONA  
A DIVISION OF THE GARRETT CORPORATION  
PHOENIX, ARIZONA

TABLE 4-1  
TURBINE EXHAUST DIRECTIVITY INDEX (db)  
GTP331-30 WITH STRAIGHT EXHAUST DUCT

NO LOAD CONDITION

DUCT POSITION MICROPHONE LOCATION	51.5	PREFERRED OCTAVE BAND CENTER FREQUENCY CPS								
		63	125	250	500	1000	2000	4000	8000	16000
-- 6°	5	6	3	5	7	8	8	7	9	10
-- 17°	6	6	6	7	8	5	7	9	9	8
-- 30°	5	6	7	8	6	4	10	7	7	8
-- 45°	5	6	6	6	7	4	1	1	2	2
-- 64°	7	1	-2	3	2	6	0	4	6	4
-- 90°	7	1	-2	0	1	1	-1	3	3	1
-- 116°	9	5	2	4	2	5	4	7	6	5
-- 135°	8	5	6	6	5	4	0	2	4	3
-- 150°	9	9	9	7	8	5	7	4	3	4
-- 163°	5	10	9	8	7	9	6	10	7	6
-- 174°	3	6	9	8	8	9	9	6	7	8

FULL LOAD CONDITION

DUCT POSITION MICROPHONE LOCATION	51.5	63	125	250	500	1000	2000	4000	8000	16000
-- 6°	8	6	3	4	8	7	5	6	9	11
-- 17°	9	7	4	7	9	7	8	10	10	11
-- 30°	7	7	7	7	8	7	10	11	8	9
-- 45°	7	8	7	5	3	3	-1	1	1	0
-- 64°	7	5	4	3	0	2	-4	-4	-5	-7
-- 90°	7	5	4	2	-1	-3	-7	-7	-9	-12
-- 116°	7	5	7	4	-2	0	-4	-5	-6	-7
-- 135°	6	6	7	7	4	4	4	1	0	-1
-- 150°	5	7	7	8	8	9	9	5	6	5
-- 163°	2	6	9	8	7	10	6	9	10	7
-- 174°	3	5	6	8	8	7	9	5	7	6



TABLE 4-2

TURBINE EXHAUST DIRECTIVITY INDEX (db) GTP331-30  
WITH RIGHT ANGLE EXHAUST DUCT-NO LOAD CONDITION

DUCT POSITION MICROPHONE LOC.	31.5	PREFERRED OCTAVE	125	250	500	1000	2000	4000	8000	16000
0°/6°	5	6	5	3	2	-3	-5	-6	-5	-4
0°/17°	4	7	5	9	8	3	4	4	5	3
0°/30°	4	7	7	11	10	5	12	10	10	9
0°/45°	4	8	9	9	7	13	14	13	13	12
0°/64°	8	8	8	6	7	8	10	10	12	12
0°/90°	8	6	2	4	8	5	4	6	7	7
0°/116°	7	5	3	4	8	3	-1	-2	-1	1
0°/135°	5	4	4	4	7	2	0	-4	-4	-3
0°/150°	7	6	4	5	6	2	1	-4	-5	-5
0°/163°	5	5	5	6	4	0	2	-3	-4	-8
0°/174°	2	2	2	7	9	-1	0	-5	-6	-8
30°/6°	6	7	7	7	5	6	2	2	1	2
30°/17°	4	7	7	10	9	9	8	7	7	7
30°/30°	4	7	9	10	7	6	11	11	10	10
30°/45°	4	8	10	9	7	10	12	13	13	12
30°/64°	7	7	9	6	7	8	8	10	12	12
30°/90°	5	6	3	4	8	6	3	4	6	7
30°/116°	6	4	2	3	7	4	-1	-1	1	2
30°/135°	7	6	3	4	6	4	1	-2	-2	-2
30°/150°	6	6	3	4	6	4	1	-3	-4	-4
30°/163°	5	6	3	5	4	1	2	-1	-4	-6
30°/174°	3	2	1	7	7	-2	-1	-2	-4	-7
60°/6°	4	6	7	7	6	5	4	8	7	7
60°/17°	5	5	8	8	8	1	9	8	8	8
60°/30°	5	7	10	8	6	8	9	11	10	9
60°/45°	5	9	11	6	6	8	10	11	11	10
60°/64°	7	8	10	4	6	8	5	7	9	10
60°/90°	6	5	5	4	8	7	2	4	7	8
60°/116°	8	5	5	3	5	6	3	1	4	5
60°/135°	8	6	5	3	4	7	3	1	2	3
60°/150°	8	7	5	4	5	8	1	-1	-2	0
60°/163°	6	7	5	6	3	1	2	-1	-2	-2
60°/174°	4	3	2	6	6	-1	-1	-2	-3	-3



AIRESEARCH MANUFACTURING COMPANY OF ARIZONA  
A DIVISION OF THE GARRETT CORPORATION  
PHOENIX, ARIZONA

TABLE 4-2 (Contd.)

TURBINE EXHAUST DIRECTIVITY INDEX (db) GTP331-30  
WITH RIGHT ANGLE EXHAUST DUCT-NO LOAD CONDITION

DUCT POSITION MICROPHONE LOC.	31.5	63	125	250	500	1000	2000	4000	8000	16000
90°/6°	3	5	7	2	5	1	-2	1	3	3
90°/17°	1	5	7	5	7	-1	4	3	4	5
90°/30°	2	7	9	5	5	4	5	5	5	6
90°/45°	4	9	10	3	6	6	6	6	7	7
90°/64°	7	9	10	3	5	7	2	4	6	7
90°/90°	6	7	6	4	5	6	-	4	6	6
90°/116°	7	5	5	3	5	8	4	5	6	7
90°/135°	7	6	5	5	4	10	5	7	7	7
90°/150°	6	7	6	6	6	8	4	6	5	5
90°/163°	5	7	7	8	4	1	1	2	4	4
90°/174°	4	4	4	9	7	-1	0	4	3	4
120°/6°	2	3	5	3	6	-2	-4	-2	-3	-2
120°/17°	4	5	4	4	6	-1	2	0	-1	1
120°/30°	4	5	7	4	4	2	1	2	0	3
120°/45°	4	7	10	1	4	0	1	1	2	6
120°/64°	7	8	8	2	5	5	1	1	3	6
120°/90°	6	6	5	3	7	6	3	4	6	9
120°/116°	8	5	6	4	5	8	6	8	10	10
120°/135°	8	7	5	6	7	12	7	11	11	11
120°/150°	9	8	6	8	8	8	6	7	8	8
120°/163°	6	7	6	9	6	8	4	4	4	5
120°/174°	3	5	5	3	8	4	5	5	4	3
150°/6°	2	3	4	4	5	1	-2	-2	-4	-6
150°/17°	4	5	5	6	6	-1	3	1	-2	-4
150°/30°	4	6	7	6	4	2	2	-1	-2	-3
150°/45°	11	7	8	2	6	1	3	-3	-2	-1
150°/64°	14	7	8	4	7	4	1	-1	1	1
150°/90°	10	6	3	4	6	5	3	6	7	7
150°/116°	11	6	5	5	6	11	10	10	11	11
150°/135°	11	7	5	8	8	14	12	14	13	12
150°/150°	8	9	6	12	10	5	15	11	10	9
150°/163°	8	8	6	8	10	13	11	7	6	3
150°/174°	6	7	5	4	4	-2	1	1	0	-3



AIRESEARCH MANUFACTURING COMPANY OF ARIZONA  
A DIVISION OF THE BARRETT CORPORATION  
PHOENIX, ARIZONA

TABLE 4-3

TURBINE EXHAUST DIRECTIVITY INDEX (db) GTP331-30  
WITH RIGHT ANGLE EXHAUST DUCT FULL LOAD CONDITION

DUCT POSITION MICROPHONE LOC.	PREFERRED OCTAVE BAND CENTER FREQUENCY-CPS									
	31.5	63	125	250	500	1000	2000	4000	8000	16000
0°/6°	5	6	4	1	-5	-8	-10	-9	-11	-12
0°/17°	4	8	6	7	6	-1	-3	-3	-1	-1
0°/30°	4	7	10	10	12	6	8	7	7	6
0°/45°	5	8	9	11	11	10	14	12	12	11
0°/64°	8	9	8	6	4	9	11	12	13	10
0°/90°	6	8	6	3	6	7	5	7	8	10
0°/116°	8	6	6	2	5	4	1	0	1	3
0°/135°	5	5	6	4	4	3	3	-2	-2	1
0°/150°	7	7	5	5	6	2	2	-1	-2	0
0°/163°	3	6	7	6	4	-1	4	-1	-2	-2
0°/174°	3	3	5	7	8	-2	1	-3	-4	-3
30°/6°	7	7	4	4	3	-4	-5	-4	-4	-5
30°/17°	5	9	8	7	4	-2	-2	0	1	1
30°/30°	7	9	9	10	10	6	10	9	7	4
30°/45°	6	8	9	10	7	12	12	13	11	8
30°/64°	8	9	8	5	4	11	10	11	11	11
30°/90°	8	8	6	2	6	9	5	8	9	8
30°/116°	8	4	5	2	6	7	1	1	2	3
30°/135°	7	5	6	3	5	6	2	1	-1	2
30°/150°	5	6	4	3	5	3	3	0	-1	1
30°/163°	4	6	8	6	2	3	3	0	-3	-2
30°/174°	2	3	6	8	4	0	-1	-1	-4	-4
60°/6°	7	6	4	6	7	3	2	6	5	5
60°/17°	5	8	6	8	8	1	6	8	8	7
60°/30°	5	6	8	9	9	4	9	9	8	8
60°/45°	5	8	9	7	7	9	9	11	10	10
60°/64°	8	8	7	5	5	10	6	8	10	11
60°/90°	7	7	5	4	6	10	4	6	8	8
60°/116°	8	4	5	3	5	8	3	4	4	5
60°/135°	8	4	6	4	5	6	3	3	3	4
60°/150°	6	5	5	4	4	6	5	3	2	3
60°/163°	5	4	7	6	2	4	3	1	0	1
60°/174°	3	2	6	5	6	-1	0	0	0	1



AIRESEARCH MANUFACTURING COMPANY OF ARIZONA  
A DIVISION OF THE GARRETT CORPORATION  
PHOENIX, ARIZONA

TABLE 4-3 (Contd.)

DUCT POSITION MICROPHCN LOC.	31.5	PREFERRED OCTAVE		BAND CENTER	FREQUENCY-CPS	3000	8000	16000
		63	125					
90°/6°	3	5	1	4	6	3	1	4
90°/17°	4	8	4	6	6	1	4	5
90°/30°	5	6	6	6	7	3	7	7
90°/45°	5	8	6	4	4	5	9	7
90°/64°	7	8	5	3	4	9	5	6
90°/90°	8	6	5	3	6	11	4	7
90°/116°	10	4	5	3	4	8	4	6
90°/135°	7	5	5	5	5	8	6	7
90°/150°	6	8	7	6	8	6	5	6
90°/163°	4	6	8	9	5	4	3	4
90°/174°	4	3	6	7	9	2	4	6
120°/6°	4	3	1	2	4	0	-1	0
120°/17°	4	5	5	4	4	0	4	2
120°/30°	6	6	6	4	3	2	5	4
120°/45°	4	7	6	2	5	2	7	4
120°/64°	6	6	4	2	5	7	3	4
120°/90°	8	6	5	2	5	10	3	7
120°/116°	8	5	5	5	4	11	7	10
120°/135°	7	6	6	8	6	11	8	10
120°/150°	9	9	8	8	9	5	7	7
120°/163°	7	8	10	8	6	8	6	4
120°/174°	6	5	7	8	6	0	3	3
150°/6°	4	2	0	4	5	0	0	1
150°/17°	4	2	3	5	5	-2	4	2
150°/30°	6	4	7	5	3	1	4	3
150°/45°	9	5	5	3	6	0	4	1
150°/64°	8	6	5	1	5	5	2	3
150°/90°	10	6	7	3	5	8	4	7
150°/116°	11	6	6	7	4	12	11	13
150°/135°	9	7	9	10	8	12	14	13
150°/150°	11	9	8	13	12	12	12	8
150°/163°	7	7	8	7	9	8	6	4
150°/174°	5	4	5	4	1	-1	-4	-3



Along with the low-frequency hump is a pure-tone spike in the 100-cps third-octave band at the no-load condition. At the full-load condition the pure-tone spike either disappears or decreases in magnitude. This spike has been observed once before on another Model 331 unit, but occurred in the 125-cps band.

The remaining noise spectrum above the 800-cycle band has some small humps which are generally attributed to aerodynamic sources. There is evidence of a turbine blade passage pure-tone fundamental in the 20,000-cycle band. The fundamental actually is just within the bandwidth of the 25,000-cps third-octave band.

#### 4.4 Reverberant-Room Engine Noise Test

##### 4.4.1 Determination of Sound Power

The remaining engine noise, less the turbine exhaust noise, was analyzed by the reverberant-field method. Briefly stated, when a noise source is placed within a room that contains little sound absorption a steady-state condition occurs whereby the energy absorbed by the room boundary surfaces equals the energy delivered by the sound source. In this state of equilibrium there exists a reverberant field where the sound level is relatively uniform and essentially independent of the distance from the noise source. This assumes that the room is large compared to the noise source and a reverberant field exists that is not dominated by the direct near field. The "reverberant field" is the sound energy in a room after the first reflection. Energy that has not undergone a reflection is called the "direct field."



The sound pressure level measured in the reverberant field is proportional to the acoustic power output of the noise source. The factor of proportionality (room constant) is related to the geometry of the room and the amount of sound absorption present. The room constant is determined by a room calibration process in which the decay rate of sound is measured as a function of frequency.

#### 4.4.2 Reverberant-Room Measurements

Filtered third-octave band random noise was used to calibrate the measuring room. The reverberation time (decay rate) was recorded for each third-octave band in the frequency range of 100 cps to 20,000 cps. Sabine's reverberant-field formula was used to determine the room constant.

$$T = \frac{0.049V}{Sa}$$

T = reverberation time in seconds

a = average room absorption coefficient

V = room volume in cubic feet

$$R = \frac{Sa}{1-a}$$

S = room surface area in square feet

R = room constant in feet

The room was calibrated for each test run because of changes in the room atmosphere (temperature and humidity), and the enclosure used for the engine noise separation.



Third-octave-band sound pressure levels were measured at three locations in the reverberant field for each test run. From these measurements a space average sound pressure level "SPL" was computed. The sound power level "PWL" radiated from the test specimen was computed from the space average "SPL" and the room constant proportionality factor "R" as follows.

$$PWL = SPL + 10 \log_{10} R - 6.5 \text{ db.}$$

#### 4.4.3 Engine Noise Test

The test engine was placed in a special enclosure as mentioned in Section 4.2. Figure 4-6 shows the enclosure, which is constructed of 1 1/2-inch-thick plywood. An air silencer was placed on top of the enclosure for the compressor air inlet, and air duct silencers were placed on the vent air openings in the turbine section. All enclosure joints were sealed. Special gasketing material was placed on the three panels that divided the engine sections between the engine surface and the panel. This minimized transmission of engine vibration to the enclosure and isolated the noise between engine sections. Preliminary sound measurements were made with the engine operating within the sealed enclosure to establish its effectiveness and locate any noise leaks. These results dictated placement of sound absorption on the inner sides of the removable panels. Thus, a minimum noise base-line was established, which set the lower limit of the measurable noise from the individual engine sections. Shown in Figure 4-7 is the enclosure configuration with all outer panels removed. Sound measurements made in the room with the above enclosure configuration established the total engine radiated noise (bare engine) less the exhaust noise. Reverberant-field measurements were made at the no-load and full-load engine operating condition for all enclosure configurations tested.



FIGURE 4-6

GT-7615-R  
Page 4-26

GTP31-30 REVERBERANT ROOM TEST  
ENGINE COMPLETELY ENCLOSED  
WITH AIR INLET SILENCERS  
PHOTO NO. P-26163-2  
 AMESKARCH MANUFACTURING COMPANY

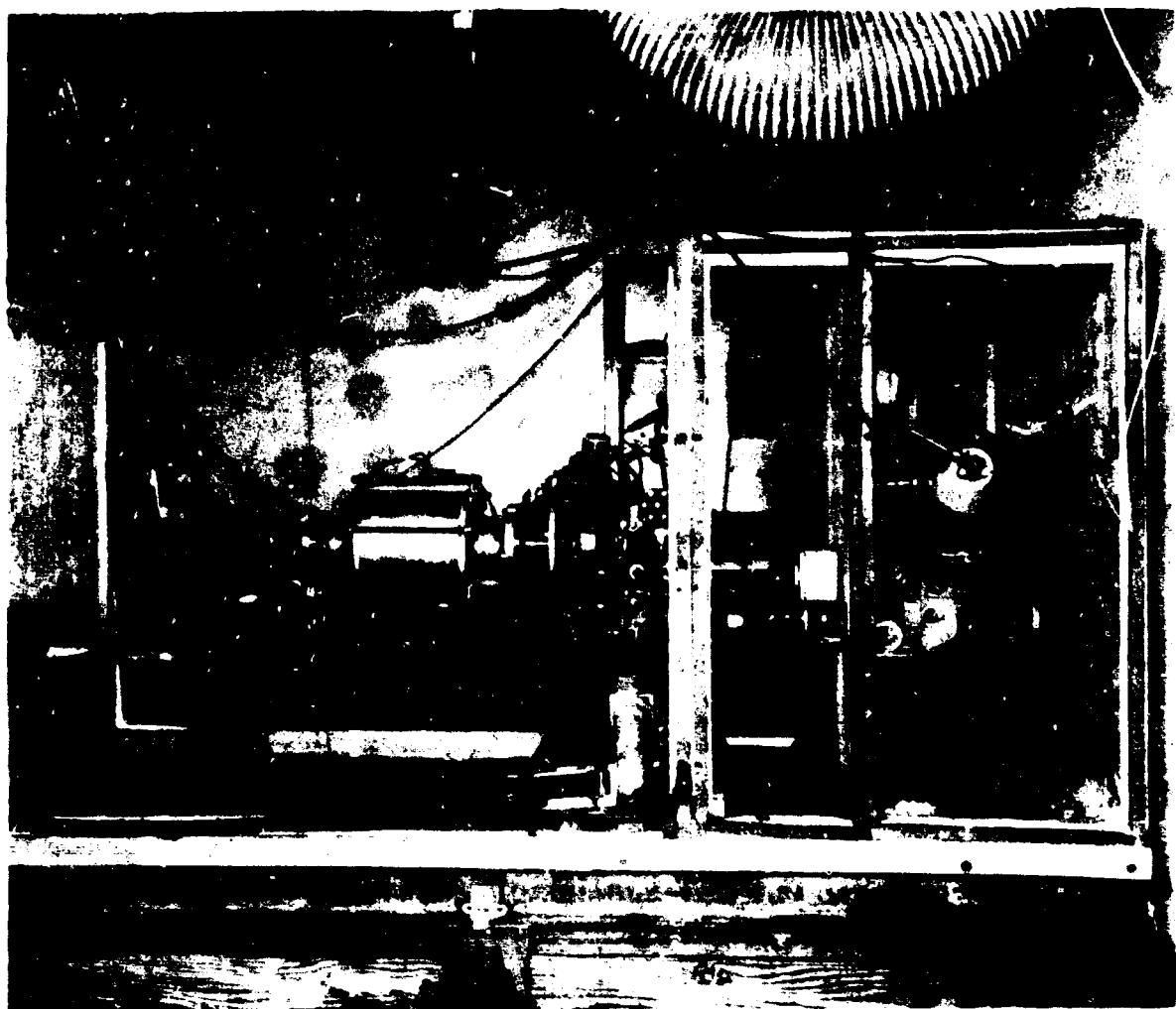


FIGURE 4-7

GT-7615-R  
Page 4-37

GTP331-30 REVERBERANT ROOM TEST  
BARE ENGINE, PANELS (SIDES AND TOP)  
REMOVED FROM ENCLOSURE  
PHOTO NO. P-26172-3  
AEROSPACE MANUFACTURING COMPANY





AIRESEARCH MANUFACTURING COMPANY OF ARIZONA  
A DIVISION OF THE GARRETT CORPORATION  
PHOENIX, ARIZONA

The enclosure configuration for each engine section is shown in the following figures: the turbine plenum sections, Figure 4-8; the compressor air inlet section, Figure 4-9; and the accessory gear case section with the water dynamometer, Figure 4-10.

The acoustic power radiated from each engine section is presented in the following graphs. The turbine plenum, Graphs 4-3 and 4-4; the compressor inlet, Graphs 4-5 and 4-6; the accessory section without the oil-cooler fan, Graphs 4-7 and 4-8. Also presented in each of the above graphs is the total sound power radiated from the bare engine (with all enclosure exterior panels removed) and the enclosed engine. The turbine exhaust noise is excluded. The engine was operated throughout the base-line survey with an external water-cooled oil heat exchanger.

A special test run of the accessory case was performed with an oil-cooler fan assembly. The fan was attached to and driven from an output drive pad of the accessory case; the oil reservoir of the cooler was filled and capped to simulate the damping effect of the engine oil. The acoustic power spectrum of the accessory case with and without the oil-cooler fan is presented in Graph 9.

#### 4.4.4 Oil-Cooler-Fan Acoustic Power Level

A third phase was initiated as a check to redetermine the oil-cooler fan acoustic power. This phase consisted of the measurement of the direct near field or close-in field. Although this method is approximate and has certain limitations, it can serve to estimate a particular noise source, especially if the source is not masked by other noise components.



FIGURE 4-8

GT-7615-R  
Page 4-29

NP 11740

GT-7615-30 REVERBERANT ROOM TEST  
TURBINE PLENUM SECTION

PHOTO NO. P-26167-1  
AEROCARSH MANUFACTURING COMPANY

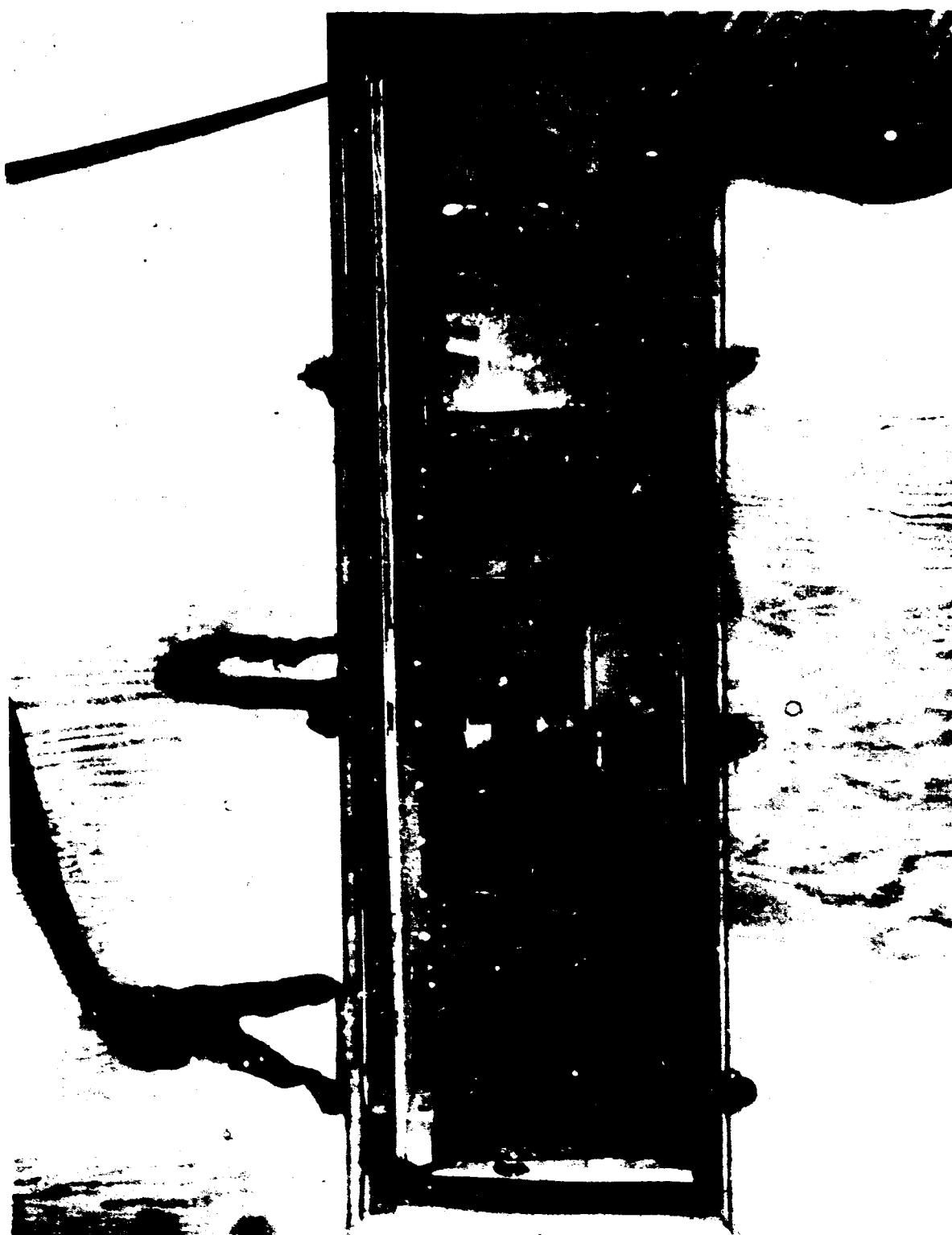


FIGURE 4-9

GT-7615-R  
Page 4-30

GT P331-30 REVERBERANT ROOM TEST  
COMPRESSOR SECTION

PHOTO NO. P-26172-1  
*Approved for public release under the terms of the  
Freedom of Information Act*



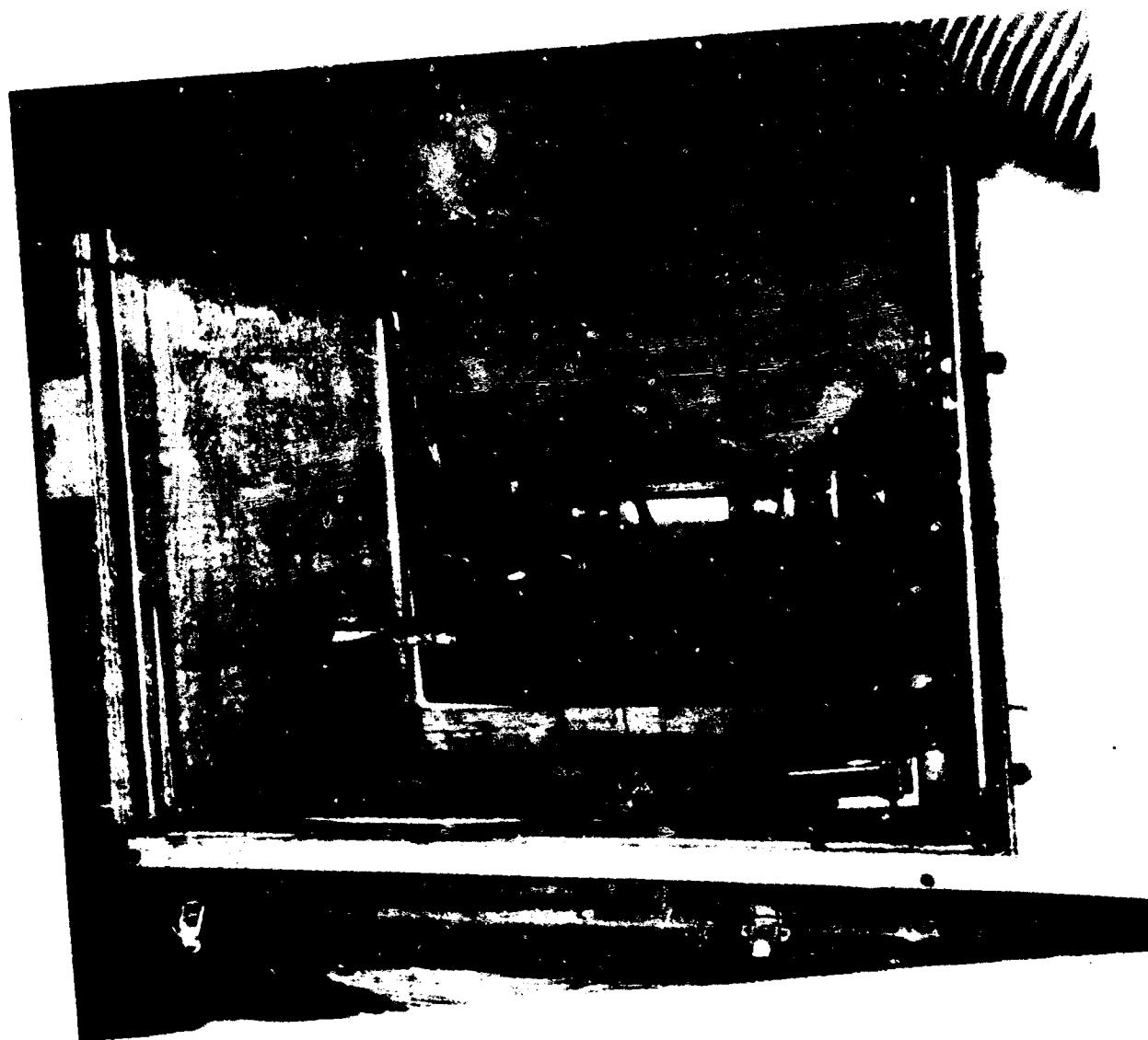


FIGURE 4-10

GT-7615-R  
Page 4-31

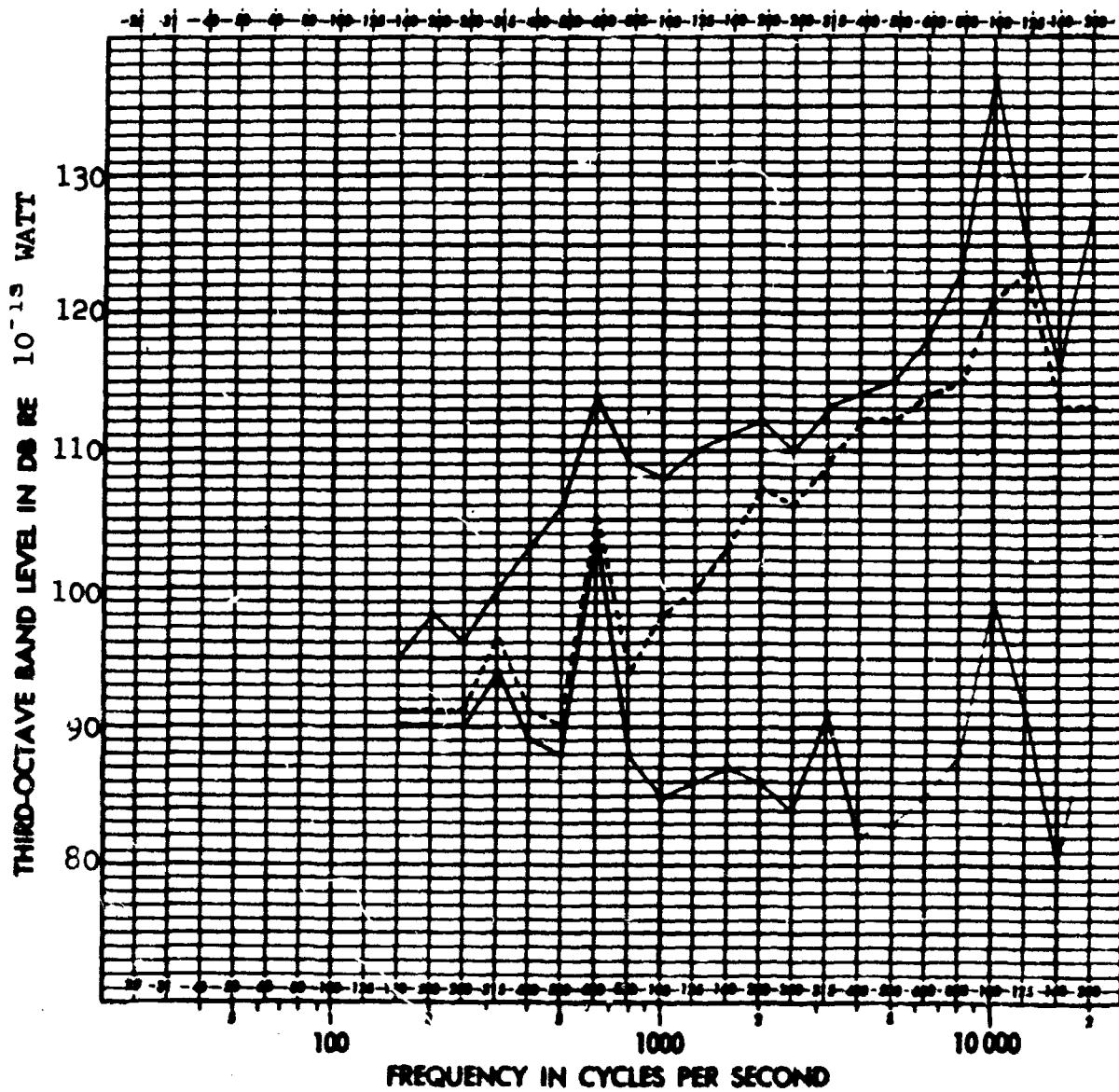
GTP351-30 REVERBERANT ROOM TEST  
ASSEMBLY SECTION

PHOTO NO. P-26172-4  
AEROSPACE MANUFACTURING COMPANY



AIRESEARCH MANUFACTURING COMPANY OF ARIZONA  
A DIVISION OF THE GARRETT CORPORATION  
PHOENIX, ARIZONA

Form No. PX1942



GRAPH 4-3

1/3 OCTAVE BAND SOUND POWER LEVEL SPECTRUM OF  
GTP331-30 TURBINE PLENUM RADIATED NOISE  
NO LOAD CONDITION

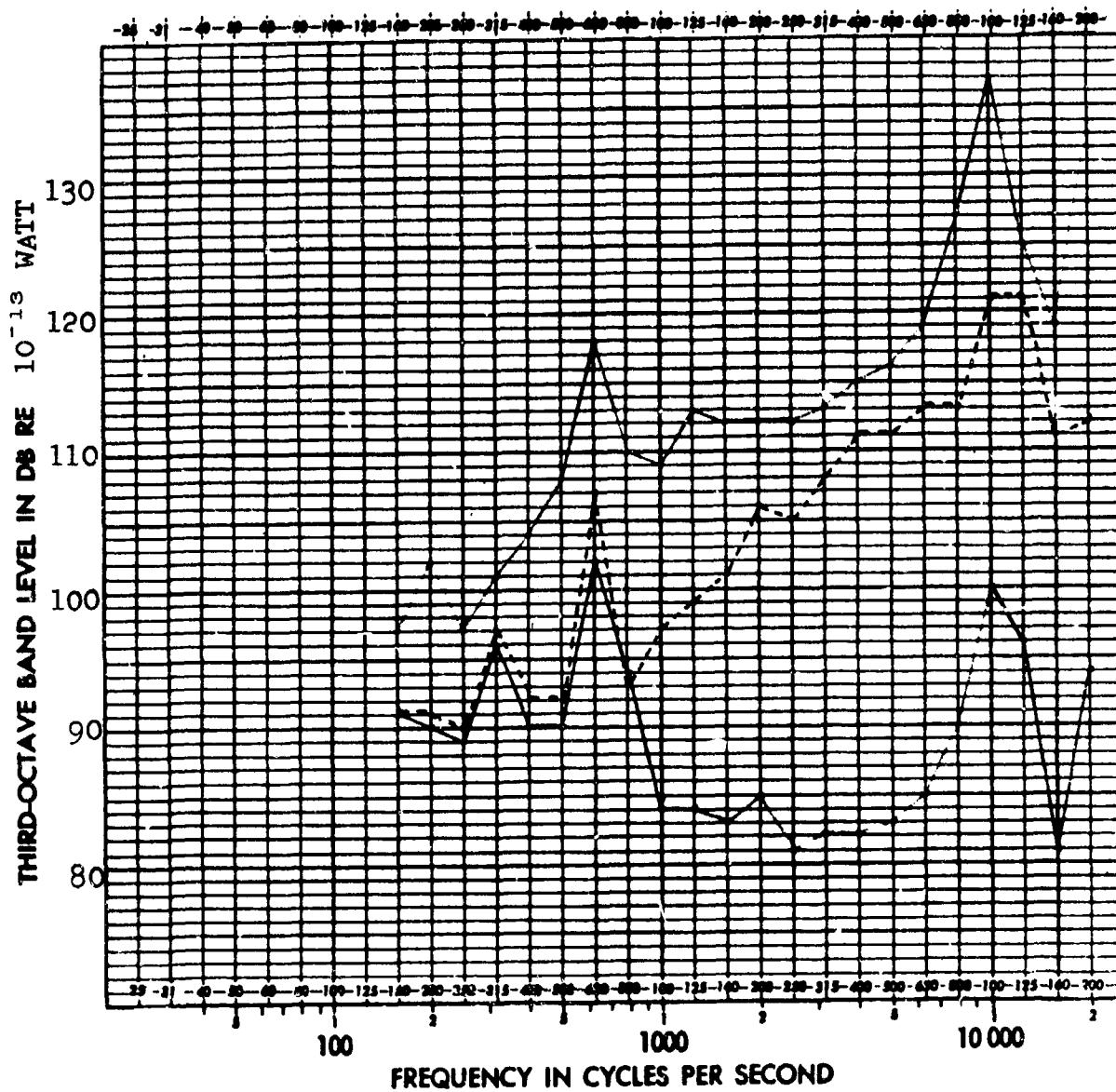
EXHAUST NOISE EXCLUDED

— UPPER TOTAL POWER BARE ENGINE  
- - - MIDDLE TURBINE PLENUM  
— LOWER TOTAL POWER ENCLOSED ENGINE



AIRESEARCH MANUFACTURING COMPANY OF ARIZONA  
A DIVISION OF THE GARRETT CORPORATION  
PHOENIX, ARIZONA

Form No. PX1842



GRAPH 4-4

1/3 OCTAVE BAND SOUND POWER LEVEL SPECTRUM  
GTP331-30 TURBINE PLENUM RADIATED NOISE  
FULL LOAD CONDITION

EXHAUST NOISE EXCLUDED

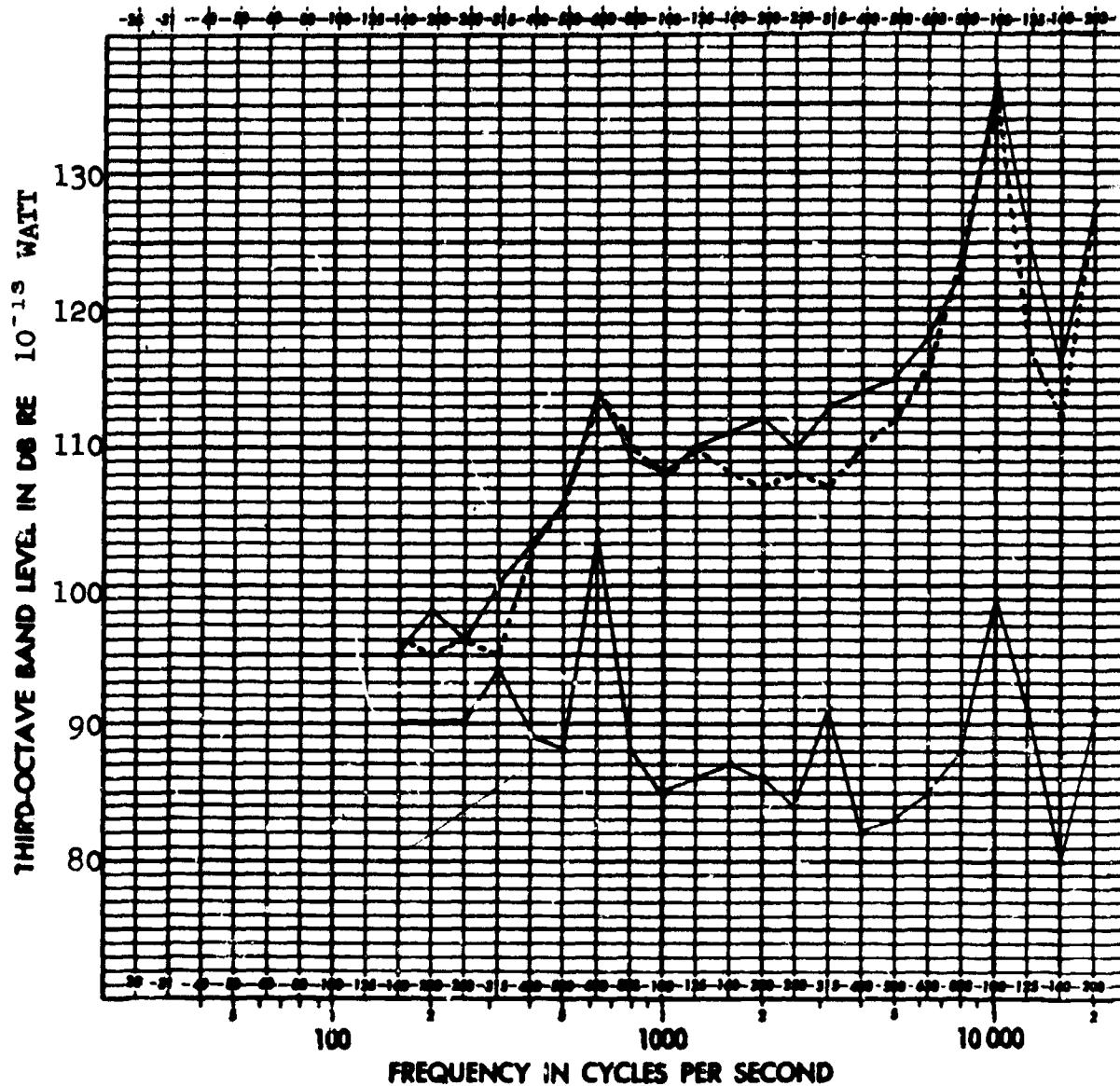
Upper TOTAL POWER BARE ENGINE  
— TURBINE PLENUM  
Lower TOTAL POWER ENCLOSED ENGINE

GT-7615-R  
Page 4-33



AIRSEARCH MANUFACTURING COMPANY OF ARIZONA  
A DIVISION OF THE GARRETT CORPORATION  
PHOENIX, ARIZONA

Form No. PX1842



GRAPH 4-5      1/3 OCTAVE BAND SOUND POWER LEVEL SPECTRUM  
GTP331-30 COMPRESSOR INLET NOISE  
NO LOAD CONDITION

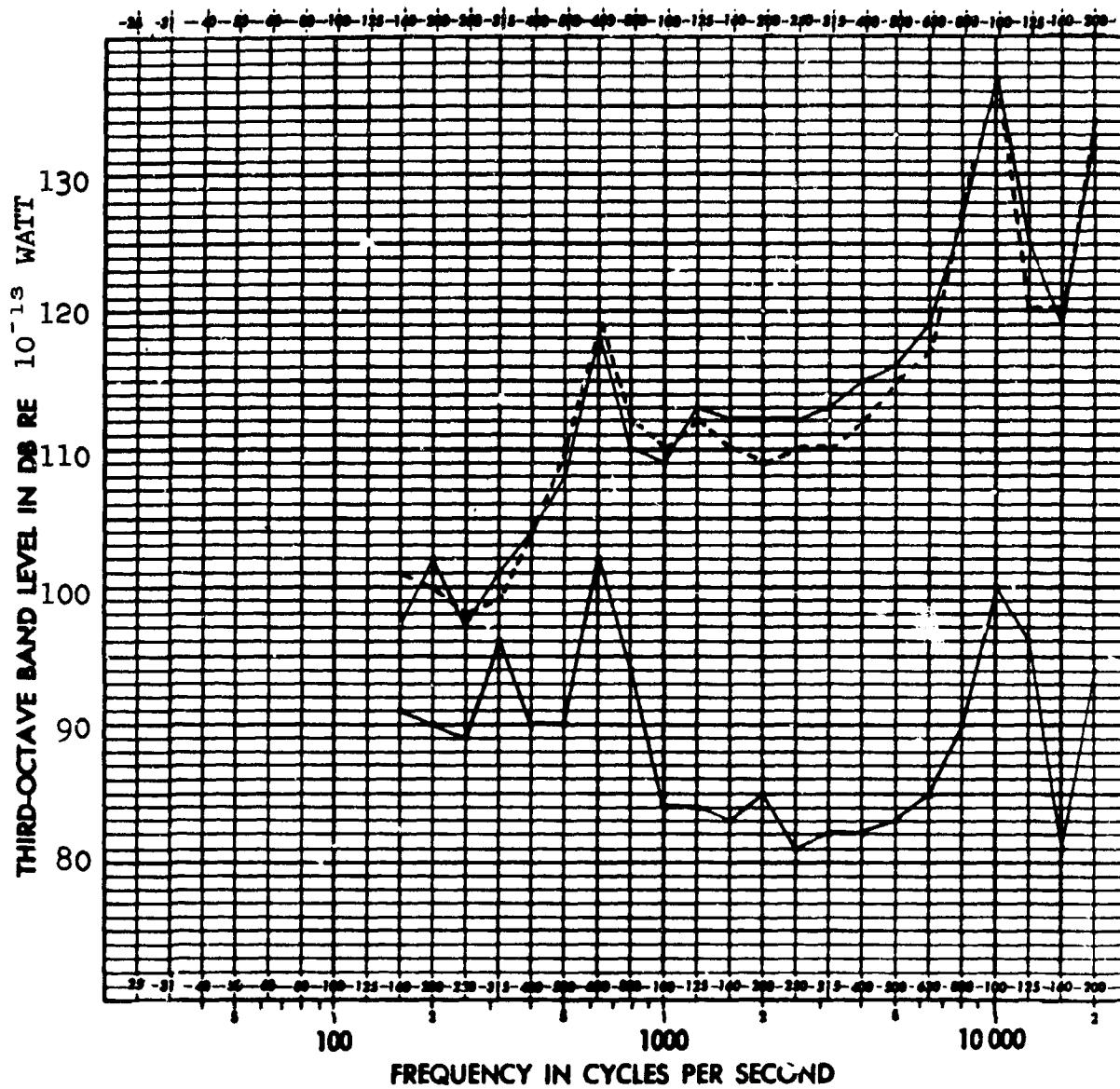
EXHAUST NOISE EXCLUDED

Upper TOTAL POWER BARE ENGINE  
— — — COMPRESSOR INLET  
Lower TOTAL POWER ENCLOSED ENGINE



AIRESEARCH MANUFACTURING COMPANY OF ARIZONA  
A DIVISION OF THE GARRETT CORPORATION  
PHOENIX, ARIZONA

Form No. PX1842



GRAPH 4-6      1/3 OCTAVE BAND SOUND POWER LEVEL SPECTRUM  
GTP331-30 COMPRESSOR INLET NOISE  
FULL LOAD CONDITION

EXHAUST NOISE EXCLUDED

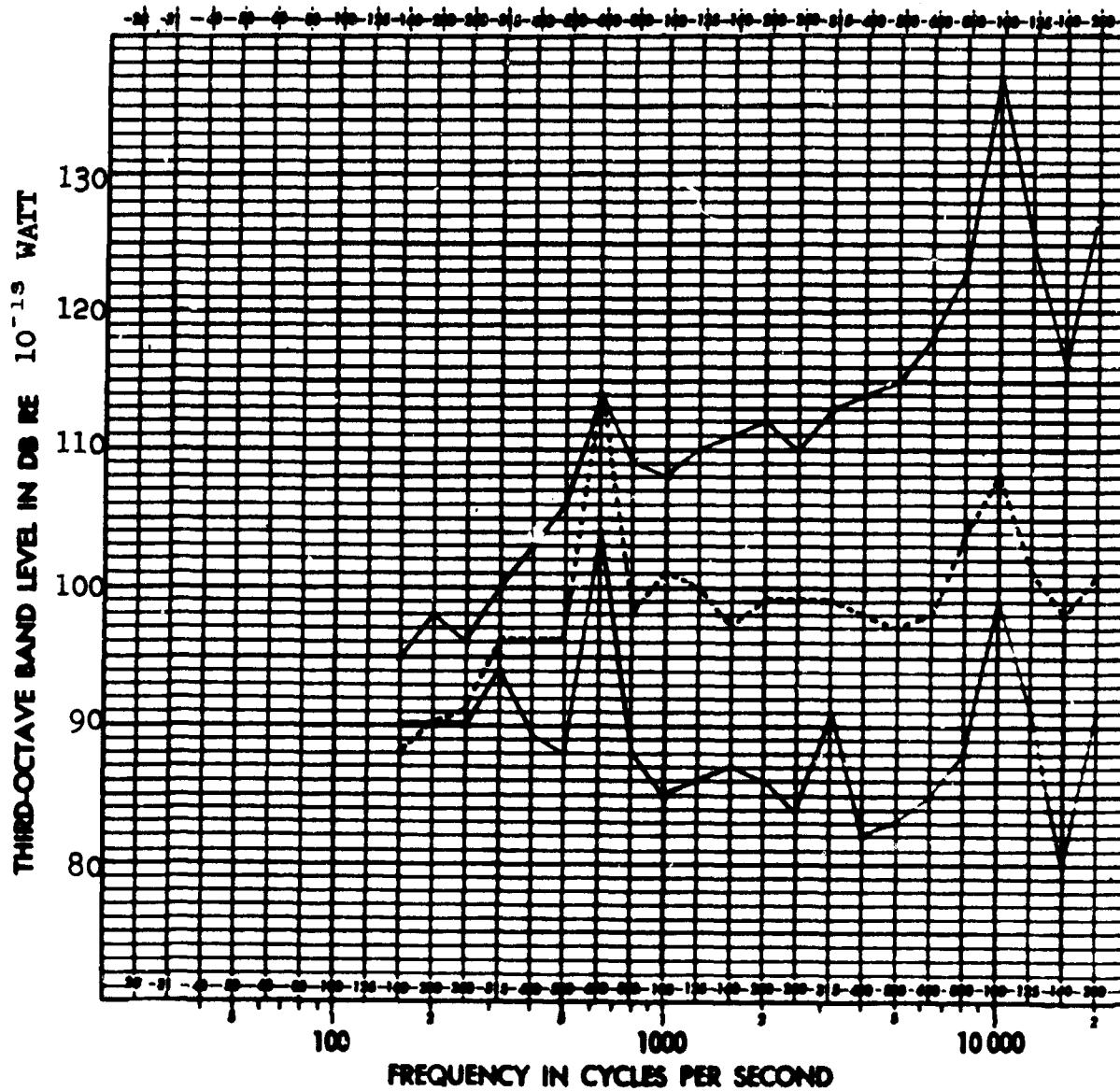
- Upper    TOTAL POWER BARE ENGINE
- COMPRESSOR INLET
- Lower    TOTAL POWER ENCLOSED ENGINE

GT-7615-R  
Page 4-35



AIRESEARCH MANUFACTURING COMPANY OF ARIZONA  
A DIVISION OF THE GARRETT CORPORATION  
PHOENIX, ARIZONA

Form No. PX1842



GRAPH 4-7      1/3 OCTAVE BAND SOUND POWER LEVEL SPECTRUM  
GTP331-30 ACCESSORY CASE NOISE  
NO LOAD CONDITION

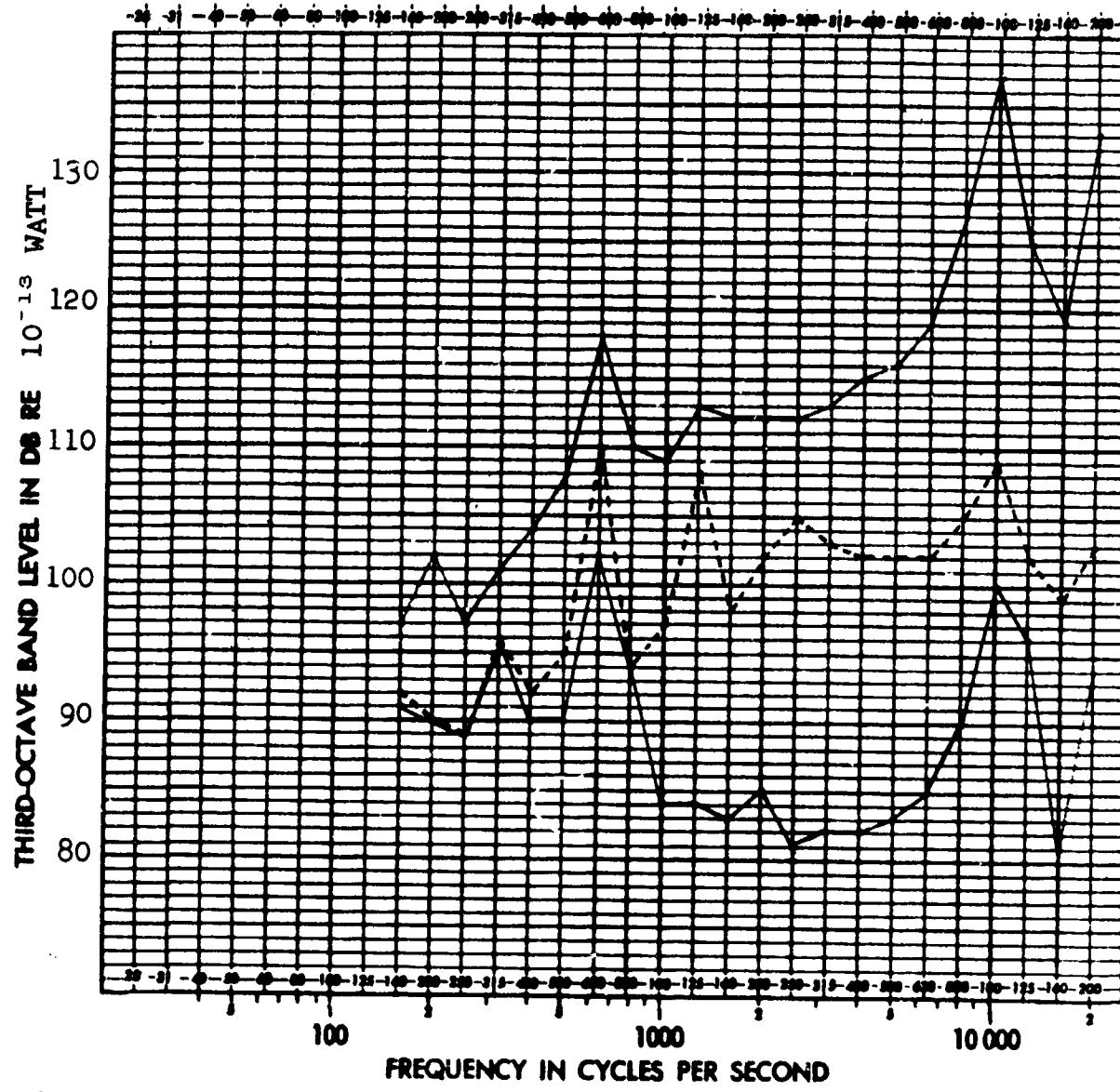
EXHAUST NOISE EXCLUDED

- Upper      TOTAL POWER BARE ENGINE
- ACCESSORY CASE (NO OIL COOLER FAN)
- Lower      TOTAL POWER ENCLOSED ENGINE



AIRESEARCH MANUFACTURING COMPANY OF ARIZONA  
A DIVISION OF THE GARRETT CORPORATION  
PHOENIX, ARIZONA

Form No. PX1842



GRAPH 4-8

1/3 OCTAVE BAND SOUND POWER LEVEL SPECTRUM  
GTP331-30 ACCESSORY CASE NOISE  
FULL LOAD CONDITION

EXHAUST NOISE EXCLUDED

UPPER

TOTAL POWER BARE ENGINE

-----

ACCESSORY CASE (NO OIL COOLER  
FAN)

LOWER

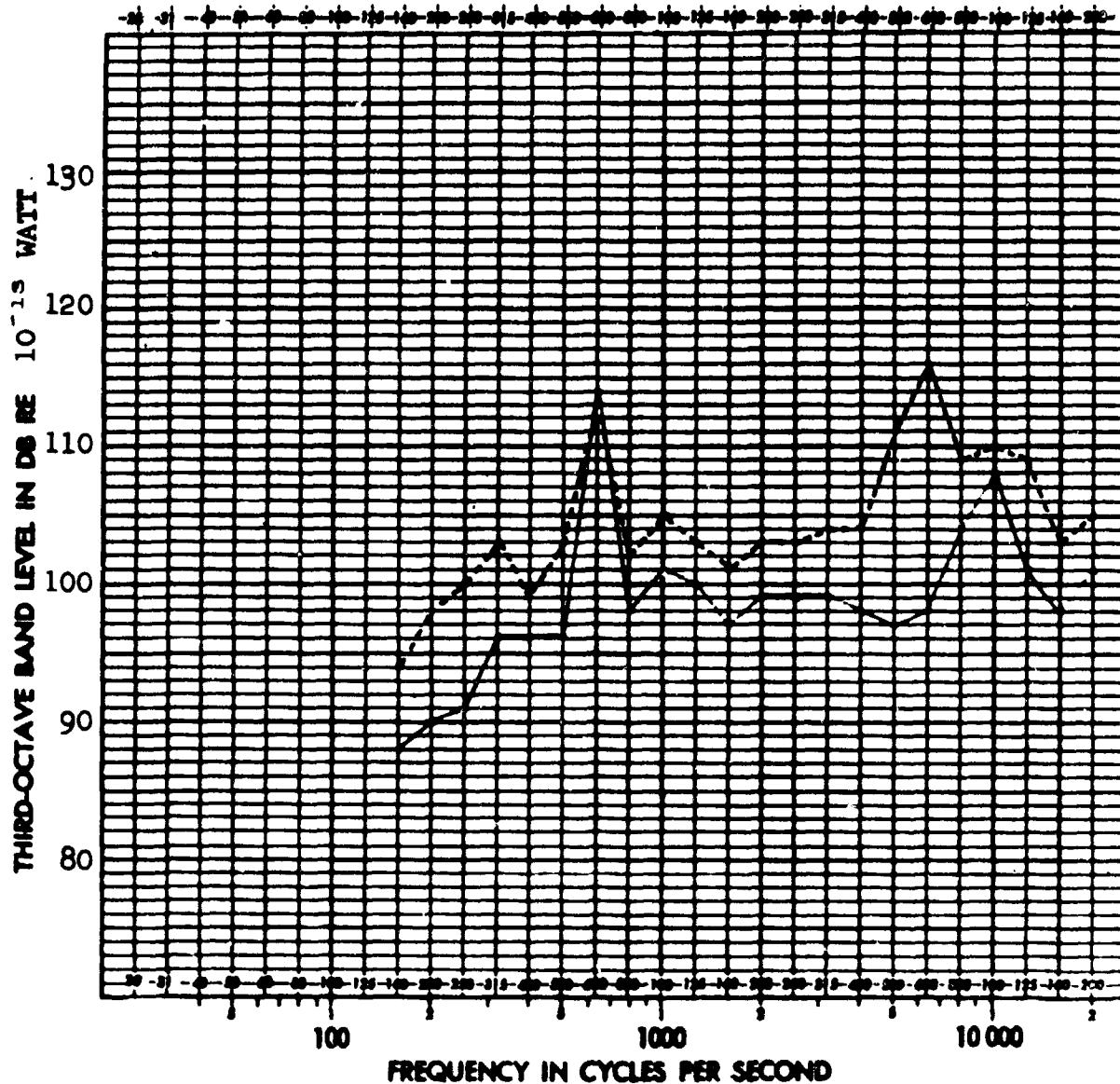
TOTAL POWER OF ENCLOSED ENGINE

GT-7615-R  
Page 4-37



AIRESEARCH MANUFACTURING COMPANY OF ARIZONA  
A DIVISION OF THE GARRETT CORPORATION  
PHOENIX, ARIZONA

Form No. PX1842



GT-7615-R  
Page 4-38



The sound-pressure-level spectrum was measured close to the air inlet and outlet of the fan. Measurements along the sides were negligible compared to the fan noise. By estimating the spherical area at the measuring locations, the acoustic power radiated through the area can then be estimated; Graph 4-10 presents this estimation.

#### 4.4.5 Interpretation of the Acoustic Power Spectra of the Bare Engine

##### Turbine Section, Graphs 4-3 and 4-4

The acoustic power radiated from the turbine plenum, which is usually the primary source of body radiation, is rated as the second major noise source in relation to the total bare engine. The turbine exhaust noise is excluded in this comparison. The spectrum increases approximately 6 decibels per octave from the 800 cps to the 8,000 cps third-octave band, which is believed due to aerodynamics of the air passages in the engine. The compressor-blade-passage pure tones from the first- and second-stage impellers, which lie within the 10,000 and 12,500 cycle bands, respectively, persist and dominate the overall acoustic power level radiated from the plenum. The noise level below the 800-cycle band is low and somewhat masked due to the limitation of the enclosure.

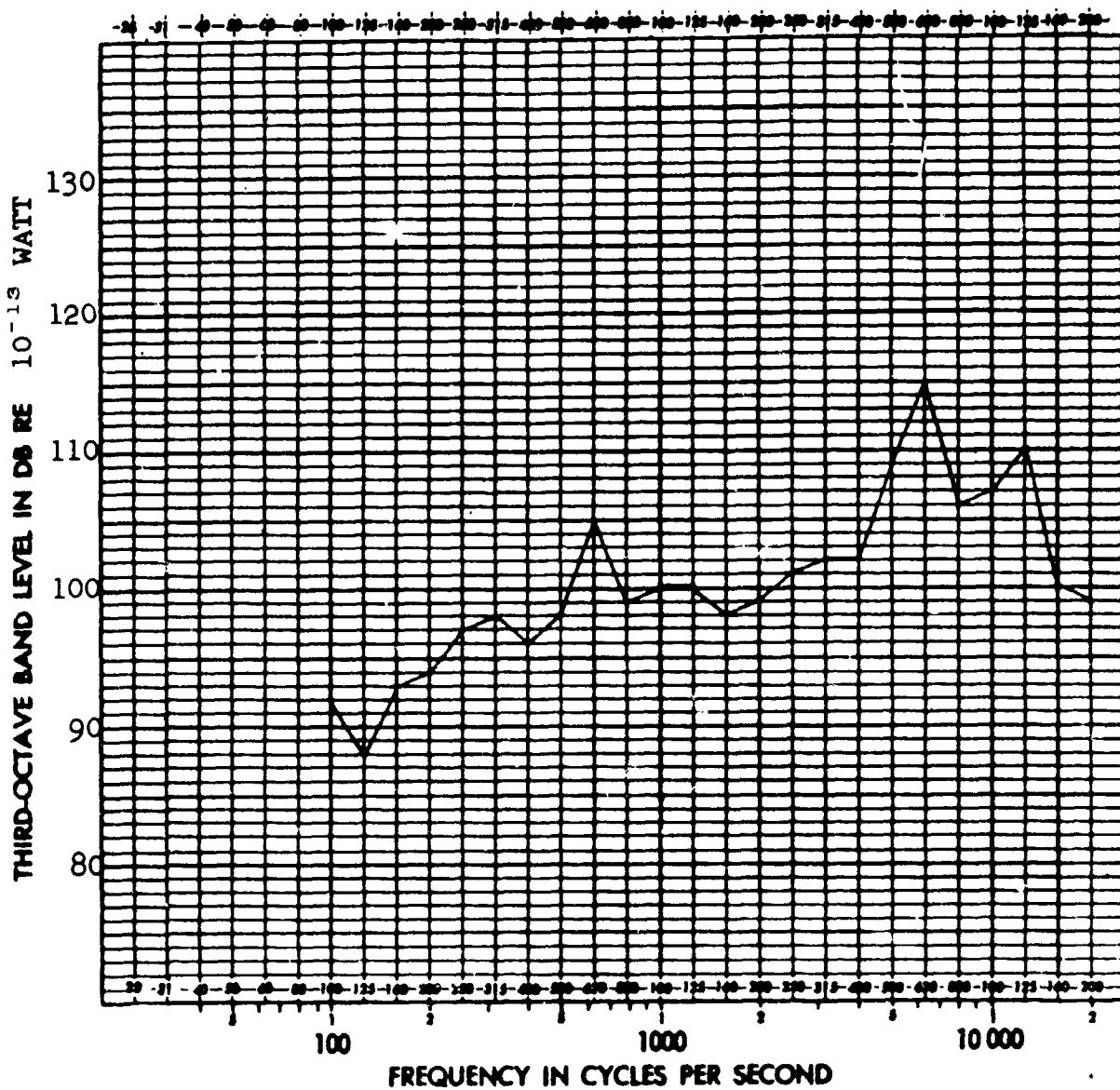
##### Compressor Section, Graphs 4-5 and 4-6

The compressor section is the predominant noise source radiating from the bare engine (excluding exhaust noise). The broad-band character of the noise in the mid-frequency range is believed due to air turbulence. The compressor-blade-passage pure-tone fundamental of the first-stage impeller dominates the overall acoustic power level. Its second harmonic is also significant. The turbine shaft-speed component emitted from the compressor section is about equal to that emitted from the bare engine.



AIRESEARCH MANUFACTURING COMPANY OF ARIZONA  
A DIVISION OF THE BARRETT CORPORATION  
PHOENIX, ARIZONA

FORM No. PX1842



GRAPH 4-10      1/3 OCTAVE BAND SOUND POWER LEVEL SPECTRUM  
GTP331-30 OIL COOLER FAN  
DETERMINED BY CLOSE-IN MEASUREMENT

GT-7615-R  
Page 4-40



Accessory Section, Graphs 4-7, 4-8, 4-9, and 4-10

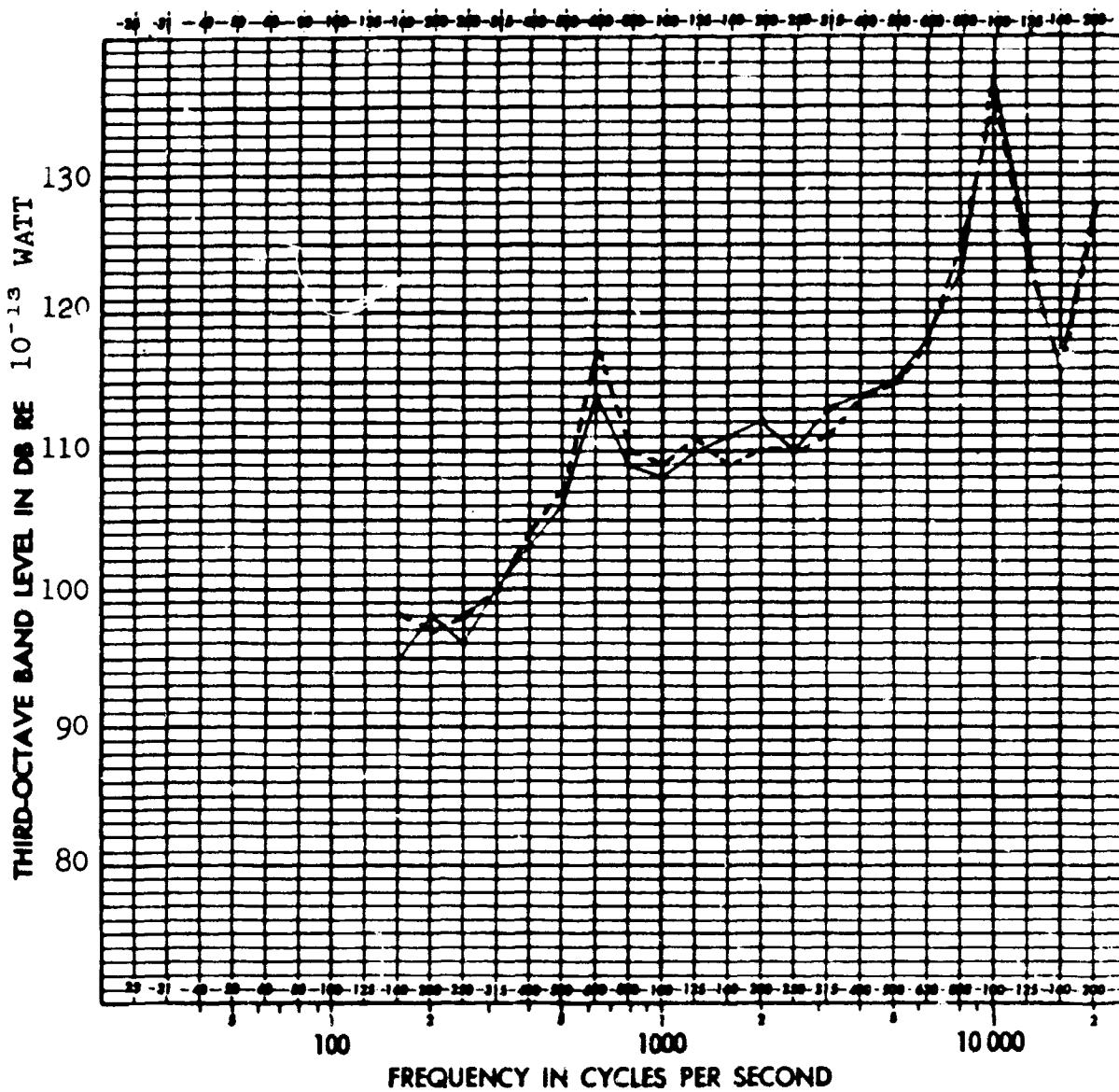
The acoustic power radiated by the accessory case without the oil-cooler fan is below that of the compressor inlet and turbine plenum radiation. As presented in Graphs 4-7 and 4-8, the turbine shaft-speed component, in the 630-cycle third-octave band is the predominant peak. At the no-load condition it is equal in magnitude to that radiated from the bare engine. A second and fourth order of shaft speed is evident only at the full-load condition (1,250-cycle and 2,500-cycle third-octave bands, respectively). A peak at the 10,000 cycle band occurs at both load conditions. Section 4.5 identifies this as being composed of the 14th and 15th order of shaft speed, the 15th order being the compressor first-stage impeller-blade-passage pure tone. Presented in Graph 4-9 is a comparison of the acoustic power radiated from the accessory case at the no-load condition with and without the oil-cooler fan. The first order of shaft speed (in the 6,300-cycle band) is the same for both, but with the oil-cooler fan the remaining spectrum does increase. The oil-cooler-fan blade-passage pure tone is quite evident in the 6,300-cycle band. An acoustic power estimation determined by close-in measurements of the oil-cooler fan is presented in Graph 4-10. The three peaks shown are the first order of turbine shaft speed and the oil-cooler-fan blade-passage pure-tone fundamental and second harmonic, respectively. The fan fundamental is the greatest in magnitude.

A comparison of the acoustic power level spectra, obtained by adding the individual power level of the three engine sections to that of the bare engine, is presented in Graphs 4-11 and 4-12. The agreement is close enough to give considerable credence to the method used in separating the three engine sections. A minor discrepancy occurs at the turbine-shaft-speed component, which is plus 3 decibels for the summation of the engine sections. Reviewing Graphs 4-5, 4-6, 4-7,



AIRESEARCH MANUFACTURING COMPANY OF ARIZONA  
A SUBSIDIARY OF THE GATES CORPORATION  
PHOENIX, ARIZONA

Form No. PX1842



GRAPH 4-11      1/3 OCTAVE BAND SOUND POWER LEVEL SPECTRUM  
GTP331-30 BARE ENGINE NOISE  
NO LOAD CONDITION

EXHAUST NOISE EXCLUDED

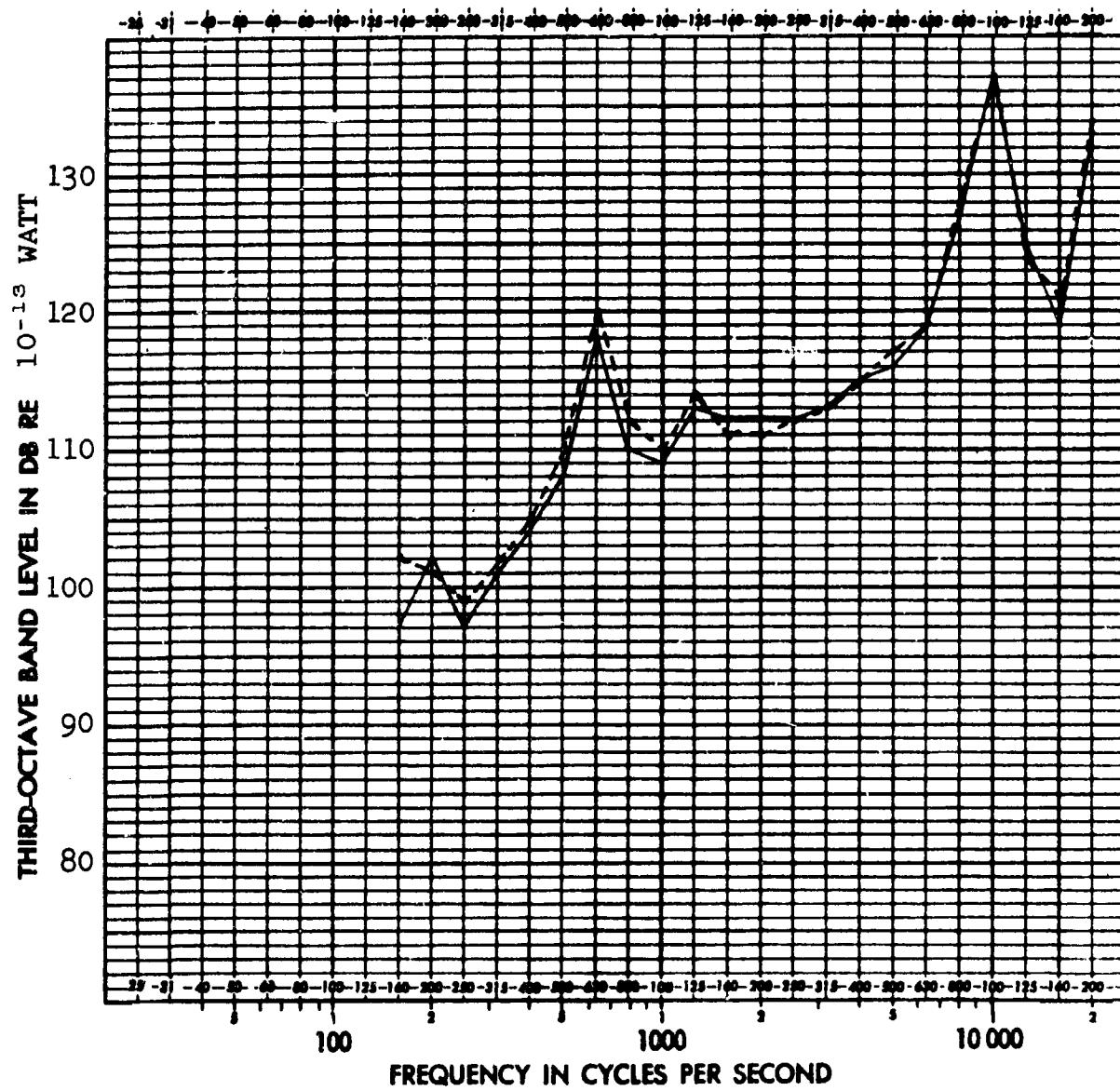
BARE ENGINE AS MEASURED

SUMMATION OF THE TURBINE PLEN &  
COMPRESSOR INLET AND  
ACCESSORY CASE MEASURED  
SEPARATELY. (NO OIL COOLER F.)



AIRESEARCH MANUFACTURING COMPANY OF ARIZONA  
A DIVISION OF THE GARNETT CORPORATION  
PHOENIX, ARIZONA

Form No. PX1842



GT-7615-R  
Page 4-43



AIRESEARCH MANUFACTURING COMPANY OF ARIZONA  
A DIVISION OF THE GARRETT CORPORATION  
PHOENIX, ARIZONA

and 4-8 shows the shaft-speed component radiated from the compressor and accessory sections to be equal in magnitude to that radiated from the total bare engine. The addition of two equal powers is a 3-decibel increase. This could indicate that the shaft speed component is not radiated totally from the compressor or accessory sections, but is a structurally-borne reradiation from the enclosure. Although the engine was vibration-isolated at all possible locations, structural ties could have existed.

Graph 4-13 compares the acoustic power level spectra of the accessory case with the oil cooler fan, arrived at by two methods. The solid line presents the acoustic power level as measured directly by the reverberant method. The broken line shows the summation of the accessory case and oil cooler fan measured separately. The former, by the reverberant method, and the latter, by the close-in method. The agreement is good enough to give credence to the close-in method used in obtaining the oil-cooler-fan acoustic power level.

The summation of the total noise radiated from the complete engine is presented in Graph 4-14. The curves represent the exhaust noise added to the bare-engine noise.

#### 4.5 Frequency Analyses of the Engine Components

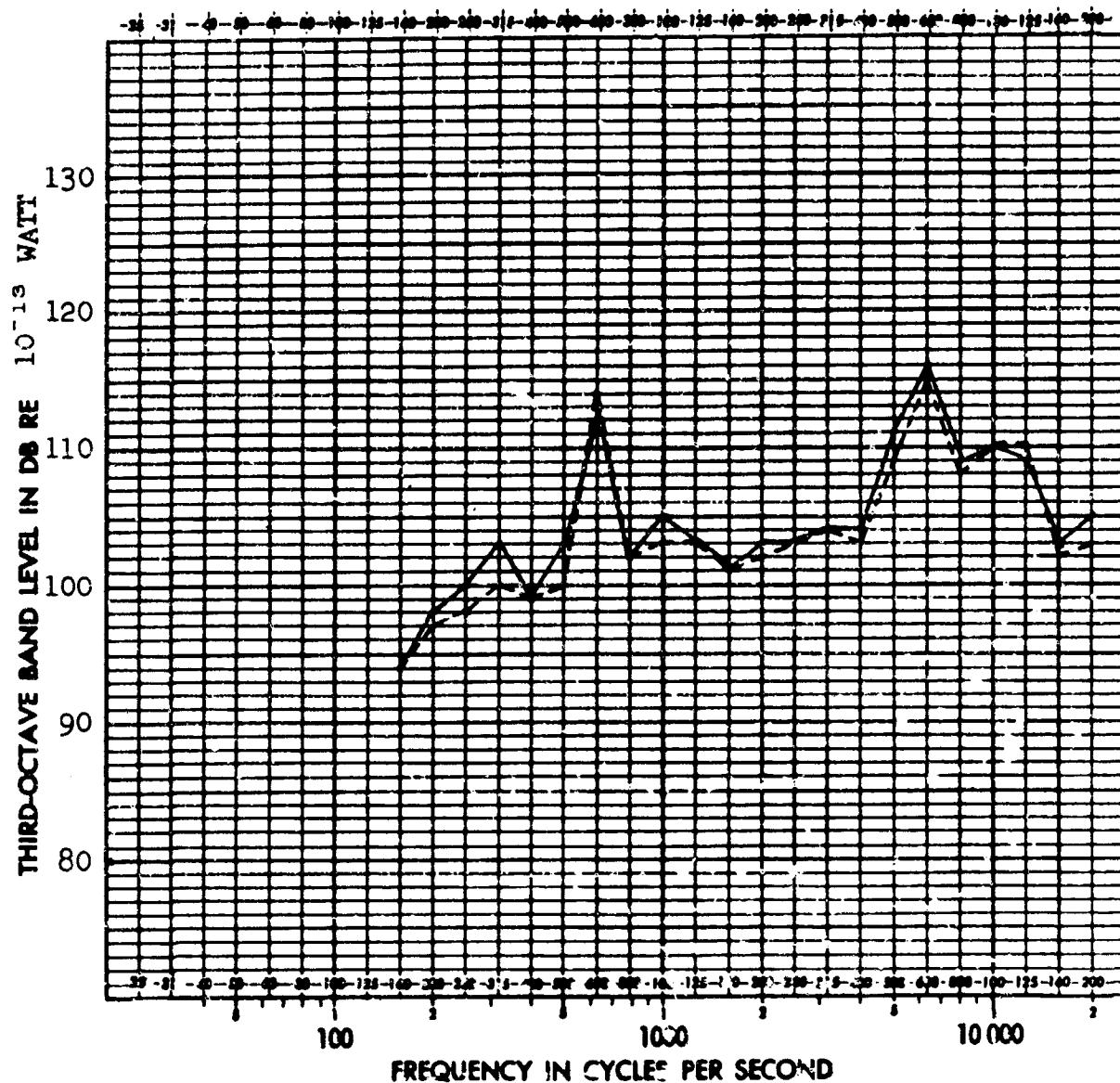
Tape recordings of the direct-near-field (close-in) noise were made of the turbine and compressor sections. The accessory case noise, with and without the oil-cooling fan, was recorded in the reverberant field because of the multitude of sources.

Playback of the recordings were made through a continuous constant-percentage band-pass frequency analyzer to a graphic level recorder. The analyses of the three engine sections are presented in Graphs 4-15 through 4-21. The results are shown on a frequency scale



AIRESEARCH MANUFACTURING COMPANY OF ARIZONA  
A DIVISION OF THE GARRETT CORPORATION  
PHOENIX, ARIZONA

Form No. PX1842



GRAPH 4-13      1/3 OCTAVE BAND SOUND POWER LEVEL SPECTRUM  
GTP331-30 ACCESSORY CASE WITH  
OIL COOLER FAN  
NO LOAD CONDITION

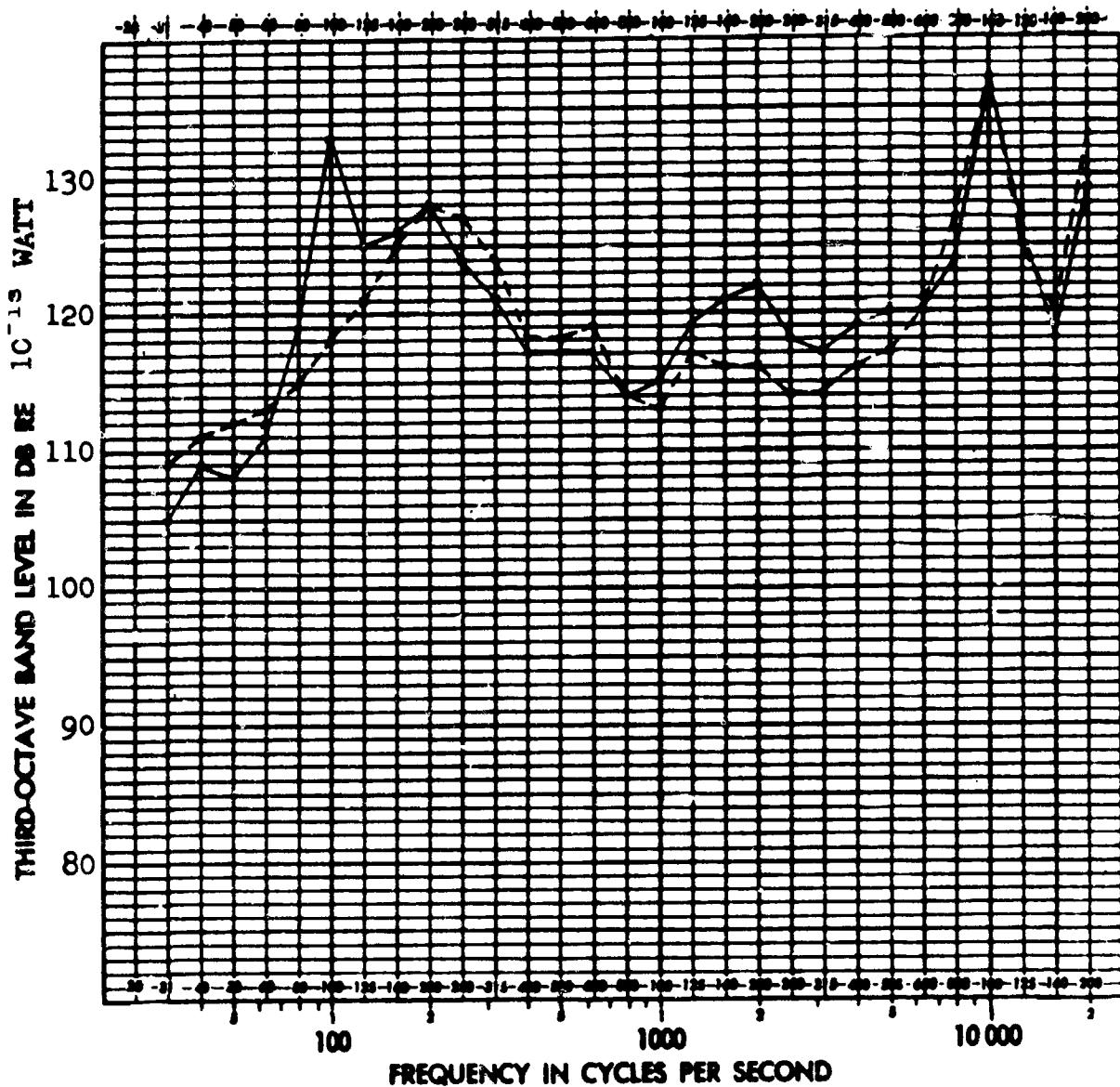
— ACCESSORY CASE WITH OIL COOLER  
FAN AS MEASURED BY REVERBERANT  
METHOD

- - - - SUMMATION OF THE ACCESSORY CASE  
WITHOUT OIL COOLER FAN (BY  
REVERBERANT METHOD) AND OIL  
COOLER FAN (BY CLOSE-IN METHOD)



AIRESEARCH MANUFACTURING COMPANY OF ARIZONA  
A DIVISION OF THE GARRETT CORPORATION  
PHOENIX, ARIZONA

Form No. PX1842



GRAPH 4-14

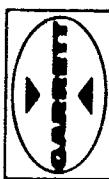
1/3 OCTAVE BAND SOUND POWER LEVEL SPECTRUM  
OF THE TOTAL POWER RADIATED FROM MODEL GTP331-30

INCLUDES

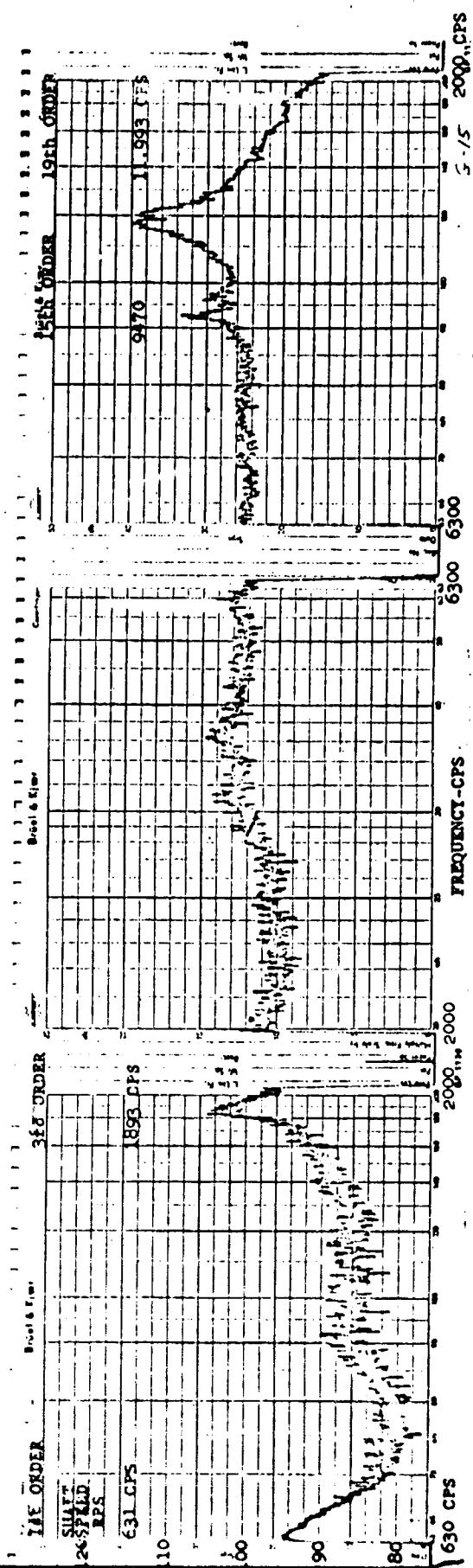
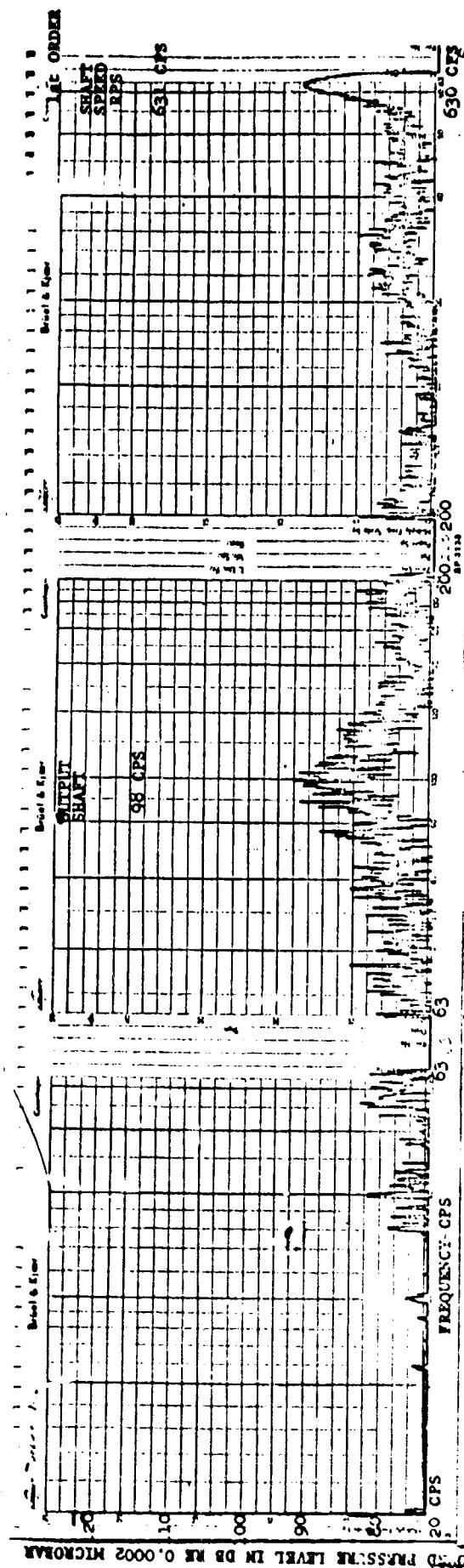
TURBINE EXHAUST WITH STRAIGHT  
EXTENSION PLUS REMAINING  
BARE ENGINE NOISE

— NO LOAD

--- FULL LOAD



**AIR RESEARCH MANUFACTURING COMPANY OF ARIZONA**  
A DIVISION OF THE GARRETT CORPORATION

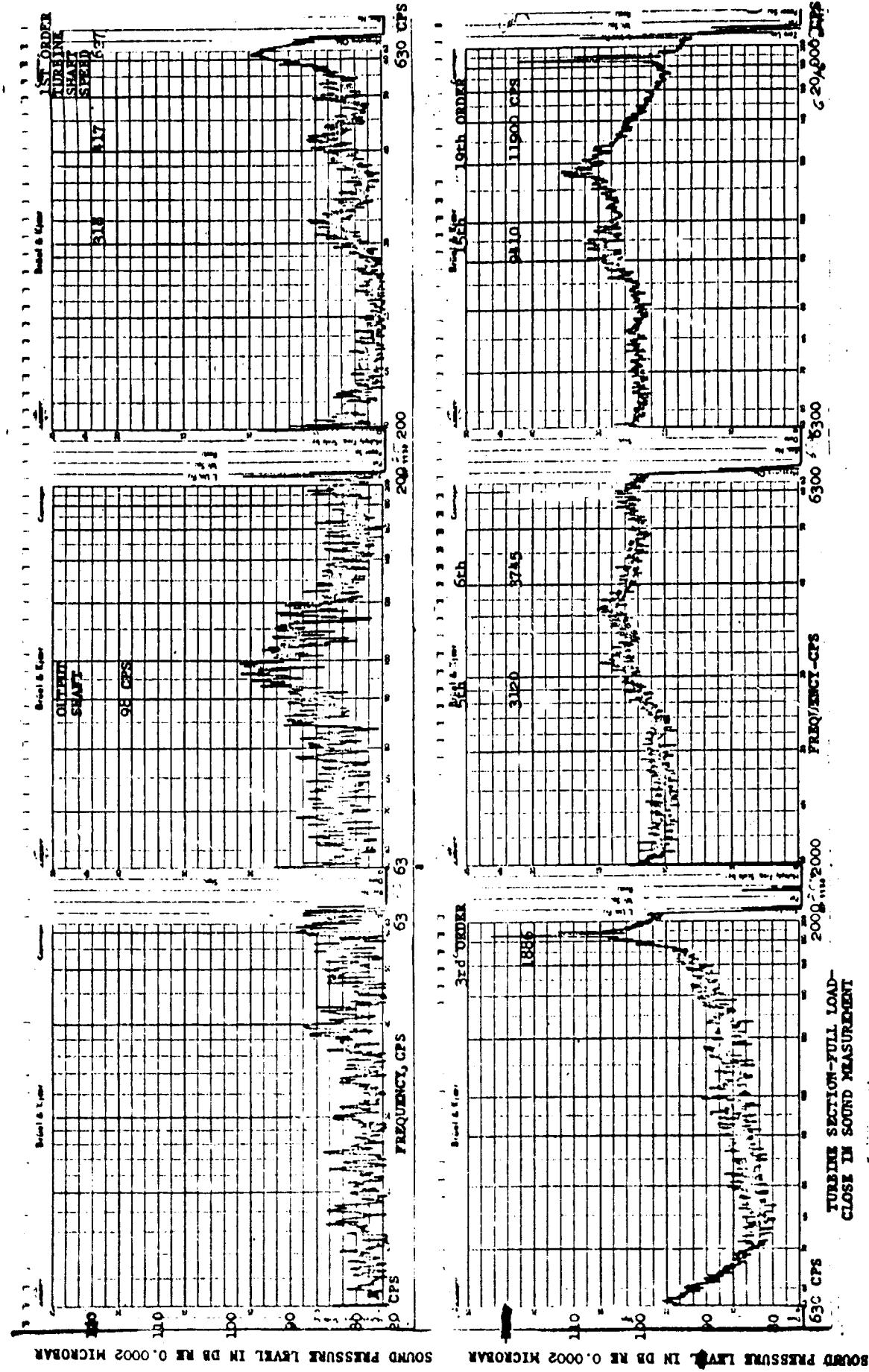
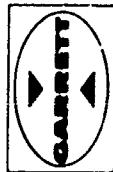


CLOSE IN SOUND MEASUREMENT  
TRUE IN SECTION - NO LOAD

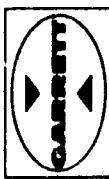
63188 1 - 1E

SOUND PRESSURE LEVEL IN dB IS 0.0002 MICROBAR

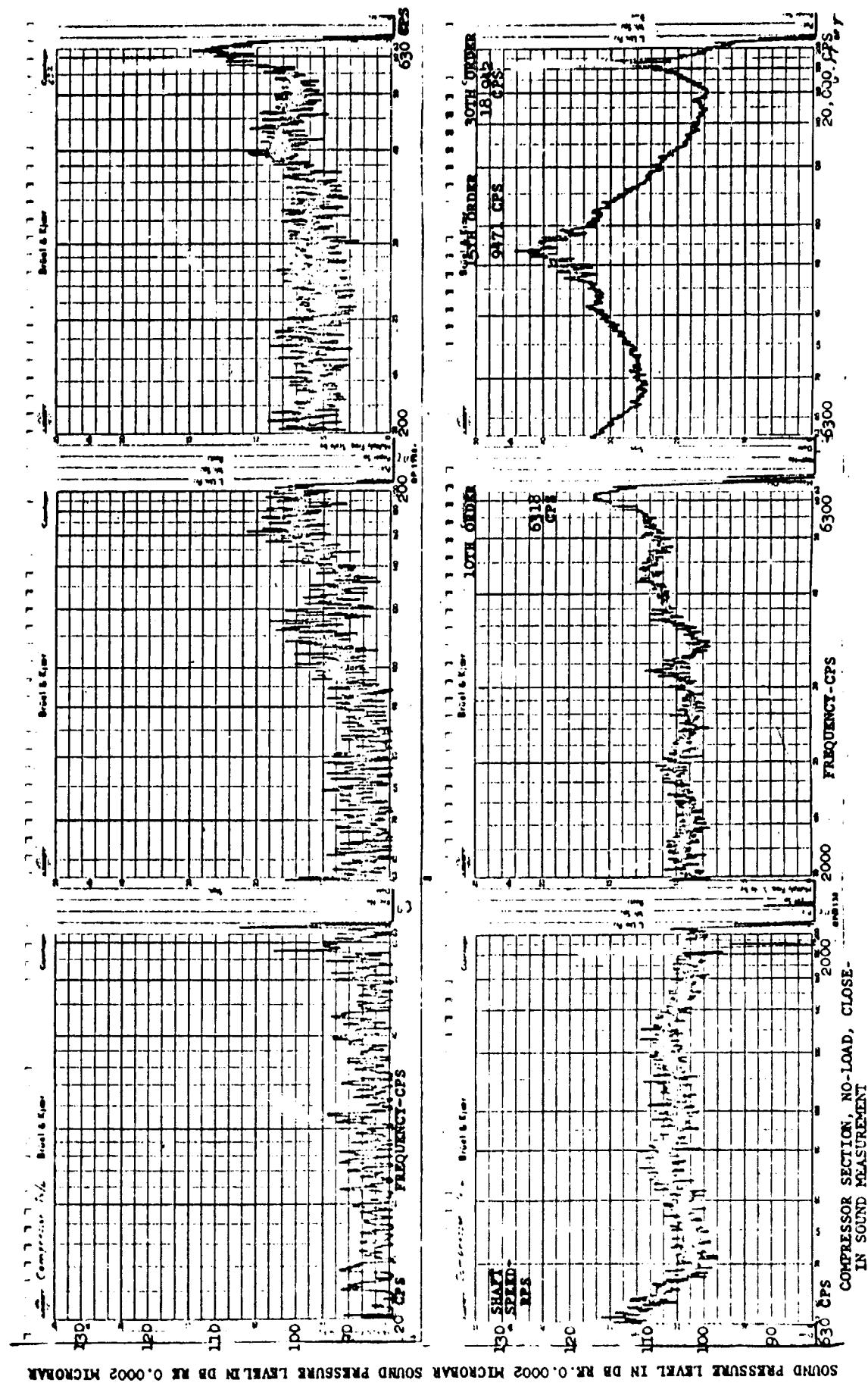
GT-7615-R  
Page 4-47



GT-7615-R  
 Page 4-48



AIRESEARCH MANUFACTURING COMPANY OF ARIZONA  
A DIVISION OF THE GARRETT CORPORATION  
PHOENIX, ARIZONA

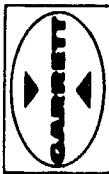


COMPRESSOR SECTION, NO-LOAD, CLOSE-IN SOUND MEASUREMENT

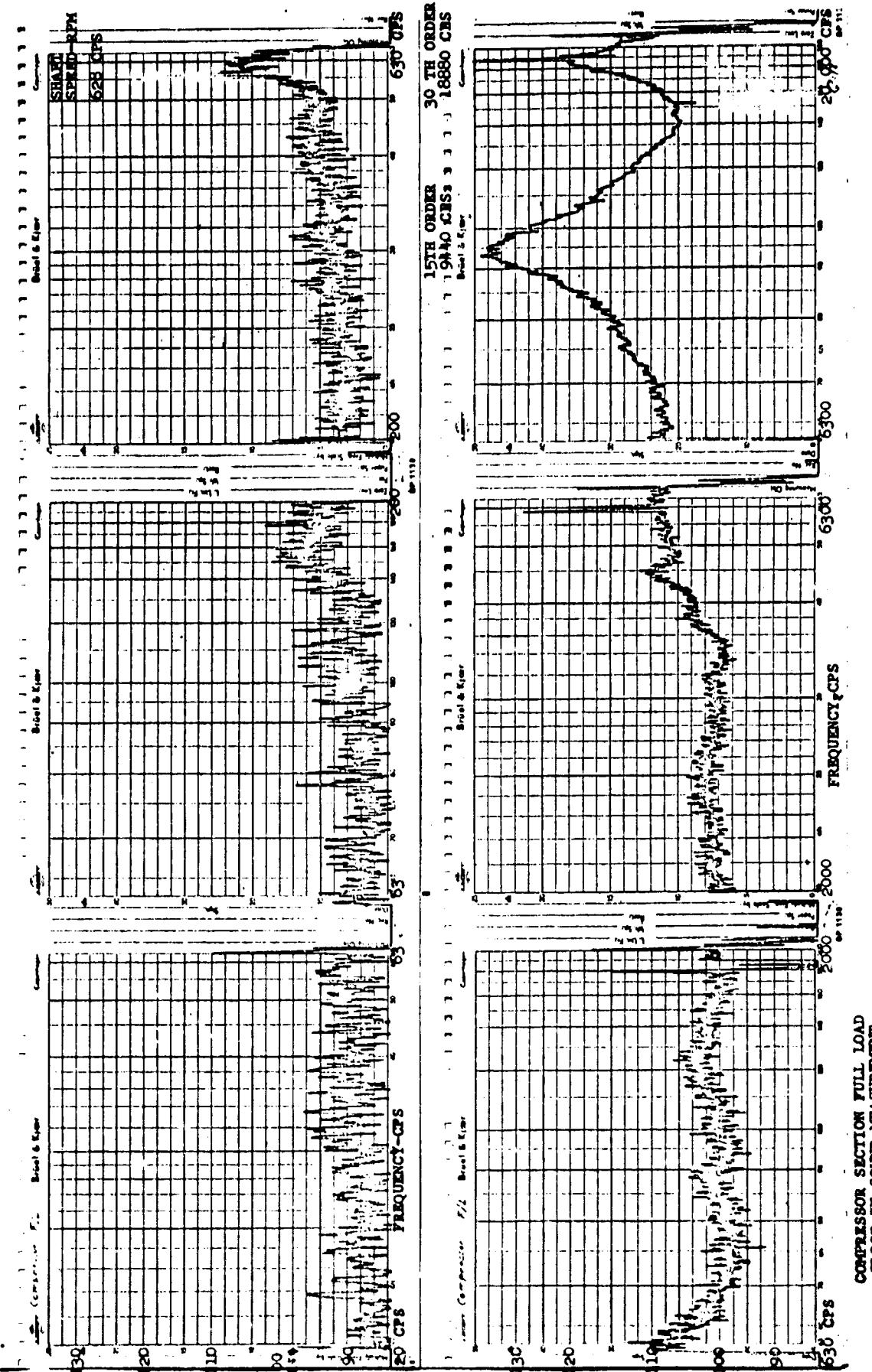
GRAPH 4-17

GT-7615-R  
Page 4-49

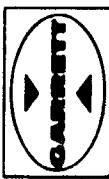
AIRESEARCH MANUFACTURING COMPANY OF ARIZONA  
A DIVISION OF THE GARRETT CORPORATION  
PHOENIX, ARIZONA



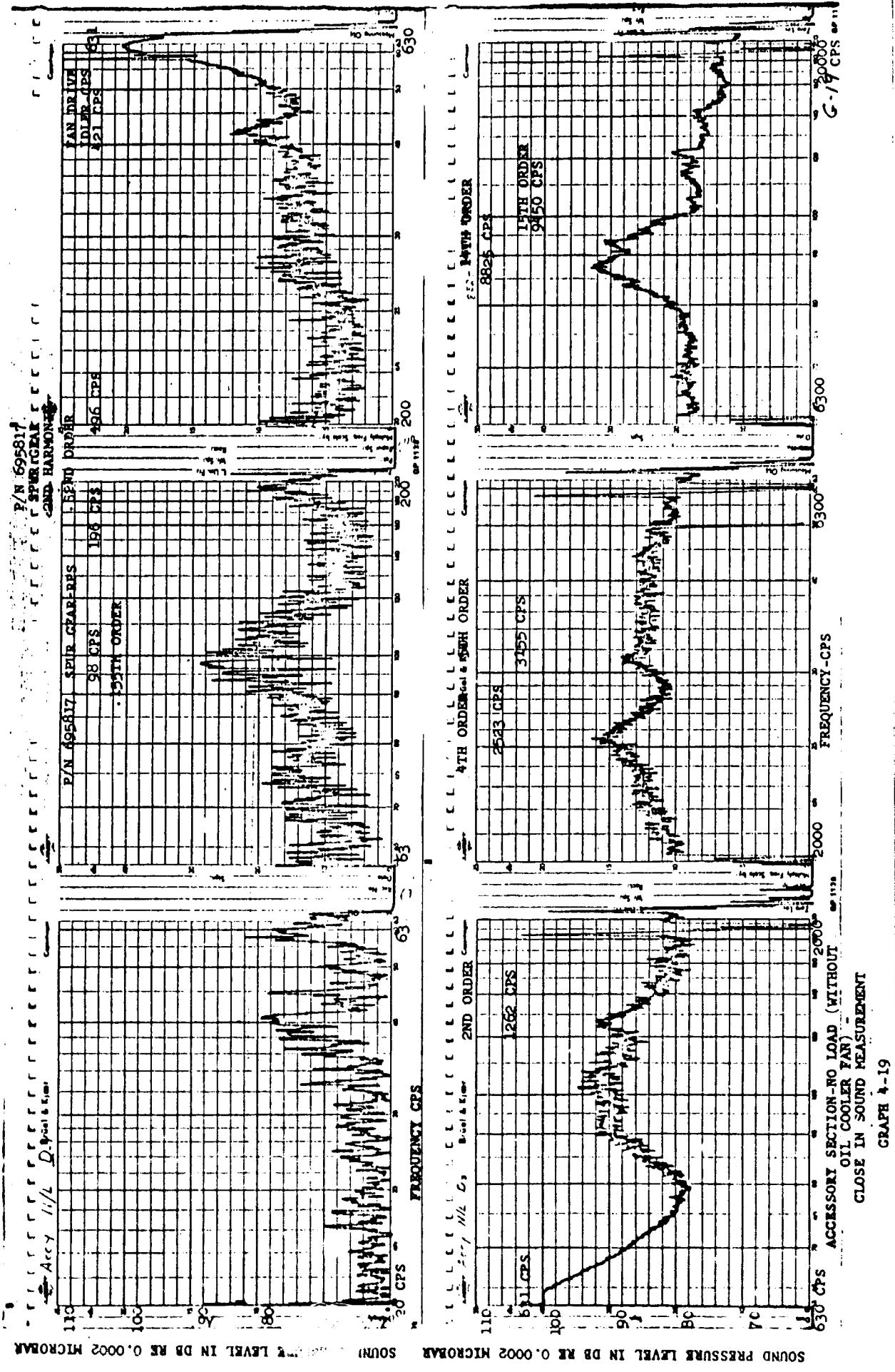
SOUND PRESSURE LEVEL IN DB RE 0.0002 MICRORAM



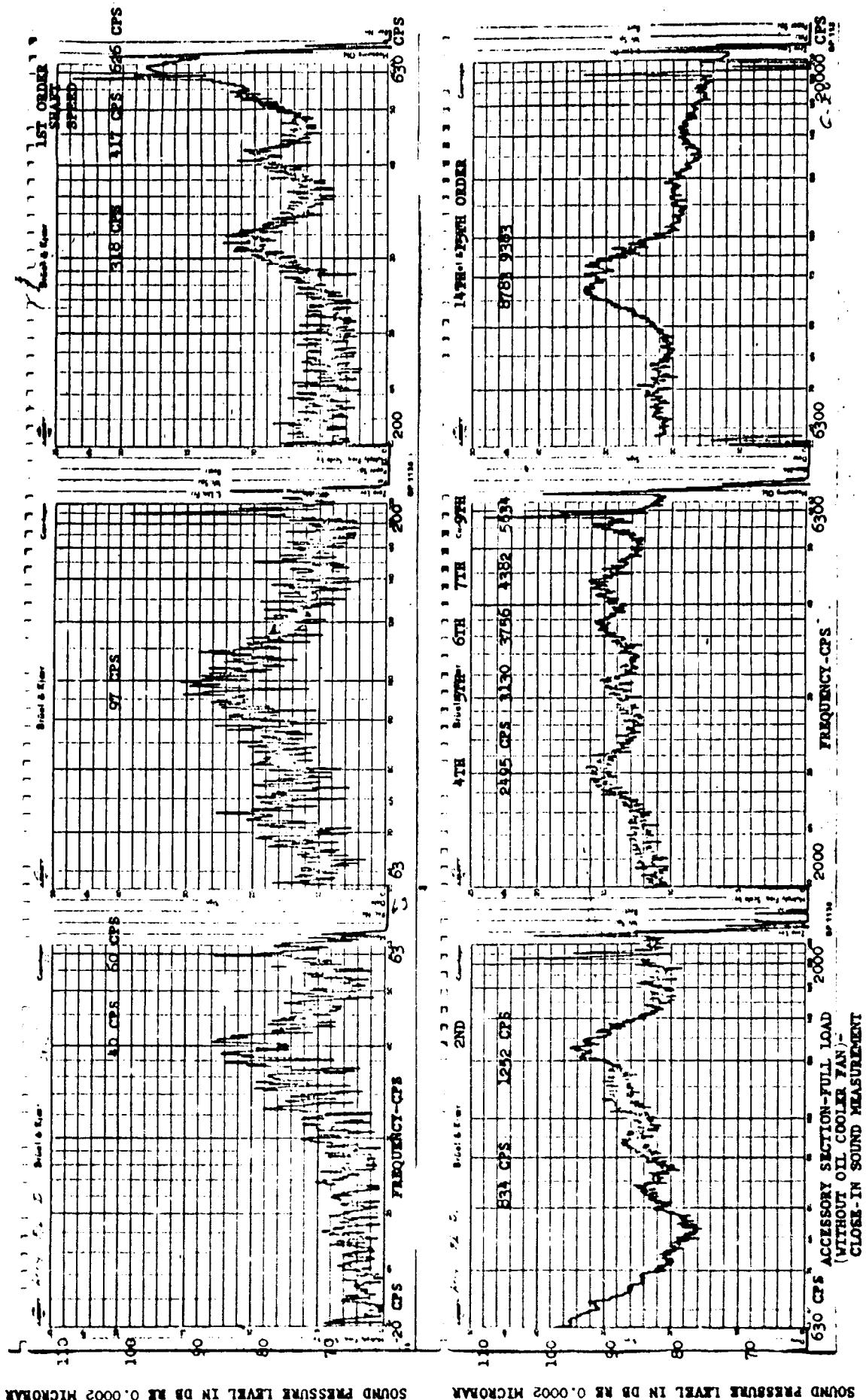
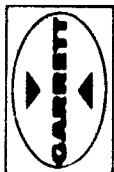
GRAPH 18



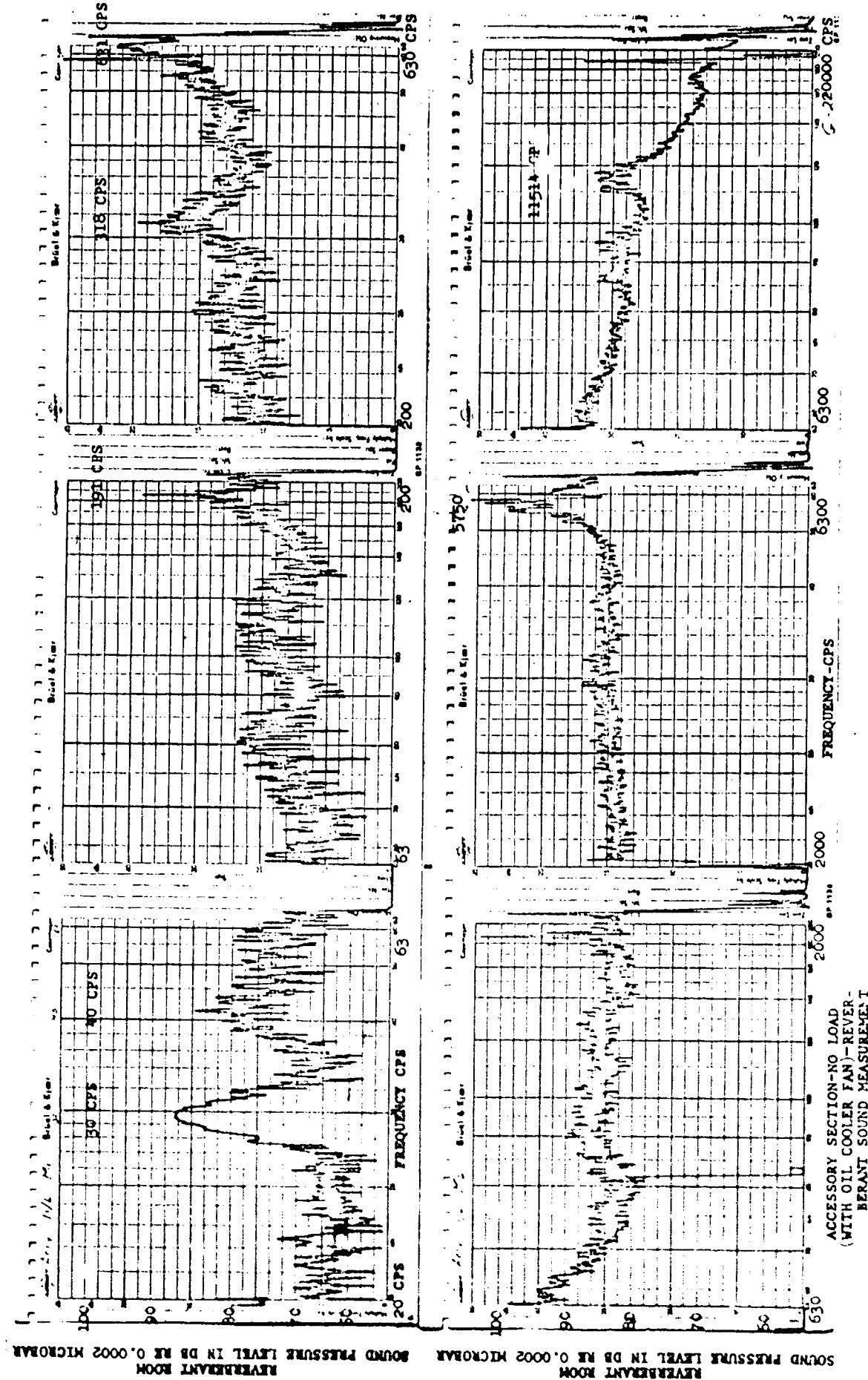
**AIRSEARCH MANUFACTURING COMPANY OF ARIZONA**  
A DIVISION OF THE DARTY CORPORATION



GT-7615-R  
Page 4-51



AIRESEARCH MANUFACTURING COMPANY OF ARIZONA  
A DIVISION OF THE GARRETT CORPORATION  
PHOENIX, ARIZONA



GRAPH 4-21



AIRESEARCH MANUFACTURING COMPANY OF ARIZONA  
A DIVISION OF THE BARRETT CORPORATION  
PHOENIX, ARIZONA

in cps plotted against amplitude in decibels (uncorrected sound pressure level). A constant bandwidth of 6 percent was used. The frequency scale is in steps of 20 to 63 cps, 63 to 200 cps, 200 cps to 630 cps, etc., to 20,000 cps. The component frequency identification was verified by either an x-y axis Lissajous figure with one axis of a known frequency, or the z axis modulation of the Lissajous figure.

#### 4.5.1 Component Summary

To facilitate the frequency identification of the graphs, the noise-generating components used in the engine are listed below:

<u>Component</u>	<u>Blade Count</u>	<u>Order of Shaft Speed</u>
<u>Compressor and turbine section</u>		
First-stage impeller	15	15
Crossover duct	8	
Second-stage impeller	19	19
Second-stage diffuser	24	
First-stage stator	22	
First-stage turbine	36	36
Second-stage stator	29	
Second-stage turbine	36	36
Third-stage stator	29	
Third-stage turbine	36	36



AIRESEARCH MANUFACTURING COMPANY OF ARIZONA  
A DIVISION OF THE BARRETT CORPORATION  
PHOENIX, ARIZONA

Accessory Section

<u>Component</u>	<u>Number of Teeth</u>	<u>Gear Speed*</u> <u>(rev/sec.)</u>	<u>Gear Mesh</u> <u>Frequency*(cps)</u>
------------------	------------------------	---	--

Bolt-on Gearbox

Spur pinion	25	630	15,750
Spur gear	161	98	15,750

Accessory Housing

Bevel pinion	24	630	15,120
Bevel gear	47	322	15,120
Spur	22	322	7,077
Oil-pump gear	101	70	7,077

Fan Assembly

Idler	54	131	7,077
Drive gear	16	442	7,077

\*Calculated at 630 rev per sec. turbine shaft speed.

The oil-cooler fan has 13 blades and rotates at 442 revolutions per second. The fan-blade-passage pure tone is approximately 5,746 cps.



AIRESEARCH MANUFACTURING COMPANY OF ARIZONA  
A DIVISION OF THE GARRETT CORPORATION  
PHOENIX, ARIZONA

#### 4.5.2 Frequency Analysis

Tabulated below are the frequencies identified for each engine section.

<u>Observed Frequency</u> (cps)	<u>No Load</u>	<u>Full Load</u>	<u>Turbine Shaft Order Number</u>	<u>Component</u>
<u>Turbine Section, Graph 4-1 and 4-16</u>				
98		98	0.155	Accessory output speed
		315	0.5	
		417	0.66	
631		627	1.	Turbine shaft
1,893		1,886	3	
		3,120	5	
		3,745	6	
9,470		9,410	15	First-stage impeller blade passage
11,993		11,900	19	Second-stage impeller blade passage
<u>Compressor Section, Graph 4-17 and 4-18</u>				
632		628	1	Turbine shaft
6,318			10	
9,471		9,440	15	First stage impeller blade passage
18,942		18,880	30	Second harmonic of first-stage impeller



AIRESEARCH MANUFACTURING COMPANY OF ARIZONA  
A DIVISION OF THE GARRETT CORPORATION  
PHOENIX, ARIZONA

Observed Frequency  
(cps)

No Load	Full Load	Oil-Cooling Fan	Turbine Shaft Order Number	Component
<u>Accessory Section, Graphs 4-18, 4-20, and 4-21</u>				
		30		
	40	40		
98	97			Accessory output speed
196		191		Second harmonic of accessory output
	318	318	0.52	Spur-bevel gear speed
421	417		0.665	
631	626	631	1	Turbine shaft
	834		1.33	Second harmonic of the .665th order
1,262	1,252		2	Second harmonic of turbine shaft
2,523	2,504		4	
3,155	3,128		5	
	3,756		6	
	4,381		7	
	5,632		9	
		5750	9.1	Oil-cooling fan blade passage
8,825	8,783		14	
9,450	9,383		15	
		11514	18.2	Second harmonic of oil-cooling fan

GT-7615-R  
Page 4-21



## 5.0 SOUND AND VIBRATION DAMPING COATINGS

### 5.1 Groundwork

#### 5.1.1 State of the Art Survey

No greater disservice can be rendered to the sponsors of research effort than to duplicate work already done. To insure against this, the state of the art for damping coatings in the 600°F to 2000°F range was carefully determined. This effort was divided into three initial phases, as follows:

- (a) Fresh contacts by phone and letter with a number of persons and organizations active in the field of vibration-damping coatings.
- (b) A canvass by mail of vendors of coating materials, and vendors of materials possibly usable as coatings.
- (c) An intensive search for relevant literature.

These activities were conducted in parallel, since considerable overlap existed. For example, the letter to the vendors asked for literature citations. The literature survey revealed what authors were currently active and, thus, who might be profitably contacted by phone or letter etc.

#### 5.1.1.1 Active Researchers

The results of fresh contacts with recent writers, recognized authorities, and organizations active in the vibration damping field were completely negative insofar as uncovering parallel activity was concerned.



AIRESEARCH MANUFACTURING COMPANY OF ARIZONA  
A DIVISION OF THE GARRETT CORPORATION  
PHOENIX, ARIZONA

By the time these contacts were made, the possible value of a suitably experienced consultant had been realized. Each person contacted disclaimed the necessary qualifications, but several mentioned Prof. B. J. Lazan as eminent in a fairly closely related field--the study of damping inherent in structural materials. Discussion of contact with Prof. Lazan is deferred to a later paragraph.

None of the persons contacted would venture serious speculation as to candidate coating materials.

#### 5.1.1.2 Vendor Canvass

As a first step toward a methodical canvass of vendors, a mailing list was drawn from Thomas Register and Aviation Week Buyers Guide. Attention was divided into two broad classes of material--metallic and nonmetallic. In the case of a specific classification, such as "high-temperature coatings," every vendor listed was placed on the list. In the case of a more general classification such as "alloys," only the largest companies were contacted, on the theory that they were likely to have the largest and most generally informed technical staffs.

The compiled list of vendors deemed possible sources of help totaled 580 organizations.

A two-page letter of inquiry was composed, which sketched the nature of the investigation, stated the general physical properties conducive to a good damping coating, and requested product data, literature citations, etc.



AIRESEARCH MANUFACTURING COMPANY OF ARIZONA  
A DIVISION OF THE GARRETT CORPORATION  
PHOENIX, ARIZONA

Out of 160 answers received, virtually no new data on the damping characteristics of possible coating materials was received. Several respondents mentioned the anomalous damping of manganese-copper alloys and cited Dean's book on Electrolytic Manganese (Ref. 9).

A particularly valuable contribution to the literature search was made by the Beryllium Corporation, which provided a copy of "Mechanical Properties of Engineering Ceramics", by R. Chang. (Ref. 7). This reference is presented in Appendix III.

Some information received lent support to the potential usefulness of vitreous coatings. Tiltman Langley, Ltd., described an attempt to correct a resonant condition in hot sheet metal with the use of sand-filled porcelain enamel; no data was taken, but "it seemed to work". Another vendor related how aircraft exhaust manifolds produced during the war were found to be no longer subject to fatigue failure of their mounting brackets when vitreous enamel was applied to them to increase their corrosion resistance. Bausch and Lomb pointed to the concept that glasses should be "lossy" in their transition region and mentioned the infinite variety of properties obtainable by compounding glass. Finally, both the O'Hommel Company and the Chicago Vitreous Corporation supplied viscosity data on vitreous enamels at elevated temperatures.

The National Lead Company cited a recent paper in the British publication New Scientist entitled "Silent Metal" (Reference 13). This brief article outlines intensive activity by the Admiralty Research Facility into the damping properties of manganese copper.

The lack of data on what is becoming recognized as a basic engineering property of material, plus widespread lack of understanding of what damping is, became apparent.



AIRESEARCH MANUFACTURING COMPANY OF ARIZONA  
A DIVISION OF THE GARRETT CORPORATION  
PHOENIX, ARIZONA

### 5.1.1.3 Literature Search

Vibration damping is of interest to a wide range of technologies, from acoustics and structural engineering to metallurgy, organic chemistry, physical chemistry, and solid-state physics. As a result, the literature is scattered, and its systematic survey presents a formidable task.

The ideal answer to such a problem is the existence of a good and recent monograph on the subject of interest.

Preliminary scanning of recent literature showed Prof. B. J. Lazan to be a prolific writer on the fundamental aspects of damping. His name was also mentioned by several of the other authorities in the damping field. Contact with Prof. Lazan disclosed that he had just completed such a monograph, which was scheduled for publication late in 1965. He expressed an immediate willingness to provide AiResearch with a copy of the manuscript. This generous action was an invaluable contribution to the success of this project. The monograph is entitled "Damping of Material and Members in Structural Mechanics," and its comprehensive nature is indicated by the fact that in final published form it will fill 600 pages. Special features include a multiply cross-indexed bibliography citing several thousand references extending back to the 18th century. In addition, the monograph presents in graphical form a vast compilation of material damping data.

This survey of literature and data appears to be devoid of reference to damping coatings for operation at elevated temperatures. The compilation of data served the valuable function of eliminating literally thousands of possible candidate materials. It also showed data on the "anomalous" damping of manganese copper alloys.



Because this monograph will be available shortly after the appearance of this report, it was unnecessary to include with this report a massive, parallel bibliography. Instead, the references cited are limited to those having major relevance to the present work, or those encountered that do not appear in Prof. Lazan's bibliography.

Considering the foregoing, vitreous enamels and manganese alloys were tentatively selected for evaluation. In addition, aluminum-alumina cermets were chosen, because their unusually high room temperature damping was a promise of the possibility of good damping at elevated temperature. Once tentative selections were made of the types of material to be tested, then literature covering other properties of these materials became relevant. Fortunately, an excellent and recent monograph was available on the subject of vitreous enamels (Ref. 20). This otherwise comprehensive work did not discuss damping characteristics. The manganese alloys are discussed in great detail in Ref. 9, and considered further in Ref. 10, 11, 12, and 14. Behavior of the manganese alloys is little understood in spite of more than 20 years of work principally by the U. S. Bureau of mines. Information concerning the aluminum-alumina cermets is sparse and mostly proprietary in character. Ref. 19 summarizes most of the physical properties and contains a bibliography.

#### 5.1.1.4 Consultants

The bulk of the vibration-damping data to be found in the literature is the result of ad hoc test procedures which generate comparative data only. In many cases it is impossible to deduce from this data the actual properties of the material being tested. The Geiger test is of this sort (Ref. 6). It is not feasible to take the results of a Geiger test and predict the behavior of another system to which the test coating is applied.



AIRESEARCH MANUFACTURING COMPANY OF ARIZONA  
A DIVISION OF THE GARRETT CORPORATION  
PHOENIX, ARIZONA

It was evident that if more fundamental data were to be obtained, which measured the true damping characteristic of the coating material itself, sophisticated apparatus and data analysis would be required. The need to operate the apparatus over a wide range of temperatures created significant technical problems. Contacts with Prof. Lazan revealed that he had many years of experience in the design and operation of apparatus used for similar measurement of damping in structural material. Much of this apparatus operated at elevated temperatures.

AiResearch acquired Prof. Lazan's services as consultant for this study. His contributions included conceptual design of the apparatus, specifications of data reduction procedures, source-of-error analyses, the screening of candidate materials, and the tentative identification of damping micromechanisms.

#### 5.1.1.5 Analysis

The review of current knowledge reveals that structural damping as an engineering tool is a very new field. Acute space-age problems, such as structural fatigue in critical jet-engine components, have motivated rapid progress in the consideration of internal damping in high-temperature structural materials, including ceramics. The alternate approach of providing the requisite damping in the form of a specialized coating is in widespread use on all kinds of vehicles and appliances in response to pressure from a noise-conscious public, and this is accomplished at ordinary temperatures by the use of specialized organic coatings. This investigation appears to be one of the first attempts to extend the coating approach to elevated-temperature vibration problems by means of inorganic coatings.



Correspondence with producers of inorganic coatings and materials revealed unfamiliarity with structural damping concepts, which manifested itself as a lack of data on internal friction as a material property.

The literature survey and tabulation of data appearing in Professor Lazan's monograph made possible the elimination of a great many candidate materials for test. The literature survey also revealed that understanding of the mechanics of structural damping is in its infancy. Professor Lazan's monograph focuses attention on the lack of an adequate mathematical model to relate stress and strain in the case of complex material behavior. This lack may be an impediment to understanding of fundamental micro-mechanisms, such as those of manganese alloys.

### 5.1.2 Materials Selection

#### 5.1.2.1 Review of Viscoelasticity

Prior to describing the selection of vibration damping materials, a review is made of the factors involved. The major damping mechanism prevalent in the polymeric and elastomeric materials used in organic damping coatings is called viscoelasticity. All such materials at some sufficiently low temperature exhibit a glassy structure, and upon impact will normally shatter. Their microstructure features large, elongated, and frequently branched molecules linked tightly together by a variety of chemical bonds. In this state, the materials are highly elastic. The molecular arrangement is seldom truly crystalline, in that short range ordering is present, but when considered over dimensions of several molecules an element of disorder is present. This short-range order, long range disorder



AIRESEARCH MANUFACTURING COMPANY OF ARIZONA  
A DIVISION OF THE GARRETT CORPORATION  
PHOENIX, ARIZONA

is characteristic of polar liquids such as water. When examined by X-ray diffraction techniques the imperfect ordering produces diffuse but perceptible diffraction patterns. Such elastomeric materials do not exhibit a sharply defined melting point but rather a progressive softening through a definite transition temperature range. In this range there is a progressive reduction in the stiffness moduli of the material, caused by the successive loosening of the various chemical bonds. As the bonds loosen, relative motion, still partly constrained by the remaining bonds, becomes possible, which results in internal friction. Associated with this motion and viscous loss is a characteristic strain response which lags an abruptly applied stress. The rapidity with which the material accommodates the stress may be expressed as a relaxation time. Each type of bond may have a different relaxation time, which leads to the concept of a relaxation-time spectrum.

As a consequence of these micromechanisms, elastomeric materials in their transition region exhibit a damping peak of considerable magnitude. Above the transition region the bonds are so loosened that the material flows as a liquid, or else decomposes. Once the liquid state is approached, then, even if viscous forces predominate, the moduli have become so small that the total energy dissipation is small. This illustrates an important fact that was generally overlooked prior to the work of Oberst--i.e., the energy dissipation per cycle depends on the product of the loss factor and the stiffness.



AIRESEARCH MANUFACTURING COMPANY OF ARIZONA  
A DIVISION OF THE GARRETT CORPORATION  
PHOENIX, ARIZONA

Viscoelasticity produces what is called quadratic damping, where the energy loss per cycle is proportional to the square of the maximum stress or strain. For such damping the hysteresis loop associated with vibration cycles is elliptical. The behavior of such materials may be described in terms of their complex modulus,  $E^*$ , where

$$E^* = E' + iE'' = E' (1 + i\eta)$$

$E'$  is the stiffness modulus,  $E''$  is the loss modulus,  $\eta$  is the loss factor, and  $i$  is  $\sqrt{-1}$ .  $E^*$  is a function of both temperature and frequency, and  $\eta$  may attain values of unity or even greater.

#### 5.1.2.2 Other Damping Mechanisms

Another form of quadratic damping, also associated with a relaxation time spectrum, is termed anelasticity, which occurs in metals at low stress amplitudes. Numerous mechanisms for anelastic damping exist, each associated with a particular relaxation time (see Ref. 15). A typical cause of anelasticity is viscosity at grain boundaries associated with the relative atomic disorder to be found there. Anelasticity seldom leads to values of  $\eta$  greater than 0.01. The location of anelastic damping peaks and their connection with micromechanisms in the material, has been a useful tool for solid-state physicists.

According to Zener (Ref. 15), a less common mechanism accounts for anomalously high damping in the manganese alloys. Manganese itself has a cubic crystal structure; but, when another metal is present, such as copper, the crystal is forced to become slightly tetragonal. Such crystals may form into parallel (twinned) layers which are mirror images. Theory, states that slightly tetragonal crystal



are capable of ready deformation into cubic, or mirror image shape, with associated losses. Chang (Ref. 7) found twinned structures and an apparently associated damping peak in the ceramic, zirconium hydride.

At stress levels approaching the proportionality limit, and above, metals exhibit plastic deformation involving actual slip within grains, which ultimately becomes minute cracks. The associated damping is no. quadratic and the hysteresis loops are pointed (nonlinear). Recently, complex expressions, called dislocation theories, have been formulated in connection with the study of fatigue(References 18 and 26). Serious attempts are made to correlate the changing character of the hysteresis loops with the dislocation theory of micromechanisms of fatigue. This fundamentally important use of damping appears handicapped by the lack of mathematical models for nonlinear hysteresis loops.

Lazan (Ref. 2) discusses other damping mechanisms, including dry friction (coulomb damping), anelasticity due to magnetostrictive effects, heat transfer, etc., as well as the peculiar damping found in clay, and the nonsymmetrical damping in highly stressed rubber. None of these, however, are directly relevant to this study, except for the possibility that the concepts presented in Section 6.0 may assist in their exploration.

#### 5.1.2.3 Glass

Any inorganic material that behaves in a manner similar to a polymer at some elevated temperature is a prospect for a high-temperature damping coating. Close inspection of the properties of glass reveals a surprising degree of analogy which, carries over into the nomenclature of such diverse fields as organic chemistry and the ancient art of glassworking. Plastics have a glassy phase



and exhibit a glassy fracture. The techniques of blowing and molding glass are strikingly similar to the molding processes for thermoplastics. The physical chemistry of glass is to some extent analogous (Ref. 21). The variety of ingredients used in compounding glass results in the absence of definite molecular or ionic crystalline structure. Glass exhibits the short-range order and long-range disorder characteristic of polar liquids when examined by X-ray. The lack of a sharply defined melting point in glass is well known and is the basis of glassworking.

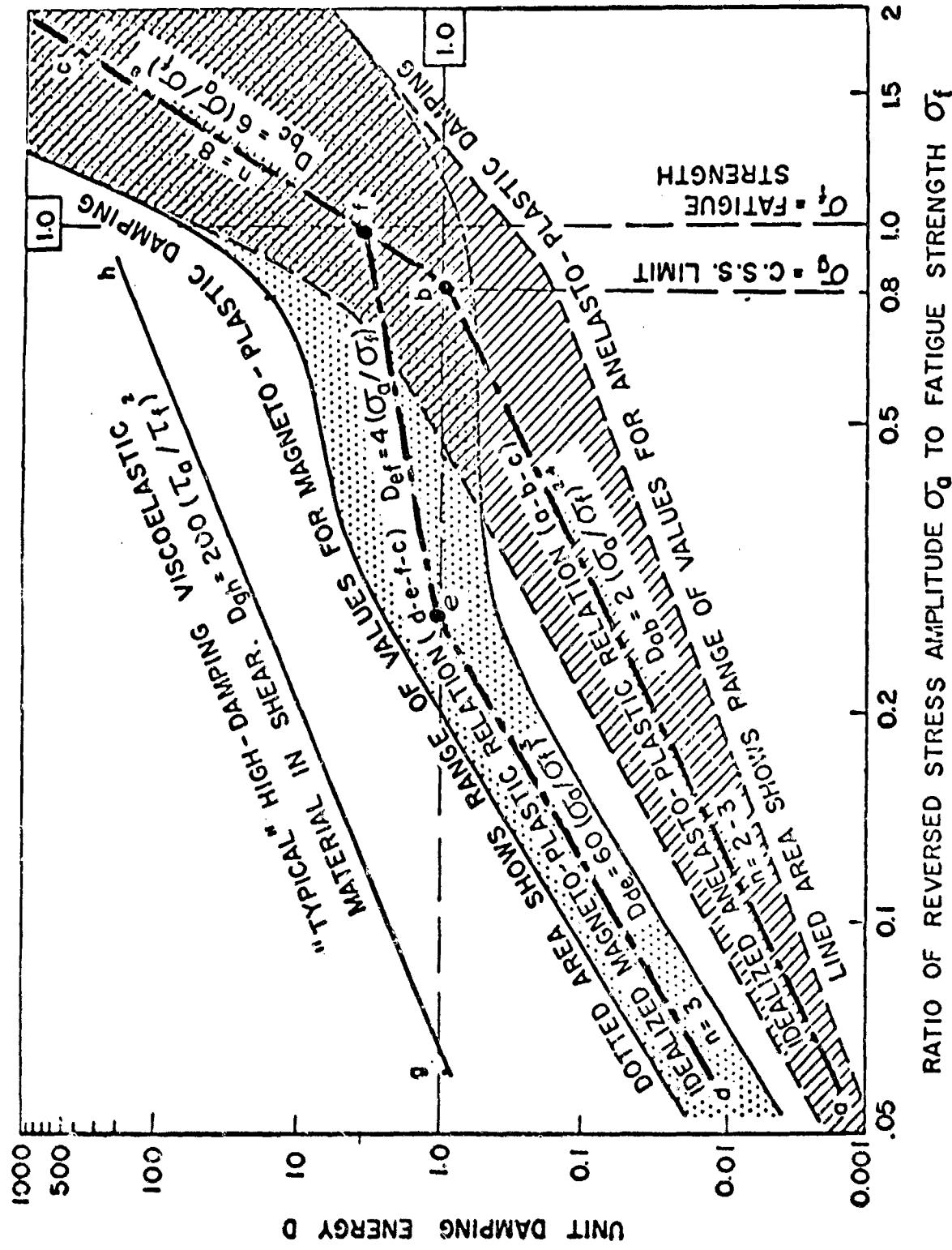
#### 5.1.2.4 Metallic Coatings

The damping materials chosen as coatings must have many desirable properties in combination, including adhesion, corrosion resistance, etc. Even disregarding these, the list of materials likely to exhibit the desirable amount of damping is limited.

Figure 5-1, reproduced from Ref. 2, shows that the damping characteristics of hundreds of metals and alloys are too low to be useful. Essentially, all materials exhibit very high damping at very high stress levels. This, however, is a pitfall as this stress is in the yield region where the fatigue life is short and, thus, the damping cannot be utilized. The materials worth exploring are those for which evidence can be found for exceptionally high damping at stress levels well below fatigue limits.

One approach that has been explored to a limited extent is the coating of structural metals with softer, more ductile metals. The American Rolling Mills Company mentioned the usefulness of copper-clad iron in this regard, but were unable to provide data. Stainless steel, "Duranel," and alloy aluminums are commercially

**AIRESEARCH MANUFACTURING COMPANY OF ARIZONA**  
A DIVISION OF THE BARRETT CORPORATION  
PHOENIX, ARIZONA



GT-7615-R  
Page 5-12



AIRESEARCH MANUFACTURING COMPANY OF ARIZONA  
A DIVISION OF THE GARRETT CORPORATION  
PHOENIX, ARIZONA

available clad with soft, relatively pure aluminum. Figure 5-2 shows data on these Alclad materials, from the Aluminum Company of America; but, neither elevated-temperature data nor fatigue-life data were available. The cladding approach is criticized by some metallurgists on the grounds that a fatigue crack in the soft cladding metal would then produce a stress concentration in the basic sheet, which could, under some circumstances, lead to a net reduction in fatigue life. This problem is complicated by the fact that most fatigue-life data is taken under conditions of constant displacement. In actual applications, however, the input is likely to be analogous to a constant driving force at resonance. The extent to which a given increase in damping might compensate a decrease in conventional fatigue life, by reducing the amplitude, could be solved only for particular conditions, perhaps with a computer program.

The best damping capabilities for clad materials, or pure metals used to coat them (copper, aluminum, etc.), do not approach those exhibited by the organic viscoelastic coatings. Therefore, to attain similar effectiveness, the search is narrowed to those few materials exhibiting truly anomalous damping.

#### 5.1.2.5 Manganese Alloys

Among the metals, manganese alloys occupy a unique position on the scale of damping (see Figure 5-3). At room temperature these metals are conspicuously "dead," but in spite of this deadness, they are strong enough to make good springs. The anomalous damping does not seem to depend critically on the composition of a particular alloy, but appears to be a property present in any high-manganese alloy. A number of high-manganese alloys were



AIRESEARCH MANUFACTURING COMPANY OF ARIZONA  
A DIVISION OF THE GARRETT CORPORATION  
PHOENIX, ARIZONA

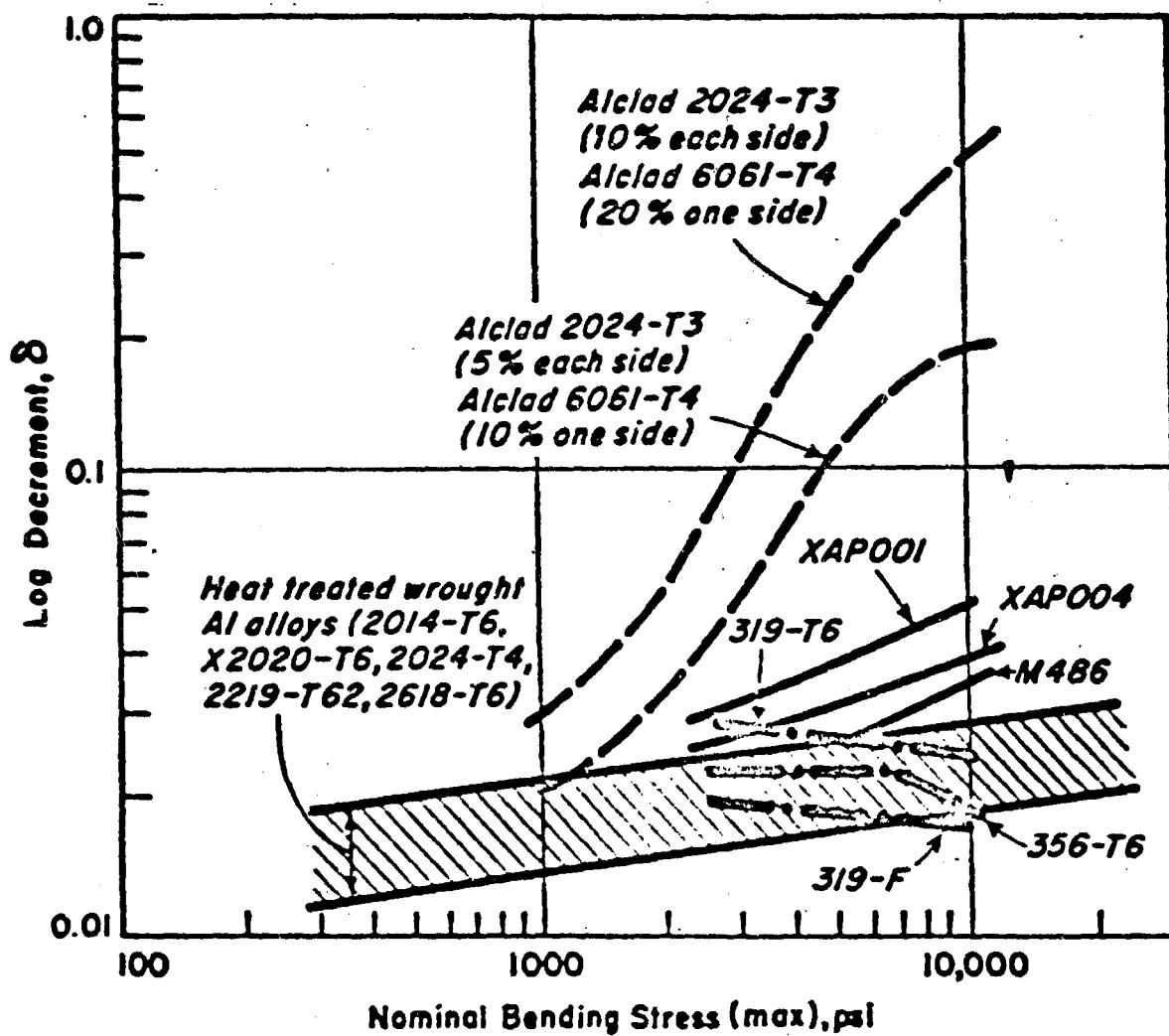


FIGURE 5-2



AIRESEARCH MANUFACTURING COMPANY OF ARIZONA  
A DIVISION OF THE GARRETT CORPORATION  
PHOENIX, ARIZONA

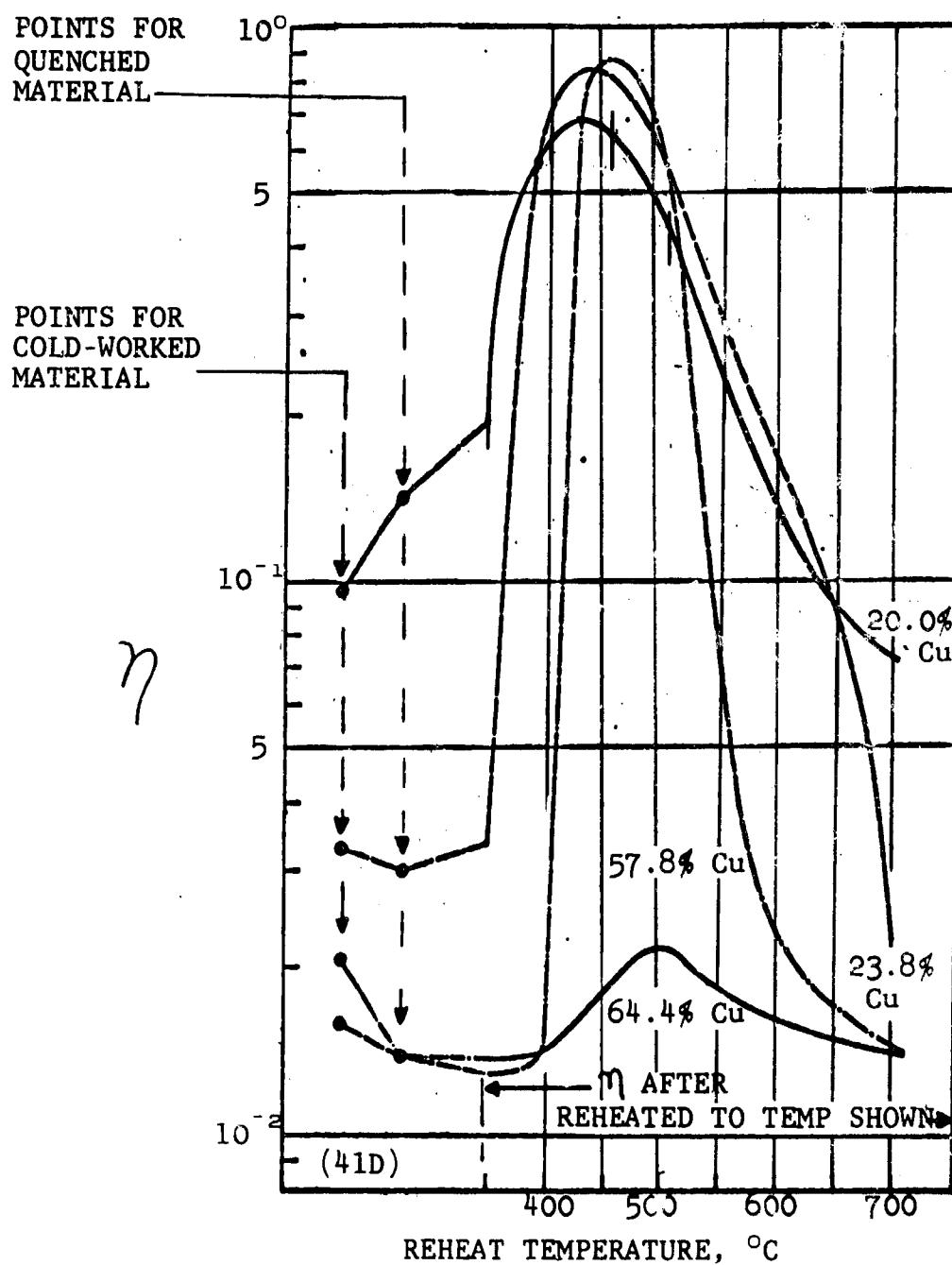


FIGURE 5-3 MANGANESE ALLOYS (COLD WORKED)

GT-7615-R, Rev. 1  
Page 5-15



patented in 1941 (Refs. 9, 10, 11, and 12), exhibiting high damping, which were recommended for such applications as "silent" gears for automobiles and "acoustical panels." The alloys later became of interest to solid-state physicists studying anelasticity. In particular, the metal was studied by Zener (Ref. 15), who built a theory to explain the anomalous damping, which has been disputed by others. Perhaps because the micromechanism is controversial, Lazan simply states (Ref. 2) that the reasons for the damping are "unknown." Although large amounts of manganese are used in both the steel industry (as a deoxidizer) and in the brass industry (as a cheap hardener), the high-manganese alloys themselves have as yet found little application except as components in bimetal strips (due to an exceptional coefficient of thermal expansion).

Interest in the almost forgotten damping characteristics seems to be reviving, as there has been recent research in damping of manganese alloys (References 13 and 14). Three high-manganese alloys, described in detail in Section 5.6, available from the Chicago Development Company, were considered representative of the manganese alloys, and were selected as candidate materials for testing.

#### 5.1.2.6 Aluminum Alloys

About 15 years ago, a peculiar group of aluminum alloys, called SAP alloys (XAP alloys by their American licensee, the Aluminum Company of America) were developed in Switzerland. Aluminum powder is ball-milled into very thin platelets and then oxidized until each particle is covered with aluminum oxide up to 14 percent by weight. The powder is then compacted in extrusion presses and forged or rolled to various shapes. These alloys are more truly cermets than metals, due to their large content of



alumina, and possess superior physical properties at elevated temperatures compared to normal aluminum alloys. Their corrosion resistance and fatigue life are claimed to be excellent. Their room-temperature damping is conspicuously large compared to soft aluminum. Figure 5-4 presents recordings of the exponential decay of cantilever beams made at AiResearch. They compare a normal aluminum alloy and an XAP alloy. Alcoa was unable to provide data on the damping of these alloys above room temperature. They do, however, provide data on the static stress-strain curves and yield points at elevated temperatures (Figure 5-5). The non-linearity of the static stress-vs-strain curves in the region below the yield point suggests, but does not guarantee, that the damping at elevated temperatures might increase rapidly.

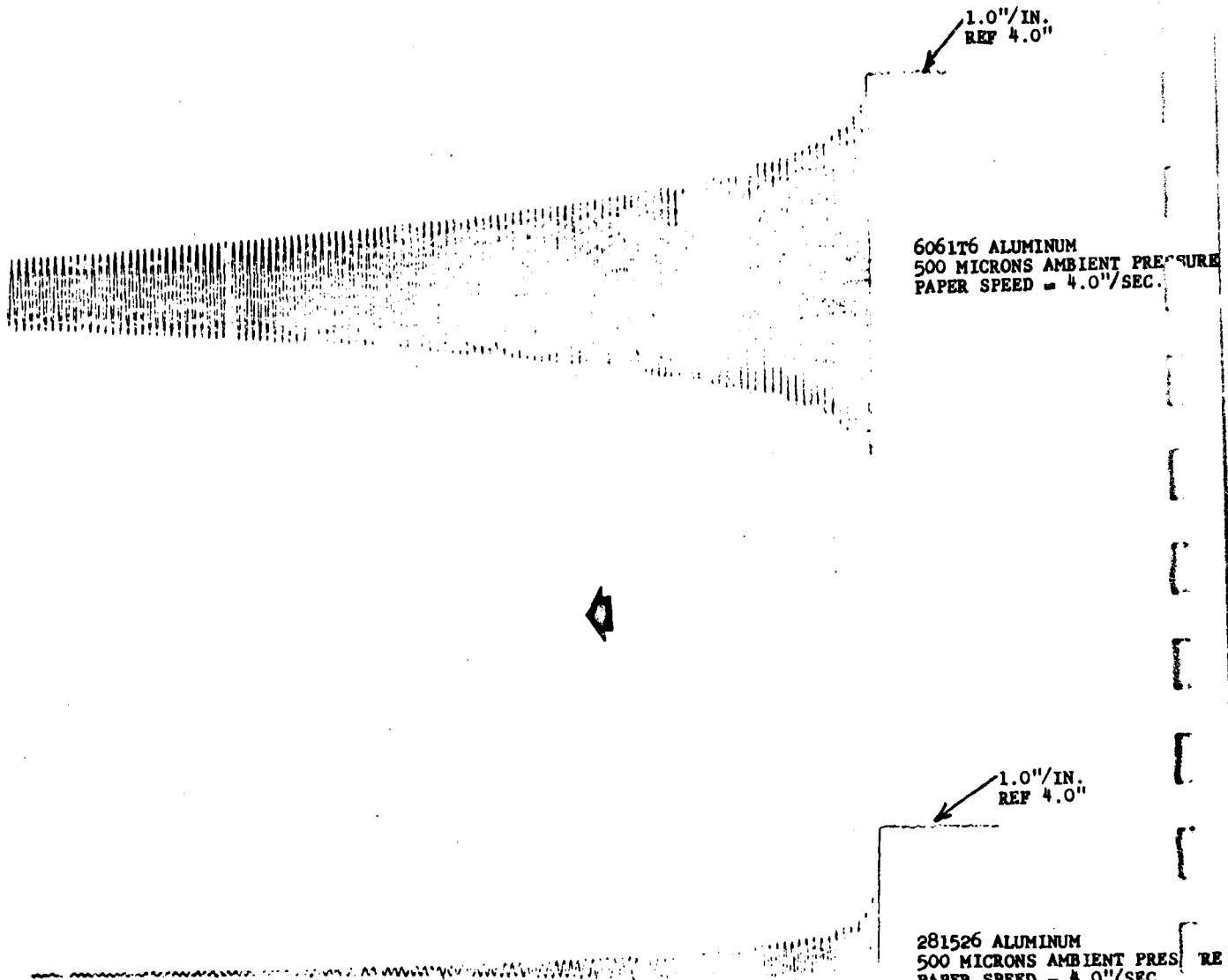
Past inquiries made to the Aluminum Swiss Company of Zurich, Switzerland, to High Duty Alloys , Slough, England, and to the Aluminum Company of America as to the cause or micromechanism of the damping obtained no satisfactory answers. These organizations apparently did not realize the usefulness of its damping for structural applications. Thus, as in the case of the manganese alloys, the micromechanism of the anomalous damping of XAP aluminum alloys is unknown.

#### 5.1.2.7 Application of Coatings

Both the manganese alloys and the XAP aluminum alloys required study for application as coatings, as none of the vendors had experience to use as a guide. Preliminary tests, indicated that the manganese alloys could be applied with the aid of flame-spraying guns, and the manganese alloys were available as wire, suitable for insertion in the guns. The XAP alloys were available only as bar stock, which was machined for use in the flame-spray gun.



AIRESEARCH MANUFACTURING COMPANY OF ARIZONA  
A DIVISION OF THE GARRETT CORPORATION  
PHOENIX, ARIZONA

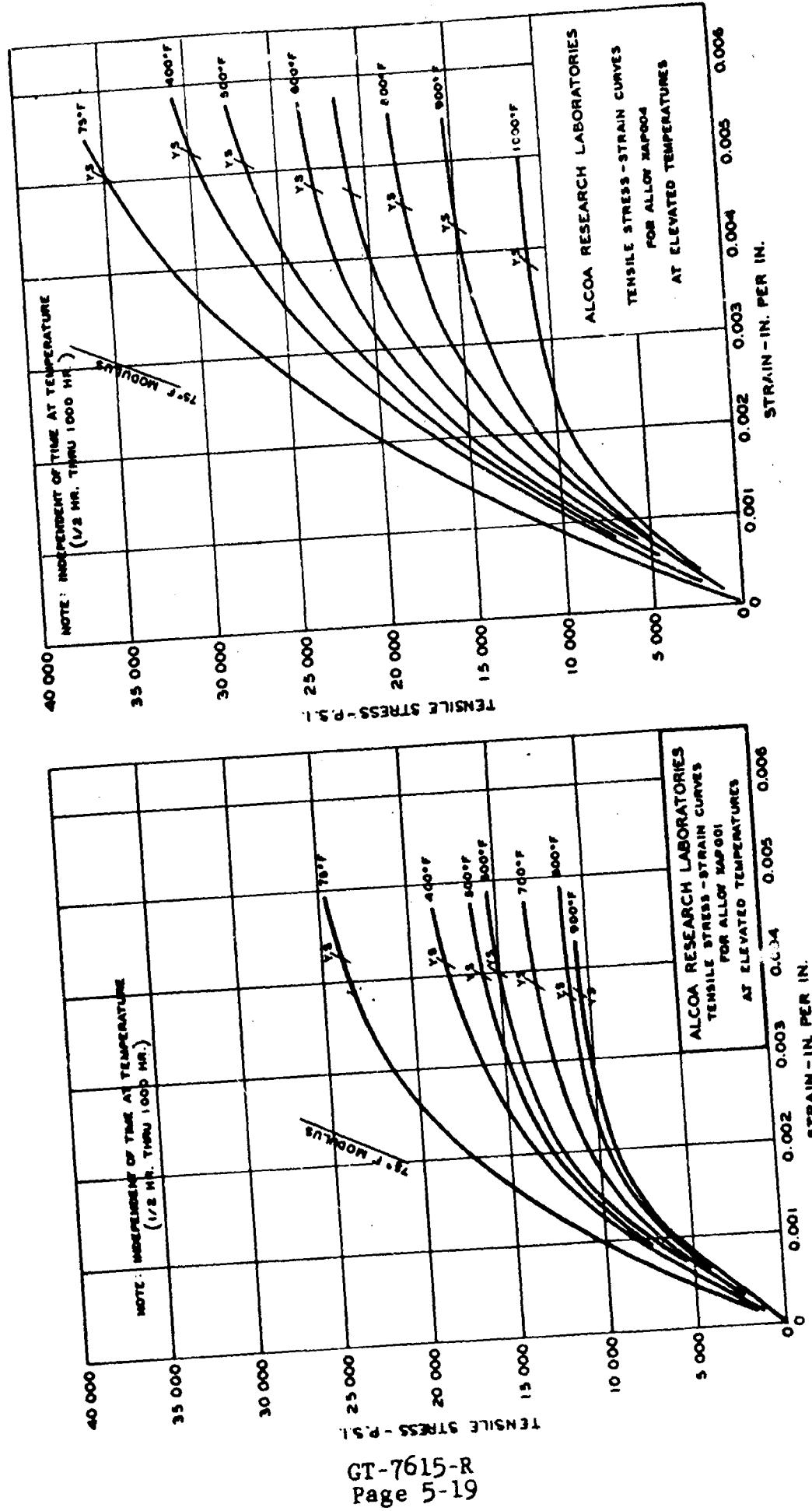
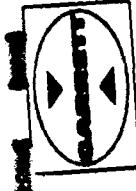


DECAY RATE OF CANTILEVER BEAMS

FIGURE 5-4

GT-7615-R  
Page 5-18

**AIRCO RESEARCH MANUFACTURING COMPANY OF ARIZONA**  
A DIVISION OF THE AIRCRAFT CORPORATION  
PHOENIX, ARIZONA



GT-7615-R  
Page 5-19

FIGURE 5-5



AIRESEARCH MANUFACTURING COMPANY OF ARIZONA  
A DIVISION OF THE GARRETT CORPORATION  
PHOENIX, ARIZONA

The high-manganese alloys and the XAP aluminum alloys were selected as candidate materials for testing because they were the most likely to be successful as simple, free-surface coatings. Other metals and alloys when used as simple coatings were considered less able to produce satisfactory damping. This does not mean that this test program was comprehensive enough to cover all possibilities; in particular, the field of constrained-layer damping, as contrasted to free-layer damping. Adhesives of organic viscoelastic nature are available which are capable of large displacements in shear without rupture. When such adhesives are used to bond metallic foils to the structure to be damped, the presence of the metal foil induces large shear loads in the adhesive. This mechanism is called constrained-layer damping and is extensively used in aircraft, where it has proved to be particularly efficient on a damping-vs-weight basis (References 16, 17, and 30). Similar mechanisms can be imagined for use at elevated temperatures. For example, stainless-steel foils could be sweat-brazed or silver-soldered to the structure to be damped. Such a structure might have the advantage of a foil layer to protect the brazing alloy or solder against its environment. However, it is not likely that brazes or solders can be readily found that are as capable as organic adhesives of deformation in shear without rupture. Such laminated structures are also inherently more expensive than free coatings. Their serious exploration has therefore been deferred in favor of free coatings.

#### 5.1.2.8 Nonmetallic Coatings

Numerous nonmetallic coatings have been developed to impart a variety of properties to the surfaces of sheet metal or other structural elements. Recently, many new refractory coatings have



AIRESEARCH MANUFACTURING COMPANY OF ARIZONA  
A DIVISION OF THE BARRETT CORPORATION  
PHOENIX, ARIZONA

been developed, some of which will withstand long term exposures of several thousand degrees. Reference 7 suggests that some of the materials used for the very-high-temperature refractory coatings may well have a useful damping temperature range, but well above that for which our measurement apparatus is designed. None of the producers of these refractory coatings could provide data on which to base an estimate of potential damping properties or the temperature at which they might occur. Ceramic-type refractory coatings were not included in the materials chosen for test because of the likelihood that any useful damping would lie above the 2000°F temperature range.

The vitreous enamels, on the other hand, are readily available, and are tailored to a wide variety of requirements and operating environments over a wide temperature range. Vitreous enamels have been developed to have such a low melting temperature that they may be applied to aluminum sheets. At the other extreme, vitreous enamels are available that are designed for operation near 2000°F and, thus, approach the operating range of refractory ceramic coatings. By definition, a vitreous material is not a true solid, but is more like an enormously viscous liquid. At some elevated temperature, perhaps just approaching that at which "softening" begins to be perceptible, a vitreous material might exhibit viscoelastic properties. The attractive possibility emerged that perhaps well-known corrosion-resistant coatings are useful dampers when properly chosen.



AIRESEARCH MANUFACTURING COMPANY  
A DIVISION OF THE GARRETT CORPORATION  
PHOENIX, ARIZONA

Four vitreous coatings were selected as candidate materials for test. The first (Type A) is an adaptation of the type used on aluminum. The object was to explore the possibility of overlapping the temperature range of 500°F to 600°F, just attainable with the most exotic organic materials. Two medium-temperature materials (Types B and Bb) were selected, based on the frits for which viscosity data was available, in the hope of finding correlation with the viscosity data. The Chicago Vitreous Corporation supplied viscosity-vs-temperature data on several basic vitreous coatings (frits) which included viscosities up to the unusually high value of  $10^{14}$  poise (Ref. 25). Finally, one high-temperature (Type C) vitreous coating was chosen, which is commonly used on such items as combustor tubes to resist corrosion up to about 1800°F.

A material advertised as a high-temperature protective coating, which can be applied with a brush, was also selected for testing, principally out of curiosity. This coating, called Sperex VHT, manufactured by the Sperex Company, was of unknown composition, and no predictions were made as to damping mechanisms that might be present. It should be emphasized that no damping claims were made by the Sperex Company for this material. Sperex VHT was selected for testing to show that most high-temperature coatings are not likely to have unrecognized damping properties. Further, it was intended to show that great care must be used in the selection of damping coatings, because useful damping is a rare property.

This completed the basic selection of coatings for detailed testing.



### 5.1.3 Tuning Fork Test

During preliminary consideration of the test methods, a simple tuning-fork design for test specimens was tried. The active parts of several of the tuning forks were coated by metal-spraying techniques with the following coatings:

(a) Metco 404	nickel aluminide
(b) Spraybond	pure Mo
(c) Cu-Mn alloys	two compositions
(d) Metco 15 and 16	brazing alloy powders (hard facing)

The shank of each tuning-fork test specimen was held firmly in a vice, and a microphone was placed near the prongs. The specimen then was struck, and the tone, or output, was received by the microphone, amplified, and indicated on a strip chart recorder. Thus, the output was recorded versus time, which enabled determination of the relative decay rates of the test specimens.

The results of coated samples then were compared with the results of uncoated specimens. In general, coatings improved the relative damping characteristics of the fork, with Metco 404 and one composition of the Cu-Mn alloy showing the best damping. This testing was not pursued further, however, when the more sophisticated flexure test device was made available.



## 5.2 Test Apparatus

### 5.2.1 Introduction

Previous discussion has pointed out that little, if any, work has been performed in the measurement of the high-temperature damping properties of coatings at temperatures above 600°F. As a result, apparatus for the testing needed to support this study had to be conceived and designed without the benefit of previous experience. This apparatus had to operate successfully throughout a temperature range from room temperature to 2000°F. The consultant, Prof. Lazan, retained to assist in material selection, was able to provide a design for test apparatus based on his work in investigating inherent damping in structural materials. The design was found to be satisfactory for use in this study; detail drawings were developed, and fabrication and procurement of the components was undertaken.

### 5.2.2 Apparatus Design

To avoid geometry changes due to differences in thermal expansion, it was necessary to use the same material for all areas of the apparatus subjected to high temperatures. Many materials were considered, and Hastelloy X was chosen because of its strength at high temperatures and resistance to scaling in an oxidizing atmosphere (the need for accessibility to the apparatus prevented use of inert atmospheres). See Figures 5-6 and 5-7.



AIRESEARCH MANUFACTURING COMPANY OF ARIZONA  
A DIVISION OF THE GARRETT CORPORATION  
PHOENIX, ARIZONA

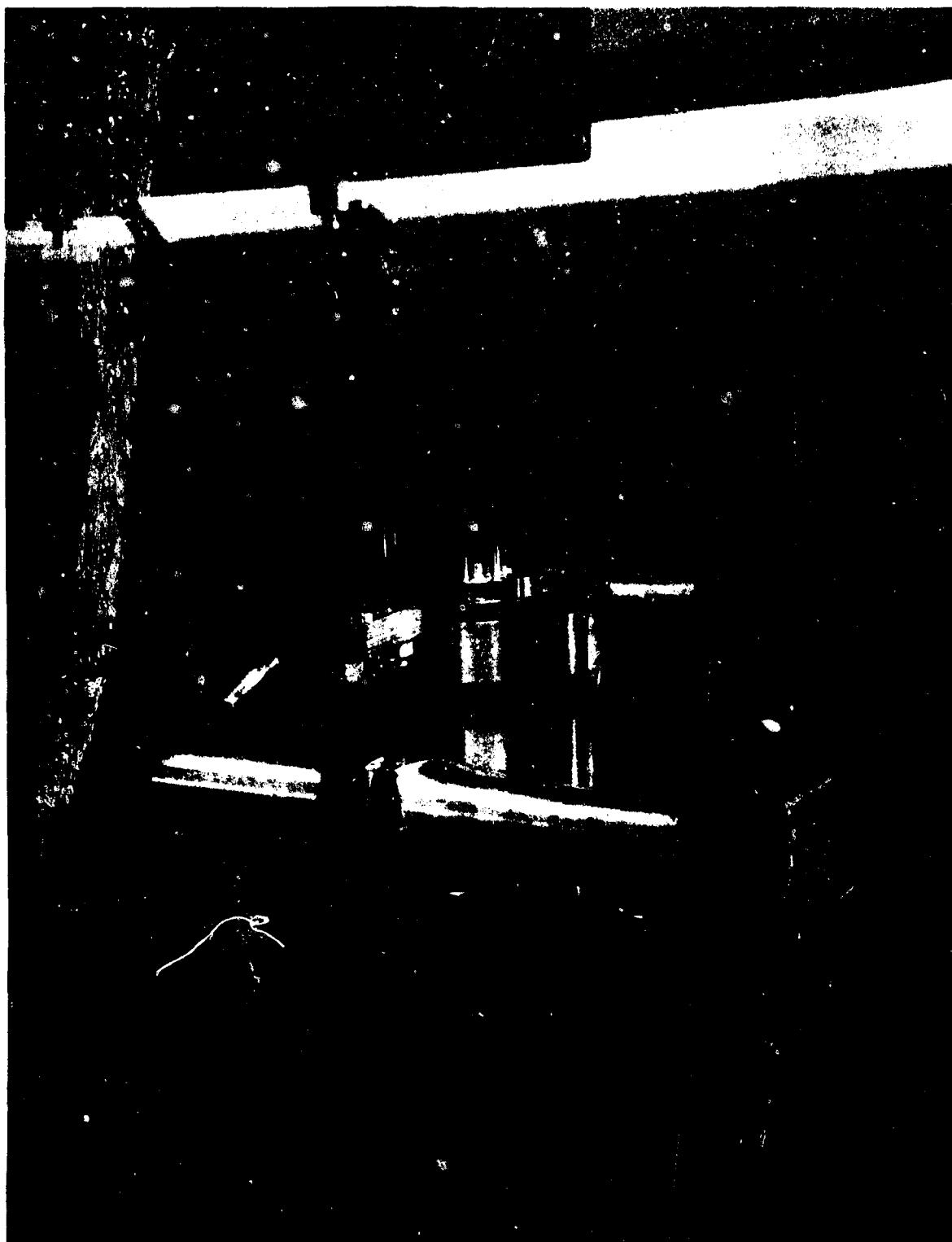


FIGURE 5-6

Photograph No. P25954-4

ERDL HIGH TEMPERATURE VIBRATION DAMPING TEST APPARATUS  
INSTRUMENTATED FOR TEMPERATURE SURVEY

WP-11759

GT-7615-R, Rev. 1  
Page 5-26



AIRESEARCH MANUFACTURING COMPANY OF ARIZONA  
A DIVISION OF THE GARRETT CORPORATION  
PHOENIX, ARIZONA

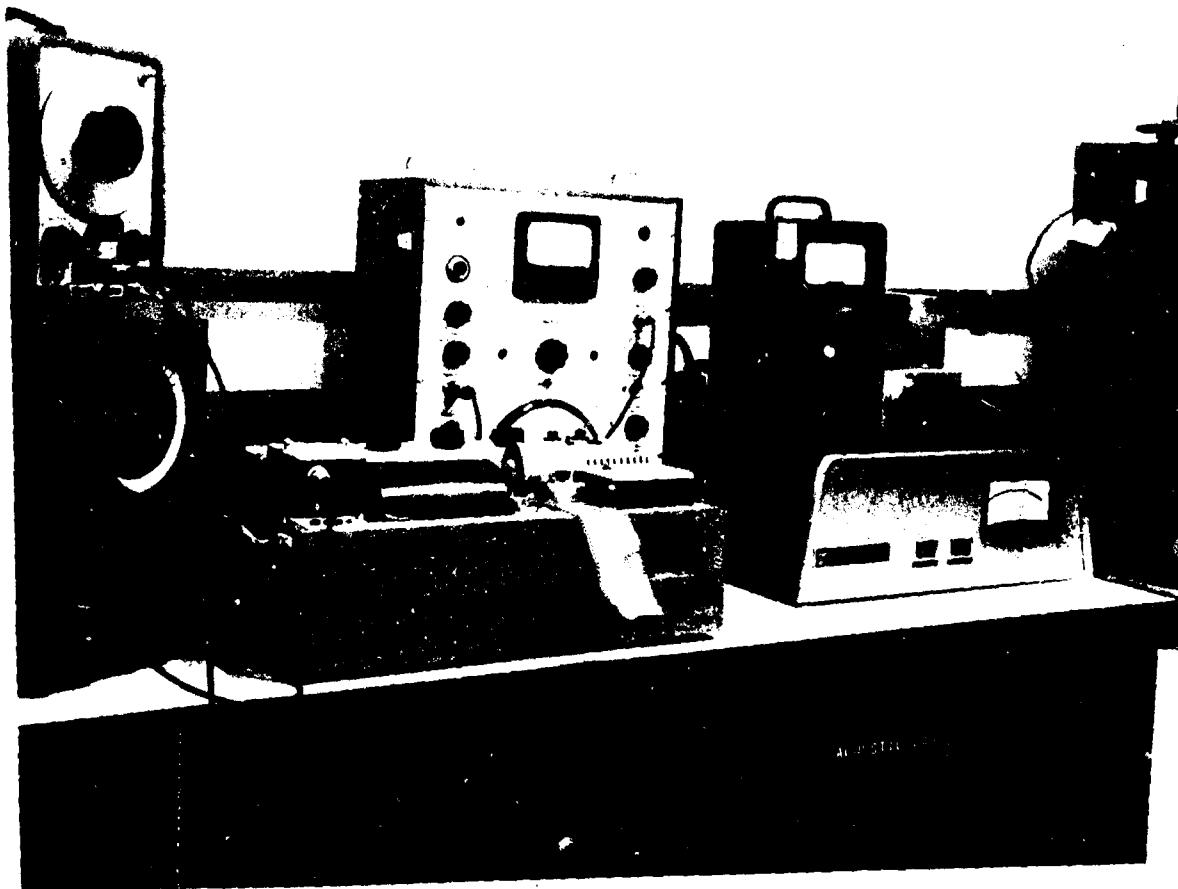


FIGURE 5-7

Photograph No. P25954-2

ERDL HIGH TEMPERATURE VIBRATION DAMPING TEST  
TEST INSTRUMENTATION

GT-7615-R, Rev. 1  
Page 5-27



AIRESEARCH MANUFACTURING COMPANY OF ARIZONA  
A DIVISION OF THE GARRETT CORPORATION  
PHOENIX, ARIZONA

### 5.2.2.1 Test Fixture Mounting

Support of the fixture was a critical consideration because of its effect on the dynamic characteristics of the overall system. Since the sensitivity of the system depends upon how its vibration energy is coupled to the support structure, several methods of suspension were analyzed. A soft spring mounting was not considered practical because it would allow excessive deflection. Total weight of the apparatus and its base plate was 84 lbs. It was decided to try a massive rigid support so that momentum interchange would be negligible. The support was a 55-gallon drum filled with concrete, which has a 24-in. x 26-in. x 2-in. steel plate firmly attached to both the concrete and the drum with epoxy adhesive. The upper (working) surface of the plate was ground to provide uniform contact with the ground surface of the test-fixture base. The weight of the support was approximately 1,400 pounds. To confirm the need for this type of mounting, tests of vibration decay rates with other support systems were made. When the fixture was placed on a lab work bench, the decay rate was 3 db per second; when located on floor-mounted bed plate, the decay rate for the fixture was 0.96 db per second. Addition of tie bolts between the fixture and the bed plate did not alter the decay rate. Since a low vibration decay rate was desired, to enable the detection of differences of effect between damping coatings, the need was confirmed for a massive support for the test apparatus. No tie-down bolts were used between the support and the apparatus, as the cohesive bond between the two ground surfaces was considered adequate retention.



#### 5.2.2.2 1020 Steel Apparatus

Prior to building the Hastelloy X apparatus it was decided that a large portion of the preliminary (low-temperature) work could be performed on apparatus made from SAE 1020 steel before final selection of the materials for the high-temperature tests. Thus, if any design shortcomings were revealed in initial testing, the parts could be revised, evaluated in steel, and then incorporated into the Hastelloy apparatus. Only those parts subjected to high temperatures were involved in the 1020-steel/Hastelloy-X evaluation.

#### 5.2.2.3 Specimen Stress Analysis

Concern arose about the stress distribution across the test specimen (herein called a flexure) as it was deflected. It was desired to have uniform stresses across the coatings--hence, across the flexure. Strain gauges were applied to the 1020 steel flexure, and the stress was found to be nearly 25 percent higher at the supported end of the test section than at the free end. A 0.007-inch taper was ground into the reduced section of the flexure, which resulted in stress equalization across the flexure. This was verified on the first Hastelloy flexure.

#### 5.2.2.4 Hastelloy X Apparatus

The addition of the taper to the flexure specimens was the only change in apparatus design found necessary in testing of the steel components. A Lindberg/Hevi-Duty Model 51222 box furnace, with a 5.25-in. x 3.75-in. x 8.00-in. chamber, and a Model 59344 temperature-control console were used to heat the test fixtures to temperatures as high as 2200°F. The furnace was modified for use with the chamber opening downward, so that it could be raised and



lowered over the test fixture (see Figure 5-8). This included making a new cover for the chamber opening that would enclose the test fixture to prevent heat loss. The cover was fabricated from Foamsil, a high-temperature silica foam insulation, which is easily worked and has better mechanical integrity than fire-brick (see Figure 5-9). This furnace originally had a hearth formed by inverting the lower heating element; this test did not need a hearth, so the element was again reversed to act as a normal element and provide a more uniform chamber heat distribution.

### 5.2.3 Instrumentation

#### 5.2.3.1 Displacement Measuring System

The displacement measuring system is a "push-pull" optical device in which an image of the moving part is projected on a pair of light-sensitive plates. Movement of the object causes more light to strike one plate and less light to strike the other. (See Figure 5-10). The device consists of the following elements:

- Light source
- Condensing lens
- Image plane and vane
- Image-forming lens system
- Light-sensitive cells
- Differential amplifier and power supply
- Readout meter

An ordinary incandescent lamp and biconvex lens provide the illumination. The image of a rod attached to the free end of the vibrating assembly (see Figure 5-6) is projected by two spaced



AIRESEARCH MANUFACTURING COMPANY OF ARIZONA  
A DIVISION OF THE GARRETT CORPORATION  
PHOENIX, ARIZONA

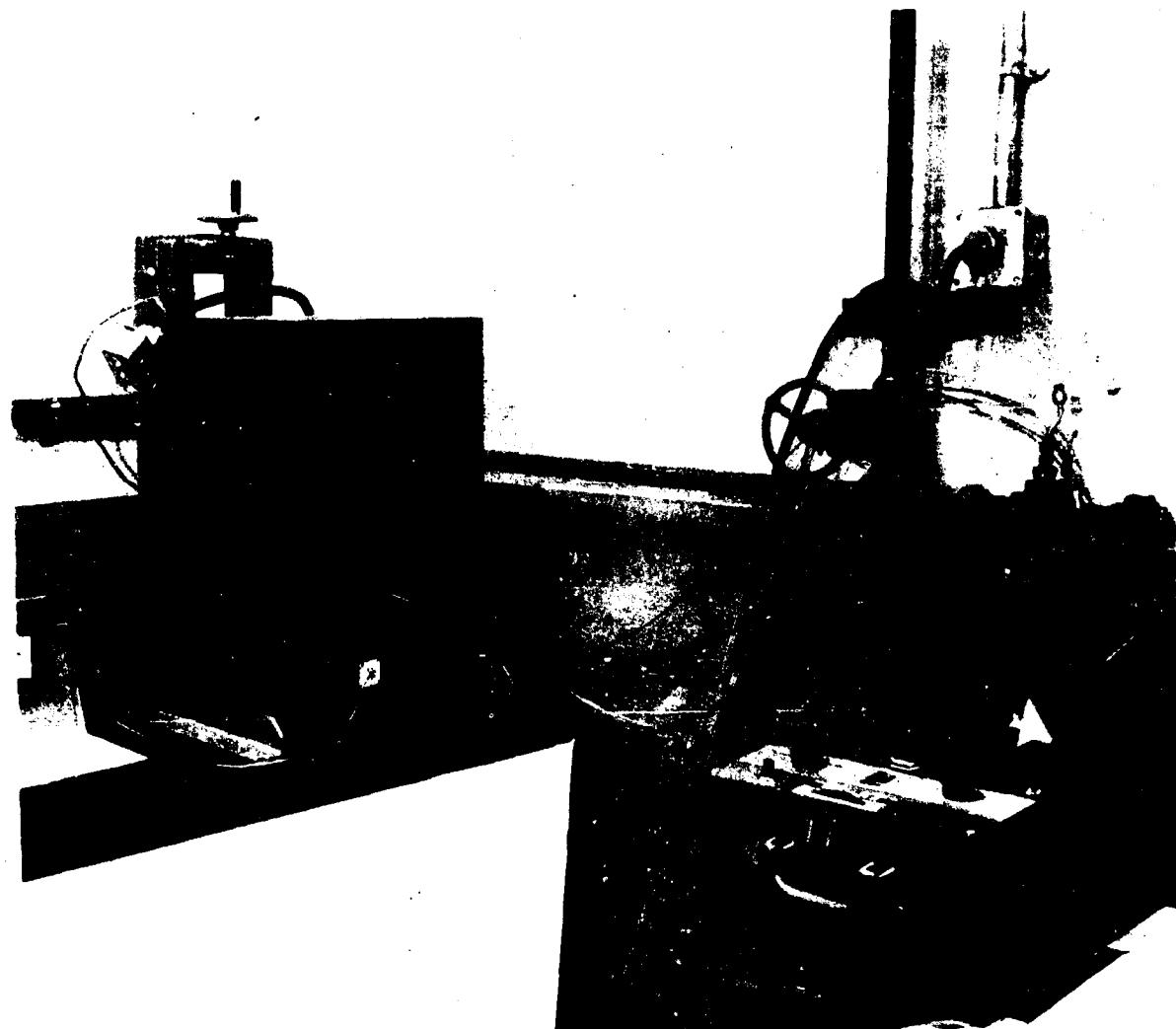


FIGURE 5-8

Photograph No. P25954-1

ERDL HIGH TEMPERATURE VIBRATION DAMPING TEST  
TEST APPARATUS WITH OVEN AND INSTRUMENTATION

GT-7615-R, Rev. 1  
Page 5-31



AIRESEARCH MANUFACTURING COMPANY OF ARIZONA  
A DIVISION OF THE GARRETT CORPORATION  
PHOENIX, ARIZONA

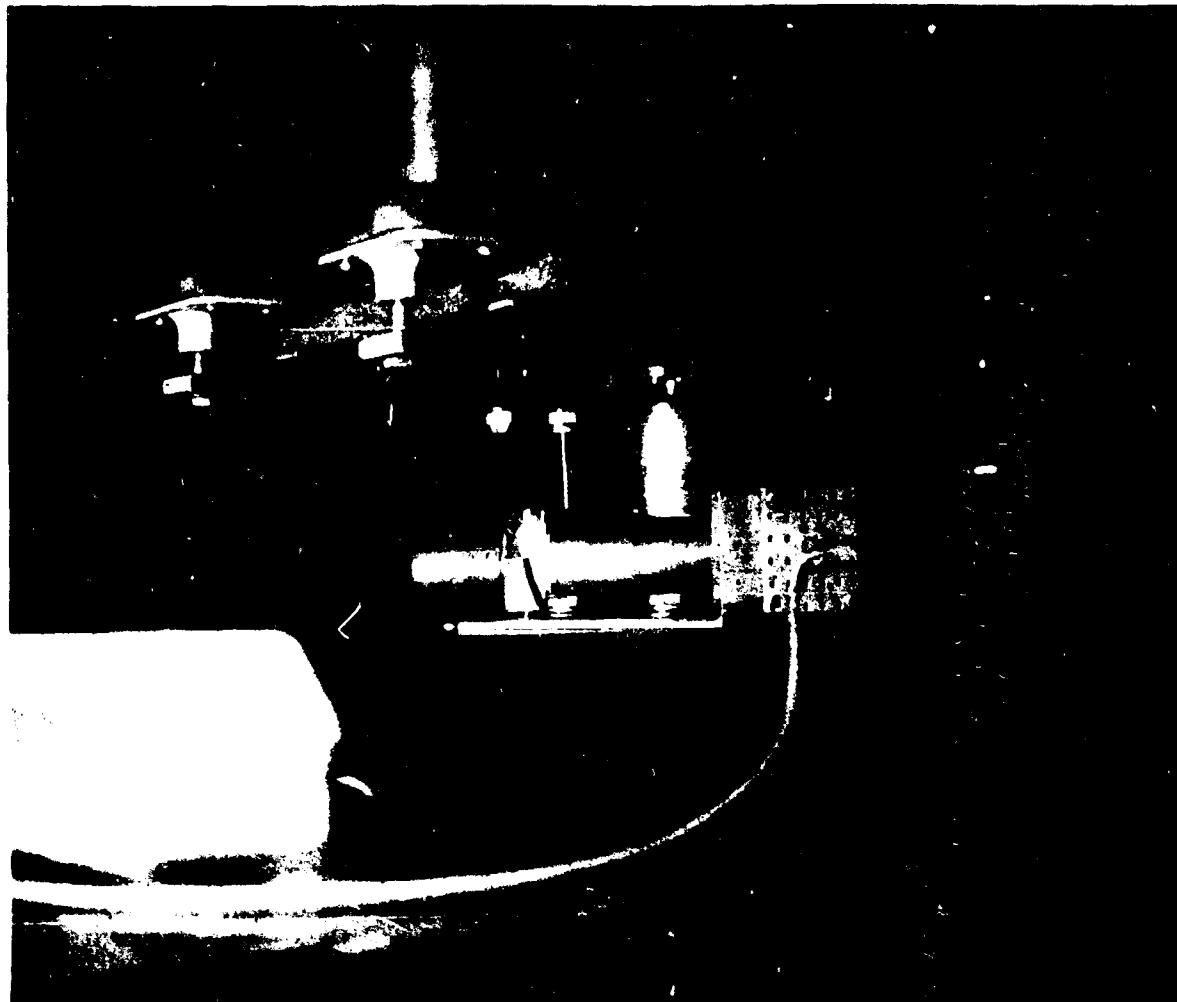


FIGURE 5-9

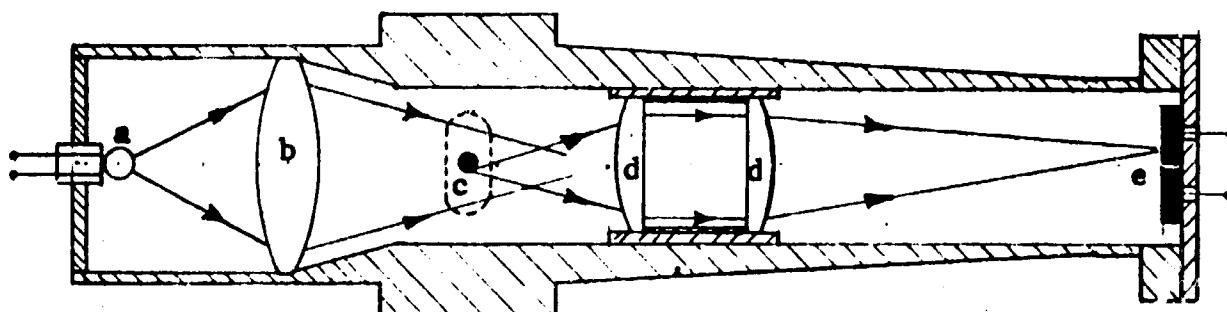
Photograph No. P25954-3  
ERDL HIGH TEMPERATURE VIBRATION DAMPING TEST  
TEST APPARATUS AND MODIFIED OVEN OPENING

GT-7615-R Rev. 1  
Page 5-32



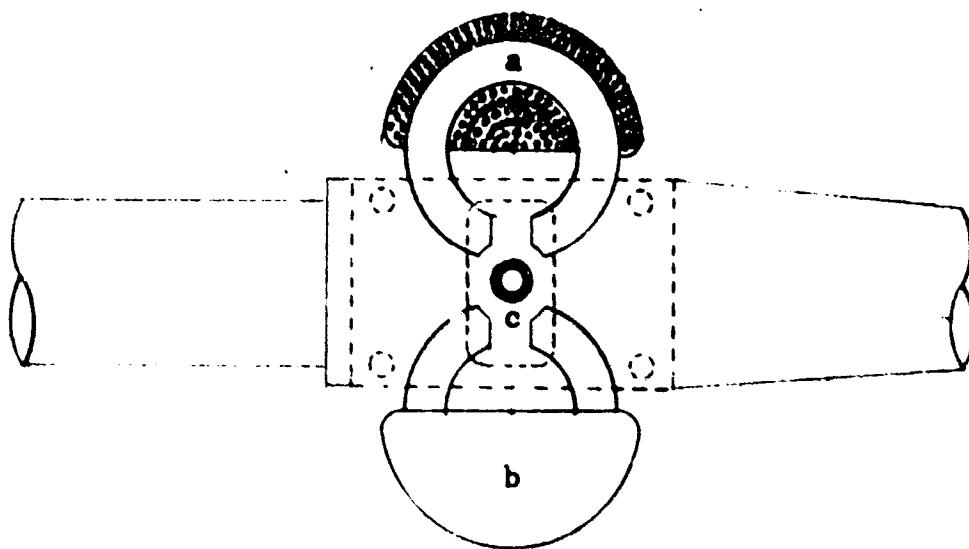
AIRESEARCH MANUFACTURING COMPANY OF ARIZONA  
A DIVISION OF THE GARRETT CORPORATION  
PHOENIX, ARIZONA

FIGURE 5-10



OPTICAL PICKUP (A)

- (a) LIGHT SOURCE
- (b) CONDENSING LENS
- (c) MOVING VANE
- (d) IMAGE FORMING LENSES
- (e) LIGHT SENSITIVE CELLS



DRIVER (B)

- (a) IRON CORE
- (b) COIL
- (c) SOFT STEEL BUTTON

GT-7615-R, Rev. 1  
Page 5 33



plano-convex lenses onto a pair of light-sensitive silicon photo cells. The light beam is carefully positioned so the image will cover the same effective area of each of the light-sensitive cells when at rest. Thus, the output of the two light cells is equal. Motion of the free end of the test assembly in a plane perpendicular to the light beam causes more light to strike one cell and less to strike the other. The difference in output of the two cells is amplified by a differential amplifier and readout on appropriate electric meters.

Calibration is carried out by displacing the rod a known amount by means of a micrometer and measuring the electrical output of the differential amplifier. The high-frequency response of the silicon photo devices used insures no loss of sensitivity in the range of frequencies to be used (50 cps).

#### 5.2.3.2 Electric Driver and Controls

The electric driver provides the alternating force required to excite and maintain constant amplitude of vibration measured at the free end of the assembly. The driver consists of a pair of magnets and associated electronic equipment (see Figure 5-10).

##### 5.2.3.2.1 Magnets

The magnets are circular powdered-iron cores with a segment removed. Each core is wound with 1,000 turns of No. 30 magnet wire.

Two opposing magnets are used so as to provide the same average force in each direction, thus causing the assembly to vibrate about its "at rest" position. The driver armature is a 0.5-inch-diameter button of soft steel attached to the rod above the displacement pickup (see Figure 5-11).



AIRESEARCH MANUFACTURING COMPANY OF ARIZONA  
A DIVISION OF THE GARRETT CORPORATION  
PHOENIX, ARIZONA

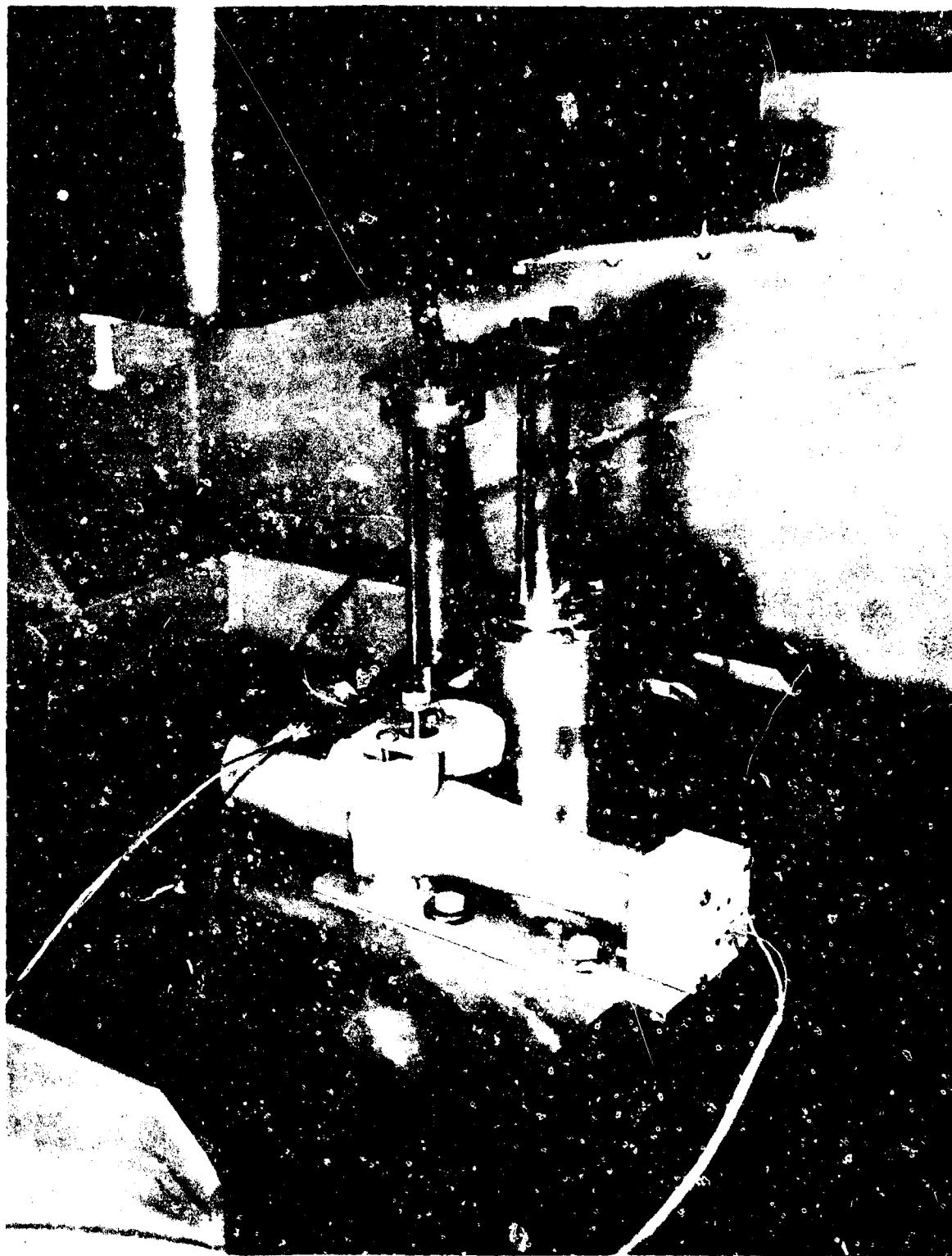


FIGURE 5-11  
Photograph No. P26240-2  
ERDL HIGH TEMPERATURE VIBRATION DAMPING TEST  
APPARATUS WITH DRIVER COILS

MP-11760

GT-7615-R, Rev. 1  
Page 5-35



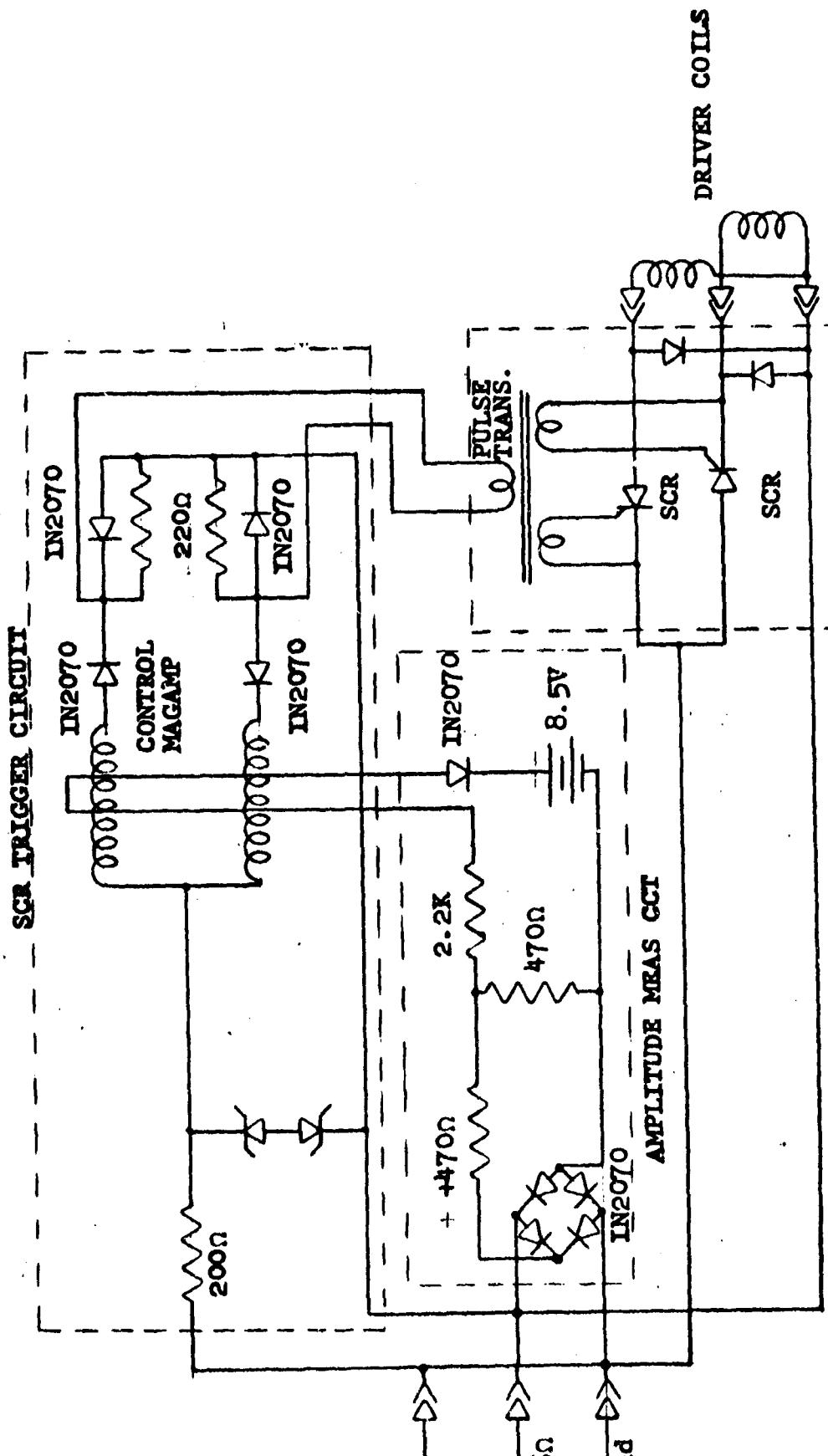
#### 5.2.3.2.2 Driver Power Supply and Control

Power is supplied to the magnets by means of a regenerative electronic system. The signal received from the optical displacement pickup is amplified with the output of the amplifier used for two purposes, to provide the necessary power to drive the vibrating assembly and to provide control of the amplitude of vibration (see Figure 5-12).

The circuit is designed so that when the amplitude of vibration, hence, voltage, measured at the output of the amplifier exceeds a fixed reference voltage, the SCR's (silicon controlled rectifiers) are phased back, which reduces the portion of the half wave that is fed to each driver coil. Equilibrium is reached when power delivered to the vibrating system by the coils is exactly that dissipated in the vibrating system. Increase in vibration results in reduction of driving power, and vice versa. The amplitude is controlled by adjusting the gain of the McIntosh amplifier. When the gain is adjusted to a low value, the overall loop gain is too low and the system will not be self-exciting, even with no phase-back in the SCR's. If the gain is increased, a threshold is reached at which the system is barely able to sustain a constant vibration. Above this gain setting, the vibration will increase until the output of the amplifier is large enough to actuate the phase-back control. The input to the amplifier is the actual amplitude of vibration, and the input level required to produce the output level that will limit the drive is inversely proportional to the amplifier gain. Therefore, increasing the gain setting above the threshold value decreases vibration level. Under most conditions the system will not be self-starting, even with high gain, but will readily build up if given an initial shock.



AIRESEARCH MANUFACTURING COMPANY  
A Division of the Honeywell Corporation  
HOHOKAM, ARIZONA



GT-7615-R  
Page 5-37

SCHEMATIC DIAGRAM OF DRIVER CIRCUIT

FIGURE 5-12



AIRESEARCH MANUFACTURING COMPANY OF ARIZONA  
A DIVISION OF THE GARRETT CORPORATION  
PHOENIX, ARIZONA

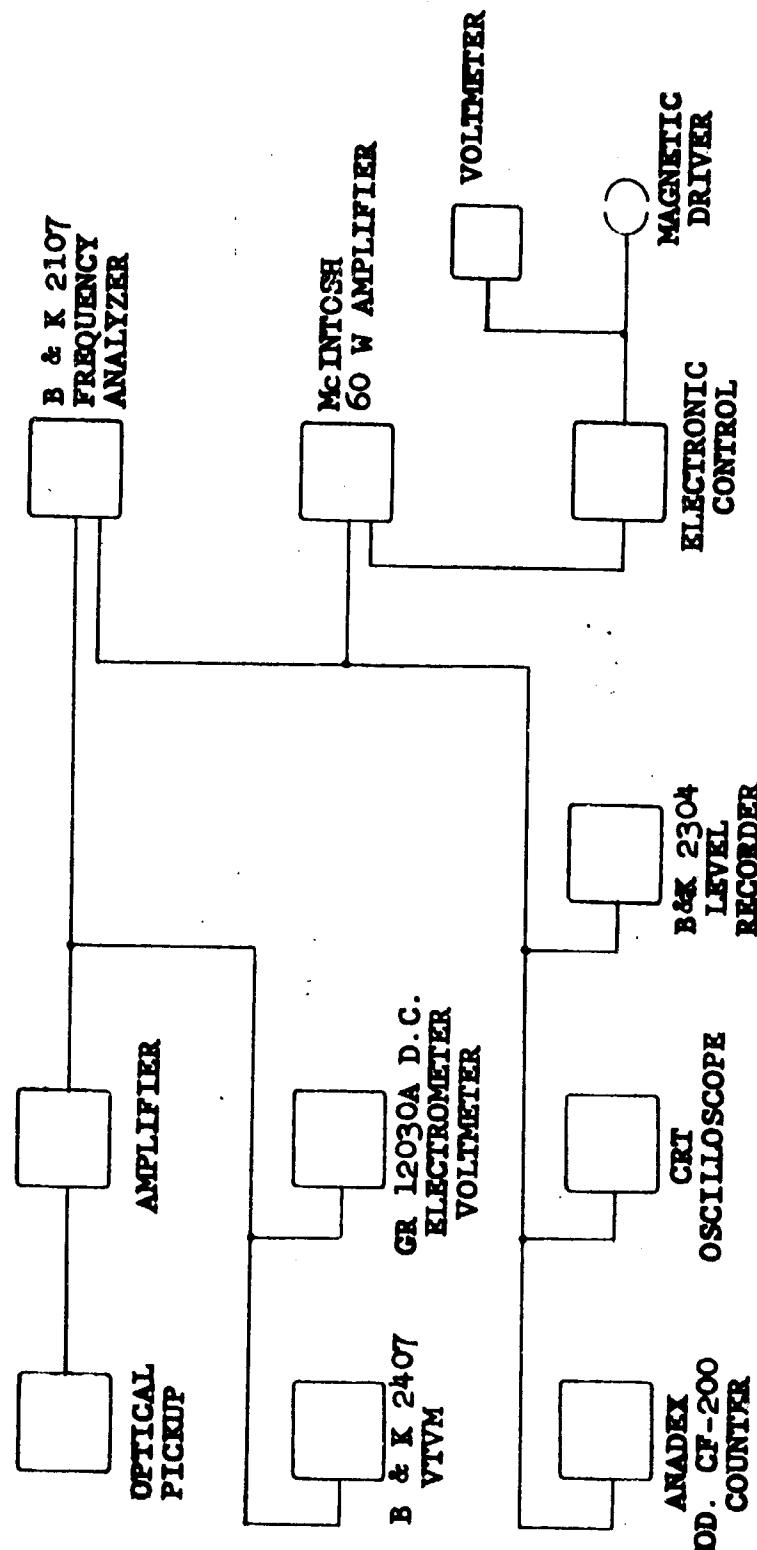
### 5.2.3.3 Readout Instruments

Figure 5-13 shows a block diagram of instrumentation used during the test program.

The optical pickup and amplifier, along with the amplitude control system, are described in the previous section.

The output of the optical system was monitored in three ways:

- (a) By using a BrueI and Kjaer Type 2407 VTVM to monitor the "peak" value of the a-c output from the optical system. This is described in more detail under the section on calibration.
- (b) By using a General Radio Type 12030A d-c electrometer voltmeter. This instrument was used to measure the d-c shift of the "Zero" in the optical system and calibration under static conditions as outlined in detail under the section on calibration.
- (c) By using a BrueI and Kjaer Type 2407 frequency analyzer. Since the natural frequency of the test flexure lay between 44 and 58 cps, it was convenient to have a narrow-bandwidth filter to remove any 60-cps noise in the system. Very little was present where, if not available, the filter would not have been needed and a phase-shifting device could be substituted in its place. Due to the characteristics of the filters, some phase distortion was present. Very minor filter adjustments were used not only to adjust for the frequency shifts due to the temperature change in the test sample, but also to phase the signal of the driver coils to the test apparatus.



GT-7615-R  
Page 5-39

INSTRUMENTATION USED  
WITH VIBRATION DAMPING TEST

FIGURE 5-13



AIRESEARCH MANUFACTURING COMPANY OF ARIZONA  
A DIVISION OF THE GARRETT CORPORATION  
PHOENIX, ARIZONA

The result of the phase adjustment was monitored on the voltmeter across the driver coils, and the filters adjusted to the lowest voltage necessary to drive the system to the required amplitude.

The signal output from the frequency analyzer provided the input for the power amplifier used in the drive system. This signal was also recorded on the Brüel and Kjaer Type 2304 level recorder as decay rates. The flexure was driven to a predetermined amplitude, and the signal to the power amplifier was interrupted. The decay in amplitude of the system at its natural frequency was then recorded on the chart paper as a logarithmic decay. This facilitates the use of a Brüel and Kjaer protractor used to read off the recorded slopes in seconds per 60 db, which is then easily converted to decibels per second.

An Anadex Model CF-200 counter was used for accurate frequency measurement. Frequency was read as period to the 5th decimal place. With proper adjustment of the filter in the frequency analyzer, the difference between frequencies while driven and during the decays would vary only in the last significant figure.

A CRT oscilloscope was also used to monitor the wave shape during testing to detect any anomalous behavior in the system.

The instrumentation is shown in Figures 5-7 and 5-8.



#### 5.2.4 Calibration

##### 5.2.4.1 Temperature Survey

Figure 5-6 shows the apparatus instrumented for the temperature survey. Since a uniform temperature distribution over the test section was necessary to obtain valid data, the first Hastelloy X flexure, Serial No. 1, was instrumented with four CA thermocouples imbedded in MgO. These thermocouples were alternated, two on top and two on the bottom of the test section. Because no instrumentation could be attached to the moving parts of this apparatus, these four thermocouples were compared to two CA thermocouples attached to the supporting column. These thermocouples were attached in a location that would place them as close as possible to the test section (see Figure 5-6).

The temperature spread was surprisingly small throughout the range from room temperature to 2000°F. The temperature spread between the upper and the lower surfaces of the test section ranged from 0 to 3°F. The temperature spread between the two thermocouples on the support column was not distinguishable. The temperature spread between the average of the four thermocouples on the flexure and the two on the column ranged from zero at room temperature to 15°F at 2000°F. This spread was not taken into consideration in the actual test, as the percentage of error was small enough not to affect the overall data.

##### 5.2.4.2 Stress-to-Displacement Relationship (Hastelloy X)

Flexure No. 32 was instrumented with two strain gauges forming a half bridge. These gauges were placed in the center of the test section--one on the upper surface and one on the lower surface. The magnetic driver shown in Figure 5-11 was replaced with a micrometer barrel. In this manner, the bolt extension protruding



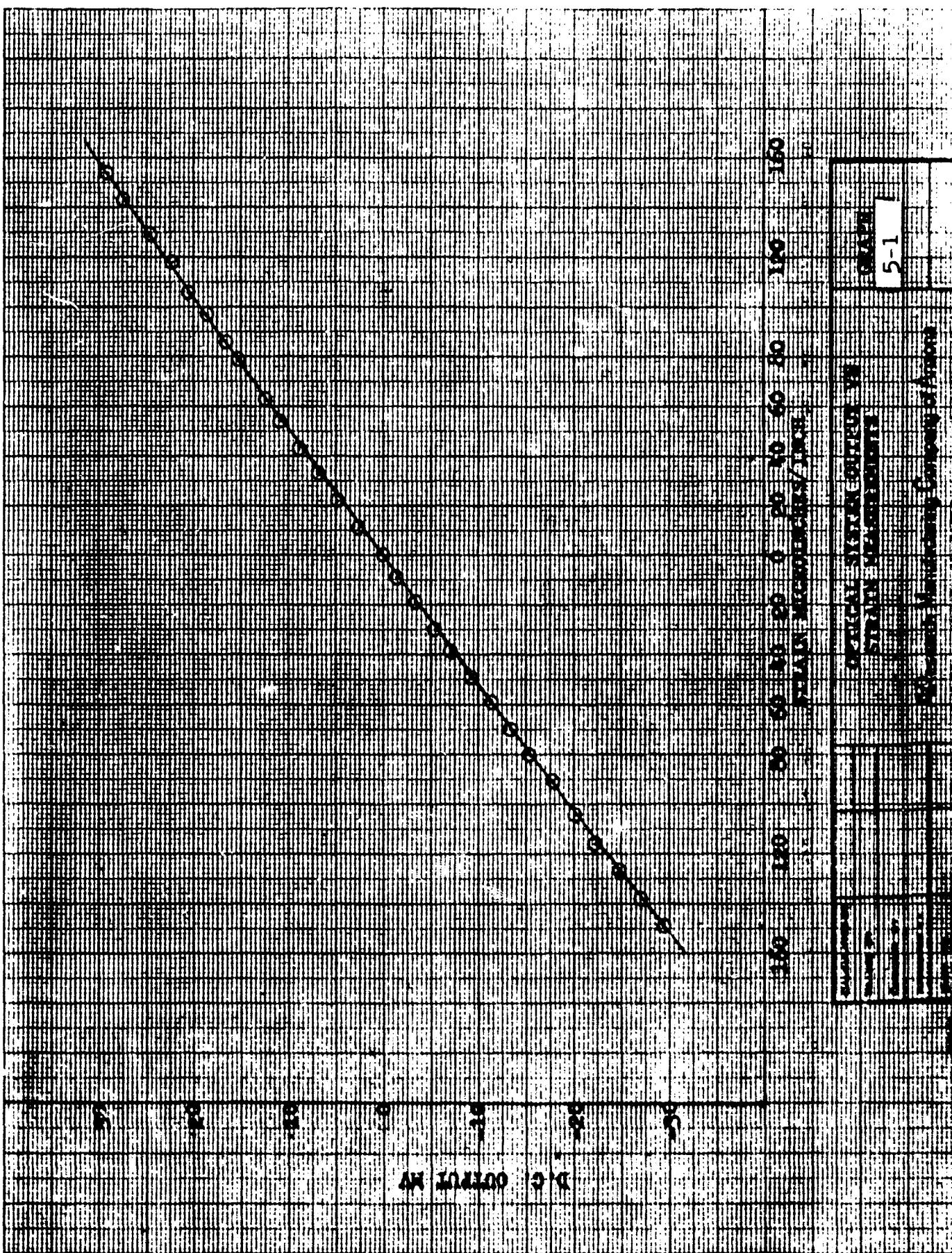
from the column on the free end could be deflected a known distance. For a known static deflection, the d-c change in the optical pick-up was measured in millivolts and the resulting strain of the flexure was measured, from zero to 0.014 inch deflection, in the positive and negative direction. The positive direction subjects the upper surface of the flexure to compressive loads and the lower surface to tension loads, and conversely for the negative direction. Static strain was read out with a Baldwin SR<sub>4</sub> Strain Indicator.

Graph No. 5-1 shows the results of these measurements. These measurements were confirmed under dynamic conditions by use of a Tectronix oscilloscope with a Type Q strain-gauge plug-in unit and a VTVM reading peak voltage.

### 5.3 Test Procedure

#### 5.3.1 Operational Procedure

Each flexure specimen was installed with considerable care being taken to maintain exactly the same fixture configuration and part location. This was necessary because of the extreme sensitivity of the system natural frequency to how it was assembled. Upon installation of the flexure specimen, the optical system was reset to a zero position. This was accomplished by adjusting the potentiometer in the optical system amplifier, or by shifting the optical system on its base. Both methods were used during the test because the range of the potentiometer was not enough to cover the shift at high operating temperatures. With the initial zero point known, temperature stabilization of the flexure could be established by observing the shift of the zero point. Calibration had shown a 4-millivolt amplitude shift for each 100°F temperature change due to thermal expansion of the flexure.



GT-7615-R

Page 5-43



AIRESEARCH MANUFACTURING COMPANY OF ARIZONA  
A DIVISION OF THE GARRETT CORPORATION  
PHOENIX, ARIZONA

Since a feedback energizing system was used, vibration was easily induced in the flexure; if very little damping were involved, the system could be excited acoustically, as sometimes occurred when doors were slammed, even at distant locations in the building. All decays (runs) were started from a peak vibration level of 30 mv (see Graph 5-1), and the tests were carried out with little effort or trouble. It was found that the insulating cover for the furnace chamber affected the decay rate. With the cover in place the decay of an uncoated Hastelloy X flexure was 0.431 db per second, and it was 0.361 db per second with the cover removed. The close fit between the cover and the free end of the flexure made viscous damping by the air itself a significant factor. At least 30 minutes was allowed for stabilization after each temperature change. For each temperature, four decay rates and period measurements were recorded. Due to the time involved--up to 16 hours for some tests--data was taken with increasing temperatures. If two tests were involved, the system was allowed to cool overnight and the test was repeated the next day.

### 5.3.2 Base-Line Test

The primary objective of this test was the study of coatings, which requires knowledge of the material being coated and of the sensitivity of the apparatus. Thirty-one test bars were fabricated from Hastelloy X; 3 of these were used for base-line tests (see tabulation in Section 5.3.2.1), and 17 were not tested. The first test was discarded, as the instrumentation had not been completely refined and the frequency measurements were subject to doubt. A second test was run on another bare flexure, and the third flexure was tested later in the test program. The results are shown as base lines on the plotted data. The frequency shown is an average (smoothed) curve of the two runs. The actual difference in frequency measured between the two bars was 0.217 cps.



The difference in decay rate was not distinguishable, with the scale used up to 1500°F. This temperature is where the Hastelloy X shows a damping phenomenon of its own. Beyond 1500°F the damping indicated a difference of  $\pm 2$  db per second from which the curve is smoothed. An explanation of this damping peak in the Hastelloy is offered in Section 5.6. A more ideal procedure, if time had permitted, would have involved a base-line test on each flexure prior to coating application.

#### 5.3.2.1 Tabulation of Flexures and Coatings Tested

Those flexures not listed were either held as spares or rejected as being defective.

##### Flexure No. 1

No coating involved; used for confirmation of stress distribution. Finally instrumented for temperature survey.

##### Flexure No. 8

Type A vitreous coating, tested from room temperature to 1006°F. Coating changed from a dark charcoal grey to white which was cross-hatched with fine fracture lines (note that this coating was subjected to tests up to firing temperature). See Graphs 5-2 and 5-17.

##### Flexure No. 9

Type A vitreous coating, tested from room temperature to 697°F. Coating changed from a dark charcoal grey to a light grey. No fracture lines visible. This was the first test performed, and due to questionable frequency measurements, the data is not presented.



AIRESEARCH MANUFACTURING COMPANY OF ARIZONA  
A DIVISION OF THE GARRETT CORPORATION  
PHOENIX, ARIZONA

Flexure No. 10

Type B vitreous coating. Two tests were performed--the first from room temperature to 930°F, and the second from 180°F to 1020°F. No change was observed in the color of the coating--a small ridge appeared in the coating after the second test. See Graphs 5-3 and 5-18.

Flexure No. 11

Type Bb vitreous coating. Two tests were performed--the first from room temperature to 1185°F; the second from room temperature to 1255°F. No change was observed in the color or texture of the coating. See Graphs 5-4 and 5-19.

Flexure No. 12

Type C vitreous coating. Two tests were performed--the first from room temperature to 1720°F; the second from 862°F to 1615°F. No change was observed in the color or texture of the coating. See Graphs 5-5 and 5-20.

Flexure No. 14

Manganese copper alloy Type CDC 780 coating. This flexure and its coating were solution-heat-treated at 850°C and cured at 450°C for 1/2 hour. This resulted in the nearly complete loss of the coating by peeling (see Figures 5-14 and 5-15). No test was performed.



AIRESEARCH MANUFACTURING COMPANY OF ARIZONA  
A DIVISION OF THE SABRETT CORPORATION  
PHOENIX, ARIZONA



FIGURE 5-14

Photograph No. P26369-1

ERDL HIGH TEMPERATURE VIBRATION DAMPING TEST  
FLEXURE NO. 14 MnCu ALLOY COATING AFTER HEAT TREAT

GT-7615-R, Rev. 1  
Page 5-47



AIRESEARCH MANUFACTURING COMPANY OF ARIZONA  
A DIVISION OF THE GARRETT CORPORATION  
PHOENIX, ARIZONA



FIGURE 5-15

Photograph No. P26369-2

ERDL HIGH TEMPERATURE VIBRATION DAMPING TEST  
FLEXURE NO. 14 MnCu ALLOY COATING AFTER HEAT TREAT

RP-11762

GT-7615-R, Rev. 1  
Page 5-48



AIRESEARCH MANUFACTURING COMPANY OF ARIZONA  
A DIVISION OF THE BARRETT CORPORATION  
PHOENIX, ARIZONA

Flexure No. 16

Manganese copper alloy Type CDC 720 coating. One test was performed from room temperature to 1660°F, as the coating peeled during this test. See Graphs 5-9 and 5-24.

Flexure No. 17

Aluminum cermet XAP003. Two tests were performed--the first from room temperature to 1000°F; the second from room temperature to 1000°F. No visible change took place in the coating on either test. See Graphs 5-11 and 5-26.

Flexure No. 18

Manganese copper alloy Type CDC 780. Three tests were performed--No. 1 from room temperature to 849°F. The temperature was held at 849°F for 1/2 hour to show the effects of aging. There was no visible change in the coating following this test.

Test No. 2 was performed from room temperature to 1712°F. Following this test the color of the coating had changed from metallic grey to a blue-gold color. The flexure was removed from the setup at this time and reinstalled later for Test No. 3.

Test No. 3 was performed from room temperature to 1850°F. The coating peeled during this test (see Figures 5-16 and 5-17). See Graphs 5-6, 5-7, and 5-22.



AIRESEARCH MANUFACTURING COMPANY OF ARIZONA  
A DIVISION OF THE GARRETT CORPORATION  
PHOENIX, ARIZONA



FIGURE 5-16

Photograph No. P26369-3

ERDL HIGH TEMPERATURE VIBRATION DAMPING TEST  
FLEXURE NO. 18 AFTER TEST NO. 3 MnCu ALLOY COATING

EP-11763

GT-7615-R, Rev. 1  
Page 5-50



AIRESEARCH MANUFACTURING COMPANY OF ARIZONA  
A DIVISION OF THE GARRETT CORPORATION  
PHOENIX, ARIZONA



FIGURE 5-17

Photograph No. P26369-4

ERDL HIGH TEMPERATURE VIBRATION DAMPING TEST  
FLEXURE NO. 18 AFTER TEST NO. 3 MnCu ALLOY COATING

GT-7615-R, Rev. 1  
Page 5-51



AIRESEARCH MANUFACTURING COMPANY OF ARIZONA  
A DIVISION OF THE GARRETT CORPORATION  
PHOENIX, ARIZONA

Flexure No. 22

Aluminum cermet XAP001. Two tests were performed--No. 1 from room temperature to 995°F. No visible change took place in the coating during this test. Test No. 2 was performed from room temperature to 1340°F. This coating changed to a dark blue-black color with a flaky appearance. See Graphs 5-10 and 5-25..

Flexure No. 23

Manganese copper alloy, CDC772. Two tests were performed-- No. 1 from room temperature to 1720°F. In this test the coating changed from a mottled black to a brassy color. There were no indications of peeling. Test No. 2 was conducted from room temperature to 1770°F. The coating peeled on this test. See Graphs 5-8 and 5-23.

Flexure No. 26

Not coated; tested as a bare bar to establish a frequency and damping base line for Hastelloy X.

Flexure No. 27

Several tests were performed on this flexure as follows:

No. 1 - Not coated; tested as a bare bar to establish a frequency and damping base line for Hastelloy X.



No. 2 - The flexure was painted with Sperex VHT coating (black). One test was performed from room temperature to 1529°F. No visible change took place in the coating. The coating was stripped off by sand-blasting following this test. See Graph 5-12.

No. 3 - With two layers of Mystik Tape No. 7402 applied to each side of the test section. Two tests were performed--No. 1 from room temperature to 480°F and No. 2 from room temperature to 475°F. No visible change took place in the tape except for some swelling of the silicone adhesive after Test No. 1. See Graphs 5-13, 5-14, and 5-27.

Flexure No. 30

No coated. Tested as a bare bar to establish a frequency and damping base line for Hastelloy X. Data rejected due to questionable frequency measurements.

Flexure No. 32

Strain-gauge test used for displacement vs strain calibration. See Graph 5-1.

Flexure No. 33

Not actually a flexure, as the blank for this flexure was used for metallurgical tests to confirm that the material used for the flexures was Hastelloy X and not a substitute.

1020 Steel Flexure

Used for system shakedown--see Section 5.2.



AIRESEARCH MANUFACTURING COMPANY OF ARIZONA  
A DIVISION OF THE BARRETT CORPORATION  
PHOENIX, ARIZONA

Pure Copper Flexure (annealed)

The Young's modulus and yield strength of copper at room temperature closely resembles that of Hastelloy X at 2000°F.

This flexure was used to estimate what the base-line frequency characteristics of the system would be before the Hastelloy flexure material choice was fixed. The resulting decay rate and period count at room temperature were 5.25 db per second and 0.02220.

5.4 Data Analysis

5.4.1 Terminology

Because vibration damping is of interest to many disciplines, ranging from structural mechanics to organic chemistry, and including the field of music, there is a bewildering array of units, terms, and test methods. A major objective of Ref. 2 was to standardize units and nomenclature (see Figure 5-18); the terms recommended therein are used throughout this report, where possible.

Most damping tests measure system damping characteristics, rather than material damping properties, because the tests are of a comparative nature. The data from such tests is difficult or impossible to use in the behavior prediction for a different system. In order to calculate the effect of a damping coating on any system, it is necessary to know the damping characteristics of the coating material, and this property must be expressed in a usable form.



AIRESEARCH MANUFACTURING COMPANY OF ARIZONA  
A Division of THE BELL & HOWELL CORPORATION  
Phoenix, Arizona

FIGURE 5-18

CLASSIFICATION OF RECOMMENDED DAMPING UNITS, THEIR INTERRELATIONS, AND THEIR RELATIONS TO THE MEASURED QUANTITIES OF DAMPING TESTING SYSTEMS

(1) Classification of type of Damping Units	(2) Preferred Name	(3) Other Name Used	(4) Symbols and Units Material	(5) Definition
(A) ABSORBTIVE ENERGY UNITS Based on c' - damped per cycle of stress.	Unit Electric Energy	Plastic energy	$U_1 = \frac{k''}{k''} U_0$	Area under $\sigma_{mid}$ - $\epsilon$ curve from 0 to $\epsilon_{max}$
Material properties: $U_0$ & $c'$ give unit values.	Total electric strain energy	Strain energy	$U_1 = U_0 \frac{\beta}{\beta + 1}$	Area under $\sigma_{mid}$ - $\epsilon$ curve from 0 to $\epsilon_{max}$
$U_0$ & $c'$ give total energy	Unit damping	Specific damping	$U_1 = U_0 \frac{\beta}{\beta + 1}$	Area within $\sigma - \epsilon$ hysteresis loop
$U_0$ & $c'$ give total values for specimen $k$ .	Spec. hysteresis	In-hydracycle	$U_1 = U_0 \frac{\beta}{\beta + 1}$	Area within $\sigma - \epsilon$ hysteresis loop
Total damping energy			$D = \frac{U_1}{U_0}$	Area within P-X
(B) COMPLEX MODULUS RELATION	Complex Modulus	$E^*, G^*, K^*, H^*$	$E^* =  E^*  e^{j\phi}$	Modulus
Appropriate for linear materials:	Absolute Modulus	$\frac{1}{k''}$	$E^* = [E^*]^2$	$E^* = \frac{1}{k''}$
Material properties:	Storage Modulus	$\frac{1}{k''} C^*, X^*, M^*$	$E' =  E^*  \cos \delta$	For linear materials
$E^* = E' + jE''$	Resonant Modulus	$\frac{1}{k''} C^*, X^*, M^*$	$E'' =  E^*  \sin \delta$	Relations Among Unit Properties of Uniform Materials
Properties of Specimen, member, or total part: $S$ .	Dissipation Modulus	$\frac{1}{k''} C^*, X^*, M^*$	$E^* = \frac{E'}{S}$	$S = \frac{E'}{E''}$
$k'' = k_x + k_y$	Loss Modulus	$\frac{1}{k''}$	$\eta = \frac{E''}{E'}$	$\eta = \frac{E''}{E'}$
(C) RELATIVE ENERGY UNITS	Loss Factor	$\eta$ (res)	$\eta = \frac{E''}{E'}$	$\eta = \frac{E''}{E'}$
Based on lossless ratios of damping energy $D$ and strain energy $U$	Damping Factor	$Q = Q \frac{E''}{E'}$	$\eta = 2\pi U$	$\eta = 2\pi U$
Properties of Materials and Structures	Storage Coef.	$Q_s = Q \frac{E''}{E'}$	$Q_s = 2\pi U_s$	$Q_s = Q$
Properties of Materials and Structures	Q Factor	$Q = \frac{E''}{D}$	$Q_s = \frac{2\pi U_s}{D_s}$	$Q_s = Q$

(D) TEMPORAL DECAY of free vibrations in members		Measured Quantities or Prop. of Systems		How Measured	
$X_0(t) = X_0(0)e^{-\Delta t}$	$\Delta_t$ (Decrement)	$\Delta_t = \ln \frac{X_0(t)}{X_0(0)}$	$\Delta_t = -\pi \frac{K_s}{D_s}$	$\Delta_t = -\pi \frac{K_s}{D_s}$	$\Delta_t = -\pi \frac{K_s}{D_s}$
$U_1 = \frac{1}{2} \log \frac{X_0(t)}{X_0(0)}$	Temporal Decay Constant	$U_t = \frac{1}{t} \ln \frac{X_0(t)}{X_0(0)}$	$U_t = -\omega \frac{D_s}{K_s}$	$U_t = -\frac{\Omega}{2} \frac{D_s}{K_s}$	$U_t = -\frac{\Omega}{2} \frac{D_s}{K_s}$
$-20 \log e^{-\Delta t} = -20 \log e^{-\Delta t}$	Decay Constant	$T_t = 0.05 U_t$	$T_t = -\frac{4\pi K_s}{D_s}$	$T_t = -\frac{4\pi K_s}{D_s}$	$T_t = -\frac{4\pi K_s}{D_s}$
	Rate With Time				
(E) SPATIAL ATTENUATION of waves in slender rods, beams, etc. having distributed parameters					
$X_0(y) = X_0(0) e^{-\Delta y}$	Attenuation	$\Delta_y = \frac{X_0(y)}{X_0(0)} e^{-\Delta y}$	$\Delta_y = \frac{D_s}{k''} \frac{U_s}{E_s}$	$\Delta_y = \frac{D_s}{k''} \frac{U_s}{E_s}$	$\Delta_y = \frac{D_s}{k''} \frac{U_s}{E_s}$
$\Delta_y = \left(\frac{1}{2}\right) \ln \left[\frac{X_0(y)}{X_0(0)}\right]$		$\Delta_y = \ln \frac{X_0(y)}{X_0(0)}$	$\Delta_y = \ln \frac{X_0(y)}{X_0(0)}$	$\Delta_y = \ln \frac{X_0(y)}{X_0(0)}$	$\Delta_y = \ln \frac{X_0(y)}{X_0(0)}$
$(\frac{1}{2}) - 20 \log \frac{X_0(y)}{X_0(0)}$					
$-20 \log e^{-\Delta y} = -20 \log e^{-\Delta y}$					
(F) FREQUENCIES OF STRUCTURAL LOADERS: single-degree-of-freedom system (linear member-mass system).					
Vibration phase angle = $\phi$ . If exciting frequency is much smaller than resonance, then $\phi = \delta$ .					
Resonance Amplitude Factor = $A_q = Q_s$ ; Res. Curve Bluntness = $B_s = \frac{1}{2}$					



For viscoelastic and anelastic materials the complex modulus ( $E^* + E' + iE''$ , see paragraph 5.1.2.2) is a suitable expression for damping. The complex modulus ( $E^*$ ) replaces Young's modulus ( $E$ ).  $E'$ , the stiffness modulus, is the ratio, of that part of the stress that is in phase with the strain, to the total strain.  $E''$ , the loss modulus, is the ratio, of that part of the stress that leads the strain by 90 degrees, to the total strain. Strictly speaking, the complex modulus applies only to materials with quadratic damping (generating elliptical hysteresis loops); but it is also used for other materials, justification for which is presented in Section 6.0.

#### 5.4.2 Objectives

The major objective of the test program was to generate data from which fundamental damping characteristics of the material could be obtained. Great care was taken in design of the test apparatus, specimens, and instrumentation to assure attainment of this objective. The material parameters desired were the stiffness modulus,  $E'_2$ , and the damping factor,  $\eta_2$ , of the coating as a function of temperature. Their product, the loss modulus,  $E''_2$ , is a suitable "figure of merit," for comparison of coatings

These quantities cannot be measured directly, they must be deduced from measurable system characteristics such as resonant frequency decay rates, and coating geometry. The following section describes the evolution of the data processing methods used.



### 5.4.3 Derivation of Data Processing Methods

#### 5.4.3.1 Oberst's Method

The original analysis of the structural damping characteristics of coatings was made by Oberst (Ref. 3), who considered a metal strip coated on one side only and subjected to pure bending waves. Following is a translation of a portion of Reference 3 covering derivations of relations for damping in coated metal strips.

"For the determination of the bending stiffness  $B$  we must first determine the location of the neutral axis. The damping can hereby be neglected. Let the origin of the rectangular coordinate system be on the neutral axis. The  $x$ -axis is in the direction of the length of the strip, the  $y$ -axis normal to the metal surface (see Figure 1).

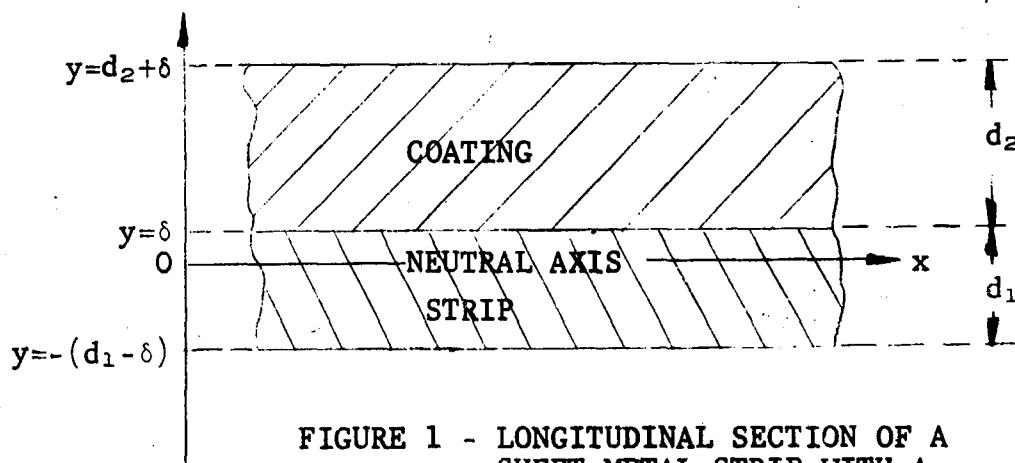


FIGURE 1 - LONGITUDINAL SECTION OF A SHEET-METAL STRIP WITH A DAMPING LAYER

"For the bending of the strip, the variation with  $y$  of the stress  $\epsilon$  along the longitudinal axes of metal and covering layers, Bernoulli's linear law holds true. The stress is equal to zero



AIRESEARCH MANUFACTURING COMPANY OF ARIZONA  
A DIVISION OF THE GARRETT CORPORATION  
PHOENIX, ARIZONA

on the neutral axis and varies linearly with  $y$ . One has

$$\epsilon = \frac{y}{j\omega} \frac{\partial w}{\partial x}, \quad (9)$$

$(1/j\omega) \partial w / \partial x$  is the variation of the angle of rotation in the  $x$ -direction.

"The normal strain in the  $x$ -direction is  $\sigma = E_i \epsilon$ ;  $i = 1$  or  $2$ , and with  $\epsilon$  from equation (9)

$$\sigma = \frac{E_i}{j\omega} y \frac{\partial w}{\partial x} \quad (10)$$

"For pure bending cases, which are to be investigated here, no longitudinal forces are transferred, that is, the force acting on the rod cross section in the  $x$ -direction is equal to zero. Therefore

$$\int_{-(d_1 - \delta)}^{d_2 + \delta} \sigma dy = 0$$

where  $\delta$  is the  $y$ -coordinate of the boundary between the covering layer and the metal (see figure 1). The integration with the aid of eq. (10) gives for  $\delta$  the expression

$$\delta = \frac{1}{2} \cdot \frac{E_1 d_1^2 - E_2 d_2^2}{E_1 d_1 + E_2 d_2} \quad (11)$$



AIRESEARCH MANUFACTURING COMPANY OF ARIZONA  
A DIVISION OF THE BARRETT CORPORATION  
PHOENIX, ARIZONA

For an uncovered sheet-metal ( $d_2 = 0$ ), the neutral axis lies in the metal center ( $\delta = d_1/2$ ). As long as  $d_1$  is comparable with  $d_2$  and  $E_2 \ll E_1$  - this is generally the case in practice - the distance of the neutral axis  $\delta$  from the coating layer is only slightly less than  $d_1/2$ . With increasing thickness ratio  $d_2/d_1$  and increasing modulus  $E_2$  the neutral axis approaches closer to the coating layer and can exceed it for large covering strips and stiffnesses such that  $\delta$  assumes negative values.

"The location of the neutral axis is thus known and the bending moment  $M$  can be calculated. We have

$$M = \int_{-(d_1 - \delta)}^{d_2 + \delta} y \sigma dy$$

Here, the damping of the covering layer must be considered, and in the expression for  $\sigma$  according to eq. (11) we use the complex value  $\bar{E}_2 = E_2(1 + j\eta_2)$  in place of  $E_2$ . With the aid of eqs. (10) and (11), one obtains for  $M$  the expression:

$$M = \frac{\bar{B}}{j\omega} \frac{\partial w}{\partial x}$$

with

$$\bar{B} = B_1 \cdot \frac{1 + 2\bar{a}(2\xi^2 + 3\xi^3 + 2\xi^4)}{1 + \bar{a}\xi^2} \quad (12)$$

$$\xi = d_2/d_1, \bar{a} = \bar{E}_2/E_1 = (E_2/E_1)(1 + j\eta_2), \\ B_1 = E_1 I_1, I_1 = d_1^3/12;$$

$I_1$  is the well-known axial moment of inertia of the cross section of rectangular rods of thickness  $d_1$ .



AIRESEARCH MANUFACTURING COMPANY OF ARIZONA  
A DIVISION OF THE GARRETT CORPORATION  
PHOENIX, ARIZONA

"With this the complex bending stiffness  $\bar{B}$  of the metal strip with covering layer are also known. It remains to separate in the expression for  $\bar{B}$  the real and the imaginary part and to determine the quantities  $B$  and  $\eta$  in  $\bar{B} = B(1 + j\eta)$  individually. With  $B$  and  $m$ , one knows the bending wave velocity according to eq. (7) and with this the bending wave-length on the covered metal strip;  $\eta$  is its loss factor which determines the damping of the bending waves.

"The separation of real and imaginary parts in the expression for  $\bar{B}$  gives

$$\frac{B}{B_1} = \frac{1 + 2a(2\xi + 3\xi^2 + 2\xi^3) + a^2\xi^4}{1 + a\xi} \quad (13)$$

$$\frac{\eta}{\eta_2} = \frac{a\xi}{1 + a\xi} \cdot \frac{3 + 6\xi + 4\xi^2 + 2a\xi^3 + a^2\xi^4}{1 = 2a(2\xi + 3\xi^2 + 2\xi^3) + a\xi^4} \quad (14)$$

$$a = E_2/E_1$$

where  $\eta_2^2$  is neglected with respect to 1.

"The ratio  $B/B_1$  and  $\eta/\eta_2$  can easily be determined by experiment,  $B/B_1$  from the measured characteristic bending frequencies. From the latter, one obtains the constants  $\sqrt{B/m}$  (for the metal strip with covering layer) and  $\sqrt{B_1/m_1}$  (for the metal strip alone) (see Section 3). However,  $B/m$  is constant only as long as the elastic modulus  $E_2$  of the layer is constant (independent of the frequency). Knowing  $m_1$  and  $m$ , one knows also  $B/B_1$  and with this and the measured values  $\xi = d_2/d_1$  one can determine by means of eq. (13) the ratio of the elastic moduli  $A = E_2/E_1$ . If one knows  $a$  and when  $\eta$  is measured, one can also determine the loss factor  $\eta_2$  of the covering layer with the aid of eq. (14).



"The method of the bending waves on small sheet-metal strips with covering layers therefore permits one to find the elastic modulus and loss factor of the damping layers. The numerical determination of  $E_2$  and  $\eta_2$  with eqs. (13) and (14) would be troublesome. Figures 2 and 3 present families of curves from which one can take these quantities directly.

"Figure 2 presents curves of  $\sqrt{B/B_1}$  as functions of  $\xi = d_2/d_1$  with  $a = E_2/E_1$  as the parameter. The latter is varied in the range from  $a = 10^{-5}$  to  $10^{-1}$ . For larger values of  $a$  the elastic modulus of the covering layer would come close to that of the steel and it is unlikely that damping materials exist which have such high rigidity with high internal losses. The value  $a = 10^{-5}$  corresponds to that for very soft rubber. For values of  $a < 10^{-5}$  one would obtain satisfactory loss factors  $\eta$  only with very large covering thicknesses (see Figure 3). The curves of Figure 2 are even valid when  $\eta_2$  is of the order 1.

"Figure 3 presents the corresponding family of curves for  $\eta/\eta_2$ . The scale on the ordinate is extended (in logarithmic presentation) downward only to  $\eta/\eta_2 = 5 \times 10^{-3}$ . Smaller values, for which  $\eta$  would also be very small, are of no practical interest. The curves increase monotonically with increasing  $\xi$  and approach the limiting value 1 when  $\xi \rightarrow \infty$ . A certain waviness of the curves can be seen, (the curves passing through some maxima and minima before attaining the limiting value), but they are not very pronounced. The curves of Figure 3 are also valid in all practical cases of interest even when  $\eta_2$  is of the order of 1. Only for comparatively large parameter values  $a$  do small deviations occur for large values of  $\xi$ , but which are generally of no significance compared to the scatter of the  $\eta$  test values."



AIRESEARCH MANUFACTURING COMPANY OF ARIZONA  
A DIVISION OF THE GARRETT CORPORATION  
PHOENIX, ARIZONA

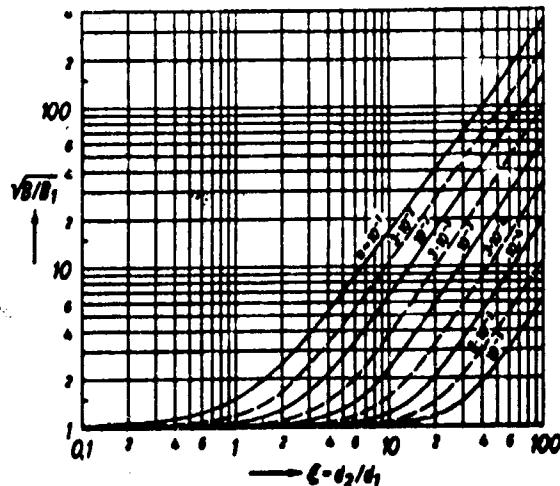


Figure 2.-Ratio of the bending stiffnesses of the covered and uncovered strips as a function of the thickness ratio.

Parameter  $a = E_2/E_1$ .

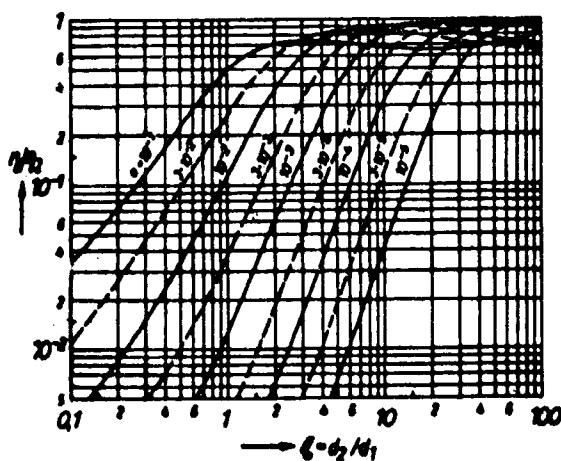


Figure 3.-Ratio of the loss factors of the covered sheet-metal and of the covering as a function of the thickness ratio.

Parameter  $a = E_2/E_1$ .



For preliminary examination of data, the consultant, Dr. Lazan, recommended use of Oberst's method as follows:

"The error in replacing the double-coated beam for calculation purposes by the single coated beam is proportional to  $1 - (H_{1,2}/H'_{1,2})^2$ . If  $h_2 = H_2/H_1$  equals 0.1 (approximate value for your beam), then the error in assuming that  $H_{1,2} = H'_{1,2}$  is only about 4%. I believe, therefore, that you can use the equations and curves given in attachment 'c'.

"In order to use Figure 34.7 in attachment 'c', it is necessary to know  $E_2/E_1$ , the ratio of the modulus of the coating to the modulus of the base or test beam. For a given test beam and free grip assembly (grip that vibrates during decay test) and assuming the inertia of the beam and coating is much smaller than the inertia of the free grip assembly, the natural frequency of the system is:

$$\frac{f^2}{n} = KEI$$

where K is a proportionality constant, E is Young's modulus, and I is moment of inertia.

For the bare test (uncoated) beam  $EI = E_1 I_1$ , the natural frequency is:

$$\frac{f^2}{n_1} = KE_1 I_1$$

For the composite beam (test beam plus coating which can be described by  $E_2 I_2$ , where  $E_2 = E^* - E'$  of coating), the natural frequency is:

$$\frac{f^2}{n_{nc}} = K(E_1 I_1 + E_2 I_2)$$

Combining these two equations:

$$\begin{aligned} \left(\frac{f_{nc}}{f_{n_1}}\right)^2 &= \frac{E_1 I_1 + E_2 I_2}{E_1 I_1} = 1 + \frac{E_2 I_2}{E_1 I_1} \\ \frac{E_2}{E_1} &= \frac{I_1}{I_2} \left[ \left(\frac{f_{nc}}{f_{n_1}}\right)^2 - 1 \right] \end{aligned}$$

Thus, to determine the ratio  $E_2/E_1$  it is necessary only to measure the natural frequencies of the system using both the uncoated beam and the coated beam keeping other features of the test constant. The moments of inertia  $I_1$  and  $I_2$  are about the centroidal axis (or central) axis of the composite beam. For reasonably thin coatings the moment of inertia of  $I_2$  is merely  $A_2 \times H_{1,2}^2$  (or  $(h_{1,2})^2$  if you wish to use the refinement mentioned above), where  $A_2$  is the cross-section of the coating."



The first data obtained on a porcelain enamel yielded values of 'a' considerably greater than that considered likely by Oberst, and indicated that  $\eta_2$  was larger than expected. Initial tests of the apparatus revealed a distinct peak for internal friction of Hastelloy X, such that the assumption made by Oberst that  $\eta_1 = 0$  might not be justified. If Oberst's method were to be used, his Figure 3 would have to be extended to the regime describing our test specimens. This would require complicated calculations with questionable assumptions, and would have results of doubtful value. Therefore, an alternative method was sought. It was found that Oberst's analytical method could be applied to the simpler case of a double-coated bar designed for uniform strain, and the result also took a simpler form. No analyses of double coatings were found in the literature. References 16, 17, 26, and 30, considered standard sources, merely copy Oberst's single-coating analysis.

#### 5.4.3.2 Derivations For Double Coating

Refer to Figure 5-19, but otherwise use Oberst's notation:

The bending moment is  $M$ ,

$$M = \frac{B^*}{j\omega} \frac{\partial W}{\partial x} = 2 \int_0^{\alpha+\beta} \sigma y \, dy$$

$$\sigma = \frac{Ei}{j\omega} y \frac{\partial W}{\partial x} \quad (\text{Oberst}) \\ \text{Eq. 10}$$

$$\frac{B^*}{j\omega} \frac{\partial W}{\partial x} = 2 \int_0^{\alpha+\beta} \frac{Ei}{j\omega} \frac{\partial W}{\partial x} y^2 \, dy$$

but since the double-coated bar has been designed for uniform surface strain,  $\frac{\partial W}{\partial x}$  is a constant and may be removed from under the integral, along with  $\frac{1}{j\omega}$ .



AIRESEARCH MANUFACTURING COMPANY OF ARIZONA  
A DIVISION OF THE GARRETT CORPORATION  
PHOENIX, ARIZONA

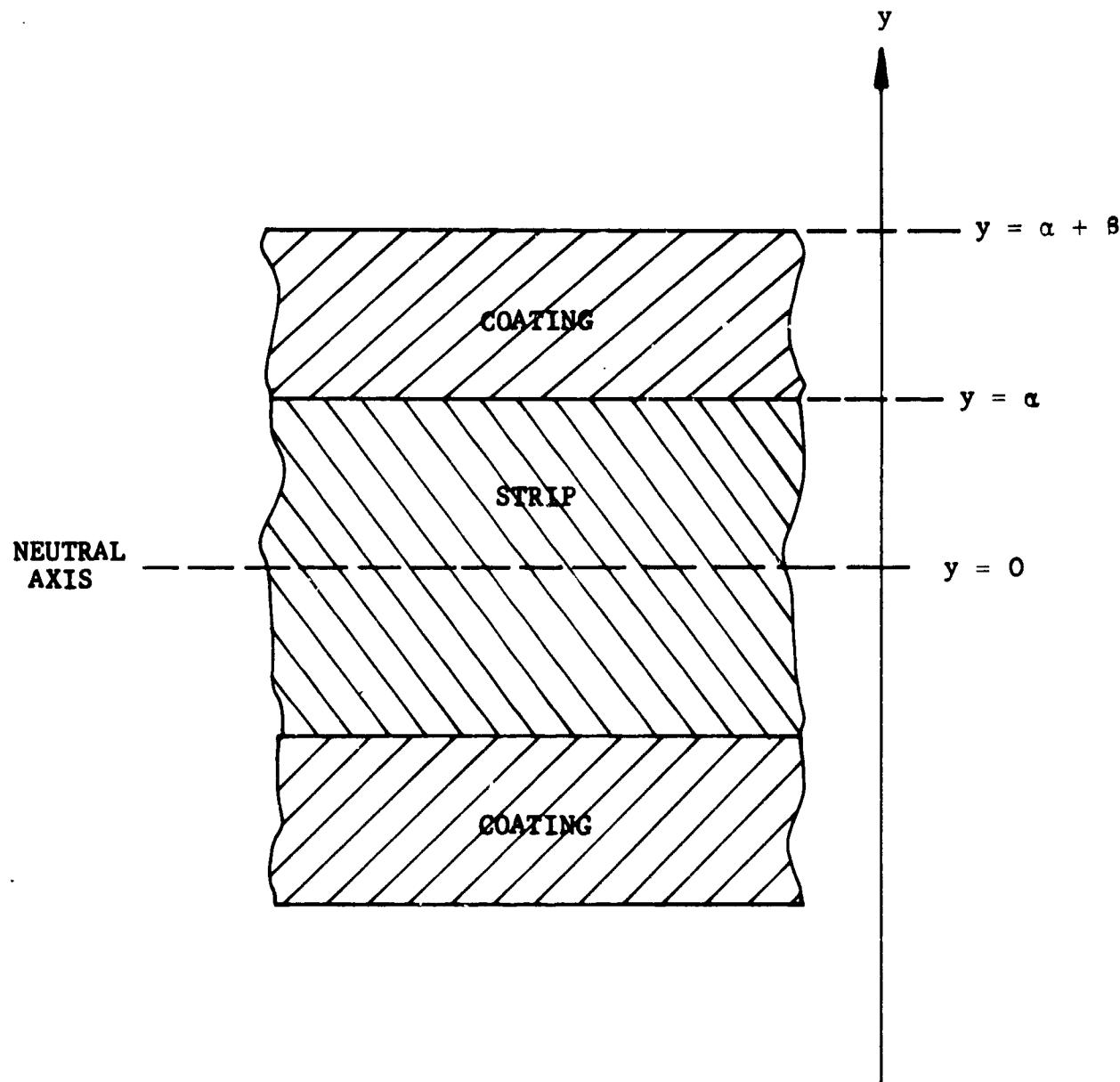


FIGURE 5-19

LONGITUDINAL SECTION OF A  
SHEET-METAL STRIP WITH TWO  
DAMPING LAYERS

GT-7615-R  
Page 5-65



AIRESEARCH MANUFACTURING COMPANY OF ARIZONA  
A DIVISION OF THE GARRETT CORPORATION  
PHOENIX, ARIZONA

$$B^* = \frac{2}{3} [E^*_{10} y^3]_0^a + E^*_{20} y^3 ]_a^\infty + \beta)$$

$$B' + i\eta B^* = \frac{2}{3} [E^*_{10} a^3 + E^*_{20} (a + \beta)^3 - E^*_{20} \alpha^3]$$

Set  $\eta_1 = 0$ , separate real and imaginary parts, and set  $\frac{E^*_{20}}{E^*_{10}} = a$ .

Then  $\frac{\eta}{\eta_2} = \frac{a(3\alpha^2\beta + 3\alpha\beta^2 + \beta^3)}{\alpha^3 + a(3\alpha^2\beta + 3\alpha\beta^2 + \beta^3)}$

If  $\xi = \frac{\beta}{a}$ , and  $C = (3\xi + 3\xi^2 + \xi^3)$ , then  $\eta_2 = \eta \frac{1 + aC}{aC}$

$C$  is determined purely by the geometry of the coating and test bar but both  $\eta$  and "a" must be determined from test data. A derivation for "a" has already appeared in the previous section.

$$a = \frac{I_1}{I_2} \left[ \left( \frac{F}{F_1} \right)^2 - 1 \right] \text{ and it may be readily shown that the ratio of the moments of inertia is } \frac{I_1}{I_2} = \frac{1}{3(\xi + \xi^2)}$$

The test instrumentation displayed period rather than frequency, so the substitution was made

$$P_n = 1/f_n$$

#### 5.4.3.3 Correction for Residual Damping

It is necessary to use a corrected value for  $\eta$  (damping coefficient of a coated bar), because the derivation of the ratio of  $\frac{\eta}{\eta_2}$  introduced the simplifying assumption that  $\eta_1 = 0$  which, due to anelasticity in Hastelloy X, is not strictly true. To avoid this difficulty, Professor Lazan derived a corrected value for  $\eta$ , which corrected the observed decay rates to what would have been observed if  $\eta_1$  were zero, as follows:



AIRESEARCH MANUFACTURING COMPANY OF ARIZONA  
A DIVISION OF THE GARRETT CORPORATION  
PHOENIX, ARIZONA

"During our recent telephone conversation you inquired about possible methods for subtracting the damping properties of the bare specimen from the overall damping so that the damping associated only with the coating can be specified. I will cover additional information on this and other points you mention in your letters in conversation at a later date.

" My personal preference for specifying the damping properties of the coating would be in terms of the damping energy dissipation rather than a dimensionless energy ratio for the base member with coating. However, most of the prior publications on this have been in terms of a dimensionless unit such as the loss coefficient or loss factor  $\eta$ . In view of this and since the material I sent you with my letter of May 25 includes analysis in terms of the loss coefficient, I believe it probably is better to analyze the coatings in terms of the loss coefficient.

"It would be possible to analyze the coating in terms of the decibel rate, such as done in the preliminary data you sent to me. However, I believe that the loss coefficient is the more accepted term for specifying damping, and I prefer this unit.

" I have very quickly derived the equations for finding the loss coefficient  $\eta_c$  that would be observed if only the coating were to dissipate energy (no energy assumed to be lost in the bare specimen). This would then show the loss coefficient that would be realized if the bare metal were to contribute nothing to the overall damping. As you recall, the graphs and other material I sent you review the subject in the context. I believe that the use of a term such as  $\eta_c$  is appropriate. Given below is the derivation and the equation, and I hope you will consider this tentative since I have not yet time to check it.



AIRESEARCH MANUFACTURING COMPANY OF ARIZONA  
A DIVISION OF THE GARRETT CORPORATION  
PHOENIX, ARIZONA

"Definitions:

$$\eta_s = \frac{D_s}{2\pi U_s} = \frac{\tau_{ts}}{27.3 f_s} \quad (\text{Eq. 1})$$

$$\eta_{sc} = \frac{D_{sc}}{2\pi U_{sc}} = \frac{D_s + D_c}{2\pi U_{sc}} = \frac{\tau_{tsc}}{27.3 f_{sc}} \quad (\text{Eq. 2})$$

$$\eta_c = \frac{D_c}{2\pi U_{sc}} \quad (\text{Eq. 3})$$

where  $\eta_s$ ,  $D_s U_s$ ,  $\tau_{ts}$  and  $f_s$  are the loss coefficient, damping energy dissipation, strain energy, decay rate, and frequency, respectively, for bare test specimen.

$\eta_{sc}$ ,  $D_{sc}$ ,  $U_{sc}$ ,  $\tau_{tsc}$  and  $f_{sc}$  are similar values for specimen with coating. Note that  $D_{sc} = D_s + D_c$  and  $U_{sc} = U_s + U_c$ .

$\eta_c$  = loss coefficient of coated specimen if bare specimen has a damping energy dissipation ( $D_s$ ) equal to zero.

$D_c$  = damping energy dissipated in coating above.

"Given: - Values Measured in Decay Apparatus.

$\tau_{ts}$ ,  $f_s$ ,  $\tau_{tsc}$  and  $f_{sc}$

"To Find: -

$\eta_c$

"Calculation: -

"Strain energy at displacement equal to vibration amplitude  $X_a$  = kinetic energy at zero displacement =  $\frac{1}{2} M V^2 = \frac{1}{2} M (2\pi f X_a)^2$



where  $V$  = velocity at zero displacement

$M$  = an effective mass for the free arm in the apparatus

$f$  = frequency of vibration-cps.

$$\frac{U_s}{U_{sc}} = \frac{2\pi^2 M f_s^2 X_a^2}{2\pi^2 M f_{sc}^2 X_a^2} = \left(\frac{f_s}{f_{sc}}\right)^2 \quad (\text{Eq. 4})$$

"From Equation 2

$$\frac{D_s}{2\pi U_{sc}} + \frac{D_c}{2\pi U_{sc}} = \frac{\tau_{tsc}}{27.3 f_{sc}} \quad (\text{Eq. 5})$$

"From Equation 1 and Equation 4

$$\frac{D_s}{2\pi U_{sc}} = \frac{D_s}{2\pi U_s} \left(\frac{U_s}{U_{sc}}\right) = \frac{\tau_{ts}}{27.3 f_s} \left(\frac{f_s^2}{f_{sc}^2}\right) = \frac{\tau_{ts}}{27.3 f_{sc}} \left(\frac{f_s}{f_{sc}}\right) \quad (\text{Eq. 6})$$

"Substituting Equations 6 and 3 in Equation 5

$$\begin{aligned} \frac{\tau_{ts}}{27.3 f_{sc}} \left(\frac{f_s}{f_{sc}}\right) + \eta_c &= \frac{\tau_{tsc}}{27.3 f_{sc}} \\ \eta_c &= \frac{1}{27.3 f_{sc}} \left[ \tau_{tsc} - \tau_{ts} \left(\frac{f_s}{f_{sc}}\right) \right] \quad (\text{Eq. 7}) \end{aligned}$$

In the present notation

$$\eta_2 = \frac{P_{12}}{27.3} \left[ \tau_{12} - \tau_1 \left(\frac{P_{12}}{P_1}\right) \right]$$

here  $\tau_{12}$  is the observed vibration decay rate in db per second for the coated bar and  $\tau$  is the observed decay rate for a bare bar.



AIRESEARCH MANUFACTURING COMPANY OF ARIZONA  
A DIVISION OF THE BARRETT CORPORATION  
PHOENIX, ARIZONA

#### 5.4.3.4 Review

Data reduction may be summarized as follows:

Given observed values of

$d_1$  = test bar thickness

$d_2$  = coating thickness (per layer)

$$(\xi = \frac{2 d_2}{d_1})$$

$\tau_n$  = decay rate db per second for the nth configuration.

$P_n$  = period of vibration (as observed at steady-state vibration) for the nth configuration

n = configuration index

1 = bare specimen

2 = coating only

$_{12}$ , or no subscript, designates the coated bar.

Calculate and plot vs. temperature.

$\eta_2$  = loss factor for coating

$E_2'$  = stiffness modulus for coating

$E_2'' = \eta_2 E_2'$  = loss modulus for coating.

To accomplish this the following relations are used:

$$\eta_2 = \eta_{12} \frac{1 + aC}{aC}$$

$$C = (3\xi + 3\xi^2 + \xi^3)$$

$$a = \frac{E_2'}{E_1} = \frac{I_1}{I_2} \left[ \left( \frac{P_1}{P_{12}} \right)^2 - 1 \right]$$

$$\frac{I_1}{I_2} = \frac{1}{3(\xi + \xi^2)}$$

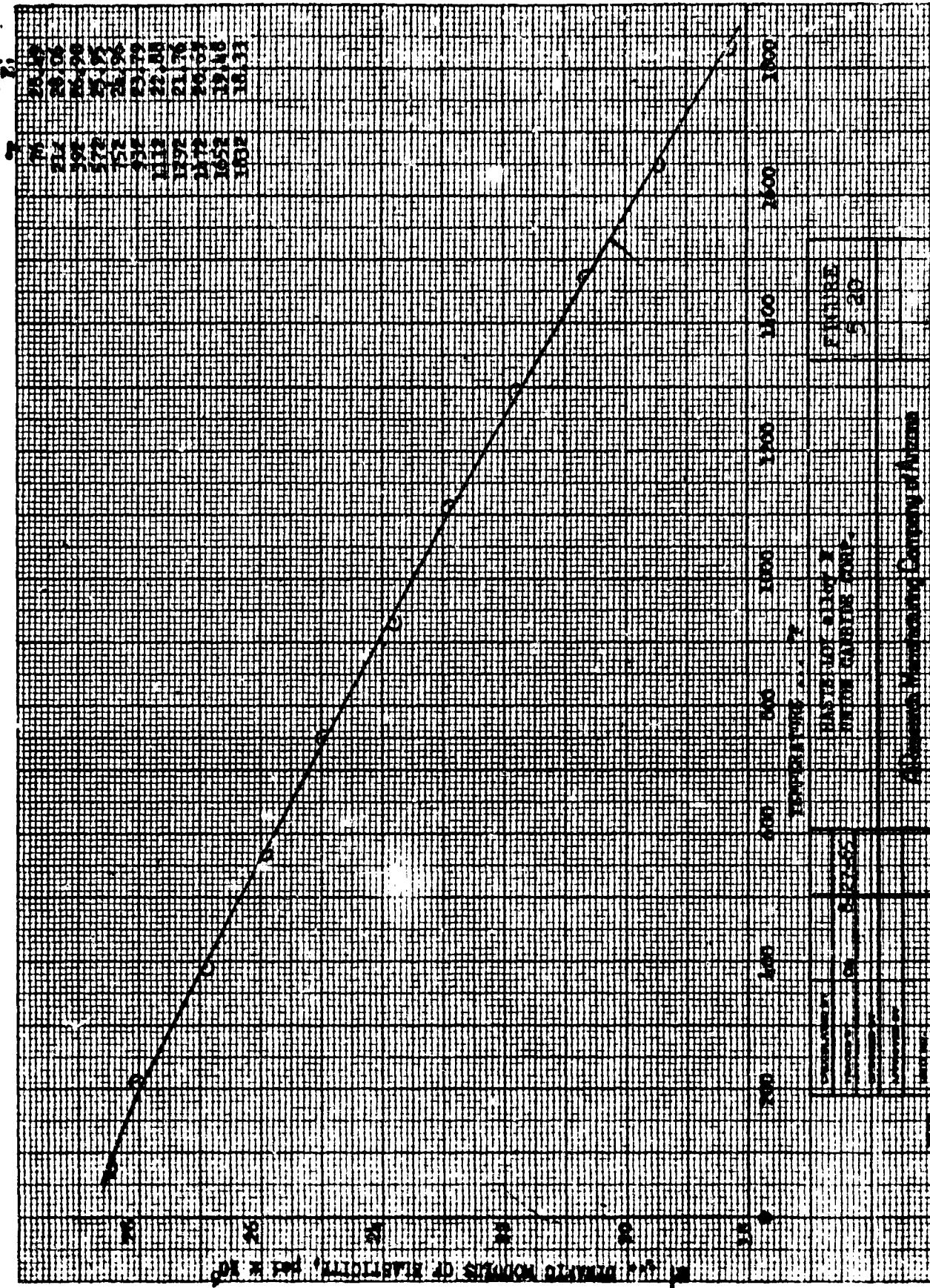
$$\eta_{12} = \frac{P_{12}}{27.3} \left[ \tau_{12} - \tau_1 \left( \frac{P_{12}}{P_1} \right) \right]$$

$E_2'$  is obtained from Figure 5-20, which is based on data published by the Union Carbide Company for Hastelloy X (Ref. 28)

$$E_2'' = \eta_2 E_2'$$



AIRESEARCH MANUFACTURING COMPANY OF ARIZONA  
A DIVISION OF THE BARRETT CORPORATION  
PHOENIX, ARIZONA



GT-7615-R  
Page 5-71



AIRESEARCH MANUFACTURING COMPANY OF ARIZONA  
A DIVISION OF THE GARRETT CORPORATION  
PHOENIX, ARIZONA

#### 5.4.4 Error Analysis

##### 5.4.4.1 Oberst's Curves Applied to Double Coatings

Reference 3 shows excellent agreement between Oberst's theoretical results and his measurements on single-coated specimens. No significant criticism of his methods was found in later literature. It was originally planned to use Oberst's methods for our testing even though double coatings were involved. Analysis of the error that would be introduced showed that for  $\xi = 0.1$  the error in  $\eta_2$  would amount to 4 percent. When it was decided to recalculate the expression for  $\eta_2$  for the double-coated bar this discrepancy disappeared.

##### 5.4.4.2 Pendulum Effect

In any damping test apparatus which mounts a test specimen as a vertical cantilever beam, an error is introduced by operation in the fundamental mode. This occurs because the beam stores energy by acting as a pendulum as well as by storing energy through its deformation. Calculations later showed that the pendulum effect in the apparatus was negligible. This point was worthy of consideration because it is a major source of error in some types of apparatus. For example, in the Brüel and Kjaer complex modulus apparatus, which incorporates Oberst's basic methods, the first mode data is rejected because of pendulum error.



#### 5.4.4.3 Decay Rates

The maximum decay rates attained are of the order of 30 db per second as contrasted to the several hundred db per second writing-speed capability of the Brüel and Kjaer level recorder used. The paper drive is by synchronous motor. For such mechanically reliable recorders error in decay rates arises from:

- (a) Nonlinear pickups
- (b) Curve decays due to variation in decay rates as a function of strain level.
- (c) Irregular decays due to excitation of several closely-spaced modes of vibration.

The push-pull optical pickup system used to detect the vibration was found to be linear for excursions considerably greater than those used. The decays recorded were in almost every case free of curvature, due to the low maximum strain level of 150 micro-inches per inch. No irregularity due to multiple mode excitation was discernible. As a result, the decay rate observations are regarded as reliable to at least, two probably three, significant figures.

#### 5.4.4.4 Period Measurement

Period measurements were made by a period counter with a five-digit display. Variations in repeated counts, in general occurred in the fifth place. The drive system was regenerative in character, and some variation in period count could be introduced by varying the phase relations in the regenerative circuits. To reduce this variation the phase was adjusted so that, for undamped specimens (bare bars), the free decay frequency corresponded to the regeneratively driven frequency. As a result, period counts are judged to be reliable to three, probably four, significant figures.



AIRESEARCH MANUFACTURING COMPANY OF ARIZONA  
A DIVISION OF THE GARRETT CORPORATION  
PHOENIX, ARIZONA

#### 5.4.4.5 Coating and Bar Thickness

As is commonly the case in this type of testing, the greatest uncertainty is in coating thickness which arises from numerous sources. The porcelain enamels have a slight thickening at the edges due to capillary effects during firing. The tapering of the test areas to attain uniform strain levels makes accurate measurement more difficult. The coatings applied by metal spray are, of necessity, nonuniform in thickness. Finally, thickness measurements are dependent on the uniformity of the test bars and the degree of precision with which their dimensions were cataloged. In retrospect, it is clear that a greater degree of precision in the grinding of the test bars would have been desirable. Tolerances no greater than  $\pm 0.0002$  inch are desired. The  $\pm .001$  tolerance used is too loose and results in considerable uncertainty concerning coating thickness. To double-check the coating and test-bar thicknesses, coatings were stripped at the center of the test sections to permit another thickness measurement. These terminal measurements were used in the calculation of  $\xi$ .

As a consequence, values of  $\xi$  and hence  $n_2$  are considered to be reliable to only one significant figure.

The most troublesome result of variations in the test bars was its influence on  $P_1$ , the natural frequency of the uncoated bar. Scheduling of the construction of the test hardware precluded any individual frequency calibration of the test bars. Bars were made and in many cases coated before the rest of the apparatus was available. Even a bare bar that is calibrated directly is subject to some uncertainty, since thermal cycling and sandblasting prior to coating tend to modify its period slightly.



The difficulty is acute only in those cases in which  $P_1$  and  $P_{12}$  come very close together. Thus, the calculation of  $a = \frac{E_2}{E_1}$  which contains the factor  $[(\frac{P_1}{P_{12}})^2 - 1]$  becomes uncertain if a reliable value for  $P_1$  is not available.

To circumvent this difficulty two bare bars were carefully calibrated for  $P_1$  vs temperature. These two calibration curves were very similar in shape but separated by 0.25 cps. Their average was used to establish the shape of the  $P_1$ -vs-T curve.

For the vitreous enamels it may be safely assumed that  $P_1 = P_{12}$  near the firing temperature, for the coating is essentially liquid and devoid of stiffness. The average  $P_1$ -vs-T curve was therefore adjusted vertically until  $P_{12}$  asymptotically approached  $P_1$  at the firing temperature. This adjusted  $P_1$  was then read off and used in the calculation of  $a$  and  $n_2$ .

For the manganese coppers and XAP specimens,  $P_1$  and  $P_{12}$  do not approach each other closely in the temperature range of interest. Therefore, the average value of  $P_1$  was used.

#### 5.4.4.6 Inherent Damping

In damping measurements, effort must be used to minimize the inherent damping in the test fixture, as inherent damping sets a lower limit to the values of  $n_2$  that can be measured. Care must be taken to prevent transmission of the test-bar vibration into surrounding structures. For the measurement of internal friction in most structural metals, it is also necessary to operate in a vacuum to avoid the damping due to acoustical radiation and viscous drag.



AIRESEARCH MANUFACTURING COMPANY OF ARIZONA  
A DIVISION OF THE GARRETT CORPORATION  
PHOENIX, ARIZONA

By providing a massive foundation it was possible to attain decay rates of 0.35 db per second in the open air at room temperature. This corresponds to an apparent  $\eta_1$  in the Hastelloy X of about  $2.5 \times 10^{-4}$ , which is a factor of 10 larger than might be expected in the metal. With the furnace in place, the decay rate increased to about 0.4 db per second, which indicated that the viscous drag of the air in the slot in the furnace floor was a limiting factor.

As the temperature of the test bars was raised above 1000°F, an unexpected increase in inherent damping occurred. This was apparently due to an anelastic resonance in the Hastelloy X. The increase was variable, with thermal cycling, from bar to bar. The value of  $T_1$  used in data reduction is an average of several such observations. The correction term  $\frac{P_{12}}{P_1}$ , applied to  $T_1$ , is nearly unity and is included to illustrate its use in cases where it might become significant.

#### 5.4.4.7 Error Review

The values for  $\eta_2$ ,  $E'_2$ , and, hence,  $E''_2$  are believed to be reliable to one significant figure. Doubts about the second significant figure are due mainly to inaccuracies in the grinding of the test bars leading to uncertainty in the values of  $\xi$  and  $P_1$ .

Those wishing to duplicate the tests in this report are admonished to grind the test bars to a precision of at least  $\pm 0.0002$  inch and to determine  $P_1$  at several temperatures for each test bar, if possible.



## 5.5 Test Results

### 5.5.1 Introduction

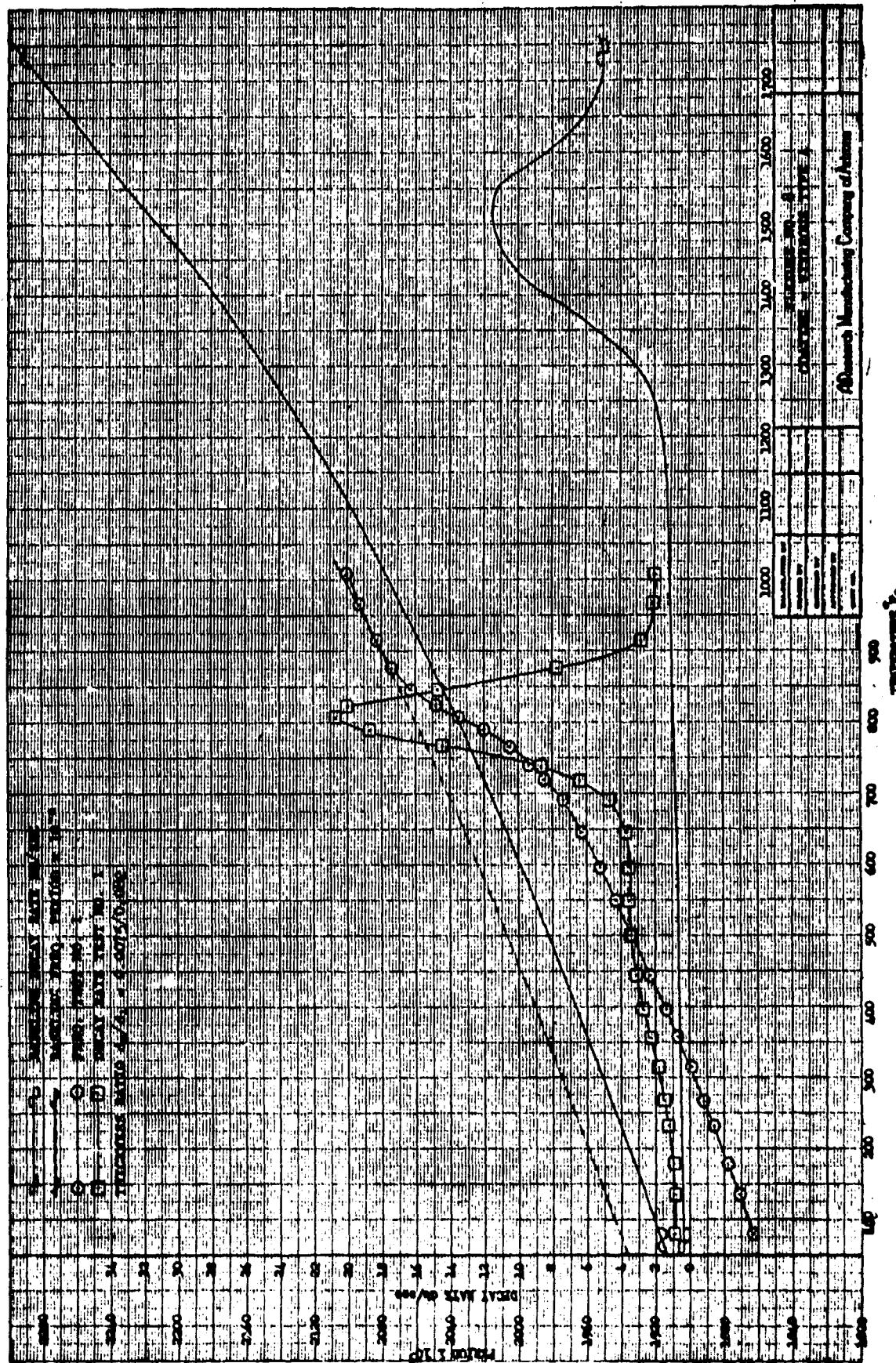
Much of the data available on vibration damping coatings was developed from apparatus and procedures designed to find comparative performance rather than material properties. If a description of the apparatus and test procedure are available, it is possible to compute material properties. This can be both laborious and uncertain unless the apparatus is designed specifically to facilitate precise calculations.

The specific objective the test program was to obtain data representing fundamental damping properties, the complex moduli; specific damping was also obtained, since it was more applicable to the materials, under consideration. This objective influenced design of the test apparatus and the data processing methods.

The data obtained from the test apparatus is presented in five phases. Graphs 5-2 through 5-14 present observations made of decay rates, as a function of corrected temperature, and the adjusted curve for period vs corrected temperatures used in subsequent data reduction. This data can serve as figures of merit for the stated coating thickness and frequency, especially if a rough compensation is made for the effects of inherent damping wherever the total decay rates approach those of the bare bar.



GRAPH 5-2

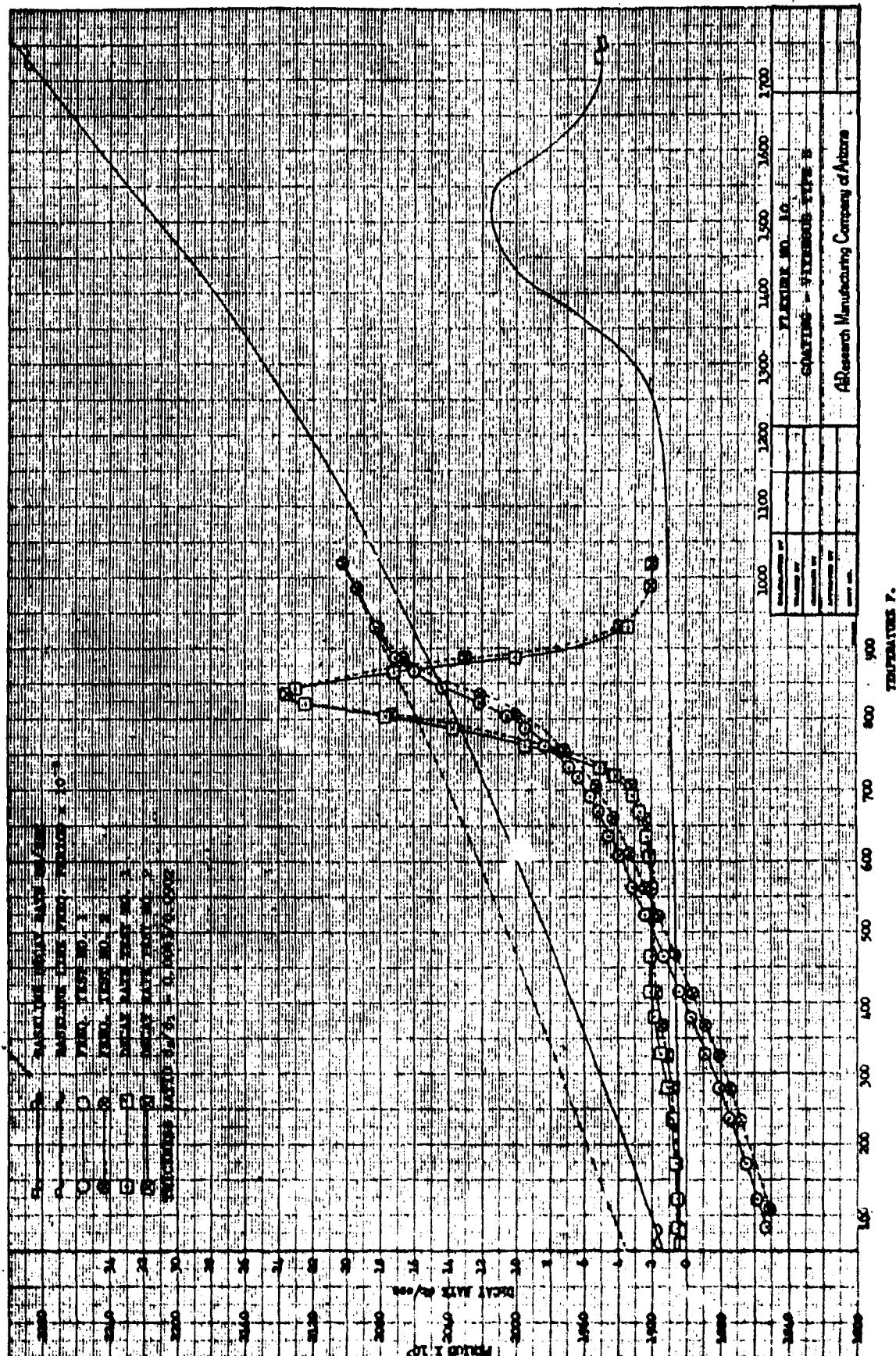


GT 7615-R  
Page 5 78



**AIRSEARCH MANUFACTURING COMPANY**  
A DIVISION OF THE MARVEL CORPORATION  
PHOENIX, ARIZONA

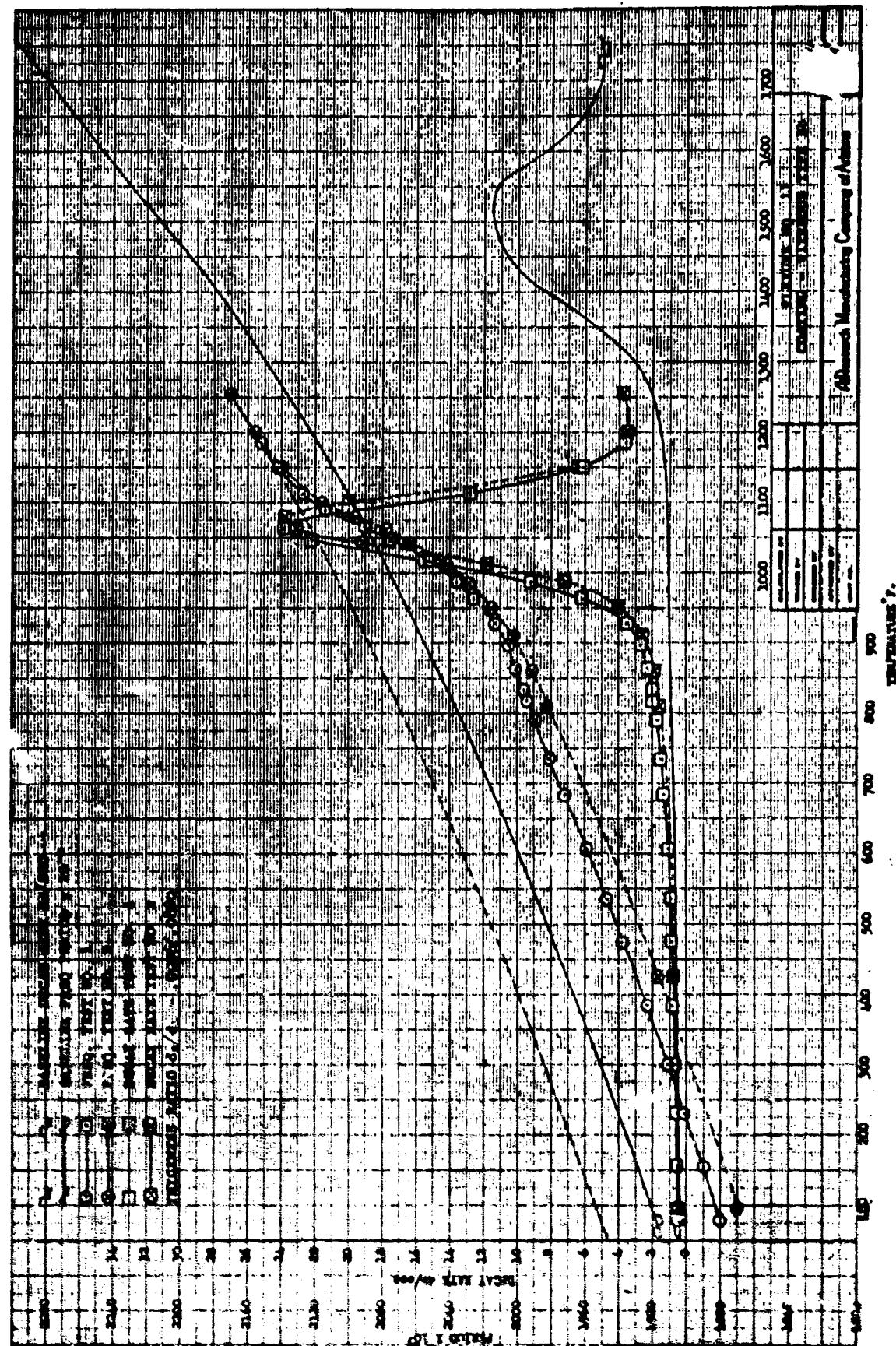
GRAPH 5-3



GT-7615-R  
Page 5-79



GRAPH 5-4

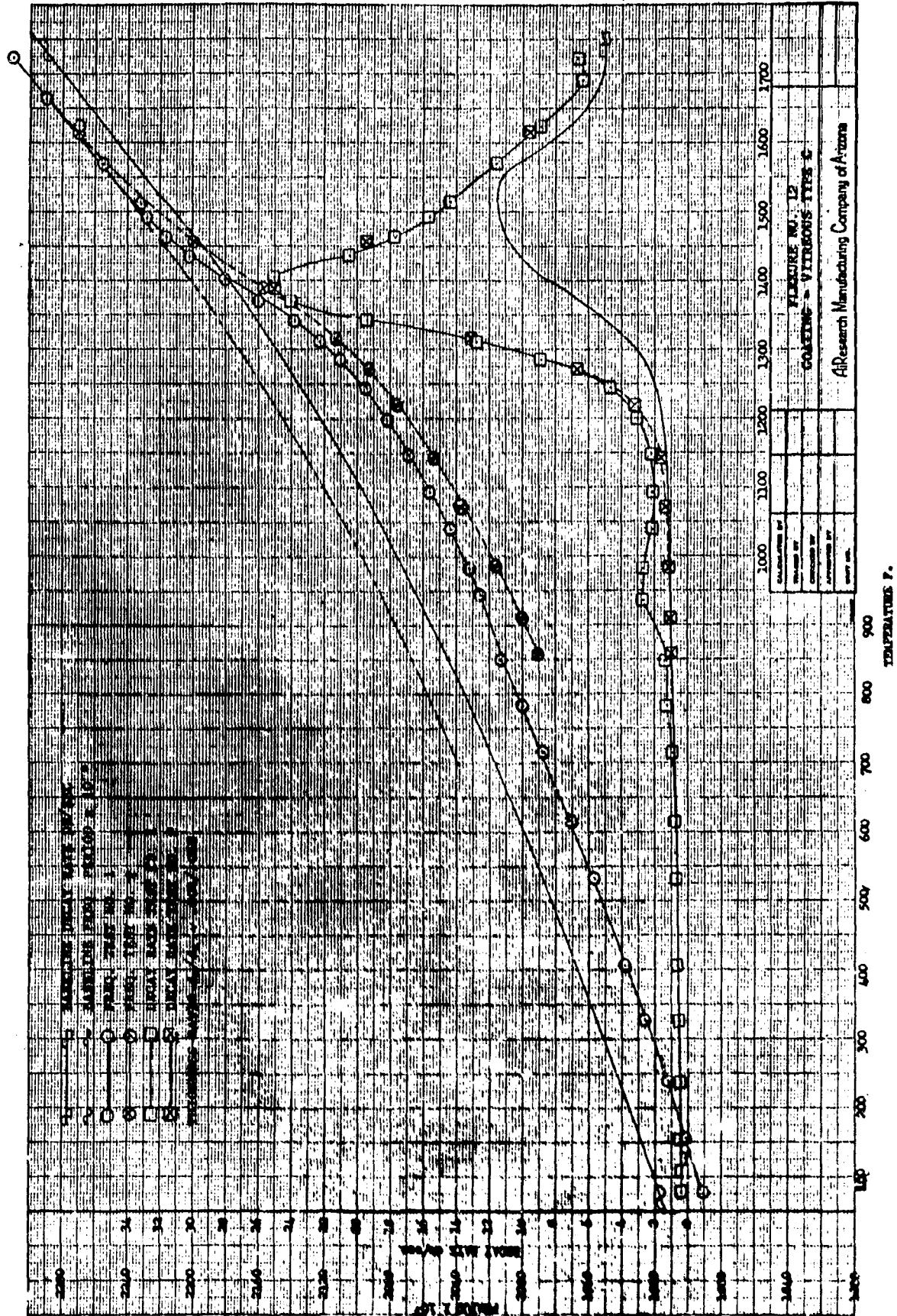


GT-7615 R  
Page 5 80



AIRSEARCH MANUFACTURING COMPANY  
A DIVISION OF THE GARRETT CORPORATION  
PHOENIX, ARIZONA

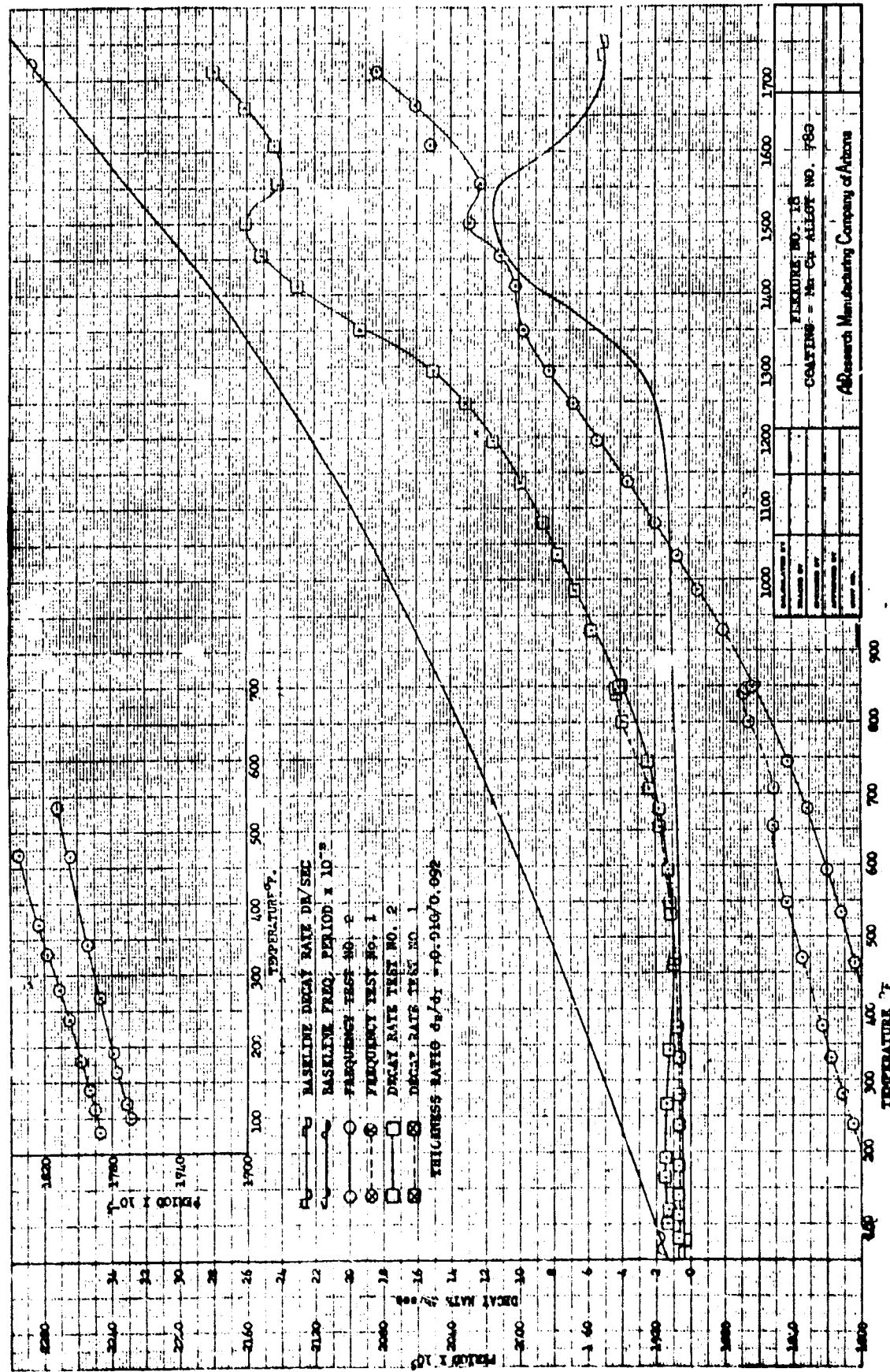
GRAPH 5-5



GT-7615-R  
Page 5-81



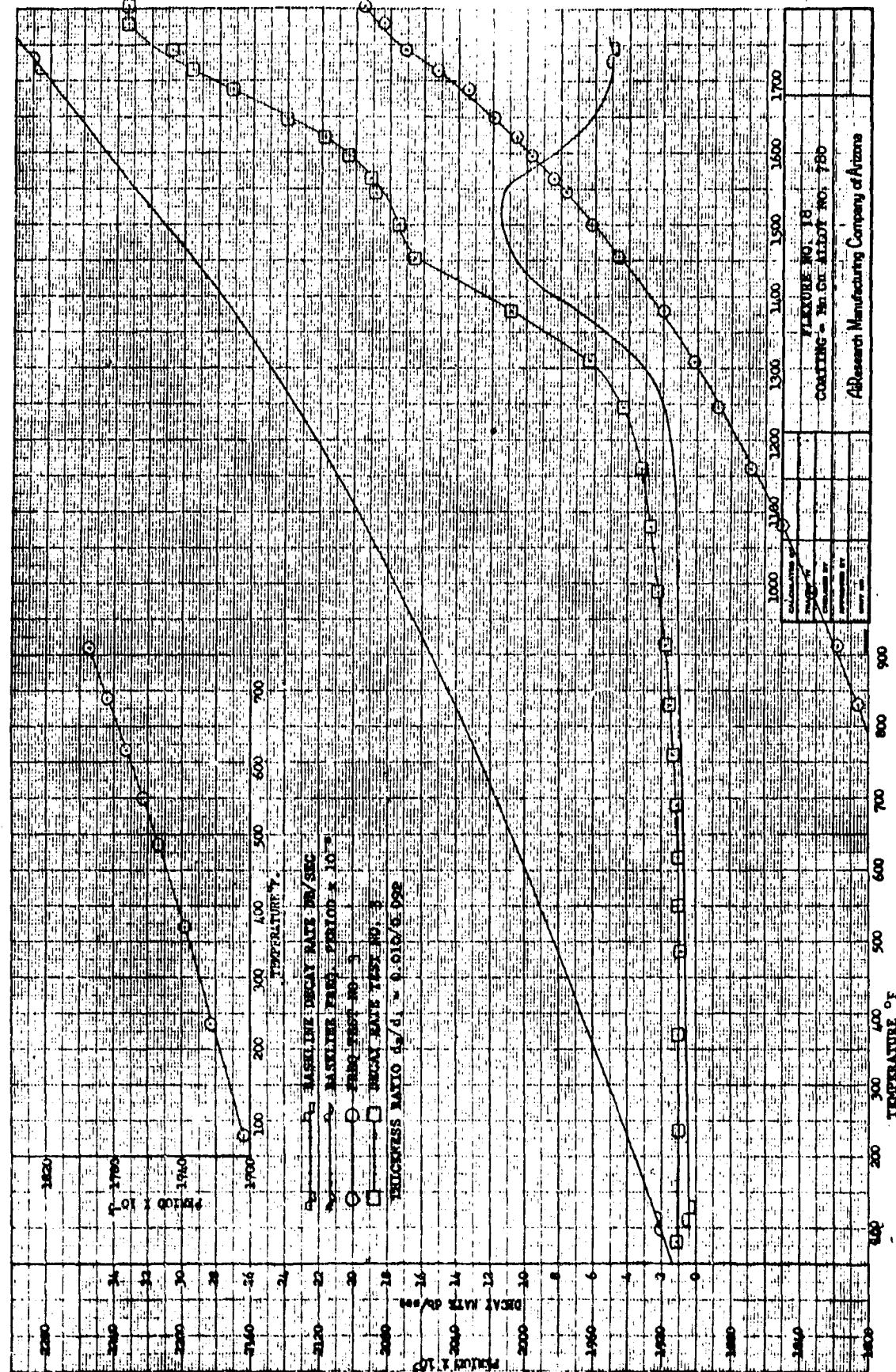
GRAPH 5-6



GT-7615-R  
Page 5 82



GRAPH 5-7

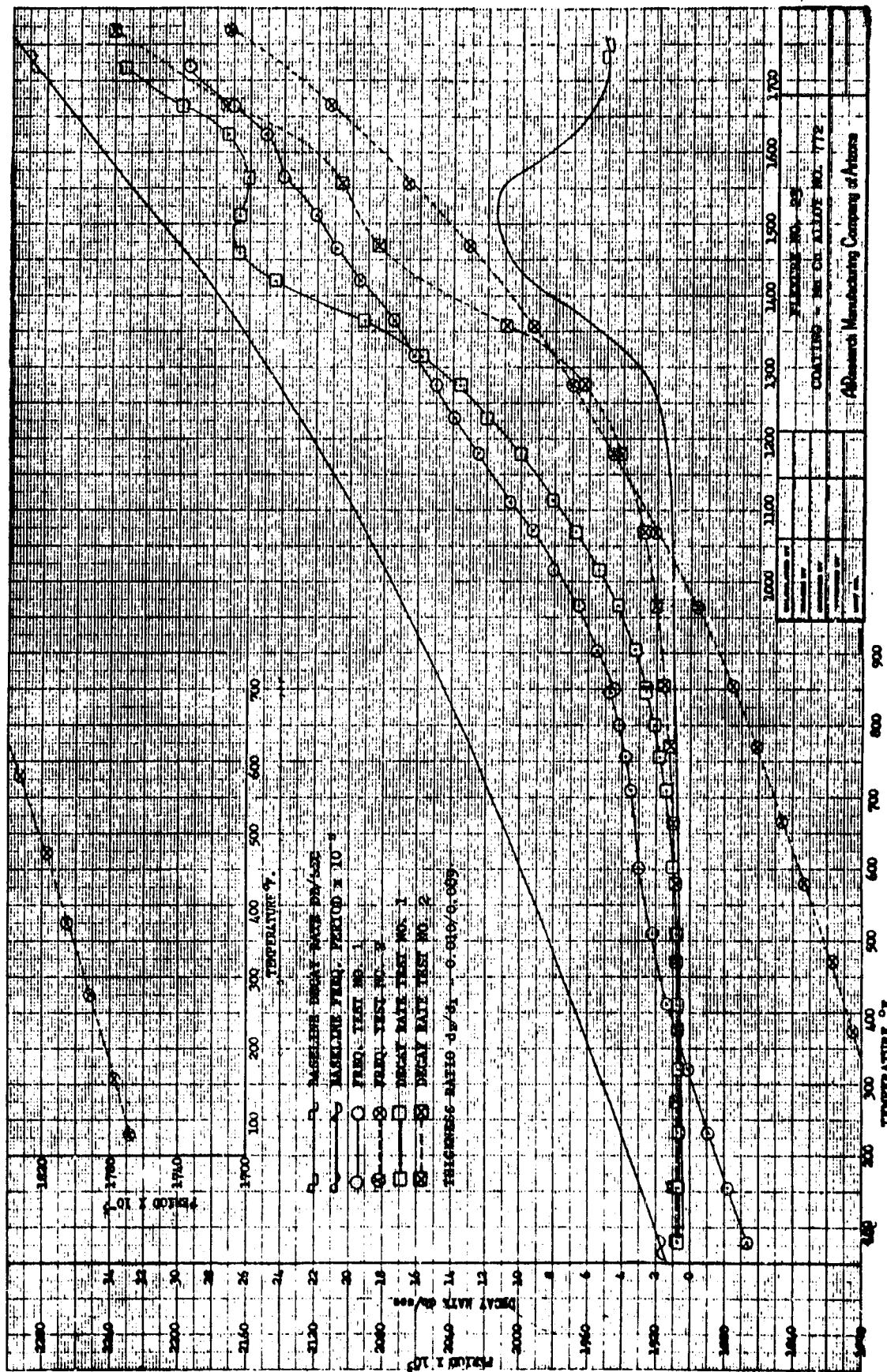


GT-7615-R  
Page 5-83



**AIRRESEARCH MANUFACTURING COMPANY OF ARIZONA**  
A DIVISION OF THE GANNETT CORPORATION

### GRAPH 5-8

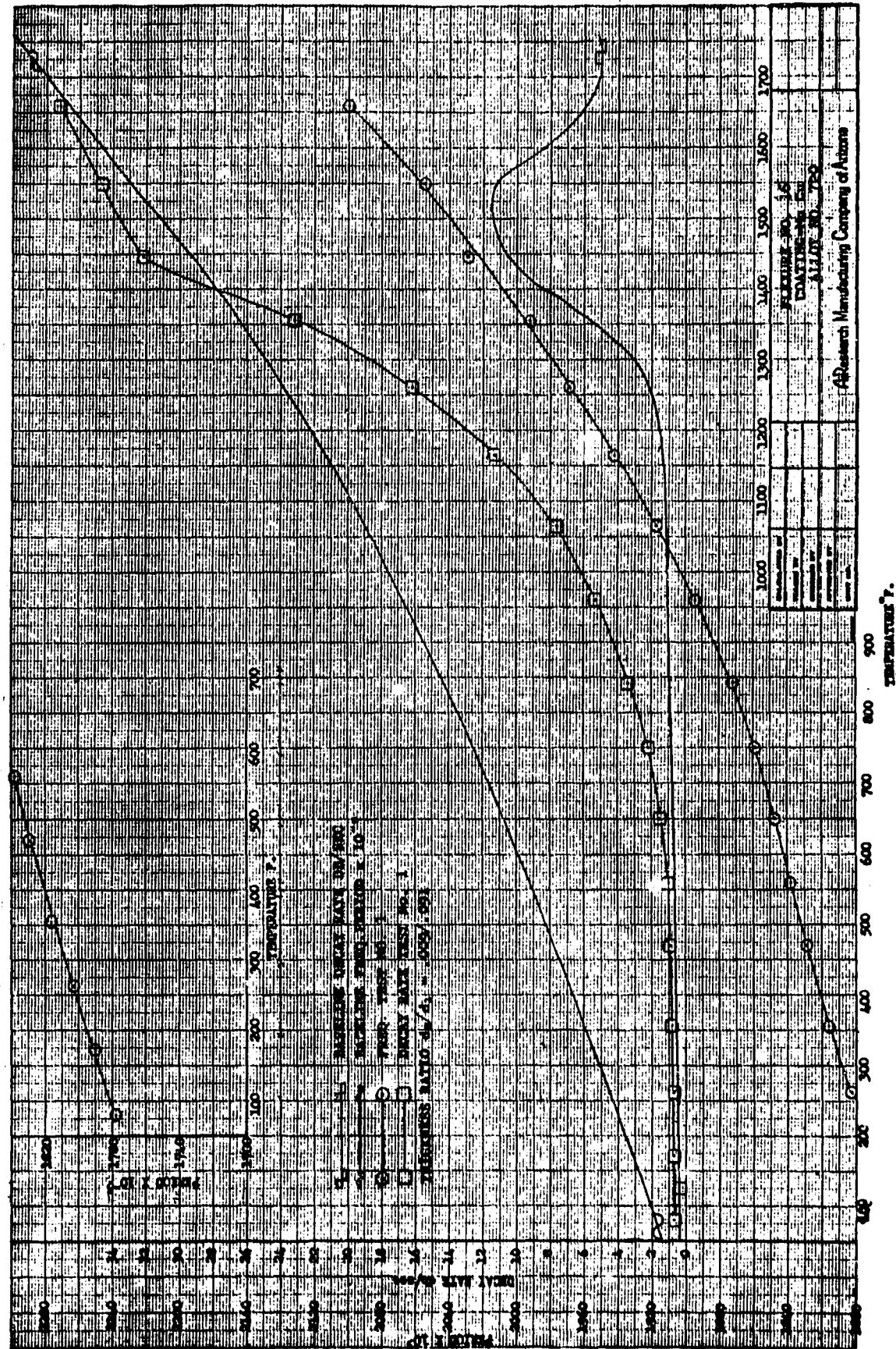


GT-7615-R  
Page 5-84

**AIRSEARCH MANUFACTURING COMPANY**  
A DIVISION OF THE BARRETT CORPORATION  
PHOENIX, ARIZONA



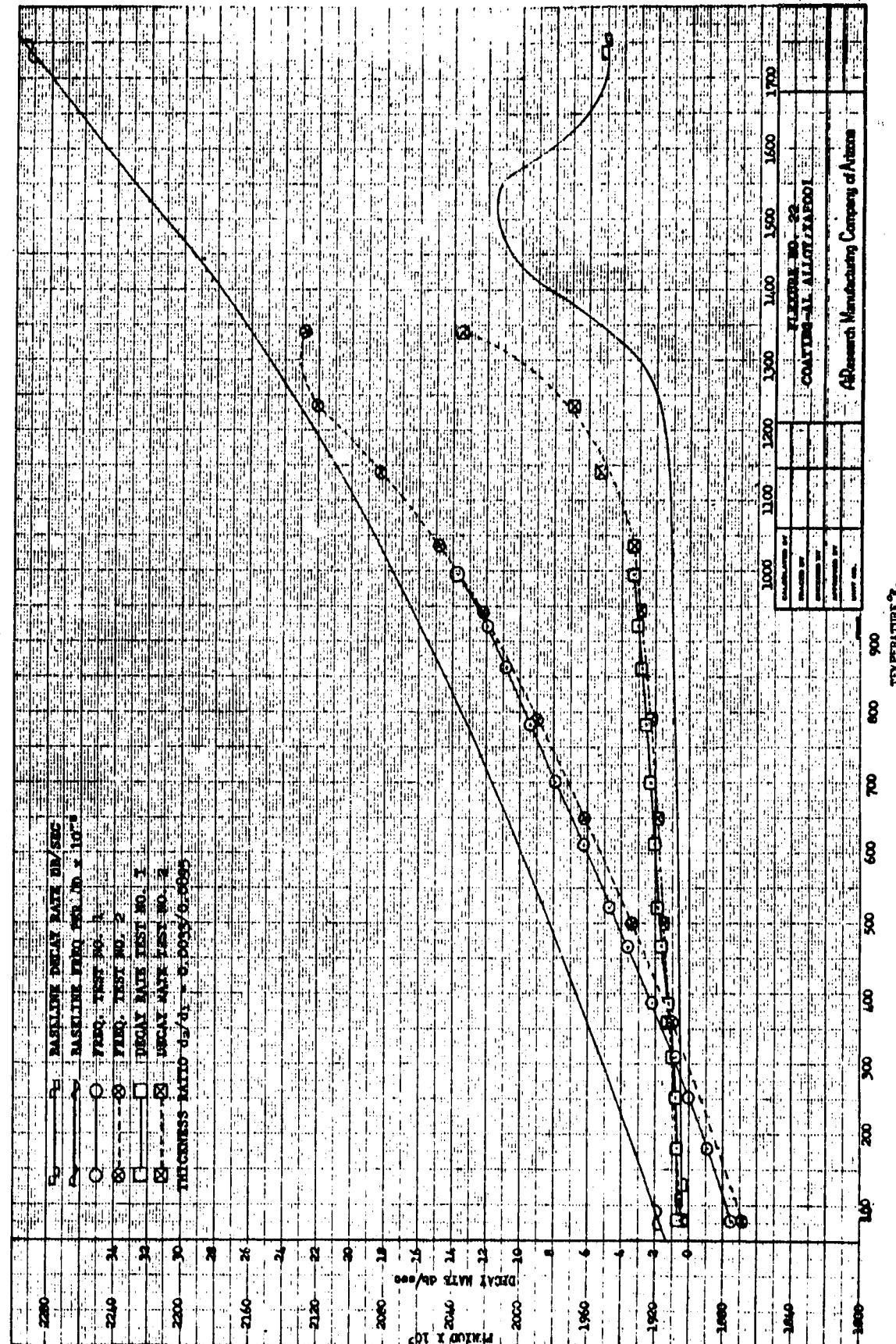
GRAPH 5-9



GT-7615-R  
Page 5-85



GRAPH 5-10

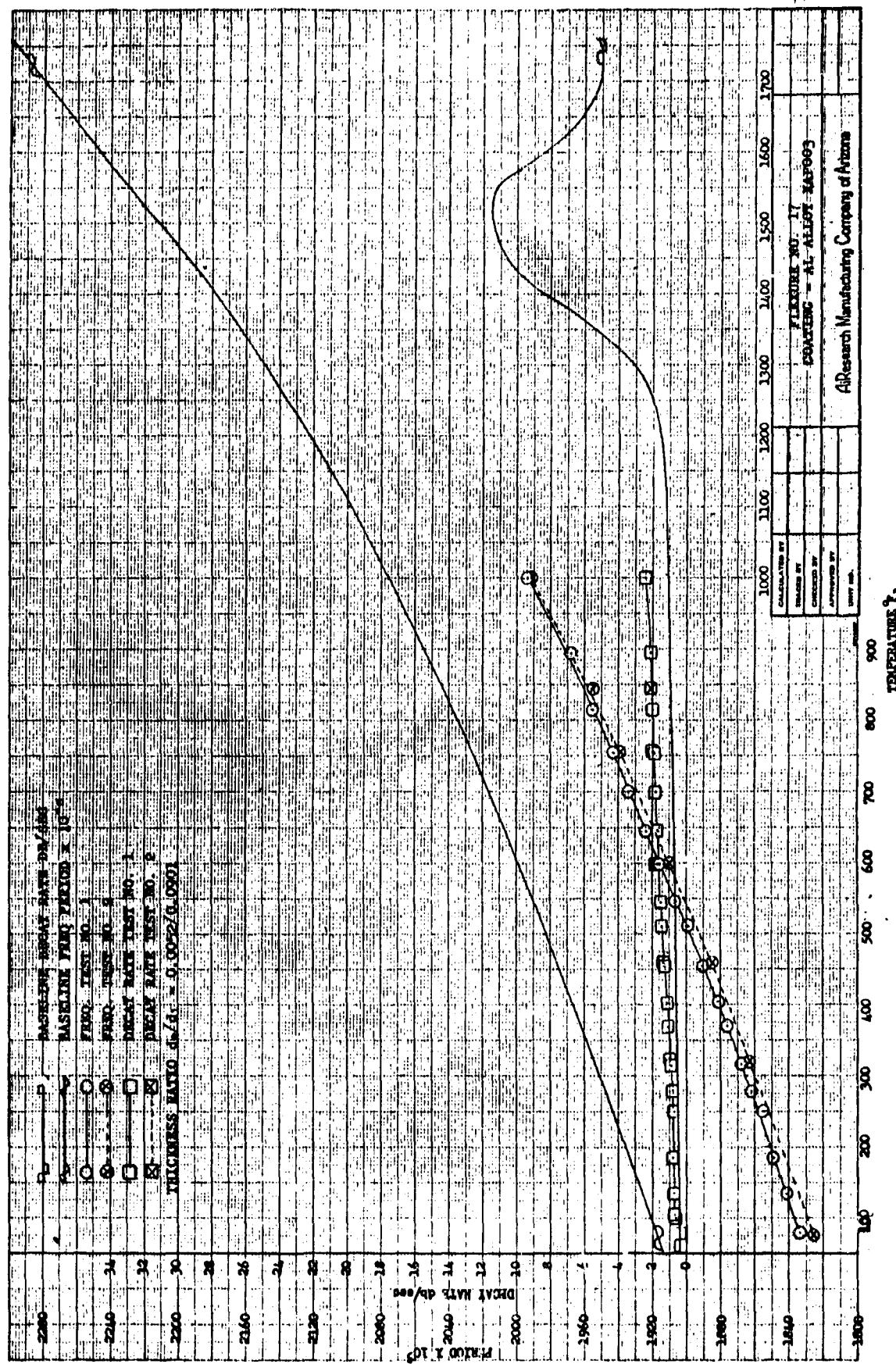


GT-7615-R  
 Page 5-86



**AIRESEARCH MANUFACTURING COMPANY OF ARIZONA**  
A DIVISION OF THE BARRETT CORPORATION

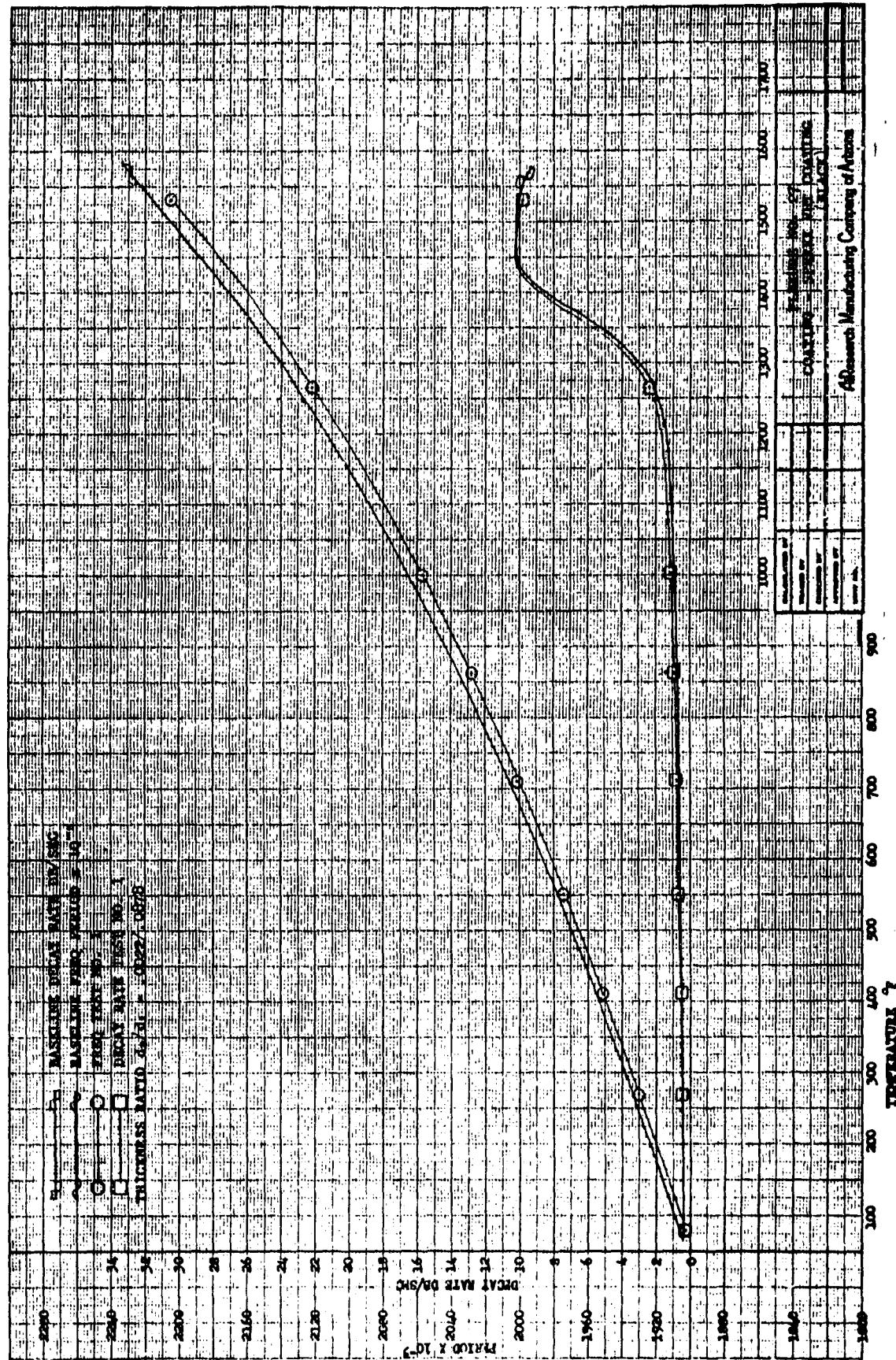
GRAPH 5-11



GT-7615-R  
Page 5-87



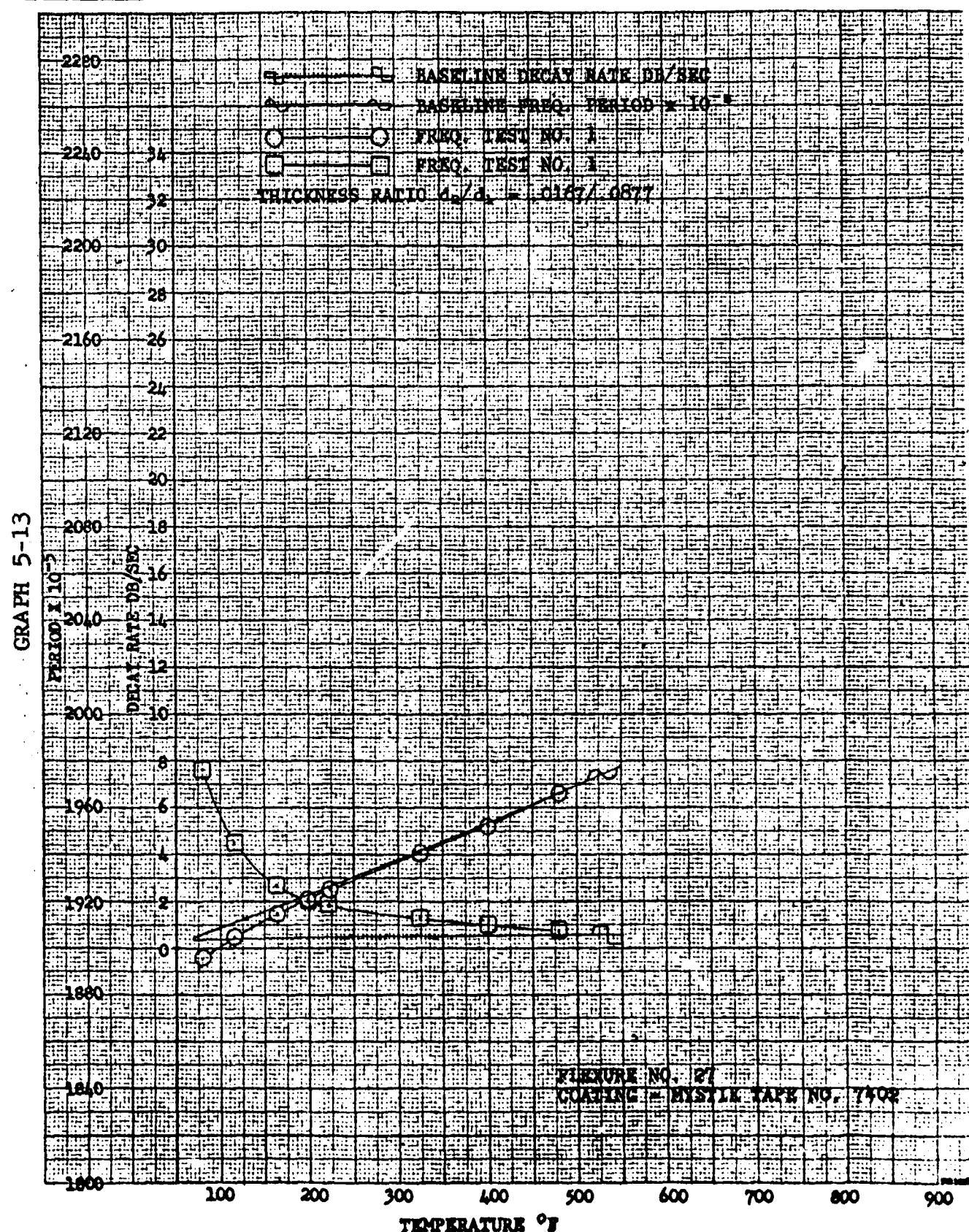
**GRAPH 5-12**



GT-7615-R  
 Page 5-88



**AIRESEARCH MANUFACTURING COMPANY OF ARIZONA**  
A DIVISION OF THE GARRETT CORPORATION  
PHOENIX, ARIZONA

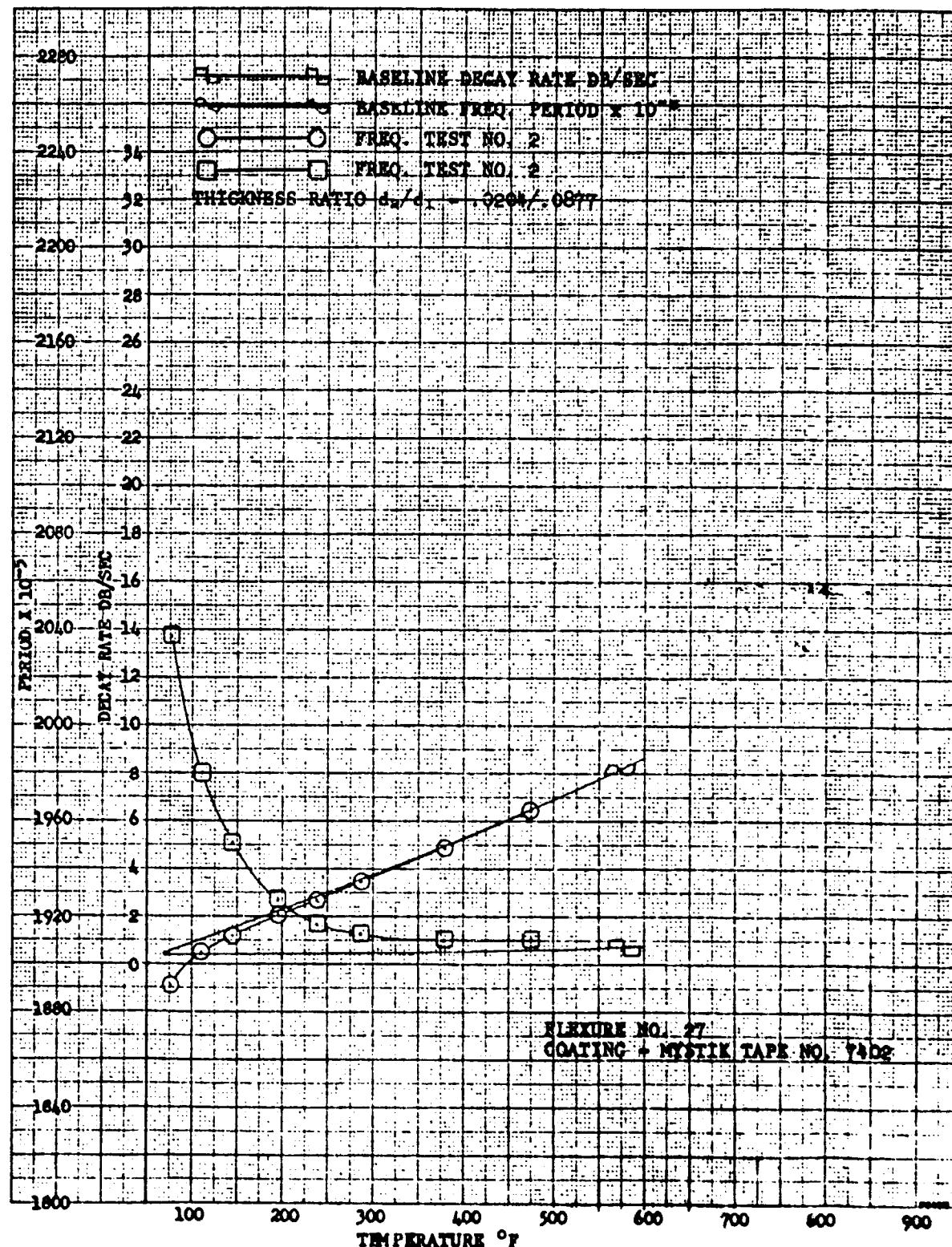


GT-7615-R  
Page 5-89



AIRESEARCH MANUFACTURING COMPANY OF ARIZONA  
A DIVISION OF THE GARRETT CORPORATION  
PHOENIX, ARIZONA

GRAPH 5-14



GT-7615-R  
Page 5-90



Figures 5-21 through 5-25 present samples of original decay rate recordings to illustrate their straightness or curvature. An essentially straight decay from the logarithmic level recorder indicates that the damping is independent of the strain level up to the maximum strain used (about 150 microinches per inch). Straight decays indicate quadratic damping such as is a result of viscoelastic and anelastic processes. The majority of decays recorded were straight; some tendency to deviate from straight-line decay was noted in manganese copper recordings. Also, some nonlinearity occurred in the case of the aluminum-foil silicone-adhesive constrained-layer damping test used to exemplify good organic damping treatment.

The important results of the test program are presented first in Figures 5-26 through 5-43, which are the printout sheets for the digital computer program, used to compute material parameters. These show both the inputs, as read from graphs 5-2 through 5-14, and the final computed data. Graphs 5-16 through 5-27 present the final data as  $E_2'$ ,  $E_2''$ , and  $\eta_2$ . This contains a redundancy, since only two of the three are strictly necessary to completely define the complex modulus. However, for different purposes, different pairs are most convenient, and the computer was available to spare the reader the task of computing the third. Not shown on these graphs, but appearing in the computer sheets, is the absolute value of  $E'$ . The phenomenological discussion of the test results centers mainly on the discussion of the variation of  $E_2'$ ,  $E_2''$  and  $\eta_2$  with temperature and choice of coating. Finally, certain comparisons among the test results are made, and comparison with the data of other observers is attempted where possible. Graphs 5-21 shows the  $E_2''$  for the four vitreous enamels plotted against percentages



AIRESEARCH MANUFACTURING COMPANY OF ARIZONA  
A DIVISION OF THE GARRETT CORPORATION  
PHOENIX, ARIZONA

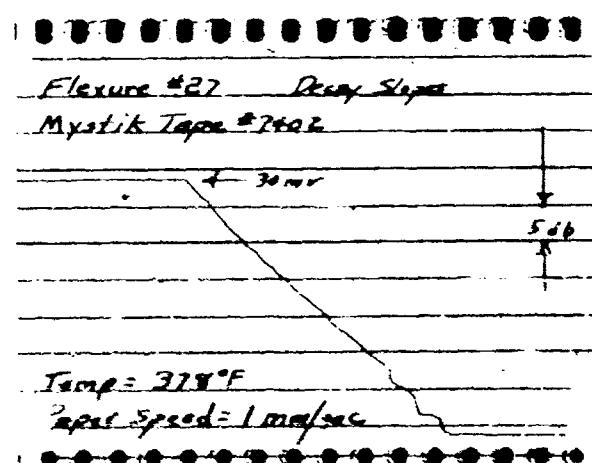
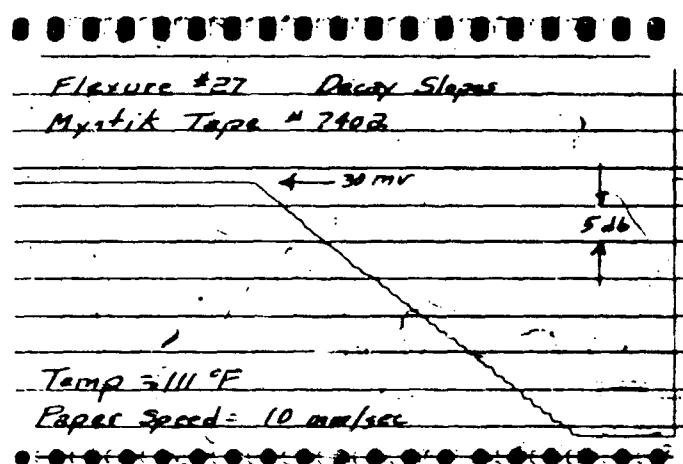
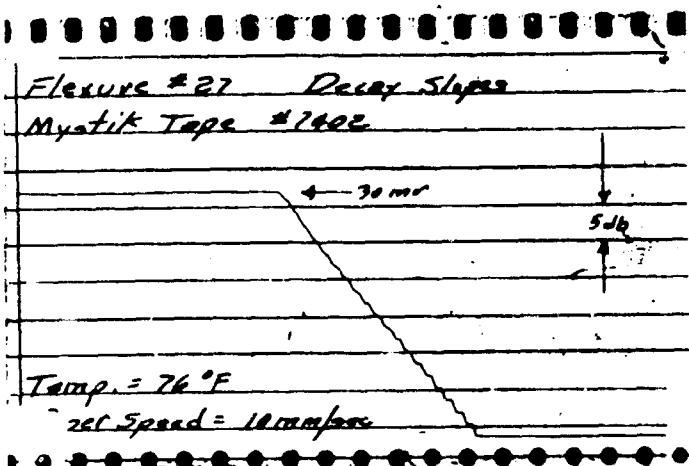


FIGURE 5-21

GT-7615-R  
Page 5-92



AIRESEARCH MANUFACTURING COMPANY OF ARIZONA  
A DIVISION OF THE GARRETT CORPORATION  
PHOENIX, ARIZONA

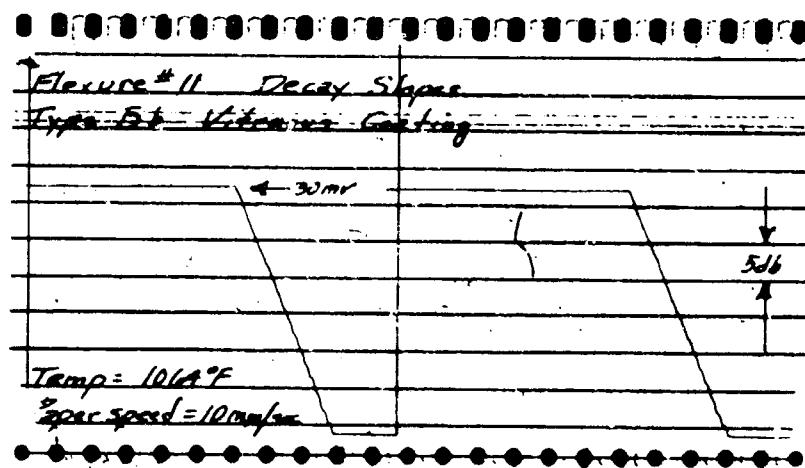
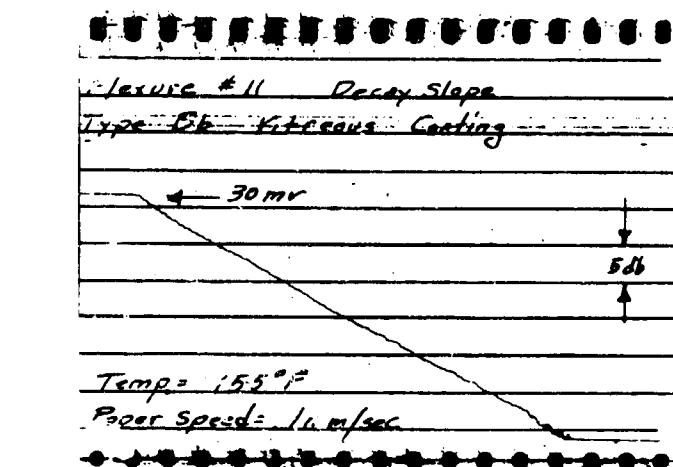
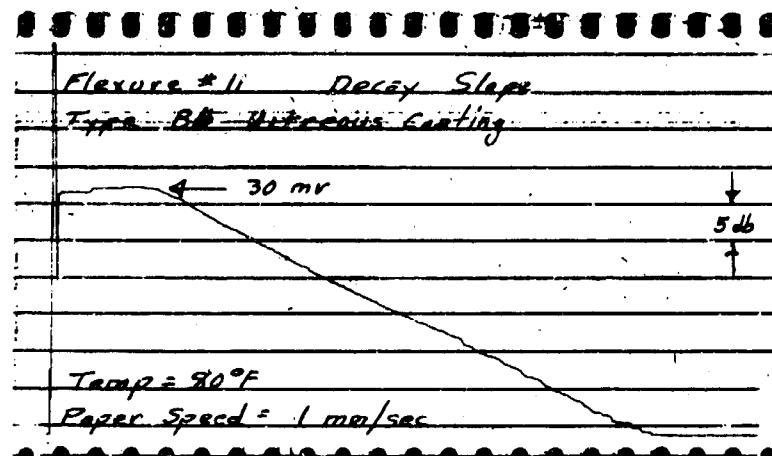


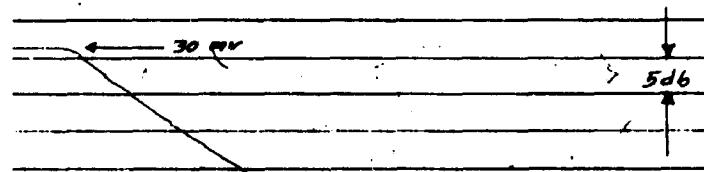
FIGURE 5-22

GT-7615-R  
Page 5-93



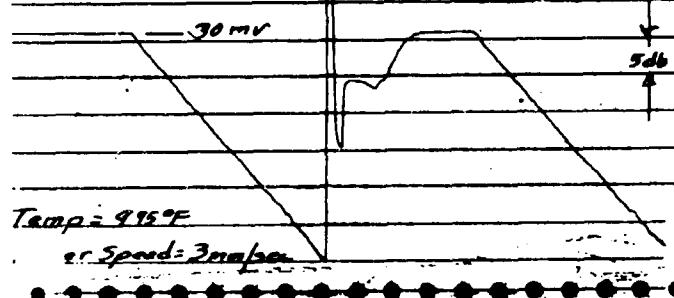
AIRESEARCH MANUFACTURING COMPANY OF ARIZONA  
A DIVISION OF THE GARRETT CORPORATION  
PHOENIX, ARIZONA

Flexure #22 Decay Slope  
Al Alloy XAP 001



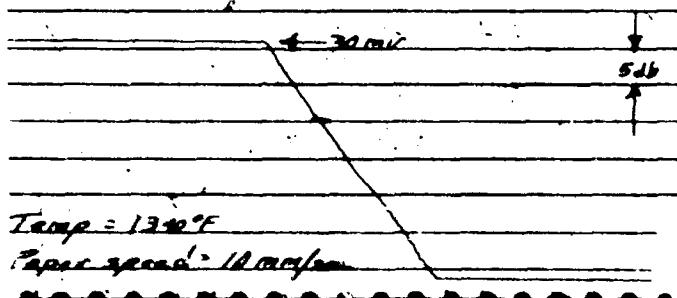
Temp = 78°F  
Paper Speed = 1 mil/sec

Flexure #22 Decay Slope  
Al Alloy XAP 001



Temp = 995°F  
Paper Speed = 3 mil/sec

Flexure #22 Decay Slope  
Al Alloy XAP 001



Temp = 1340°F  
Paper speed = 10 mil/sec

FIGURE 5-23

GT-7615-R  
Page 5-94



AIRESEARCH MANUFACTURING COMPANY OF ARIZONA  
A DIVISION OF THE GARRETT CORPORATION  
PHOENIX, ARIZONA

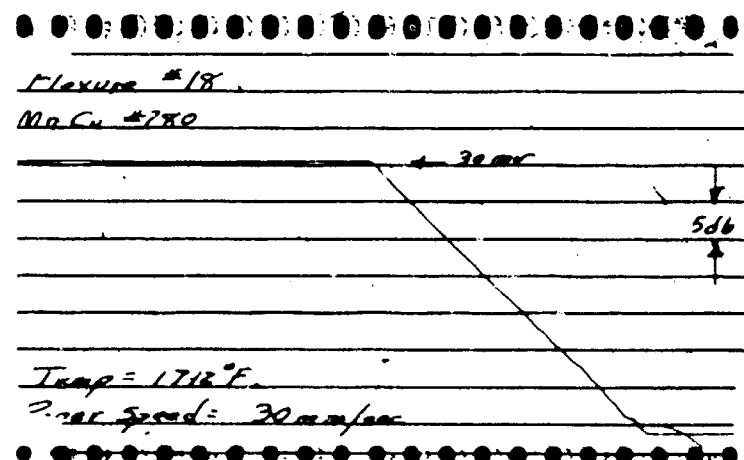
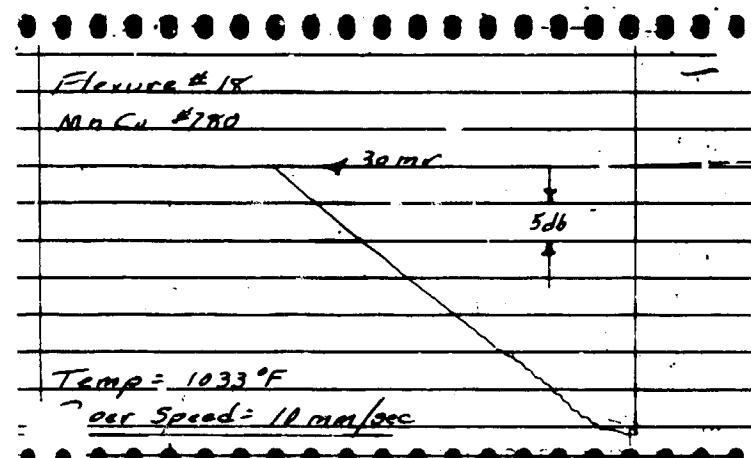
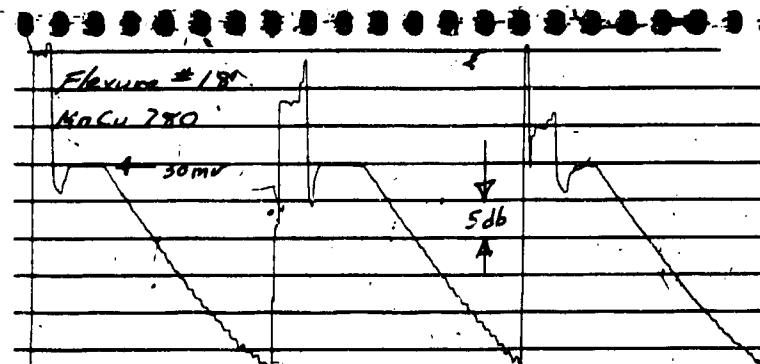


FIGURE 5-24

GT-7615-R  
Page 5-95



AIRESEARCH MANUFACTURING COMPANY OF ARIZONA  
A DIVISION OF THE GARRETT CORPORATION  
PHOENIX, ARIZONA

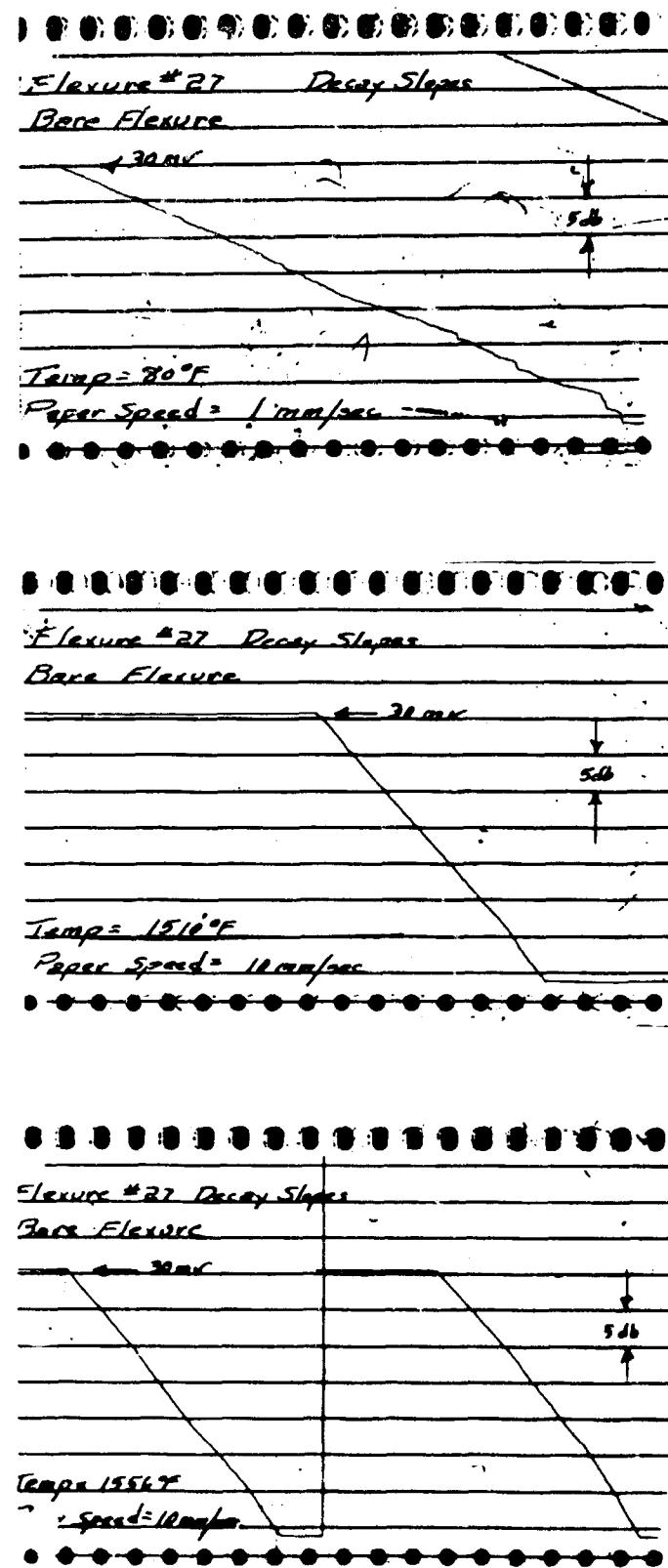


FIGURE 5-25

GT-7615-R  
Page 5-96

卷之三

EXCUSE NO. 6 SUBJECTS AND TYPES A

TEST 13: 1

GT-7615-R  
Page 5-97

FIGURE 5-26

## 1134 TEMPERATURE DATA FOR TEST 446324

## SHEAR AND IN COHESIVE STRENGTH TYPE 8

TEST NO. 1  
THICKNESS RATIO = 1.04343

T	2-12	2-1	T-1	T-12	E1-2	ETA-2	E-2P	E-2P
100.00000	0.019435	0.400000	0.550000	0.450000	0.001284	19.498061	0.025026	19.498076
200.00000	0.019565	0.450000	0.750000	0.600000	0.002443	19.379243	0.047337	19.378300
300.00000	0.019735	0.500000	1.300000	1.150000	0.006365	18.842774	0.119940	18.843156
400.00000	0.019890	0.600000	2.000000	1.850000	0.011473	17.862362	0.204937	17.863536
450.00000	0.019910	0.625000	2.100000	2.000000	0.012324	17.399853	0.214429	17.401174
500.00000	0.019940	0.650000	2.050000	2.000000	0.011949	16.933037	0.202338	16.934246
550.00000	0.019970	0.675010	2.000000	2.000000	0.011430	16.361129	0.190282	16.362236
590.00000	0.019970	0.700000	2.100000	2.000000	0.012382	16.116997	0.199554	16.118322
650.00000	0.019970	0.750000	2.450000	2.500000	0.015315	15.672798	0.240023	15.674636
700.00000	0.019970	0.800000	3.400000	3.000000	0.024235	14.937136	0.362020	14.941522
725.00000	0.020435	0.825000	4.600000	4.000000	0.036914	14.144709	0.520726	14.154291
750.00000	0.019755	0.850000	7.550000	7.900000	0.049533	13.164084	0.915301	13.195866
775.00000	0.019870	0.875000	11.550000	11.500000	0.122185	11.633296	1.446100	11.923319
800.00000	0.020380	0.900000	17.000000	24.400000	0.218165	9.896739	2.159117	10.129522
825.00000	0.020530	0.925000	23.100000	24.500000	0.427970	6.863952	2.937564	7.466132
850.00000	0.020325	0.120545	0.935000	23.400000	0.543740	5.441237	2.958617	6.193583
950.00000	0.020445	0.120680	0.950000	21.400000	0.350000	0.517362	3.267619	4.220267
975.00000	0.020640	0.120235	0.975000	14.200000	0.220000	1.395461	1.235846	1.712216
980.00000	0.020755	0.120780	1.000000	6.700000	0.070000	1.801267	0.407030	0.733170
985.00000	0.020820	0.120930	1.025000	3.000000	0.203515	0.161301	0.355446	0.390333

GT-7615-R  
Page 5-98

FIGURE 5-27

"SUSTAINABLE" INSTITUTE TYPES 9

THE JOURNAL OF CLIMATE

GT-7615-R  
Page 5-99

FIGURE 5-28

## FIGURE NO. 11 COATING TYPE VITREOUS TYPE 34

TEST NO. 11  
THICKNESS RATIO = 0.10939

T	a-12	2-1	T-1	T-12	E1-3	E1-2	E-2-3	E-2-2	E-2PP	F	a-E2
1.00	.000000	0.014700	0.019535	0.400000	0.450000	28.450000	0.000349	7.156055	0.003916	7.156056	
2.00	.000000	0.024935	0.019690	0.490000	0.500000	28.000000	0.000363	7.162466	0.004031	7.162467	
3.00	.000000	0.019543	0.019543	0.520000	0.600000	27.450000	0.000361	7.050250	0.004238	7.050251	
4.00	.000000	0.019995	0.019995	0.600000	0.700000	26.800000	0.001374	6.890829	0.007128	6.890833	
5.00	.000000	0.020155	0.020155	0.650000	0.750000	26.350000	0.001163	6.736257	0.007158	6.736260	
6.00	.000000	0.019440	0.020320	0.700000	0.800000	25.700000	0.001392	6.573217	0.007175	6.573221	
6.50	.000000	0.019225	0.020405	0.750000	1.000000	25.500000	0.002383	6.475407	0.015444	6.475426	
7.00	.000000	0.020495	0.020495	0.800000	1.200000	25.220000	0.003462	6.412963	0.023613	6.413006	
7.50	.000000	0.020590	0.020590	0.850000	1.300000	24.930000	0.004161	6.307989	0.026249	6.308042	
8.00	.000000	0.019800	0.020690	0.900000	1.500000	24.600000	0.005540	6.1669229	0.034170	6.1669324	
8.25	.000000	0.020735	0.020735	0.925000	1.600000	24.500000	0.006131	6.227179	0.038189	6.227296	
8.50	.000000	0.019890	0.020760	0.950000	1.700000	24.350000	0.006950	6.137911	0.042044	6.138055	
8.75	.000000	0.019660	0.020930	0.975000	1.800000	24.220000	0.009495	5.943647	0.056439	5.943915	
9.00	.000000	0.020980	0.020980	1.000000	2.000000	24.025000	0.011302	5.963987	0.067405	5.964366	
9.25	.000000	0.020700	0.020925	1.025000	2.900000	23.930000	0.017346	5.7366830	0.1006661	5.737713	
9.50	.000000	0.020980	0.020980	1.050000	4.000000	23.780000	0.026375	5.505401	0.156306	5.510618	
9.75	.000000	0.021030	0.021030	1.075000	5.450000	23.640000	0.044259	5.183404	0.229410	5.188478	
1.00	.000000	0.021055	0.021055	1.100000	9.300000	23.500000	0.059369	4.727105	0.425294	4.746198	
1.025	.000000	0.020500	0.021185	1.125000	1.125000	23.350000	0.165777	4.079405	0.676272	4.135081	
1.050	.000000	0.020855	0.021195	1.150000	21.200000	23.200000	0.316374	3.190662	1.017420	3.346950	
1.075	.000000	0.020150	0.021255	1.175000	23.600000	23.070000	0.516242	2.177507	1.125644	2.451247	
1.100	.000000	0.020940	0.021265	1.160000	23.800000	23.030000	0.608466	1.859978	1.132106	2.177426	
1.125	.000000	0.021165	0.021315	1.200000	20.000000	22.920000	1.036335	0.898216	0.930584	1.293359	
1.150	.000000	0.021290	0.021375	1.250000	12.600000	22.770000	1.131267	0.501914	0.567799	0.757835	
1.175	.000000	0.021395	0.021460	1.300000	6.800000	22.620000	1.024760	0.262426	0.266923	0.375746	
1.200	.000000	0.021480	0.021500	1.400000	4.200000	22.470000	1.181040	0.115334	0.136214	0.178483	
1.225	.000000	0.021550	0.021565	1.550000	3.500000	22.320000	1.103545	0.085634	0.094501	0.127529	
1.250	.000000	0.021620	0.021625	1.750000	3.500000	22.170000	2.957363	0.028254	0.034406	0.089010	
1.275	.000000	0.021690	0.021700	2.000000	3.700000	22.010000	1.461376	0.0555926	0.0996033	0.0996130	

## FLEXURE TESTS ON CANTILEVER BEAMS TYPE A

TEST NO. 1  
THICKNESS FATIGUE = 0.13390

T	2-12	2-1	T-1	T-12	E-12	E-1	E-2	E-20	E-2PP	E+2
100.00000	0.40000	0.45000	0.45000	0.45000	28.43000	0.001395	5.979061	0.009536	5.979068	5.979068
200.00000	0.40000	0.45000	0.45000	0.45000	25.00000	0.001396	5.966845	0.009581	5.966852	5.966852
300.00000	0.40000	0.45000	0.45000	0.45000	27.00000	0.001393	5.929233	0.009694	5.929241	5.929241
400.00000	0.40000	0.45000	0.45000	0.45000	26.80000	0.001214	5.760347	0.012462	5.760361	5.760361
500.00000	0.40000	0.45000	0.45000	0.45000	26.35000	0.001221	5.677526	0.012442	5.677540	5.677540
600.00000	0.40000	0.45000	0.45000	0.45000	25.70000	0.001375	5.467901	0.020525	5.467940	5.467940
650.00000	0.40000	0.45000	0.45000	0.45000	25.50000	0.001471	5.425273	0.025931	5.425335	5.425335
700.00000	0.40000	0.45000	0.45000	0.45000	25.00000	0.001632	5.340797	0.033939	5.340905	5.340905
750.00000	0.40000	0.45000	0.45000	0.45000	24.93000	0.001739	5.328217	0.041867	5.328381	5.328381
800.00000	0.40000	0.45000	0.45000	0.45000	24.64000	0.001926	5.352233	0.049696	5.352463	5.352463
825.00000	0.40000	0.45000	0.45000	0.45000	24.50000	0.010364	5.416467	0.038951	5.416728	5.416728
850.00000	0.40000	0.45000	0.45000	0.45000	24.35000	0.012359	5.407147	0.058044	5.407575	5.407575
875.00000	0.40000	0.45000	0.45000	0.45000	24.00000	0.014284	5.400589	0.077144	5.401139	5.401139
900.00000	0.40000	0.45000	0.45000	0.45000	24.00000	0.017122	5.496462	0.094113	5.497268	5.497268
925.00000	0.40000	0.45000	0.45000	0.45000	24.02500	0.023550	5.345657	0.126427	5.347152	5.347152
950.00000	0.40000	0.45000	0.45000	0.45000	24.90000	0.039315	5.087316	0.202567	5.091348	5.091348
975.00000	0.40000	0.45000	0.45000	0.45000	23.64000	0.072294	4.699564	0.339749	4.71829	4.71829
1000.00000	0.40000	0.45000	0.45000	0.45000	23.50000	0.130394	4.217980	0.552108	4.253960	4.253960
1025.00000	0.40000	0.45000	0.45000	0.45000	23.35000	0.232220	3.581582	0.831717	3.676885	3.676885
1050.00000	0.40000	0.45000	0.45000	0.45000	23.20000	0.413900	2.642519	1.093740	2.859926	2.859926
1065.00000	0.40000	0.45000	0.45000	0.45000	23.16000	0.544435	2.089780	1.136961	2.379046	2.379046
1075.00000	0.40000	0.45000	0.45000	0.45000	23.07000	0.758473	1.429094	1.053938	1.793664	1.793664
1100.00000	0.40000	0.45000	0.45000	0.45000	22.92000	0.956693	1.241297	0.740670	0.951123	0.951123
1125.00000	0.40000	0.45000	0.45000	0.45000	22.77000	1.712557	0.264972	0.453866	0.525499	0.525499
1150.00000	0.40000	0.45000	0.45000	0.45000	22.62000	2.05435	0.116429	0.239245	0.266071	0.266071
1172.00000	0.40000	0.45000	0.45000	0.45000	22.47000	-4.724121	-0.429783	0.135976	0.138949	0.138949

GT-7615-R  
Page 5-101

FIGURE 5-30

HIGH TEMPERATURE CERAMIC TEST PROGRAM

FIGURE VI. 12 - G-111. TYPE C VITREOUS

TEST NO. 1

THICKNESS RATIO = 0.84345

	T-12	T-1	T-1	T-12	E1-2	E1-2	E-23	E-23	E-2PP	□	△	○	◆
780.000000	0.019870	1.0201590	0.800000	0.900000	25.220000	0.001739	9.381409	0.016316	9.381423				
759.000000	0.020445	0.020445	0.850000	1.101000	24.930000	0.003425	9.321095	0.036582	9.321167				
089.000000	0.120345	0.120345	0.900000	1.305000	24.640000	0.005353	9.527236	0.056720	9.527405				
056.000000	0.120278	0.120278	0.950000	1.305000	24.350000	0.005265	9.464369	0.049843	9.464490				
086.000000	0.120575	0.120575	1.000000	2.000000	24.070000	0.013321	9.749936	0.135729	9.750660				
086.000000	0.120775	0.120775	1.075000	2.707000	23.750000	0.021498	10.106910	0.220618	10.109317				
054.000000	0.020270	0.020270	1.075000	2.550000	23.500000	0.018375	10.193330	0.193423	10.195165				
084.000000	0.020350	0.020350	1.100000	2.200000	2.200000	0.013900	10.178237	0.140448	10.178206				
105.000000	0.020440	0.020440	1.150000	2.105000	2.105000	0.011345	10.06401	0.120424	10.061120				
118.000000	0.020570	0.020570	1.200000	2.250000	2.250000	0.012764	9.890886	0.126238	9.890692				
115.000000	0.020265	0.020265	1.300000	2.300000	2.300000	0.019594	9.619381	0.189440	9.621246				
120.000000	0.020270	0.020270	1.350000	2.320000	2.320000	0.019594	9.619381	0.189440	9.621246				
129.000000	0.020270	0.020270	1.400000	2.350000	2.350000	0.044198	9.957845	0.395921	9.966590				
127.000000	0.021350	0.021350	1.450000	2.450000	2.450000	0.071724	8.558978	0.613888	8.560965				
136.000000	0.021270	0.021270	1.500000	2.500000	2.500000	0.120554	9.012690	0.965966	9.012706				
132.000000	0.021290	0.021290	1.500000	2.500000	2.500000	0.192303	7.184280	1.381594	7.315920				
139.000000	0.021470	0.021470	1.550000	2.550000	2.550000	0.317755	6.150805	1.954451	6.453858				
129.000000	0.021350	0.021350	1.550000	2.550000	2.550000	0.450921	4.800082	2.164460	5.265518				
127.000000	0.021350	0.021350	1.600000	2.600000	2.600000	0.645590	3.138291	2.026362	3.735641				
136.000000	0.022210	0.022210	1.650000	2.650000	2.650000	0.950709	1.742721	1.534828	2.322234				
132.000000	0.022210	0.022210	1.700000	2.700000	2.700000	0.974249	0.990859	0.965342	1.363361				
139.000000	0.022215	0.022215	1.750000	2.750000	2.750000	0.600000	1.238561	0.645150	0.629181				
129.000000	0.022215	0.022215	1.800000	2.800000	2.800000	0.450921	2.156771	0.417760	0.46104				
127.000000	0.022215	0.022215	1.850000	2.850000	2.850000	0.729000	2.214223	0.127003	0.281214				
136.000000	0.022215	0.022215	1.900000	2.900000	2.900000	1.140000	1.303279	0.125988	0.163676				
132.000000	0.022215	0.022215	1.950000	2.950000	2.950000	1.300000	1.313164	0.124156	0.163037				
139.000000	0.022215	0.022215	2.000000	3.000000	2.000000	1.000000	1.301164	0.061299	0.202358				
129.000000	0.022215	0.022215	2.050000	3.050000	2.050000	1.200000	1.300000	0.060564	0.207240				
127.000000	0.022215	0.022215	2.100000	3.100000	2.100000	1.400000	1.299000	0.059835	0.171977				
136.000000	0.022215	0.022215	2.150000	3.150000	2.150000	1.600000	1.298000	0.059124	0.125570				
132.000000	0.022215	0.022215	2.200000	3.200000	2.200000	1.800000	1.297000	0.029214	0.136211				
139.000000	0.022215	0.022215	2.250000	3.250000	2.250000	2.000000	1.296000	0.028913	0.180814				
129.000000	0.022215	0.022215	2.300000	3.300000	2.300000	2.200000	1.295000	0.028913	0.180814				
127.000000	0.022215	0.022215	2.350000	3.350000	2.350000	2.400000	1.294000	0.028913	0.180814				
136.000000	0.022215	0.022215	2.400000	3.400000	2.400000	2.600000	1.293000	0.028913	0.180814				
132.000000	0.022215	0.022215	2.450000	3.450000	2.450000	2.800000	1.292000	0.028913	0.180814				
139.000000	0.022215	0.022215	2.500000	3.500000	2.500000	3.000000	1.291000	0.028913	0.180814				
129.000000	0.022215	0.022215	2.550000	3.550000	2.550000	3.200000	1.290000	0.028913	0.180814				
127.000000	0.022215	0.022215	2.600000	3.600000	2.600000	3.400000	1.289000	0.028913	0.180814				
136.000000	0.022215	0.022215	2.650000	3.650000	2.650000	3.600000	1.288000	0.028913	0.180814				
132.000000	0.022215	0.022215	2.700000	3.700000	2.700000	3.800000	1.287000	0.028913	0.180814				
139.000000	0.022215	0.022215	2.750000	3.750000	2.750000	4.000000	1.286000	0.028913	0.180814				
129.000000	0.022215	0.022215	2.800000	3.800000	2.800000	4.200000	1.285000	0.028913	0.180814				
127.000000	0.022215	0.022215	2.850000	3.850000	2.850000	4.400000	1.284000	0.028913	0.180814				
136.000000	0.022215	0.022215	2.900000	3.900000	2.900000	4.600000	1.283000	0.028913	0.180814				
132.000000	0.022215	0.022215	2.950000	3.950000	2.950000	4.800000	1.282000	0.028913	0.180814				
139.000000	0.022215	0.022215	3.000000	4.000000	3.000000	5.000000	1.281000	0.028913	0.180814				
129.000000	0.022215	0.022215	3.050000	4.050000	3.050000	5.200000	1.280000	0.028913	0.180814				
127.000000	0.022215	0.022215	3.100000	4.100000	3.100000	5.400000	1.279000	0.028913	0.180814				
136.000000	0.022215	0.022215	3.150000	4.150000	3.150000	5.600000	1.278000	0.028913	0.180814				
132.000000	0.022215	0.022215	3.200000	4.200000	3.200000	5.800000	1.277000	0.028913	0.180814				
139.000000	0.022215	0.022215	3.250000	4.250000	3.250000	6.000000	1.276000	0.028913	0.180814				
129.000000	0.022215	0.022215	3.300000	4.300000	3.300000	6.200000	1.275000	0.028913	0.180814				
127.000000	0.022215	0.022215	3.350000	4.350000	3.350000	6.400000	1.274000	0.028913	0.180814				
136.000000	0.022215	0.022215	3.400000	4.400000	3.400000	6.600000	1.273000	0.028913	0.180814				
132.000000	0.022215	0.022215	3.450000	4.450000	3.450000	6.800000	1.272000	0.028913	0.180814				
139.000000	0.022215	0.022215	3.500000	4.500000	3.500000	7.000000	1.271000	0.028913	0.180814				
129.000000	0.022215	0.022215	3.550000	4.550000	3.550000	7.200000	1.270000	0.028913	0.180814				
127.000000	0.022215	0.022215	3.600000	4.600000	3.600000	7.400000	1.269000	0.028913	0.180814				
136.000000	0.022215	0.022215	3.650000	4.650000	3.650000	7.600000	1.268000	0.028913	0.180814				
132.000000	0.022215	0.022215	3.700000	4.700000	3.700000	7.800000	1.267000	0.028913	0.180814				
139.000000	0.022215	0.022215	3.750000	4.750000	3.750000	8.000000	1.266000	0.028913	0.180814				
129.000000	0.022215	0.022215	3.800000	4.800000	3.800000	8.200000	1.265000	0.028913	0.180814				
127.000000	0.022215	0.022215	3.850000	4.850000	3.850000	8.400000	1.264000	0.028913	0.180814				
136.000000	0.022215	0.022215	3.900000	4.900000	3.900000	8.600000	1.263000						

FIGURE 5-32 FLEXURE IN. 42 STAINLESS STEEL TYPE C

FLEXURE IN. 42 STAINLESS STEEL TYPE C  
THICKNESS RATIO = 0.04545

T	2-12	2-1	T-1	T-12	E1-2	E1-2	E-22	E-2PP	E-2
975.000000	0.020723	0.975000	0.975000	24.220000	13.825544	13.825545	0.005014	13.825545	13.825545
900.000000	0.020725	1.000000	1.000000	24.070000	13.796271	13.796272	0.005143	13.796272	13.796272
850.000000	0.020724	1.050000	1.050000	23.750000	13.656717	13.656722	0.011999	13.656722	13.656722
1000.000000	0.020725	1.050000	1.050000	23.500000	13.336372	13.336372	0.018685	13.336372	13.336372
1050.000000	0.020725	1.100000	1.100000	23.000000	13.400545	13.400545	0.025247	13.400545	13.400545
1100.000000	0.020725	1.150000	1.150000	23.000000	13.003123	13.003123	0.038161	12.600912	12.600912
1150.000000	0.020725	1.200000	1.200000	22.620000	12.599943	12.599943	0.031066	12.194693	12.194693
1200.000000	0.020725	1.300000	1.300000	22.620000	12.034189	12.034189	0.031066	12.034189	12.034189
1250.000000	0.020725	1.550000	1.550000	22.320000	9.010355	11.714478	0.128095	11.715178	11.715178
1295.000000	0.020725	2.000000	2.000000	22.010000	9.030923	10.922032	0.336650	10.922032	10.922032
1375.000000	0.020725	2.450000	2.450000	21.980000	9.035504	10.419127	0.581434	10.419127	10.419127
1390.000000	0.020725	3.100000	3.100000	21.700000	9.039542	9.767929	0.973298	9.767929	9.767929
1320.000000	0.020725	4.000000	4.000000	21.530000	9.015733	9.83446	0.391346	9.83446	9.83446
1350.000000	0.020725	5.350000	5.350000	21.200000	21.380000	7.766124	1.967861	8.011564	8.011564
1375.000000	0.020725	6.213547	6.213547	21.240000	9.037953	4.451749	2.180390	6.810224	6.810224
1400.000000	0.020725	8.350000	8.350000	21.070000	9.046359	5.027103	2.045219	5.42217	5.42217
1425.000000	0.020725	9.700000	9.700000	20.920000	9.043259	5.585531	1.551454	5.906795	5.906795
1450.000000	0.020725	10.650000	10.650000	20.770000	9.036173	2.529921	0.976948	2.712012	2.712012
1475.000000	0.020725	11.150000	11.150000	20.600000	9.0312197	2.10557	0.655788	2.200544	2.200544
1500.000000	0.020725	12.2225	12.2225	20.450000	9.025345	1.683956	0.426880	1.737221	1.737221
1525.000000	0.020725	12.2225	12.2225	20.290000	9.022521	1.277722	0.287765	1.309726	1.309726
1550.000000	0.020725	12.2225	12.2225	20.140000	9.019938	0.882645	0.167601	0.98417	0.98417
1575.000000	0.020725	12.2225	12.2225	19.990000	9.01241367	0.684974	0.155656	0.704653	0.704653
1600.000000	0.020725	12.2225	12.2225	19.820000	9.0145359	0.491530	0.204162	0.532244	0.532244

FIGURE 5-32

卷之三

TEST NO. 1  
THICKNESS EATION = 0.05597  
EXPOSURE = 241524 (APRIL 1974)

GT-7615-R  
Page 5-10

FIGURE 5-33

HIGH TENSILE - 3E LAMINATE TEST 2-03-A4

FLEXURE NO. 22 SCATTERING FREQ 4.224Y 291526 (XAPRINT) TWST A7.2  
THICKNESS AT 12 = 0.035637

	2-12	2-1	1	T-12	E1-2	E1-2	E-22	E-2PP	E-2
80.00000	0.0124601	0.0124718	0.0124718	0.4000000	0.5900000	28.4500000	0.06225	15.136950	0.035817
100.00000	0.0124715	0.0124715	0.0124715	0.4000000	0.5900000	28.4500000	0.062593	13.295855	0.035874
200.00000	0.0124715	0.0124715	0.0124715	0.4500000	0.5500000	28.0000000	0.062593	12.983755	0.035874
300.00000	0.0124715	0.0124715	0.0124715	0.5500000	1.0000000	27.4500000	0.065344	12.756295	0.031437
400.00000	0.0124717	0.0124717	0.0124717	0.5500000	1.3000000	26.8500000	0.061025	12.009987	0.123617
500.00000	0.0124717	0.0124717	0.0124717	0.5500000	1.3000000	26.3400000	0.013565	11.663369	0.158230
600.00000	0.0124720	0.0124720	0.0124720	0.5500000	1.7000000	25.7500000	0.016462	10.952150	0.179615
700.00000	0.0124715	0.0124715	0.0124715	0.5500000	2.0000000	25.2200000	0.016319	10.153142	0.202245
800.00000	0.0124715	0.0124715	0.0124715	0.5500000	2.3500000	24.6400000	0.025365	9.423572	0.240278
900.00000	0.0124715	0.0124715	0.0124715	0.5500000	2.7500000	24.0700000	0.031474	9.957815	0.295523
1000.00000	0.0124715	0.0124715	0.0124715	0.5500000	3.1000000	23.5000000	0.043753	7.609951	0.332995
1100.00000	0.0124715	0.0124715	0.0124715	0.5500000	4.2000000	22.9200000	0.030440	5.642897	0.453913
1200.00000	0.0124715	0.0124715	0.0124715	0.5500000	6.2000000	22.3200000	0.232119	3.051463	5.661124
1300.00000	0.0124715	0.0124715	0.0124715	0.5500000	10.2000000	21.7000000	0.333269	3.209892	1.059855
1400.00000	0.0124715	0.0124715	0.0124715	0.8500000	13.5000000	21.4500000	0.232519	5.631064	1.309312

GT-7615-R  
Page 5-105

FIGURE 5-34

HIGH TEMPERATURE COATING TEST 242744

FIGURE 10. 17 COATING TYPE AL 4-LJN 230483 (XAP0r3) THICKNESS RATIO : 0.02771 TEST NO. 1

T	T-12	T-1	T-1	T-12	E1-a	ETA-2	E-2a	E-2PP	E-2
100.00000	0.013870	0.0119210	0.400700	0.650000	28.450000	0.002112	14.533194	0.030551	14.533226
200.00000	0.015310	0.0119355	0.450000	0.750000	28.000000	0.002535	14.276103	0.036198	14.279149
300.00000	0.018655	0.0119510	0.550000	0.850000	27.430000	0.003281	14.055435	0.036277	14.055482
400.00000	0.018610	0.0119555	0.600000	1.000000	26.880000	0.004302	13.484510	0.058008	13.484635
500.00000	0.019820	0.0119325	0.650000	1.400000	26.340000	0.0016475	13.092688	0.04770	13.092962
575.00000	0.019070	0.0119305	0.675000	1.550000	26.050000	0.0032475	12.730349	0.097762	12.730715
650.00000	0.019160	0.0119990	0.700000	1.600000	25.770000	0.008011	12.455451	0.099786	12.456651
650.00000	0.019245	0.020250	0.750000	1.700000	25.590464	0.0095776	20.637204	0.144517	22.433481
700.00000	0.019335	0.020165	0.800000	1.800000	25.220000	0.009165	12.077943	0.109483	12.078439
725.00000	0.019380	0.020210	0.825000	1.950000	25.090000	0.0094334	11.982423	0.111849	11.982945
750.00000	0.019425	0.020255	0.850000	2.000000	24.930000	0.0119605	11.882586	0.114148	11.883136
775.00000	0.019470	0.020370	0.675000	1.950000	24.790000	0.0092340	11.787979	0.11788555	11.788666
800.00000	0.019307	0.020350	0.900000	2.000000	24.640000	0.010161	11.686016	0.118746	11.686619
825.00000	0.019370	0.020393	0.925000	2.030000	24.500000	0.010343	11.538054	0.119192	11.538675
850.00000	0.019390	0.020450	0.950000	2.067000	24.350000	0.010371	11.562055	0.119910	11.562677
875.00000	0.019510	0.020493	0.975000	2.100000	24.220000	0.0103623	11.327347	0.120334	11.327996
900.00000	0.019570	0.020550	1.000000	2.150000	24.070000	0.010954	11.297519	0.122620	11.298184
925.00000	0.019770	0.020500	1.025000	2.200000	23.930000	0.011145	11.242818	0.124656	11.235513
950.00000	0.019825	0.020450	1.050000	2.250000	23.790000	0.011505	11.032840	0.126947	11.033970
975.00000	0.019860	0.020700	1.075000	2.350000	23.640000	0.012343	10.869362	0.134162	10.870130
1000.00000	0.019340	0.020755	1.100000	2.450000	23.500000	0.013204	10.704768	0.141344	10.705702

GT-7615-R  
Page 5-106

FIGURE 5-35

FIGURE 5-36. 2-D STRESSING TABLE FOR ALLOY 231423 ((YAPJ03))  
THICKNESS RATIO = 7.05771 TEST NO. 11

T	E-12	E-1	T-1	T-12	E-1	E-12	E-1								
100.	0.00300	0.01192210	0.410000	0.630000	28.450000	6.011327	16.022675	0.030875	16.022704	0.036521	15.950842	0.036558	15.026545	0.036558	15.026545
200.	0.00300	0.0119365	0.450000	0.750000	28.450000	6.011327	15.530793	0.032143	15.530793	0.036521	15.950842	0.036558	15.026545	0.036558	15.026545
300.	0.00300	0.0119510	0.550000	0.830000	27.450000	5.032433	15.026501	0.034145	14.425903	0.058364	14.426021	0.058364	14.426021	0.058364	14.426021
400.	0.00300	0.0119555	0.600000	0.910000	26.290000	6.011327	14.006166	0.056214	14.006166	0.056214	14.006425	0.056214	14.006425	0.056214	14.006425
500.	0.00300	0.0119325	0.650000	1.400000	26.340000	6.011327	13.629213	0.098187	13.629213	0.098187	13.628568	0.098187	13.628568	0.098187	13.628568
551.	0.00300	0.0119325	0.675000	1.550000	26.650000	6.011327	13.420369	0.106327	13.420369	0.106327	13.420743	0.106327	13.420743	0.106327	13.420743
500.	0.00300	0.0119305	0.700000	1.600000	25.770000	5.037175	13.007070	0.034300	13.007070	0.034300	13.007561	0.034300	13.007561	0.034300	13.007561
500.	0.00300	0.0119105	0.700000	1.600000	25.500000	5.037175	12.777674	0.035505	12.777674	0.035505	12.778146	0.035505	12.778146	0.035505	12.778146
550.	0.00300	0.0119195	0.720750	1.750100	25.500000	5.037175	12.599154	0.035311	12.599154	0.035311	12.599654	0.035311	12.599654	0.035311	12.599654
700.	0.00300	0.0119290	0.800000	1.800000	25.220000	5.037175	12.392222	0.039222	12.392222	0.039222	12.417973	0.039222	12.417973	0.039222	12.417973
725.	0.00300	0.0119340	0.820210	1.825000	25.090000	5.037175	12.319500	0.039495	12.319500	0.039495	12.319554	0.039495	12.319554	0.039495	12.319554
750.	0.00300	0.0119360	0.820255	1.850000	24.930000	5.037175	12.319500	0.039495	12.319500	0.039495	12.319554	0.039495	12.319554	0.039495	12.319554
775.	0.00300	0.0119475	0.820300	1.950000	24.790000	5.037175	12.319500	0.039495	12.319500	0.039495	12.319554	0.039495	12.319554	0.039495	12.319554
900.	0.00300	0.0119485	0.820450	2.000000	24.640000	5.037175	12.211962	0.039753	12.211962	0.039753	12.212443	0.039753	12.212443	0.039753	12.212443
900.	0.00300	0.0119485	0.820450	2.000000	24.640000	5.037175	12.191241	0.039753	12.191241	0.039753	12.191241	0.039753	12.191241	0.039753	12.191241
925.	0.00300	0.0119545	0.820595	2.025000	24.500000	5.037175	11.964590	0.039790	11.964590	0.039790	11.965167	0.039790	11.965167	0.039790	11.965167
450.	0.00300	0.0119590	0.820450	2.050000	24.350000	5.037175	11.931199	0.016373	11.931199	0.016373	11.931793	0.016373	11.931793	0.016373	11.931793
475.	0.00300	0.0119615	0.820495	2.075000	24.220000	5.037175	11.693049	0.016313	11.693049	0.016313	11.693662	0.016313	11.693662	0.016313	11.693662
500.	0.00300	0.0119695	0.820350	2.100000	24.070000	5.037175	11.660126	0.016545	11.660126	0.016545	11.660773	0.016545	11.660773	0.016545	11.660773
525.	0.00300	0.0119752	0.820500	2.125000	2.200000	5.037175	11.490996	0.016485	11.490996	0.016485	11.490996	0.016485	11.490996	0.016485	11.490996
550.	0.00300	0.0119815	0.820550	2.105000	2.250000	5.037175	11.317542	0.011237	11.317542	0.011237	11.318257	0.011237	11.318257	0.011237	11.318257
575.	0.00300	0.0119861	0.820700	2.107500	2.350000	5.037175	11.151345	0.012153	11.151345	0.012153	11.152156	0.012153	11.152156	0.012153	11.152156
600.	0.00300	0.0119920	0.820755	2.110000	2.450000	5.037175	10.984095	0.012391	10.984095	0.012391	10.985008	0.012391	10.985008	0.012391	10.985008

## FLEXURE NO. 27 CLOTHING TEST ANGLE TAPE 7402

TEST VJ. 1

THICKNESS RATIO = 0.23241

T	2-12	2-1	T-1	T-12	E1-2	E1-3	E1-2	E-2B	E-2PP	E-2	+E-2
75.00000	0.010910	1.0112153	0.3900001	13.700000	28.500000	0.339593	0.310080	0.305841	0.304744	0.303443	0.303443
100.00000	0.010915	2.0119160	0.4000000	9.3100000	28.430000	0.779110	0.261431	0.203736	0.203736	0.203736	0.203736
125.00000	0.010923	3.0119123	0.4100000	6.5500000	28.150000	1.012610	0.136303	0.140047	0.140047	0.140047	0.140047
150.00000	0.010930	4.0119150	0.4200000	4.7500000	26.220000	0.355977	0.102961	0.098437	0.142461	0.142461	0.142461
175.00000	0.010936	5.0119195	0.4300000	3.4500000	26.150000	0.503173	0.085263	0.068473	0.109354	0.109354	0.109354
200.00000	0.010942	6.0119230	0.4400000	2.5000000	28.050000	0.537150	0.067817	0.046614	0.082293	0.082293	0.082293
225.00000	0.0109250	7.0119270	0.4500000	1.9000000	27.870000	0.495375	0.067362	0.032736	0.074693	0.074693	0.074693
250.00000	0.0109283	8.0119300	0.4600000	1.5000000	27.750000	0.456171	0.050170	0.023398	0.059354	0.059354	0.059354
275.00000	0.0109350	9.0119343	0.4700000	1.3000000	27.590100	0.373914	0.049801	0.018616	0.036204	0.036204	0.036204
300.00000	0.0109402	1.0119377	0.4800000	1.1500000	27.450010	0.434175	0.032964	0.014971	0.035029	0.035029	0.035029
325.00000	0.0109405	2.0119415	0.4900000	1.0500000	27.310000	0.381111	0.032732	0.012475	0.035029	0.035029	0.035029
350.00000	0.0109445	3.0119453	0.5000000	1.0250000	27.150000	0.478220	0.024389	0.011659	0.027025	0.027025	0.027025
375.00000	0.0109485	4.0119493	0.5250000	1.0250000	27.540000	0.457540	0.024205	0.011070	0.026616	0.026616	0.026616
400.00000	0.0109525	5.0119530	0.5500000	1.0000000	26.890000	0.619765	0.016007	0.009921	0.018632	0.018632	0.018632
425.00000	0.0109565	6.0119570	0.5750000	1.0000000	26.730000	0.597756	0.015897	0.009344	0.016440	0.016440	0.016440
450.00000	0.0109607	7.0119610	0.6000000	1.0000000	26.620000	1.110757	0.015792	0.008267	0.01796	0.01796	0.01796
475.00000	0.0109647	8.0119650	0.6250000	1.0000000	26.470000	1.045537	0.007532	0.008189	0.011332	0.011332	0.011332

FIGURE 5-38. LF DATA AS TATE IN C AL-CV CMC 780

	T	2-12	2-1	T-1	T-12	E1-2	ETA-2	E-2a	E-2PP	+E+2
60.0000000	1.17465	1.117179	1.4000000	0.7200000	26.490000	0.001714	12.004993	0.020574	12.005011	
150.0000000	1.17345	1.112293	1.4250000	0.6500000	28.220000	0.001247	12.046009	0.015023	12.046017	
250.0000000	1.17245	1.111353	1.4500000	0.6500000	24.000000	0.001130	12.040513	0.013616	12.040521	
350.0000000	1.17150	1.111251	1.4500000	0.6500000	27.430000	0.000721	11.921102	0.010979	11.921114	
450.0000000	1.17060	1.111242	1.4500000	0.6500000	26.690000	0.001182	11.775375	0.012781	11.775382	
500.0000000	1.17030	1.111235	1.4500000	0.6500000	26.340000	0.001199	11.906110	0.022608	11.906132	
550.0000000	1.17010	1.111235	1.4500000	0.6500000	25.770000	0.001532	12.016367	0.042327	12.016442	
600.0000000	1.16990	1.1114492	1.4500000	0.7000000	25.490000	0.001532	12.016367	0.042327	12.016442	
700.0000000	1.16970	1.1114502	1.4500000	0.8000000	2.200000	0.001526	13.103809	0.082082	13.104066	
800.0000000	1.16950	1.1114662	1.4500000	0.9000000	3.870000	0.012344	13.009473	0.166331	13.009627	
900.0000000	1.16930	1.1114675	1.4500000	0.9200000	4.250000	0.014175	13.247028	0.197777	13.248359	
947.0000000	1.16910	1.1114760	1.4500000	0.9400000	4.280000	0.014012	13.457849	0.158575	13.459170	
949.0000000	1.16900	1.1114764	1.4500000	0.9500000	4.150000	0.013201	13.733590	0.161294	13.734787	

GT-7615-R  
Page 5-109

FIGURE 5-38

SECTION 154-1 TEST PLAN - FLEXURE TESTS

FLEXURE TESTS

TEST NO. 2

		Y						Z					
		2+12		2+1		T-1		T-12		E1-2		ETA-2	
		E-2B		E-2P		E-2PP		E-2B		E-2P		E-2PP	
100.0000000	1.012963	0.4000000	0.4501003	-0.3300000	28.430000	0.004496	14.072602	0.057639	14.073020	0.064646	14.102436	14.102436	14.102436
200.0000000	1.012432	0.4501003	0.5000000	-28.090000	28.450000	0.004584	14.102289	0.057639	14.102436	0.064646	14.102436	14.102436	14.102436
300.0000000	1.012012	0.5000000	0.5500000	-27.780000	27.450000	0.003521	14.252574	0.051609	14.252667	0.051609	14.252667	14.252667	14.252667
400.0000000	1.011723	0.6000000	0.6000000	-27.380000	26.890000	0.002237	14.320558	0.029176	14.320566	0.029176	14.320566	14.320566	14.320566
500.0000000	1.011442	0.5500000	0.5500000	-26.980000	26.340000	0.001321	14.723014	0.022392	14.723031	0.022392	14.723031	14.723031	14.723031
600.0000000	1.011211	0.7000000	0.7000000	-25.770000	25.032589	14.616217	0.037837	14.616266	0.037837	14.616266	14.616266	14.616266	14.616266
700.0000000	1.011063	0.8000000	0.8000000	-24.930000	24.220000	0.004725	14.344712	0.057773	14.344872	0.057773	14.344872	14.344872	14.344872
800.0000000	1.010950	0.9000000	0.9000000	-24.640000	24.090000	0.008913	14.107860	0.125817	14.108441	0.125817	14.108441	14.108441	14.108441
900.0000000	1.010852	0.9500000	0.9500000	-24.350000	24.030000	0.012491	13.863474	0.173170	13.864556	0.173170	13.864556	13.864556	13.864556
1000.0000000	1.010753	1.0000000	1.0000000	-24.070000	24.010000	0.016447	13.524748	0.222985	13.525886	0.222985	13.525886	13.525886	13.525886
1100.0000000	1.010656	1.1000000	1.1000000	-23.300000	23.000000	0.025283	12.660874	0.320106	12.664920	0.320106	12.664920	12.664920	12.664920
1200.0000000	1.010559	1.2000000	1.2000000	-22.920000	22.920000	0.035314	11.832136	0.417841	11.839511	0.417841	11.839511	11.839511	11.839511
1300.0000000	1.010451	1.3000000	1.3000000	-22.320000	22.320000	0.047283	11.069549	0.523466	11.069553	0.523466	11.069553	11.069553	11.069553
1400.0000000	1.010350	1.4000000	1.4000000	-21.700000	21.700000	0.061555	10.327855	0.636790	10.347468	0.636790	10.347468	10.347468	10.347468
1500.0000000	1.010251	1.5000000	1.5000000	-22.350000	21.070000	0.059170	10.698617	0.740024	10.724180	0.740024	10.724180	10.724180	10.724180
1600.0000000	1.010152	1.6000000	1.6000000	-20.770000	20.770000	0.059133	11.067890	0.764048	11.094231	0.764048	11.094231	11.094231	11.094231
1700.0000000	1.010054	1.7000000	1.7000000	-20.430000	20.430000	0.072522	10.639880	0.771628	10.667823	0.771628	10.667823	10.667823	10.667823
1800.0000000	1.009956	1.8000000	1.8000000	-20.000000	20.290000	0.057122	11.173411	0.749977	11.198553	0.749977	11.198553	11.198553	11.198553
1900.0000000	1.009858	1.9000000	1.9000000	-20.140000	20.140000	0.058343	11.919604	0.701464	11.940926	0.701464	11.940926	11.940926	11.940926
2000.0000000	1.009760	2.0000000	2.0000000	-20.990000	19.990000	0.051594	12.143885	0.747984	12.166829	0.747984	12.166829	12.166829	12.166829
2100.0000000	1.009662	2.1000000	2.1000000	-20.820000	19.820000	0.058783	12.035615	0.827917	12.064057	0.827917	12.064057	12.064057	12.064057
2200.0000000	1.009564	2.2000000	2.2000000	-19.500000	19.500000	0.055321	11.522293	0.983095	11.364156	0.983095	11.364156	11.364156	11.364156
2300.0000000	1.009466	2.3000000	2.3000000	-19.000000	19.000000	0.055353	10.615813	1.124760	10.675234	1.124760	10.675234	10.675234	10.675234
2400.0000000	1.009368	2.4000000	2.4000000	-18.500000	18.500000	0.055385	10.155953	1.124760	10.675234	1.124760	10.675234	10.675234	10.675234

GT-7615-R  
Page 5-110

FIGURE 5-39

FIGURE 4C. IN-DEPTH PROFILE OF CLOTHING LAYER SECTION

FIGURE 4C. IN-DEPTH PROFILE OF CLOTHING LAYER SECTION  
TEST NO. 3  
TEST FABRIC = P.110972

T	3-12	3-1	T-1	T-12	E-1	E-12	E-T-2	E-2P	E-2P
30.00000	1.17015	1.119175	0.401000	28.450000	0.052193	21.631687	0.644254	21.631737	0.644254
280.00000	1.17125	3.119135	0.450000	2d.359000	1.001323	20.998737	0.040151	20.998775	0.040151
300.00000	1.17245	3.119310	0.500000	1.000000	0.701212	20.693734	0.031260	20.693757	0.031260
400.00000	1.17420	3.119355	0.600000	0.990000	0.301353	20.302464	0.027599	20.302482	0.027599
500.00000	1.17576	3.119325	0.650000	0.980000	0.101203	20.028501	0.024087	20.028515	0.024087
600.00000	1.17710	3.119393	0.700000	1.020000	0.001193	19.637515	0.023525	19.637532	0.023525
700.00000	1.17855	3.120135	0.800000	1.180000	0.021424	19.217928	0.022737	19.217947	0.022737
800.00000	1.17946	3.120350	0.900000	1.400000	0.031939	19.764454	0.034503	18.764486	0.034503
900.00000	1.18175	3.120350	1.000000	1.750000	0.092539	19.536997	0.049912	18.537062	0.049912
1000.00000	1.18200	3.119345	1.100000	2.250000	0.033214	18.200500	0.071240	18.200639	0.071240
1100.00000	1.182560	3.120375	1.200000	2.800000	0.005430	17.571735	0.095416	17.571994	0.095416
1200.00000	1.18762	3.121223	1.500000	3.620000	0.007053	17.273337	0.121631	17.273767	0.121631
1250.00000	1.19376	3.121355	2.000000	4.430000	0.008400	17.024470	0.143008	17.025070	0.143008
1300.00000	1.19669	3.121490	3.000000	5.900000	0.010944	16.763193	0.168033	16.764038	0.168033
1350.00000	1.19669	3.121490	3.100000	5.900000	0.010944	16.763193	0.168033	16.764038	0.168033
1400.00000	1.19275	3.121775	6.500000	12.300000	0.015953	16.119019	0.257157	16.121070	0.257157
1450.00000	1.19438	3.121940	10.650000	16.250000	0.022497	15.741541	0.354143	15.745524	0.354143
1500.00000	1.19616	3.122115	11.450010	17.400000	0.024342	15.330437	0.373173	15.334979	0.373173
1550.00000	1.19745	3.122293	11.200000	18.590000	0.029349	15.031209	0.441754	15.037698	0.441754
1600.00000	1.19765	3.122452	8.350000	20.500000	0.045751	14.445928	0.660912	14.460938	0.660912
1650.00000	1.19801	3.122520	6.150000	24.000000	0.057204	13.757620	0.924561	13.766522	0.924561
1700.00000	1.19845	3.122793	5.100000	28.400000	0.091184	12.864643	1.173050	12.918016	1.173050
1750.00000	1.19845	3.122963	5.100000	32.000000	0.112305	11.762664	1.326903	11.837269	1.326903

GT-7615-R  
Page 5-111

FIGURE 5-40

HIGH TEMPERATURE LUMINESCENCE 245

TEST 3: 1  
TICKNESS PAT/C = 0.22520  
TEST NO. 22116 TEST NO. 2 AL-20 CDC 120

T	P-12	a-1	T-1	T-12	E1-3	ET4-2	E-2P	E-2PP	*E*2
80.000000	1.17774	1.19175	0.400000	0.670000	26.450000	-0.001302	-1.4299191	-0.019755	1.4269204
260.000000	1.17365	1.191355	0.450000	0.730000	28.000000	0.001365	1.5914409	0.021771	1.3914426
360.000000	1.16022	1.191510	0.550000	0.600000	27.450000	0.001340	1.58022642	0.018795	1.3802255
460.000000	1.14210	1.191695	0.600000	0.630000	26.850000	0.001328	1.5803149	0.017517	1.3603160
560.000001	1.13210	1.191925	0.650000	0.960000	26.340000	0.001317	1.5819574	0.024022	1.31816595
660.000001	1.14420	1.191993	0.700000	1.200000	25.770000	0.002475	1.4047641	0.034769	1.4047684
760.000000	1.15330	1.1920165	0.800000	1.700000	25.220000	0.002457	1.4209457	0.060004	1.42252650
860.000000	1.16562	1.1920350	0.900000	2.000000	24.640000	0.002465	1.44289574	0.120999	1.4429086
960.000000	1.17740	1.1920550	1.000000	2.300000	24.070000	0.014213	1.48102753	0.200468	1.48104177
1060.000000	1.18310	1.1920755	1.100000	2.180000	23.500000	0.022303	1.53704200	0.303591	1.53707670
1160.000000	1.19255	1.1920975	1.200000	2.700000	22.920000	0.034347	1.53119894	0.4560634	1.53127631
1260.000000	1.20915	1.1921225	1.300000	2.120000	22.320000	0.052211	1.522715	0.54023232	1.5227588
1360.000000	1.22790	1.1921490	1.400000	2.170000	21.700000	0.075401	1.51925622	0.899200	1.51925947
1460.000000	1.24610	1.1921778	1.500000	2.279000	21.070000	0.099264	1.51376272	1.129256	1.51382162
1560.000000	1.26450	1.1922135	1.600000	2.323000	20.770000	0.111245	1.511187520	1.2445565	1.51125636
1660.000000	1.28240	1.1922415	1.700000	33.600000	20.430000	0.114945	1.5110455	1.266203	1.511097753
1760.000000	1.30030	1.1922462	1.800000	35.800000	19.420000	0.14555	1.51041076	1.510516382	1.510520334
1860.000000	1.31820	1.1922562	1.900000	37.200000	19.430000	0.172314	1.5106026	1.510669382	1.510670490
1960.000000	1.33610	1.1922647	2.000000	32.200000	21.770000	0.214259	1.51114259	1.511144090	1.511144562

GT-7615-B  
Page 5-112

Figure 5-41

STRUCTURE NO. 23 COATING TYPE A1 C1 AL31 SDC772 THICKNESS RATIO = 0.11235

	P-12	2-1	1-1	7-12	F1-3	ET4-2	E-23	E-2PP	E-E2
00.0000000	0.019670	1.112175	0.400070	0.700070	25.490000	0.004749	4.189658	0.016963	4.189703
150.0000000	0.114770	2.112291	0.425100	0.650000	28.220000	0.053101	4.145481	0.012652	4.145501
280.0000000	0.324545	0.121293	0.450030	0.650000	-28.400016	-0.002312	4.066575	0.011479	4.096591
300.0000000	0.118703	2.012351	1.550000	0.750000	27.430010	0.002813	4.104936	0.011508	4.104952
480.0000000	0.019555	2.012353	1.500000	0.775000	26.680000	0.002445	4.107635	0.010126	4.107648
500.0000000	0.019240	2.012355	0.650000	0.625000	26.340000	0.002274	4.492121	0.010216	4.492133
680.0000000	0.119362	0.019362	0.700000	1.000000	25.770000	0.003365	5.002102	0.016837	5.002131
700.0000000	0.119365	0.020165	0.900000	1.420000	25.220000	0.005749	5.860039	0.033695	5.860036
600.0000000	0.119420	2.020350	0.900000	2.100000	24.640000	0.009351	6.444696	0.063490	6.444696
640.0000000	0.019436	2.020356	0.940000	2.600000	24.390000	0.023124	6.614802	0.066814	6.615372
645.0000000	0.019470	2.020450	0.950000	2.600000	24.350000	0.012918	6.842046	0.084647	6.842093
750.0000000	0.022350	0.022350	0.900000	3.220000	24.070000	0.016581	6.807788	0.114925	6.808758
1000.0000000	0.019745	2.020753	1.100000	5.000000	23.510000	0.030142	6.575846	0.198339	6.578836
1100.0000000	0.020220	2.020975	1.200000	7.050000	22.920000	0.033420	5.970936	0.318965	5.979449
1200.0000000	0.020115	2.021225	1.550000	10.000000	22.320000	0.082315	5.452430	0.448932	5.470880
1300.0000000	0.020545	2.021490	3.100000	15.050000	21.700000	0.110094	5.20057	0.572563	5.232818
1400.0000000	0.020645	2.021775	4.350000	22.600000	21.070000	0.137319	5.025362	0.690080	5.072528
1450.0000000	0.021140	2.021940	10.550000	24.300070	20.770000	0.153749	4.840337	0.744195	4.897212
1480.0000000	0.021125	2.022045	11.200000	27.000000	20.590000	0.133465	4.884763	0.749792	4.941973
1500.0000000	0.021175	2.022115	11.450000	26.900000	20.450000	0.148052	4.949753	0.732820	5.003707
1550.0000000	0.021190	2.022190	10.620000	26.100000	20.050000	0.147025	4.891769	0.717742	4.934250
1600.0000000	0.021240	2.022240	8.350000	26.420000	19.180000	0.154947	5.132488	0.846589	5.201840
1700.0000000	0.021950	2.022795	5.100000C	32.400000	19.040000	0.295543	4.266424	1.210332	4.436970
1720.0000000	0.021962	2.022865	5.000000C	33.400000	19.040000	0.296103	4.261596	1.261860	4.444490

GT-7615-A  
Page 5-113

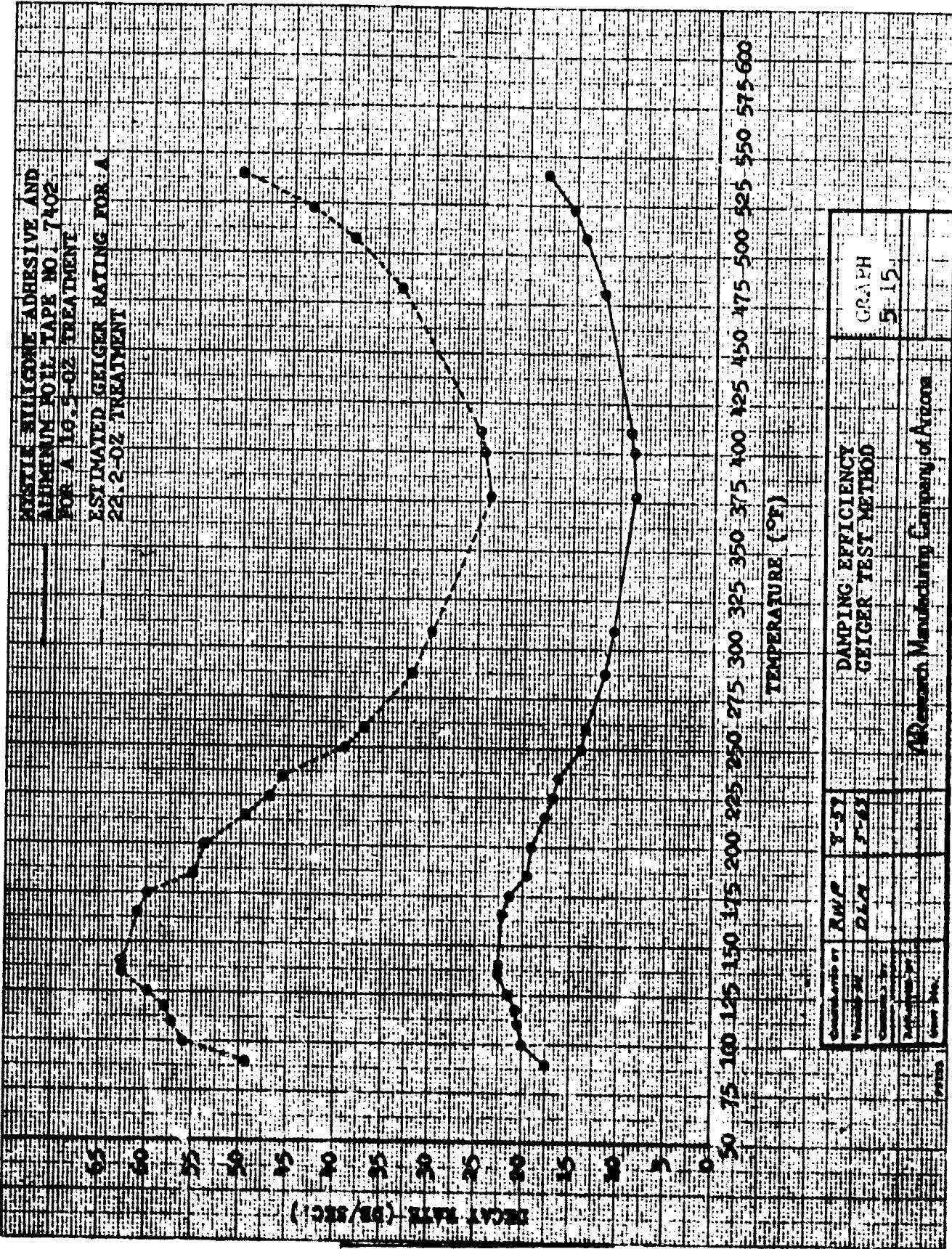
FIGURE 5-42

אַתָּה תְּבִרְכֵנִי בְּעֵדוֹת אֶתְנוּן

TEST NO. C-2  
THICKNESS RATIO = 0.11236

ANSWER

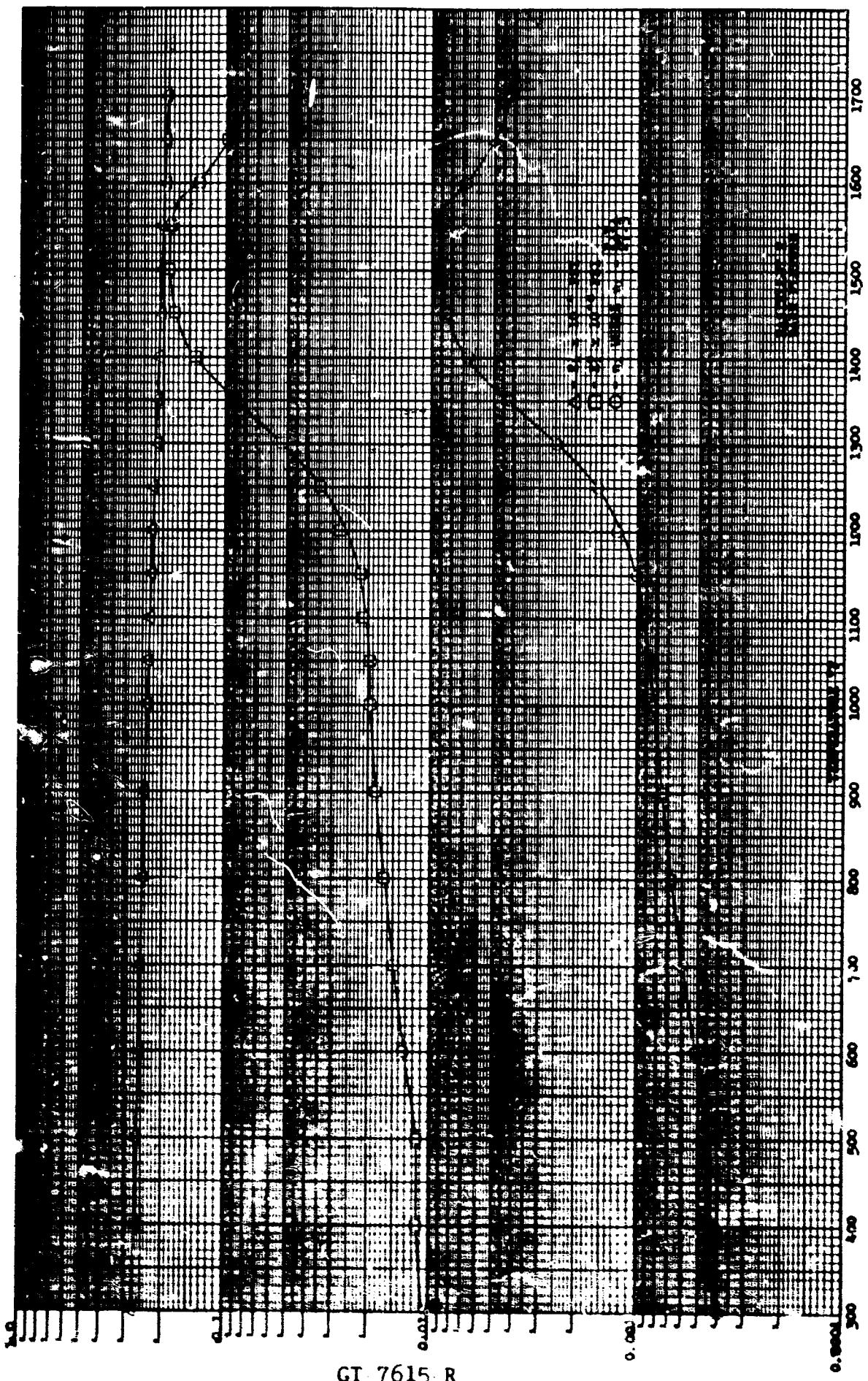
GT-7615-a  
Page 5-14



GT-7615-R  
Page 5-115



GRAPH 5-16

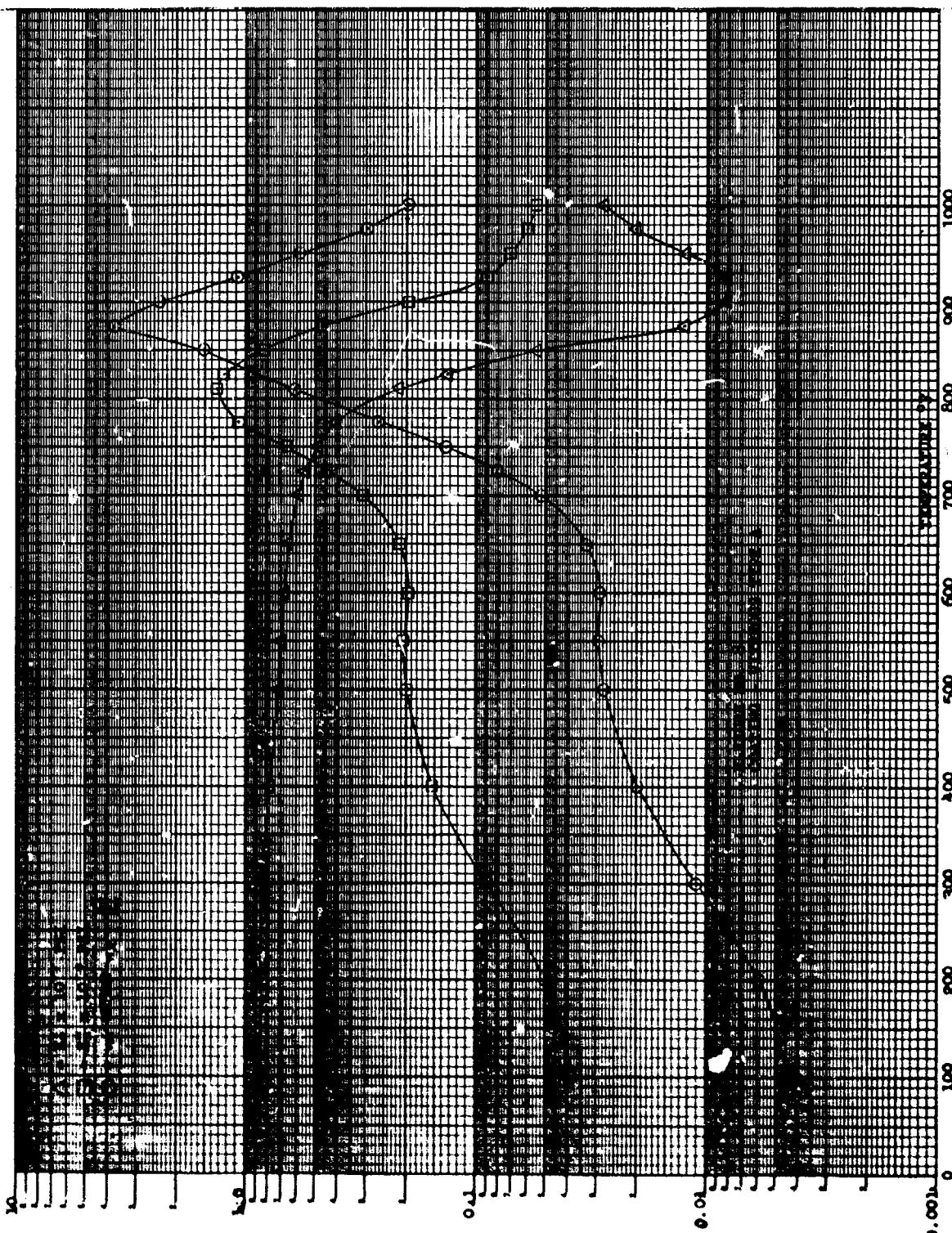


GT 7615 R  
Page 5-116



AIRESEARCH MANUFACTURING COMPANY  
A DIVISION OF THE AMETEK CORPORATION  
PHILADELPHIA, PENNSYLVANIA

GRAPH 5-17

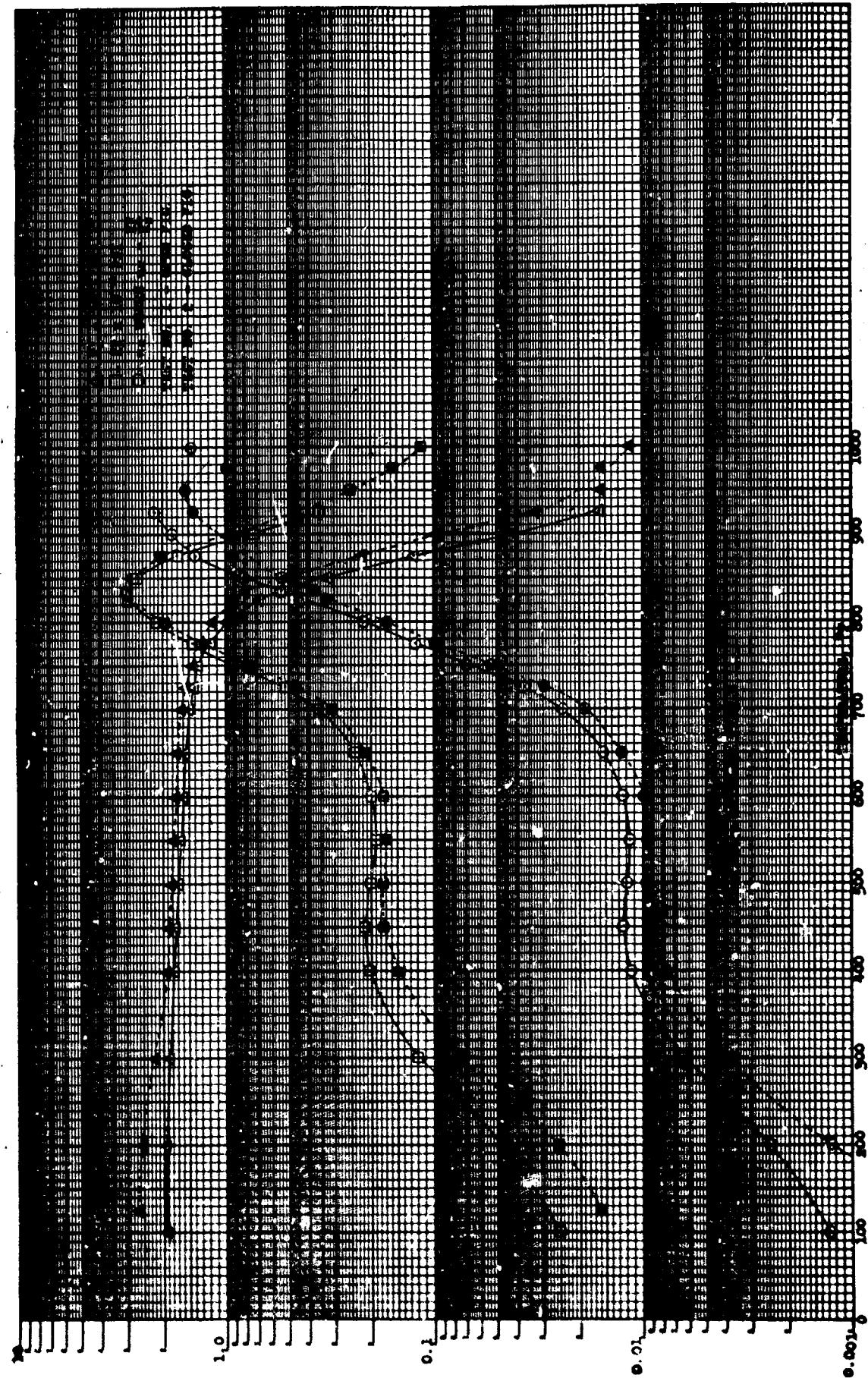


GT-7615-R  
Page 5-117

**AIRSEARCH MANUFACTURING COMPANY**  
A division of the Quality Corporation



GRAPH 5-18

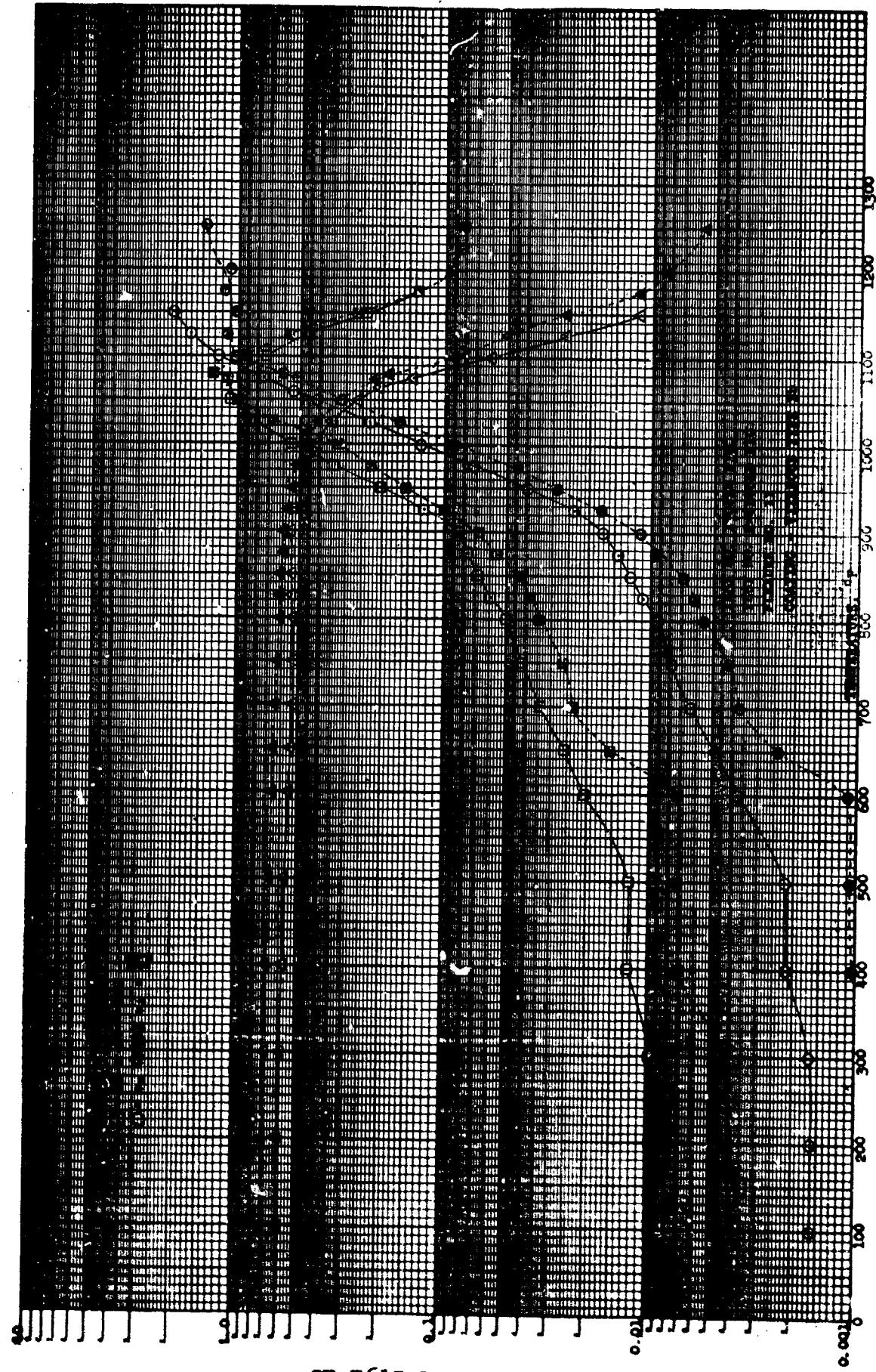


GT-7615-R  
Page 5-118



AIRESEARCH MANUFACTURING COMPANY  
DIVISION OF THE GOODYEAR CORPORATION

GRAPH 5-19

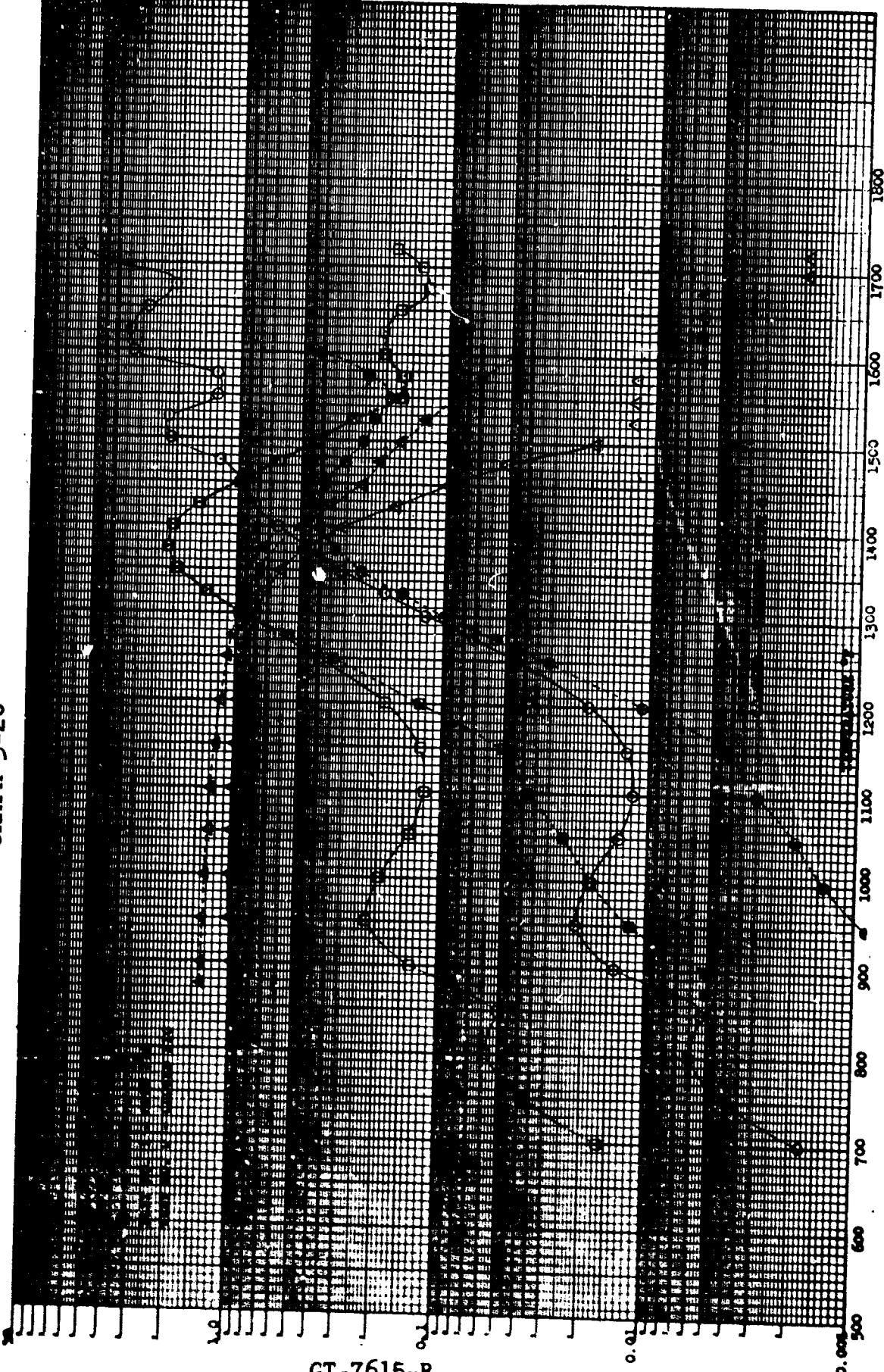


GT-7615-R  
Page 5-119

AIR RESEARCH MANUFACTURING COMPANY  
A Division of the Quality Assurance Corporation



GRAPH 5-20

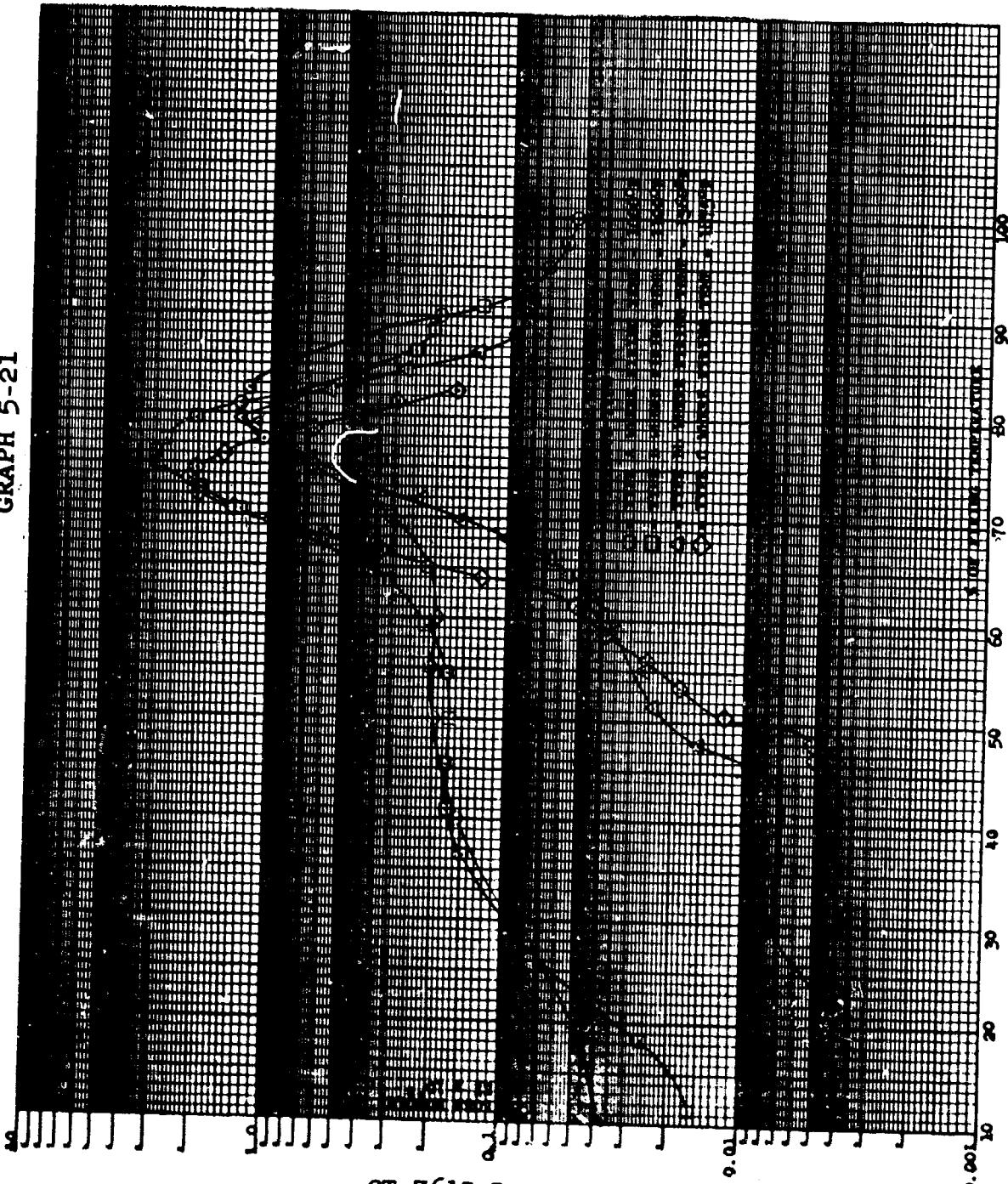


GT-7615-R  
Page 5-120



AIRESEARCH MANUFACTURING COMPANY  
A division of THE DOW CHEMICAL COMPANY

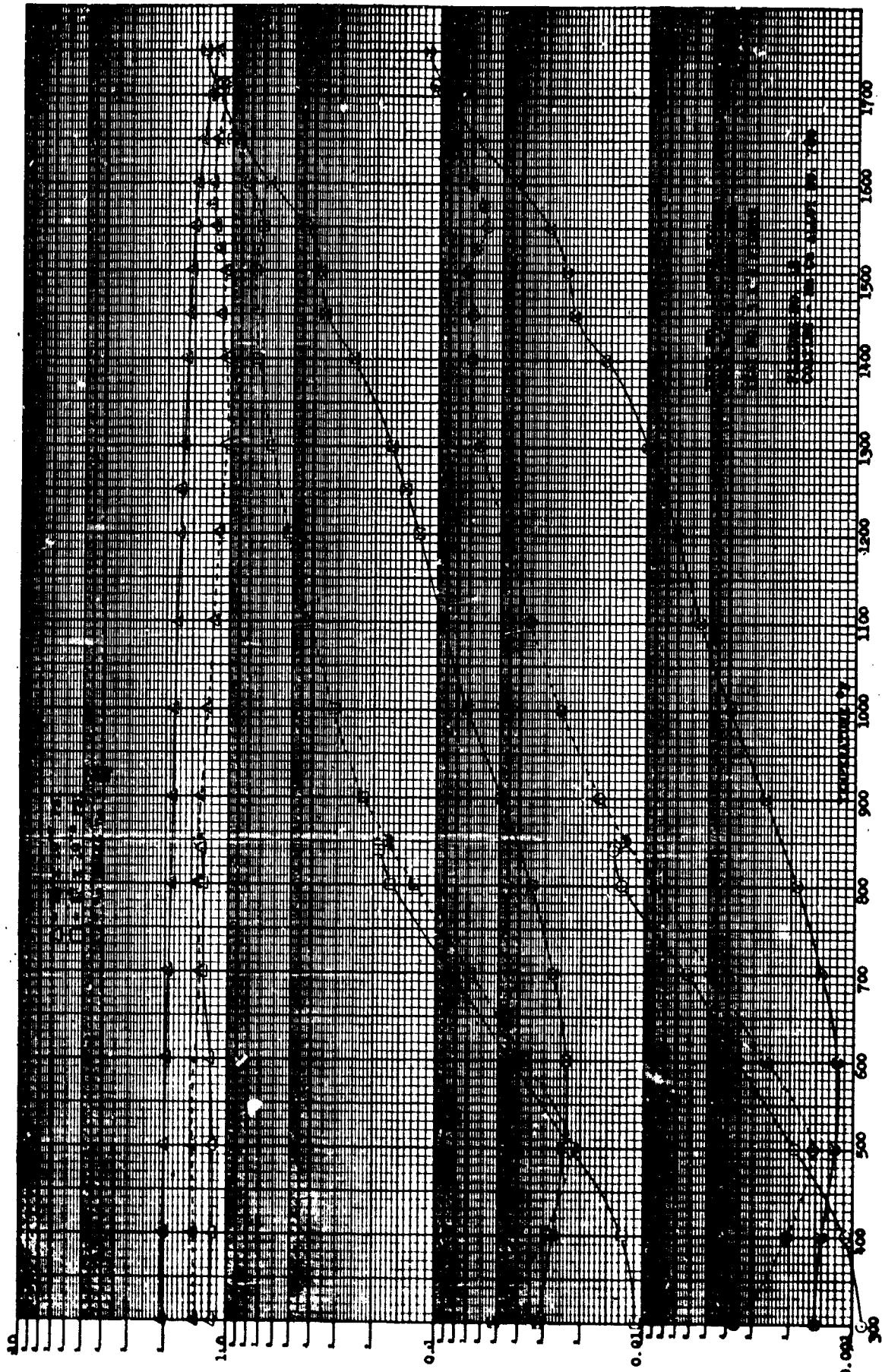
GRAPH 5-21



GT-7615-R  
Page 5-121



GRAPH 5-22

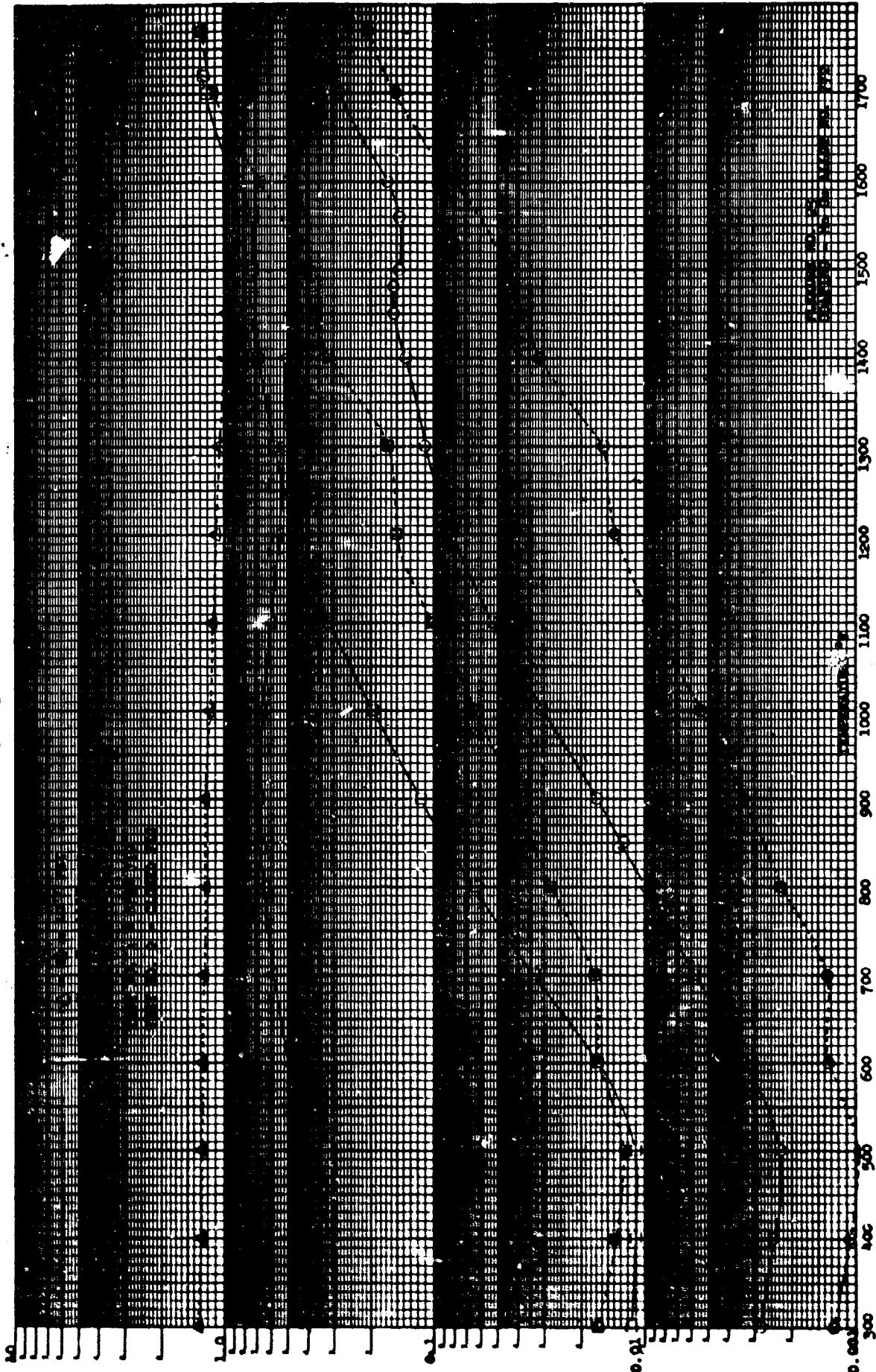


GT-7615-R  
Page 5-122



AIRESEARCH MANUFACTURING COMPANY  
A Division of the Goodyear Corporation

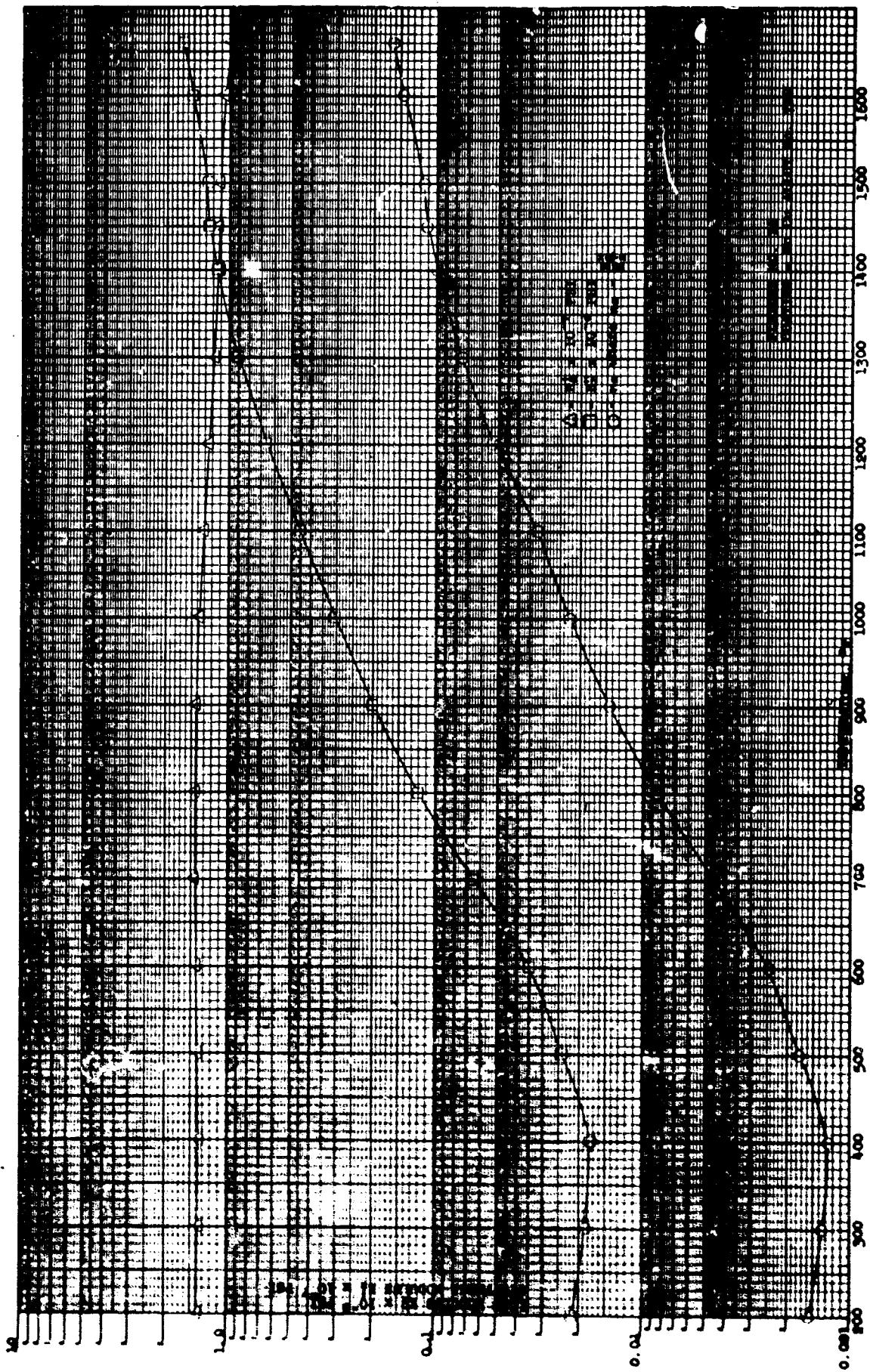
GRAPH 5-23



GT-7615-R  
Page 5-123



GRAPH 5-24

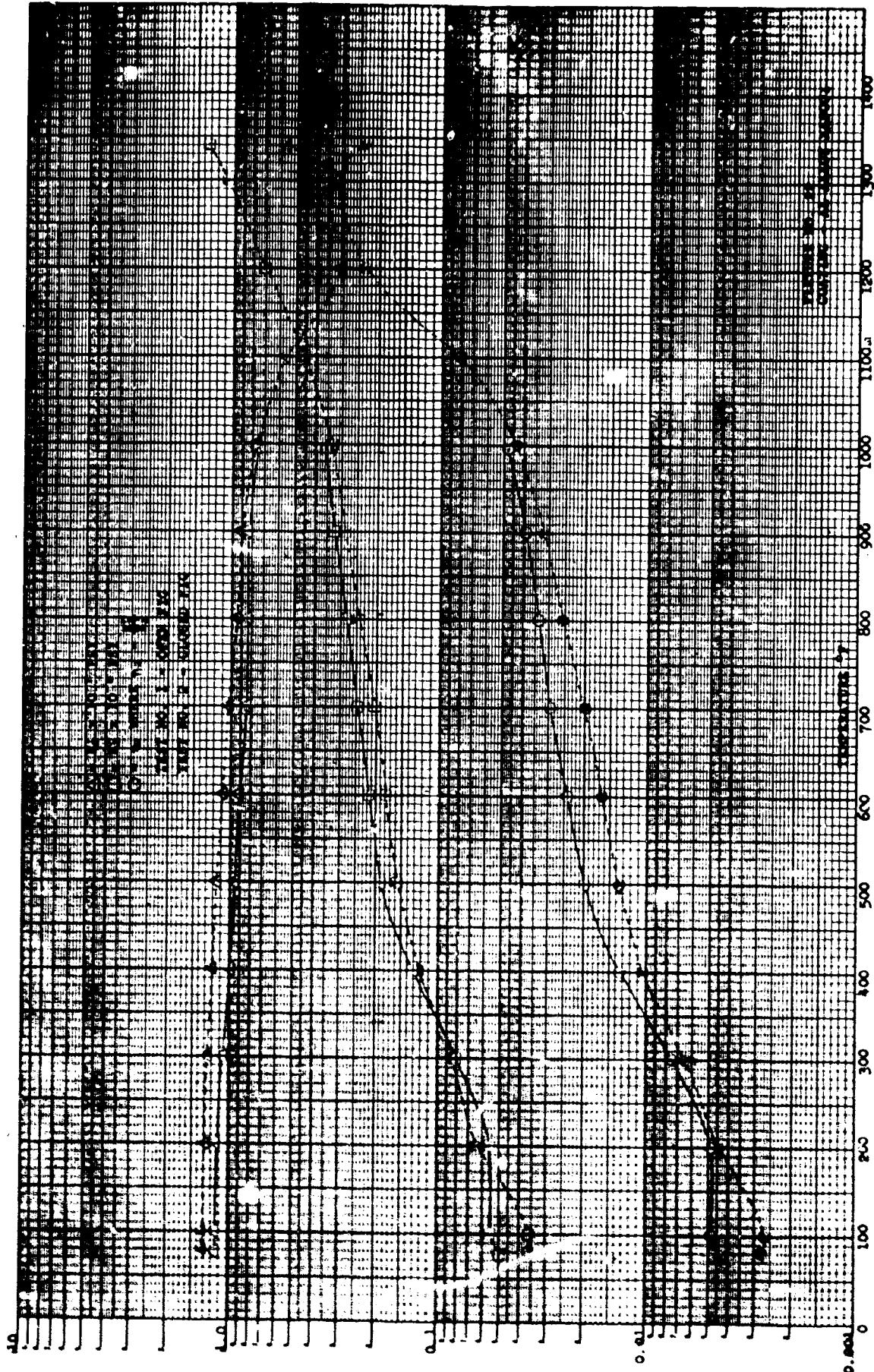


GT 7615 R  
Page 5-124



AIRESEARCH MANUFACTURING COMPANY  
A Division of The Goodyear Aerospace

GRAPH 5-25

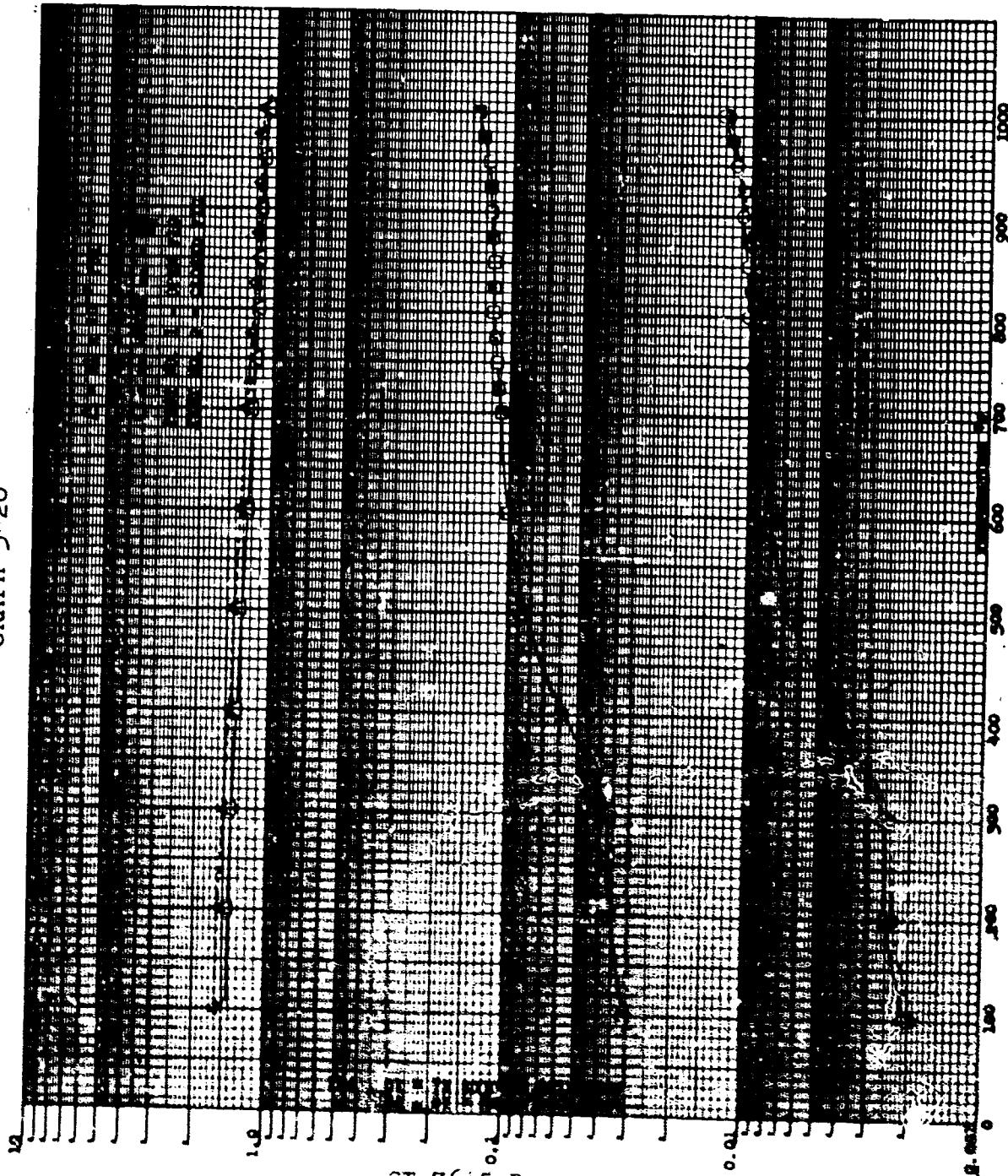


GT-7615-R  
Page 5-125

**AIRESEARCH MANUFACTURING COMPANY**  
A Division of The Goodyear Aerospace Corporation



GRAPH 5-26



GT-7615 R  
Page 5 126

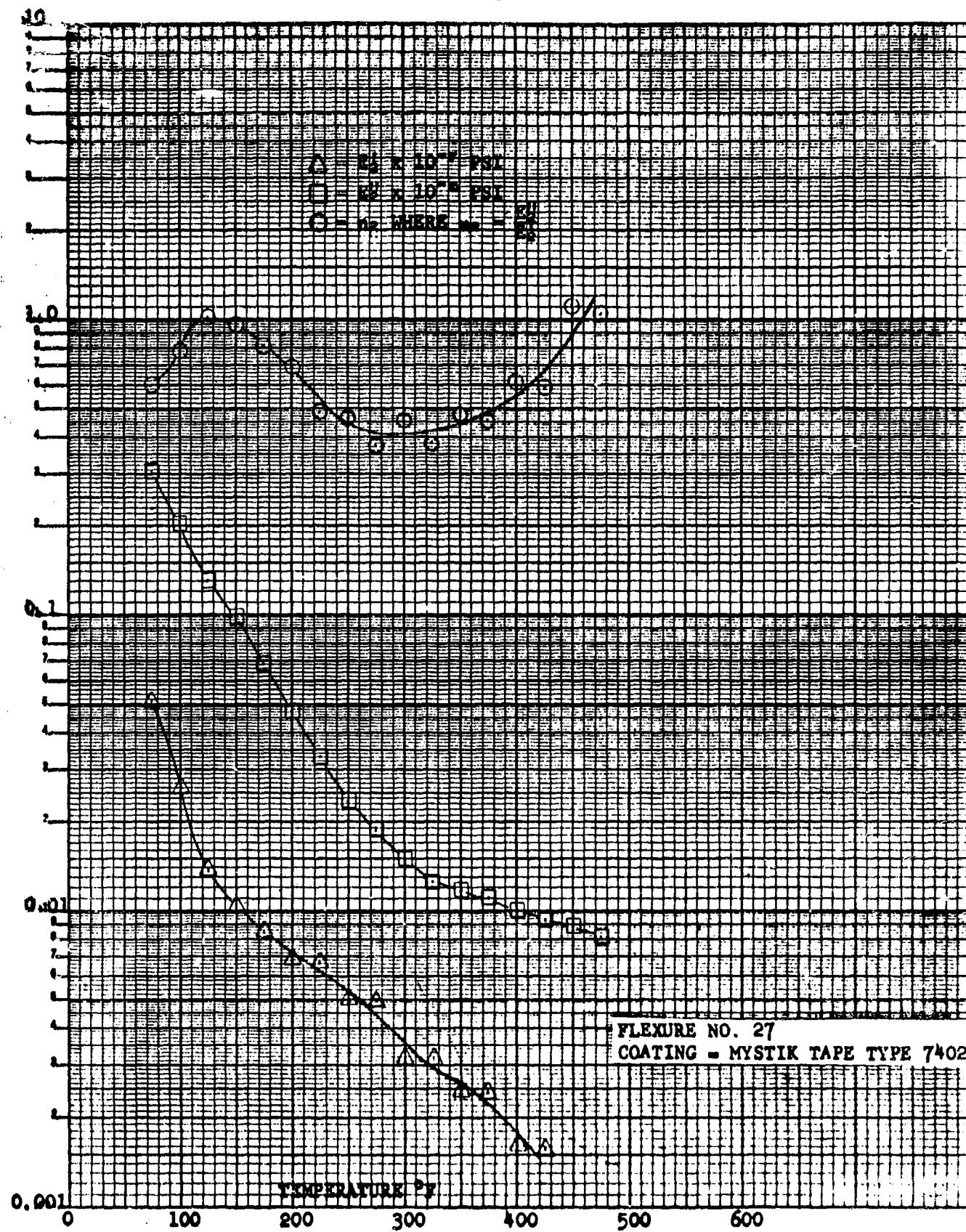


AIRESEARCH MANUFACTURING COMPANY OF ARIZONA

A DIVISION OF THE JARRETT CORPORATION

PHOENIX, ARIZONA

GRAPH 5 27



GT-7615-R  
Page 5-127



AIRESEARCH MANUFACTURING COMPANY OF ARIZONA  
A DIVISION OF THE GARRETT CORPORATION  
PHOENIX, ARIZONA

of their firing temperatures. Graph 5-28 shows the comparison of the damping observed in manganese copper with data reported by other observers.

#### 5.5.2 Observations

The decay rate and period, as functions of temperature, are averaged for two bare flexures and appear as a reference on all graphs presenting original observations--Graphs 5-2 through 5-14. The monotonic rise in period reflects mainly the progressive loss of stiffness with increasing temperature. No attempt was made to correct for the slight increase in moment of inertia due to thermal growth. The pronounced damping increase that appeared between 1300°F and 1700°F was unexpected and required modification of the data-reduction procedure to remove its influence on the coating material parameters. That the apparatus could map this internal friction peak shows its possible usefulness for the investigation of such peaks in other high-temperature alloys.

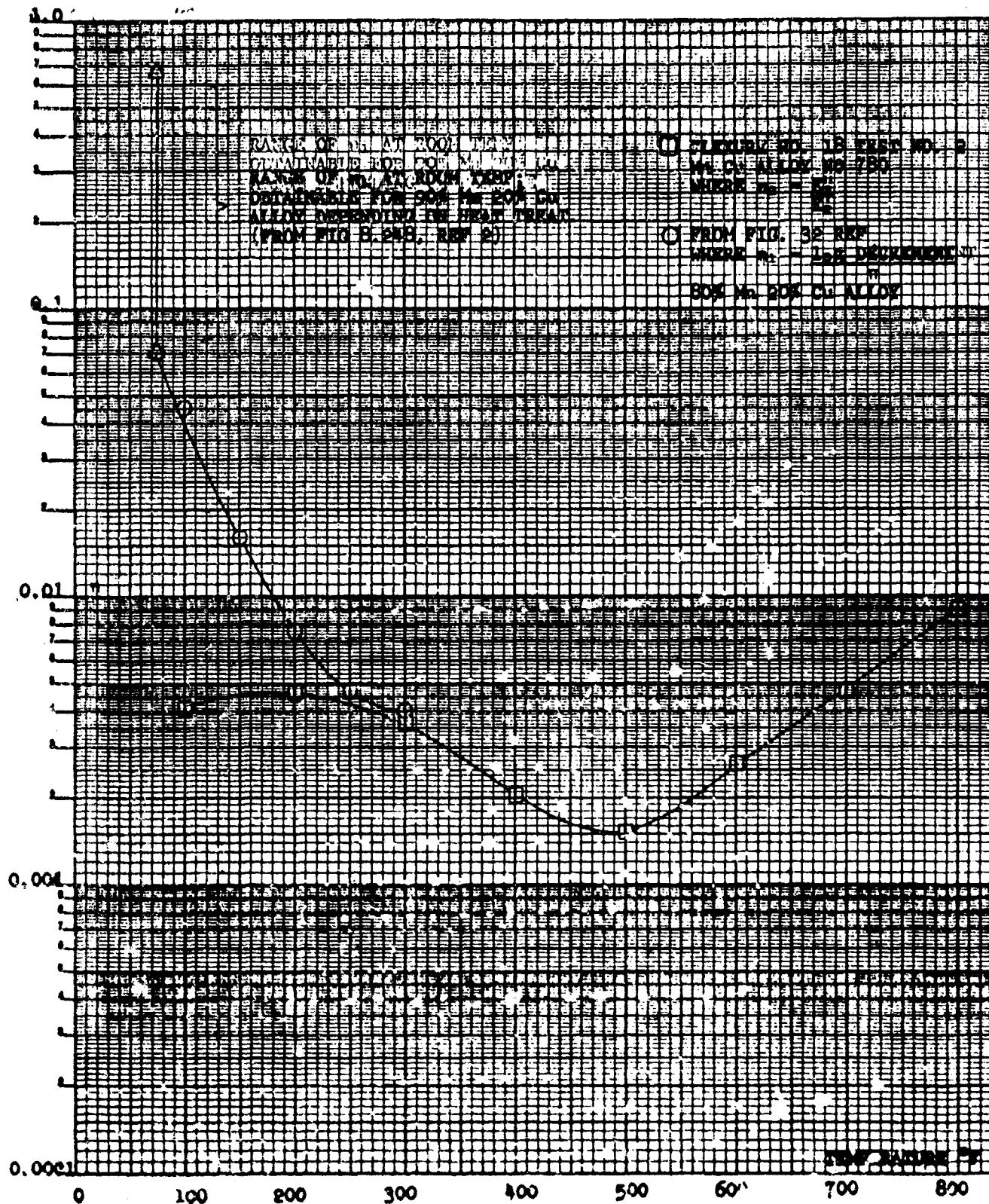
##### 5.5.2.1 Vitreous Enamels

Graphs 5-2 through 5-5 present the decay rates observed on the four vitreous enamels and also show the period curve used in data reduction. This period curve is drawn parallel to the average period curve from the bare-bar tests, but its height is adjusted to coincide with the coated-bar period at the firing temperature of the vitreous enamel. This was necessary because the data depended critically on the period, yet the exact bare-bar frequency for each



AIRESEARCH MANUFACTURING COMPANY OF ARIZONA  
A DIVISION OF THE GARRETT CORPORATION  
PHOENIX, ARIZONA

GRAPH 5-28



GT-7615-R  
Page 5-129



AIRESEARCH MANUFACTURING COMPANY OF ARIZONA  
A DIVISION OF THE GARRETT CORPORATION  
PHOENIX, ARIZONA

specimen was in doubt. The only assumptions necessary were that the stiffness of the enamel was negligible at its firing temperature and that the effect of the coating mass on the period was negligible. The first assumption stands on its own merits. The second assumption was checked directly by the addition of mass to the center of a test bar. Two grams were necessary to change one digit in the fifth significant figure of the period.

The extraordinary decay rates attained at the peaks of the vitreous enamel damping curves were greater than expected. In fact, it is fortunate that the coatings were thin. Had the coatings been much thicker, the damping would have exceeded the maximum values that could be regeneratively driven by the forcing system (about 35 db per second maximum decay rate). The appearance of the small initial plateau in the decay rates at about 450°F in Types A and B was also unexpected and offered the promise of useful damping at temperatures lower than expected. The initial appearances and later disappearances of such a plateau in the type of coating indicated a possible chemical change during the first thermal cycle.

#### 5.5.2.2 Manganese Alloys

The behavior of the manganese alloys was considerably more complicated than that of the vitreous enamels. The periods are well removed from the bare-bar periods; hence, the average bare-bar periods were used in the data reduction. Decay rates and periods both were affected strangely by thermal history. Alloy No. 78C shows a modest initial decay rate which nearly disappears at 400°F. It should be noted here that this amount of room-temperature damping has made this manganese alloy notable as a "dead metal." Processing of this data to obtain material parameters had a smothering effect on the curves, and further discussion of the complicated behavior of the manganese coatings is deferred to Section 5.6.



AIRESEARCH MANUFACTURING COMPANY OF ARIZONA  
A DIVISION OF THE GARRETT CORPORATION  
PHOENIX, ARIZONA

The comparison made in Graph 5-28 is one illustration of the complicated behavior of a manganese alloy.

The band presented from Dean's data, which is shown also in Figure 5-3 illustrates the variation in damping at low stress levels, depending on heat treatment.

Figure 32 of Ref. 14 was the only other data available at this time showing the damping characteristics at elevated temperature, and was taken at high stress levels. These two tests were performed on carefully prepared metallurgical samples with controlled heat treatment, while the information obtained in this program was the result of measurements made on flame-sprayed coatings where no attempt was made to determine the metallurgical changes that took place in the material.

#### 5.5.2.3 Aluminum Cermets

Both of the aluminum cermets exhibited similar and consistent period and decay rate curves. The periods were usually well removed from those of the bare bar, and no period correction was attempted. Both display a barely perceptible damping at room temperature. This is the room temperature anomalous damping for which these alloys are famous. As temperature increases, decay rates climb linearly to slightly higher values. The periods also increase linearly to about 1000°F.

#### 5.5.2.4 Sperex VHT

Graph 5-12 shows the observations on the commercial high-temperature protective material, Sperex VHT Coating (black). Both the period and decay rate curves parallel the bare bar curves.



Thus, it is concluded that the coating had no appreciable effect on either stiffness or damping. This data was not processed further. No criticism of the coating is made, since no claims of damping or stiffness are made by the manufacturer.

#### 5.5.2.5 Aluminum-Silicone Tape

The results of two tests on a constrained-layer damping tape, that is known to be effective are shown in Graphs 5-13 and 5-14. The decay rates are significantly higher on the second test than on the first, which reflects a curing of the silicone adhesive. The period rises abruptly at first, which suggests a rapid loss or stiffness in the adhesive. The damping curves show maximum damping at 80°F, the lowest temperature tested. This same material was evaluated, by the Geiger test method (160 cps), previously.

The Geiger test (Graph 5-15) showed a peak damping at 140°F which disagrees with the present tests as to the location of the peak. What may have occurred in the intervening years in the way of changes in the formulation of the adhesive is not known.

It is regarded as probable that the damping observed at 75°F is at or near the maximum for the present-day material. Note that the total tip thickness is about 0.010 inch--more than twice as thick as the vitreous enamels.

#### 5.5.3 The Refined Data

##### 5.5.3.1 Hastelloy X

Graph 5-16 presents the stiffness modulus  $E'_1$ , the loss modulus,  $E''_1$ , and the ratio of loss modulus to stiffness modulus,  $\eta_1$ , for the annealed Hastelloy X. Because the stiffness modulus is relatively



constant, the  $E''_1$  curve essentially parallels the  $\eta_1$  curve. At low temperatures the values of  $\eta_1$ , hence  $E''_1$ , are too high because the damping originates in the viscous drag of air on the portion of the fixture that protrudes through the furnace floor. In the region of the damping increase, however, internal friction in the Hastelloy X is clearly predominant. The peak value of  $\eta_1$  is 0.0093, which means that a force of nearly one percent of the stiffness is out of phase with the strain. This shows that at this temperature a Hastelloy X structure is as "dead" as though it were made of hardwood, even if no other damping mechanism is present. This is presumed to be an anelastic peak (see Section 5.7).

#### 5.5.3.2 Vitreous Enamels

The four vitreous enamels generally behaved alike, but differences in detail were significant. For Type A (Graph 5-17) the stiffness modulus,  $E'_2$ , decreases very gradually with increasing temperature and then abruptly at about  $700^{\circ}\text{F}$ . The apparent increase in stiffness above  $900^{\circ}\text{F}$  is probably erroneous and should be disregarded unless future studies confirm its existence.

The loss factor,  $\eta_2$ , shows an initial climb beginning at  $200^{\circ}\text{F}$  and attains a plateau of approximately 0.03 at  $500^{\circ}\text{F}$ . Since the glass is so stiff ( $E'_2 \approx 7 \times 10^8$  psi at  $500^{\circ}\text{F}$ ), this plateau represents useful damping for many applications. At  $650^{\circ}\text{F}$ ,  $\eta_2$  climbs rapidly to form a major damping peak with a maximum of about 0.4 at  $875^{\circ}\text{F}$ . Above  $875^{\circ}\text{F}$  the loss coefficient drops in a symmetrical manner. The loss modulus is at first parallel to  $\eta_2$ , and is 200,000 psi in the plateau region. The peak value of  $E''_2$  occurs at a lower temperature ( $800^{\circ}\text{F}$ ) than does the peak in  $\eta_2$  because of the rapid loss of stiffness in this region. The  $E''_2$  peak is also symmetrical.



AIRESEARCH MANUFACTURING COMPANY OF ARIZONA  
A DIVISION OF THE GARRETT CORPORATION  
PHOENIX, ARIZONA

The pattern just described is characteristic of viscoelastic materials. The peak value of  $E_2''$  of nearly 2,000,000 psi is, however, unprecedented and is an order of magnitude greater than that attainable in organic polymers.

The Type B vitreous enamel exhibits an  $E_2'$ ,  $E_2''$ , and  $\eta_2$  similar in character to those of Type A. A second test revealed a small increase in stiffness and a tendency for  $\eta_2$  to shift downward and toward higher temperatures. The peak value of  $E_2''$ , however, remains essentially unchanged. These differences suggest that the coating had not completely stabilized chemically during its brief application firing. The peak value of  $E_2''$  is about 3,000,000 psi at 825°F, but useful damping is present above 400°F. Unlike the Type A material,  $\eta_2$  for Type B climbs continuously as the firing temperature is approached and reaches values above unity (see Graph 5-18).

Type Bb vitreous enamel also shows stiffening and a greater loss of  $\eta_2$  during a second test;  $\eta_2$  and  $E_2''$  exhibit both a plateau and a region of moderate climb before the major peak is attained. Peak values of  $E_2''$  exceed 1,000,000 psi and  $\eta_2$  climbs continuously to values in excess of unity. The  $E_2''$  peak occurs at about 1050°F (see Graph 5-19).

Type C vitreous enamel exhibited the same general pattern, but also more complexity in detail and more difference between the first and the second test. There was exact duplication of the  $E_2''$  peak in the first and the second test. During the first run the stiffness actually increased for a few hundred degrees, which indicated a possible chemical change toward the significantly stiffer material observed in the second test. During the first run, two maximums of  $\eta_2$  and  $E_2''$  occurred below 1100°F. This was replaced by a single moderate upward slope in the second test. Above the major  $E_2''$  peak,



$\eta_2$  in the first test climbed in an undulating manner to a value in excess of five. During the second test an  $\eta_2$  maximum occurred that was considerably less than unity. As in all previous cases, the change in stiffness seemed to compensate the change in loss factor and led to a virtually unchanged  $E''$  peak. In this case, the peak value of  $E''_2$  was about 2,000,000 psi (see Graph 5-20).

The similarity among the four vitreous enamels is shown in Graph 5-21, which shows  $E''_2$  as a function of percent of firing temperatures. The peaks all occur between 73 and 81 percent of firing temperature. All are symmetrical and of nearly the same width. Peak values of  $E''_2$  are all of the same order of magnitudes. Two have major plateaus; two do not.

#### 5.5.3.3 Manganese Alloys

The manganese alloys were more regular in their behavior than the original data indicated when plotted as  $E'_2$ ,  $E''_2$ , and  $\eta_2$  (see Graphs 5-22 through 5-24). The CDC alloy No. 720, containing 20 percent Mn, shows a nearly constant stiffness modulus having a maximum near 700°F. As a result of this flatness the  $\eta_2$  and  $E''_2$  curves are parallel. Both exhibit a minimum at 400°F then rise monotonically. The loss coefficient,  $\eta_2$ , finally reaches 0.15 at 1650°F, and the loss modulus exceeds 1,500,000 psi at this point. This broad damping characteristic can be useful if application problems can be solved.

Alloy No. 772 (72 percent manganese) exhibited pronounced heat-treatment effects. The stiffness modulus is more than 100 percent greater on the second test. During the first test,  $\eta_2$  shows a slight minimum at 500°F and then climbs smoothly to 1450°F. Above 1450°F two apparent discontinuities appear. The second test shows  $\eta_2$  to be significantly lower. The same minimum occurs near 500°F, but new discontinuities in slope occur at 1200°F and 1300°F. The loss modulus,  $E''_2$ , is greater during the second test below 500°F



AIRSEARCH MANUFACTURING COMPANY OF ARIZONA  
A DIVISION OF THE BARRETT CORPORATION  
PHOENIX, ARIZONA

but appreciably less above 500°F. The value of loss modulus for tests one and two converges at 1700°F at a value in excess of 1,000,000 psi. Useful broad-band damping is indicated if application techniques can be evolved.

Graph 5-22 shows the results of three tests on alloy No. 780 (80 percent Mn, the high-damping alloy). For test 1, the initial value of  $\eta_2$  was low and then rose steadily to near 800°F, where it rolled off abruptly to a slightly lower value of 850°F. This temperature is the heat-treatment temperature used to bring out maximum room-temperature damping in this alloy.

The second test showed a much higher initial value of  $\eta_2$ , which then fell steadily to a minimum near 500°F. The loss coefficient,  $\eta_2$ , then rose smoothly to 1300°F and leveled off until 1500°F, above which it became irregular.

The third test showed the loss coefficient to be low in its initial value, and its minimum occurred near 600°F. The loss coefficient,  $\eta_2$ , then climbed steadily, except for a minor peak at 1450°F. During this climb its value was lower than during Test 2, but finally attained the same value near 1700°F.

Again, the effect of the increased stiffness partly compensated for the reduction in  $\eta_2$ , so that useful damping was present over a considerable temperature range.

#### 5.5.3.4 Aluminum Cermets

Two tests each were run on the two alloys, XAP001 and XAP003 (see Graphs 5-25 and 5-26). The XAP003 was heated only to 1000°F, which is below the melting point of aluminum. Its stiffness



modulus, loss modulus, and loss coefficient were repeatable. Since the stiffness declined slowly, the  $\eta_2$  and  $E''_2$  curves are parallel. The damping is appreciable at room temperature, then rises slowly to 300°F. There, an abrupt discontinuity in slope occurs, and the damping rises rapidly in a smooth monotonic manner, becoming nearly constant as 1000° is approached.  $E''_2$  exceeds 100,000 psi above 500°F, which is comparable to the best organic dampers. The material adhered well and retained its bright finish; and it appears to be potentially very useful.

The XAP001 material was first tested to 1000°F; then a second test was conducted to 1350°F, which is above the melting point of aluminum. The first test showed appreciable initial damping and an irregular increase in slope of  $E''_2$  and  $\eta_2$  at 200°F. The loss parameters then rose smoothly at a decreasing rate to 1000°F. The second test showed some increase in stiffness below 1000°F and a falloff of stiffness above 1000°F, which then abruptly flattened out again at 1200°F. Above 1000°F,  $\eta_2$  showed a fairly rapid rise and a small peak at 1275°F (about the melting point of aluminum). The loss modulus at this point attained 1,000,000 psi and exceeded 100,000 psi everywhere above 350°F. The coating separated from the bar sometime during the second test, which was probably the result of overheating. This material resisted oxidation well and appears to be useful.

#### 5.5.3.5 Damping Tape

Prior to this study the only damping material known to be useful at temperatures above about 150°F was aluminum-foil tape with a silicone adhesive. To establish a bridge between the present study and past Geiger testing, this tape (total thickness, 0.010 inch) was tested to 450°F. The data was processed by the



same computer program, but these results (Graph 5-27) apply only to the 150-microinch-per-inch surface strain level. The decays recorded showed substantial curvatures (see Figure 5-21), such that, at lower strain levels, the damping was appreciably less. This, plus possible formulation changes in the adhesive, may explain discrepancies between the Geiger test results (Graph 5-15) and the present test results.

Starting at 75°F, the loss coefficient rose from an initial value of 0.6 to a value of unity at 125°F. It then fell to 0.4 at 300°F and rose again to unity at 450°F. The stiffness modulus fell off very rapidly from an initial value of 500,000 psi to 15,000 psi at 450°F. The loss modulus fell more slowly from 300,000 psi to 9,000 psi. These test results should not be taken as more than an indication of the maxima to be expected from an efficient organic damping structure. Details of end attachment of the tape, etc., as well as the strain levels used, can profoundly affect the shape of the curves.

### 5.6 Other Physical Properties

The following is a brief description of general physical properties drawn mainly from vendor-supplied data. Vendor catalogue information is presented in Appendix II.



AIRESEARCH MANUFACTURING COMPANY OF ARIZONA  
A DIVISION OF THE GARRETT CORPORATION  
PHOENIX, ARIZONA

### 5.6.1 Base Material

Hastelloy X, a nickel-base alloy, was used in the construction of the test apparatus and test bars. It was chosen for its high-temperature strength, oxidation resistance, and machinability. See Appendix II.

### 5.6.2 Coatings

#### 5.6.2.1 Aluminum-Alumina Cermets

Two of a series of sintered aluminum powder alloys (aluminum-alumina cermets) developed by the Aluminum Swiss Company were utilized as coatings during this investigation. The alloys, designated XAP001 and XAP003, offer high mechanical properties in the temperature range from 600° to 1000°F. Other attractive characteristics of the aluminum powder alloys XAP001 and XAP003 are as follows:

- (a) Stable properties at temperature regardless of the length of exposure time at temperature.
- (b) Retention of original room-temperature properties after repeated elevated-temperature exposures.
- (c) High modulus of elasticity at both room and elevated temperatures.



AIRESEARCH MANUFACTURING COMPANY OF ARIZONA  
A DIVISION OF THE GARRETT CORPORATION  
PHOENIX, ARIZONA

The alloys exhibit excellent resistance to creep and stress-rupture over the temperature ranges investigated (up to 1000°F). Appendix II presents information on specific gravity, electrical conductivity, thermal conductivity, coefficient of thermal expansion, melting range, specific heat, and damping. Table 5 shows typical mechanical properties of extruded XAP001. It is believed that the good strength and ductility of XAP001, particularly in the transverse direction, is due to a uniform oxide dispersion.

It is claimed that the general corrosion resistance of the alloys is better than that of aluminum alloys 7075-T6 and 2024-T4 and is comparable to that of 6061-T6. Stress-corrosion tests indicate that XAP001 and XAP003 exhibit excellent resistance to stress-corrosion cracking.

#### 5.6.2.2 Manganese Alloys

Three manganese alloys developed by the Chicago Development Corporation were applied to the test specimens as coatings to determine their damping capacities versus temperature. They are designated C.D.C. Manganese Alloys No.720, 772, and 780. The nominal chemical composition of the alloys, various physical properties, and typical room-temperature mechanical properties of the manganese alloys, are shown in Appendix II.

Alloy No. 720 is a manganese alloy that responds to hardening by heat treatment. It has high tensile and fatigue strength, wide hardness range, and excellent corrosion-resisting characteristics. It is a soft, ductile metal which can be hot- or cold-formed readily. It is hardened by heating in the range of 500 to 900°F. This alloy differs from precipitation-hardening alloys in that



AIRESEARCH MANUFACTURING COMPANY OF ARIZONA  
A DIVISION OF THE GARRETT CORPORATION  
PHOENIX, ARIZONA

TABLE 5-1

## TYPICAL MECHANICAL PROPERTIES OF SINTERED ALUMINUM POWDER EXTRUSIONS AT PROGRESSIVELY ELEVATED TEMPERATURES

<u>Temperature</u>	<u>Property<sup>1</sup></u>	<u>XAP001<sup>2</sup></u>	
		<u>L</u>	<u>T</u>
Room	Ultimate strength, psi	37,000	32,000
	Yield strength, psi	27,000	22,000
	Elongation, %	13	9
400°F	Ultimate strength, psi	23,000	22,000
	Yield strength, psi	19,000	17,000
	Elongation, %	13	9
600°F	Ultimate strength, psi	16,000	14,000
	Yield strength, psi	14,000	12,000
	Elongation, %	11	7
800°F	Ultimate strength, psi	11,000	10,000
	Yield strength, psi	10,000	9,000
	Elongation, %	4	3
1000°F	Ultimate strength, psi	6,000	5,000
	Yield strength, psi	5,000	4,000
	Elongation, %	6	4

NOTES: 1. These properties are independent of time at temperature.  
 2. Upon cooling to room temperature, the original room-temperature properties apply.



AIRESEARCH MANUFACTURING COMPANY OF ARIZONA  
A DIVISION OF THE GARRETT CORPORATION  
PHOENIX, ARIZONA

PREVIOUS PAGE WAS BLANK, THEREFORE NOT FILMED |

dependable and uniform hardening response does not involve critical control of chemical composition, fabricating technique, or heat treatment. Hardening produces a high ratio of yield strength and proportional limit to tensile strength. Negligible distortion occurs during the precipitation hardening.

Manganese Alloy No. 772 offers a combination of high strength and ductility. It has a high thermal coefficient of expansion, low thermal conductivity, and high vibration damping constant. The combination of high strength and a high specific damping constant makes the alloy desirable in applications that cannot incorporate rubber or plastics to reduce vibrations. It is especially useful in eliminating sustained resonance of metallic members due to intermittent shock. The damping rate of the alloy is about 25 times greater than for hardened steel when compared at low stresses.

Alloy 780 possesses an unusual combination of mechanical and thermal properties. Its extremely low shear modulus with high damping capacity provides excellent wear resistance and low noise level.

#### 5.6.2.3 Vitreous Enamels

All test bars were annealed at 1400°F in an exothermic atmosphere for 5 minutes and then sandblasted to produce a mechanical etch.



AIRESEARCH MANUFACTURING COMPANY OF ARIZONA  
A DIVISION OF THE GARRETT CORPORATION  
PHOENIX, ARIZONA

#### 5.6.2.4 Coating Application

Methods of application of the metallic materials were considered, and metal spraying was selected for the following reasons:

- (a) It has little effect on the physical properties of the test flexures.
- (b) It is apparently the only simple way of applying the XAP Alloys and manganese alloys.
- (c) This appeared to be the best general method for applying the materials to parts, and it was therefore desirable to gain experience in this area.



AIRESEARCH MANUFACTURING COMPANY OF ARIZONA  
A DIVISION OF THE GARRETT CORPORATION  
PHOENIX, ARIZONA

As with any coating, surface cleanliness and physical condition are important to obtain adhesion. The best procedure for metal spraying is to sandblast with a 60-grit nominal-size abrasive for cleaning and surface conditioning.

Because thin sections, such as sheet-metal parts, could be distorted by sandblasting, this type of metal spraying might not be practicable. The equipment used for metal spraying is that provided by Metco, Inc. Recommended procedures of Metco were utilized initially and then varied to obtain the desired results--i.e., a uniformly thick layer that exhibited complete adhesion. Since the Mn-Cu alloys are not listed by Metco, their recommended wire-feed speed for copper was used. This proved to be satisfactory, and slightly faster or slower speeds did not appear to alter the coated layer significantly. In the case of XAP Alloys the recommended speed for aluminum proved to be completely unworkable. The metal came out of the gun in large globules and was deposited as a few isolated bumps on the test flexure.

It appeared that either or all of the following was occurring:

- (a) The wire feed rate was too fast.
- (b) The material was not hot enough to atomize.
- (c) Gas pressures to the gun nozzle were too low.
- (d) The gas flow rate was too slow.

The wire-feed speed was slowed to the lowest speed of the gun and gas pressure was increased, as well as gas flow rate. These changes in technique resulted in satisfactory coating of the XAP Alloys.



AIRESEARCH MANUFACTURING COMPANY OF ARIZONA  
A DIVISION OF THE GARRETT CORPORATION  
PHOENIX, ARIZONA

Although the vitreous coatings were not actually applied by AiResearch, there did not appear to be any difficulty encountered. It is pointed out that the firing temperature should not affect the mechanical properties of the base metals because the ultimate usable temperature of the ceramic coating is always lower than the firing temperature.

#### 5.6.3 Fabrication Philosophy

The preparation of the test flexures and the applied coatings developed some problems that were overcome, but also indicated potential difficulties if these materials are to be applied to equipments or parts of equipments. These problems could be:

- (a) Coating application difficulties.
- (b) Deleterious effect of coatings on base metals.
- (c) Effect of potential service environments on coated parts.

Metal spraying, even though a versatile process, would have limitations for coating parts with complex configurations. The difficulty of obtaining a uniformly thick layer in recesses, internal diameters, etc., is inherent with any spray operation. Experience in this area should be gained by processing typical parts that could then be metallurgically examined for coating quality.



AIRESEARCH MANUFACTURING COMPANY OF ARIZONA  
A DIVISION OF THE GARRETT CORPORATION  
PHOENIX, ARIZONA

It would appear that sheet metal previously clad with the coating would simplify fabrication of parts. A determination of the ability to clad various sheet metals with the Mn-Cu alloys should be made. Studies and tests of form bility and other fabrication methods of clad sheet metal would be necessary.

Consideration must be given to the effect of the coating materials on the base metal due to dissimilar metal potentials, which could promote corrosion of the base metal. Diffusion of elements of the coating alloys, as a result of temperature, could result in embrittlement or other changes in mechanical properties of the base metal.

In addition to the above, the effects of service environments on the coatings must be known, such as the capability of coatings to withstand the effects of temperature cycling, thermal shock, and addition of moisture and chlorides in combination with temperature variations. Oxygen, carbon, sulfur, and lead, either singly or in combination, are generally associated with high-temperature applications. A study of coated parts in these environments would have to precede design adaptations to any equipment.



## 5.7 Discussion

### 5.7.1 Temperature Band Width

#### 5.7.1.1 Viscoelastic Materials

Both viscoelastic damping and several anelastic damping mechanisms are ultimately caused by relaxation mechanisms. These relaxation processes are temperature-dependent, and the damping they produce is a function of temperature. Characteristically, the damping exhibits a symmetrical peak when plotted against temperature. The width of the peak depends on the details of the relaxation time distribution function. In this same temperature region other material parameters, such as the stiffness modulus, undergo an abrupt transition to considerably different values.

The simpler materials, having narrow relaxation time spectra, exhibit large values of damping but over such a narrow temperature range that their usefulness is limited in many applications where a range of temperatures may be encountered. In many cases the compounding of the material may be changed to produce a broader relaxation time spectrum and a correspondingly broader temperature characteristic. For example, this is accomplished in polymers by the incorporation of plasticizers. Invariably, a reduction in peak damping accompanies the broadening of the temperature range. Oberst (Ref. 5) has reduced this subject to simple terms, which are approximations, but which appear satisfactory for engineering use.

He shows that the area under an  $\frac{E''}{E_g}$  vs T curve is constant; furthermore, this area is approximated well by a rectangle having  $\frac{E''_{\max}}{E_g}$  as its height, and the width,  $\Delta T$ , measured at the points



AIRESEARCH MANUFACTURING COMPANY OF ARIZONA  
A DIVISION OF THE BARRETT CORPORATION  
PHOENIX, ARIZONA

where  $\frac{E''}{E_g} = \frac{1}{2} \frac{E''_{\max}}{E_g}$ . This leads to the relation

$$\frac{E''_{\max}}{E_g} \Delta T \cong 6^\circ$$

Here

$E''_{\max}$  is the peak value of the loss modulus

$E_g$  is the value of Young's modulus below the transition region

$\Delta T$  is the "half-value" band width of the  $E''$  vs  $\Delta T$  curve

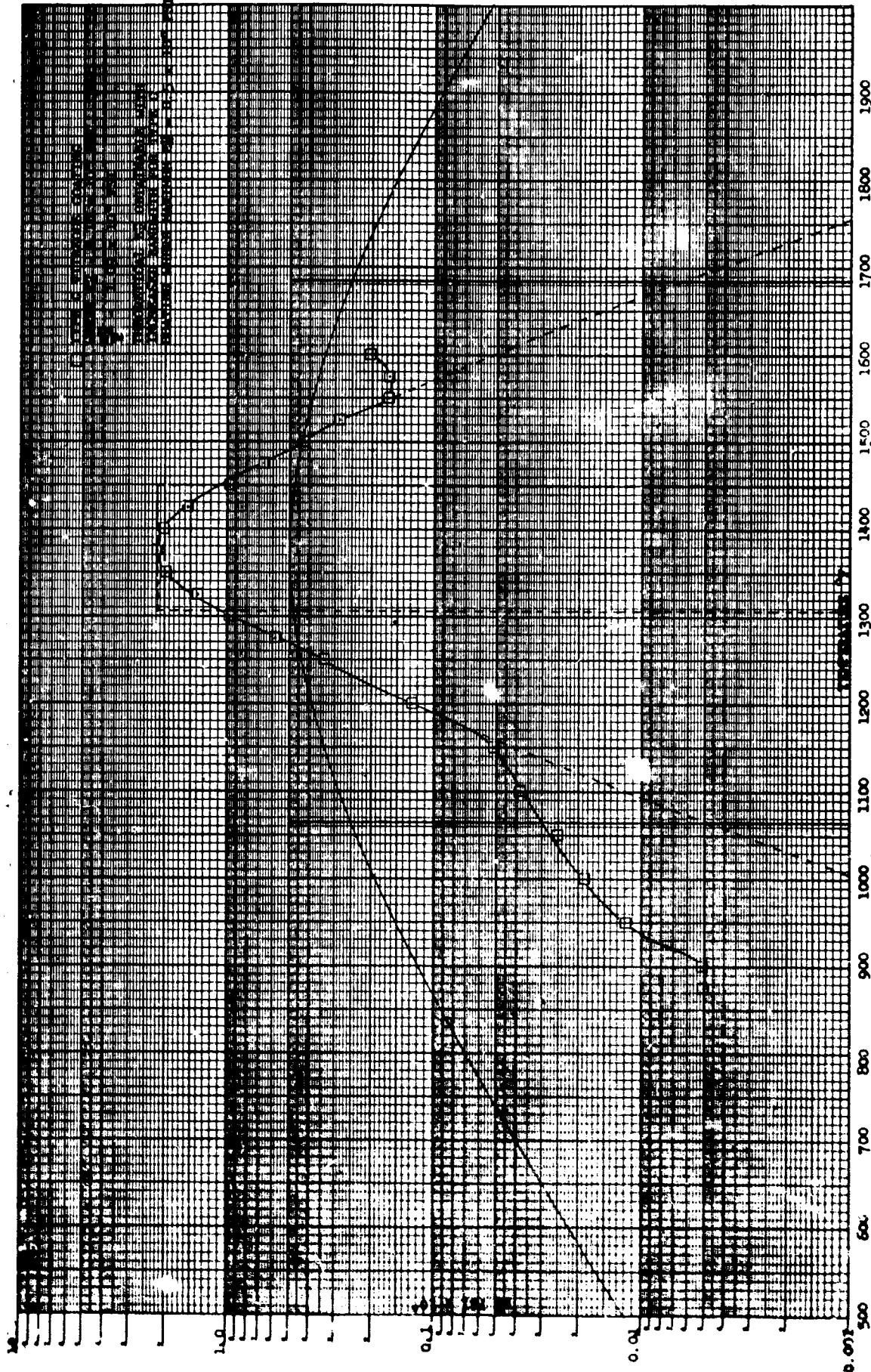
The value  $6^\circ$  assumes measurement of  $\Delta T$  as change in the absolute-temperature Kelvin scale.

Oberst shows that the nominal constant  $6^\circ$  may vary from about  $5^\circ$  to  $7^\circ$ , but the value  $6^\circ$  leads to predictions satisfactory for most engineering purposes.

Although Oberst's work was devoted to polymeric organic materials, his assumptions only invoke a relaxation time mechanism. The behavior of the vitreous materials in their transition region resembles the classic behavior of the organic polymers so closely that there seems little reason to doubt that their behavior is truly viscoelastic and that Oberst's formula holds. Figure 5-44 shows that tradeoff of peak damping for temperature band width according to Oberst's relation.



FIGURE 5-44



GT-7615 R  
Page 5 153



### 5.7.1.2 The Harrison Test

All four vitreous enamels tested showed similar damping peaks. This is illustrated in Figure 5-21, which shows that if  $E_2''$  is plotted against percentage of firing temperatures, the curves for the four enamels nearly superimpose on each other.

The peak damping attained is much greater than that of the best organic materials. This results from the greater stiffness of glass as compared to plastics. The moderate bandwidths, however, are narrower than desirable in many applications in which a range of temperatures are encountered.

It seems reasonable to believe that vitreous enamels having much broader bandwidths (and correspondingly lower peak values) can be compounded. There is a possibility that conventional vitreous enamel's have evolved along lines leading to narrow bandwidths, since well-defined fusion temperatures, rather than a sluggish transition, could be a convenience to the applicator.

To facilitate the compounding of enamel frits having broader temperature bandwidths, a simple screening test is needed. Otherwise, a prospective enamel composition would have to be made and applied to a test bar and a complete damping test conducted for each formulation. The total effort involved in such an approach would be staggering.

Vitreous enamelers and frit manufacturers have paid considerable attention to defining and measuring a fusion temperature for their coatings. Harrison (Ref. 34) at the U.S. Bureau of Standards evolved a test procedure about 35 years ago intended to



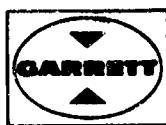
redefine a fusion point. This test has found little or no use among frit makers or enamelers but appears to provide a simple screening test for damping bandwidth.

The Harrison test consists of preparing a small sample of a proposed formulation and melting it in a crucible. While molten, a thermocouple junction is potted in the sample. After cooling, the crucible is placed in a hot furnace and the thermocouple voltage is recorded as a function of time.

The results of such a test are shown in Figure 5-45. The temperature or thermocouple voltage is plotted against the reciprocal of temperature-rate-of-change,  $\frac{\text{seconds}}{2.5^\circ\text{C}}$ . A material having a constant specific heat will generate a simple exponential heating curve as shown in the figure.

A material that is undergoing a progressive loosening of a variety of chemical bonds will not exhibit a constant specific heat. It is undergoing a distributed melting, and each type of bond breakage has an associated latent heat of fusion. The result is a variable reciprocal of temperature-rate-of-change as shown in the figure. It appears almost certain that this test procedure will lead to results having a direct correlation to damping tests, particularly with regard to bandwidth. It should also answer questions of chemical stability in terms of the repeatability after prolonged heating. The Harrison test is therefore recommended for exploration as a screening test for the study of the effect of frit compounding on temperature bandwidth.

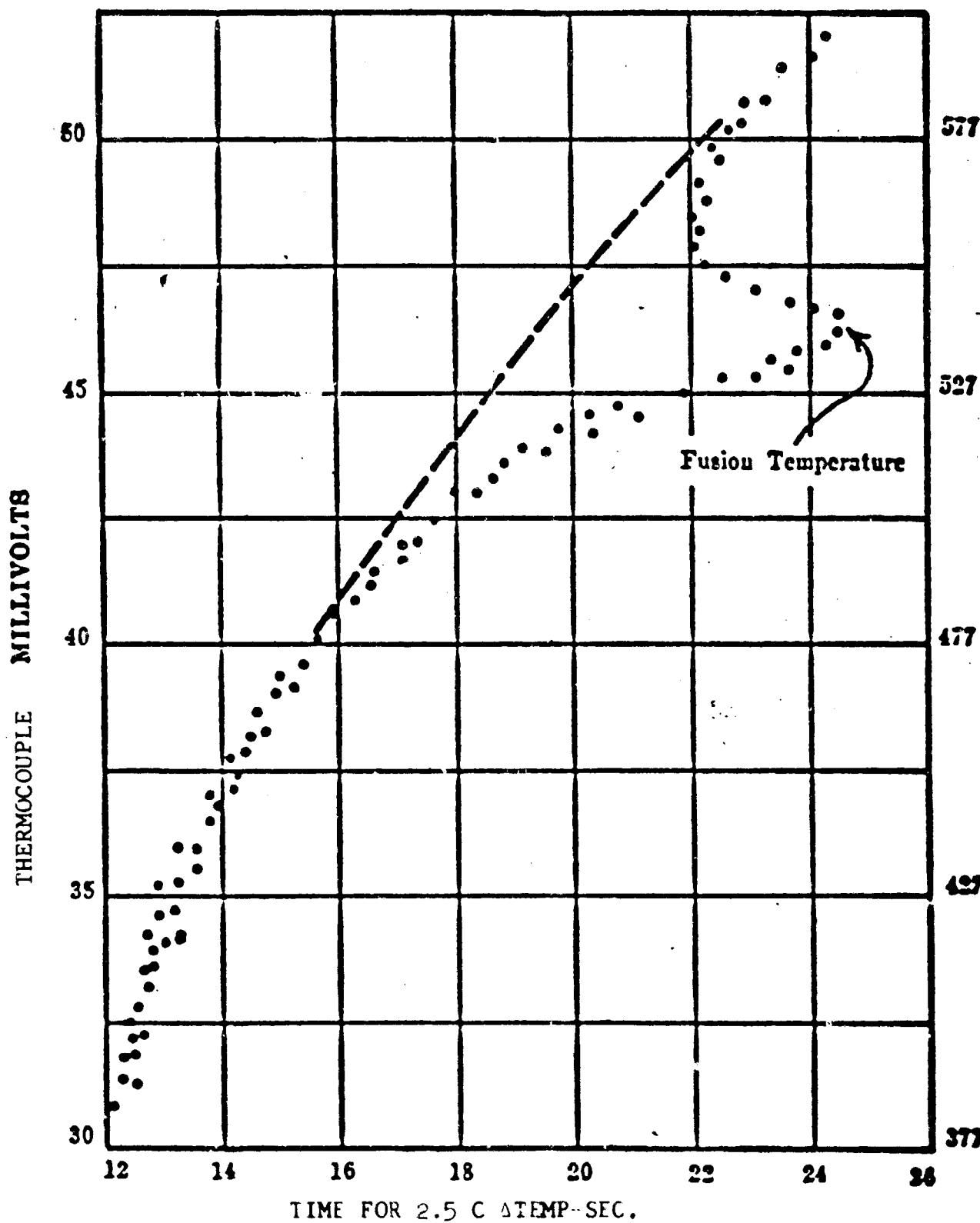
Both Type A (low-temperature) and Type C (high-temperature) enamels showed some indication of broadening of the response curve. The Type A coating exhibits a minor rise in damping near  $500^\circ\text{F}$ ,



AIRESEARCH MANUFACTURING COMPANY OF ARIZONA  
A DIVISION OF THE GARRETT CORPORATION  
PHOENIX, ARIZONA

TYPICAL HARRISON TEST RESULTS  
FOR A PORCELAIN ENAMEL

FIGURE 5-45



GT 7615-R, Rev. 1  
Page 5-156



which levels out as a plateau before the major peak occurs. The Type C material showed a similar tendency on the initial run, but the effect was absent as temperature was decreased. This indicated that minor chemical changes occurred during the thermal cycle. The Type B material showed no such tendencies. The Type B frits were basic frits--probably involving the least elaborate compounding.

#### 5.7.1.3 Manganese Alloys and Cermets

Both the manganese alloys and the aluminum cermets exhibit a broad and increasing damping characteristic as temperature increases. There is no clearly defined symmetrical peak that characterizes viscoelasticity or anelasticity. The decay rates showed little curvature, which leads one to infer that the damping was quadratic from 150 microinches per inch on down.

The broadness of the damping characteristic as a function of temperature is the outstanding merit of the metallic coatings. For many applications, the range of possible operating temperatures is wide, and protection against resonance may be needed at all temperatures. This problem is difficult to cope with if the damping coating is too temperature-dependent. Thus, coatings of XAP alloys can be very useful, since they provide moderate but significant damping from room temperature or below up to 1000°F or more.

For both the manganese alloys and the aluminum cermets the damping mechanisms are unknown. In the absence of some knowledge of the micromechanisms it is impossible to speculate as to the probable effects of composition changes.



AIRESEARCH MANUFACTURING COMPANY OF ARIZONA  
A DIVISION OF THE GARRETT CORPORATION  
PHOENIX, ARIZONA

## 5.7.2 Frequency Bandwidth

### 5.7.2.1 Introduction

Any damping mechanism associated with a relaxation time spectrum is, of necessity, rate-dependent (i.e., frequency-dependent). Thus, it is possible to conduct vibration damping tests at constant temperature and vary the frequency. The result on a viscoelastic material is a resonance curve which, when plotted to the properly chosen frequency scale, is essentially identical with those plotted to a temperature scale.

Such constant-temperature tests are seldom performed, because of the experimental difficulties involved.

Any damping mechanism associated with relaxation spectra will follow a predictable pattern of frequency dependence. An increase in temperature has the same effect on damping as a decrease in frequency, and vice versa. In general, it is observed that a small change in temperature is the equivalent of a large change in frequency. Thus, in many cases, frequency dependence is neglected as a small effect compared to other uncertainties. A material showing good damping at a frequency in the audio range will in all probability be as useful elsewhere in the audio range. Nonetheless, for true optimization of a damping treatment the general magnitude of the frequency dependence should be known, as well as its direction of change.



AIRESEARCH MANUFACTURING COMPANY OF ARIZONA  
A DIVISION OF THE GARRETT CORPORATION  
PHOENIX, ARIZONA

### 5.7.2.2 The Arrhenius Equation

A fundamental relation used by physical chemists to explain the temperature dependence of chemical reactions is the Arrhenius equation:

$$\ln K = - \frac{A_e}{RT}$$

Here

R = gas constant

T = absolute temperature

$A_e$  = activation energy

K = reaction rate

The reaction rate is considered to be proportional to the frequency of collisions involving energy greater than  $A_e$ .

The same form has been found to be valid for relating the frequency and temperature dependence of relaxation damping mechanisms.

$$\ln f = + \frac{A_e}{RT}$$

$$\log_{10} \frac{f}{f_0} = \frac{.43 A_e}{R} \left( \frac{1}{T} - \frac{1}{T_0} \right)$$



AIRESEARCH MANUFACTURING COMPANY OF ARIZONA  
A DIVISION OF THE GARRETT CORPORATION  
PHOENIX, ARIZONA

Here a material having a maximum value of  $F''_2$  at  $T_0$  when tested at  $f_0$  will show max  $E''_2$  at T if tested at frequency f.

This relation holds only in the transition region of the material. Just as the physical chemist must calculate his activation energy,  $A_e$ , from reaction rates measured at two or more temperatures, it is necessary to calculate  $A_e$  from measurements of damping peaks at two or more frequencies.

The Arrhenius equation shows that  $\log_{10} \frac{f}{f_0}$  is proportional to  $(\frac{1}{T_0} - \frac{1}{T})$ . The fact that large changes in frequency are required to produce small changes in the temperature at which  $E''_{max}$  occurs presents appreciable experimental difficulty in the measurements of  $A_e$ .

#### 5.7.2.3 Oberst's Relation

Oberst (Ref. 5) provided convenient bench marks for frequency-temperature interdependence. He derived not only an expression for the bandwidth of  $\frac{E''}{E_g}$  vs temperature, but also an identical expression for the bandwidth of  $\frac{E''}{E_g}$  vs  $\log_{10} \frac{f}{f_0}$ .

$$\frac{E''}{E} \Delta T \approx 6^\circ \text{ Kelvin}$$

$$\frac{E''}{E_g} \Delta \log_{10} \frac{F}{F_0} \approx .68$$

The subscript g infers values typical for its glassy state.



Thus, it is possible to write

$$\Delta \log_{10} \frac{f}{f_0} \cong .11 \Delta T \quad (\text{T in degrees Kelvin})$$

Although originally derived to deal with organic polymer materials, Oberst's assumptions seem general enough to be valid for vitreous materials.

#### 5.7.2.4 Practical Effect

Figure 5-46 shows the application of the above relation to the test results on the Type C vitreous enamel. It shows the great range of frequency that would have to be swept to generate just the portion of the damping curve between the half-value points if the temperatures were held constant at  $1375^{\circ}\text{F}$  ( $747^{\circ}\text{C}$ ). Thus, it can be seen why the frequency dependence is probably of greater theoretical than engineering importance.

#### 5.7.3 Applications

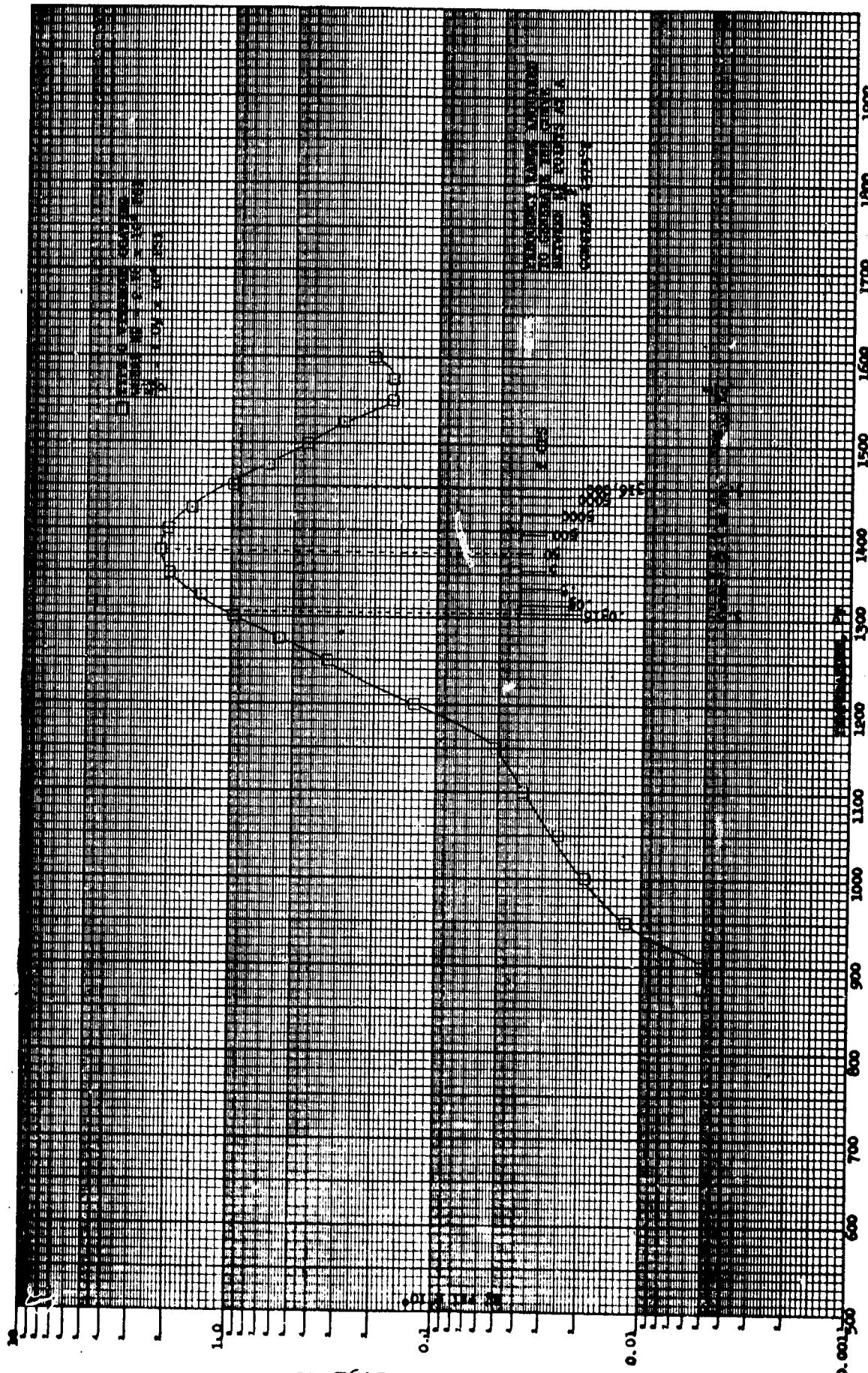
##### 5.7.3.1 Motivations

Vibration-damping coatings are often misapplied, which leads to disappointing results. This is symptomatic of the newness of damping as an engineering tool and the general lack of working knowledge and experience. Vibration-damping coatings are not a cure-all for vibration, noise, and fatigue problems. It is still best to reduce excitation forces or "detune" structures, if possible. Vibration-damping coatings cannot significantly reduce forced vibration. They cannot "absorb" sound in the usual sense of the word. Furthermore, some structures for which damping is



AIRESEARCH MANUFACTURING COMPANY  
A Division of The Goodyear Tire & Rubber Company  
Cleveland, Ohio

FIGURE 5-46



GT 7615 R  
Page 5-162



appropriate already possess enough damping, so that additional damping shows little improvement. The following discussion is intended to provide general guide lines for selecting the cases for which a damping coating is appropriate. These criteria apply to both ordinary temperatures and high temperatures.

#### 5.7.3.2 Exciting Forces

Damping may be appropriate if broadband excitation processes have already been reduced to practical minima and objectionable vibration of sheet metal persists. Broadband excitation forces are becoming increasingly common. Examples are jet and rocket noise, aerodynamic noise, and impact noise.

#### 5.7.3.3 Structure Detuning

The classic approach to a structural resonance that responds to a single frequency-excitation force has been a structural change to move the resonance away from the pure-tone exciting frequency (detuning). There are several types of circumstances in which this solution fails. The structure cannot be detuned if the excitation frequency varies or sweeps over a wide range. Many structures, particularly sheet metal, exhibit numerous closely spaced resonances such that detuning is impractical. A particularly troublesome type of vibration is the self-excited vibration in which a feedback mechanism exists. These excitations occur at resonance frequencies, and if structural tuning changes, they may simply move to the new frequency. Numerous aerodynamic excitations and frictional excitations take this form.



#### 5.7.3.4 Structural Transmission

It is not uncommon to find sheet metal in resonant response to remote excitation forces. The driving signal is "telegraphed" through connecting structure. If decoupling (isolation) is not practical, damping may be indicated. Structural resonances can also lead to a significant reduction in acoustic transmission loss. This occurs commonly in thin ducting. Damping can correct such an acoustical "transparency" of the duct. Even if the criteria above seem to apply, the damping inherent in the structure should be considered. Mechanical joints that are bolted or riveted, or even press joints, can contribute significant coulomb damping. Supplemental damping will have appreciable effect only if its value can be quite large compared to the damping inherent in the structure. Other acoustical or thermal treatments such as glass fiber packs often contribute major amounts of damping as a side benefit. Thus, the use of a damping coating in such an area can become redundant.

Except in certain obvious cases of extremely live structures, all-welded sheet-metal structures, etc., it is desirable to evaluate the inherent damping. This may range from a simple knuckle rapping and subjective judgement of tinniness to an elaborate measurement of vibration decay rates and the computation of system damping factors.

If system damping factors due to inherent damping are known, then the effect of supplemental damping may be estimated or calculated by means that are the reverse of those used in processing test data on coatings. Ref. 2, Chapter 9, is devoted to this general topic.



### 5.7.3.5 Fatigue Failures

Chronic or sporadic fatigue cracking of sheet-metal parts after prolonged operation is an indication that damping is needed. In the case of sheet-metal parts that operate hot, these failures are often complicated by effects of corrosion. The vitreous enamels appear to offer an excellent solution to such combination corrosion and fatigue problems.

The sheet-metal structures in the turbine end of light-weight gas turbines, including jet engines, appear to offer combinations of the above criteria that strongly suggest the usefulness of vitreous damping coatings. Turbine plenums operate at temperatures above 500°F. These have occasionally exhibited fatigue cracks and are known to respond to damping as a means of moderately increasing their high-frequency acoustical transmission loss to the high-intensity noise they contain. They are also subjected to high-velocity airflow with its attendant excitation effects due to turbulence and boundary-layer processes.

Combustor tubes are made of sheet metal and are exposed to high velocity flow of corrosive combustion products. They are frequently subject to cracking. Type C coatings have been successfully used on combustor tubes for many years as corrosion protection. In some cases inadvertent damping must have also been attained but was not clearly recognized. The sheet-metal ducting that conducts the products of combustion to the turbine nozzles is subject to an adverse corrosion and vibration environment. Fatigue failures are common in these areas. Vibration damping by vitreous coatings is strongly indicated.



AIRESEARCH MANUFACTURING COMPANY OF ARIZONA  
A DIVISION OF THE GARRETT CORPORATION  
PHOENIX, ARIZONA

The accurate evaluation of the possible benefits of vibration damping is often difficult and requires elaborate statistics or careful experimentation to answer the question, "How much do we gain?" The gains are frequently worth while but seldom dramatic or glamorous. In the case of fatigue failures, it may require prolonged field operation and careful overhaul statistics to show that parts designed for a 2,000-hour life show a 99-percent reliability if coated, instead of 88 percent, if uncoated. To predict such a result from prototype tests requires a careful strain-gauge study.

Acoustical benefits are even more difficult to predict. In common with many other acoustical treatments, careful isolation of noise sources is required for true evaluation. This point is so commonly misunderstood that an example is in order.

Suppose a machine such as a gas turbine possesses six noise-generating mechanisms of roughly the same strength. Examples might be the compressor inlet, exhaust duct, body radiation, cooler fan, etc. Now, suppose a separate treatment is designed for each individual noise source that accomplishes its complete silencing. If these are applied one at a time to the gas turbine, each time leaving the other five sources unattenuated, the first conclusion reached would be that none of the silencing devices were any good, since none accomplished a significant noise reduction--this in spite of the fact that the use of all six would render the machine completely silent!



AIRESEARCH MANUFACTURING COMPANY OF ARIZONA  
A DIVISION OF THE BARRETT CORPORATION  
PHOENIX, ARIZONA

This unhappy error is an everyday occurrence which mars a vast amount of acoustical testing that is not designed with sufficient discrimination. The useful testing of an acoustical component such as a damping coating can be meaningful only if all other extraneous noise processes are eliminated for the purpose of the test.

Another pitfall is the common discrepancy between objective and subjective measurements. This discrepancy seems particularly large in the case of the effects of damping. The measurable differences between the noise in an automobile with a damped vs undamped body structure are small and require careful frequency analysis under well-controlled test conditions to be revealed. Nonetheless, because of subjective judgments of "tinniness," a car with an undamped body is subject to a severe sales handicap. Such subjective factors as this introduce a semi-intuitive aspect into engineering decisions regarding damping.

The commonest criterion for what constitutes a well-damped engineering structure is a system damping factor of 0.01 to 0.1. This is a value typical for wooden structures assembled with mechanical fastenings in which Coulomb damping is present (nails, bolts, etc.). Thus, the criterion for adequate damping is to produce a modern engineering structure that is as well damped as the engineering structures of previous centuries.



## 6.0 MICROMECHANISMS AND MODELS

### 6.1 Introduction

The study of carefully selected vibration damping coatings, which was the subject of Section 3.0, was almost purely phenomenological in character. The apparatus and test methods were designed to provide as accurate an evaluation as possible of the damping characteristics of the coatings themselves. Speculative consideration of possible micromechanisms of damping entered only into the selection of the materials tested.

The testing was also limited to low stress levels. Virtually all materials exhibit fairly high damping at high stress levels but only by processes associated with the fatigue and self-destruction of the material. High damping at low stress levels has been shown to be such a rare property of structural materials that it is often designated by the adjective "anomalous."

Now that a few such "anomalous" materials have been shown to exist, the "center of gravity" of future investigations should shift closer to investigation of micromechanisms. Only by a better understanding of the micromechanisms of damping operative in the materials can they be shaped and modified to optimum characteristics, and other useful materials found.

Section 6.2 presents a brief sketch of the various micromechanisms leading to vibration damping.



Section 6.3 presents a brief discussion of what little is known about the micromechanisms acting in the specimens tested. Some of this is almost purely speculative in character. In some cases, not enough is known to provide a basis for speculation.

Section 6.4 deals briefly with the micromechanisms of damping at high stress levels and their relation to fatigue. This vitally important subject deals mainly with nonlinear stress-strain relations. The major tool for studying the damping associated with these processes is the study of the hysteresis loop. Here the study of damping becomes a major research tool. Attempts are made to correlate the magnitudes and shapes of the hysteresis loops with micrographic and X-ray spectrographic observations on the specimens. Finally, these data are considered in a framework of theory generally designated as "dislocation" theory. This entire branch of materials engineering and science is scarcely two decades old.

Section 6.4 also describes briefly the apparent reasons why damping studies have fallen short of expectations in the study of micromechanisms in general and the micromechanisms of fatigue in particular. These shortcomings appear to result from the lack of an adequate mathematical model for the hysteresis loop and, in particular, the nonlinear hysteresis loop.

Section 6.5 is devoted to the sketching of such a mathematical model suggested by analogous difficulties recently overcome in the field of shaft dynamics.



## 6.2 Some Known Micromechanisms

### 6.2.1 Anelasticity

A sizable group of micromechanisms that produce linear damping (elliptical hysteresis loops) in response to low-level stress or strain inputs is designated by the term "anelasticity." In general, anelasticity produces rather well-defined peaks at particular combinations of temperature and frequency. These peaks are almost always very modest in magnitude. Values of the loss factor  $\eta$  are limited to less than 0.01, except for slightly higher values occasionally found in light metals such as aluminum or magnesium.\*

One mechanism for energy dissipation involves heat transfer from regions heated by compression to other regions less heated (or even cooled by expansion). These effects may be macroscopic, such as by heat transfer through a bar, or may be microscopic due to uneven stresses in a material. The magnitude of such damping is small and is frequency-dependent.\*

The anelastic mechanism that usually produces the largest damping peak is called "boundary layer viscosity." The molecules within a grain or crystal are quite regular in their lattice structure. At the grain boundary, however, an abrupt transition occurs from one lattice to a differently oriented lattice, and the arrangement of boundary atoms is disordered in a manner somewhat analogous to the partial disorder in a vitreous material. At a particular combination of temperature and frequency a viscous-type damping can occur.\*

\*Reference 2



AIRESEARCH MANUFACTURING COMPANY OF ARIZONA  
A DIVISION OF THE GARRETT CORPORATION  
PHOENIX, ARIZONA

Another anelastic mechanism occurs in various metals and alloys because of magnetostrictive effects. Periodic stress variations produce periodic magnetic fields. These, in turn, induce eddy currents in the material that lead to energy dissipation. This mechanism characteristically vanishes at the Curie point of the material.\*

A very rare anelastic mechanism occurs in manganese alloys and zirconium hydride. These materials have a cubic phase and a phase that is only slightly tetragonal. The tetragonal lattice can occur in parallel layers that are minor images of each other. This leads to a "herringbone" appearance on micrographic specimens, as well as characteristic double peaks in X-ray diffraction patterns. Such a structure can show large values of Young's modulus, yet since a "lossy" distortion can occur in which the long axes of the tetragonal units change, anomalous damping occurs.\*\*

Numerous other mechanisms have been isolated as causes for minor anelastic peaks, particularly in metals. The location and identification of these peaks furnish a useful tool to the solid state physicist.

#### 6.2.2 Viscoelasticity

Viscoelasticity is a term commonly applied to quadratic damping mechanisms in which a relaxation mechanism is involved. At high frequencies (or low temperatures), the material acts elastically because there is insufficient time for the relaxation processes to occur. At very low frequencies (or high temperatures) there is plenty of time for the relaxation to be complete, and the material

\*Reference 2

\*\*References 7, 14 and 15



is then quite plastic but with a smaller Young's modulus. At intermediate frequencies (or temperatures) a transition occurs in which a large and symmetrical damping peak occurs. In the past, this behavior has been mainly associated with polymeric organic compounds. The microstructure of such polymers consists essentially of long chain modules capable of an endless variety of side or cross linkages. The transition region has been associated with the progressive loosening of the side linkages, with the chain links remaining essentially intact. Vast amounts of data on polymeric materials have been taken, and it is clear how measurements of damping are a valuable tool to the organic physical chemist. The wealth of data on polymeric materials and knowledge of the effects of compounding have led to the present-day abundance of organic vibration damping coating materials.\*

#### 6.2.3 Nonlinear Damping

Nonlinear damping produces hysteresis loops that are not elliptical but which usually are pointed figures. Almost always it is associated with higher stress levels. These stress levels are almost always high enough that the material has a finite fatigue life. The detailed mechanisms are multitudinous, complex, and little understood. Examples of attempts to correlate the nonlinear hysteresis loops and micrographic data are the subject of Section 6.3.\*\*

\*References 2, 3, 4, 5, and 6

\*\*References 2, 8, and 26



### 6.3 Micromechanisms in the Specimens Tested

The purpose of this section is to set forth what little is known, plus some speculations, concerning micromechanisms of the damping found in the specimens.

#### 6.3.1 Hastelloy-X

The damping peak exhibited by the bare test bars at temperatures near  $1350^{\circ}\text{F}$  has been tentatively attributed to grain boundary viscosity. This anelastic mechanism is normally the source of the largest anelastic peaks. The peak damping observed in the Hastelloy-X corresponds to a loss factor  $\eta$  of a little less than 0.01. This is in agreement with Reference 2, which sets 0.01 as a nominal damping limit for  $\eta$  for this type of damping. The straightness of the logarithmic decay curves indicates quadratic dependence on stress amplitude. The temperature of the peak damping agrees with the empirical equicohesive temperature (about  $1/2$  the melting temperature). The equicohesive temperature is defined as the temperature at which grain strength and grain boundary strength are equal. Below this temperature, fracture occurs across grains. Above this temperature, fracture occurs along grain boundaries. It is therefore quite reasonable to expect viscous effects to manifest themselves in such a transition temperature range.

#### 6.3.2 Vitreous Enamels

In the region of the major damping peak, the behavior of all four vitreous enamels fits the classic model of viscoelasticity. The "E" hump is very symmetrical, which justifies the use of Oberst's frequency temperature relations. The appearance of the



hump coincides with an abrupt decline in stiffness modulus. The loss factor  $\eta$  attains values in excess of unity, as is true of many polymers. The simplest summary seems to be to list (probably) all glasses as viscoelastic materials.

The vitreous enamels were selected for test because of suspicions that this was the state of affairs, as mentioned previously. Vitreous materials are known to have a type of partial disorder in their atomic lattice.\* Silicon chains are the counterparts of carbon chains even in such polymeric materials as silicone rubber. Glass has no fixed molecular formula but rather may be compounded in endless variety from a wide selection of oxides in a manner analogous to the freedom with which one modifies the polymers.

Inspection of the vitreous enamel damping below the major peak shows interesting effects. In some cases the results differ between the increasing temperature run and the decreasing temperature run. In one case the stiffness modulus actually increases for the first few hundred degrees of the first run. One may infer that the enamel has not completely stabilized chemically during the rather brief (15 minutes) firing process that originally applied it to the test bar. These transitions show the relation of composition to the width of the damping characteristics and support the hope that stable compositions having broadened characteristics can be found.

The appearance of the minor peaks and plateaus suggests the presence of various types of bonds that loosen at very different temperatures. This would suggest that the approach to broader temperature characteristics is the use of a considerable number

\*Reference 21



of ingredients having markedly different bond-loosening temperatures. This clue may be of value to the glass compounders. It is clear from the tests that the measurement of damping could serve the glass industry by indicating, for example, the completeness, or stability, of the chemical arrangements.

With glass having been classified as a viscoelastic material, the striking similarities in nomenclature and fabricating technology between glass and plastics should no longer seem remarkable.

#### 6.3.3 Manganese Alloys

The anomalous damping of the manganese alloys seems explainable by Zener's model\* only up to 300°F.\*\* Above this temperature the material is supposed to have a purely cubic structure, and the twining of the slightly tetragonal units is no longer possible. Thus, what is known about the micromechanisms explains only the modest initial damping and its minimum at 300°F. The reasons for the substantially greater damping found as the temperature was increased must be listed as completely unknown. This temperature region should provide a challenge to research in these alloys. The metal spray specimens provide a poor basis for even speculation because of their probable lack of homogeneity and their uncertain condition of heat treatment and working.

#### 6.3.4 Aluminum Cermets

The aluminum cermets show lower temperature tendencies unlike those of the manganese alloys. Starting from "modest" damping at room temperature (anomalously high by most standards),

\*Reference 15

\*\*Reference 14



they show a tendency to attain a plateau at 300°F and then begin a slow steady rise. Thus, they show useful damping over a very wide temperature range. The micromechanisms that produce this behavior are not known.

#### 6.4 Micromechanisms and Fatigue

Aside from simple noise control, the chief use for vibration damping coatings is protection against metal fatigue due to excitation of resonances. This becomes critically important at times, partly because fatigue processes are so imperfectly understood and, hence, poorly predictable.

The systematic study of fatigue is a very new science, dating back, at most, about two decades. Powerful new tools have become available for these studies. These include the use of electron microscopy which provides magnification orders of magnitudes greater than those possible by optical means.

The stress-strain relations that prevail while the fatigue process proceeds from initial plastic deformation to ultimate rupture are changing but always nonlinear hysteresis loops. These have been carefully observed in numerous studies. Certain tendencies and trends are discernible, and some success has been attained in correlating these with micrographic observations.

Reference 8 is an example of recent (1960) thorough work in the field. Numerous carefully prepared specimens of high-purity aluminum were subjected to prolonged cyclic stress. The changing patterns of the hysteresis loops were recorded. The surface of the specimens was studied by both optical and electron-beam micrographs as the



tests proceeded. The enormous magnification made possible by the electron microscope shows in remarkable detail the progress of fatigue from early slip bands to the microscopic cracks that precede rupture. These details are not at all discernible by optical methods.

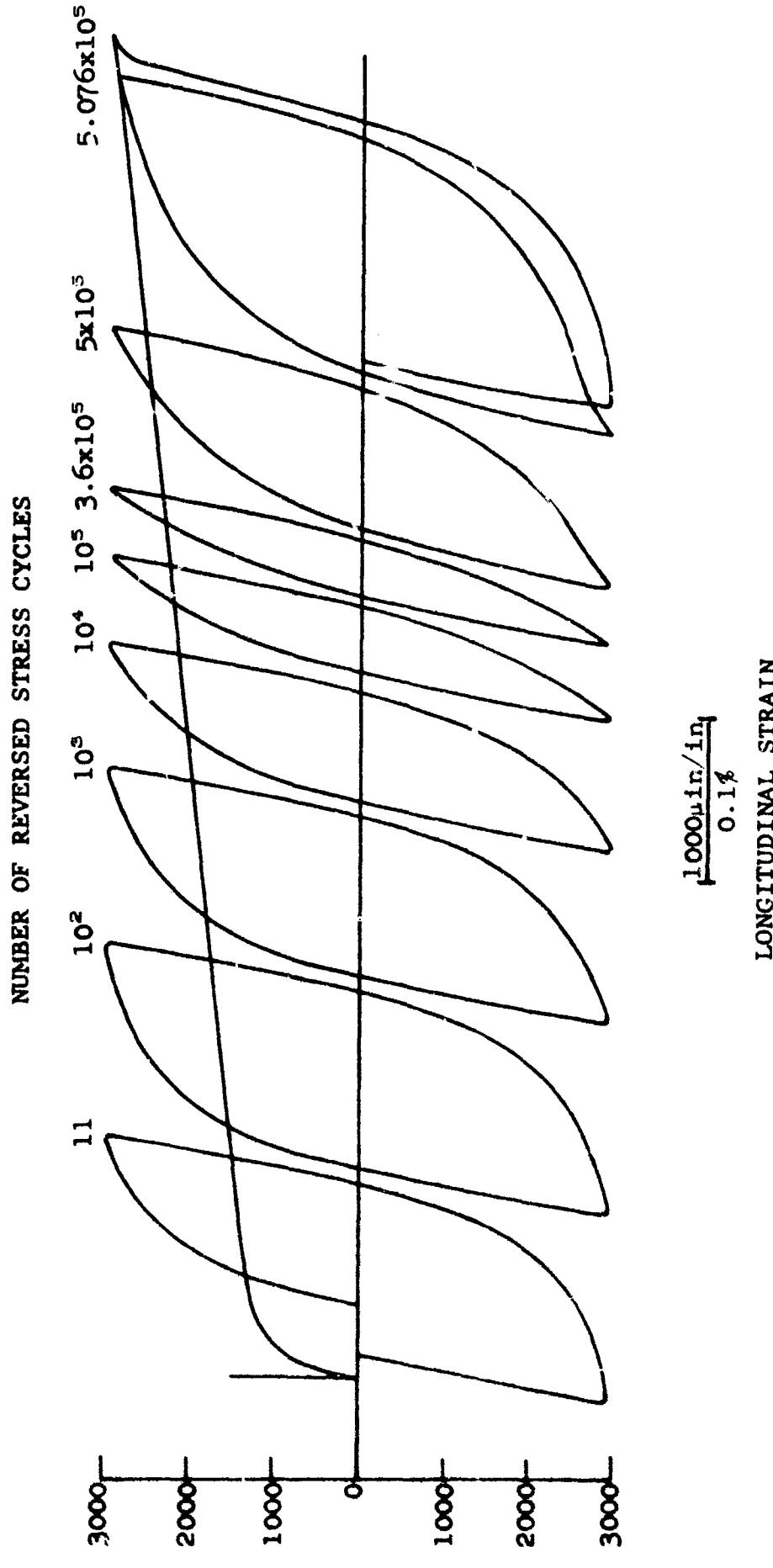
Figures 6-1, 6-2, 6-3, 6-4, and 6-5, reproduced from Reference 8, are presented as samples of the hundreds that appear in this reference. Figure 6-1 shows typical changes in the hysteresis loop as the number of cycles increases. Figure 6-2 shows the typical surface condition of a specimen before application of cycle stress. Figures 6-3, 6-4, and 6-5 show the progressive fatigues from early slip bands to advanced stages of damage, which would eventually be a microscopic crack.

Concurrent with this type of advanced observations, solid-state physicists are attempting to construct theoretical models of the microprocesses involved. These attempts are designated as dislocation theory. Any discussion of these theories is far beyond the scope of this work. However, interested persons will find a discussion and summary of the present state of dislocation theory, as well as additional references, in Reference 2.

Since the recorded hysteresis loops are quantitative measurements of stress-strain relations and show trends that parallel micrographic observations and features of dislocation theory, it is natural to seek quantitative relations between theory and measured stress-strain patterns. In fact, the term "theory" is not quite properly applied until some quantitative agreements are demonstrated. Serious difficulties as to method have arisen to obstruct these attempts. The difficulty is the lack of an adequate mathematical model for a nonlinear hysteresis loop.



AIRESEARCH MANUFACTURING COMPANY OF ARIZONA  
A Division of The Garrett Corporation  
Phoenix, Arizona

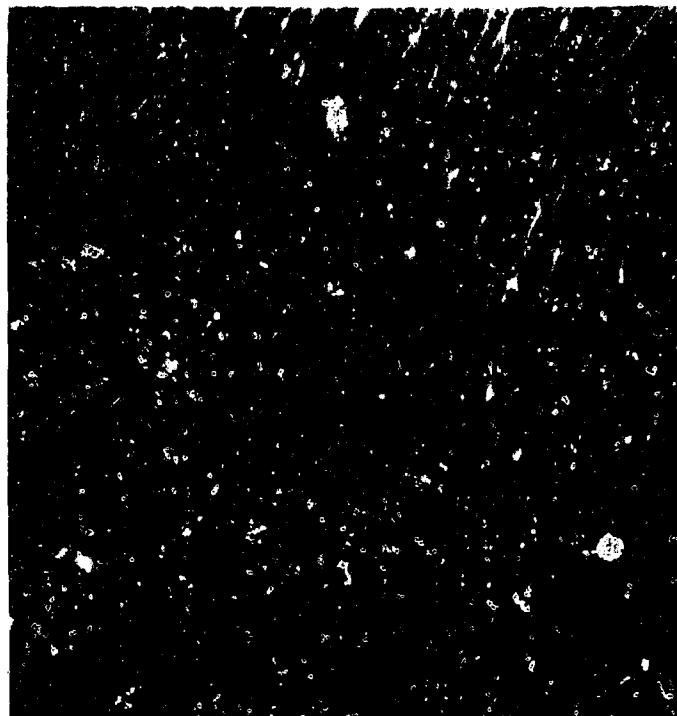


GT-7615-R  
Page 6-11

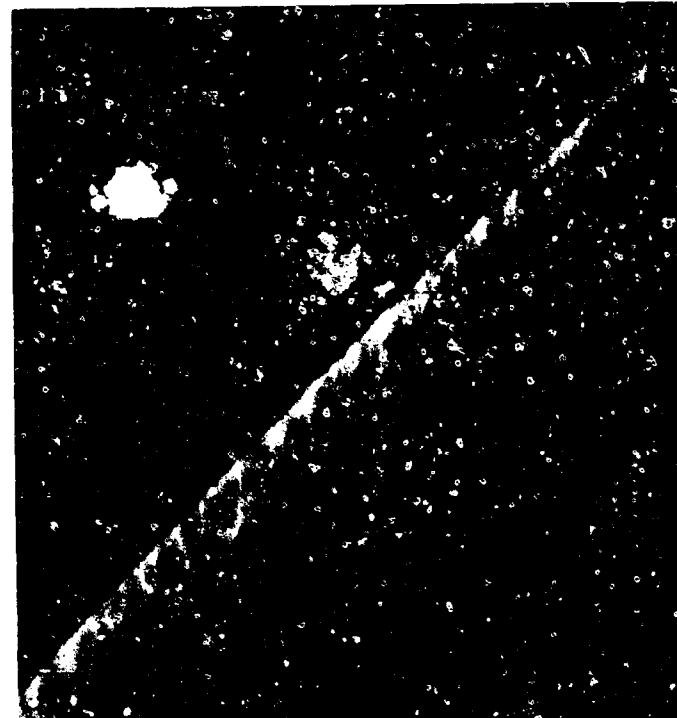
FIGURE 6-1  
TYPICAL CHANGES IN STRESS-STRAIN HYSTESIS LOOPS  
OCCURRING WITH TYPE BC SPECIMEN DURING FATIGUE  
TEST AT HIGH STRESS AMPLITUDE,  $\pm 2940$  PSI  
(REPRODUCED FROM REFERENCE 8)



AIRESEARCH MANUFACTURING COMPANY OF ARIZONA  
A DIVISION OF THE BARRETT CORPORATION  
PHOENIX, ARIZONA



— 1 $\mu$  UNTESTED X 8000



— 1 $\mu$  BE  $\pm$ 900 PSI, 500,000 C X 8250

FIGURE 6-2  
ELECTRON MICROGRAPHS OF CHEMICALLY POLISHED  
SPECIMENS SHOWING GRAIN BOUNDARIES  
(REPRODUCED FROM REFERENCE 8)  
GT-7615-R  
Page 6-12



AIRESEARCH MANUFACTURING COMPANY OF ARIZONA  
A DIVISION OF THE GARRETT CORPORATION  
PHOENIX, ARIZONA

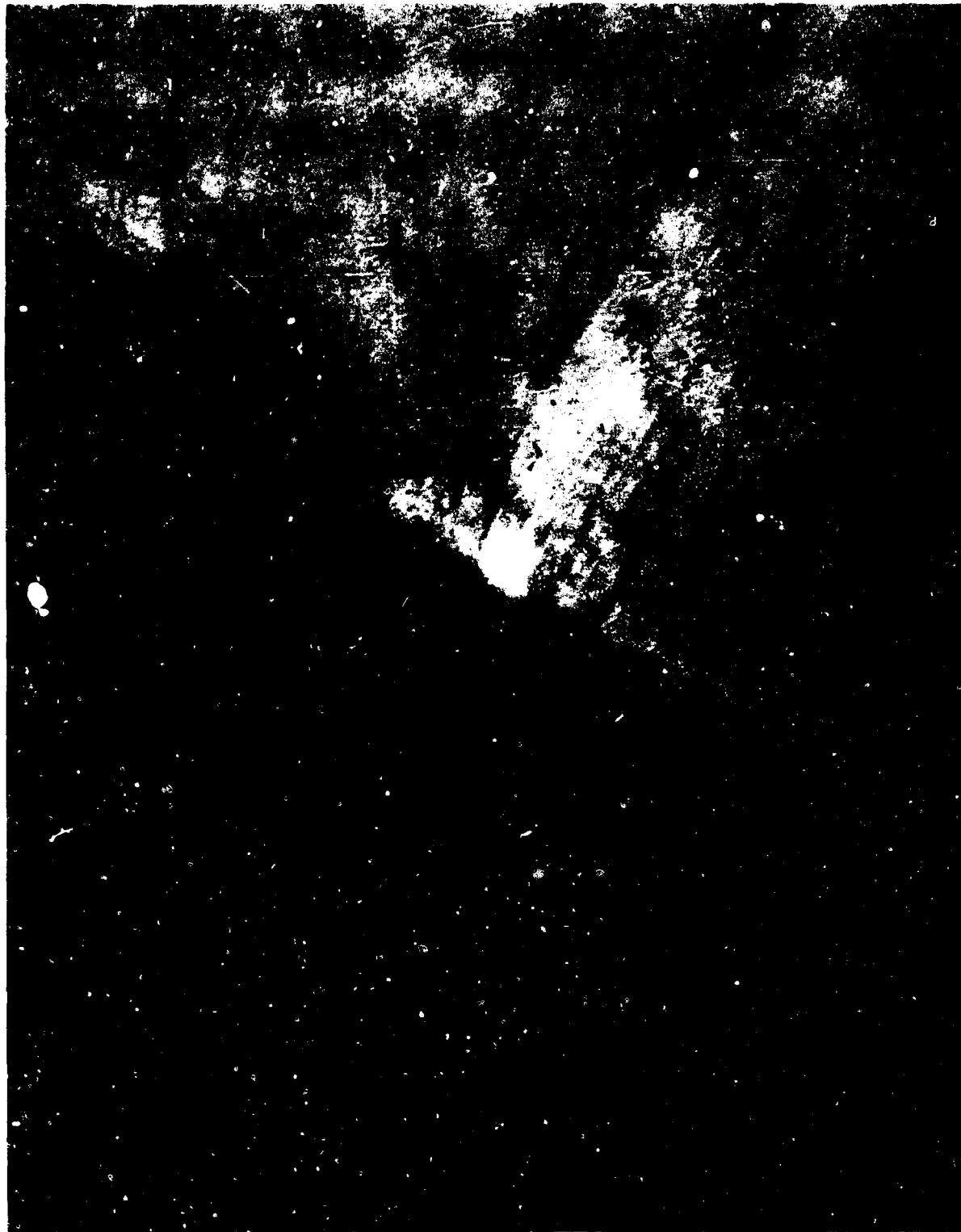


FIGURE 6-3  
ELECTRON MICROGRAPH FROM SURFACE REPLICA OF TAPERED SPECIMEN  
AT  $\pm 2500$  PSI LEVEL, AFTER 1000 CYCLES; SHOWING DISPLACEMENT  
ON LINES OF A SLIP SYSTEM DUE TO INTERSECTING SLIP BAND  
(REPRODUCED FROM REFERENCE 8)

GT-7615-R  
Page 6-13



AIRESEARCH MANUFACTURING COMPANY OF ARIZONA  
A DIVISION OF THE GARRETT CORPORATION  
PHOENIX, ARIZONA



1 $\mu$  —

X 15,500

FIGURE 6-4  
ELECTRON MICROGRAPH FROM SURFACE REPLICA OF TAPERED  
SPECIMEN AT  $\pm 2500$  PSI LEVEL, AFTER  $10^4$  CYCLES;  
SHOWING STRUCTURE OF BROAD SLIP BAND AND NEARBY FINE SLIP  
(REPRODUCED FROM REFERENCE 8)

GT-7615-R  
Page 6-14



AIRESEARCH MANUFACTURING COMPANY OF ARIZONA  
A DIVISION OF THE BARRETT CORPORATION  
PHOENIX, ARIZONA



FIGURE 6-5  
ELECTRON MICROGRAPH FROM SURFACE REPLICA OF TAPERED  
SPECIMEN AT  $\pm 2500$  PSI LEVEL, AFTER  $10^5$  CYCLES; SHOWING  
REGIONS OF COARSE SLIP BANDS GIVING EVIDENCE OF EXTRUSIONS  
(REPRODUCED FROM REFERENCE 8)

GT-7615-R  
Page 6-15



AIRESEARCH MANUFACTURING COMPANY OF ARIZONA  
A DIVISION OF THE GARRETT CORPORATION  
PHOENIX, ARIZONA

Professor Lazan describes the lack of such equations in these words.\*

"Unfortunately, general rheological equations for defining stress-strain-time relations of material are unavailable in almost all cases. Only under restricted conditions, such as for linear viscoelasticity, is such an approach now feasible. Even if general rheological equations were available for the more general types of materials systems, which are usually nonlinear, they would probably be too complicated to be mathematically tractable. Only in relatively few cases can rheological equations be found that are general, valid (that is, compatible with engineering realistics), and also mathematically tractable."

It is pointed out in the following section that an apparently suitable mathematical model capable of representing any hysteresis loop has existed for about 2,000 years--in elegantly refined form for over a century.

\*Reference 2 Chapter 2



AIRESEARCH MANUFACTURING COMPANY OF ARIZONA  
A DIVISION OF THE GARRETT CORPORATION  
PHOENIX, ARIZONA

## 6.5 Rheological Epicycles

### 6.5.1 Introduction

#### 6.5.1.1 The Need for a Stress-Strain-Time Equation

"An explicit stress-strain-time equation, if it exists, would provide a particularly powerful approach for studying rheological behavior under complicated stress histories involving many loadings and unloadings . . . . . Unfortunately, all efforts to describe the rheological properties of solid materials by explicit stress-strain-time equations of this type have, with very few and highly restricted exceptions, been unsuccessful."\*

The very few and highly restricted exceptions to which Professor Lazan refers include the following stress-strain-time rheological equations:

##### A. Perfect elasticity:

$$\frac{\text{stress}}{\text{strain}} = E_0 = \text{Young's modulus}$$

##### B. Quadratic damping independent of time:

$$\frac{\text{stress}}{\text{strain}} = E' + iE''$$

##### C. Quadratic damping which may be dependent on rate or temperature:

$$\frac{\text{stress}}{\text{strain}} = E'(\omega T) + iE''(\omega T)$$

$\omega$  = circular frequency

T = temperature

\*Reference 2, Chapter 1.



Case C represents viscoelasticity and anelasticity. Both generate elliptical hysteresis loops, the geometry of which depends on frequency and temperature. Case C includes A and B as special cases.

In all cases the moduli may also be long-range functions of other variables such as stress history, magnetic fields, and the like.

The bulk of the materials or systems of engineering interest is nonlinear. These generate hysteresis loops that are pointed even for sinusoidal inputs. They can also be unsymmetrical. For Coulomb-type damping mechanisms, such as dry friction, they can be quadrilateral in shape.

These have been stone walls that have defied satisfactory representation as functions of stress-strain-time, not to mention temperature, stress history, etc.

#### 6.5.1.2 Prior Attempts to Derive the Equation

The attempts that have been made to represent the hysteresis loops as stress-strain functions are discussed by Professor Lazan in Chapter 4 of Reference 2. These include the Davidenkov representation and the very similar expressions of Halford and Morrow.

These expressions appear to be clever curve fittings. The loading and unloading branches of the hysteresis loops must be dealt with separately. As a result of their empirical nature, they must at best be approximate and lack the physical meaning essential for them to be truly useful.



#### 6.5.1.3 Requirements

To meet the need indicated above, a stress-strain-time relation is required that is capable of representing the hysteresis loop resulting from any stress or strain wave-shape input in the presence of any arbitrary preload. The same expression should represent any part of either branch of the hysteresis loop. Above all, it should be both mathematically tractable and capable of meaningful physical interpretation and, hence, representation by physical models. If its parameters are simple and relatively few in number, then chances are increased that they can be expressed as functions of temperature and the long-range variables. These parameters should be amenable to simple, direct measurement and geometric representation. Finally, the general expression must include all previously solved cases (cases A, B, and C above) as special cases.

#### 6.5.1.4 The Need for Communication

"Although communication within a given field is generally reasonably effective, communication among different disciplines, which often utilize different nomenclatures, is generally quite difficult."\*

Once such communication is established, the various branches of natural science profitably borrow mathematical models from each other. For example, the wave equation is common to optics, mechanics, electricity, and acoustics. The pure mathematician is frequently the contact man between the various sciences.

The acoustician is also strategically disposed to serve as a contact, since his science is a hybrid of nearly all the others.

\*Reference 2, Chapter 2.



In industry, sound and vibration are frequently lumped together as a single activity. This is quite natural, since the instruments and concepts are much the same. Vibration may be regarded as sound that is not yet airborne, and a vibrating machine can be considered to be merely a peculiar type of loudspeaker.

This customary lumping of activity is true at AiResearch. For turbomachinery builders, most vibration problems originate as symptoms of complex shaft-dynamics problems.

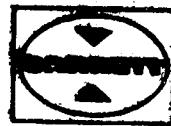
#### 6.5.1.5 A New Approach

A routine procedure in the study of anomalous shaft motions is to display them as Lissajous figures such as those shown in Figure 6-6.

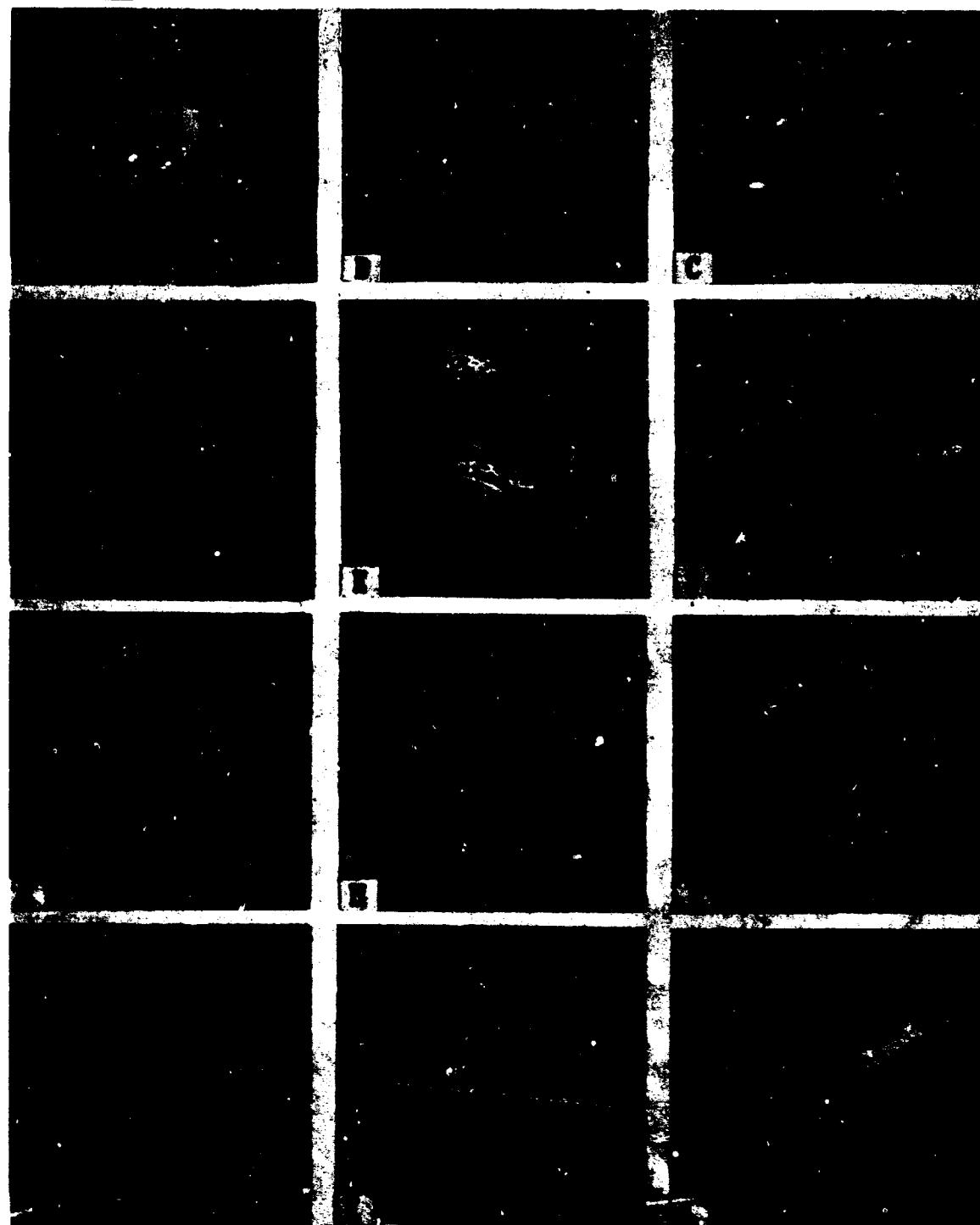
The simpler patterns frequently bear a resemblance to hysteresis loops--i.e., ellipses, double-pointed loops, or quadrilaterals. For many years, these figures (shaft excursions) were also considered too complex to respond to any simple mathematical representation.

Within the last decade the work of Professor Tashio Yamamoto of Nagoya University, Japan (Ref. 35), has resulted in a simple and lucid representation for such figures. Furthermore, the representation is derived as the explicit solution of Newtonian equations.

The essence of this representation is the superposition of simple circular motions (precessions). Each may progress in either the positive or negative direction and have any angular velocity. The most complex of the motions shown in Figure 6-6 may be readily resolved into a very few such precessions.



RESEARCH MANUFACTURING COMPANY OF ARIZONA  
A DIVISION OF THE GOODYEAR CORPORATION  
Phoenix, Arizona



SHAFT MOTIONS

FIGURE 6-6

07-7615-A  
Page 6-21



An interesting feature of these superimposed motions is the fact that they are mathematically indistinguishable from the nearly 2,000-year-old kinematic system known as the Epicycles of Ptolemy.

Ptolemy kinematically explained the apparently erratic motions of the planets as the superposition of circular motions of various frequencies and directions. Such a kinematic model is in reality closely related to Fourier analysis, but is much more general, since no restrictions need be placed on the frequencies.

#### 6.5.1.6 Rheological Epicycles

The demonstrable rigorous correctness of representing a two-dimensional locus of any shape as a summation of epicycles, plus their usefulness in representing complicated loci in the field of shaft dynamics, assures in advance that hysteresis loops can be represented as a sum of epicycles.

Since hysteresis loops are very simple figures as compared to those generated by shafts, the number of epicycles required should be quite limited.

From this representation, it is easy to exhibit some remarkable facts about hysteresis loops, some of which may not have been clearly realized before. Section 6.5.2 is devoted to exhibiting an epicyclic representation and deriving such properties of the hysteresis loop as follows:

- (a) Damping occurs only by the interaction of harmonic components present in both stress (strain) input and the strain(stress) response.



- (b) The motion of the point that generates an elliptical hysteresis loop obeys Kepler's second law.
- (c) The dynamic modulus of a viscoelastic material has a dual character (i.e., there are two related dynamic moduli).
- (d) An epicyclic representation converges rapidly, so only a few terms are needed even in the extreme case of a square hysteresis loop (coulombic damping) used as an example. These parameters are easy to obtain experimentally and have a straightforward electrical analogy.
- (e) Neither sinusoidal stress inputs nor sinusoidal strain inputs generate a hysteresis loop that truly exhibits the rheological properties of a material. Neither can lead to a unique representation.

In spite of this elegance and apparent usefulness, the representation evolved proved to suffer one major weakness--i.e., it does not provide a set of parameters that are unique. This disappointment was foreshadowed by the fact that Ptolemy's epicycles, although kinematically beyond reproach, represented an earth-centered system rather than a sun-centered system, although they could equally well have represented a heliocentric model.

Late in this exercise it was realized that an equivalent unique formulation existed in the form of power series. This formulation has been only partially explored but appears to remove the defects of the Ptolemaic representation of Section 6.5.2 and yet includes all its advantages. In Section 6.5.2 some of the following properties of the final formulation that are shown are:



- (a) At any point in time a material specimen may be represented by a unique set of a few parameters such that the hysteresis loop resulting from any input may be predicted.
- (b) The stress history may be traced as the history of the parameters.
- (c) These parameters cannot be deduced from stress-strain tests as they have been conducted in the past.
- (d) The unique set of parameters for nonlinear materials leads to a representation that degenerates properly--i.e., produces essentially quadratic damping at low stress and exhibits progressively greater distortion as the stress levels increase.

The type of interrelation that exists between stress-strain-time and the long-range and environmental variables has counterparts in several other fields. Nonlinear hysteresis loops occur in magnetics, electricity, mechanics, acoustics, etc. In these fields the inadequacy of single-input experiments to define the system characteristics has been repeatedly recognized (see Reference 36). It is therefore hoped that the epicyclic representation can prove useful in any field that must cope with time-dependent nonlinear hysteresis loops.



### 6.5.2 A Ptolemaic Formulation

#### 6.5.2.1 Parametric Equations

In any material, stress is a function of strain, and vice versa. In such a case, the most natural representation is by means of parametric relations.

$$\epsilon = F_1(\sigma) \quad (6-1)$$

$$\sigma = F_2(\epsilon) \quad (6-2)$$

So,

$$\epsilon = F_3(\theta) \quad (6-3)$$

$$\sigma = F_4(\theta) \quad (6-4)$$

where  $\theta$  is a parameter. For time-independent cases, a convenient parameter is a polar angle. For any time-dependent case we set

$$\theta = \omega t \quad (6-5)$$

#### 6.5.2.2 Complex Notation

The representation for hysteresis loops which is formulated is basically a vector representation. For this purpose it proves to be convenient to utilize the isomorphism of two-dimensional vectors and complex-number algebra. The complex stress-strain plane is therefore established as follows:

$$Z' = \epsilon' + i\sigma' \quad (6-6)$$



It should be emphasized that the complex-number notation is chosen purely to facilitate vector manipulation and has no other significance.

Materials engineers are accustomed to a real stress-strain plane for all types of hysteresis loops. To discuss anelasticity or viscoelasticity, however, they resort to complex notation in order to cope with a dynamic modulus

$$E^* = E' + iE'' = E' (1 + i\eta) \quad (6-7)$$

This creates a second plane having coordinates  $E'$  and  $iE''$  to supplement the real  $\epsilon$ ,  $\sigma$  plane.

One of the conveniences of a complex stress-strain plane is the fact that  $E^*$  may also be presented in this same plane.

The creation of the complex stress-strain plane encounters one difficulty. The physical units of stress and strain are different, and as a result, the physical units of any vector that is not parallel to a coordinate axis are not consistent. This defect is equally present in a real stress-strain plane whenever significance is attached to the length of oblique lines such as the various moduli (see Figure 3.14 in Reference 2).

The obvious solution to this difficulty is normalization to dimensionless stress (strain is already dimensionless). This may be accomplished in a variety of ways. In this presentation the stress is normalized by dividing it by the absolute value of the dynamic modulus of the material. Thus, unit strain is associated with unit stress, which is dimensionless. How this applies to nonlinear materials will become evident later.



At this point the primes are dropped to signify that the normalization of the coordinates axes has been accomplished.

$$Z = \epsilon + i\sigma \quad (6-8)$$

where

$$\sigma = \frac{\sigma'}{|E^*|} \quad (6-9)$$

A hysteresis loop is now a closed locus of Z in the  $\epsilon$ ,  $\sigma$  plane as shown in Figure 6-7.

#### 6.5.2.3 A Rheological Theorem

##### 6.5.2.3.1 Theorem I

Given any closed hysteresis loop that is periodically traced in the complex plane  $Z = \epsilon + i\sigma$ , then it may be represented as being traced by the tip of a moving vector  $\bar{H}$  where

$$\bar{H} = \sum_{n=0}^{n=\infty} R_n e^{in\theta} + \bar{R}_n e^{-in\theta} \quad (6-10)$$

$$\bar{R}_n = R_n e^{ia_n} \quad (6-11)$$

$$\bar{R}_n = R_n e^{is_n} \quad (6-12)$$

$R_n$ ,  $R_n$ ,  $a_n$ ,  $s_n$  are all real arbitrary constants.  $\theta$  is a polar angle that may be set equal to  $\omega t$  where

$$\omega = 2\pi f \quad (6-13)$$

t = time

The term f is the fundamental frequency for the periodic traverse of the locus (see Figure 6-7).



AIRESEARCH MANUFACTURING COMPANY OF ARIZONA  
A DIVISION OF THE GARDNER CORPORATION  
PHOENIX, ARIZONA

16

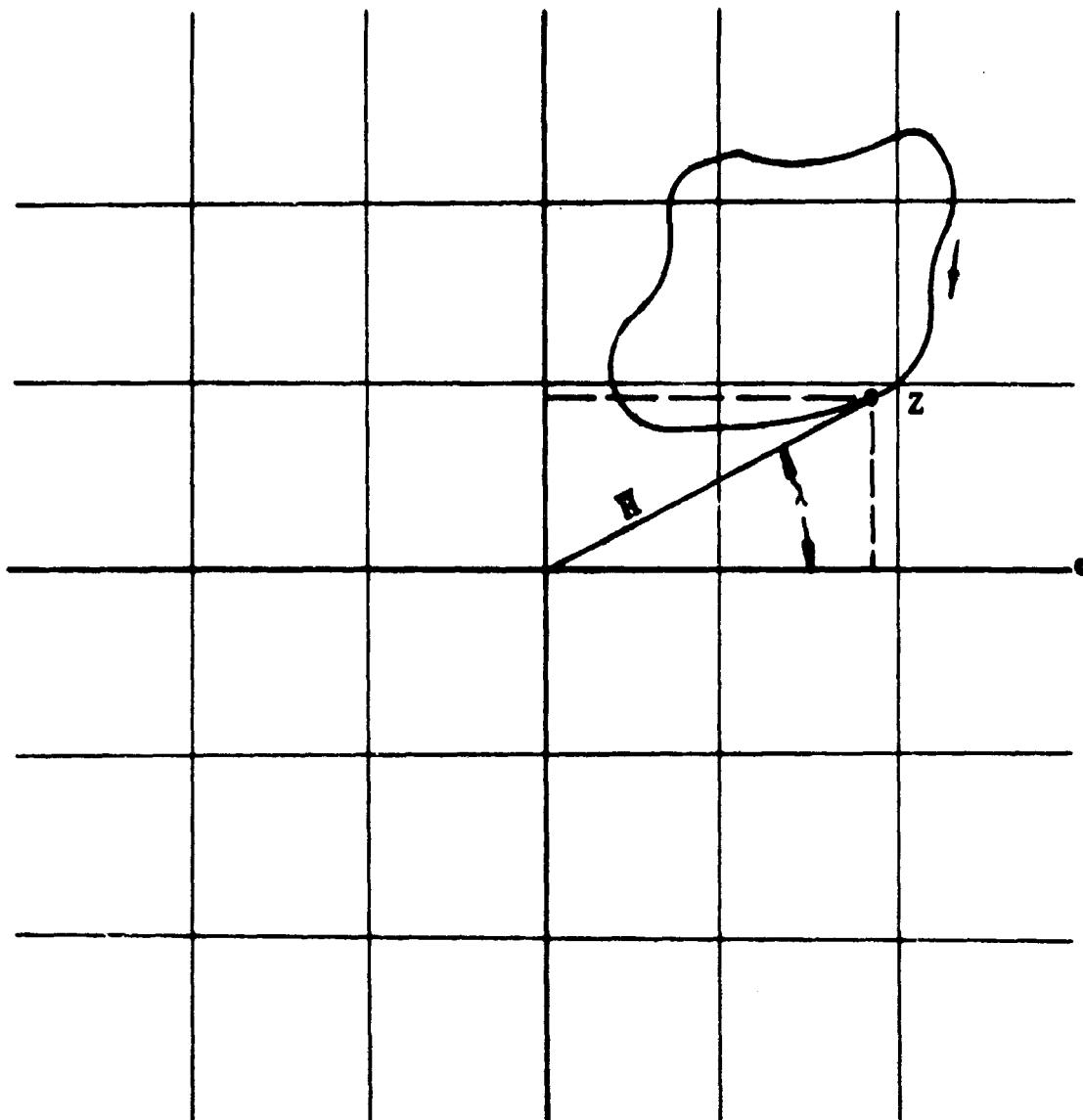


FIGURE 6-7

AN ARBITRARY HYSTERESIS LOOP  
IN A COMPLEX PLANE

B11010

GT-7615-R, Rev. 1  
Page 6-28



### 6.5.2.3.2 Notes on the Theorem

This theorem simply states that any physically realizable closed hysteresis loop resulting from any arbitrary periodic stress or strain input with any preload may be expressed as the sum of a series of  $n$  paired counterrotating vectors. Each of these vectors has a constant length,  $R_n$  or  $\bar{R}_n$ , rotates with a constant angular velocity,  $n\omega$  or  $-n\omega$ , and has a particular initial angular displacement,  $a_n$  or  $\theta_n$ , at time zero.

$R_n$ ,  $\bar{R}_n$ ,  $a_n$ , and  $\theta_n$  are to be regarded as short-term steady-state constants. They may be functions of long-term variables such as temperature and stress history.

The vectors  $\bar{R}_n$  rotate in the positive (counterclockwise) direction, since  $n\omega$  is positive.

The vectors  $\bar{R}_n$  rotate in the negative (clockwise) direction, since  $-n\omega$  is negative.

The symbol  $\bar{R}$  is a Russian letter pronounced "ya" and is chosen because its shape, a backward R, suggests its rotation in the backward direction.

It will be shown in later sections that the vectors  $\bar{R}_n$  and  $\bar{\theta}_n$  have a simple physical meaning leading to simple model representation and to a simple electrical analog representation. As a result, they lead to certain striking conclusions concerning energy relations that may have been overlooked in the past. Finally, the representation seems to settle once and for all the classic controversy over whether it is better to use stress inputs or strain inputs.



### 6.5.2.3.3 An Informal Proof of the Theorem

In Figure 6-7, the point Z, which is the tip of a radius vector  $\bar{H}$ , traces out the arbitrary closed loop in a periodic manner in the normalized  $\epsilon + i\sigma$  plane. The radius vector  $\bar{H}$ , in general, has a variable length and a variable angular velocity. As is evident from the figure, the locus of the tip of  $\bar{H}$  is the locus of the complex number  $\epsilon + i\sigma$ , that is:

$$\bar{H} = \epsilon + i\sigma \quad (6-14)$$

Since the locus of the tip of  $\bar{H}$  is traversed periodically, both  $\epsilon$  and  $i\sigma$  are periodic functions of  $\theta$  and may be written as Fourier series. Fourier series may be written in many forms, including the rather straightforward forms shown below.

$$\epsilon(\theta) = \sum_{n=0}^{\infty} \epsilon_n \cos(n\theta + \phi_n) \quad (6-15)$$

$$i\sigma(\theta) = i \sum_{n=0}^{\infty} \sigma_n \sin(n\theta + \phi_n) \quad (6-16)$$

But by the identities shown in Appendix 1,

$$\cos(n\theta + \phi_n) = \frac{1}{2} \left[ e^{i(n\theta + \phi_n)} + e^{-i(n\theta + \phi_n)} \right] \quad (6-17)$$

$$i \sin(n\theta + \phi_n) = \frac{1}{2} \left[ e^{i(n\theta + \phi_n)} - e^{-i(n\theta + \phi_n)} \right] \quad (6-18)$$



AIRESEARCH MANUFACTURING COMPANY OF ARIZONA  
A DIVISION OF THE BARRETT CORPORATION  
PHOENIX, ARIZONA

These identities show that the trigonometric functions themselves may be expressed as the sum of two counterrotating vectors. For each value of n there are four such vectors:

$$\frac{\epsilon_n}{2} e^{i(n\theta + \psi_n)} \quad \frac{\sigma_n}{2} e^{i(n\theta + \phi_n)}$$

$$\frac{\epsilon_n}{2} e^{-i(n\theta + \psi_n)} \quad - \frac{\sigma_n}{2} e^{-i(n\theta + \phi_n)}$$

These may be combined into a single positive rotating and single negative rotating vector simply by addition. These sums serve as the definition of the vectors  $\bar{R}_n$  and  $\bar{\sigma}_n$ .

$$\bar{R}_n e^{in\theta} = \frac{\epsilon_n}{2} e^{i(n\theta + \psi_n)} + \frac{\sigma_n}{2} e^{i(n\theta + \phi_n)} \quad (6-19)$$

$$\bar{\sigma}_n e^{-in\theta} = \frac{\epsilon_n}{2} e^{-i(n\theta + \psi_n)} - \frac{\sigma_n}{2} e^{-i(n\theta + \phi_n)} \quad (6-20)$$

Thus,

$$\bar{H} = \epsilon + i\sigma = \sum_{n=0}^{\infty} \bar{R}_n e^{in\theta} + \bar{\sigma}_n e^{-in\theta} \quad (6-21)$$



#### 6.5.2.4 Kinematics

##### 6.5.2.4.1 The Zero-Order Vectors

It is evident that the zero-order vectors  $\bar{R}_n$  and  $\bar{R}_o$  are nonrotating and when added represent any initial preload. Thus, the preload is a stationary vector which serves to shift the center of the coordinates axes (see Figure 6-8). It is convenient here to consider  $\bar{H}$  as the sum of components  $\bar{H}_n$ .

$$\bar{H} = \sum_{n=0}^{n=\infty} \bar{H}_n \quad (6-22)$$

where

$$\bar{H}_n = \bar{R}_n e^{in\theta} + \bar{R}_o e^{-in\theta} \quad (6-23)$$

$$\bar{H}_o = \bar{R}_o + \bar{R}_o \quad (6-24)$$

It can also be shown that

$$R_o e^{ia_o} = R_o e^{is_o} \quad (6-25)$$

Hence,  $R_o = R_o$  and  $a_o = s_o$

To simplify the exposition, henceforth consider no preload to be present; i.e.,

$$\bar{H}_o = 0,$$

and proceed to examine the nature of a typical  $\bar{H}_n$  term

$$\bar{H}_n = \bar{R}_n e^{in\theta} + \bar{R}_n e^{-in\theta} \quad (6-26)$$



AIRESEARCH MANUFACTURING COMPANY OF ARIZONA  
A DIVISION OF THE GARRETT CORPORATION  
PHOENIX, ARIZONA

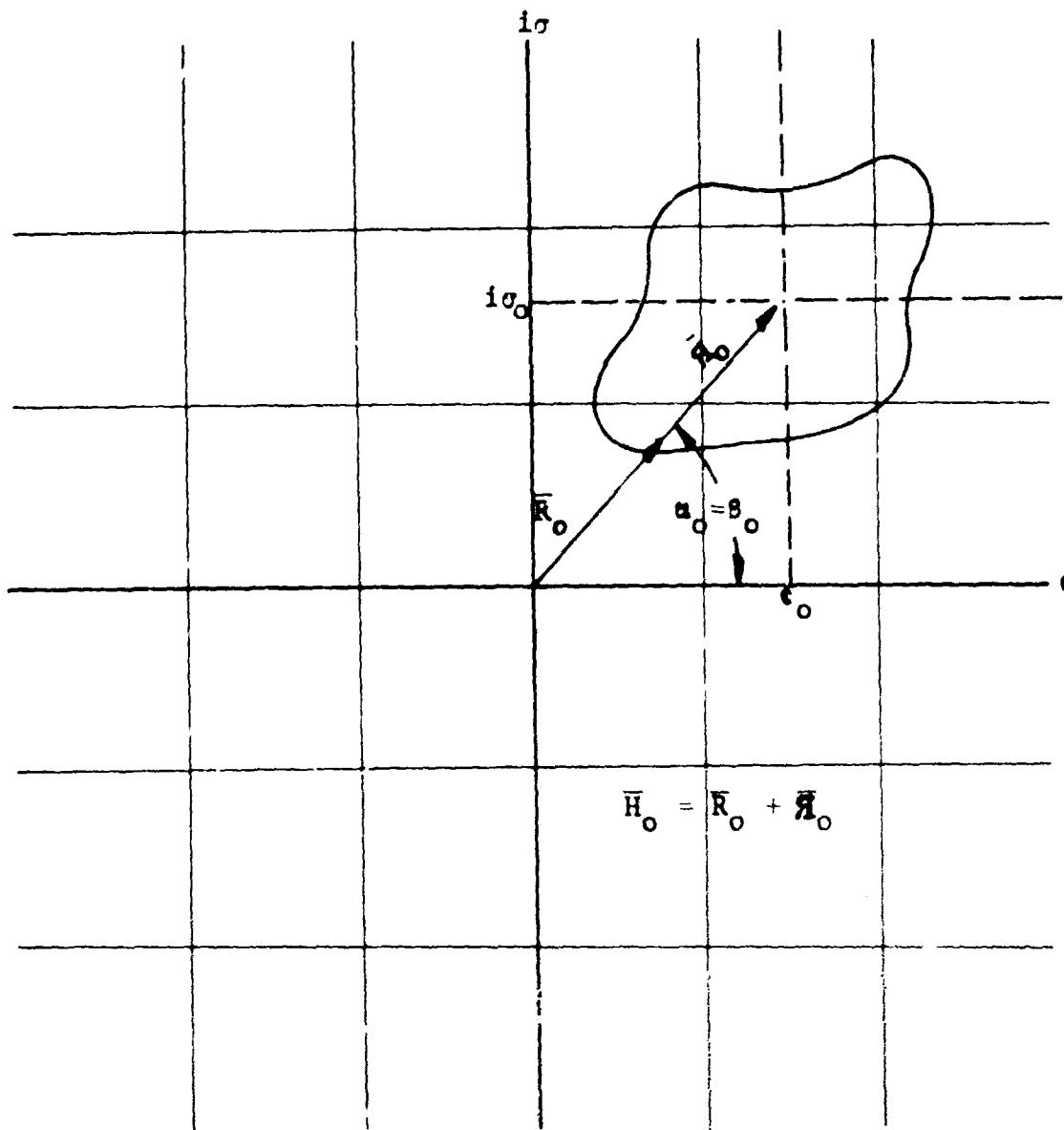


FIGURE 6-8

THE ZERO ORDER TERM WHICH  
REPRESENTS THE PRELOAD

B11009

GT-7615-R  
Page 6-33



#### 6.5.2.4.2 The $n^{\text{th}}$ Order Vector

For any "lossy" material, stress leads strain by some angle  $\delta$ . It is not possible to show  $\delta$  directly in the real stress-strain plane.

In the complex stress-strain plane,  $\bar{R}_n$  is formed as the sum of the positive rotating stress component vector and the positive rotating strain component vector.

$$\bar{R}_n = \frac{\epsilon_n}{2} e^{(i\psi_n)} + \frac{\sigma_n}{2} e^{(i\phi_n)} \quad (6-27)$$

The angle between these two components of  $\bar{R}_n$  is

$$\phi_n - \psi_n = \frac{\pi}{2} + \delta_n > \frac{\pi}{2} \quad (6-28)$$

as shown in Figure 6-9.

The vector  $\bar{R}_n$  is formed as the sum of the negative rotating stress component vector and the negative rotating strain component vector

$$\bar{R}_n = \frac{\epsilon_n}{2} e^{-i\psi_n} - \frac{\sigma_n}{2} e^{-i\phi_n} \quad (6-29)$$



AIRESEARCH MANUFACTURING COMPANY OF ARIZONA  
A DIVISION OF THE GARRETT CORPORATION  
PHOENIX, ARIZONA

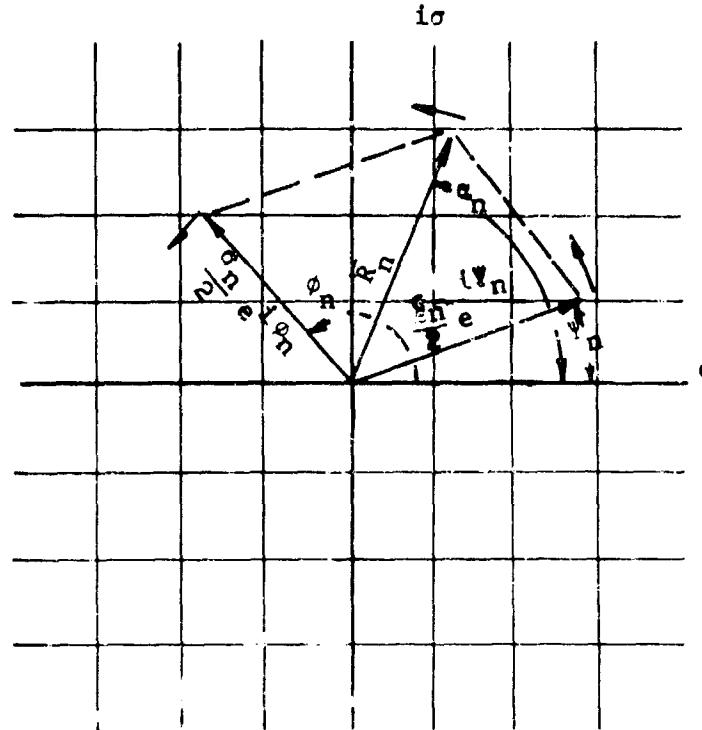


FIGURE 6-9  
THE COMPONENTS OF  $\bar{R}_n$  AT  $t = 0$

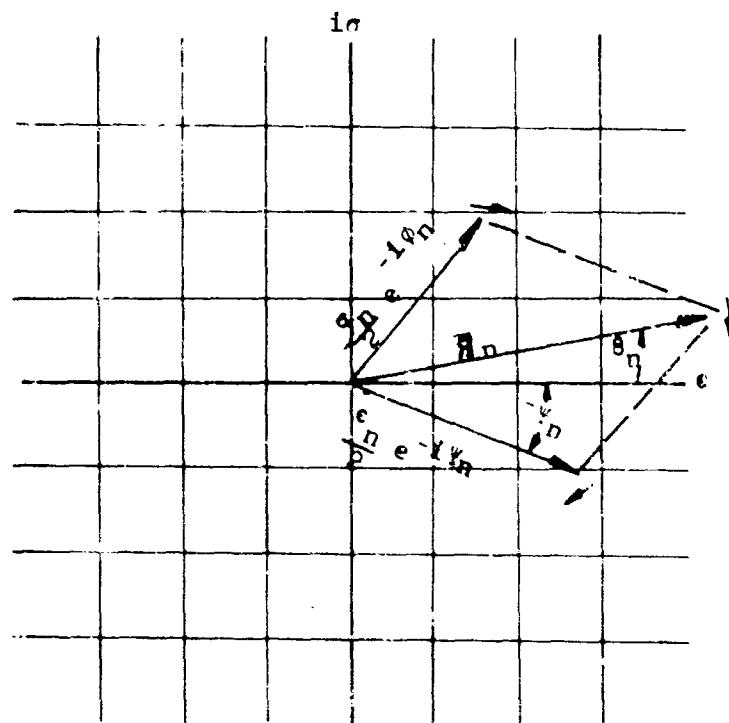


FIGURE 6-10  
THE COMPONENTS OF  $\bar{R}_n$  AT  $t = 0$

B10998

GT-7615-R, Rev. 1  
Page 6-35



AIRESEARCH MANUFACTURING COMPANY OF ARIZONA  
A DIVISION OF THE GARRETT CORPORATION  
PHOENIX, ARIZONA

As can be seen in Figure 6-10, the stress component again leads the strain component (stress vector attains the vertical before the strain vector attains the horizontal as the pair rotate in the clockwise direction).

The angle between them is less than  $\frac{\pi}{2}$ .

$$\psi_n - \phi_n = \frac{\pi}{2} - \delta < \frac{\pi}{2} \quad (6-30)$$

Thus, stress leads strain by the same amount for either direction. Also,  $\bar{R}$  and  $\bar{R}$  are both formed from components having the same absolute values. The angle between the positive rotating component vectors is always obtuse. The angle between the negative components is always acute. Therefore,

$$R_n > \bar{R}_n$$

if energy is dissipated by the  $n^{\text{th}}$  term. Careful inspection of Figures 6-9 and 6-10 will clarify this point.

Recall that

$$\bar{R}_n = R_n e^{i\alpha_n} \quad (6-32)$$

$$R_n = R_n e^{i\theta_n} \quad (6-33)$$

If  
 $\theta = \omega t$  (6-34)

it is clear that the tip of  $R_n e^{i\omega n t}$  sweeps out a circle (epicycle) at constant angular velocity,  $n\theta = \omega n t$ , in the positive (counter-clockwise) direction.



Similarly,  $\bar{R}_n e^{-in\theta}$  sweeps out a circle of radius  $R_n$  at constant angular velocity  $-n\omega t$  (i.e., in the clockwise direction).

$$\bar{H}_n = \bar{R}_n e^{in\theta} + \bar{R}_n e^{-in\theta} \quad (6-35)$$

must therefore generate an ellipse having semimajor axis  $R_n + R_n$  and semiminor  $R_n - R_n$ , since it was shown  $R_n < R_n$ . These ellipses generated by  $\bar{H}_n$  include as special cases the circle (if  $R_n = 0$ , or  $R_n = 0$ ) and the straight line (if  $R_n = R_n$ ).

Since

$$\bar{H}_n = \sum_{n=0}^{\infty} \bar{H}_n, \quad (6-36)$$

it is clear that the most nonlinear hysteresis loop may be resolved into the sum of  $n$  linear elliptical hysteresis loops.

#### 6.5.2.4.3 The Semi-Major Axis

It is evident from Figure 6-11 that at some particular time  $t_n$  the counterrotating vectors  $\bar{R}_n$  and  $\bar{R}_n$  will have the same direction angle (often called the "argument"), and this angle must be the average of  $\alpha_n$  and  $\beta_n$ . It is also evident from the figure that

$$\frac{\alpha_n + \beta_n}{2} \quad (6-37)$$

is always the angle of inclination for the principal axis of the  $n^{th}$  ellipse.

$$e^{i(n\theta+\alpha_n)} = e^{-i(n\theta-\beta_n)} \quad (6-38)$$



AIRESEARCH MANUFACTURING COMPANY OF ARIZONA  
A DIVISION OF THE GARRETT CORPORATION  
PHOENIX, ARIZONA

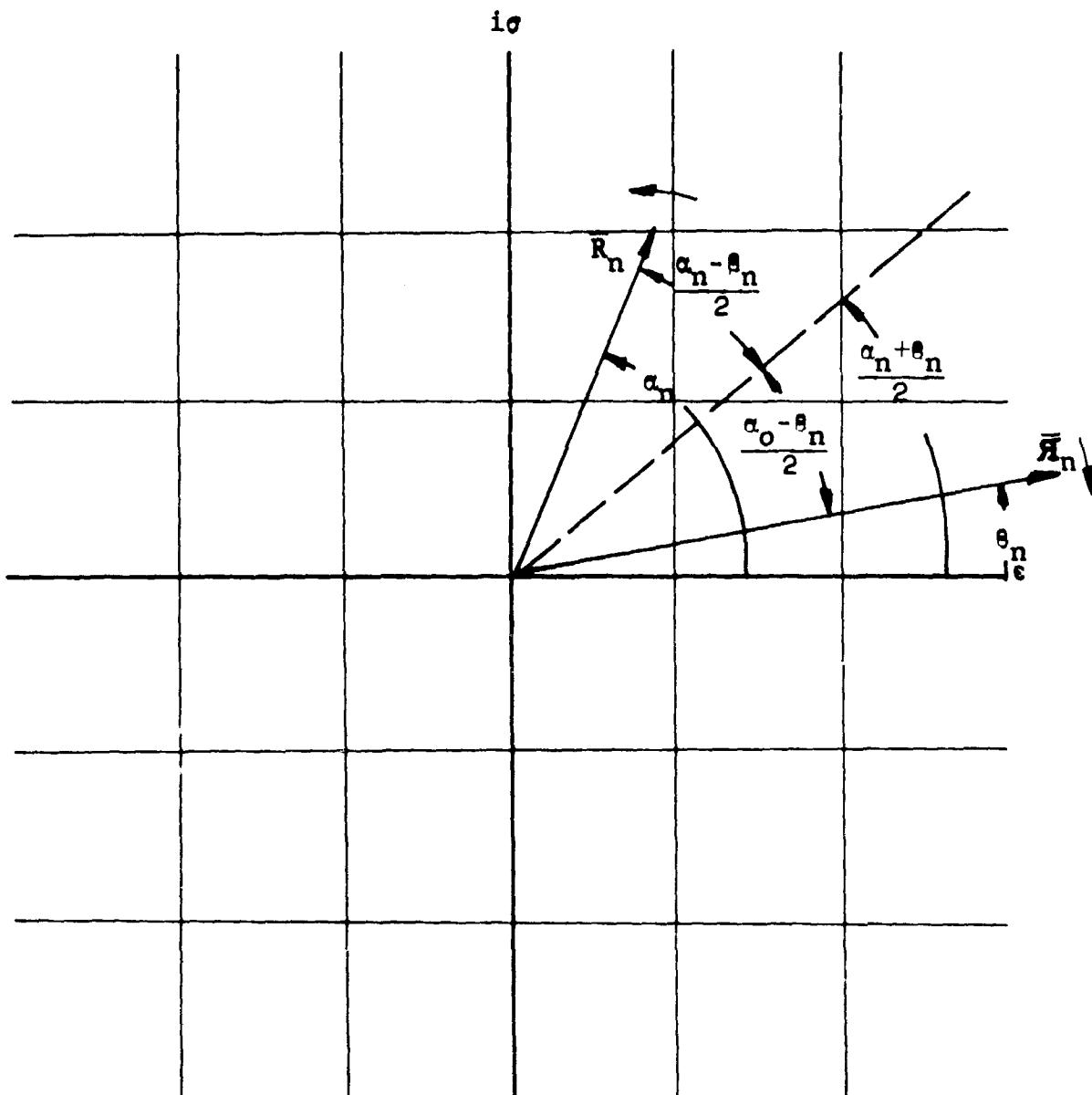


FIGURE 6-11  
ANGULAR RELATIONS OF  $\bar{R}_n$  AND  $M_n$



This occurs when

$$n\theta = \frac{\theta_n - \alpha_n}{2} = n\omega t \quad (6-39)$$

#### 6.5.2.4.4 Kepler's Second Law

The motion of the point that generates any elliptical hysteresis loop obeys Kepler's second law. This conclusion may have been overlooked in the past.

As the tip of  $\bar{H}_n$  sweeps out the ellipse, both its angular velocity and length must vary. Kepler's second law, formulated to describe the motion of planets around the sun in their elliptical orbits, states that the motion varies in such a way that the radius vector sweeps out equal areas in equal intervals of time. This is sometimes stated as follows:

Areal velocity = constant

It is clear that the areal velocity of either  $R_n e^{in\theta}$  or  $\bar{R}_n e^{-in\theta}$  is constant, since their lengths and angular velocities are constant. It is therefore intuitively plausible that their resultant

$$\bar{H}_n = \bar{R}_n e^{in\theta} + \bar{R}_n e^{-in\theta}$$

should also have a constant areal velocity.



This may be proved by the use of vector cross-product notation.

$$\bar{H}_n = R_n e^{i(n\theta + \alpha_n)} + \bar{R}_n e^{-i(n\theta - \beta_n)} \quad (6-40)$$

$$d\bar{H}_n = nR_n e^{i(n\theta + \alpha_n + \frac{\pi}{2})} d\theta + n\bar{R}_n e^{-i(n\theta - \beta_n + \frac{\pi}{2})} d\theta \quad (6-41)$$

$$\bar{H}_n \times d\bar{H}_n = (n R_n^2 - n \bar{R}_n^2) d\theta \quad (6-42)$$

$$\begin{aligned} &+ n R_n \bar{R}_n \sin(-2n\theta + \beta_n - \alpha_n - \frac{\pi}{2}) d\theta \\ &+ n \bar{R}_n R_n \sin(2n\theta - \beta_n + \alpha_n + \frac{\pi}{2}) d\theta \end{aligned}$$

$$\bar{H}_n \times d\bar{H}_n = (R_n^2 - \bar{R}_n^2) nd\theta \quad (6-43)$$

$$d(\text{area}) = dA = \frac{1}{2} (\bar{H}_n \times d\bar{H}_n) = \frac{1}{2} (R_n^2 - \bar{R}_n^2) nd\theta \quad (6-44)$$

$$A = \frac{1}{2} (R_n^2 - \bar{R}_n^2) \int_0^{2\pi} nd\theta \quad (6-45)$$

$$A = \pi R_n^2 - \pi \bar{R}_n^2 \quad (6-46)$$

Equation (6-44) shows that

$$\frac{dA}{d\theta} = \text{constant}$$

which proves that Kepler's second law applies to the  $n^{\text{th}}$  ellipse.



AIRESEARCH MANUFACTURING COMPANY OF ARIZONA  
A DIVISION OF THE GARRETT CORPORATION  
PHOENIX, ARIZONA

The integration of  $dA$  verifies that the area of the  $n^{\text{th}}$  ellipse is indeed the difference in area of the circles swept by  $\bar{R}_n$  and  $\bar{R}_n$ . Note that the area emerges as a negative value, since the vector  $\bar{H}$  sweeps the area in the negative direction, as shown in Figure 6-12.

#### 6.5.2.4.5 Dynamic Moduli

Historically the most important material parameter is Young's modulus, which is the ratio of stress to strain with the material assumed to be perfectly elastic or, alternatively, statically strained so that no loss processes are involved. Young's modulus can be portrayed directly in a conventional, real, stress-strain plane.

As the significance of loss processes in materials became known, the concept of a dynamic modulus evolved. Dynamic modulus is normally written  $E^*$ , although this designation is unfortunate since the more common meaning of the asterisk is to denote the complex conjugate of a complex number. Since there will be occasion to denote the complex conjugate of moduli, the classic dynamic modulus shall be denoted as  $E$  and the more usual meaning of complex conjugate assigned to the asterisk.

$$\text{Dynamic modulus} = E = E' + iE'' \quad (6-47)$$

where

$E'$  = stiffness modulus

$E''$  = loss modulus

The concept of the dynamic modulus applies only to materials generating elliptical hysteresis loops such



AIRESEARCH MANUFACTURING COMPANY OF ARIZONA  
A DIVISION OF THE GARRETT CORPORATION  
PHOENIX, ARIZONA

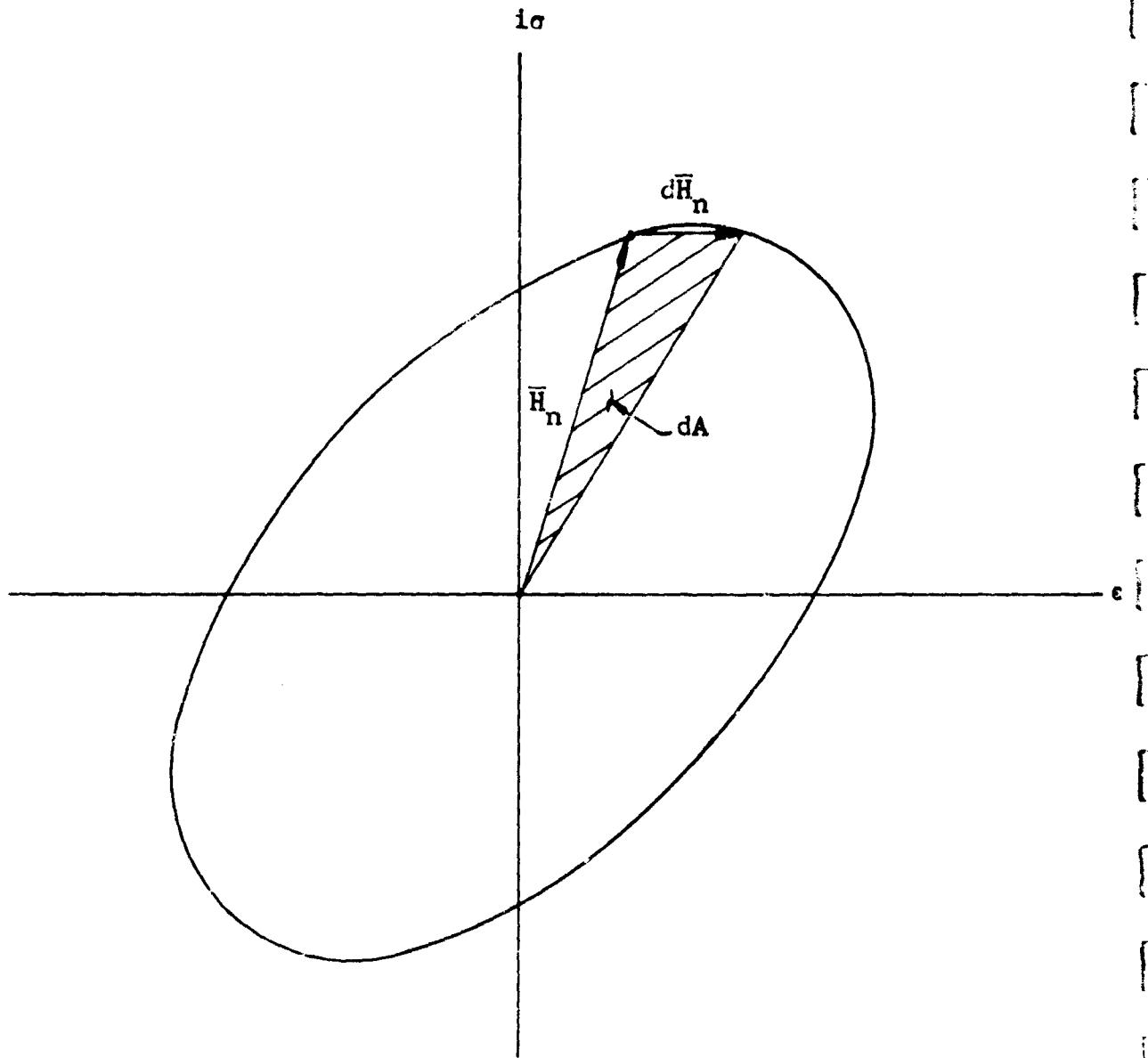
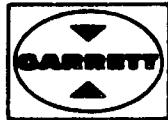


FIGURE 6-12  
INCREMENT OF AREA SWEPT OUT  
BY THE VECTOR  $\bar{H}_n$

GT-7615-R  
Page 6-42

B11011



AIRESEARCH MANUFACTURING COMPANY OF ARIZONA  
A DIVISION OF THE GARRETT CORPORATION  
PHOENIX, ARIZONA

as viscoelastic materials. It is sometimes applied to materials having nonelliptical hysteresis loops by first "linearizing" the material. This is done by assuming an elliptical hysteresis loop having the same area as the nonelliptical loop.

$E$  cannot be represented in a real stress-strain plane because it is a complex number, so a separate  $E' + iE''$  plane must be imagined. The magnitude of  $E'$  and  $E''$ , however, may be obtained from the real plane ellipse by certain geometric constructions.

For all "lossy" materials, stress leads strain by some angle  $\delta$ , and

$$\frac{E''}{E'} = \tan \delta \quad (6-48)$$

The dynamic modulus is therefore sometimes defined as

$$E = \frac{\sigma_{\max}}{\epsilon_{\max}} e^{i\delta} \quad (6-49)$$

In the complex stress-strain plane all phase angles are measured from the real axis in the counterclockwise direction. Thus

$$\sigma_{\max} = i\sigma_1 \quad (6-50)$$

In the complex plane,  $E$  may be represented directly as

$$E = \frac{i\sigma_1}{\epsilon_1} e^{i\delta} = \frac{\sigma_1}{\epsilon_1} e^{i(\delta + \frac{\pi}{2})} \quad (6-51)$$



AIRESEARCH MANUFACTURING COMPANY OF ARIZONA  
A DIVISION OF THE GARRETT CORPORATION  
PHOENIX, ARIZONA

The dynamic modulus must be a constant (nonrotating) vector which represents the (constant) ratio of stress to strain.  $E$  may be written as the ratio of the stress component of  $\bar{R}_1$  to the strain component of  $\bar{R}_1$ .

$$\overset{+}{E}_1 = \frac{\frac{1}{2} \sigma_1 e^{i\phi_1}}{\frac{1}{2} \epsilon_1 e^{i\psi_1}} = \frac{\sigma_1}{\epsilon_1} e^{i(\phi_1 - \psi_1)} \quad (6-52)$$

Then

$$\frac{\sigma_1}{\epsilon_1} e^{i(\phi_1 - \psi_1)} = \frac{\sigma_1}{\epsilon_1} e^{i(\delta + \frac{\pi}{2})} \quad (6-53)$$

$$\phi_1 - \psi_1 = \delta + \frac{\pi}{2} \quad (6-54)$$

This relation is illustrated in Figure 6-13, page

A dynamic modulus vector can also be formed from the stress and strain components of  $\bar{R}_1$ .

$$\bar{E}_1 = \frac{\frac{1}{2} \sigma_1 e^{-i\phi_1}}{\frac{1}{2} \epsilon_1 e^{-i\psi_1}} = \frac{\sigma_1}{\epsilon_1} e^{i(\psi_1 - \phi_1)} \quad (6-55)$$

Note that the dynamic modulus derived from  $\bar{R}_1$  has been designated as  $\overset{+}{E}_1$  and the modulus derived from  $\bar{R}_1$  as  $\bar{E}_1$ .

If the stress and strain components of  $\bar{R}_1$  are considered as they rotate in the clockwise (negative) direction, it is found that the stress attains its maximum before the strain and that this stress also leads the strain by the amount  $\delta$ .



AIRESEARCH MANUFACTURING COMPANY OF ARIZONA  
A DIVISION OF THE GARRETT CORPORATION  
PHOENIX, ARIZONA

$\bar{E}_1$  is therefore just as valid a definition of dynamic modulus as  $\dot{E}_1$  although they are not the same vector (see Figure 6-13).

The relation of  $\dot{E}_1$  and  $\bar{E}_1$  is clearly as follows

$$\bar{E}_1 = -\dot{E}_1^* \quad (6-56)$$

where the asterisk means complex conjugate.

Thus is revealed an astonishing duality in the dynamic modulus.

By analogy the dynamic moduli for any of the  $n$  component ellipses of a nonlinear hysteresis loop are now defined as

$$\dot{E}_n = \frac{\sigma_n}{\epsilon_n} e^{i(\phi_n - \dot{\phi}_n)} \quad (6-57)$$

$$\bar{E}_n = -\frac{\sigma_n}{\epsilon_n} e^{i(\dot{\phi}_n - \phi_n)} \quad (6-58)$$

$$\bar{E}_n = -\dot{E}_n^* \quad (6-59)$$

Note that there are two "degenerate" cases for which  $\dot{E}_n$  and  $\bar{E}_n$  cannot be defined. If  $\epsilon_n = 0$ , the moduli are not defined. If  $\sigma_n = 0$ , the direction of  $\dot{E}$  and  $\bar{E}$  cannot be defined.

An apparently serious difficulty arises at this point because for any sinusoidal stress input  $\sigma_n = 0$  if  $n > 1$ , and



AIRESEARCH MANUFACTURING COMPANY OF ARIZONA  
A DIVISION OF THE GARRETT CORPORATION  
PHOENIX, ARIZONA

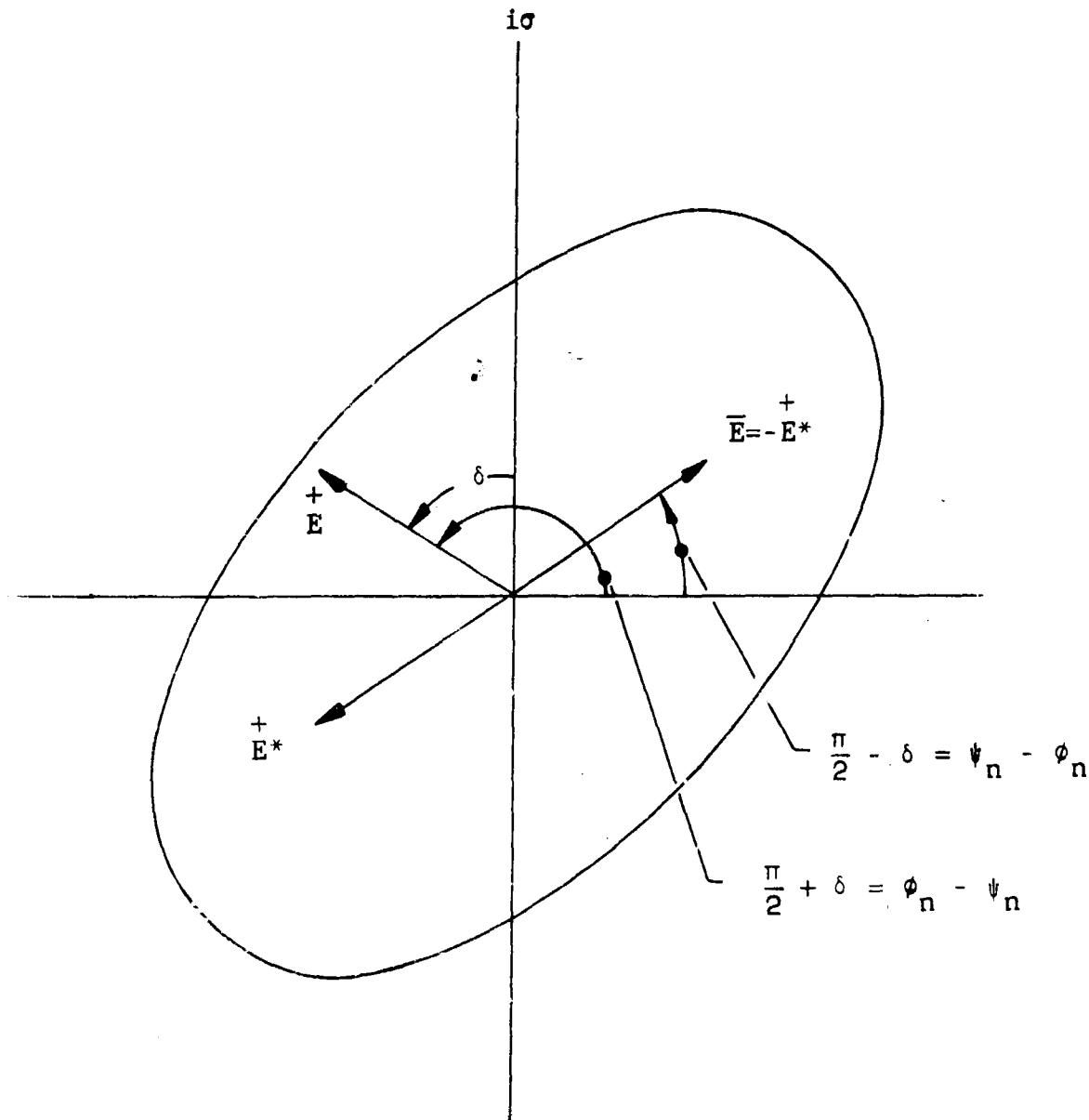


FIGURE 6-13

RELATIVE POSITION OF  $\vec{E}$ ,  $\vec{E}^*$   
AND  $\bar{E}$  VECTORS



AIRESEARCH MANUFACTURING COMPANY OF ARIZONA  
A DIVISION OF THE GARRETT CORPORATION  
PHOENIX, ARIZONA

for any sinusoidal strain input test  $\epsilon_n = 0$  if  $n > 1$ . A way of circumventing this difficulty is presented in Section 6.5.2.9

Figure 6-14 shows how the direction of  $E_n^+$  and  $E_n^-$  may be obtained by an elemental geometric construction. The tip of  $H_n$  is located as shown in Figure 6-14 at time  $t = -\psi_n$ . At this time both of the counterrotating strain components lie on the real ( $\epsilon$ ) axis.  $H_n$  may then be completed by constructing the two vectors  $\frac{\sigma_n}{2}$  as shown. Their directions must be the directions of  $E_n^+$  and  $E_n^-$ .

### 6.5.2.5 Energy Considerations

#### 6.5.2.5.1 Circular Hysteresis Loops

A circular hysteresis loop in a real stress-strain plane would have a direct meaning. The dynamic modulus must be as follows: (See Figure 6-15.)

$$E = \frac{\text{max stress}}{\text{max strain}} e^{i\frac{\pi}{2}} \quad (6-60)$$

or

$$E = iE', E' = 0 \quad (6-61)$$

and

$$\frac{S_1}{S_2} \frac{\text{max stress}}{\text{max strain}} = 1 \quad (6-62)$$

where  $S_1$  and  $S_2$  are the scale factors to which the figure is drawn.



AIRESEARCH MANUFACTURING COMPANY OF ARIZONA  
A DIVISION OF THE GARRETT CORPORATION  
PHOENIX, ARIZONA

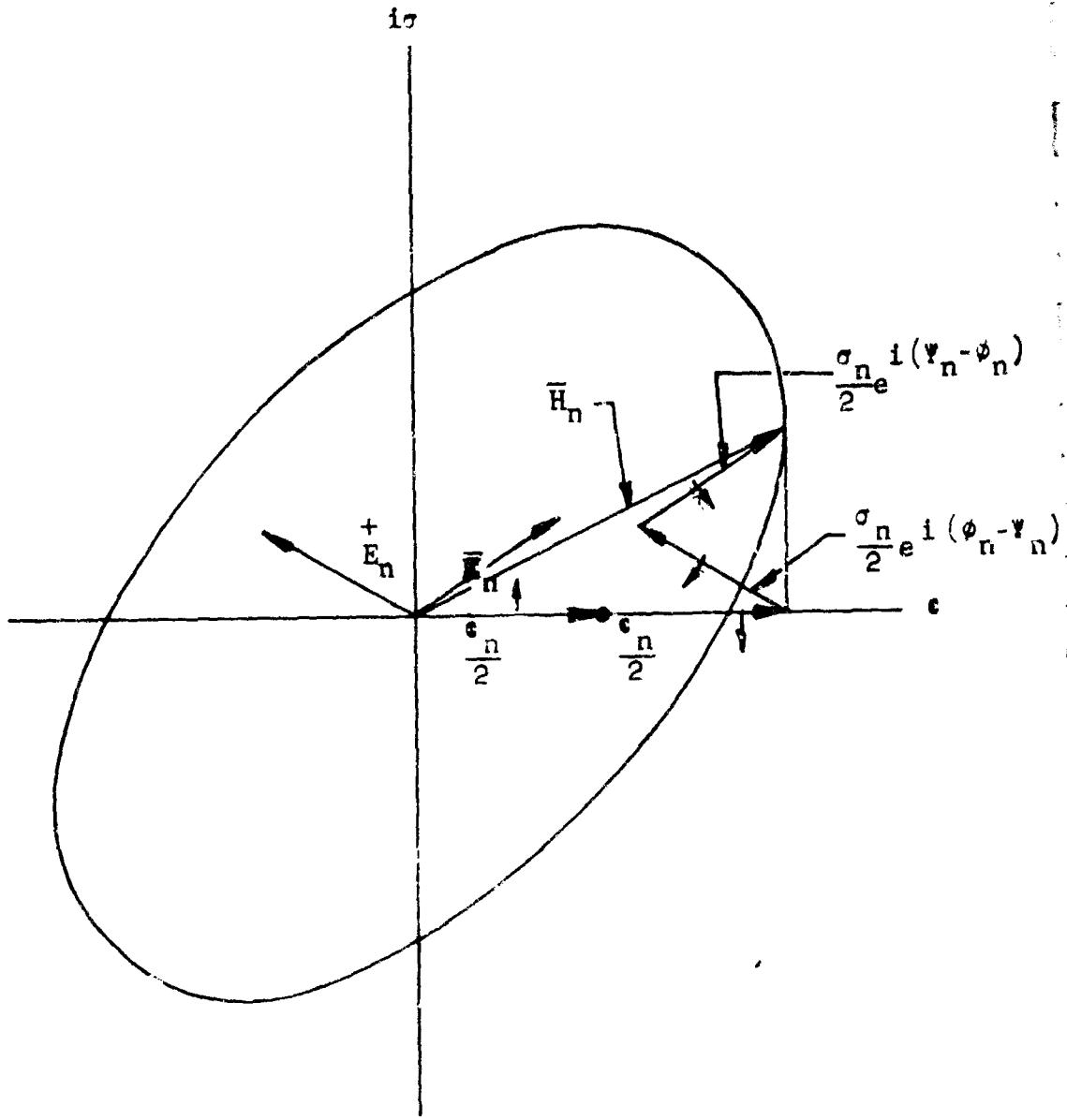


FIGURE 6-14

DETERMINATION OF DIRECTION  
OF  $\bar{E}_n$  AND  $E_n$

GT-7615-R, Rev. 1  
Page 6-48

811013



AIRESEARCH MANUFACTURING COMPANY OF ARIZONA  
A DIVISION OF THE GARRETT CORPORATION  
PHOENIX, ARIZONA

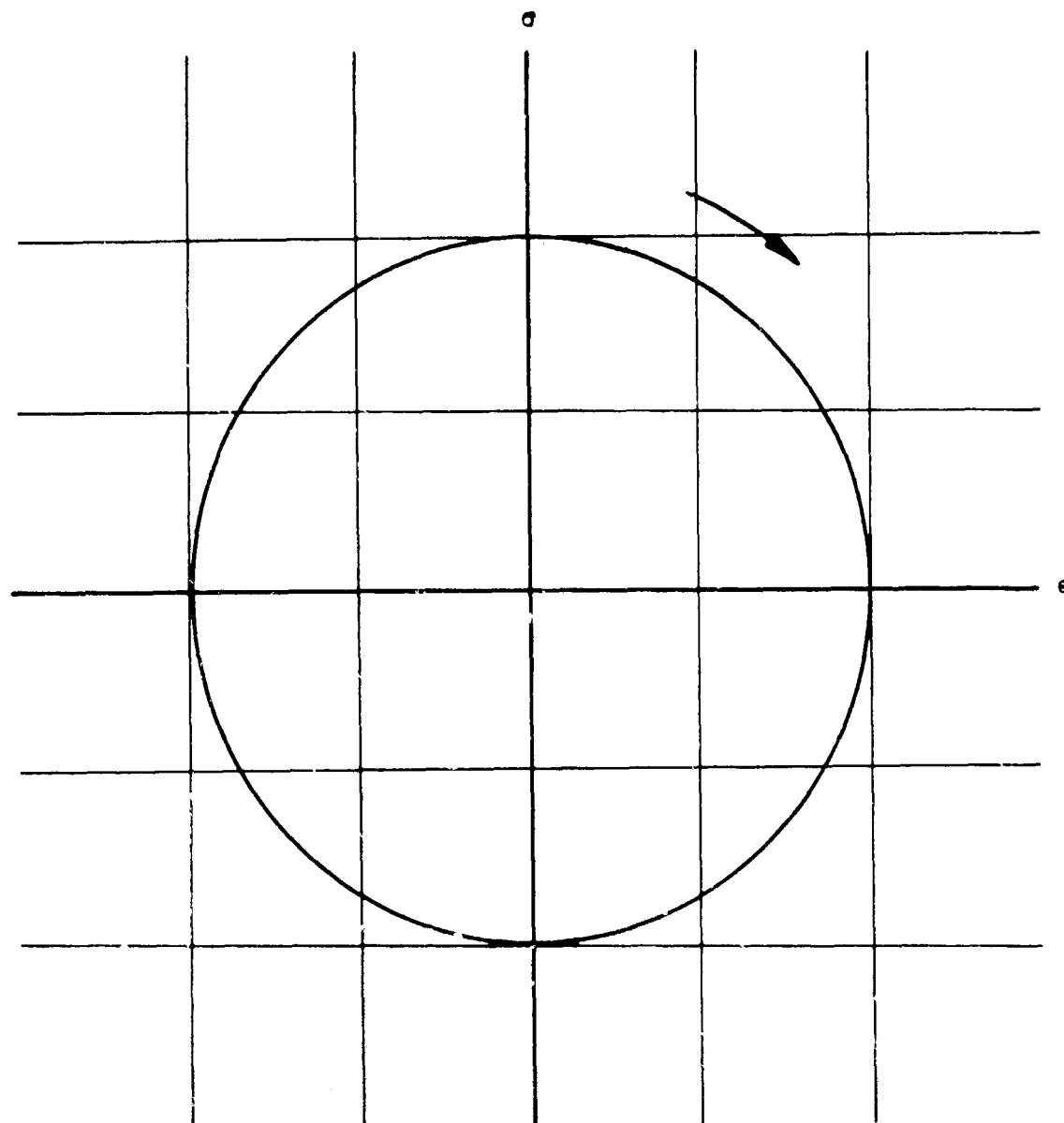


FIGURE 6-15

A CIRCULAR HYSTERESIS LOOP IN  
A REAL STRESS-STRAIN PLANE

B11014

GT-7615-R  
Page 6-49



AIRESEARCH MANUFACTURING COMPANY OF ARIZONA  
A DIVISION OF THE GARRETT CORPORATION  
PHOENIX, ARIZONA

The model for such a material is simply a linear dashpot. Such loops actually occur as in the case of a loop observed at the resonant peak of a mass-spring-dashpot system. In this case, at resonance, the mass inertia has just cancelled out the stiffness of the spring, which leaves only the dashpot to influence the system.

An equally simple electrical analogy is apparent--that of a single linear resistor.

Since the circular hysteresis loops can be traversed in either direction, it is necessary to postulate negative dashpots or negative resistors. Negative resistance is a common tool to the electrical engineer and is occasionally used by mechanical engineers. A negative resistance simply means an energy source, whereas a positive resistance is an energy dissipation device or energy sink.

A regenerative electrical circuit is conveniently represented as the sum of a positive and a negative resistance in series. The positive resistance supplies the losses in the circuit. The negative resistance supplies the power such as is done by an amplifier.

It is thus natural to associate a normal clockwise traverse of a circular loop with power received by the material from its driving source. Conversely, the traverse of a circular hysteresis loop in the reverse direction, counterclockwise, may represent



the flow of stored energy out of the specimen. Since for any material there is a net dissipation of energy, more must flow in than is returned; hence, the difference, which is the dissipation, is always such that the resultant traverse of the loop is in the clockwise direction.

As shown in Figure 6-16, the semimajor axis of the  $n^{\text{th}}$  elliptical loop is  $R_n + \bar{R}_n$  and its semiminor axis is  $\bar{R}_n - R_n$ . The area of the loop must equal  $\pi$  times the product of the semi-axes and must represent the energy loss per cycle. Thus, the area of the ellipse is the difference in area of the two circles of radius  $\bar{R}_n$  and  $R_n$ .

It has been shown that  $\bar{R}_n$  is associated with energy put into the material and  $R_n$  is associated with energy returned by the material, so that the difference must represent the loss per cycle as shown in Figure 6-17.

#### 6.5.2.5.2 A Corollary

The harmonic-type analysis used here reveals a fact that may not be clearly recognizable in terms of the real plane analyses. It seems important enough to state as a corollary to Therorem 1.



AIRESEARCH MANUFACTURING COMPANY OF ARIZONA  
A DIVISION OF THE GARRETT CORPORATION  
PHOENIX, ARIZONA

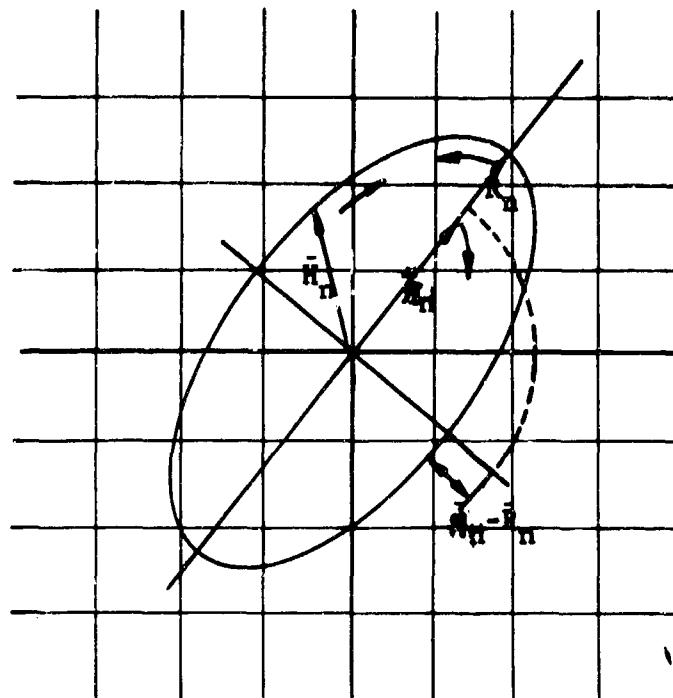


FIGURE 6-16

$$\text{AREA} = \pi(\bar{R}_h + \bar{R})(\bar{R}_l - \bar{R}) = \pi\bar{R}_h^2 - \pi\bar{R}_l^2$$

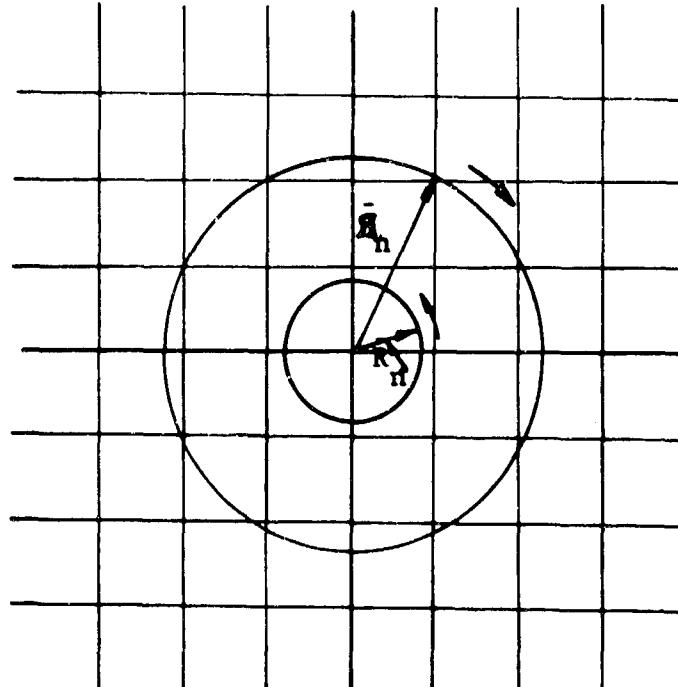


FIGURE 6-17

THE AREA OF THE ELLIPSE OF FIGURE 6-16  
EQUALS THE DIFFERENCE IN THESE CIRCULAR  
AREAS

B11007

GT-7615-R  
Page 6-52



### Corollary I

Given a hysteresis loop,  $Z = \epsilon + i\sigma$ , then energy can be dissipated only by the interaction of harmonic components common to both the stress and the strain axis (real and imaginary axes).

### Informal Proof of Corollary I

It has already been shown that the stress and the strain may each be expressed as Fourier series.

$$\epsilon = \sum_{n=0}^{n=\infty} \epsilon_n \cos (n\theta + \psi_n) \quad (6-63)$$

$$\sigma = \sum_{n=0}^{n=\infty} \sigma_n \sin (n\theta + \phi_n) \quad (6-64)$$

Also, by classic definition, the loss per cycle equals:

$$\oint \sigma d\epsilon \quad (6-65)$$

The product  $\sigma d\epsilon$  consists of a double summation over m and n of terms having the form

$$[-n\epsilon_n \sin (n\theta + \psi_n)] [\sigma_n \sin (n\theta + \phi_n)] \quad (6-66)$$



or the Fourier series can always be rewritten to eliminate the phase angles  $\psi_m$  and  $\phi_n$  yielding an  $\epsilon$  and  $\sigma$  terms of the form

$$d\epsilon_m = a \cos m\theta + b \sin m\theta \quad (6-67)$$

$$\sigma_n = c \cos n\theta + d \sin n\theta \quad (6-68)$$

where  $a$ ,  $b$ ,  $c$ ,  $d$  are constants.

Product terms are of one of three forms containing

- (1)  $\cos m\theta \cos n\theta$
- (2)  $\cos m\theta \sin n\theta$
- (3)  $\sin m\theta \sin n\theta$

But the integral over one cycle of  $\theta$  is always zero for Type 2 and is zero for both Types 1 and 3 unless  $m = n$ .

These vanishing integrals are a fundamental property of all sets of orthogonal functions.

#### 6.5.2.6 The Effect of Phase

For each value of  $n$  there are four parameters ( $R_n$ ,  $\Re_n$ ,  $\alpha_n$ , and  $\beta_n$ ). It is reasonable to expect that many materials may exhibit similar values for  $R_n$  and  $\Re_n$  yet may differ greatly in their phase parameters  $\alpha_n$  and  $\beta_n$ .

This is evident from the three ellipses shown in Figure 6-18, which all have the same values of  $R_n$  and  $\Re_n$ , but for which  $\alpha_n$  and  $\beta_n$  are very different.



AIRESEARCH MANUFACTURING COMPANY OF ARIZONA  
A DIVISION OF THE GARRETT CORPORATION  
PHOENIX, ARIZONA

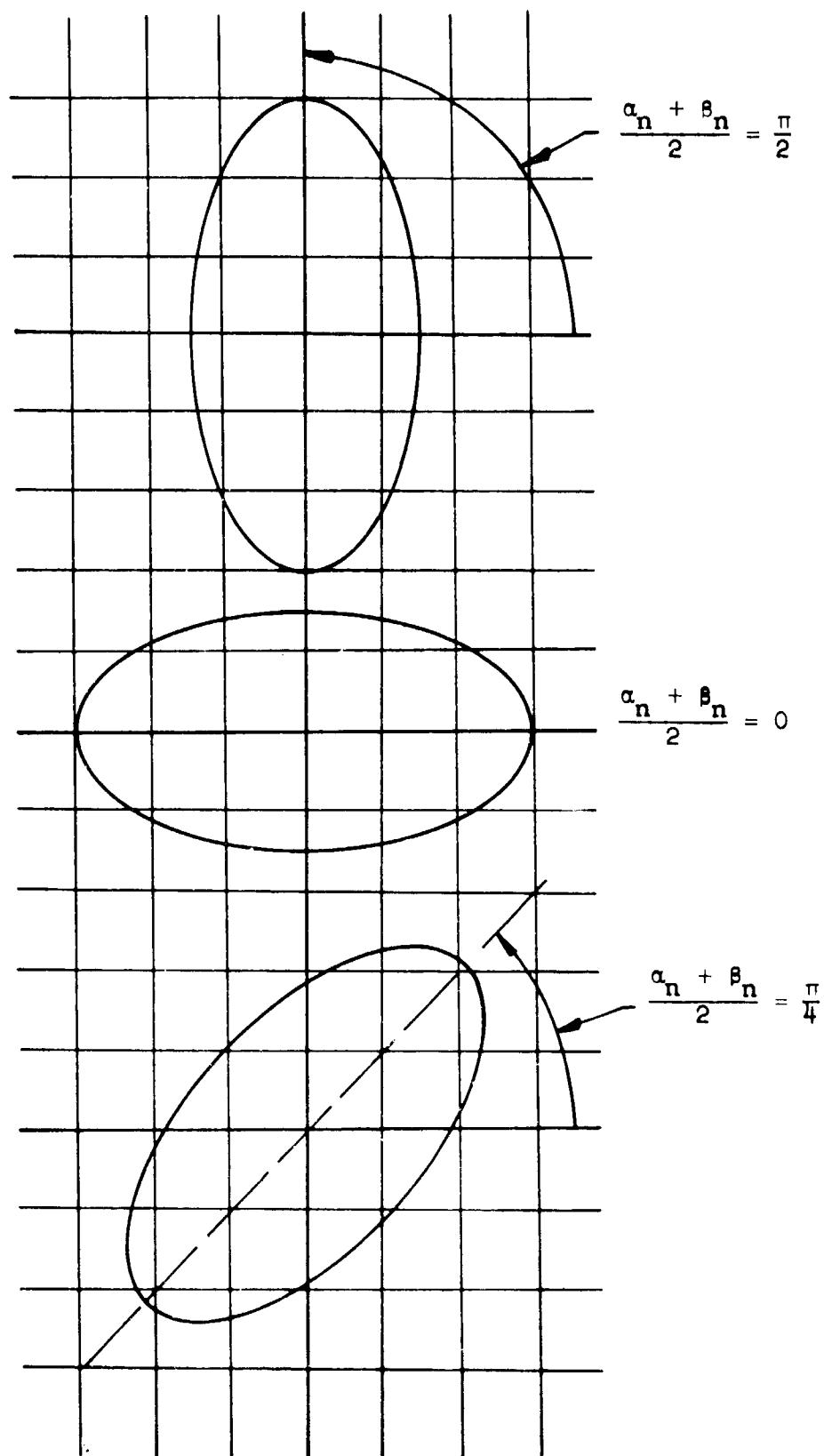


FIGURE 6-18

EFFECT OF PHASE PARAMETERS,  $\alpha_n$  and  $\beta_n$

B11004

GT-7615-R  
Page 6-55



As previously shown, the angle between the principal axis of the ellipse and the strain axis is equal to  $\frac{\alpha_n + \beta_n}{2}$  regardless of the time base chosen. A second relation is needed to actually determine  $\alpha_n$  and  $\beta_n$ .

Fortunately, the direct measurement of  $\alpha_n$  and  $\beta_n$  is accomplished with ease with the aid of modern instrumentation procedures. As a matter of routine, the strain is measurable directly with strain transducers. Likewise, the stress is measurable with force transducers. The most natural display for the transducer signals is to form the hysteresis loop as a Lissajour figure on a cathode ray oscilloscope.

With the aid of band-pass filters, it is then elemental to display separately each of the  $n$  component ellipses in turn. By forming a sharp pulse out of a signal derived in any convenient manner from the fundamental driving frequency  $\omega$ , a common time marker may be applied to each of the  $n$  ellipses. The pulse is used to mark a spot on the ellipse by modulation of the  $Z$  axis. The angles  $\alpha_n$  and  $\beta_n$  may then be obtained directly from a photograph of the  $n$ th ellipse by the geometric construction shown in Figure 6-19.  $R_n$  and  $R_m$  are, of course, already known by measuring the major and minor semi-axes of the ellipse.

The crucial role of phase angle is shown in the Lissajour figures of section 6.5.2.8. By addition of a small amount of third harmonic to the strain axis an elliptical loop is changed to a nonlinear loop. A shaft of  $90^\circ$  in the phase of this third harmonic transforms the figure from a sharply pointed loop characteristic of metals to a blunted shape characteristic of clay.

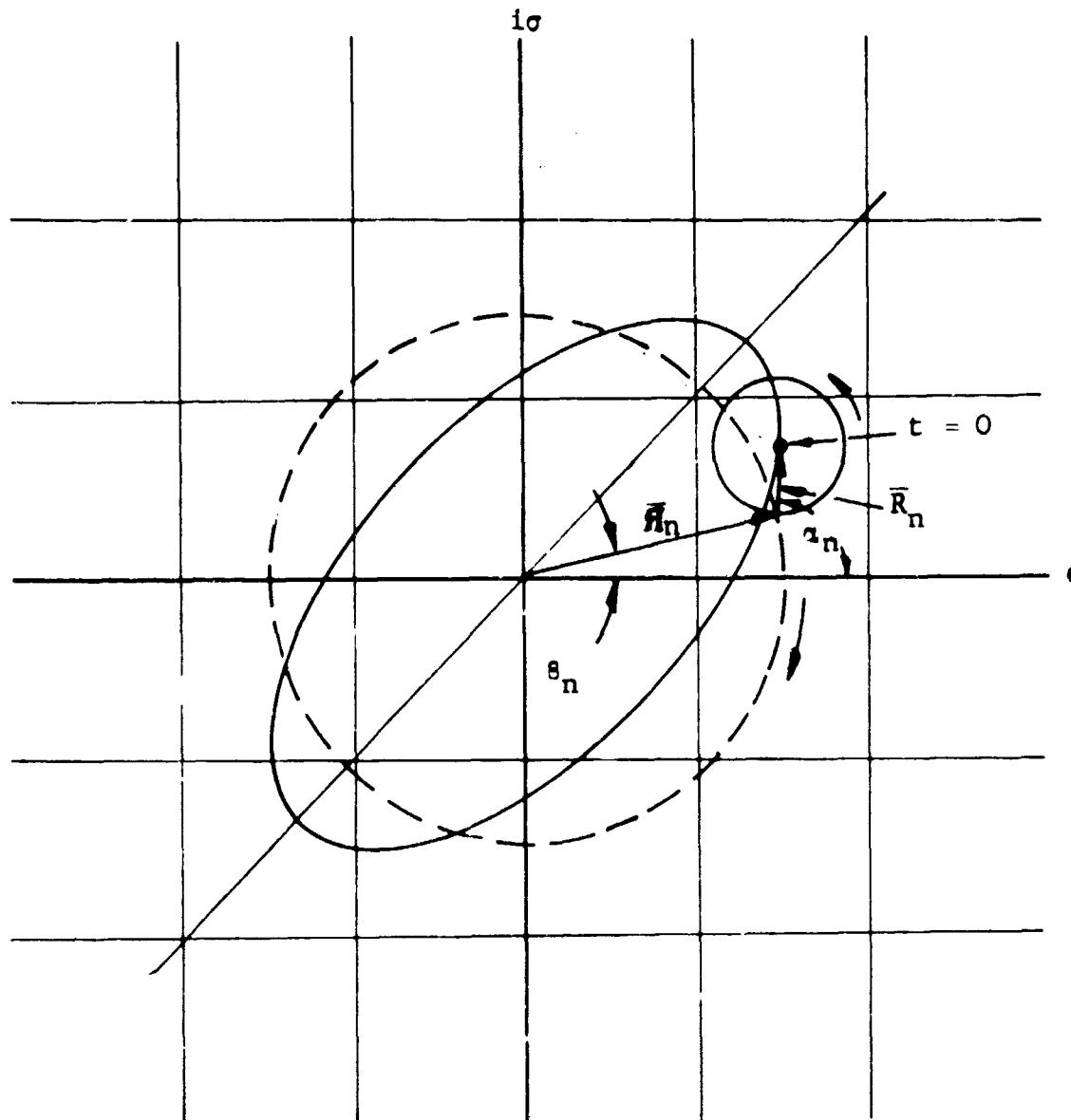


FIGURE 6-19

CONSTRUCTION OF  $\bar{R}_n$  AND  $R_n$  FROM  
A TIME MARK ON THE  $n^{\text{th}}$  ELLIPSE



AIRESEARCH MANUFACTURING COMPANY OF ARIZONA  
A DIVISION OF THE GARRETT CORPORATION  
PHOENIX, ARIZONA

#### 6.5.2.7 Coulomb Damping

As an illustrative exercise, consider the case of a material or system having zero stiffness and pure coulomb damping. This leads to a square hysteresis loop which is certainly an extreme case of nonlinearity and would seem not too amenable to expression as a sum of linear (viscous) damping terms.

Figure 6-20 shows the mechanical model, the resulting hysteresis loop, and a plot of the sinusoidal strain input and the stress as indicated by tension in the connecting rod.

The analysis proves to be simple and converges so rapidly that very few harmonic terms (pairs of epicycles) are needed.

This extreme example serves to clearly illustrate most of the important features of analysis by rheological epicycles. Since the strain input is sinusoidal, the entire energy dissipation (area of the square) must occur by interaction of  $n = 1$  terms. Indeed, the computed area is correct. To accommodate this, all  $R_n$  and  $\dot{R}_n$  become equal for  $n > 1$  and their counterrotation merely generates straight lines having no area and lying on the stress axis. Since coulombic damping is inherently independent of rate, the angle  $\theta$  is used as parameter.

$$\epsilon = \epsilon_1 \cos \theta = \cos \theta \text{ (by assumption)} \quad (6-69)$$

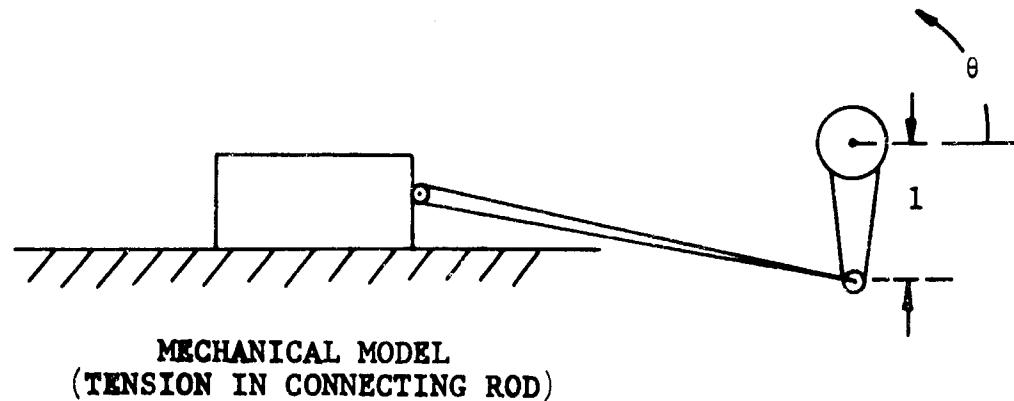
The Fourier expansion for a square wave is well known and may be written as

$$\begin{aligned} \sigma = -\frac{\pi}{4} [\sin \theta + 1/3 \sin 3\theta \\ + \frac{1}{5} \sin 5\theta + \dots + \frac{1}{n} \sin n\theta] n = 1, 3, 5, \dots \end{aligned} \quad (6-70)$$

Note that only odd values of  $n$  appear.



AIRESEARCH MANUFACTURING COMPANY OF ARIZONA  
A DIVISION OF THE GARRETT CORPORATION  
PHOENIX, ARIZONA



MECHANICAL MODEL  
(TENSION IN CONNECTING ROD)

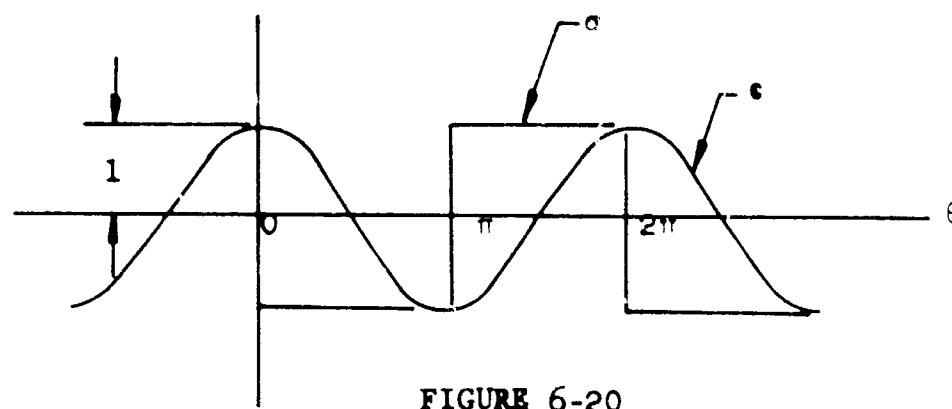
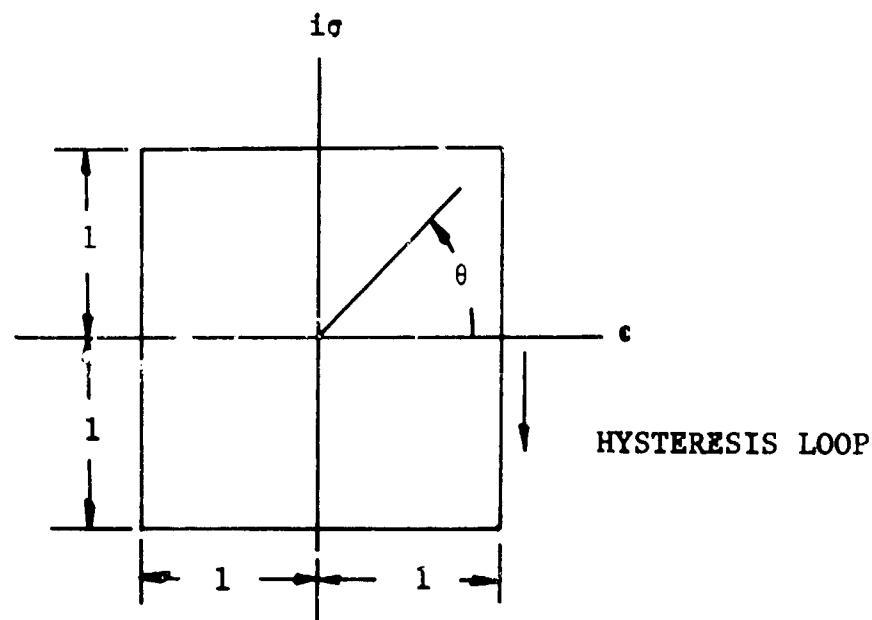


FIGURE 6-20  
COULOMB DAMPING

B11006

GT-7615-R  
Page 6-59



AIRESEARCH MANUFACTURING COMPANY OF ARIZONA  
A DIVISION OF THE GARRETT CORPORATION  
PHOENIX, ARIZONA

Note also that for the coordinates chosen, there are no cosine terms or phase angles. The negative sign appears only because of the convention choice of tension in the rod as a positive force.

$$\bar{R}_n e^{in\theta} = R_n e^{i(n\theta + \alpha_n)} \quad (6-71)$$

$$= \frac{\epsilon_n}{2} e^{i(n\theta + \psi_n)} + \frac{\sigma_n}{2} e^{i(n\theta + \phi_n)}$$

But because  $\epsilon$  and  $\sigma$  are even and odd functions, respectively, both  $\psi_n$  and  $\phi_n$  are all zero.

Also, no static stress or strain is possible, so  $\bar{R}_0$  and  $R_0$  are zero.  $R_n$ ,  $\alpha_n$ , and  $\theta_n$  may be evaluated at any convenient value of  $\theta$ , so for  $\theta = 0$ :

$$[\bar{R}_1]_{\theta=0} = R_1 e^{i\alpha_1} = \left(\frac{1}{2} - \frac{2}{\pi}\right) \quad (6-72)$$

Note that

$$[\bar{R}_1]_{\theta=0} \text{ is a real number} = -0.1365 \quad (6-73)$$

$$R_1 \cos \alpha_1 + i R_1 \sin \alpha_1 = -0.1365 \quad (6-74)$$

$$R_1 = 0.1365, \alpha_1 = \pi \quad (6-75)$$

$$\epsilon_0 = \epsilon_3 = \epsilon_5 = \epsilon_n = 0 \quad n \neq 1 \quad (6-76)$$

So all other  $\bar{R}_n$  may be written

$$[\bar{R}_n]_{\theta=0} = R_n e^{i\alpha_n} = -\frac{2}{n\pi} + 0i \quad (6-77)$$



AIRSEARCH MANUFACTURING COMPANY OF ARIZONA  
A DIVISION OF THE GARRETT CORPORATION  
PHOENIX, ARIZONA

$$R_n = \frac{2}{n\pi}, \alpha_n = \pi \quad (6-78)$$

$$n = 3, 5, 7, \dots$$

Similarly

$$\bar{R}_n = R_n e^{i\theta_n} \quad (6-79)$$

$$\bar{R}_n = \frac{\epsilon_n}{2} - \frac{\sigma_n}{2} \quad (\text{a real number}) \quad (6-80)$$

For  $n = 1$

$$R_1 e^{i\theta_1} = 1.1365 + i0 \quad (6-81)$$

$$\epsilon_1 = 1.1365 \quad \theta_1 = 0 \quad (6-82)$$

For all other values of  $n$

$$R_n = \frac{2}{n\pi} \quad (6-84)$$

Values of  $R_n$ ,  $\bar{R}_n$ ,  $\alpha_n$ , and  $\theta_n$  are shown in Table I.



AIRESEARCH MANUFACTURING COMPANY OF ARIZONA  
A DIVISION OF THE GARRETT CORPORATION  
PHOENIX, ARIZONA

TABLE I

<u>n</u>	<u>R<sub>n</sub></u>	<u>α<sub>n</sub></u>	<u>R<sub>n</sub></u>	<u>S<sub>n</sub></u>	<u>(Area)</u>
0	0		0		
1	0.1365	π	1.1365	0	3.997
2					
3	0.2122	π	0.2122	0	0
4					
5	0.1273	π	0.1273	0	0
6					
7	0.0909	π	0.0909	0	0
8					
9	0.0707	π	0.0707	0	0

Note that the area is correct for the number of significant figures used.

Figures 6-21, 6-22, and 6-23 show  $R_n$  and  $R_n$  and their resultant ellipses for  $n = 1, 3, 5$ . Figure 6-24 shows successive approximations of the square hysteresis loop as  $n$  is increased.

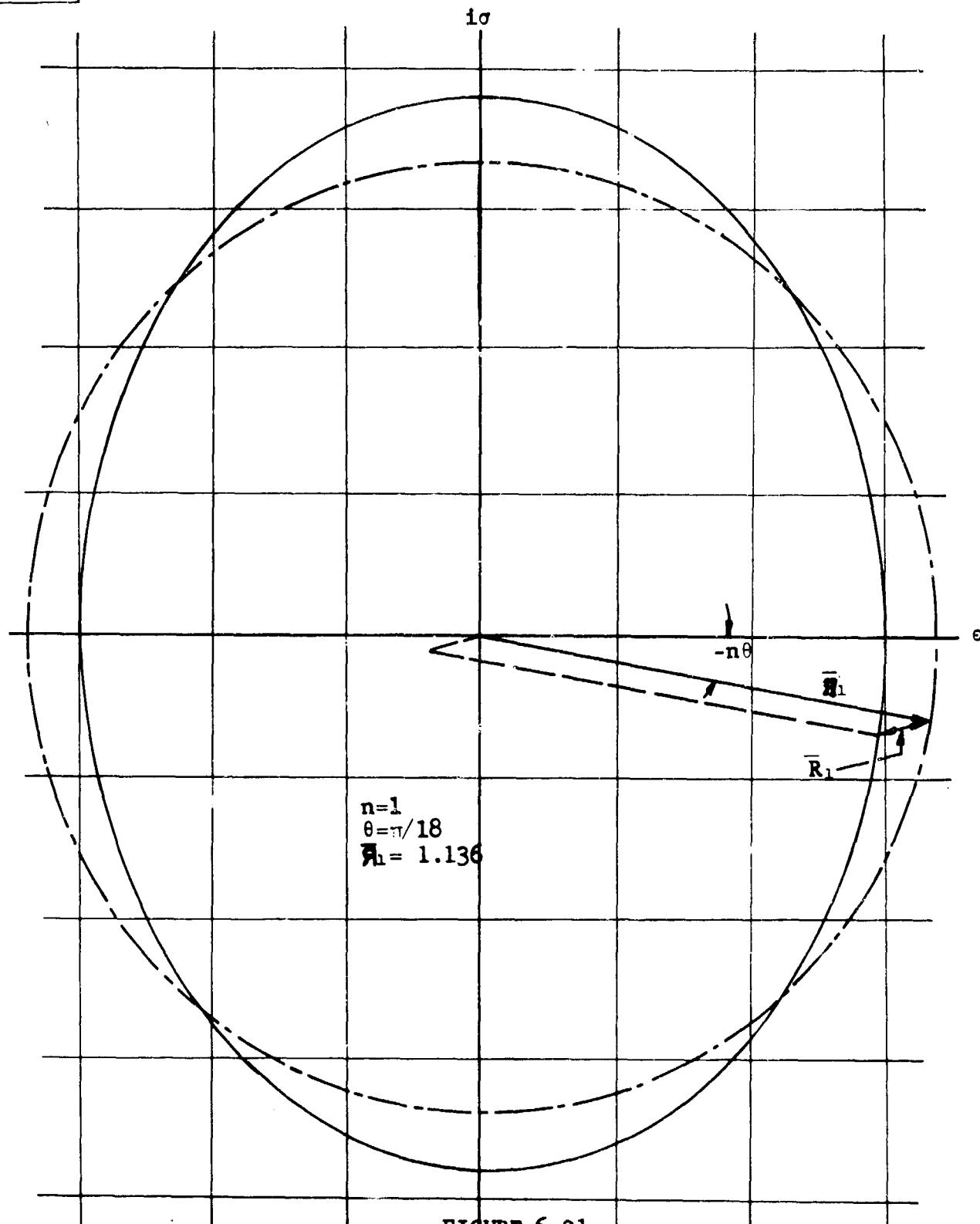


FIGURE 6-21  
FIRST COMPONENT ELLIPSE  
FOR A SQUARE HYSTERESIS  
LOOP

GT-7615-R, Rev. 1  
Page 6-63

B11005

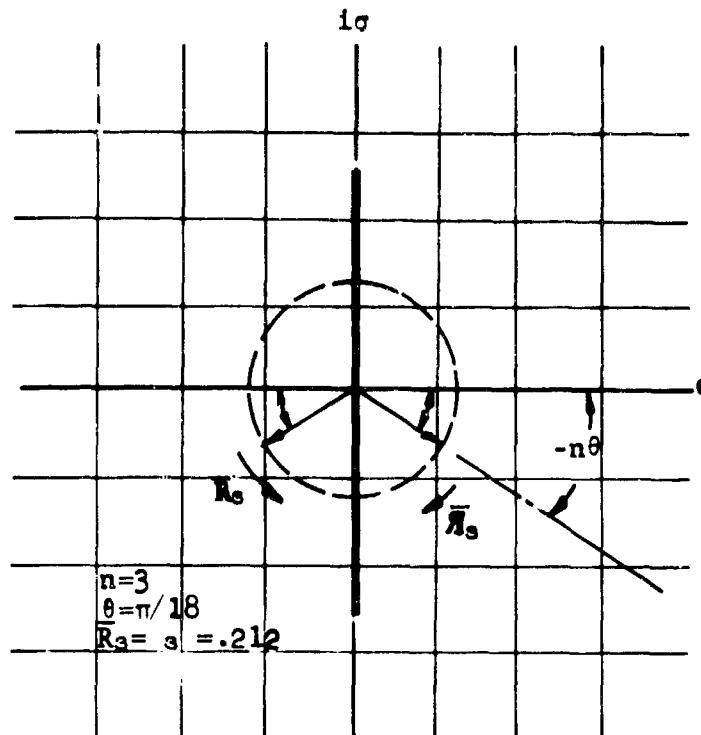


FIGURE 6-22

THE  $n=3$  COMPONENT OF A SQUARE HYSTERESIS LOOP

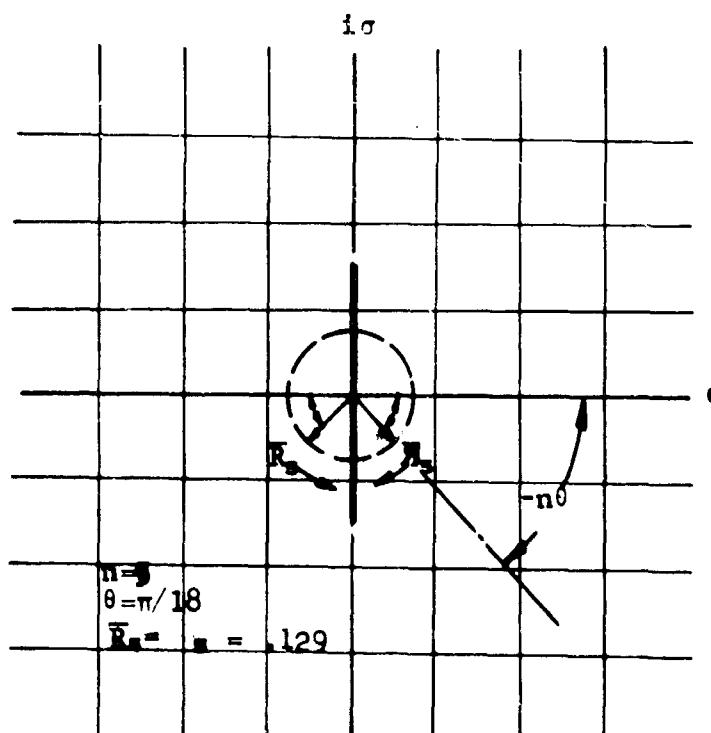


FIGURE 6-23

THE  $n=5$  COMPONENT OF A SQUARE HYSTERESIS LOOP



AIRESEARCH MANUFACTURING COMPANY OF ARIZONA  
A DIVISION OF THE GARRETT CORPORATION  
PHOENIX, ARIZONA

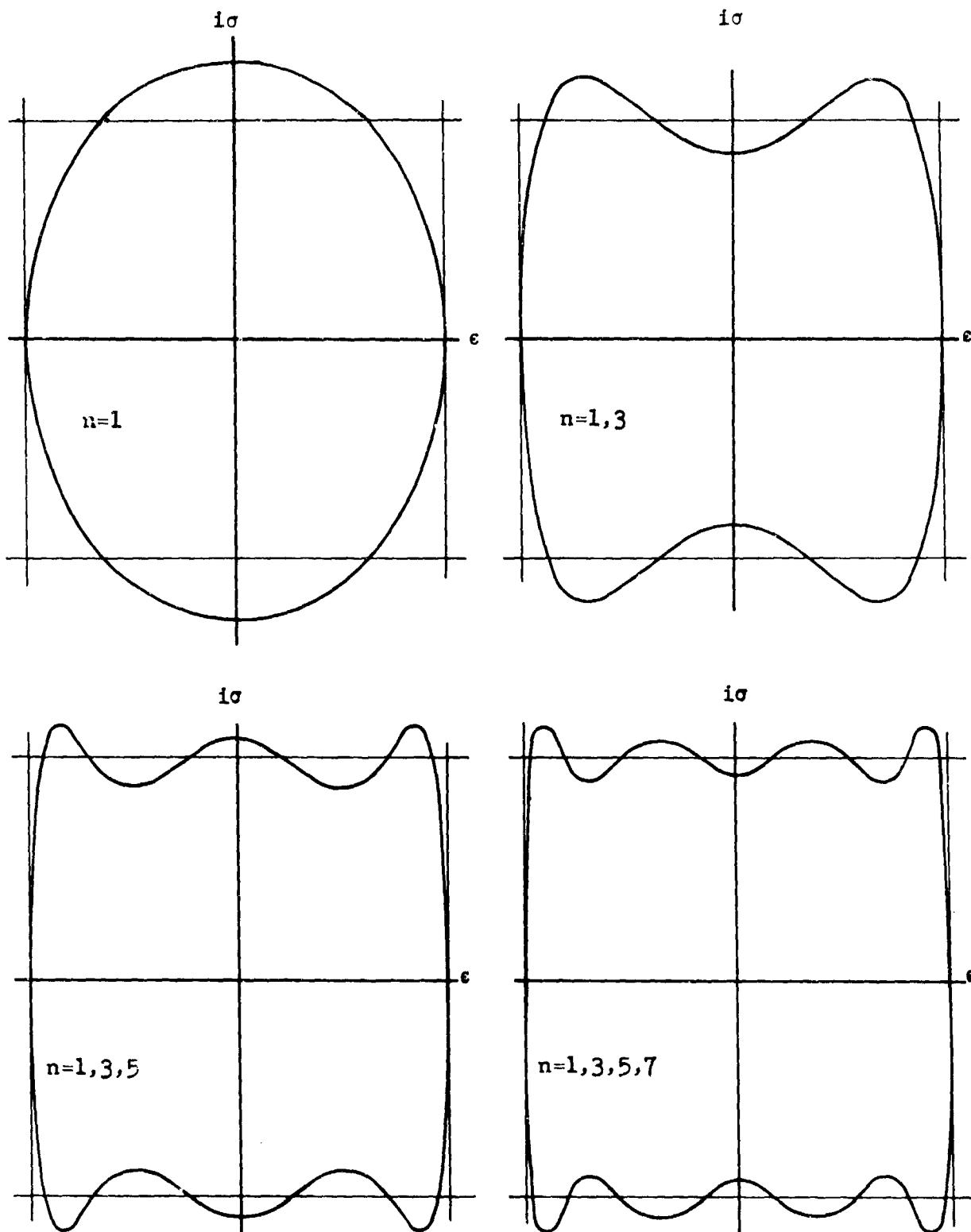


FIGURE 6-24

SUCCESSIVE APPROXIMATIONS OF A  
SQUARE HYSTERESIS LOOP AS  $n$   
INCREASES FROM 1 TO 7

B11003

GT-7615-R  
Page 6-65



AIRESEARCH MANUFACTURING COMPANY OF ARIZONA  
A DIVISION OF THE BARRETT CORPORATION  
PHOENIX, ARIZONA

### 6.5.3 Synthesis of Hysteresis Loops by Means of a Computer

#### 6.5.3.1 Introduction

The process of resolving hysteresis loops into a number of circular motions can be reversed--i.e., the hysteresis loops can be formed by combining the component circular motions. The generation and addition and subtraction of the rotating vectors that constitute the circular motions is a procedure readily performed by an analog computer. The effect of harmonics and particularly of the phase relationship between fundamental and harmonics is demonstrated.

#### 6.5.3.2 Equipment

A PACE-TRIO Analog Computer with repetitive-operation capability (see Figure 6-25) was used to generate and combine the sinusoidal voltages that represent the vector components of the hysteresis loops. This computer is a precise and stable unit capable of producing sinusoidal voltages by means of a simulation of an undamped second order system. The repetitive operation feature makes it possible to use a conventional oscilloscope for display. A Dumont Type 304-A dual-beam oscilloscope was used for this display.

#### 6.5.3.3 Computer Mechanization

The  $R_n$  and  $\bar{R}_n$  vectors rotate at the same angular velocity and describe circles that may be of equal or different radii. The rotation of  $\bar{R}$  is counterclockwise and that of  $R$  clockwise. Figure 6-26 shows the  $\bar{R}$  circle (upper) and the  $R$  circle (lower).



AIRESEARCH MANUFACTURING COMPANY OF ARIZONA  
A DIVISION OF THE GARRETT CORPORATION  
PHOENIX, ARIZONA

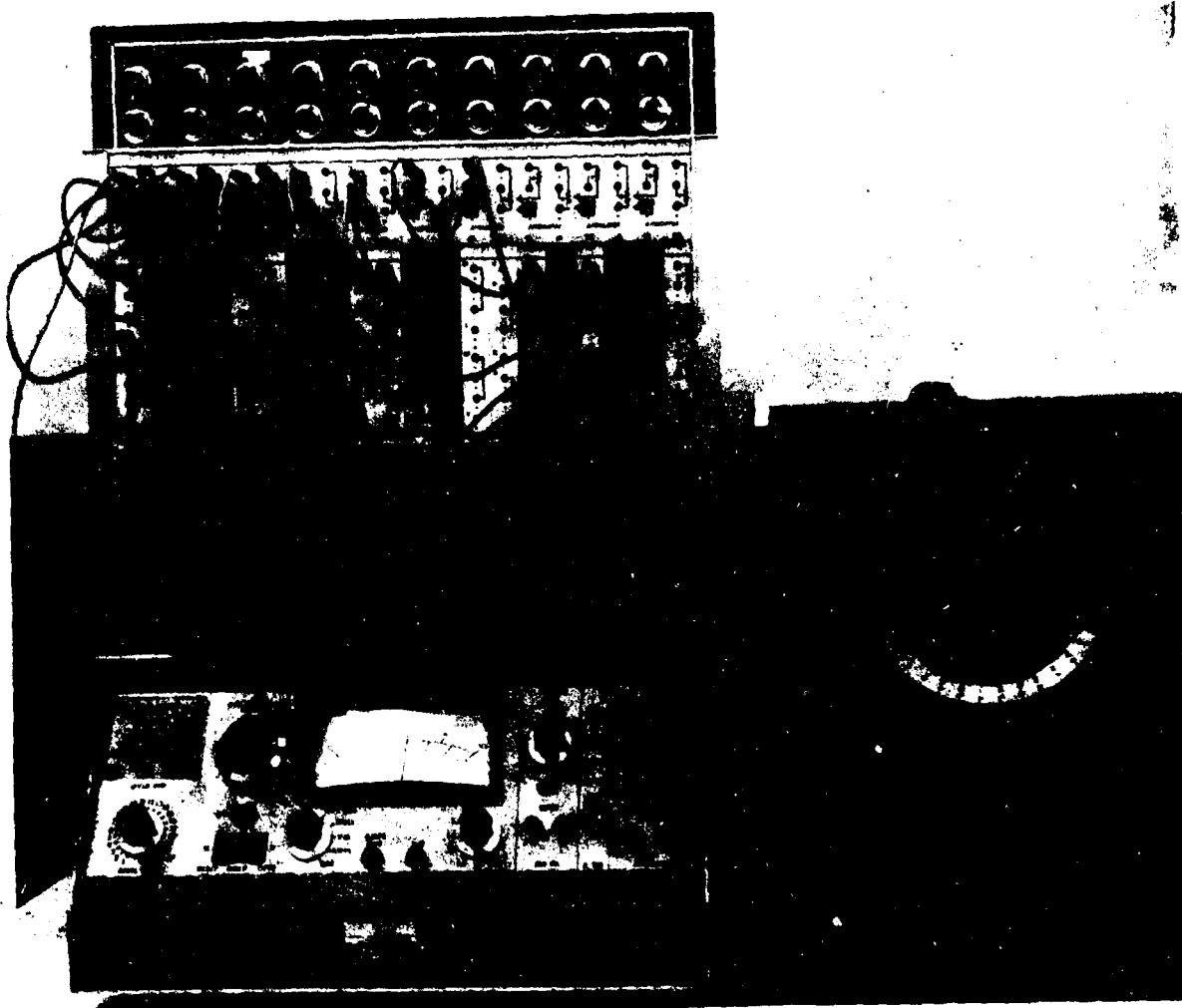


FIGURE 6-25  
ANALOG COMPUTER

GT-7615-R  
Page 6-67



AIRESEARCH MANUFACTURING COMPANY OF ARIZONA  
A DIVISION OF THE GARRETT CORPORATION  
PHOENIX, ARIZONA

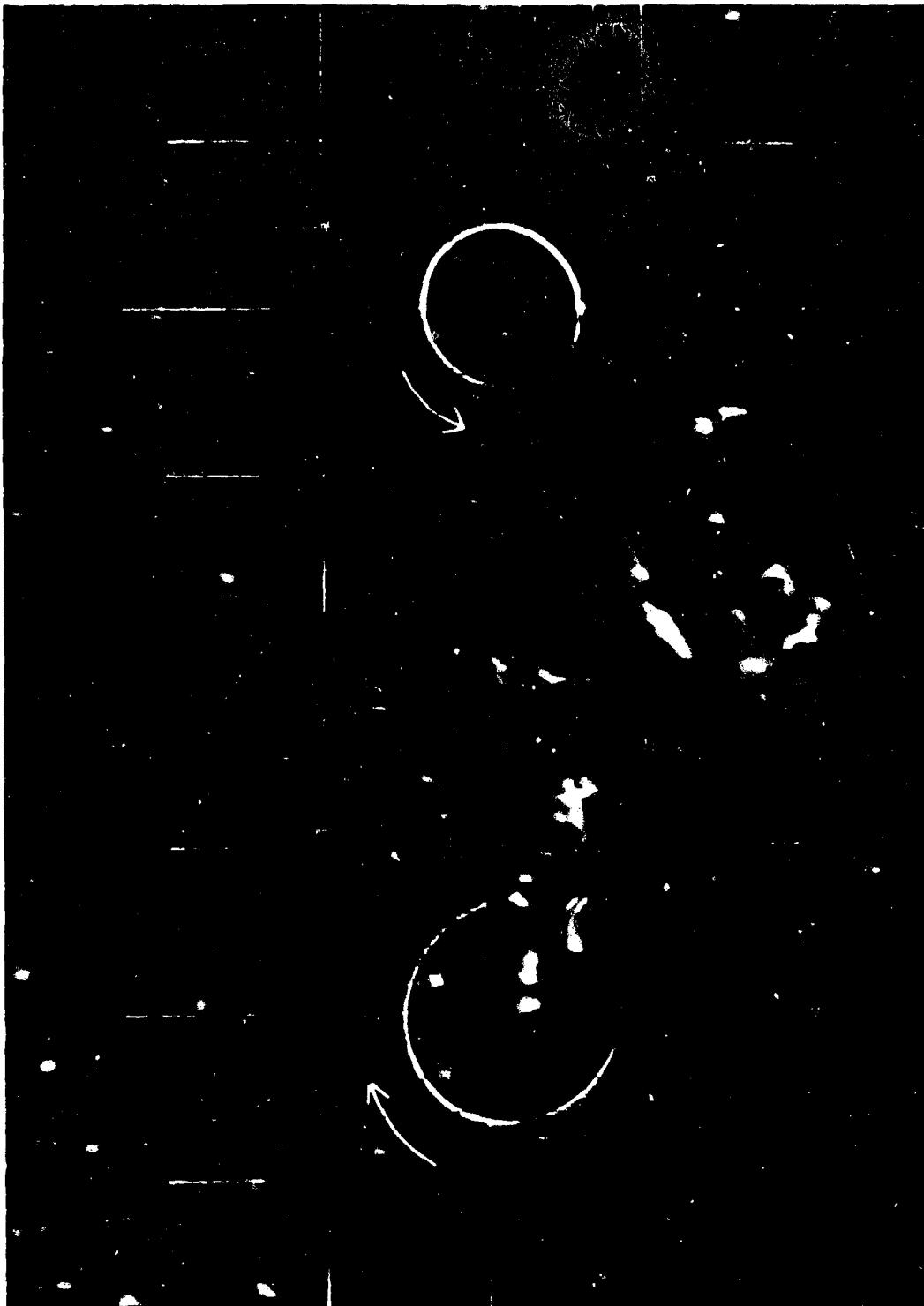


FIGURE 6-26  
 $\bar{R}_1$  CIRCLE (UPPER) AND  $\bar{R}_2$  CIRCLE (LOWER)

GT-7615-R,  
Page 6-68



The  $\vec{R}$  vector is produced by the following simulation:

The computer is set up to solve the equation,

$$y = \ddot{ax} + bx \quad (6-85)$$

When the proper initial conditions are established, the computer solution of this equation is a sine wave of constant peak amplitude dependent on initial condition, and of frequency

$$\omega = \sqrt{\frac{b}{a}} \quad (6-86)$$

This solution may then be written:

$$x = A \sin(\omega t) \quad (6-87)$$

The computer also conveniently generates the quadrature component which can be adjusted to have the same peak amplitude and is described:

$$\dot{x} = A \cos(\omega t) \quad (6-88)$$

The vector  $\vec{R}$  is then simulated by

$$\vec{R} = A (\sin \omega t + j \cos \omega t) \quad (6-89)$$

The computer mechanization for this simulation is shown in Figure 6-27. When the two components  $x$  and  $\dot{x}$  are connected to horizontal and vertical axes of an oscilloscope, the result is a circle described by a spot that moves in a counterclockwise direction about the center of the screen and at a distance from the center,  $A = R_1$ . The spot starts from a position on the horizontal axis.



AIRESEARCH MANUFACTURING COMPANY OF ARIZONA  
A DIVISION OF THE GARRETT CORPORATION  
PHOENIX, ARIZONA

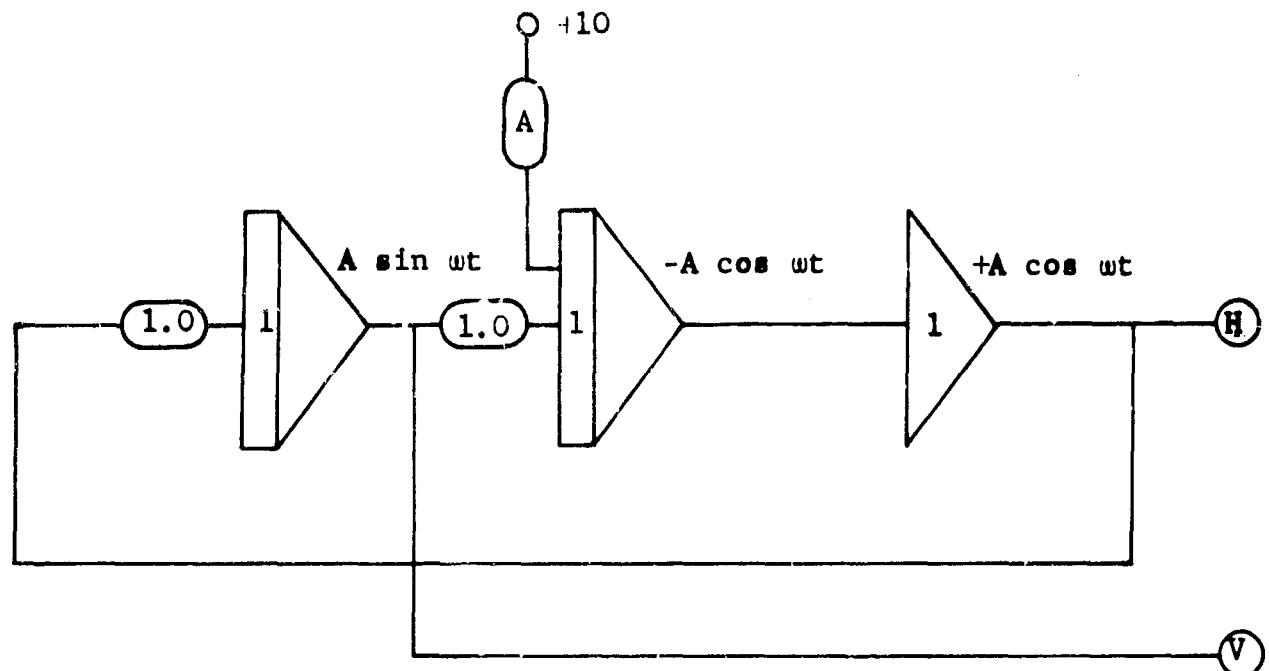


FIGURE 6-27

COMPUTER MECHANIZATION FOR  
SIMULATION OF  $\bar{R} = A(\sin \omega t + j \cos \omega t)$



A similar mechanization (see Figure 6-28) is used to generate the vector  $\bar{R}_1$  except that the sign of the cosine term is changed. This causes the vector to rotate in the opposite direction. The negative cosine component is connected to the vertical axis and the sine to the horizontal axis, with the result that the spot starts from the vertical axis.

The two vectors  $\bar{R}_1$  and  $\bar{R}_1$  are combined by adding the sine term of  $\bar{R}_1$  to the cosine terms of  $\bar{R}_1$  in one summing amplifier and the cosine term of  $R_1$  to the sine term of  $R_1$  in another. These two amplifiers then provide the horizontal and vertical signals to the oscilloscope. By adjusting the magnitude of the initial conditions, the combination of  $\bar{R}_1$  and  $R_1$  will appear on the oscilloscope as a circular pattern rotating counterclockwise when  $R_1$  is 0, as a straight line inclined  $45^\circ$  to the horizontal when  $R_1 = R_1$ , and a circular pattern with clockwise rotation when  $\bar{R}_1 = 0$ . For all other relative magnitudes of  $\bar{R}_1$  and  $R_1$  the pattern will be elliptical with clockwise rotation if  $R_1$  is larger and counterclockwise if  $\bar{R}_1$  is larger. For the conventions normally used in stress-strain curves,  $R_1$  is larger and rotation is clockwise. Figure 6-29 shows the combined circles, which describe an ellipse.

The elliptical pattern formed by  $\bar{R}_1$  and  $R_1$  is distorted into the forms commonly seen in hysteresis loops by addition of  $\bar{R}_3$  and  $R_3$ , the third harmonic. Figure 6-30 shows the  $\bar{R}_3 + R_3$  ( $R_3 = R_3$ ) component (lower) and the figure traced when all components are added. Since the distortion is assumed to affect only the horizontal (strain) axis corresponding to a distorted strain that results from a sinusoidal stress input, only one sinusoidal component of third harmonic frequency need be generated. This component is formed by a circuit identical with that used for  $\bar{R}_1$ .



AIRESEARCH MANUFACTURING COMPANY OF ARIZONA  
A DIVISION OF THE GARRETT CORPORATION  
PHOENIX, ARIZONA

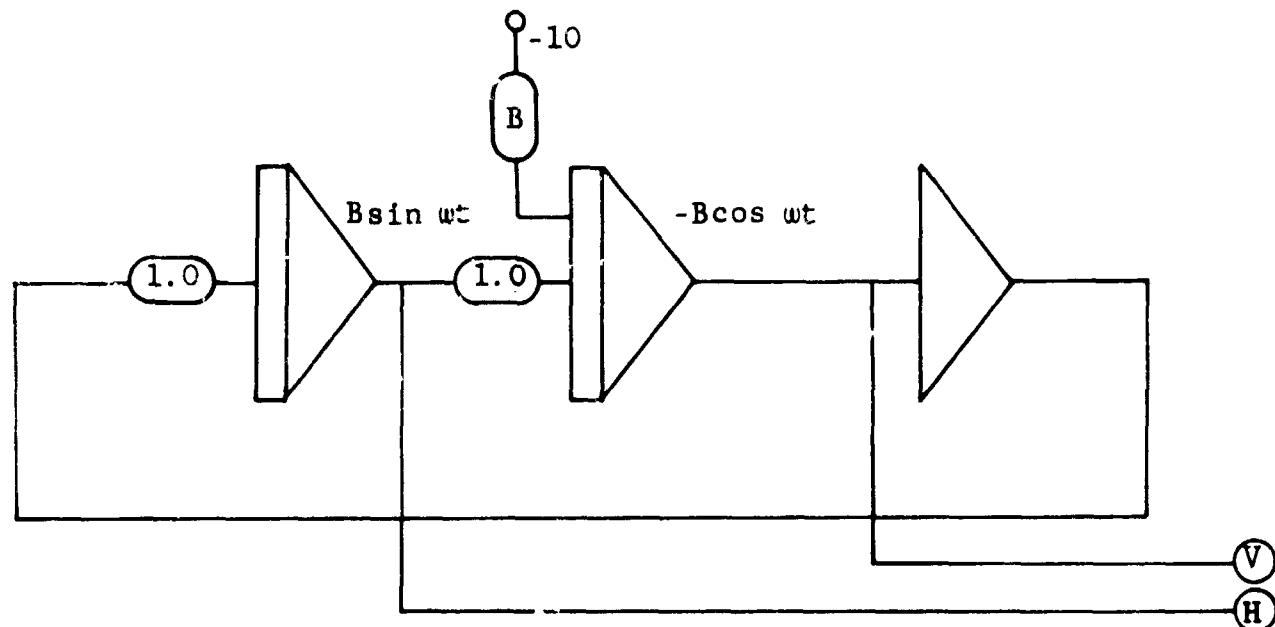


FIGURE 6-28

COMPUTER MECHANIZATION FOR  
SIMULATION OF  $\bar{R} = B(\sin \omega t + j \cos \omega t)$

GT-7615-R, Rev. 1  
Page 6-72

B11001



AIRESEARCH MANUFACTURING COMPANY OF ARIZONA  
A DIVISION OF THE GARRETT CORPORATION  
PHOENIX, ARIZONA

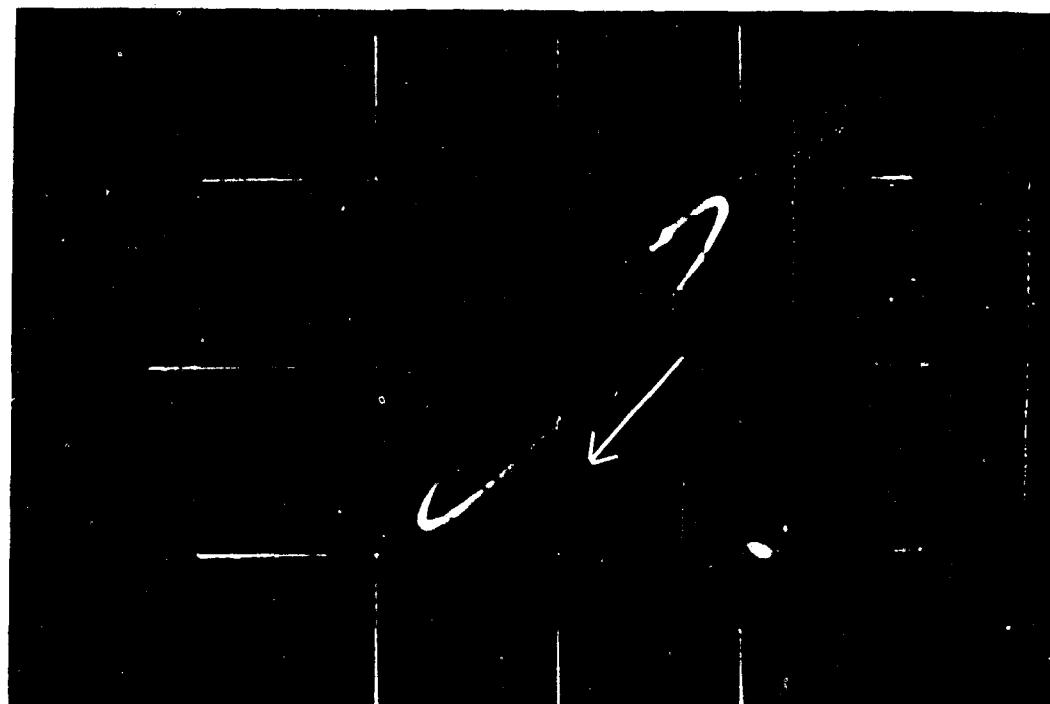


FIGURE 6-29  
COMBINED R AND S CIRCLES

GT-7615-R,  
Page 6-73



AIRESEARCH MANUFACTURING COMPANY OF ARIZONA  
A DIVISION OF THE GARRETT CORPORATION  
PHOENIX, ARIZONA

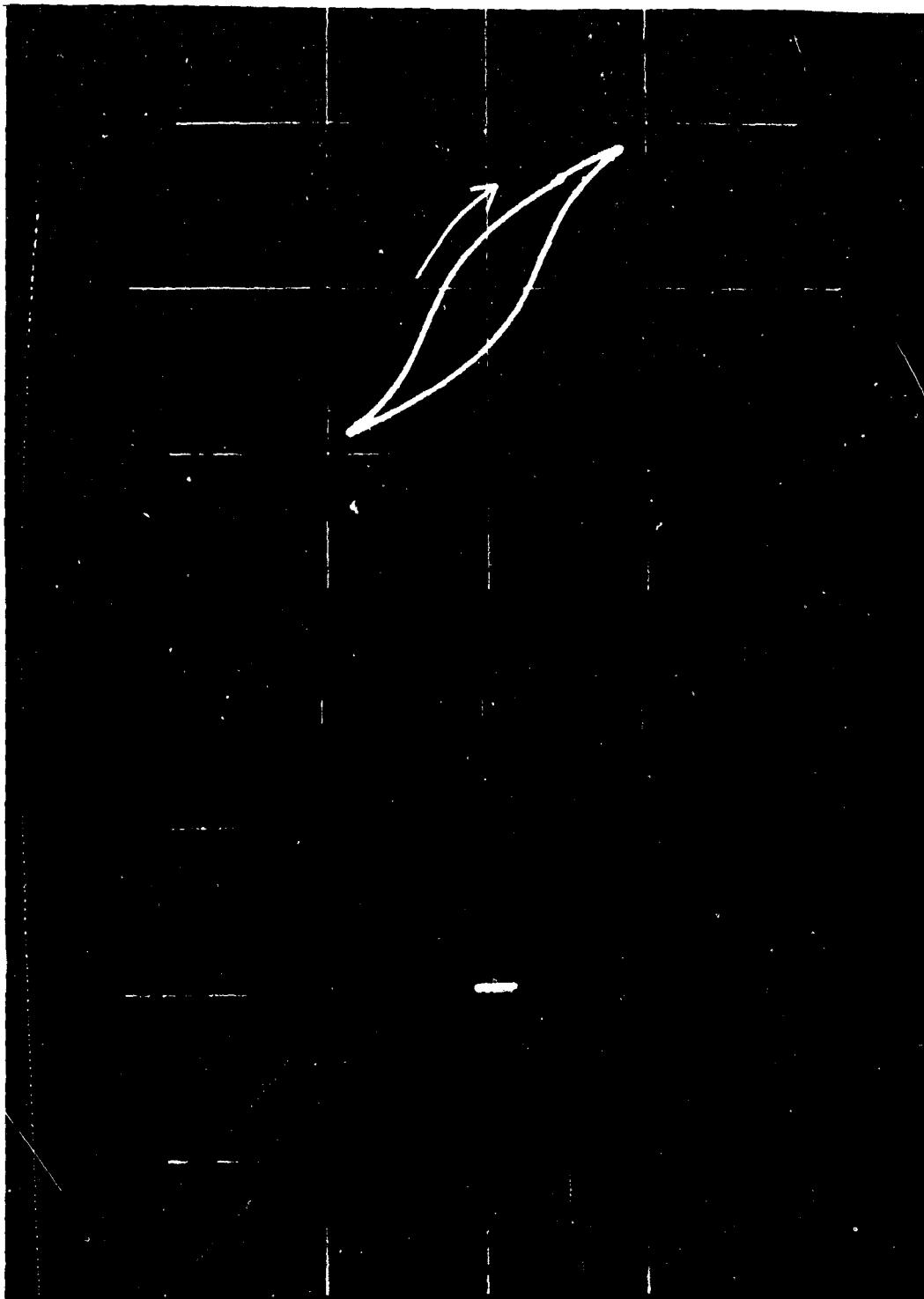


FIGURE 6-30

LOWER: THE THIRD HARMONIC  $\bar{R}_3 + \bar{R}_3$ , ( $R_3 = R_3$ )  
UPPER: EFFECT OF ADDING THE THIRD HARMONIC TO  
THE COMBINED  $\bar{R}$  AND  $\bar{R}$  CIRCLES

GT-7615-R,  
Page 6-74



and  $\bar{R}$  except that the frequency is three times as great, and provision is added for inserting initial conditions so as to shift the phase of the wave. The computer mechanization is shown in Figure 6-31. This component is then described as:

$$x_3 = A_3 \sin (3\omega t + e) \quad (6-90)$$

It is added to the horizontal axis through the same summing amplifier used for  $\bar{R}$  and  $\bar{R}_3$  (see Figure 6-32).

Figures 6-33 through 6-36 show the effect of change in phase of the  $\bar{R}_3 + \bar{R}_3$  component on the shape of the figure. In order to show clearly the phase relation of the third harmonic, this component was expanded and displayed with a linear horizontal time base. The flat section at the beginning of each three cycles, or one cycle of the fundamental, with respect to the horizontal axis represents the value of  $\bar{R}_3 + \bar{R}_3$  at the instant the problem is started. The positions correspond to:

$$\bar{R}_3 + \bar{R}_3 = A_3 \sin (3\omega t + 0) \quad (\text{Figure 6-33})$$

$$\bar{R}_3 + \bar{R}_3 = A_3 \sin (3\omega t - 30^\circ) \quad (\text{Figure 6-34})$$

$$\bar{R}_3 + \bar{R}_3 = A_3 \sin (3\omega t - 60^\circ) \quad (\text{Figure 6-35})$$

$$\bar{R}_3 + \bar{R}_3 = A_3 \sin (3\omega t - 90^\circ) \quad (\text{Figure 6-36})$$

These synthetic figures exhibit how little third harmonic is required to generate the type of hysteresis loop that is characteristic of heavily stressed metals. For this same amount of third harmonic, the figure passes from metallic-type loops to a type of loop that is characteristic of clay.



AIRESEARCH MANUFACTURING COMPANY OF ARIZONA  
A DIVISION OF THE GARRETT CORPORATION  
PHOENIX, ARIZONA

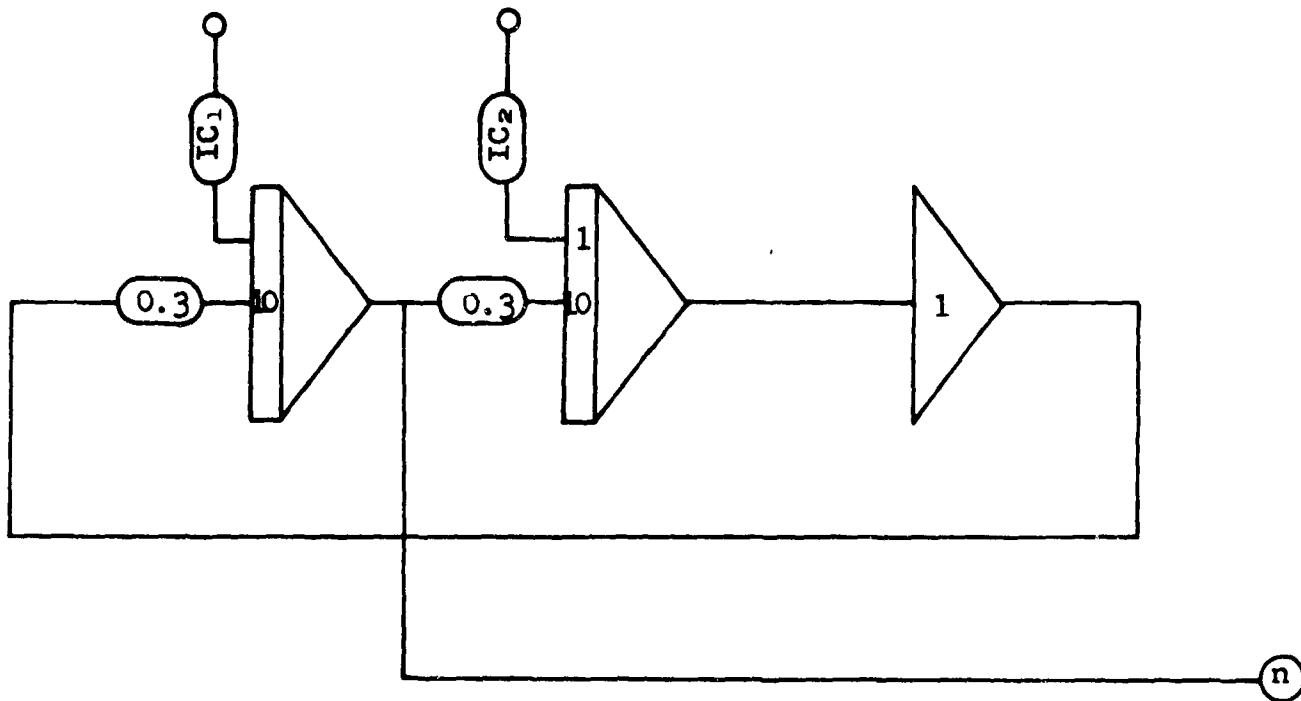


FIGURE 6-31

COMPUTER MECHANIZATION FOR SIMULATION OF:

$$R_s + R_a = A_s [\sin(3\omega t + \alpha) + j \cos(3\omega t + \alpha)]$$

$$\alpha = \tan^{-1} \frac{IC_1}{IC_2}$$

$$A_s = \sqrt{IC_1^2 + IC_2^2}$$



AIRESEARCH MANUFACTURING COMPANY OF ARIZONA  
A DIVISION OF THE GARRETT CORPORATION  
PHOENIX, ARIZONA

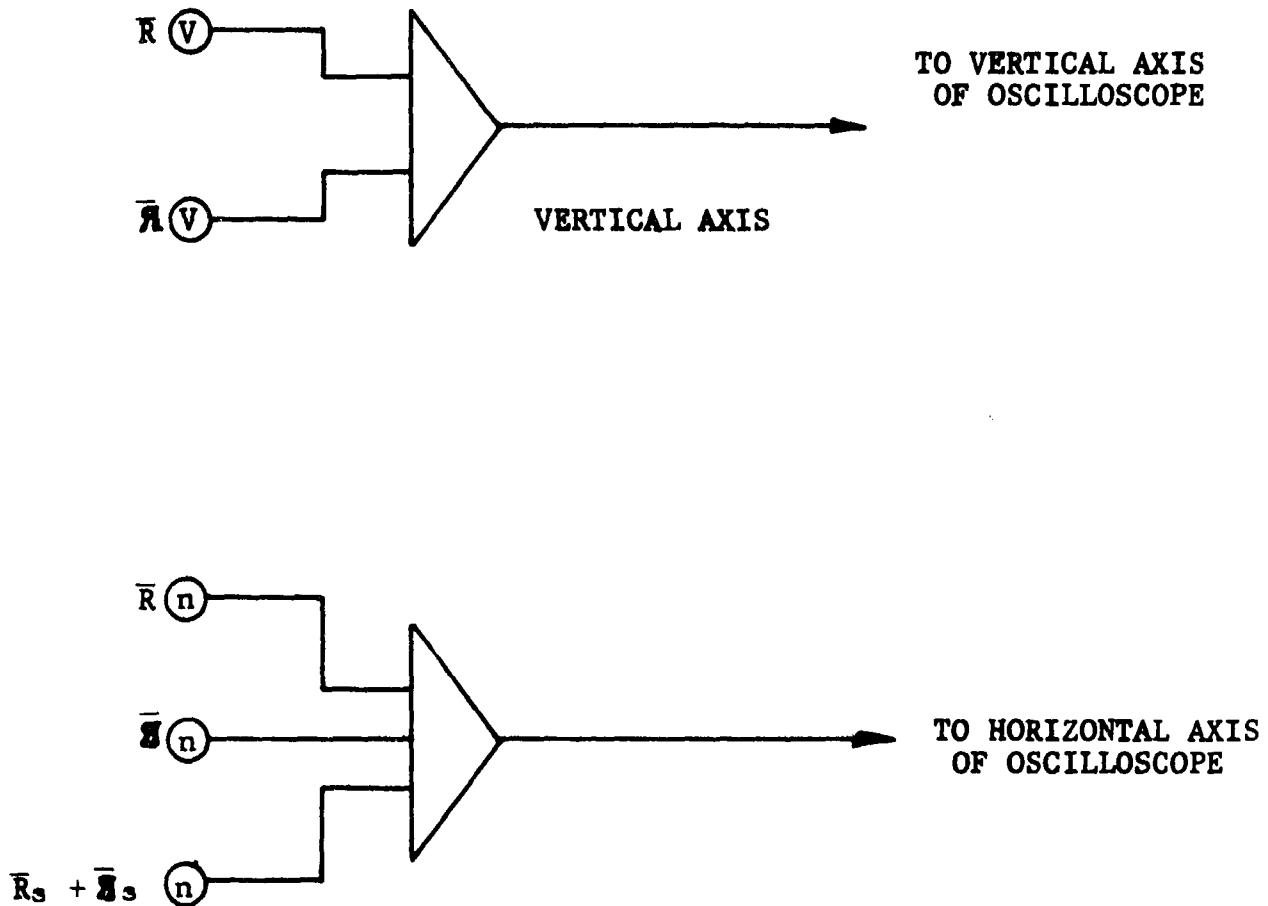


FIGURE 6-32  
SUMMING AMPLIFIERS

B10999

GT-7615-R  
Page 6-77



AIRESEARCH MANUFACTURING COMPANY OF ARIZONA  
A DIVISION OF THE GARRETT CORPORATION  
PHOENIX, ARIZONA

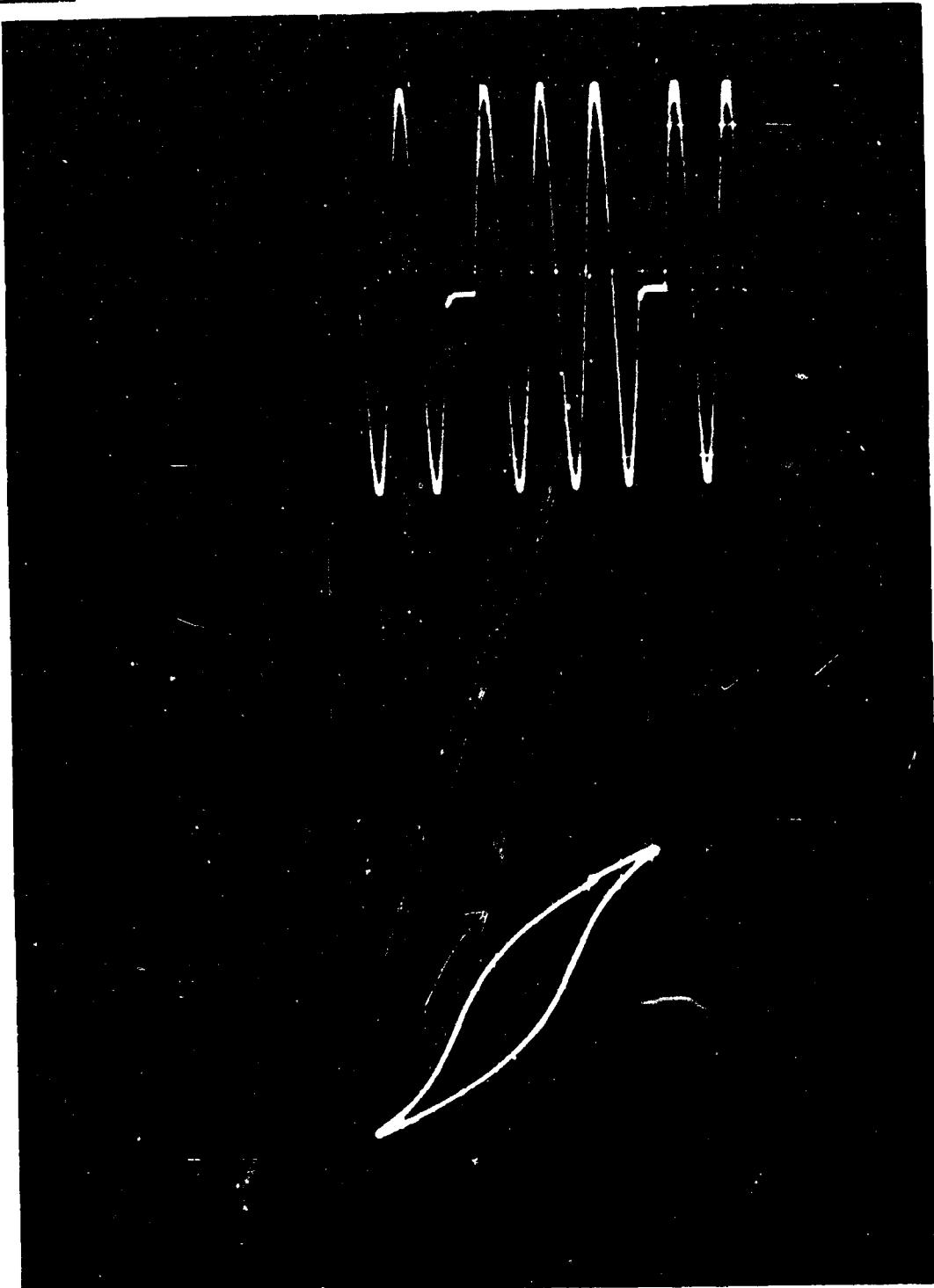


FIGURE 6-33  
EFFECT OF  
 $\bar{R}_3 + \bar{R}_3 = A_3 \sin (3\omega t + 0)$

GT-7615-R,  
Page 6-78



AIRESEARCH MANUFACTURING COMPANY OF ARIZONA  
A DIVISION OF THE GARRETT CORPORATION  
PHOENIX, ARIZONA

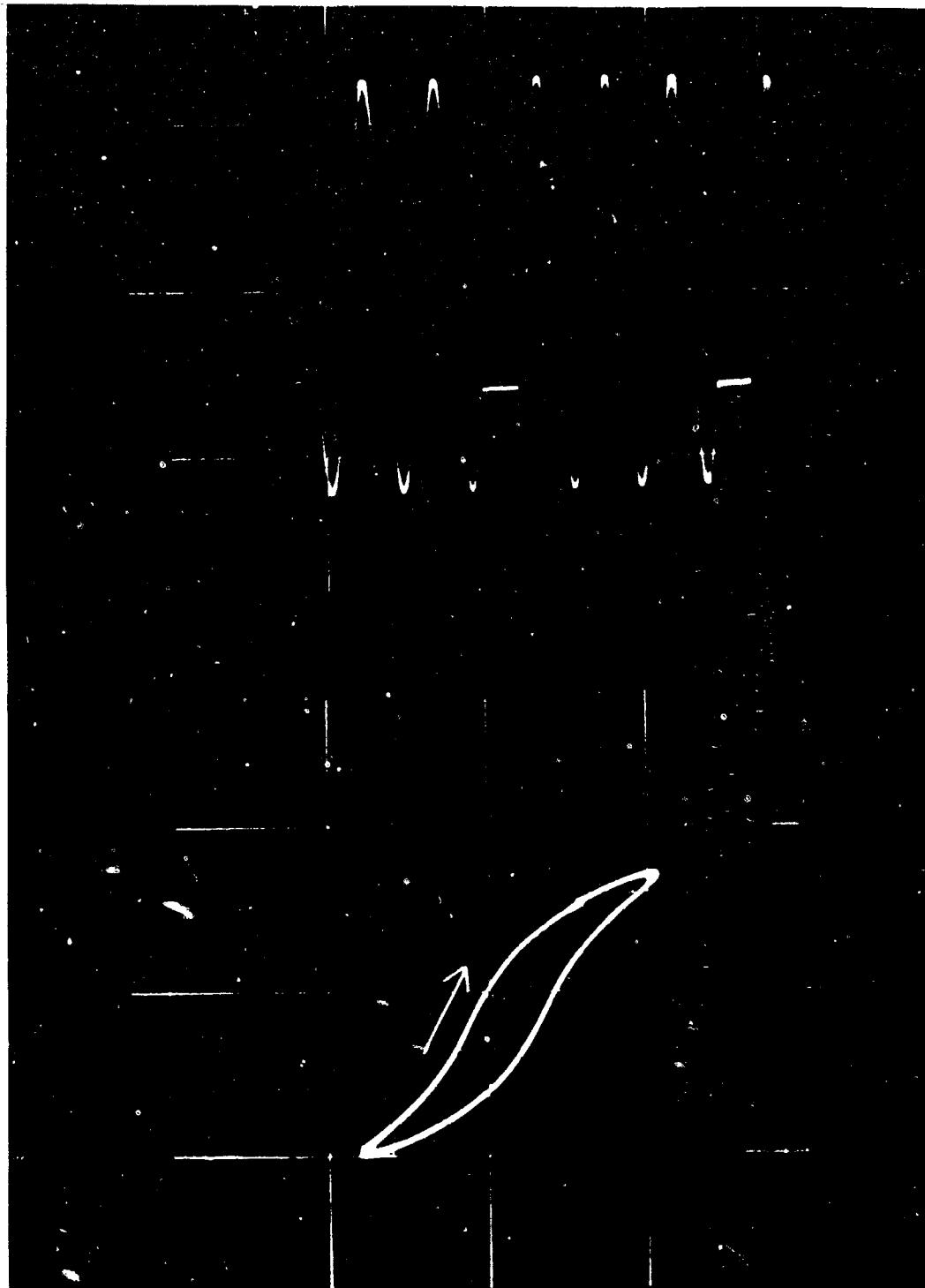


FIGURE 6-34

EFFECT OF

$$\bar{R}_3 + \bar{R}_3 = A_3 \sin (3\omega t - 30^\circ)$$

GT-7615-R,  
Page 6-79



AIRESEARCH MANUFACTURING COMPANY OF ARIZONA  
A DIVISION OF THE GARRETT CORPORATION  
PHOENIX, ARIZONA

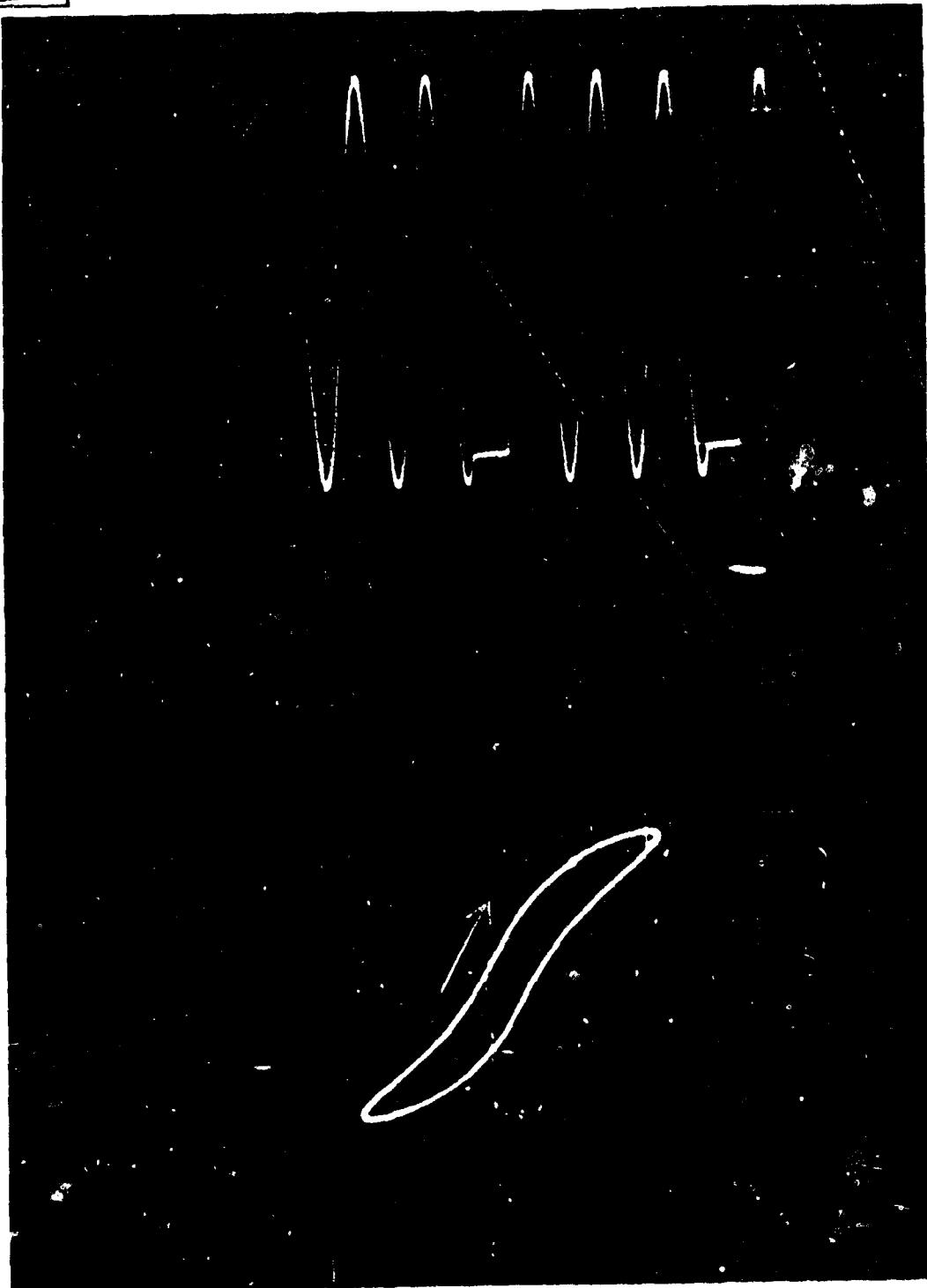


FIGURE 6-35

$$R_3 + \bar{R}_3 = A_3 \sin (3\omega t - 60^\circ)$$

GT-7615-R,  
Page 6-80



AIRSEARCH MANUFACTURING COMPANY OF ARIZONA  
A DIVISION OF THE BARRETT CORPORATION  
PHOENIX, ARIZONA

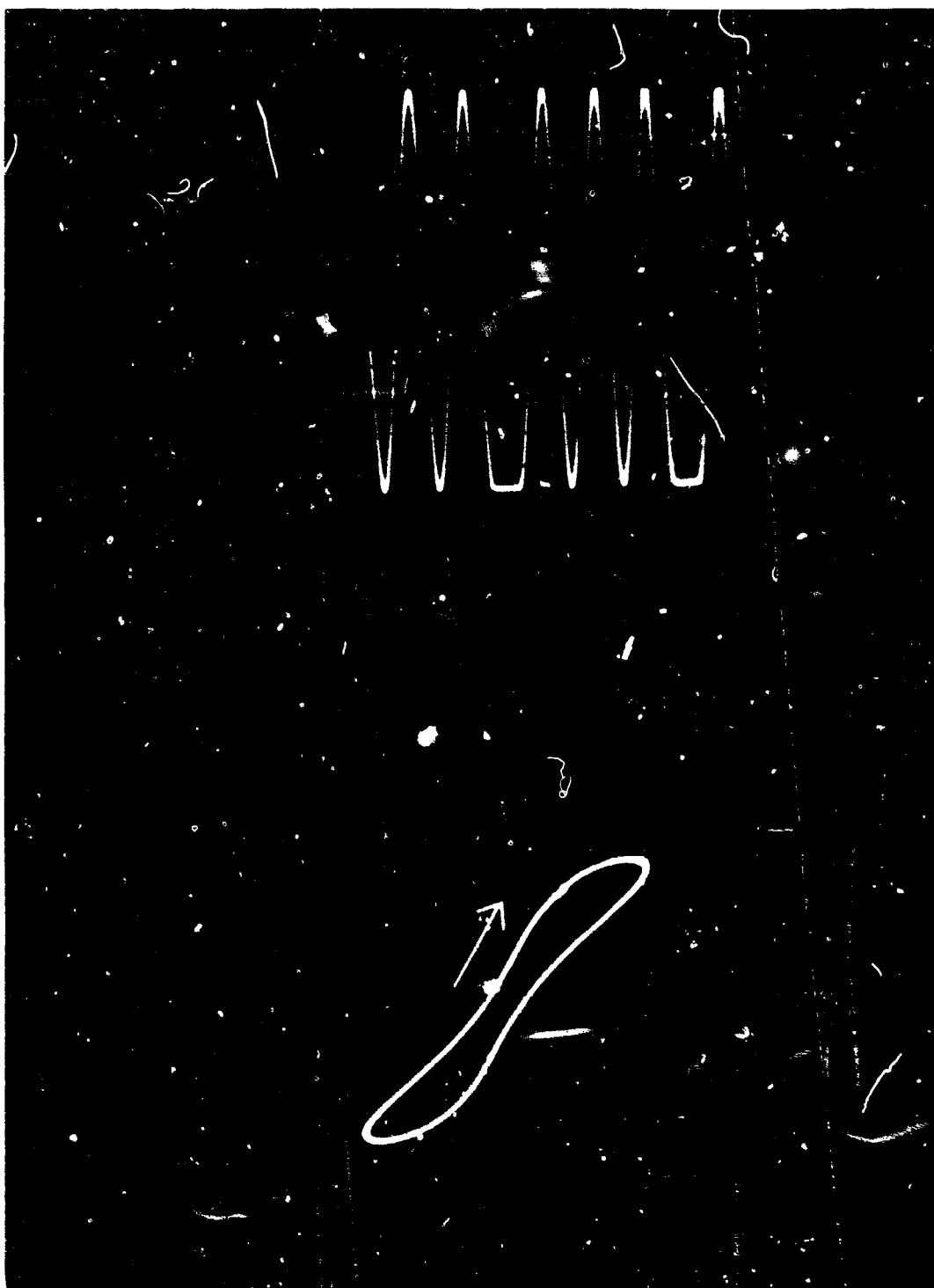


FIGURE 6-36  
 $\bar{R}_3 + \bar{S}_3 = A_3 \sin (3\omega t - 90^\circ)$

GT-7615-R,  
Page 6-81



AIRESEARCH MANUFACTURING COMPANY OF ARIZONA  
A DIVISION OF THE BARRETT CORPORATION  
PHOENIX, ARIZONA

#### 6.5.3.4 Stress Inputs Versus Strain Inputs for Generation of Hysteresis Loops

It has been seen that a sinusoidal stress input  $\sigma_1$  will in any nonlinear material produce strain outputs of  $\epsilon_1, \epsilon_2, \dots \epsilon_n$ .

Similarly, a sinusoidal strain input  $\epsilon_1$  will produce a stress output  $\sigma_1\sigma_2 + \sigma_n^+$ . In either case  $E_1 = \frac{\sigma_1}{\epsilon_1} e^{i(\phi_1 - \psi_1)}$  is presumed to be the same. In neither case, however, can any of the other  $E_n^+$  be defined. Whenever a nonlinear material of any sort produces a distorted strain output in response to a pure sinusoidal stress input  $\sigma_1$  or a distorted stress output in response to a pure sinusoidal strain input  $\epsilon_1$ ,  $E_n^+, n > 1$  cannot be defined by a single experiment.

If  $\sigma_n = 0$ ,  $|E_n| = 0$  and no direction can be assigned to it.

If  $\epsilon_n = 0$ ,  $E_n^+$  is not defined. The effect on  $R_n$  and  $\bar{R}_n$  is to produce the 'degenerate' cases.

For  $\sigma_n = 0$ ,

$$\frac{\alpha_n + \beta_n}{2} = 0, \quad \alpha_n = -\beta_n \quad (6-91)$$

$$R_n = \bar{R}_n = \frac{\epsilon_n}{2} \quad (6-92)$$



AIRESEARCH MANUFACTURING COMPANY OF ARIZONA  
A DIVISION OF THE GARRETT CORPORATION  
PHOENIX, ARIZONA

If  $\epsilon_n = 0$ ,

$$\frac{\alpha_n + \beta_n}{2} = \frac{\pi}{2} \quad (6-93)$$

$$R_n = R_n = \frac{\sigma_n}{2} \quad (6-94)$$

These conclusions follows from the definitions of  $\bar{R}_n$  and  $\bar{R}_n$

$$\bar{R}_n = R_n e^{i\alpha_n} = \frac{\epsilon_n}{2} e^{i\psi_n} + \frac{\sigma_n}{2} e^{i\phi_n} \quad (6-95)$$

$$\bar{R}_n = R_n e^{i\theta_n} = \frac{\epsilon_n}{2} e^{-i\psi_n} - \frac{\sigma_n}{2} e^{-i\phi_n} \quad (6-96)$$

Suppose now that two experiments are performed on the same test bar.

#### Experiment 1

Apply a sinusoidal stress  $\sigma_1$  and observe each resulting pair  $\bar{R}_{n_1}$ ,  $\bar{R}_{n_1}$  with the aid of the oscilloscope. Carefully note the proportion and time base of the  $n = 1$  ellipse.

Then  $\bar{R}_{n_1} = \frac{\epsilon_{n_1}}{2} e^{i\psi_{n_1}} = R_{n_1} e^{i\alpha_{n_1}}$  (6-97)

$$\bar{R}_{n_1} = \frac{\epsilon_{n_1}}{2} e^{-i\psi_{n_1}} = R_{n_1} e^{i\theta_{n_1}} \quad (6-98)$$

for all cases  $n > 1$



AIRESEARCH MANUFACTURING COMPANY OF ARIZONA  
A DIVISION OF THE BARRETT CORPORATION  
PHOENIX, ARIZONA

### Experiment 2

Apply a sinusoidal strain  $\epsilon_1$  and adjust its magnitude to obtain precisely the same  $n = 1$  ellipse having the same time base as in Experiment 1.

$$\text{Then each } \bar{R}_{n_2} = \frac{\sigma_{n_2}}{2} e^{i\phi_{n_2}} = R_{n_2} e^{i\alpha_{n_2}} \quad (6-99)$$

$$\bar{R}_{n_2} = \frac{\sigma_n}{2} e^{-i\phi_n} = R_{n_2} e^{i\theta_{n_2}} \quad (6-100)$$

Then let

$$\bar{R}_n = \bar{R}_{n_1} + \bar{R}_{n_2} \quad (6-101)$$

$$\bar{R}_n = R_n e^{i\alpha_n} \quad (6-102)$$

$$\bar{R}_n = \frac{\epsilon_{n_1}}{2} e^{i\psi_{n_1}} + \frac{\sigma_{n_2}}{2} e^{i\phi_{n_2}} \quad (\text{at } t = 0) \quad (6-103)$$

$$\text{and, similarly } \bar{R}_n = \bar{R}_{n_1} + \bar{R}_{n_2} = R_n e^{i\theta_n} \quad (6-104)$$

$$\bar{R}_n = \frac{\epsilon_{n_1}}{2} e^{-i\psi_{n_1}} - \frac{\sigma_{n_2}}{2} e^{-i\phi_{n_2}} \quad (6-105)$$

$$\text{Then } E_n^+ = \frac{\sigma_n}{\epsilon_n} e^{i(\phi_n - \psi_n)} \quad (6-106)$$



AIRESEARCH MANUFACTURING COMPANY OF ARIZONA  
A DIVISION OF THE GARRETT CORPORATION  
PHOENIX, ARIZONA

It is hoped that a long-standing controversy among materials engineers can be resolved. One school of thought prefers the use of sinusoidal stress inputs to generate hysteresis loops. To accomplish this, a voice coil-type force generator (ideally zero mechanical impedance source) may be used. Strain may then be recorded as detected by a strain gauge.

Another school of thought prefers sinusoidal strain inputs to generate hysteresis loops. These are conveniently attained by use of a motor-driven cam or crank (infinite impedance source). Stress may then be measured by means of a force transducer such as a load cell. Each school of thought has had its partisans.

It is now apparent that to define clearly the parameters  $R_n$ ,  $\alpha_n$ ,  $\beta_n$  and the modulus  $E_n^+$  it is necessary to use both a stress input and a strain input in two separate experiments.

The figure corresponding to this unique set of parameters is some sort of "generalized" hysteresis loop. An attempt to explore a few of the implications of these concepts will be undertaken in the next section.



#### 6.5.4 The Generalized Hysteresis Loop and Its Representation by Power Series

##### 6.5.4.1 Introduction

"Mathematical Research does not proceed in a series of rigorous little steps from the known into the unknown. Instead, the first step is to fling all rigor to the winds and proceed with uninhibited abandon. Only if you encounter something of interest do you retrace your steps to plug the loopholes with rigor."

(Quoted by memory from a classroom lecture by Professor Copeland, University of Michigan, Mathematics Department, about 1949).

Professor Copeland's prescription provides the method used in this section. No pretense is made of rigor. Intuition, plausibility, and analogy are freely substituted for it without apology.

The results are indeed interesting and vindicate the method. A generalized hysteresis loop is found that appears to truly represent any material, whether it be linear or nonlinear.

The generalized loop is shown to be expressible as a power series that is an expansion of any desired input. The power series has the desirable characteristic of increasing the influence of the nonlinearities as the magnitude of the input increases.

The existence of the power series representation for the generalized loop leads to the hypothesis that a single set of unique coefficients, usually few in number, may represent the behavior of a material for any input and over a wide range of input magnitudes. Further, if coefficients vary, their history represents the stress history of the specimen.

Time limitations have precluded the completion of the last step, the provision of rigor, or even experimental verifications. It is hoped that others in the field will find the results interesting enough to explore them further.



AIRESEARCH MANUFACTURING COMPANY OF ARIZONA  
A DIVISION OF THE GARRETT CORPORATION  
PHOENIX, ARIZONA

It is hoped that a long-standing controversy among materials engineers can be resolved. One school of thought prefers the use of sinusoidal stress inputs to generate hysteresis loops. To accomplish this, a voice coil-type force generator (ideally zero mechanical impedance source) may be used. Strain may then be recorded as detected by a strain gauge.

Another school of thought prefers sinusoidal strain inputs to generate hysteresis loops. These are conveniently attained by use of a motor-driven cam or crank (infinite impedance source). Stress may then be measured by means of a force transducer such as a load cell. Each school of thought has had its partisans.

It is now apparent that to define clearly the parameters  $R_n$ ,  $\alpha_n$ ,  $\beta_n$  and the modulus  $E_n^+$  it is necessary to use both a stress input and a strain input in two separate experiments.

The figure corresponding to this unique set of parameters is some sort of "generalized" hysteresis loop. An attempt to explore a few of the implications of these concepts will be undertaken in the next section.



#### 6.5.4.2 Normalization

Careful normalization of the stress-strain plane greatly simplifies the vector manipulations that follow. Experience has shown that the normalization to be preferred is that shown in Figure 6-37. For the viscoelastic or  $n = 1$  ellipse, the maximum strain is adjusted to equal the maximum (dimensionless) stress in magnitude. This magnitude is designated "a". Furthermore, zero time is chosen such that for a sinusoidal strain input, the component strain vectors lie on the real axis as shown. Then the positive rotating stress vector component is located at an angle  $\delta$  past the  $i\sigma$  axis and points in the direction of  $\dot{E}_1$ . The angle of inclination of the ellipse is  $\frac{\pi}{4}$ .  $\dot{E}_1$  is a unit vector

$$\dot{E}_1 = e^{i(\delta + \frac{\pi}{2})} \quad (6-107)$$

where  $\delta$  is the conventional angle by which stress leads strain. Finally, both the stress components and the strain components all have the magnitude  $\frac{a}{2}$ .

#### 6.5.4.3 Relation of Stress and Strain

The Ptolemaic model made no sharp distinction between stress and strain but simply accepted them as found. This was justified by their parametric relations. The apparently obvious distinction between stress and strain tends to disappear when subjected to close scrutiny. Yet the results of sinusoidal stress or sinusoidal strain inputs differ for nonlinear materials. For both, all distortion terms appear in quadrature. This point is at least partly resolved in the following paragraphs.



AIRESEARCH MANUFACTURING COMPANY OF ARIZONA  
A DIVISION OF THE GARRETT CORPORATION  
PHOENIX, ARIZONA

NOTES:

1. OPEN POINTS: STRESS COMPONENTS
2. CLOSED POINTS: STRAIN COMPONENTS
3. VECTORS ROTATE IN THE DIRECTION INDICATED BY THE CORNER OF THE HALF POINT

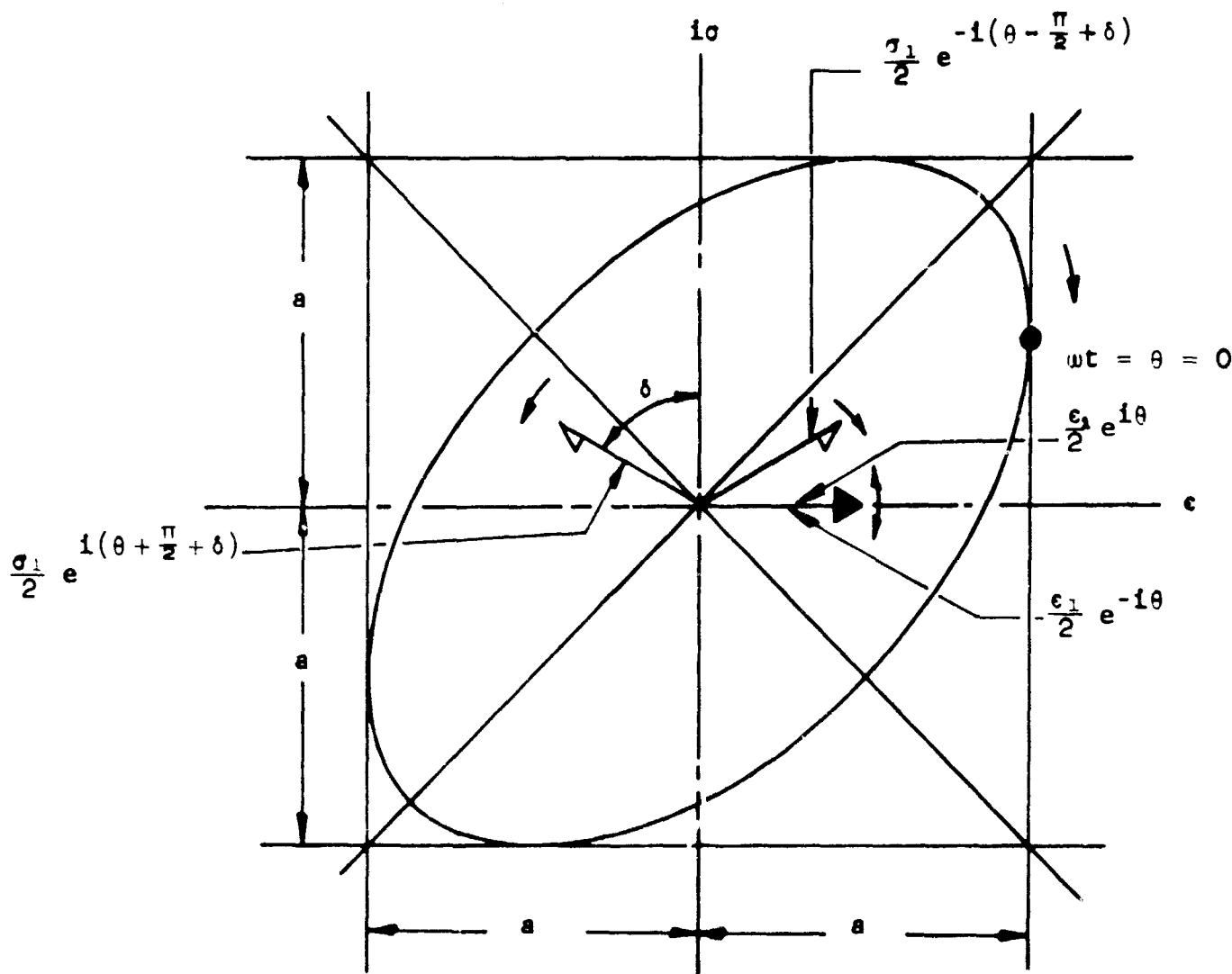


FIGURE 6-37  
NORMALIZATION OF THE FIRST ORDER ELLIPSE,  
SHOWN FOR INPUT  $\epsilon = a \cos \theta$



Referring to Figure 6-38b, the vector  $a e^{i\theta}$  is considered to rotate with angular velocity  $\theta = \omega t$ . Its vertical projection defines a sinusoidal strain input, and the result of its application to a viscoelastic material is shown in Figure 6-38c. Note the time mark and the position of the stress component and strain component vectors.

The horizontal projection of the same vector corresponds to a sinusoidal stress input. Figure 6-38a shows its effect on a viscoelastic material. Note the revised position of the stress component and strain component vectors and the time mark. For a viscoelastic material this appears to be the only distinction possible, since both ellipses are identical. It is, however, the needed distinction.

Figure 6-39 shows the vectors  $\bar{R}_{\epsilon_1}$  and  $\bar{R}_{\epsilon_1}$  which may be constructed from the component vectors and the time mark for sinusoidal strain input. Notice the use of the subscript  $\epsilon$  to designate strain input as well as the usual numerical subscript to designate order number. Similarly, Figure 6-39a shows the vectors  $\bar{R}_{\sigma_1}$  and  $\bar{R}_{\sigma_1}$  constructed from the component vectors and the time mark for a stress input. Note also that the generating vector is designated differently for stress and strain inputs:

$$[\bar{F}]_{\theta=0} = \bar{R}_{\epsilon_1} + \bar{R}_{\epsilon_1} \quad (6-108)$$

$$[\bar{G}]_{\theta=0} = \bar{R}_{\sigma_1} + \bar{R}_{\sigma_1} \quad (6-109)$$

With this as preparation, a single loop will be constructed to represent both cases. This will be designated as generated by the resultant vector  $\bar{H}$ .



AIRESEARCH MANUFACTURING COMPANY OF ARIZONA  
A DIVISION OF THE GARRETT CORPORATION  
PHOENIX, ARIZONA

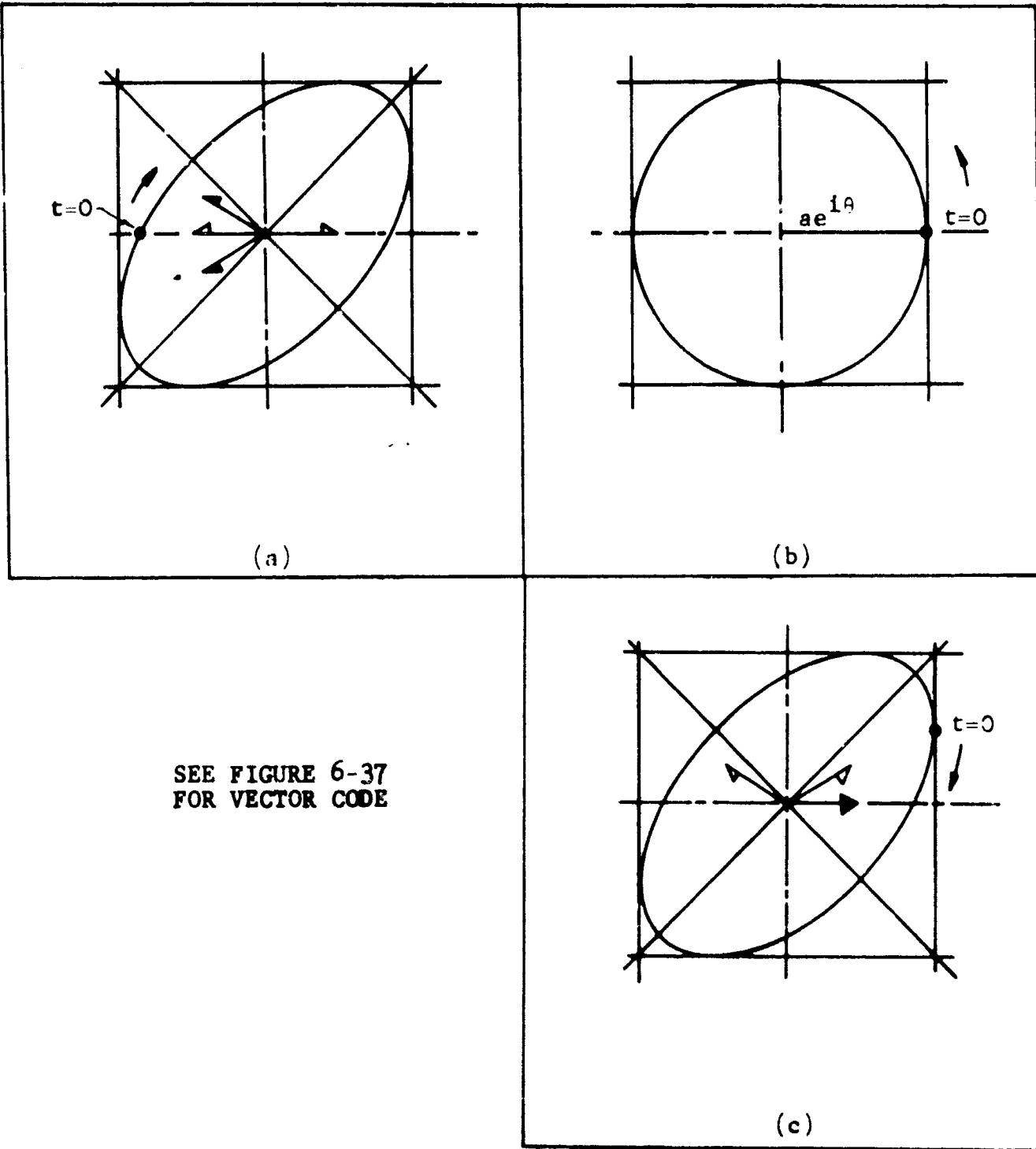


**FIGURE 6-38**  
**RELATION OF STRESS INPUT TO STRAIN INPUT**  
**FOR A VISCOELASTIC MATERIAL**

GT-7615-R, Rev. 1  
Page 6-90



AIRESEARCH MANUFACTURING COMPANY OF ARIZONA  
A DIVISION OF THE GARRETT CORPORATION  
PHOENIX, ARIZONA

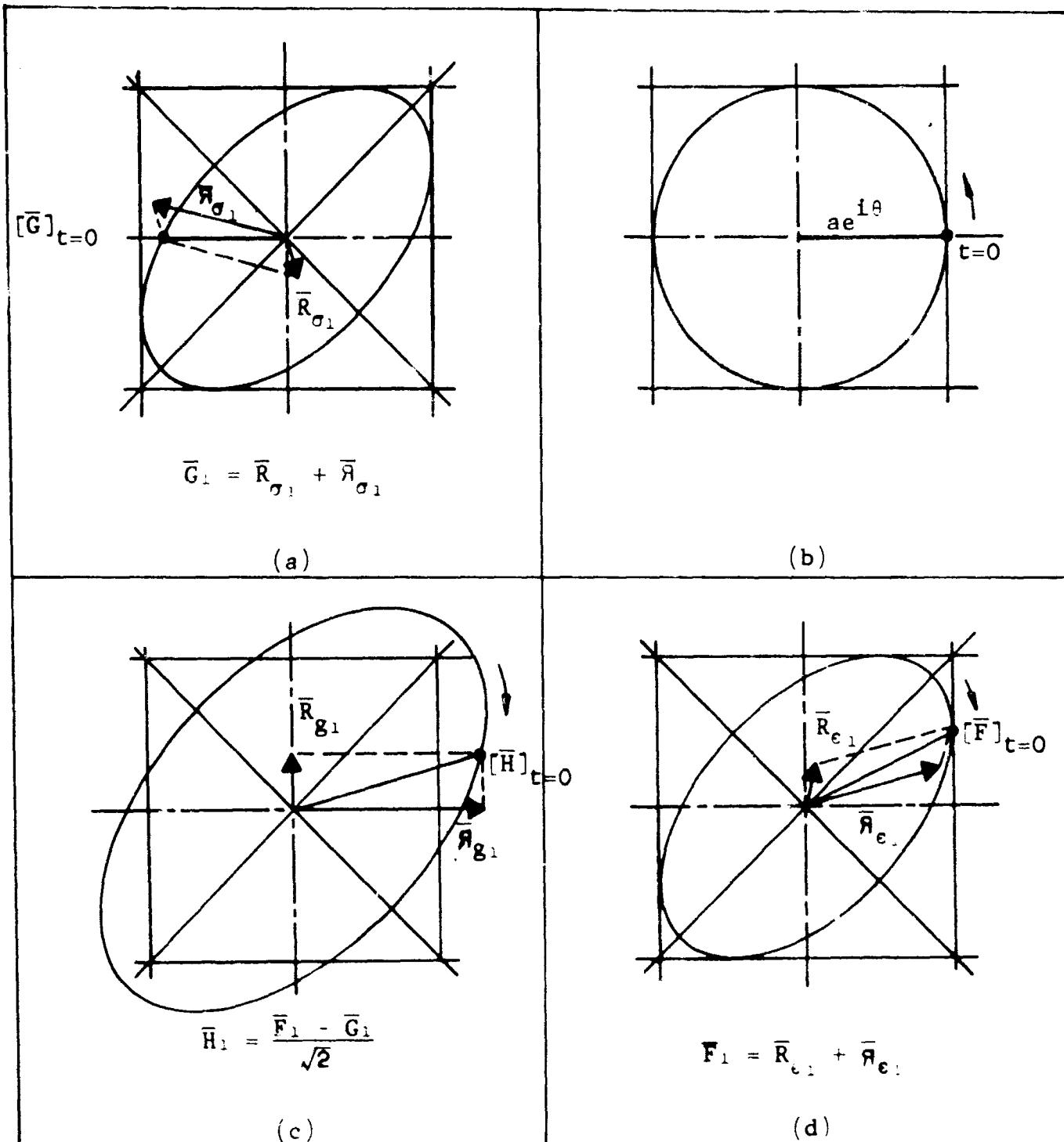


FIGURE 6-39

THE CONSTRUCTION OF  $\bar{F}$ ,  $\bar{G}$ , AND  $\bar{H}$  AT  $t = 0$

GT-7615-R, Rev. 1  
Page 6-91



AIRESEARCH MANUFACTURING COMPANY OF ARIZONA  
A DIVISION OF THE GARRETT CORPORATION  
PHOENIX, ARIZONA

#### 6.5.4.4 The Generalized Loop

##### 6.5.4.4.1 The Viscoelastic Case

The shape of a periodic stress-strain loop depends on the shape and nature of the driving signal. Test machines normally use sinusoidal strain generated by a source having very high mechanical impedance (cams, etc.) or sinusoidal stress generated by a source having near zero mechanical impedance (voice coils, etc.). These are idealizations seldom encountered in real machinery.

Mathematically there is no difficulty in simultaneously subjecting the specimen to sinusoidal stress and sinusoidal strain. This can be approximated on conventional test apparatus by superimposing the results of alternate stress input and strain input tests. The immediate purpose is to perform this superposition on a viscoelastic material.

Let  $\bar{F}_1$  represent the vector that generates the elliptical loop for a viscoelastic material subjected to sinusoidal strain.

$$\bar{F}_1 = \epsilon_1 \cos (\theta + \psi_1) + i\tau_1 \sin (\theta + \phi_1) \quad (6-110)$$

For the normalization shown in Figure 6-37,

$$\epsilon_1 = \tau_1 = a \quad (6-111)$$

$$\psi_1 = 0 \quad (6-112)$$

$$\phi_1 = \frac{\pi}{2} + \delta \quad (6-113)$$



AIRSEARCH MANUFACTURING COMPANY OF ARIZONA  
A DIVISION OF THE GARRETT CORPORATION  
PHOENIX, ARIZONA

$$\bar{F}_1 = R_{\epsilon_1} e^{i\theta} + \bar{R}_{\epsilon_1} e^{-i\theta} \quad (6-114)$$

$$\bar{R}_{\epsilon_1} = \frac{a}{2} \left[ 1 + e^{i(\frac{\pi}{2} + \delta)} \right] \quad (6-115)$$

$$\bar{R}_{\epsilon_1} = \frac{a}{2} (1 + \dot{E}_1) \quad (6-116)$$

$$\bar{R}_{\epsilon_1} = \frac{a}{2} \left[ 1 - e^{-i(\frac{\pi}{2} + \delta)} \right] \quad (6-117)$$

$$\bar{R}_{\epsilon_1} = \frac{a}{2} (1 - \dot{E}_1^*) = \frac{a}{2} (1 + \bar{E}_1) \quad (6-118)$$

Let  $\bar{G}$  represent the vector which generates the elliptical loop for a sinusoidal stress input. In general form  $\bar{G}_1$  would be written

$$\bar{G}_1 = i\sigma_1 \sin (\theta + \phi'_1) + \epsilon_1 \cos (\theta + \psi'_1) \quad (6-119)$$

Here the primed phase angles simply indicate a dependence of the phase angle on the choice of input. The real and imaginary terms have been reversed from their usual order also.

After normalization,  $\bar{G}$  may be written

$$\bar{G}_1 = R_{\sigma_1} e^{i\theta} + \bar{R}_{\sigma_1} e^{-i\theta} \quad (6-120)$$

$$R_{\sigma_1} = \frac{a}{2} (1 + \dot{E}_1^*) \quad (6-121)$$

$$\begin{aligned} \bar{R}_{\sigma_1} &= \frac{a}{2} (-1 + \dot{E}_1) = \frac{a}{2} (-1 - \dot{E}_1^*) \\ &= \frac{a}{2} (-1 - \bar{E}_1^*) \end{aligned} \quad (6-122)$$



$[\bar{F}]_{\theta=0}$  and  $[\bar{G}]_{\theta=0}$  are shown in Figure 6-39.

It would seem logical to simply add  $\bar{F}$  and  $\bar{G}$  to try for a generalized generating vector  $\bar{H}$ , but it turns out not to behave properly in limiting cases. Note that Equation 6-110, if normalized, becomes

$$\bar{F} = a \cos \theta + \text{quadrature term} \quad (6-123)$$

and Equation 6-119 may be written

$$\bar{G} = ia \sin \theta + \text{quadrature term} \quad (6-124)$$

then

$$\bar{F} + \bar{G} = ae^{i\theta} + \text{other terms} \quad (6-125)$$

In each case, the first term describes the input. But it was seen in the Ptolemaic formulation that the vector  $e^{-i\theta}$  is associated with the process of energy entering the material. The correct choice will prove to be:

$$\bar{F} - \bar{G} = ae^{-i\theta} + \text{other terms} \quad (6-126)$$

The vector  $\bar{F}$  is the result of applying the forcing function

$$\epsilon = \epsilon_1 \cos \theta \quad (6-127)$$

to the specimen. The vector  $\bar{G}$  is the result of applying the forcing function

$$\sigma = \sigma_1 \sin \theta \quad (6-128)$$

to the specimen, presumably in a separate experiment.



These two inputs are in quadrature. An electrical analogy would involve two equal sinusoidal voltages applied in quadrature to the same circuit. The vector addition of these voltages would be larger than either single voltage by a factor of  $\sqrt{2}$ . Then the total power dissipation would be twice as great as for a single voltage, since power is proportional to the square of the voltage. This analogy suggests the factor  $\sqrt{2}$  in the definition of  $\bar{H}$ . Thus,

$$\bar{H} = \frac{\bar{F} - \bar{G}}{\sqrt{2}} \quad (\text{see Figure 6-39}) \quad (6-129)$$

The locus of the tip of  $\bar{H}$  is designated as the generalized hysteresis loop.

Figure 6-39 shows  $[\bar{H}]_{\theta=0}$  for the case  $\delta = \frac{\pi}{3} = 50^\circ$ . Before examining this figure in detail, it is instructive to consider the limiting cases.

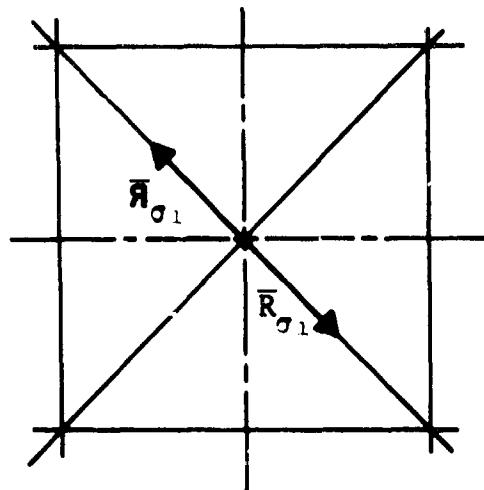
If  $\delta = 0$ , the material is perfectly elastic and no energy dissipation occurs. As a result

$$\bar{R}_{g_1} = \bar{R}_{-g_1} = \frac{\sqrt{2}}{2} a \quad (6-130)$$

Figure 6-40 shows the hysteresis loop for strain input and stress input, as well as their zero time marks. Each is simply the diagonal of the square having sides  $2a$ . Figure 6-40c shows the locus of  $\bar{H}$  and the location of  $\bar{R}_{g_1}$  and  $\bar{R}_{-g_1}$  at time equals 0. The locus of  $\bar{H}$  is identical with that of  $\bar{F}$  or  $\bar{G}$  except for the location of the zero time mark.

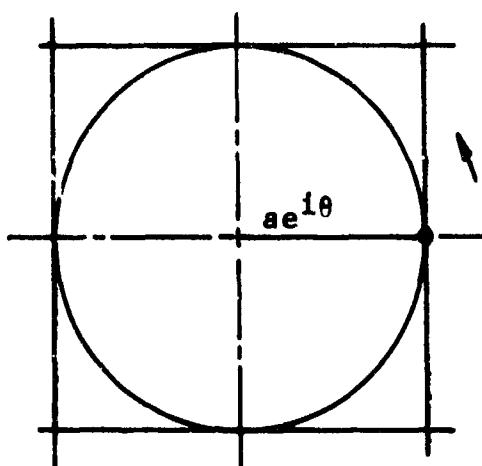


AIRESEARCH MANUFACTURING COMPANY OF ARIZONA  
A DIVISION OF THE GARRETT CORPORATION  
PHOENIX, ARIZONA

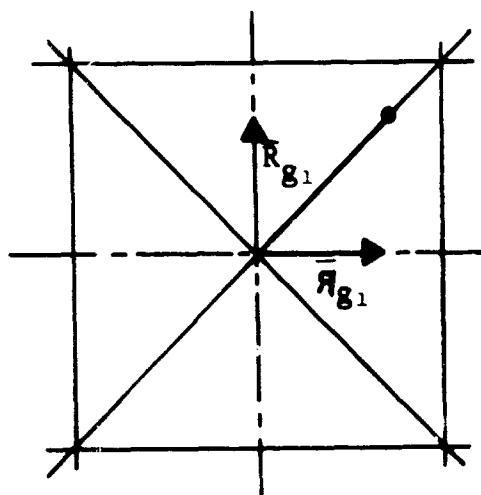


$$[\bar{G}]_{\theta=0} = \bar{R}_{\sigma_1} + \bar{R}_{\bar{\sigma}_1}$$

(a)

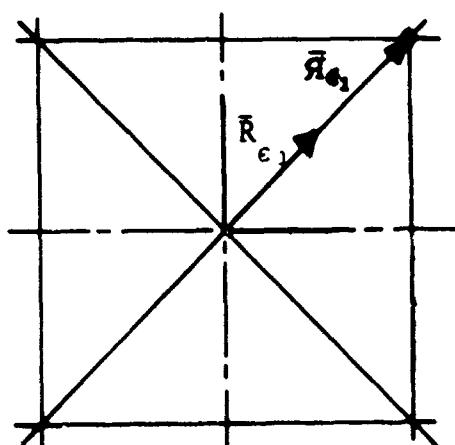


(b)



$$[\bar{H}]_{\theta=0} = \bar{R}_{g_1} + \bar{R}_{\bar{g}_1} = \frac{\bar{F} - \bar{G}}{\sqrt{2}}$$

(c)



$$[\bar{F}]_{\theta=0} = \bar{R}_{\epsilon_1} + \bar{R}_{\bar{\epsilon}_1}$$

(d)

FIGURE 6-40  
 $\bar{F}$ ,  $\bar{G}$  AND  $\bar{H}$  FOR THE CASE  $\delta = 0$



AIRESEARCH MANUFACTURING COMPANY OF ARIZONA  
A DIVISION OF THE GARRETT CORPORATION  
PHOENIX, ARIZONA

Define

$$\bar{R}_{g_1} = \frac{\bar{R}_{\epsilon_1} - \bar{R}_{\sigma_1}}{\sqrt{2}} \quad (6-131)$$

$$\bar{R}_{g_1} = \frac{\bar{R}_{\epsilon_1} - \bar{R}_{\sigma_1}}{\sqrt{2}} \quad (6-132)$$

and note that  $\bar{R}_{g_1}$  and  $\bar{R}_{g_1}$  are on the coordinate axes. By careful inspection of the figure it is apparent that the function

$$\bar{H}^* = \frac{\bar{F} + \bar{G}}{\sqrt{2}} \quad (6-133)$$

would have produced an identical figure except for the interchange of the axes on which  $R_{g_1}$  and  $R_{g_1}$  are located.

Figure 6-41 shows the hysteresis loops traced by  $\bar{F}$ ,  $\bar{G}$ , and  $\bar{H}$  for the case  $\delta = \frac{\pi}{2} = 90^\circ$ . This is the case of a material or structure having pure viscous damping and no stiffness. All three vectors generate circles.

Note that

$$R_{\epsilon_1} = R_{\sigma_1} = R_{g_1} = 0 \quad (6-134)$$

Since

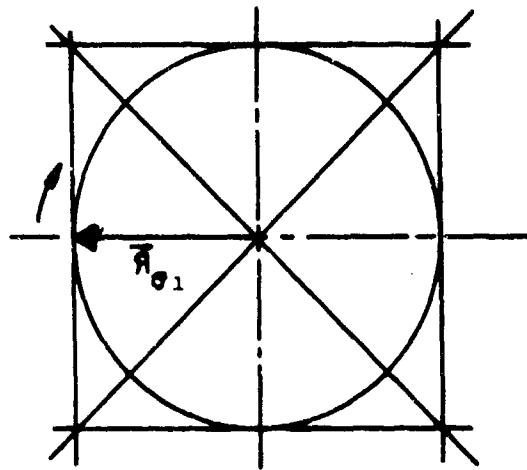
$$R_{\epsilon_1} = R_{g_1} = a \quad (6-135)$$

$$\bar{R}_{g_1} = \sqrt{2} R_{\epsilon_1} = \sqrt{2}a \quad (6-136)$$

Thus, the locus of  $\bar{R}_{g_1}$  circumscribes the square of sides  $2a$  and has an area (energy dissipation) twice that of the circle swept by either  $\bar{F}$  or  $\bar{G}$ .

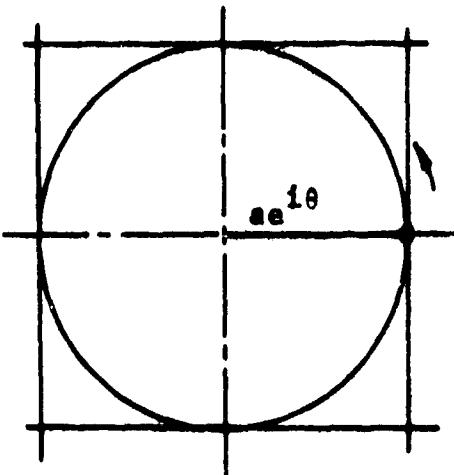


AIRESEARCH MANUFACTURING COMPANY OF ARIZONA  
A DIVISION OF THE MARRETT CORPORATION  
PHOENIX, ARIZONA

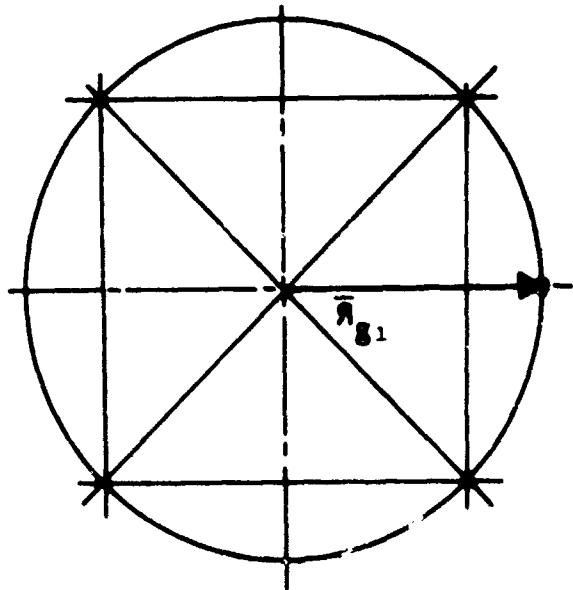


$$\bar{G} = \bar{R}_{\sigma_1}$$

(a)

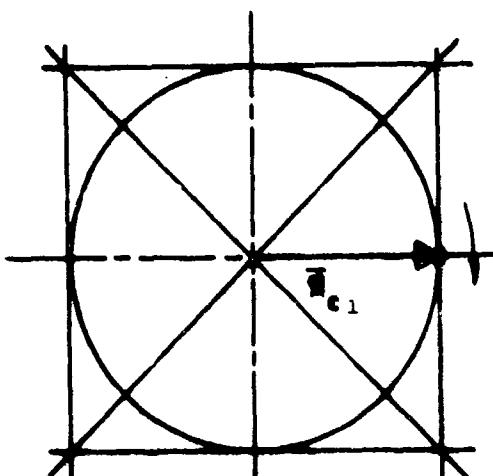


(b)



$$[H]_{\theta=0} = \frac{\bar{F} - \bar{G}}{\sqrt{2}} = \bar{R}_{g_1}$$

(c)



$$\bar{F} = \bar{R}_{e_1}$$

(d)

FIGURE 6-41  
 $\bar{F}$ ,  $\bar{G}$ , AND  $\bar{H}$  FOR THE CASE  $\delta = \frac{\pi}{2}$



By inspection of Figure 6-41 it is clear that for the function

$$\bar{H}^* = \frac{\bar{F} + \bar{G}}{\sqrt{2}} \quad (6-137)$$

both  $\bar{R}_{g_1}$  and  $\bar{R}_{g_1}$  equal zero. This appears to be consistent with the fact that no energy is returned in this case.

Returning to the general viscoelastic case as illustrated in Figure 6-39, the behavior is intermediate. The locus of  $\bar{H}_1$  is elliptical but is not a full  $\sqrt{2}$  larger than the stress or strain ellipses. Again  $\bar{R}_{g_1}$  and  $\bar{R}_{g_1}$  lie on the imaginary and real axes, respectively. This will prove to be extremely convenient for computations later.

It is important to emphasize at this point that the only reason it is possible to construct the generalized hysteresis loop for the viscoelastic case is that the behavior of the specimen is known for both a sinusoidal stress and a sinusoidal strain input. Without this knowledge,  $\bar{H}$  cannot be constructed.

By use of Equations 6-116 and 6-118 for  $\bar{R}_{\epsilon_1}$  and  $\bar{R}_{\epsilon_1}$ , combined with Equations 6-121 and 6-122 for  $R_{\sigma_1}$  and  $R_{\sigma_1}$ , we are able to calculate the location and magnitude of  $\bar{R}_{g_1}$  and  $\bar{R}_{g_1}$ . The results are as follows:

$$\bar{R}_{g_1} = \frac{\bar{R}_{\epsilon_1} - \bar{R}_{\sigma_1}}{\sqrt{2}} \quad (6-138)$$

$$\bar{R}_{g_1} = \frac{a}{2\sqrt{2}} \left[ (1 + \frac{+}{E_1}) - (1 + \frac{+}{E^*}) \right] \quad (6-139)$$



$$\bar{R}_{g_1} = i \frac{a}{\sqrt{2}} \text{Im } \bar{E} = i \frac{a}{\sqrt{2}} \cos \delta \quad (6-140)$$

$$\bar{\eta}_{g_1} = \frac{\bar{\eta}_{e_1} - \bar{\eta}_{\sigma_1}}{\sqrt{2}} \quad (6-141)$$

$$\bar{\eta}_{g_1} = \frac{a}{2\sqrt{2}} [(1 + \bar{E}_1) - (-1 - \bar{E}^*)] \quad (6-142)$$

$$\bar{\eta}_{g_1} = \frac{a}{\sqrt{2}} (1 + \text{Re } \bar{E}) = \frac{a}{\sqrt{2}} (1 + \sin \delta) \quad (6-143)$$

The area of the generalized ellipse is, of course, pi times the product of the semiaxes.

$$\text{Area} = \pi (R_{g_1} + \eta_{g_1})(R_{g_1} - \eta_{g_1}) \quad (6-144)$$

$$\text{Area} = \pi a^2 (\sin^2 \delta + \sin \delta) \quad (6-145)$$

for  $\delta = 0$  (perfect elasticity)

$$\text{Area} = 0 \quad (6-146)$$

for  $\delta = \frac{\pi}{2}$  (viscous damping)

$$\text{Area} = 2\pi a^2 \quad (6-147)$$

It is clear that the generalized hysteresis loop for the viscoelastic case is very simple and well behaved for all values of  $\delta$ . The next objective is to generalize it to the case of non-linear materials.



#### 6.5.4.4.2 The Nonlinear Case

The characteristic peculiarity of hysteresis loops produced by sinusoidal strain is the appearance of all distortion terms on the stress axis. Conversely, for stress inputs, all distortion appears on the strain axis. But Equation 6-123 shows that even the first order stress resulting from sinusoidal strain may be regarded as a distortion term in quadrature with the input. Similarly, Equation 6-124 shows first-order strain due to stress input to be of the ratio of a distortion term in quadrature.

It therefore seems quite natural to generalize  $\bar{F}$  and  $\bar{G}$  as follows:

$$\bar{F} = \epsilon_1 \cos \theta + i \sum_{n=1}^{\infty} \sigma_n \sin (n\theta + \phi_n) \quad (6-148)$$

$$\bar{G} = i\sigma_1 \sin \theta + \sum_{n=1}^{\infty} \epsilon_n \cos (n\theta + \psi_n) \quad (6-149)$$

Again, let

$$\bar{H} = \frac{\bar{F} - \bar{G}}{\sqrt{2}} \quad (6-150)$$

Then

$$\bar{H} = \frac{1}{\sqrt{2}} \left[ a e^{-i\theta} - \sum_{n=1}^{\infty} \epsilon_n \cos (n\theta + \psi_n) - \sigma_n i \sin (n\theta + \phi_n) \right] \quad (6-151)$$



For the manipulations that follow it is more convenient to write  $\bar{F}$ ,  $\bar{G}$ , and  $\bar{H}$  as follows:

$$\bar{F} = \sum_{n=1}^{\infty} \bar{R}_{\epsilon_n} e^{in\theta} + \bar{R}_{\sigma_n} e^{-in\theta} \quad (6-152)$$

$$\bar{G} = \sum_{n=1}^{\infty} \bar{R}_{\sigma_n} e^{in\theta} + \bar{R}_{\epsilon_n} e^{-in\theta} \quad (6-153)$$

$$\bar{H} = \frac{1}{\sqrt{2}} \sum_{n=1}^{\infty} \bar{R}_{g_n} e^{in\theta} + \bar{R}_{g_n} e^{-in\theta} \quad (6-154)$$

where

$$\bar{R}_{g_n} = \frac{\bar{R}_{\epsilon_n} - \bar{R}_{\sigma_n}}{\sqrt{2}} \quad (6-155)$$

$$\bar{R}_{g_n} = \frac{\bar{R}_{\epsilon_n} - \bar{R}_{\sigma_n}}{\sqrt{2}} \quad (6-156)$$

The argument presented in Section 6.5.2.9 assures that, in general,  $\bar{R}_{g_n}$  and  $\bar{R}_{g_n}$  will produce an ellipse and permit definition of an  $E_n$ .

Again, to construct the generalized hysteresis loop, the results of both a strain input test and a stress input test are required, preferably with the tests conducted in succession on the same specimen. We do not know of any such data. Hence, the first generalized hysteresis loop for a real test bar of a non-linear material has yet to be drawn.



#### 6.5.4.5 Power Series Representation

##### 6.5.4.5.1 Properties

So far, the model is purely a kinematic representation. The higher order terms are to be found by paired experiments, and the results of these experiments are to be plotted as a generalized loop. No prediction is possible for the shape of the generalized loop under some other magnitude or kind of input.

As a final step, knowledge will be sought of the  $n^{\text{th}}$  terms as a function of the input--i.e., as a function of the parameters "a" and " $\delta$ ".

Equation 6-154 is strongly suggestive of a power series and, in particular, is like a Laurent series because of the presence of terms in both  $e^{in\theta}$  and  $e^{-in\theta}$ .

A power-series representation, if it exists, would have several attractive features. As the magnitude of the input increases, the influence of the higher terms increases. This is analogous to the behavior of most materials which are essentially linear in their behavior at small stress levels but show more and more nonlinearity as stress levels grow larger. Power series are quite tractable mathematically. There usually exist integrals by which the coefficients may be determined. Finally, most differential equations for nonlinear systems introduce the nonlinearity as the first few terms of a power series. For example, a nonlinear spring may be represented as having a spring constant K where

$$K = K_1 + aK_1^3 + \dots \quad (6-157)$$



#### 6.5.4.5.2 Derivation

It is a simple matter to formally express  $\bar{H}$  as a power series.

Let

$$Z' = ae^{i\theta} \quad (6-158)$$

$$Z^* = ae^{-i\theta} \quad (6-159)$$

$$\bar{H} = \sum_{n=1}^{\infty} \bar{R}_n g_n e^{in\theta} + \bar{R}_n g_n e^{-in\theta} \quad (6-160)$$

$$\bar{H} = \sum_{n=1}^{\infty} \frac{\bar{R}_n}{a^n} Z'^n + \frac{\bar{R}_n}{a^n} Z^{*n} \quad (6-161)$$

Define  $\bar{R}_n = \frac{\bar{R}_n}{a^n}$  (6-162)

$$\bar{R}_n = \frac{\bar{R}_n}{a^n} \quad (6-163)$$

$$\bar{H} = \sum_{n=1}^{\infty} \bar{R}_n Z'^n + \bar{R}_n (\bar{Z}^*)^n \quad (6-164)$$

Laurent's series are power series in  $Z$  and  $1/Z$ . They are a unique representation of analytic functions and serve the function of mapping "inputs" such as unit circles into other closed figures. No attempt will be made here to discuss these series in detail, since they are dealt with extensively in many standard works on complex variables.



AIRESEARCH MANUFACTURING COMPANY OF ARIZONA  
A DIVISION OF THE GARRETT CORPORATION  
PHOENIX, ARIZONA

Laurent's series may be written as

$$F(z) = A_0 + \sum_{n=1}^{\infty} A_n (z - z_0)^n + B_n (z - z_0)^{-n} \quad (6-165)$$

where  $A_n = \frac{1}{2\pi i} \oint_C \frac{F(z') dz'}{(z' - z_0)^{n+1}}$  (6-166)

$$B_n = \frac{1}{2\pi i} \oint_C \frac{F(z') dz'}{(z' - z_0)^{-n+1}} \quad (6-167)$$

The integrations are carried out in the counterclockwise direction over a closed path around  $z_0$ , such as over a unit circle centered at  $z_0$ .

For  $z_c = 0$ , which is the only case we are considering, the  $A_0$  term vanishes, and

$$F(z) = \sum_{n=1}^{\infty} A_n z^n + B_n z^{-n} \quad (6-168)$$

$$A_n = \frac{1}{2\pi i} \oint_C \frac{F(z') dz'}{(z')^{n+1}} \quad (6-169)$$

$$B_n = \frac{1}{2\pi i} \oint_C \frac{F(z') dz'}{(z')^{-n+1}} \quad (6-170)$$

It is clear that Equations 6-161 and 6-168 differ only in the use of  $\bar{z}$  or  $z^{-1}$ , which differ in their absolute values.



AIRESEARCH MANUFACTURING COMPANY OF ARIZONA  
A DIVISION OF THE GARRETT CORPORATION  
PHOENIX, ARIZONA

Thus, Equation 6-168 is a Laurent's series in  $e^{i\theta}$  if  $a = 1$ . Equation 6-168 is a Laurent's series in  $ae^{i\theta}$  if the coefficients A and B are functions of "a" as follows.

$$\text{Let } A_n z^n = \bar{R}_n z^n = \frac{\bar{g}_n}{a^n} z^n \quad (6-171)$$

$$B_n z^{-n} = \bar{R}_n z^{-n} = \bar{g}_n a^n z^{-n} \quad (6-172)$$

Thus, in power series form, any term consists of the input raised to a power and multiplied by a vector multiplier which adjusts its phase angle and magnitude to its proper value.

As a simple example, consider a viscoelastic material for which  $\delta = 60^\circ$  as shown in Figure 6-38.

$$\bar{H} = R_{g_1} e^{i\theta} + \bar{g}_{g_1} e^{-i\theta} \quad (6-173)$$

$$R_{g_1} = \frac{ia}{\sqrt{2}} \cos \delta = i 0.354a \quad (6-174)$$

$$\bar{g}_{g_1} = \frac{a}{\sqrt{2}} (1 + \sin \delta) = 1.319a \quad (6-175)$$

Written as a Laurent series

$$\bar{H} = i 0.354 (ae^{i\theta}) + 1.319 a^2 (ae^{i\theta})^{-1} \quad (6-176)$$

$$A_1 = i 0.354 \quad (6-177)$$

$$B_1 = 1.319 a^2 \quad (6-178)$$



AIRESEARCH MANUFACTURING COMPANY OF ARIZONA  
A DIVISION OF THE GARRETT CORPORATION  
PHOENIX, ARIZONA

It is interesting to compute  $B_1$  from the integral formula (6-170).

$$B_1 = \frac{1}{2\pi i} \int_C \bar{H}(Z') dZ' \quad (6-179)$$

$$Z' = ae^{i\theta} \quad (6-180)$$

$$dZ' = iae^{i\theta} d\theta \quad (6-181)$$

$$B_1 = \frac{1}{2\pi i} \int_0^{2\pi} (R_{g_1} e^{i\theta} + \bar{R}_{g_1} e^{-i\theta}) iae^{i\theta} d\theta \quad (6-182)$$

$$B_1 = \frac{aR_{g_1}}{2\pi} \int_0^{2\pi} e^{i2\theta} d\theta + \frac{a\bar{R}_{g_1}}{2\pi} \int_0^{2\pi} d\theta \quad (6-183)$$

$$B_1 = a\bar{R}_{g_1} = a^2 R_1 = 1.319 a^2 \quad (6-184)$$

as in Equation 6-172.

Table 2 presents a tabulation of  $\bar{R}_1$  and  $\bar{R}_1$  for values of  $\delta$  from 0 to  $90^\circ$ . These represent viscoelastic materials for any input level "a". Presumably, values of  $\bar{R}_n$  and  $\bar{R}_n$  can be obtained by experiment to represent any nonlinear materials.



AIRESEARCH MANUFACTURING COMPANY OF ARIZONA  
A DIVISION OF THE GARRETT CORPORATION  
PHOENIX, ARIZONA

TABLE 6-2

<u><math>\delta</math></u>	<u><math>\bar{R}_1</math></u>	<u><math>\bar{R}_2</math></u>
0°	0.707111	0.70711
10°	0.696371	0.82990
20°	0.664461	0.94895
30°	0.612381	1.06066
40°	0.541671	1.16163
50°	0.454521	1.24878
60°	0.353551	1.31949
70°	0.241851	1.37157
80°	0.122791	1.40348
90°	-0-	1.41421

#### 6.5.4.6 Generalized Inputs to the Generalized Loop

So far the only inputs used here have been sinusoidal strain, used to generate  $\bar{F}$ , sinusoidal stress used to generate  $\bar{G}$ , and  $a e^{-i\theta}$  used to generate  $\bar{H}$ , where

$$\bar{H} = \frac{\bar{F} - \bar{G}}{\sqrt{2}} \quad (6-185)$$

In Section 6.5.4.4 an alternate definition for  $\bar{H}$  was specified as

$$\bar{H}^* = \frac{\bar{F} + \bar{G}}{\sqrt{2}} \quad (6-186)$$

$\bar{H}^*$  was laid aside temporarily because it corresponded to an input of  $a e^{i\theta}$  which is associated with energy returned to the drive system rather than energy supplied by the drive system.  $\bar{H}^*$  will now be called the conjugate of  $\bar{H}$ .



To be truly general in character we must be able to introduce any driving function and obtain the resulting loop from our power series that defines the properties of the material.

This process must include the ability to obtain the original hysteresis loops that are due to sinusoidal stress or strain, if these inputs are supplied to the power series representation.

It is even hoped that if inputs are used that have components not harmonically related, the proper nonrepetitive or rotating figures might be obtained. If this is true, then the power-series representation will become as universal as Ptolemy's Epicycles (which were not limited to harmonically related frequencies) and the representation can, for example, be used in shaft dynamics because it can represent figures of the sort shown in Figure 6-6.

Recall that Equations 6-123 through 6-126 showed the vectors (perhaps better called vector operators),  $\bar{F}$ ,  $\bar{G}$ ,  $\bar{H}$ , and  $\bar{H}^*$  to have a peculiar characteristic--that of always consisting of the sum of the input and terms that expressed the reaction of the material to the input.

$$\bar{F} = a \cos \theta + i \operatorname{Im} F = \sum \bar{R}_{\epsilon_n} e^{i\theta} + \bar{R}_{\epsilon_n} e^{-i\theta} \quad (6-187)$$

$$\bar{G} = ia \sin \theta : \operatorname{Re} F = \sum \bar{R}_{\sigma_n} e^{i\theta} + \bar{R}_{\sigma_n} e^{-i\theta} \quad (6-188)$$

$$\bar{H} = \frac{1}{\sqrt{2}} [ae^{-i\theta} + \text{reaction}] = \frac{\bar{F} - \bar{G}}{\sqrt{2}} \quad (6-189)$$



AIRESEARCH MANUFACTURING COMPANY OF ARIZONA  
A DIVISION OF THE GARBETT CORPORATION  
PHOENIX, ARIZONA

$$\bar{H}^* = \frac{1}{\sqrt{2}} [ae^{i\theta} + \text{reaction}] = \frac{\bar{F} + \bar{G}}{\sqrt{2}} \quad (6-190)$$

Since  $\theta = \omega t$ , inputs at various frequencies may be considered, i.e.,  $\theta_1 = \omega_1 t$ ,  $\theta_2 = \omega_2 t$ , etc., and each may have its own amplitude  $a_1$ ,  $a_2$ , etc.

Then combinations of  $a_1 e^{i\theta_1}$ ,  $a_2 e^{i\theta_2}$ , etc., may be used to define any physically attainable input. The vectors, or rather power-series vector operators  $\bar{H}$  and  $\bar{H}^*$  are additive; hence, we may build the loop for any conceivable input as follows:

(a) Express the input as a sum of terms

$$\text{input} = \sum_n a_n e^{+i\theta_n} + b_n e^{-i\theta_n} \quad (6-191)$$

(b) To all terms of the type  $b_n e^{-i\theta_n}$  apply the operator  $\bar{H}$ ; i.e., write

$$\bar{H}_{\theta_n} = \sum R_n e^{in\theta_n} + R_n^* e^{-in\theta_n} \quad (6-192)$$

(c) To all terms of the form  $a_n e^{i\theta_n}$  apply the operator  $\bar{H}^*$ ; i.e., write

$$\bar{H}_{\theta_n}^* = \sum R_n^* e^{in\theta_n} + R_n e^{-in\theta_n} \quad (6-193)$$

(d) Finally, sum the power series

$$\bar{H} = \sum \bar{H}_{\theta_n} + \bar{H}_{\theta_n}^* \quad (6-194)$$



Note that

$$\bar{R}_n^* = \frac{\bar{R}_{\epsilon_n} + \bar{R}_{\sigma_n}}{a^n \sqrt{2}} \quad (6-195)$$

$$\bar{R}_n^* = \frac{\bar{R}_{\epsilon_n} + \bar{R}_{\sigma_n}}{a^n \sqrt{2}} \quad (6-196)$$

For cases in which  $\bar{R}_n$  and  $\bar{R}_n^*$  are functions of  $\theta$ , then the values used would of course be chosen accordingly. As a trivial example consider a material for which  $R_{\epsilon_n}$ ,  $R_{\sigma_n}$ ,  $\bar{R}_{\epsilon_n}$ , and  $\bar{R}_{\sigma_n}$  are all known by test. Then we may reconstruct the hysteresis loop corresponding to a sinusoidal strain input,  $\bar{F}$ , as follows:

$$\text{input} = a \cos \theta = \frac{a}{2} e^{i\theta} + \frac{a}{2} e^{-i\theta} \quad (6-197)$$

$$\bar{H} \left( \frac{a}{2} e^{-i\theta} \right) = \frac{\bar{F} (a \cos \theta) - \bar{G} (ai \sin \theta)}{\sqrt{2}} \quad (6-198)$$

$$\bar{H}^* \left( \frac{a}{2} e^{i\theta} \right) = \frac{\bar{F} (a \cos \theta) + \bar{G} (ai \sin \theta)}{\sqrt{2}} \quad (6-199)$$

$$\frac{\bar{H} + \bar{H}^*}{\sqrt{2}} = \bar{F} (a \cos \theta) \quad (6-200)$$

Thus, the method is both universal and reversible. In connection with reversibility, it might be observed that although the simultaneous application of a sinusoidal stress and a sinusoidal strain seems difficult to attain in order to directly plot a generalized hysteresis loop, the reverse operation is in principle practiced as follows:



If  $\bar{H}$  is known, we may easily imagine a forcing device with servo-type controls that will cause the stress-strain dot to trace the generalized loop in the proper manner. In this mode of operation we may rest quite certain that the actual input to the system is described by  $se^{-1\theta}$ .

#### 6.5.4.7 Some Hypotheses

The following hypotheses are presented in the hope that interested people may profitably explore them.

- I. For fixed environmental conditions, the rheological behavior of many materials may be represented over a wide range of input levels by a power series having as coefficients  $R_n$  and  $\bar{R}_n$  which remain constant.
- II. The effect of environmental conditions may be meaningfully represented by coefficients  $R_n$  and  $\bar{R}_n$ , which are functions of the environmental conditions.
- III. The stress history of a material specimen may be represented as the history of the power-series coefficients  $R_n$  and  $\bar{R}_n$  which represent the material.
- IV. Power-series representations may exist for individual micromechanisms in the material. The sum of these contributions may be the observed  $R_n$  and  $\bar{R}_n$ .
- V. The rheological properties of a material cannot be determined by either a sinusoidal strain test or a sinusoidal stress test but can be determined as a result of both types of tests.



Hypothesis I is based on the ability of a power series to approach linearity for small values of the independent variable and then to become more and more nonlinear for larger values of the independent variable as the significance of the higher order terms increases. This is a tendency of almost all materials. Thus, nominally viscoelastic materials finally show distortion for very large inputs. This can be represented by the presence of very small coefficients of high order in their power series representation.

Hypothesis II needs little discussion. Certainly material properties are functions of temperature, etc. To represent their effects by observing how the coefficients  $R_n$  and  $\dot{R}_n$  vary will provide a fresh look which could be meaningful.

Hypothesis III is presented as a means for exploring the effects of stress history. At present, this is a particularly troublesome phase of rheology. It may be meaningful to observe which coefficients change, and in what manner.

Hypothesis IV may help interpret changes in the coefficients that occur as a result of stress history, environment, or input level. This is one possible approach to correlation with micro-mechanisms. Suppose, for example, that six coefficients are required to represent a material, but they are grossly variable with input level; then, simultaneous equations can be written to express the power series as the sum of other power series with fixed coefficients. Each of the fixed-coefficient power series may correlate with a particular micromechanism.

Hypothesis V is left as a hypothesis because although the preceding sections indicate its probability, it is not believed that the point is quite proven.



#### 6.5.4.8 Conclusion

The discussion of hysteresis loops presented in the preceding sections was only nominally directed to those of rheology. Actually, hysteresis loops are a phenomenon common to almost every branch of science in which energy dissipation occurs in a cyclic manner. It is hoped that these efforts will prove useful in such diverse fields as transformer design, tape recorder theory, and mechanics, as well as in rheology.

The representation of periodic loci by systems of rotating vectors is both ancient and widely used in many guises. It is, therefore, a little surprising that these concepts have not been more widely used to represent hysteresis loops. The use of the isomorphism between two dimensional vectors and complex numbers is a particularly powerful tool. Its use for mapping complicated electrical and magnetic fields and the solution of elaborate boundary value problems in heat transfer, etc., attest to the power of these methods. This massive and elegant tool has been available now for over a century. Its use, however, has been much more limited on dynamic problems than on static or potential distribution type problems.

The pure mathematician insists that vectors and complex numbers are two totally different systems that happen to be isomorphic. In application, however, this distinction seems meaningless. Thus, forebearance is asked for the indiscriminate mixing of vector and complex-number notation.



AIRESEARCH MANUFACTURING COMPANY OF ARIZONA  
A DIVISION OF THE GARRETT CORPORATION  
PHOENIX, ARIZONA

The tentative conclusion that single-input (sinusoidal stress or sinusoidal strain) tests cannot define rheological properties of materials has a striking parallel in both mechanisms and electricity. It has been recognized in both fields that two tests are needed. For example, the electrical properties of an unknown "black box" cannot be defined by a constant-current (infinite source impedance) test. A constant-voltage test (zero source impedance) is equally ineffectual to completely determine the characteristic of the possible nonlinear black box. Both types of tests must be performed. It is possible that the complex-number power-series representation can be useful in setting forth the characteristics of such electrical or mechanical systems. As of this moment, no power series has been constructed from any data taken on a real material. It is unlikely that any old data can be found from which such series might be constructed. There remain to be explored challenging questions concerning the power series themselves. The writer is not at all satisfied that the formulations presented are the best; rather, this work merely indicates that useful things appear to exist awaiting methodical exploration.



AIRESEARCH MANUFACTURING COMPANY OF ARIZONA  
A DIVISION OF THE GARRETT CORPORATION  
PHOENIX, ARIZONA

Conclusions and Recommendations are presented  
in Section 3.0 of this document.

GT 7615-R  
Page 7-1



AIRESEARCH MANUFACTURING COMPANY OF ARIZONA  
A DIVISION OF THE GARRETT CORPORATION  
PHOENIX, ARIZONA

## APPENDIX I

### REVIEW OF POLAR FORMULAS (8 pages)

GT-7615-R, Rev. 1  
Appendix I



## APPENDIX I

### REVIEW OF POLAR FORMULAS

#### 1. General

The relations evolved in Section 6 are relations between geometric vectors in a plane. By far the most convenient and comprehensive representation for these vectors is polar representation in a complex plane. Due to the possibility that some materials engineers may not have a day-to-day familiarity in the use of the complex variable, it is appropriate to include a brief review of the elements of polar representation and at least state the chief identities used.

#### 2. Polar Form of Z

Given a complex plane having axes  $x$  and  $iy$ :

Then, any point  $z = x + iy$  may be represented as the tip of a radius vector of length  $r$  at some angle  $\theta$ .

Then

$$x = r \cos \theta$$

$$iy = ir \sin \theta$$

It may also be shown by the addition of infinite power series that

$$z = x + iy = re^{i\theta} = r \cos \theta + ir \sin \theta$$

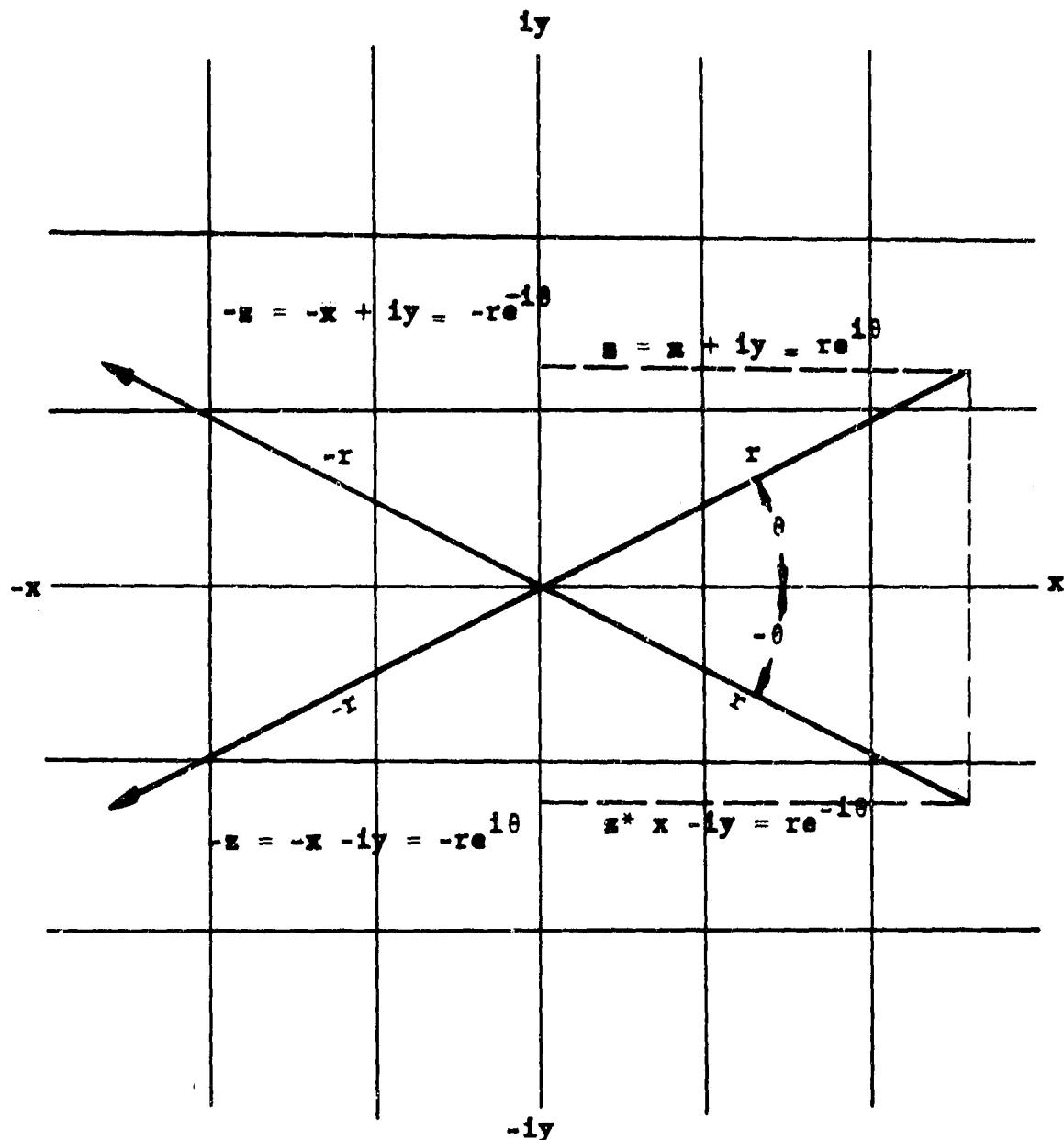
$$z^* = x - iy = e^{-i\theta} = r \cos \theta - ir \sin \theta$$

where  $z^*$  is called the complex conjugate of  $z$ .

Finally,  $-re^{i\theta}$  extends in the opposite direction to  $+re^{i\theta}$ . All of these relations are illustrated in Figure 1.



AIRESEARCH MANUFACTURING COMPANY OF ARIZONA  
A DIVISION OF THE GARRETT CORPORATION  
PHOENIX, ARIZONA



THE POLAR FORM OF THE COMPLEX NUMBERS  $z$ ,  $-z$ ,  $z^*$ ,  $-z^*$

FIGURE 1  
GT-7615-R  
Appendix I  
Page 2 of 8



Products

$$z_1 z_2 = r_1 e^{i\theta_1} r_2 e^{i\theta_2} = r_1 r_2 e^{i(\theta_1 + \theta_2)}$$

Figure 2

Ratios

$$\frac{z_1}{z_2} = \frac{r_1 e^{i\theta_1}}{r_2 e^{i\theta_2}} = \frac{r_1}{r_2} e^{i(\theta_1 - \theta_2)}$$

Figure 3

3. Trigonometric Functions

Relation of trigonometric functions to  $z$ :

$$r \cos \theta = \frac{r}{2} (e^{i\theta} + e^{-i\theta})$$

Figure 4

$$ir \sin \theta = \frac{r}{2} (e^{i\theta} - e^{-i\theta})$$

Figure 5

If  $r$  is constant and  $\theta = \omega t$ , then the constant-length vector will rotate at the (uniform) angular velocity  $\omega$  or  $-\omega$ .

As shown in Figures 4 and 5, the resultant of the two counter-rotating vectors is a linear sinusoidal motion--i.e., the sine or cosine function. This method of representing a rectilinear motion will be used repeatedly. Recall that mechanical vibration generators usually generate rectilinear vibration by means of counterrotating unbalanced rotors.

Fourier expansions can take many forms. For present purposes the following forms are most convenient:

$$\begin{aligned} x &= x_0 \cos (\theta + \psi_0) + x_1 \cos (\theta + \psi_1) + \\ &\quad + x_2 \cos (\theta + \psi_2) + \dots + x_n \cos (\theta + \psi_n) + \dots \end{aligned}$$



AIRESEARCH MANUFACTURING COMPANY OF ARIZONA  
A DIVISION OF THE GARRETT CORPORATION  
PHOENIX, ARIZONA

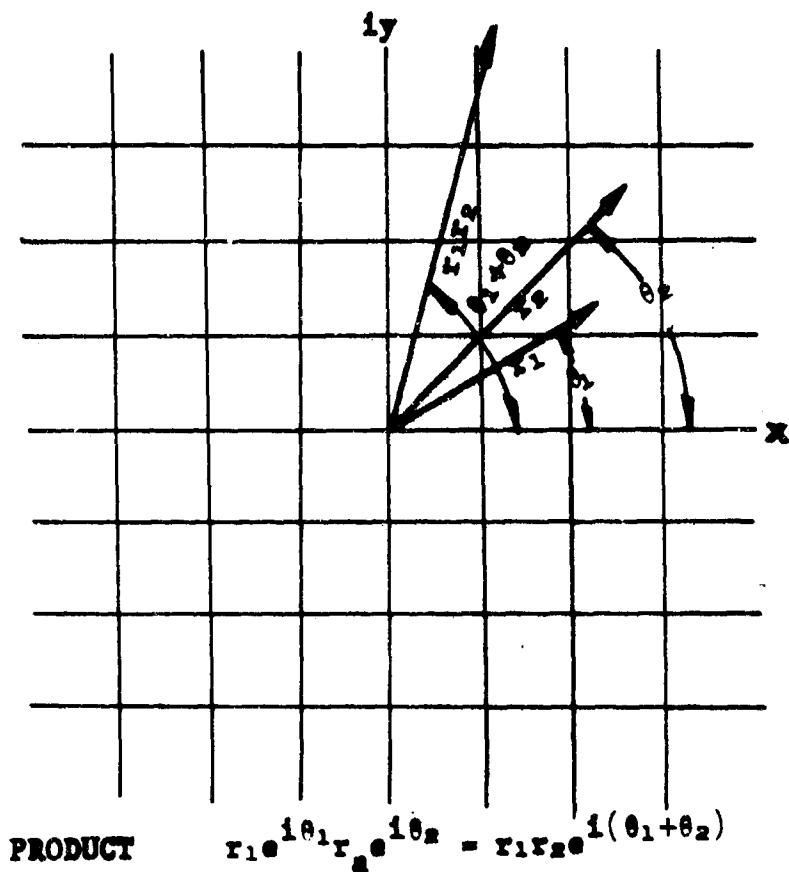
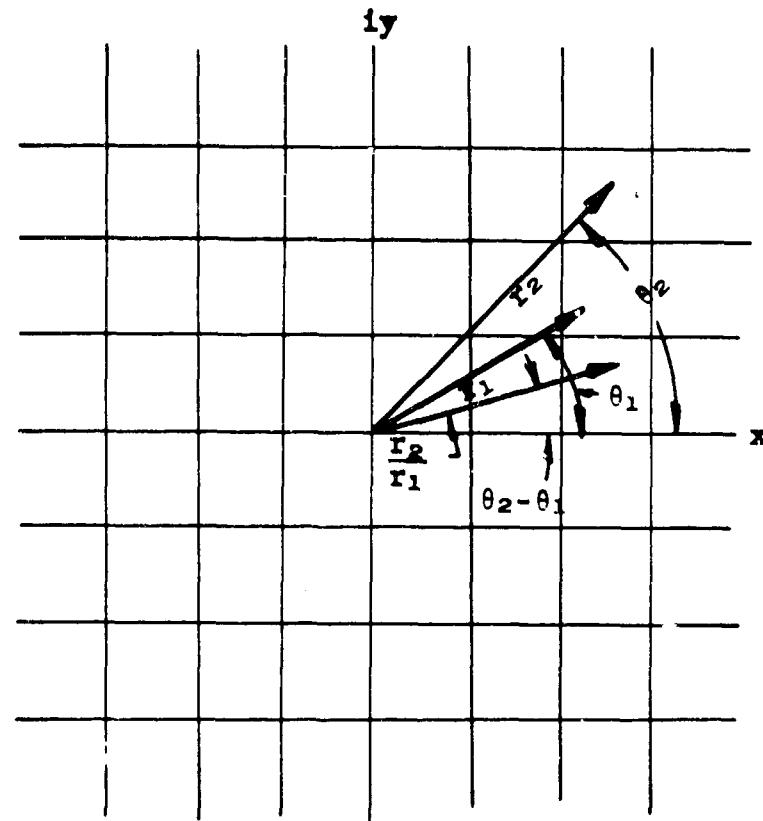


FIGURE 2

GT-7015-R  
Appendix I  
Page 4 of 8



AIRESEARCH MANUFACTURING COMPANY OF ARIZONA  
A DIVISION OF THE GARRETT CORPORATION  
PHOENIX, ARIZONA

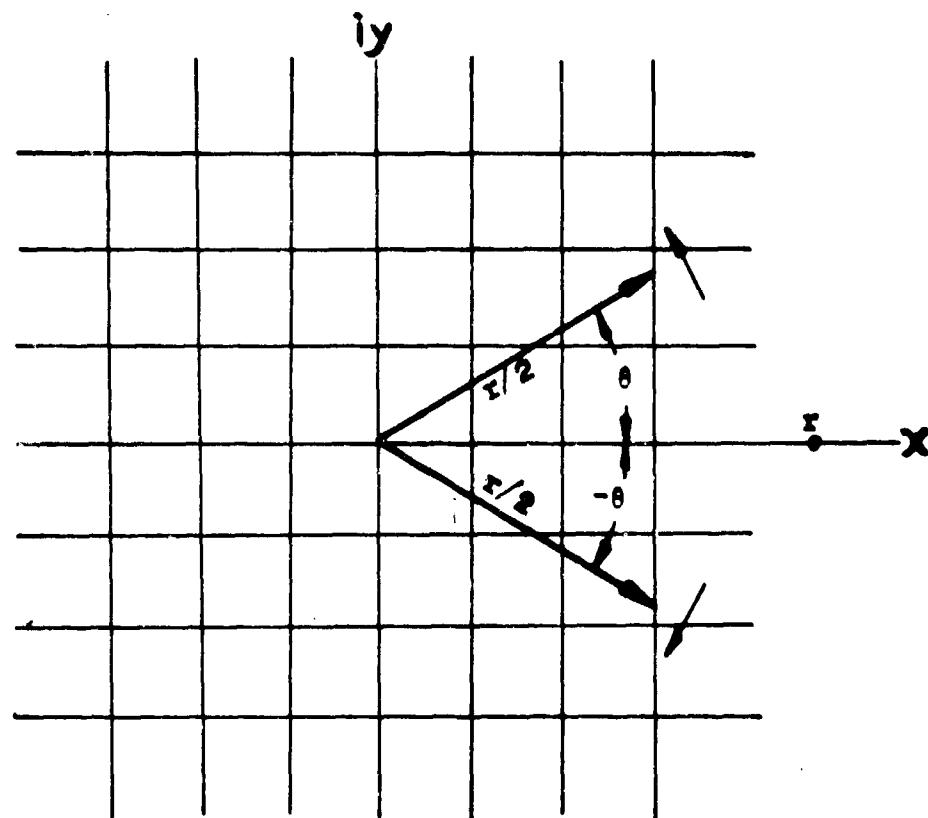


$$\text{QUOTIENT } \frac{r_2 e^{i\theta_2}}{r_1 e^{i\theta_1}} = \frac{r_2}{r_1} e^{i(\theta_2 - \theta_1)}$$

FIGURE 3



AIRESEARCH MANUFACTURING COMPANY OF ARIZONA  
A DIVISION OF THE GARRETT CORPORATION  
PHOENIX, ARIZONA



$$r \cos \theta = r/2 e^{i\theta} + r/2 e^{-i\theta}$$

FIGURE 4

GT-7615-R  
Appendix I  
Page 6 of 8



AIRESEARCH MANUFACTURING COMPANY OF ARIZONA  
A DIVISION OF THE GARRETT CORPORATION  
PHOENIX, ARIZONA

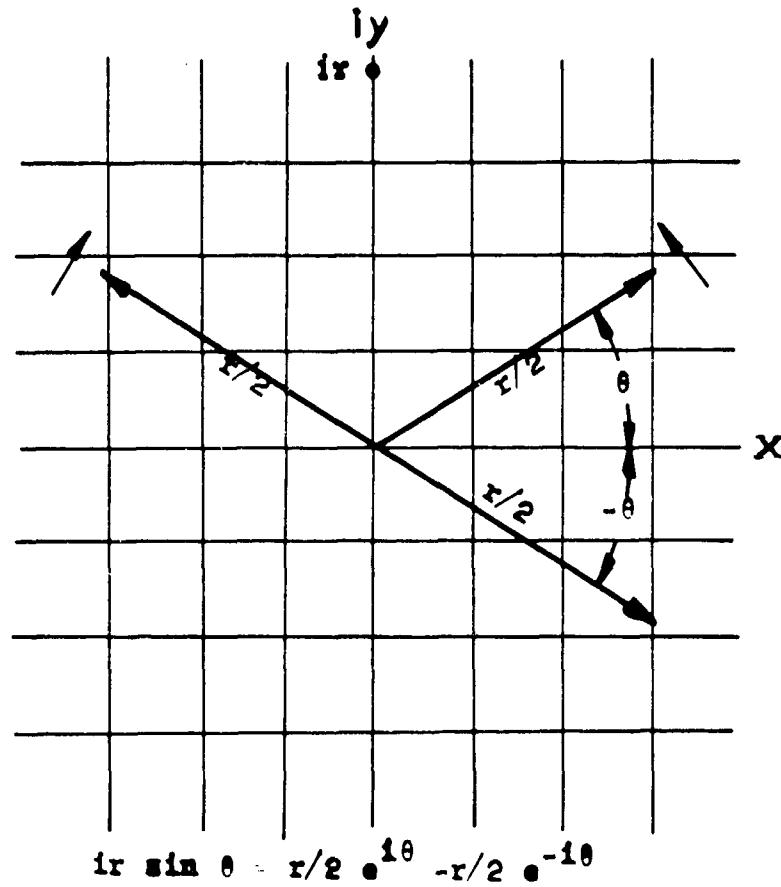


FIGURE 5

GT-7615-R  
Appendix I  
Page 7 of 8



AIRESEARCH MANUFACTURING COMPANY OF ARIZONA  
A DIVISION OF THE GARRETT CORPORATION  
PHOENIX, ARIZONA

$$y = y_0 \cos (\theta + \phi_0) + y_1 \cos (\theta + \phi_1) + \\ y_2 \cos (2\theta + \phi_2) + \dots + y_n \cos (n\theta + \phi_n) + \dots$$

also, recall that

$$\int_{-\pi}^{\pi} \cos m\theta \sin n\theta d\theta = 0$$
$$\int_{-\pi}^{\pi} \cos m\theta \cos n\theta d\theta = \begin{cases} 0 & \text{if } m \neq n \\ \pi & \text{if } m = n \end{cases}$$
$$\int_{-\pi}^{\pi} \sin m\theta \sin n\theta d\theta = \begin{cases} 0 & \text{if } m \neq n \\ -\pi & \text{if } m = n \end{cases}$$

#### Cross Products

$$\mathbf{A} \times \mathbf{B} = |\mathbf{A}| |\mathbf{B}| \sin C$$

where C is the angle between A and B.

The cross product is not commutative; i.e.,

$$\mathbf{A} \times \mathbf{B} = - \mathbf{B} \times \mathbf{A}$$



AIRESEARCH MANUFACTURING COMPANY OF ARIZONA  
A DIVISION OF THE GARRETT CORPORATION  
PHOENIX, ARIZONA

## APPENDIX II

- Aluminum Company of America Data Sheet (1 page)
- California-Doran Heat Treating Company (2 pages)
- Chicago Vitreous Corporation Data Sheet 12-165 (2 pages)
- Chicago Vitreous Corporation Data Sheet 15-361 (5 pages)
- Chicago Development Corporation Manganese Alloy No. 720  
(2 pages)
- Chicago Development Corporation Manganese Alloy No. 722  
(1 page)
- Chicago Development Corporation Manganese Alloy No. 780  
(1 page)
- Union Carbide Corporation Hastelloy Alloy X (3 pages)



AIRESEARCH MANUFACTURING COMPANY OF ARIZONA  
A DIVISION OF THE BARRETT CORPORATION  
PHOENIX, ARIZONA

PHYSICAL PROPERTIES OF ALCOA'S APM ALLOYS

	XAP001	XAP005	XAP002	XAP003	XAP004
<u>Specific Gravity</u>	2.74	2.74	2.75	2.77	
<u>Density, lb/cu. in.</u>	0.099	0.099	0.099	0.100	
<u>Electrical Conductivity</u>					
at 25°C (77°F) % IACS	47	44	39	34	
<u>Thermal Conductivity</u>	75° F	0.43	0.40	0.36	0.32
CG Units (Calculated on Basis of Electrical Conductivity)	400° F	0.44	0.43	0.39	0.36
	500° F	0.45	0.43	0.40	0.37
	600° F	0.45	0.43	0.41	0.38
	700° F	0.45	0.44	0.41	0.38
	800° F	0.45	0.44	0.42	0.39
	900° F	0.45	0.44	0.42	0.40
	1000° F	0.45	0.44	0.42	0.40
<u>Average Coefficient of Thermal Expansion</u>					
per °F x 10 <sup>-6</sup>					
Temp. Range, °F	68-212	12.0	11.8	11.5	11.1
	68-392	12.6	12.4	12.0	11.7
	68-572	13.1	12.9	12.5	12.1
	68-752	13.6	13.3	12.8	12.3
	68-842	13.9	13.8	13.0	12.5
<u>Melting Range</u>					
of Aluminum Phase (°F):					
		Solidus for All Alloys = 1180 - 1200			
		Liquidus for All Alloys = 1215			
		Oxide Phase Melts at 3700 (approx.)			
<u>Specific Heat (cal/g):</u>					
(Calculated)					
68°F	0.215	0.212	0.211	0.210	
212°F	0.225	0.224	0.223	0.223	
<u>Damping</u>					

Tests made at Aircor Research Laboratories on 0.250" thick XAP001 and XAP004 plate showed that these alloys have 1½ - 2½ times as much damping capacity as other bare wrought aluminum alloys. Alclad products also exhibit unusually high damping capacity.

**CALIFORNIA-DORAN HEAT TREATING CO.**LARGEST COMMERCIAL HEAT  
TREATING FACILITIES IN THE WEST

2830 E. Washington Blvd., Los Angeles 22, California, phone: AN 1-9121

May 26, 1965

Mr. Lester S. Wirt  
Airesearch Manufacturing Company  
402 South 36th Street  
Phoenix, Arizona 85034

Dear Mr. Wirt:

We are sending the completed flextures under separate cover to your attention. The following data should enable you to duplicate what we have accomplished on these test bars.

Surface Preparation:

All test bars were annealed at 1400° F in an exothermic atmosphere for five minutes and then sandblasted to produce a mechanical etch.

Coating Thickness:

It was difficult to establish an exact coating thickness due to the bilateral taper in the reduced cross section of the test bars, and the unconformity of thickness from test bar to test bar. Using micrometers before and after coating we feel the thickness range is between 0.003 and 0.005 on all coated areas except the edges where capillary action during the application produces a ridge.

Coatings:

Type A - flextures #2X, 8, 9 (Frit-AL-2 Ferro Corporation)

Formula

Frit AL-2	100	parts by weight
Boric Acid	3	" " "
KOH	2.5	" " "
Kasil #6	2	" " "
"O" Sod. Sil.	2	" " "
H <sub>2</sub> O	30	" " "

fineness .1 - .2 g on a 325 mesh screen using a 50 cc sample of slip.  
firing temperature 1000° F for 10 - 12 minutes

Type B - flextures #3X, 4X, 10 (Frit-145-S Chicago Vitreous Enamel Co.)

Formula

Frit 145-S	100	parts by weight
Q Clay	5	" " "
Bentonite	0.0625	" " "
NaNO <sub>2</sub>	0.0625	" " "
H <sub>2</sub> O	50	" " "

fineness 2 - 4 g on a 200 mesh screen. using a 50 cc sample of slip  
firing temperature 1100° F for 10 - 12 minutes.

Mr. Lester S. Wirt  
Airesearch Manufacturing Company

May 26, 1965  
Page 2

Type Eb - flextures #5X, 6X, 10 (Frit 325 Chicago Vitreous Enamel Co.)

Formula

Frit 325	100	parts by weight
Q Clay	5	" " "
Bentonite	0.0625	" " "
NaNO <sub>2</sub>	0.0625	" " "
H <sub>2</sub> O	50	" " "

fineness 2 - 4 g on a 200 mesh screen using a 50 cc sample of slip.  
firing temperature 1360° F for 10 - 12 minutes.

NOTE: Add 2 cc UREA solution for each 100 cc slip prior to applying  
enamel to eliminate tearing during firing operation.

Type C - flextures #7X, 12, 13 (Frit XG201 Ferro Corp.)

NBS - A - 418

Formula

Frit XG 201	70	parts by weight
Chrome Oxide	30	" " "
Green Label Clay	5	" " "
H <sub>2</sub> O	50	" " "

fineness trace - .1 g on a 325 mesh screen using a 50 cc sample of  
slip. firing temperature 1875 ± 25° F for 10 ~ 15 minutes.

If you have any further questions regarding this project, please contact  
me.

Yours truly

CALIFORNIA DORAN HEAT TREATING CO.

*Donald R. Van Sant*  
Donald R. Van Sant  
Ceramic Technician

DRVS  
ms



RESEARCH AND  
DEVELOPMENT  
LABORATORY

*Chicago Vitreous* CORPORATION  
A Division of The Eagle-Picher Company  
1425 South 55th Court • Cicero, Illinois 60650

Data Sheet 12-165

#### VISCOSITY CHARACTERISTICS OF SELECTED PORCELAIN ENAMEL FRITS

##### Description:

Frit is a granular material produced by quenching molten glass. Glasses do not exhibit a definite melting point, but are characterized by decreasing viscosity with increasing temperature. The listed porcelain enamel frits are proprietary formulations in the alkali-alumina-borosilicate field. They were selected to cover a range of temperature-viscosity relationships.

##### Properties:

Frit Designation	Specific Gravity	Linear Coef. of Exp. $\times 10^6 / ^\circ F.*$	Temperatures in "F. at which Glass Attains Indicated Viscosity **				
			$10^{14}$	$10^{11}$ (in Poises)	$10^7$	$10^3$	$10^{2.5}$
CV-145-S	2.94	6.5	756	837	1100	1200	1225
801	2.98	5.8	842	937	1300	1415	1450
325	2.84	5.3	850	975	1360	1525	1570
1106	2.70	6.0	848	966	1480	1725	1800
1100	2.50	5.9	896	990	1520	1750	1840
1502	2.65	5.7	936	1040	1540	1800	1880
15-M-1185	2.47	5.3	869	1013	1580	1850	1930
15-S-184	3.42	4.1	1202	1319	1700	1925	2150
6600	2.50	4.3	914	1067	1800	2050	2200

\* Coefficient of thermal expansion in./in./ $^\circ F.$  in the temperature range 97° - 637° F. as determined by the interferometer method.

\*\* Estimated viscosity based on interferometer determinations, molten viscosity measurements and behavior of glass when applied as a porcelain enamel.

##### Availability:

Stocked as frit (particles ranging in size from approximately 1/4 inch to minus 100 mesh) in 100-lb. multi-ply bags of 1-1/4 cu. ft. capacity. Crushed granules graded to customer specification on orders of 2000 lb. or more.

5/25/53

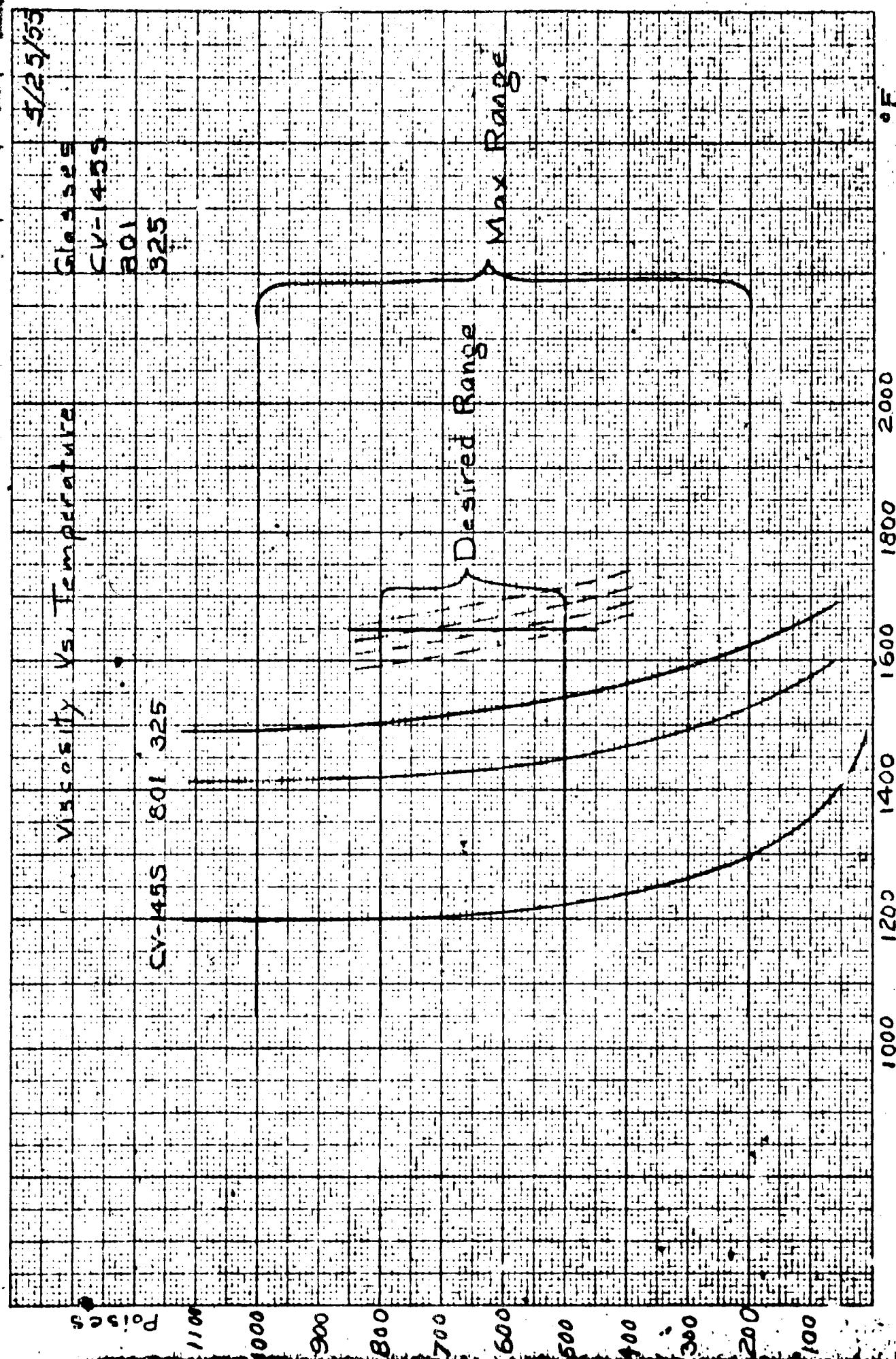
Class 225

C.V. = 45.5

301

325

Viscosity Vs. Temperature



1000 1200 1400 1600 1800 2000  $^{\circ}$ F



RESEARCH AND  
DEVELOPMENT  
LABORATORY

*Chicago Vitreous* CORPORATION

A Division of the Eagle-Picher Company  
1425 South 55th Court • Cicero 50, Illinois

CERAMICS COATINGS

Data Sheet 15-361

(4 Pages)

### CERAMIC COATINGS

#### Purpose:

To protect metals and alloys subjected to high temperatures and/or chemical corrosion, gaseous diffusion and erosion. To a limited extent, certain coatings also provide thermal or electrical insulation to metals.

#### Description:

Ceramic coatings are a special group of functional inorganic, essentially non-metallic finishes on metal components designed for service at temperatures in the 800° to 2000 F. range. Some types have a glossy green appearance and others a dull or full-mat gray finish. They are glass hard, relatively thin (one to ten thousandths of an inch) finishes for cast or formed metals of various sizes and shapes.

#### Composition:

The basic ingredients include a wide variety and combination of materials such as porcelain enamel frits, refractory oxides and in some instances, metal powders.

#### Representative Ceramic Coatings:

Some of the formulations which have been developed along with their processing instructions are listed in the accompanying tables under Chicago Vitreous Corporation code designation. The purpose of the listing is to illustrate the variety of metals and service conditions encompassed by ceramic coatings. It does not include all of the coatings which have been used or can be developed, since each coating must be designed for the specific metal, and service condition of the part being coated.

#### Coating Process

The coating of the metal part requires processing of the basic ingredients into a condition suitable for application by either the dip or spray method. This processing is accomplished by ball milling the dry ingredients with water as the vehicle. The resultant liquid suspension of finely ground solids, called slip, is applied to clean metal surfaces and then dried. Surfaces to receive the slip can be either chemically or mechanically cleaned, but should be free of scale and organic soils. In the dried state, the coating, which is composed of powdery particles, can be easily removed in those areas where the coating is not desired. The coating is matured by heating the metal part in a furnace (usually an oxidizing atmosphere) for sufficient time and at a suitable temperature to bring about fusion of the glassy constituents. Although multiple layers can be built up by repeating the application and fusing process, ceramic coatings are generally achieved in a single, thin application.

Representative Ceramic Coatings

<u>Coating</u>	<u>Appearance</u>	<u>Base Metal for Which Coating was Developed*</u>	<u>Service Temp., °F.</u>
SL-10162-E	Gray, mat	Low carbon & low alloy steels	1400
SL-13309	Black, mat	" "	1400
SL-14706	Black, mat	" "	1100
SL-17073	Black, semi-mat	" "	1100
SL-17153-D	Blue, semi-mat	" "	1200
SL-17385	Black, glossy	" "	1000
SL-18104	Blue, glossy	" "	1100
SL-18161	Black, semi-mat	" "	1200
SL-18691	Black, semi-glossy	" "	1100
SL-13943-W	Blue, glossy	Timken Alloy 17-22A(S) & low carbon steels	1000
SL-13943-W-1	Gray, semi-glossy	" "	900 to 1000
SL-16695-**	Gray, semi-mat	" "	1400
SL-13055-B	Green, glossy	Inconel & stainless steels of the 300 & 400 series	1800
SL-13290-B	Green, glossy	" "	1800
SL-14007-B	White, mat	" "	1600
SL-14230-C	Green, semi-glossy	" "	1900 to 2100
SL-14367-A	Brown, semi-glossy	" "	1800
SL-14875	Black, semi-glossy	" "	1900
SL-15356	White, semi-mat	" "	1800
SL-15864	Metallic	" "	2000
SL-16285**	Blue	Cast Iron	1600
CL-18340	Blue, glossy	" "	1200
SL-13969	Blue, glossy	Titanium	1800

\* Sandblasting recommended as method for metal preparation.  
Pickling may be satisfactorily employed in some instances.

\*\* Fire in controlled atmosphere.

Processing Instructions for Ceramic Coatings

Application Weight <u>Grams/sq.ft.</u>	Optimum Fired Thickness <u>(Mils)</u>	Firing* Temp. °F.	Time Min.
SL-10162-E	15	2.0	1600 5
SL-13309	15	2.0	1600 4
SL-14706	20	3.5	1650 3-1/2
SL-17385	25	4.0	1500 3
SL-18104	45	8.0	1540 8
SL-18161	20	4.0	1560 5
SL-18691	16	3.0	1500 4
SL-17153-D	22	4.0	1500 4-1/2
SL-17073	22	4.0	1500 4
SL-13943-W	15	2.0	1750 4
SL-13943-W-1	15	2.0	1100 10
SL-16695	15	2.0	1740** 20
SL-13055-B	15	2.0	1850 10
SL-13290-B	15	2.0	1800 10
SL-14007-B	20	3.0	1700 6
SL-14230-C	15	2.0	1900 15
SL-14367-A	15	2.0	1800 15
SL-14875	15	2.0	1900 20
SL-15356	15	2.0	2000 10
SL-15864	30	1.5	2000 10
SL-16285	15	2.0	1540** 25
CL-18340	35	6.0	1500 25
SL-13969	15	2.0	1800 6

\* Firing temperatures and times given for 18 - 20 ga. stock, except as noted.

\*\* Timken Alloy 17-22A(S) drawn for 6 hr. at 1165°F. after coating is fired.

\*\*\* Cast Iron.

Applications for Ceramic Coatings

<u>Coating</u>	<u>Suggested Applications</u>
SL-10162-E	Heat exchangers, space heater units, exhaust pipes, fire walls.
SL-14309	Heat exchangers, grates, space heaters, exhaust stacks.
SL-14706	Burner grates, exhaust pipes, heat exchangers.
SL-17385	Heat exchangers, storage bins.
SL-18104	Hot water storage tanks.
SL-18161	Heat exchangers, exhaust systems.
SL-18691	Automobile mufflers* and heat exchangers.
SL-17073	Burner grates, exhaust pipes, heat exchangers.
SL-17153-D	Heat exchangers, burner grates, exhaust stacks.
SL-13943-W	Compressor blades for superchargers and jets.
SL-13943-W-1	Grates, coal chutes, tote boxes.
SL-16695	Compressor blades, engine cowling.
SL-13055-B	Jet engine combustion chamber inner liners, transition liners.
SL-13290-B	Jet engine tail cones, tail pipes and afterburner sections.
SL-14007-B	Fire walls, exhaust systems.
SL-14230-C	Jet engine combustion and exhaust parts, heat treating tools.
SL-14367-A	Fuel tubes and engine parts subject to lead bromide attack.
SL-14875	Fuel injection tubes and jet engine parts.
SL-15356	Engine components subject to vanadium attack.
SL-15864	Continuous furnace shoe plates, fuel injection tube nozzles.
SL-16285	Cast iron thermocouple protection tubes.
CL-18340	Exhaust systems.
SL-13969	Aircraft components fabricated from titanium and its alloys.

\*May be blended 80/20 with SL-18162 white enamel for gray, acid resistant muffler enamel.

# C.D.C. Manganese Alloy No. 720

(Heat-Treatable, Corrosion Resistant Alloy)

C. D. C. MANGANESE ALLOY No. 720 is a manganese alloy that responds to hardening by heat treatment. It has high tensile and fatigue strength, wide hardness range and excellent corrosion resisting characteristics.

Composition	Nominal	Physical Constants	Soft	Hard
Copper	60	Specific Gravity, g./cc	8.03	8.20
Nickel	20	Density, lb./cu. in.	0.297	0.299
Manganese	20	Melting point, °F	1910	1910
		Specific heat, cal/g./°C(15-25 °C)	0.12	0.11
		Thermal conductivity, cal./sec./cm <sup>2</sup> /°C/cm	0.047	0.077
		Thermal coef. of expan. /°C (75-200°C)	0.0000150	0.0000173
		Electrical resistivity, microhms/cm <sup>2</sup> at 25°C	83-88	60-75
		Electrical conductivity, %IACS	2.1-1.97	3.5-2.3
		Temp. coef. elect. resist /°C (25-150°C)	-0.000125	+0.00024
		Modulus of elasticity, psi	18,000,000	21,000,000
		Torsion modulus, psi	6,700,000	7,100,000
		Magnetic permeability-200 oersteds	1.0030	1.0015

## PROPERTIES

Table 1 - As Rolled Properties

Cold Reduction %	Tensile Strength psi	Yield Strength (0.1%) psi	Proportional Limit psi	Vickers Hardness	Elongation 2 inch.
Annealed	98000	80000	36000	140	0
10	108000	90000	55000	90	8
20	115000	10000	65000	200	4
50	138000	115000	70000	260	2
80	150000	130000	75000	280	1.5

Table 2 - As Hardened Properties

Cold Reduction %	Tensile Strength psi	Yield Strength (0.1%), psi	Proportional Limit psi	Vickers Hardness
Annealed	200000	160000	120000	475
10	205000	165000	135000	480
20	210000	170000	140000	480
50	216000	185000	150000	485
80	220000	190000	160000	515

## Heat Treatment

Hardening: Heat to 500-600°F for a time interval which will produce the desired hardness indicated in Table 3.

Table 3 - Effect of Time of Aging on Hardness

Time in Hours	No Cold Work	80% Reduction
0	150	300
3	300	450
6	375	480
9	415	495
12	435	510
15	450	515
18	465	518
21	470	521
24	475	524

Table 4 - Effect of Aging Temperature on Hardness

(Samples had no cold work before hardening)  
(Hardness for various times at indicated temps.)

Temp. °F	2 hours	6 hours	12 hours	24 hours
500	138	138	138	138
600	190	225	375	450
700	230	365	435	463
800	185	330	420	465
900	150	170	180	470

Annealing: Heat to 1000-1200°F, air cool or water quench.

Softening of Hardened Material: Heat to 1050-1100°F, air cool or water quench.

To eliminate the light adherent scale during hardening, heat in a neutral or reducing atmosphere furnace, or in a hardening salt bath.

### Machinability:

Best machinability when in the annealed condition. C.D.C. Manganese Alloy No. 720 is satisfactorily machinable, and it machines similarly to Monel. Because of its great toughness, cutting speeds are somewhat slower and feeds lighter than those for mild steel. Tools should be of high speed steel, especially the cobalt type, ground with sharper angles than for steel. Sulphurized cutting oil should be used abundantly as a lubricant for boring, drilling, tapping, etc., and is preferred for all work, though water-soluble oils suffice for lathe work. In turning screw machine parts a good finish is obtained by using carbon tetrachloride as a coolant. Below are given some general recommendations of speed for cutting this alloy:

Operation	Speed sfpm	Depth of Cut, in.	Feed, Inch
Turning	45-65	1/8-1/16	1/8-1/16
Drilling	40-60		Same as for steel
Milling	50-65		0.005-0.010 in/tooth
Tapping	20-25		
Thread Chasing	20-25		
Reaming	25-35		

For high production, carbide-tipped tools should be used. All cutting tools should be ground to sharp cutting edges, and the speeds and feeds should be moderate. Standard twist drills should have polished flutes and must be kept feeding into the work. Spiral-fluted, high speed steel reamers with narrow lands and well polished flutes are used and are kept sharp at all times.

### Workability:

Alloy No. 720 is a soft, ductile metal which can be hot or cold formed readily. Finishing temperatures for hot forging should be 1000-1250°F. The maximum forging temperature is 1650°F. At 1750°F the alloy is hot short and can neither be hot rolled or forged at this or a higher temperature.

### Weldability:

Can be silver-soldered and then hardened. The strength of brazes is actually increased by the hardening treatment, ap-

parently resulting from the diffusion of the precipitate in the interface. By using a low melting point solder (1000-1100°F) soldering can be done at 1200-1300°F which approximates the annealing temperature of the No. 720 Alloy. Hardening can then be done in the usual manner for annealed alloy.

### Corrosion Resistance:

Highly corrosion resistant.

### General Characteristics:

This alloy differs from precipitation hardening alloys in that dependable and uniform hardening response does not involve critical control of chemical analysis, fabricating technique, or heat treatment. Hardening produces a high ratio of yield strength and proportional limit to tensile strength. It shows no appreciable drop in hardness even after several days of continuous heating at the hardening temperature. Any overaging, from a practical consideration, is primarily a function of temperature as shown in Table 1. Maximum hardening takes place between 700-800°F. Negligible distortion occurs during precipitation hardening. Cold rolled parts show no tendency toward springback or drift at the heat treatment temperature.

This soft, ductile alloy is particularly adopted for use in springs, diaphragms, and other parts in which design requirements make it desirable first to shape the part and then heat treat it to attain the desired hardness, tensile strength and fatigue strength.

### Forms Available:

Wire, strip, forgings, bars.

### Applications:

Springs, diaphragms

Available from: Chicago Development Corporation  
Riverdale, Maryland

# C.D.C. Manganese Alloy No. 772

C. D. C. MANGANESE ALLOY No. 772 offers a combination of high strength and ductility. It has a high temperature coefficient of expansion, high electrical resistivity, low thermal conductivity, and high vibration damping constant.

## Composition:

	Nominal	Range
Manganese	72	71.75-72.25
Copper	18	17.90-18.10
Nickel	10	9.90-10.10

## Physical Constants:

Specific gravity, g/cc	7.21
Density, lb./cu.in.	0.26
Electrical resistivity, ohms per cir mil ft.	1050
Temperature coefficient of expansion, °C (25-150°C)	0.0006275
Temperature coefficient of resistance, °C (25-150°C)	.000141
Thermal conductivity, cal/sec/cm²/°C/cm	0.02
Emissivity, as rolled, %	28
Specific heat, cal/g/°C (15-35 °C)	0.126
Vibrating damping constant, %	2.3
Magnetic characteristic	nonmagnetic
Modulus of elasticity, psi	18,000,000

## PROPERTIES

Table 1

Typical Mechanical Properties	
Tensile strength, psi	115000
Yield strength, psi (0.1% set)	95000
Proportional limit, psi	50000
Elongation, % in 2"	6.5
Vickers hardness (50% cold reduction)	220

Table 2

Temp. °F	Effect of Elevated Temperatures			
	Tensile Strength psi	Yield Proportional Strength 0.1% set, psi	Limit Elongation psi	% in2"
0	115000	92000	48000	6
100	112000	92000	48000	6
200	110000	91000	47000	5.8
300	108000	90000	45000	5.5
400	104000	88000	40000	5.0
500	97000	84000	35000	4.5
600	91000	76000	30000	4.0

Table 3

Temp. °F	Effect of Elevated Temperatures	
	Expansion Coefficient	Resistivity ohms/cir mil ft.
0	0.0000148	1035
100	0.0000151	1055
200	0.0000154	1062
300	0.0000166	1070
400	0.0000175	1075
500	0.0000188	1080
600	0.0000200	1080

## Machinability:

C.D.C. MANGANESE ALLOY No. 772 is satisfactorily machinable, and it machines similarly to Monel. Because of its great toughness, cutting speeds are somewhat slower and feeds lighter than those for mild steel. Tools should be of high speed steel, especially the cobalt type, ground with sharper angles than for steel. Sulphurized cutting oil should be used abundantly as a lubricant for boring, drilling, tapping, etc., and is preferred for all work, though water-soluble oils suffice for lathe work. In turning screw machine parts a good finish is obtained by using carbon tetrachloride as a coolant. Below are given some general recommendations of speeds for cutting this alloy:

Operation	Speed sfpm	Depth of Cut, in.	Feed, inch
Turning	45-65	1/8-1/16	1/8-1/16
Drilling	40-60		Same as for steel
Milling	50-65		0.005-0.010 in/tooth
Tapping	20-25		
Thread Chasing	20-25		
Reaming	25-35		Twice drill speeds

For high production, carbide-tipped tools should be used. All cutting tools should be ground to sharp cutting edges, and the speeds and feeds should be moderate. Standard twist drills should have polished flutes and must be kept feeding into the work. Spiral-fluted, high speed steel reamers with narrow lands and well polished flutes are used and are kept sharp at all times.

## Workability:

This alloy can be readily stamped, drawn, and extruded. Its hot working temperature range is 1600-1650°F.

Available from: Chicago Development Corporation  
Riverdale, Maryland

## Weldability:

Can be spot welded, butt welded, or silver brazed to itself or steel. It can be atomic hydrogen welded, electric arc welded, resistance welded, and oxyacetylene torch welded effectively. After welding, no thermal or chemical (passivation) treatments are necessary or recommended to retain or restore corrosion resistance.

## General Characteristics:

The exceptionally high electrical resistivity, low temperature coefficient of resistance, and excellent physical properties are a combination which makes the alloy ideally suited for low temperature resistor applications. Also in electrical apparatus, parts located in a varying magnetic field are free from eddy current losses, if made of the No. 772 alloy, due to its high electrical resistivity. The combination of high strength and a high specific damping constant makes the alloy desirable in applications which cannot incorporate rubber or plastics to reduce vibrations. It is especially useful in eliminating sustained resonance of metallic members due to intermittent shock. The damping rate of the alloy is about twenty-five times greater than for hardened steel when compared at low stresses. The electrical resistivity value is not affected by annealing procedure, cold working, or by cooling to minus 100°F. The alloy is nonmagnetic. Low thermal conductivity combined with high strength makes the alloy useful in power transmission where heat flow must be minimized.

## Forms Available:

Sheet, strip, hot-rolled round bars, extruded tubing, special shapes.

## Applications:

Low temperature resistor applications — rheostats, auxiliary for circuit breakers — electrically heated expansion elements, electrical appliances, low thermal transmission couplings.

# C.D.C. Manganese Alloy No. 780

C.D.C. MANGANESE ALLOY 780 possesses an unusual combination of mechanical, electrical and thermal properties.

Its extremely low shear modulus gives a high degree of surface conformity in cam and gear assembly which with high damping capacity provides excellent wear resistance and low noise level.

Low thermal conductivity combined with high yield in the cold worked alloy provide conditions for good power transmission with minimum heat transmission.

## C.D.C. Manganese Alloy 780

Nominal Composition	Mn 80% Cu 20%
Composition Range	Mn 78-82% Cu Balance
Electrical Resistivity ohm Cm at 20°C	149x10 <sup>-6</sup>
Density lbs. /cu. in.	2.6
Thermal Coefficient of Expansion /°C	20x10 <sup>-6</sup>
Heat Conductivity Cal/Sec./°C/SqCm/Cm	0.02
Temp. Coefficient of Electrical Resistance /°C	0.1x10 <sup>-4</sup>

### Mechanical Properties Quenched from 850°C

Tensile Strength psi	68000
Yield Strength psi	24000
Proportional Limit	13000
Elongation in 2" — %	35
Reduction of Area — %	49
Rockwell Hardness	B-55
Endurance Limit 1 x 10 <sup>8</sup> cycles psi	17000
Tensile Modulus psi	13500000
Shear Modulus	4000000
Poissons Ratio	0.7
Damping Capacity Low Stress %	7.0
Small Increment on 5000 psi %	20.0
10000 psi %	80.0
Internal Friction Q, (for comparison Q. for Beryllium Copper = 5)	1750

### Mechanical Properties Hot Rolled

Damping Capacity Low Stress %	17.0
Safe Load Factor K, lbs/Sq.in.of face on Cam Follower (for comparison Cast Iron K = 750)	3000

### Mechanical Properties Cold Rolled

Tensile Strength psi	10% Reduction	90000
	30% Reduction	130000
Yield Strength psi	10% Reduction	89000
	30% Reduction	115000
Elongation % in 2"	10% Reduction	10
	30% Reduction	9
Working Range	1600 - 1650° F	
	Room Temperature to 500° F	
	Brittle from 500 - 1500° F	

Available in hot or cold rolled bars, forgings, wire, strip, special heat treated parts and neutron flux wires and foils.

Available from: Chicago Development Corporation  
Riverdale, Maryland

### Strong and Oxidation Resistant to 2200 Deg. F.

HASTELLOY alloy X is a nickel-base alloy with a low strategic alloy content. It possesses exceptional strength and oxidation resistance up to 2200 deg. F. The alloy has excellent forming and welding characteristics.

### Useful Properties for Aircraft and Furnace Parts

HASTELLOY alloy X is recommended especially for use in furnace applications because it has unusual resistance to oxidizing, reducing, and neutral atmospheres. Furnace rolls made of this alloy were still in good condition after operating for 8700 hours at 2150 deg. F. Furnace trays, used to support heavy loads, have been exposed to temperatures up to 2300 deg. F. in an oxidizing atmosphere without bending or warping.

Alloy X is equally suitable for use in jet engine tailpipes, afterburner components, turbine blades, nozzle vanes, cabin heaters, and other aircraft parts.

### Easily Fabricated

HASTELLOY alloy X can be forged and, because of its good ductility, can be cold-worked. It can be welded by both manual and automatic welding methods including metallic-arc, inert-gas-shielded arc, submerged-melt, and SIGMA methods. Alloy X can also be resistance-welded.

### Available in Wrought and Cast Form

HASTELLOY alloy X is available in the form of sheet, plate, bar, wire, welding rod, and billets for forging. It can also be obtained as sand and investment castings and as remelt stock produced to a certified chemistry.

### Simple Heat-Treatment

All wrought forms of HASTELLOY alloy X are furnished in the solution heat-treated condition unless otherwise specified. The standard heat treatment is at 2150 deg. F. followed by either a rapid air-cool or a water quench.

### Boiler Code

The use of HASTELLOY alloy X sheet, plate, rod and bar in the construction of unfired pressure vessels in accordance with the requirements of the ASME Boiler and Pressure Vessel Code Section VIII has been approved under Case 1321 (Special Ruling). Alloy X is approved for use at temperatures up to 1650 deg. F. Design data can be found on page 28.

### Specifications

The following specifications have been established for HASTELLOY alloy X:

Bar (Solution Heat-Treated)	: AMS 5754-D
Sheet (Solution Heat-Treated)	: AMS 5536-C
Investment Castings (As-Cast)	: AMS 5390
Wire (Cold Drawn)	: AMS 5798
Coated Welding Electrodes	: AMS 5799

### Properties Data

The properties data listed in this booklet are typical or average values and should not be interpreted as guaranteed minimums or maximums except where so stated.

HASTELLOY alloy X is covered by U.S. Patent Number 2,703,277.

## CHEMICAL COMPOSITION, PER CENT

Nickel	Cobalt	Chromium	Molybdenum	Tungsten	Iron	Carbon	Silicon	Manganese
Balance	0.50-	20.50-	8.00-	0.20-	17.00-	0.05-	1.00*	1.00*
	2.50	23.00	10.00	1.00	20.00	0.15		

\* Maximum

## PHYSICAL PROPERTIES

Physical Property	Temp., deg. C.	Metric Units		Temp., deg. F.	British Units
		Metric Units	British Units		
Density	22	8.23 g./cu.cm.		72	0.297 lb./cu.in.
Melting Temperature	1260-1355			2300-2470	
Electrical Resistivity	22	118.3 microhm-cm.		72	46.6 microhm-in. (712 ohms per cir. mil-ft.)
Mean Coefficient of Thermal Expansion	26-100 26-500 26-600 26-700 26-800 26-900 26-1000	13.80 microns/m.-deg. C. 14.89 microns/m.-deg. C. 15.26 microns/m.-deg. C. 15.67 microns/m.-deg. C. 15.98 microns/m.-deg. C. 16.27 microns/m.-deg. C. 16.56 microns/m.-deg. C.		79-200 79-1000 79-1200 79-1350 79-1500 79-1650 79-1800	7.70 microinches/in.-deg. F. 8.39 microinches/in.-deg. F. 8.56 microinches/in.-deg. F. 8.76 microinches/in.-deg. F. 8.92 microinches/in.-deg. F. 9.07 microinches/in.-deg. F. 9.20 microinches/in.-deg. F.
Thermal Conductivity	20 100 300 600 700 800 900	0.097* watt-cm./cm. <sup>2</sup> -deg. C. 0.111 watt-cm./cm. <sup>2</sup> -deg. C. 0.147 watt-cm./cm. <sup>2</sup> -deg. C. 0.206 watt-cm./cm. <sup>2</sup> -deg. C. 0.228 watt-cm./cm. <sup>2</sup> -deg. C. 0.250 watt-cm./cm. <sup>2</sup> -deg. C. 0.274* watt-cm./cm. <sup>2</sup> -deg. C.		70 200 500 1100 1300 1500 1700	62.8* Btu-in./ft. <sup>2</sup> -hr.-deg. F. 76.0* Btu-in./ft. <sup>2</sup> -hr.-deg. F. 98.0 Btu-in./ft. <sup>2</sup> -hr.-deg. F. 143.5 Btu-in./ft. <sup>2</sup> -hr.-deg. F. 158.5 Btu-in./ft. <sup>2</sup> -hr.-deg. F. 173.5 Btu-in./ft. <sup>2</sup> -hr.-deg. F. 188.5* Btu-in./ft. <sup>2</sup> -hr.-deg. F.
Specific Heat	Room 315 650 870 1095	0.116 cal./g.-deg. C. 0.119 cal./g.-deg. C. 0.139 cal./g.-deg. C. 0.167 cal./g.-deg. C. 0.205 cal./g.-deg. C.		Room 600 1200 1600 2000	0.116 Btu/lb.-deg. F. 0.119 Btu/lb.-deg. F. 0.139 Btu/lb.-deg. F. 0.167 Btu/lb.-deg. F. 0.205 Btu/lb.-deg. F.
Poisson's Ratio	-78 22	0.328 0.320		-108 72	0.328 0.320
Magnetic Permeability			<1.002 at 200 oersteds		

\* Extrapolated

## IMPACT STRENGTH

Form	Condition	Test Temp., deg. F.	Typical Charpy V-Notch Impact Strength, ft.-lb.
Plate	Heat-treated at 2150 deg. F., WQ	-321	36.8
		-216	44.1
		-108	50.6
		-20	55.7
		Room	54.1
		1500	58.0
Plate	Heat-treated at 2150 deg. F., WQ, and aged:		
		168 hrs. at 1500 deg. F.	9
		168 hrs. at 1500 deg. F.	29
		500 hrs. at 1600 deg. F.	9
		500 hrs. at 1800 deg. F.	20
		50 hrs. at 1900 deg. F.	36
Investment-Cast	Heat-treated at 2150 deg. F., WQ	Room	9.8
		1500	13.8
Investment-Cast	Heat-treated at 2150 deg. F., WQ; aged 168 hrs. at 1500 deg. F.	Room	6.3
		1500	8.1

## DYNAMIC MODULUS OF ELASTICITY\*

Form	Condition	Test Temp., deg. F.	Dynamic Modulus of Elasticity, psi $\times 10^4$
Sheet	Heat-treated at 2150 deg. F., RAC	76	28.49
		212	28.06
		392	26.90
		572	25.95
		752	24.96
		932	23.79
		1112	22.88
		1292	21.76
		1472	20.67
		1652	19.48
		1832	18.33

## EFFECT OF CRYOGENIC TEMPERATURES ON TENSILE PROPERTIES

Form	Condition	Test Temp., deg. F.	Ultimate Tensile Strength, psi	Yield Strength at 0.2% offset, psi	Elongation in 2 in., per cent
Plate	Heat-treated at 2150 deg. F., WQ	-321	150,200	—	45.5
		-108	118,800	—	51.0
		72	104,500	47,000	46.2

\* Averages of two tests at temperature.

WQ - Water-Quenched

RAC - Rapid Air-Cooled



AIRESEARCH MANUFACTURING COMPANY OF ARIZONA  
A DIVISION OF THE GARRETT CORPORATION  
PHOENIX, ARIZONA

### APPENDIX III

THE ELASTIC AND ANELASTIC PROPERTIES  
OF REFRACTORY MATERIALS FOR  
HIGH-TEMPERATURE APPLICATIONS  
(13 Pages)

GT-7615-R  
Appendix III

Reprinted from

**MECHANICAL  
PROPERTIES  
OF  
ENGINEERING CERAMICS**

Proceedings of a Conference Conducted by The School of Engineering and  
the College Extension Division, North Carolina State College

In Cooperation with the Office of Ordnance Research, U. S. Army,  
at Raleigh, North Carolina, March 9-11, 1960

Edited by  
**W. WURTH KRIEGEL**  
and  
**HAYNE PALMOUR III**

**INTERSCIENCE PUBLISHERS • NEW YORK • LONDON • 1961**

---

## THE ELASTIC AND ANELASTIC PROPERTIES OF REFRACTORY MATERIALS FOR HIGH-TEMPERATURE APPLICATIONS

R. CHANG, *Atomics International, A Division of  
North American Aviation, Inc.*

### Abstract

Examples of anelastic phenomena associated with grain boundary relaxation, twin interface motion, or dislocation motion in some refractory oxides and other high-temperature materials are presented. The significance of such studies in providing fundamental information about detailed mechanisms of deformation in ceramic materials is discussed.

### I. Introduction

The theories of anelastic phenomena in crystalline solids have been treated formally by Zener [1]. When a stress is suddenly applied to a Voigt solid,\* there is no instantaneous strain, but the strain gradually approaches an asymptotic value. Conversely, when the stress is suddenly removed, the solid suffers no instantaneous recovery, but the strain gradually disappears. The tangent of the angle by which strain lags behind stress is used as a measure of internal friction. Under dynamic conditions, both the internal friction and elastic modulus are dependent on frequency. The frequency dependence is schematically illustrated in Fig. 1. It is not the purpose of this paper to go into further details of the theoretical aspects

\* A Voigt solid, or standard linear solid, is where the stress components are linear functions of both the strain and strain rates.

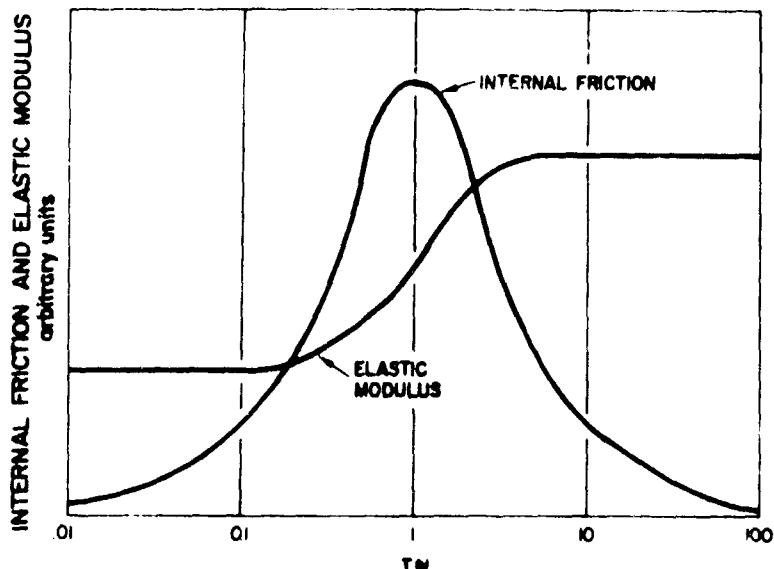


*Fig. 1.* Schematic diagram showing the frequency dependence of internal friction and elastic modulus.

of anelasticity but rather to point out the merits of studying the elastic and anelastic properties of high-temperature materials.

From a technical viewpoint, ceramic materials usually have low resistance to thermal shock. The engineering parameter measuring the thermal shock resistance of an isotropic solid is  $\sigma k/E\alpha$ , where  $\sigma$  is the fracture stress,  $k$  the thermal conductivity,  $E$  the elastic modulus, and  $\alpha$  the coefficient of thermal expansion. However, if anelastic processes occur in a solid during sudden temperature changes, and the relaxation times of these processes are short enough to cause relaxation of stress, such stress relaxation should be taken into consideration in any evaluation of thermal shock resistance of the solid.

From fundamental viewpoints, if a crystalline solid fractures by breaking of bonds without the occurrence of any complicated processes involving the generation, motion, and interaction of dislocations, things would be simpler. It would be merely necessary to know the elastic properties of the solid. In actuality, however, knowing the elastic properties of a crystalline solid is necessary but not sufficient, since dislocations are always present in a crystalline solid and fracture is intimately connected with generation, motion, and interaction of these ubiquitous dislocations. A fundamental understanding of the behavior of dislocations in a crystalline solid

is essential. One powerful way to learn the properties of dislocations in crystalline solids is by means of anelastic measurements.

The anelastic properties of metals, both in monocrystalline and polycrystalline form, have been studied in considerable detail, whereas those of ceramic materials were investigated to a small degree until very recently. In the following, several important anelastic phenomena occurring in ceramic materials will be described and compared with those found for metals. It is hoped that this paper will stimulate further interest in both experimental and theoretical investigations of the various anelastic properties of ceramic materials.

## II. Anelastic Phenomena Associated with Grain Boundary Relaxation in Polycrystalline Solids

Grain boundary phenomena in metals have been extensively studied by Ke [2] and others using anelastic methods. Similar work

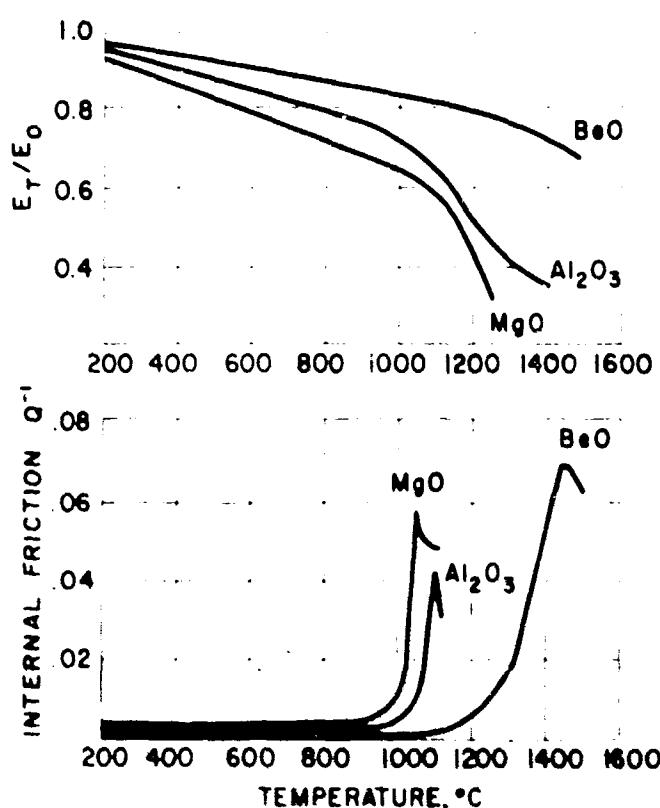


*Fig. 2.* Temperature dependence of Young's modulus and internal friction of polycrystalline BeO, Al<sub>2</sub>O<sub>3</sub>, and MgO.

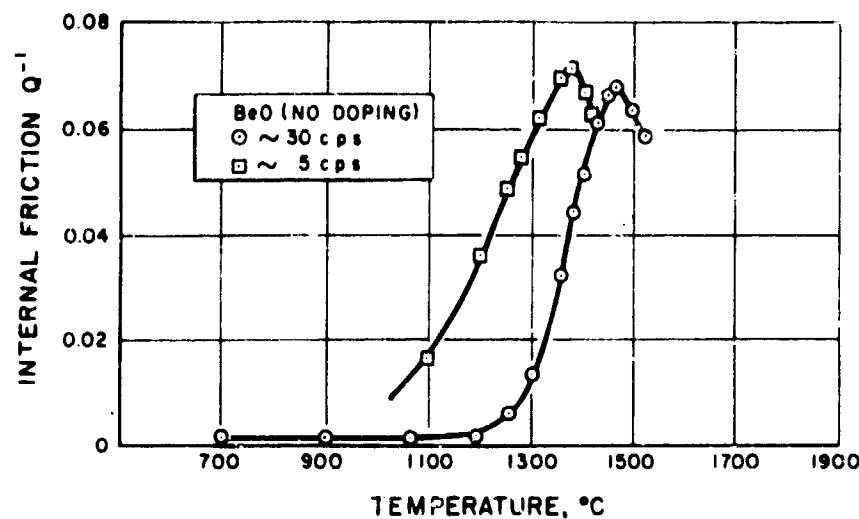


Fig. 3. Temperature dependence of internal friction of polycrystalline BeO at two frequencies.

on ceramic materials has received attention only very recently [3]. Typical examples of grain boundary phenomena are shown for pure oxides, in Figs. 2 and 3, and for oxides containing impurities in solution, in Figs. 4 and 5. The rapid decrease of Young's modulus, accompanied by an increase in internal friction, indicates that grain boundary relaxation is an important factor governing the high-temperature mechanical properties of these materials. Although several possible interpretations have appeared in the literature [4,5],

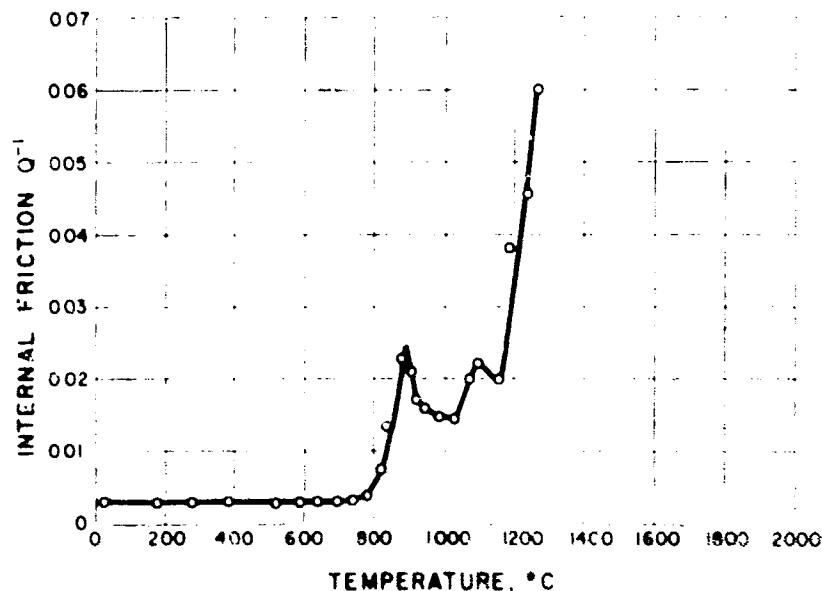


Fig. 4. Temperature dependence of internal friction of polycrystalline  $\text{Al}_2\text{O}_3$  containing 0.25 % by weight  $\text{La}_2\text{O}_3$ .

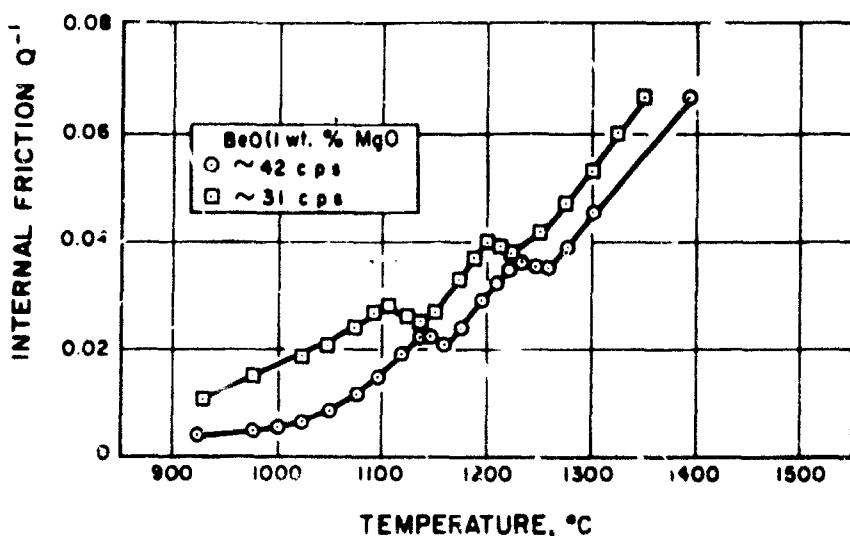


Fig. 5. Temperature dependence of internal friction of polycrystalline BeO containing 1% by weight MgO.

a completely satisfactory mechanism capable of explaining all the experimental observations is still lacking. These should be interesting fields for future investigation.

### III. Anelastic Phenomena Associated with Twin Interface Motion

Heavy twinning arising from cubic to tetragonal diffusionless transformation has been found in a number of alloys, such as AuCd [6], InTl [7], and CuMn [8]. The twin interfaces so formed are very mobile, and their motion requires only very small movements of the atoms. If, for example, the twin interfaces are locked by impurities or defects, motion of these interfaces under an applied shear stress will be controlled by the diffusion rates of the impurity or defect. Furthermore, twin interface motion may require the synchronized movement of both atom species, the rate of which may be controlled by diffusion of one of the two atom species [10]. At low temperatures the motion of the twin interfaces under dynamic conditions is so slow that no appreciable displacement occurs during a half-cycle of vibration, and the internal friction is low. On the other hand, the twin interfaces at high temperatures are so mobile that the shear stress is completely relieved at all times, so that the internal friction is again very low. Only in the intermediate temperature range, where both the displacement and the net shear stress are appreciable, is the internal friction large. The internal friction

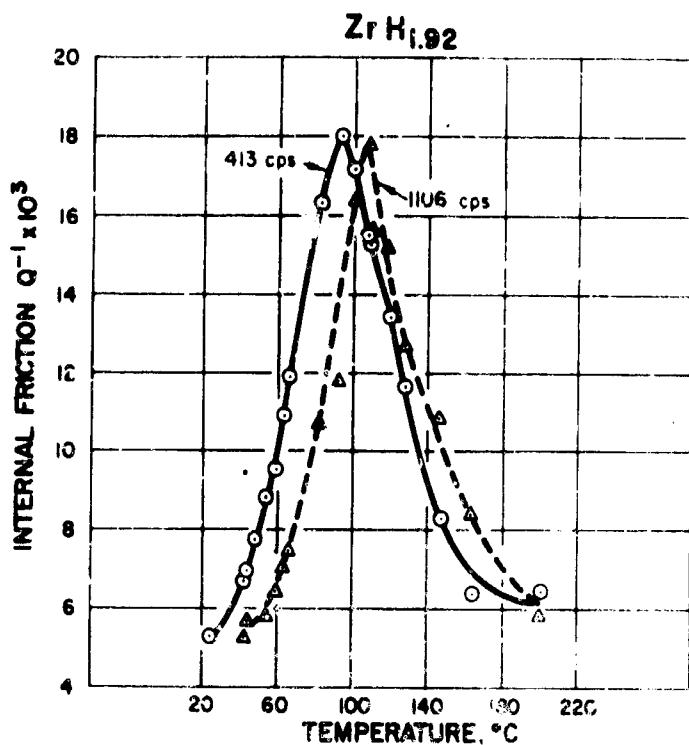


Fig. 6. Temperature dependence of internal friction of  $ZrH_2$  at two frequencies.

peak of Cu-Mn alloys ( $\sim 90\%$  Mn) found by Worrell [8] is thus interpreted by Zener [1] to arise from stress-induced movement of the twin interfaces of this alloy.

Similar cubic to tetragonal transformation, accompanied by heavy twinning, has been found in  $ZrH_2$ . The internal friction of this alloy in the twinned tetragonal state is shown in Fig. 6, and its microstructure is shown in Fig. 7. The author proposes that the

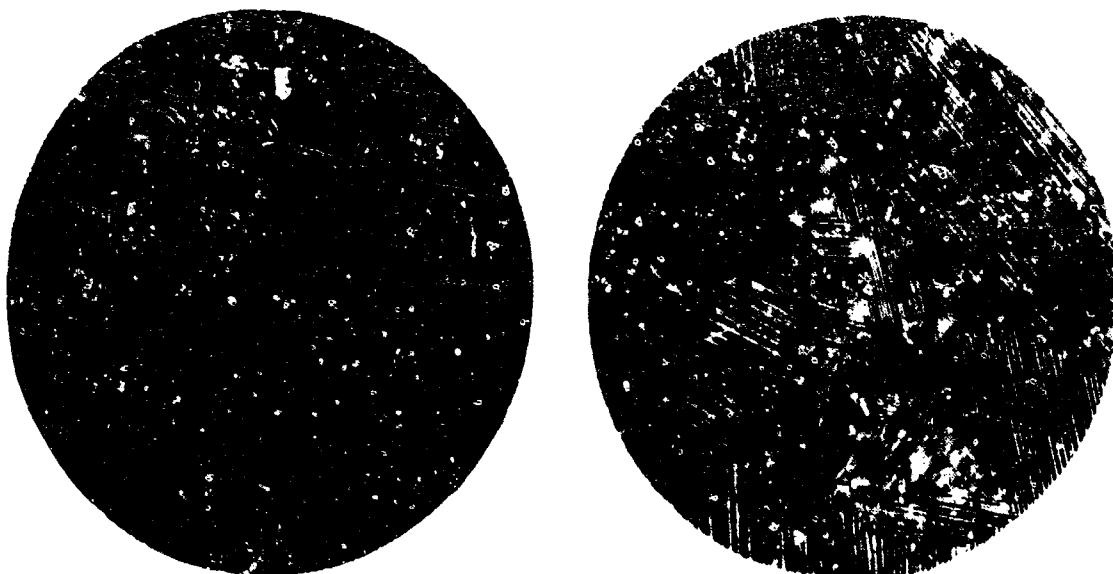


Fig. 7. Microstructure of  $ZrH_2$  at 100X and 500X.

observed internal friction peak is also associated with stress-induced movement of the twin interfaces in  $ZrH_2$ .

The Young's modulus and internal friction of partially stabilized  $ZrO_2$  are shown in Fig. 8. Although the microstructure of the material has not been investigated, it is distinctly possible that the internal friction peak is also due to stress-induced motion of the twin interfaces in the tetragonal phase of  $ZrO_2$ .

The shift of the internal friction peak with frequency yields activation energies of  $\sim 20,000$  cal/mole for  $ZrH_2$  and  $\sim 30,000$  cal/mole for  $ZrO_2$ , which are believed to be the respective activation energies for diffusion of H and O in these materials.

A closer look at the crystal structure of  $ZrH_2$  and  $ZrO_2$  suggests that the twin interface cannot be one atomic layer thick and must be composed of arrays of edge- or screw-type twinning dislocations [9]. The paths taken by atoms during twin interface motion will most likely be defined by the geometry of dislocations or partial dislocations in the lattice, in a manner suggested by Kronberg [10] for slip and twinning in sapphire. Although the details of atom movements have yet to be worked out, it is likely that such movement may require the synchronized motion of both atom species. If twinning

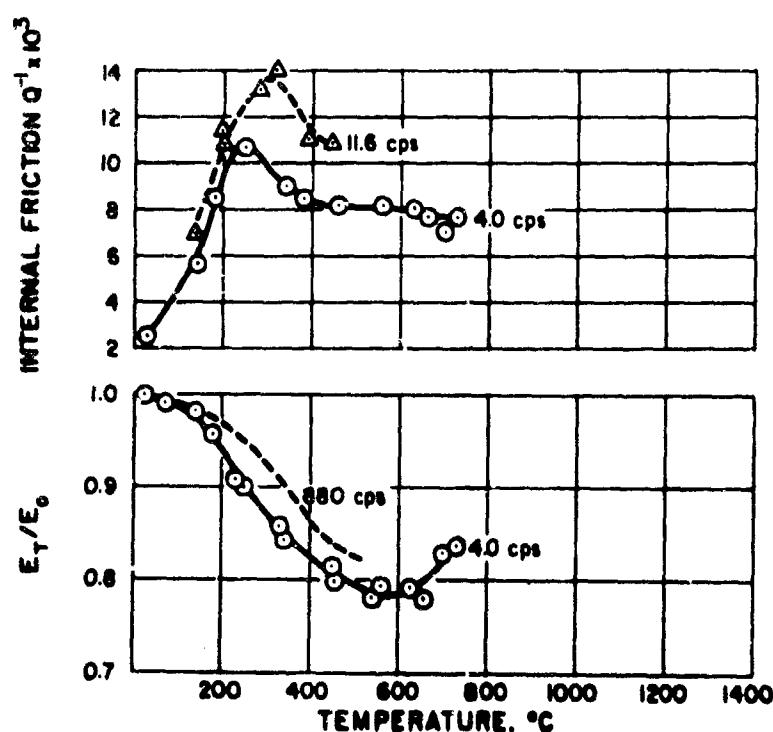


Fig. 8. Temperature dependence of modulus and internal friction of partially stabilized  $ZrO_2$ .

is to be described by the shearing of Zr atoms (or ions) in  $ZrH_2$  and  $ZrO_2$ , the synchronized motion of H and O atoms (or ions) from tetrahedral to octahedral and back to tetrahedral sites is required. Further work is needed to substantiate the hypothesis.

#### IV. Anelastic Phenomena Associated with Mechanical Relaxation in Deformed Crystals

Dynamic anelastic experiments provide an excellent method of studying dislocation motion in crystalline solids at low-stress level to which there is no other easy access. The energy losses due to dislocation motion which have been discussed in the literature are: hysteresis losses, resonance losses, and relaxation losses [11]. Typical hysteresis losses are: those in which dislocations are torn away irreversibly from pinning points by the applied stress [12]; those where moving dislocations feel a stress field due to dispersed impurities, defects, or obstacles [13]; etc. An example illustrating hysteresis losses in oxides is shown in Fig. 9 for a sapphire crystal. The dielectric losses in ionic solids are typical resonance losses which do not involve dislocations [14]. There is one process in crystals which involves dislocations only and which shows all the characteristic

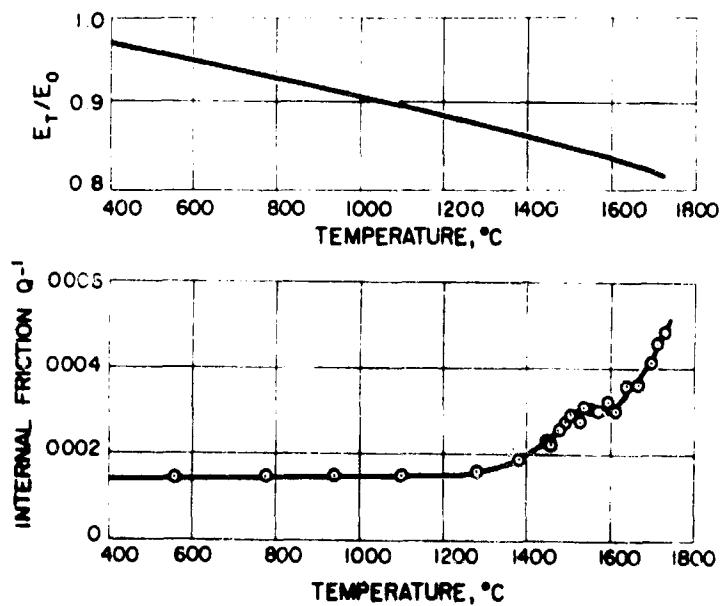


Fig. 9. Temperature dependence of elastic modulus and internal friction of sapphire crystal.

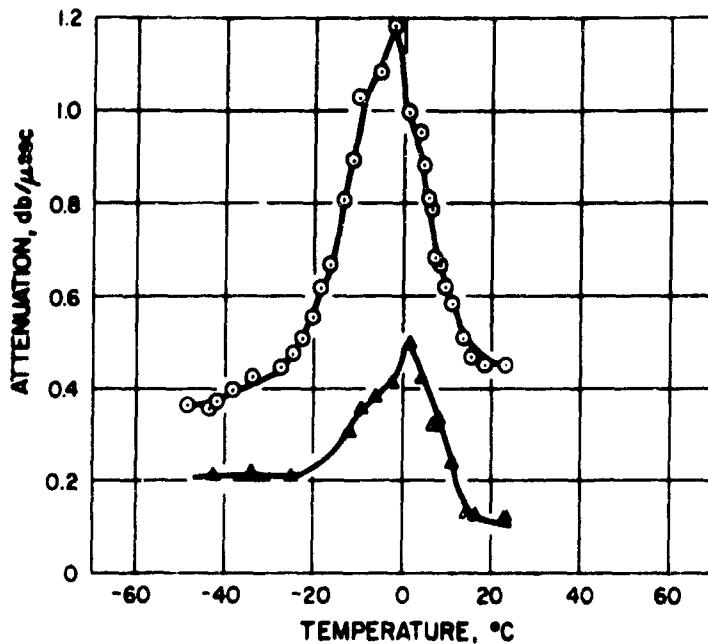


Fig. 10. Temperature dependence of attenuation of MgO single crystals due to cold work. Upper curve, cold worked ( $\sim \frac{1}{2}\%$ ); lower curve, as cleaved.

features of a relaxation mechanism, namely, that observed in various face-centered cubic metals by Bordoni [15]. Recently we have discovered a similar phenomenon in MgO single crystals. Typical examples are shown in Fig. 10. The internal friction peak is enhanced by cold work and can be decreased by annealing. Since the Peierls force may be very important in determining the plastic flow behavior of ceramic materials, further studies along this line are recommended.

## V. Summary and Conclusion

In conclusion, it is impossible to name all the anelastic phenomena occurring in high-temperature materials. The more important ones influencing the mechanical properties of these materials are briefly discussed above. This does not exclude other elastic and anelastic properties of high-temperature materials which are less clearly understood. The changes of elastic properties of commercial polycrystalline NbBe<sub>12</sub> with temperature, for example, are shown in Fig. 11. The increase in Young's modulus of NbBe<sub>12</sub> at  $\sim 1100^\circ\text{C}$  may well be an important factor influencing the high-temperature strength of the material. As another example, the changes of in-

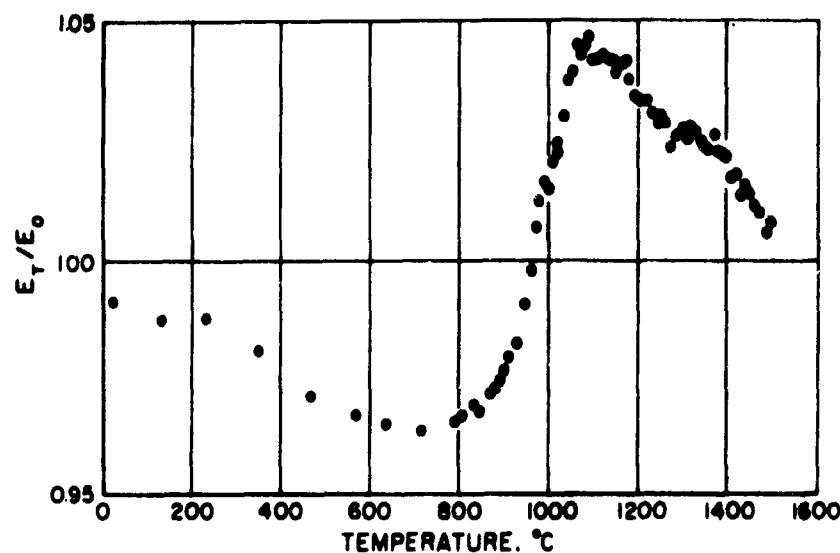


Fig. 11. Temperature dependence of Young's modulus of commercial  $\text{NbBe}_{12}$ .

ternal friction and elastic modulus of graphite with temperature are shown in Fig. 12. The gradual increase in elastic modulus of graphite with increasing temperature is reflected in increasing strength of the material with rising temperature. Fundamental understanding of the mechanism of these phenomena is essential to any scientist or engineer for an intelligent evaluation of the relative merits of existing materials and of the potentialities of new materials for high-temperature applications.

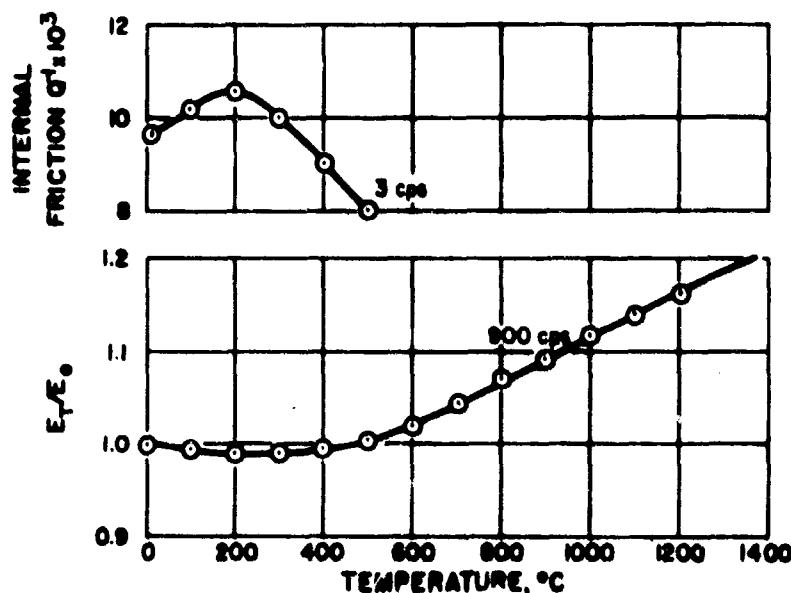


Fig. 12. Temperature dependence of internal friction and Young's modulus of commercial (ECA) graphite.

### References

1. C. Zener, *Elasticity and Anelasticity of Metals*, University of Chicago Press, Chicago, 1948.
2. T. S. Ke, *J. Appl. Phys.* **21**, 414 (1950).
3. See, for example, paper by J. B. Wachtman, Jr., and D. G. Lam, Jr., *J. Am. Ceram. Soc.* **42**, 254 (1959).
4. T. S. Ke, *Phys. Rev.* **71**, 533 (1947).
5. N. F. Mott, *Proc. Phys. Soc. (London)* **60**, 391 (1948).
6. L. C. Chang and T. A. Read, *Trans. AIME* **191**, 47 (1951).
7. M. W. Burkart and T. A. Read, *Trans. AIME* **197**, 1516 (1953).
8. F. Worrell, *Phys. Rev.* **72**, 533 (1947).
9. Z. S. Basinski and J. W. Christian, *Acta Met.* **2**, 101 (1954).
10. M. L. Kronberg, *Acta Met.* **5**, 507 (1957).
11. A. Seeger, H. Donth, and F. Pfaff, *Faraday Society Discussions* **23**, 19 (1957).
12. A. S. Nowick *Progress Metal Phys.* **4**, 1 (1953).
13. J. Weertman, *J. Appl. Phys.* **26**, 202 (1955).
14. R. G. Breckinridge, *Imperfections in Nearly Perfect Crystals*, John Wiley and Sons, 1952, p. 219.
15. P. C. Bordoni, *J. Acous. Soc. Am.* **26**, 495 (1954).

### Discussion

**R. E. Maringer (Battelle Memorial Institute):** Some metals, which contain mechanical twins, have a characteristic property which might be helpful in identifying the damping peak you found in zirconium oxide. If a tensile stress is applied to a metal containing mechanical twins and, at the same time, the internal friction is measured in torsion, the damping is observed to increase significantly. In fact, the damping becomes directly proportional to the rate of application of stress. In a material which is anisotropic in its thermal expansion, such as uranium, the stress can be supplied by a temperature change, and the internal friction becomes proportional to the rate of change of temperature. It is believed that this phenomenon is the result of the stress-induced movement of twin boundaries. The existence of this type of stress-dependent damping in zirconium oxide would provide support for the contention that the mechanism of twin boundary movement is operative and that the observed damping peak is related to this mechanism.

**Leon Green, Jr. (Aeronutronic Division, Ford Motor Co.):** In regard to Fig. 12, I would like to mention that some experiments on internal friction on ECA graphite were made at North American about ten years ago covering a higher temperature range, and we found that a peak in the internal friction data occurred, attending the peaking of the Young's

modulus, or in this case shear modulus—indicating that it was a grain boundary relaxation phenomenon which produced the drop off in modulus at high temperature.

**R. Chang:** Yes. We found the peak at around 2200°C. I am not sure whether it is due to grain boundary relaxation alone. The peak is not very sharp; it is very broad.

**P. L. Pratt** (*University of London*): Have you any idea as to what these kinks in graphite are? I wasn't quite clear on what you said.

**R. Chang:** You take very thin flakes of graphite, look at them under the electron microscope, and you will see very prominent kink bands. Also if you touch a graphite flake with the tip of a tweezer, kinks will form very easily. The geometry of kinks has been worked out by me some time ago. It is not yet published.

**S. A. Bortz** (*Armour Research Foundation*): In obtaining change in dynamic modulus with temperature in Fig. 12, did you cycle your specimens at all; and, if you did, did you observe any hysteresis loop?

**R. Chang:** I'm sorry, I haven't done that, but we do find hysteresis loops in bend tests upon cycling.



AIRESEARCH MANUFACTURING COMPANY OF ARIZONA  
A DIVISION OF THE GARRETT CORPORATION  
PHOENIX, ARIZONA

## APPENDIX IV

### LIST OF REFERENCES

GT-7615-R  
Appendix IV



AIRESEARCH MANUFACTURING COMPANY OF ARIZONA  
A DIVISION OF THE GARRETT CORPORATION  
PHOENIX, ARIZONA

## LIST OF REFERENCES

1. Engineering Report, Gas Turbine Sound Attenuation Final Report, U. S. Army, ERDL Contract Number DA-44-009-ENG-5183, AiResearch Report, SD-5011, Volume II, July 1963.
2. Lazan, Benjamin J., Damping of Materials and Members in Structural Mechanics, Pergamon Press, Inc., August 1965.
3. Oberst, Hermann, On the Damping of Bending Vibrations of Thin Sheet Metal by Adhesive Layers of Damping Materials, Akustische Beihefte, Heft 4, 1952, pp. 181 to 194.
4. Oberst, Hermann, Materials of High Internal Damping, Akustische Beihefte, Heft 1, 1956 in Vol. 6 of Acustica.
5. Oberst, H. and Linhardt, F., On the Temperature Dependence of Vibration Damping Synthetic Materials, Acustica, pp. 255-264, Vol. 11 (1961)
6. Geiger, P. H. Noise-Reduction Manual, Engineering Research Institute University of Michigan, 1956
7. Chang, R. The Elastic and Anelastic Properties of Refractory Materials for High-Temperature Applications, Proceedings of a Conference Conducted by The School of Engineering and the College Extension Division, North Carolina State College - In Cooperation with the Office of Ordnance Research, U. S. Army, at Raleigh, North Carolina, March 9-11, 1960
8. Demer, Louis J., On the Relation Between the Micro-Mechanism of Fatigue and The Macro-Rheology, with special reference to Damping, of High Purity Aluminum, Volume I, Experimental Investigation, A thesis Submitted to the Faculty of the Graduate School of the University of Minnesota, January, 1960
9. Dean, Reginald S., Electrolytic Manganese and Its Alloys, The Ronald Press Company, New York, 1952.
10. Dean, Reginald S., Manganese Alloy, Patented March 11, 1941 #2234428



AIRESEARCH MANUFACTURING COMPANY OF ARIZONA  
A DIVISION OF THE GARRATT CORPORATION  
PHOENIX, ARIZONA

11. Dean, Reginald S., Manganese Alloy, Patented October 21, 1941 #2259459
12. Reginald S. Dean and Anderson, Clarence T., Alloy, Patented December 23, 1941, #2267,300
13. Silent Metal, February New Scientist Library, 1965
14. Jensen, J. W. and Walsh, D. F., Manganese-Copper Damping Alloys, Bureau of Mines Bulletin 624, 1965
15. Zener, Clarence, Elasticity and Anelasticity of Metals, The University of Chicago Press, Chicago, 1948
16. Ross, Donald; Ungar, Eric E.; Kerwin, Jr., E. M.; Damping of Plate Flexural Vibrations by Means of Viscoelastic Laminae, a colloquium on structural damping held at the ASME annual Meeting, Atlantic City, N. J., Dec. 1959
17. Ungar, Eric E., Highly Damped Structures, Machine Design, February 14, 1963
18. Kaufman, J. G., Damping of Light Metals, reprint from Materials in Design Engineering, August 1962
19. Alcoa's Aluminum Powder Metallurgy (APM) Alloys, by Aero-Space Section Sales Development Division, New Kensington, Pa. (Not released for Publication)
20. Andrews, Andrew I., Ph.D., Porcelain Enamels, The Garrard Press, Champaign, Illinois, 1961
21. Glasstone, Samuel, D. Sc., Phd. D. Textbook of Physical Chemistry, Second Edition, Fifth Printing, D. Van Nostrand Co., Inc. New York, 1948
22. C.D.C. Manganese Alloy No. 780, Chicago Development Corporation, Riverdale, Maryland
23. C.D.C. Manganese Alloy No. 772, Chicago Development Corporation, Riverdale, Maryland
24. C.D.C. Manganese Alloy No. 720, Chicago Development Corporation, Riverdale, Maryland



25. Viscosity Characteristics of Selected Porcelain Enamel Frits, (Data Sheet No. 12-165 Chicago Vitreous Corporation, Cicero, Illinois.)
26. Internal Friction, Damping, and Cyclic Plasticity, Symposium Presented at 67 Annual Meeting American Society for Testing and Materials, Chicago, June 22, 1964
27. Demer, L. J., Bibliography of the Material Damping Field (With Abstracts and Punched Card Codings) May 1956, Wright Air Development Center
28. Hastelloy Alloy X. Union Carbide Corporation, Kokomo, Indiana, October, 1964
29. Lyle, John P. Jr. Aluminum Powder Metallurgy Products, reprint from Materials and Methods, April 1956, Reinhold Publishing Corp., New York
30. Rothbart, Harold A., Mechanical Design and Systems Handbook, McGraw-Hill Book Company, New York, 1964
31. Bibliography and Tabulation of Damping Properties of Non-Metallic Materials, Prepared under Contract No. AF 33(657)-7453, University of Minnesota, Minneapolis Minnesota; Sun Hwan Chi, Author)
32. Schlagel, A. Measurements of Modulus of Elasticity and Loss Factor For Solid Materials, B and K Technical Review, No. I, January 1958
33. Schlagel, A. Measurements of Dynamic Modulus of Elasticity and the Loss Factor for Solid Materials (Part II) B and K Technical Review, No. 2, April 1958
34. Harrison, W. N. and Sweo, B. J. Bureau of Standards Journal of Research, 10, 189, (1933).
35. Spears, Earl, The Collected Works of Toshio Yamamoto, G-5019-R, Rev. 1, AiResearch Manufacturing Company, A division of The Garrett Corporation, November 23, 1964



AIRESEARCH MANUFACTURING COMPANY OF ARIZONA  
A DIVISION OF THE GARRETT CORPORATION  
PHOENIX, ARIZONA

36. Churchill, Ruel V., Introduction to Complex Variables and Applications, McGraw-Hill Book Company, Inc. 1948.
37. Dean, R. S., Anderson, C. T., and Potter, E. V., The Alloys of Manganese and Copper: Vibration Damping Capacity Trans., Am. Soc. Metals, Vol. 29, pp. 402-414, 1941(D) Cu, Mn, 11, 20, 24, 26, 27, 32, 38.4, 41.1, 42, 42.1, 44.
38. Engineering Report, Use of Scottfelt Material for Sound-Attenuating Gas Turbines, AiResearch Report GT-7413-R, November 19, 1964.
39. Engineering Report, Use of Slitmetal for Sound Attenuation of the Exhaust of Gas Turbines, AiResearch Report GT-7492, Rev. 1, November 8, 1965.

**GT-7-66**

TAB No. 70-3

1 February 1970

IDENTIFICATION	FORMER STATEMENT	NEW STATEMENT	AUTHORITY
AD-482 069L Garrett Corp., Phoenix, Ariz. AiResearch Mfg. Div. Final engineering rept. 6 Nov 64-13 Dec 65. Rept. no. GT-7515-R- REV-1 3 Feb 66 Contract DA-41-009- AMC-838(T)	USGO: others to Commanding Officer, Army Engineer Research and Development Labs., Fort Belvoir, Va.	No limitation	USAMRDC notice, 20 Aug 69